1-ICGTMW2023

1st International Conference on Geotechnics of Tailings and Mine Waste

October 24 – 26, 2023

Ouro Preto, Brazil

www. geominouropreto.com.br/2023/icgtmw2023/

1-ICGTMW2023

1ST International Conference on Geotechnics of Tailings and Mine Waste

PREFACE

The TC221 on Tailings and Mine Waste was launched by the ISSMGE in March 2020. Its purpose is to provide a platform to discuss, exchange, and disseminate scientific advances, expert knowledge, and practical know-how in all geotechnical engineering issues related to the design, construction, and closure of the earth structures required for the storage of waste materials resulting from mining processes. The First International Conference on Geotechnics of Tailings and Mine Waste (1-ICGTMW), held from 24 to 26 October 2023, in Ouro Preto, Minas Gerais, Brazil, with a focus on the geotechnical characterization, design, stability, construction, and monitoring of tailings dams and mining waste deposits is an important step towards fulfilling the purpose of the TC221.

Mining engineers conceive mining waste structures as part of the requirements imposed by the operation of mines and mineral exploitation. However, materials characterization, design, and stability analysis are primarily addressed by geotechnical engineers. The proper technical management of tailings and mining waste and decision-making depends on geotechnical engineering analyses. The wide range of challenging geotechnical topics covers different issues going from the evaluation of the complex hydro-mechanical behavior and the characteristic mechanical properties of these particular granular materials to the verification of the long-term stability for the closure stage.

Tailings dams and rock waste dumps belong to the largest and most complex modern earth structures. As large catastrophic failures have shown in the past, they pose a huge risk for the people and the environment, and for this reason, they demand the highest technical expertise and the best level of geotechnical engineering available. By bringing together geotechnical practitioners, experts, and researchers working in the field of tailings and mining waste as well as disseminating and improving the state of the art in this field, the 1-ICGTMW has significantly contributed to the sustainable development of the extractive industry.

Prof. Fernando Schnaid
Secretary TC221
Univ. Federal do Rio Grande do Sul, Brazil

Prof. Roberto Cudmani
Vice Chair TC221
Zentrum Geotechnik, Techn. Univ. of Munich

Dr. Ramón Verdugo
Chair TC221
CMGI – Chile

Brazil, October 2023.

ABOUT 1-ICGTMW2023 Conference

The 1- ICGTMW 2023 was held from 24th to 26th, October 2023 in Ouro Preto, State of Minas Gerais, Brazil. The 1-ICGTMW 2023 is organized by the Brazilian Geotechnical Society under the auspices of the International Society of Soil Mechanics and Geotechnical. Engineering – Technical Committee TC221 on Tailings and Mine Waste. This conference aims to bring together engineers, scientists, researchers, educators and practitioners, with the purpose of generating a forum for discussion, knowledge exchange and dissemination of the best engineering practices in different geotechnical issues related to tailings storage facilities (TSF) and mine waste. The event will take place in parallel with the Geomin Symposium, a Brazilian event that attracts different stakeholders and practitioners from the mining industry. The technical program includes high-quality keynote lectures and sessions where accepted papers will be presented by their authors. The official language of the 1-ICGTMW 2023 is English.

Ouro Preto was founded at the end of the 17th century, being the focal point of the gold rush and Brazil's golden age in the 18th century. The baroque architecture, including churches, bridges, fountains, and squares, and its steep, winding cobbled streets are a testimony to its past prosperity. The city is in the State of Minas Gerais where 53% of Brazilian iron ore and 29% of ores in general are produced, including gold, zinc, phosphate and niobium. In 2020, the National Mining Agency in Brazil registered 221 tailings dams in Minas Gerais.

ACKNOWLEDGEMENTS

The TC221 on Tailings and Mine Waste acknowledges the support of the Brazilian Geotechnical Society, GEOMIN and the Zentrum Geotechnik of the Technical University of Munich in the organization of the 1st International Conference on Geotechnics of Tailings and Mine Waste.

CONTENTS

COMMITTEES

Steering Committee

Jose Campana

Roberto Cudmani

Fernando Schnaid

Luis Valenzuela

Ramón Verdugo

Fernando Saliba

Scientific Committee

The nominated members of the TC221 are appointed in the Scientific Committee of this event:

Andrés Peña Olarte, Germany

Juan de Dios Alemán Velasquez, Mexico

Rigoberto Rivera Constantino, Mexico

Christopher Beckett , United Kingdom

Antonio Carraro, United Kingdom

Shi-Jin Feng, China

Yongfeng Deng, China

Shaw Shong Liew, Malaysia

Luiz Guilherme De Mello, Brazil

Márcio Almeida, Brazil

Steven Kramer, United States

Alejandro Martinez, United States

Paolo Simonini, Italy

Koldobika Sánchez Arrotegui, Spain

Ignacio Pérez Rey, Spain

Jean-François Vanden Berghe, Belgium

Waldemar Świdziński, Poland

Andrzej Gruchot, Poland

Laura Carbone, Germany

Brahian Roman, Peru

Jun Yang, Hong Kong

Jesse Tam, Hong Kong

Alejo Sfriso, Argentina

Luciano Oldecop, Argentina

Nuno Cristelo, Portugal

Hongjie Zhou, Australia

Øyvind Torgersrud, Norway

Luca Piciullo, Norway

Mitsu Okamura, Japan

Takashi Kiyota, Japan

Mayu Tincopa, Peru

Norbert Morgenstern, Canada

Luis Valenzuela, Chile

Susumu Yasuda, Japan

Richard Jewell, Belgium

Joan Manuel Larrahondo, Colombia

Jan Laue, Sweden

Sven Knutsson, Sweden

Ioannis Zevgolis, Greece

Eoin McGrath, Ireland

Adrian Russell, Australia

Sarat Das, India

Gonzalo Suazo, Chile

Marcelo Gonzalez, Chile

Antonio Viana da Fonseca, Portugal

Mamadou Fall, Canada

Nikolay Milev, Bulgaria

1st ICGTMW - PROGRAM

Session 1: Soil Mechanics, Constitutive Models and Analysis

Tuesday, October 24, 12:00pm to 1:00pm

Chair: Alejo Sfriso

Vice-Chair: Arcesio Lizcano

1.- Assessment of advanced constitutive models to simulate the monotonic behaviour of mine tailings.

By Ana Paula Ribera, Andrés A. Peña-Olarte, Lennon Ferreira Tomasi and Roberto Cudmani.

2.- Numerical modeling of static liquefaction in tailing dams – comparison between HSS, Norsand, and MIT-S1 constitutive models.

By Nicolas A. Rivas, Mauro G. Sottile, Felipe Lopez Rivarola and Alejo O. Sfriso.

3.- Effect of principal stress direction on loading response of unsaturated iron ore tailings.

By Ana Claudia de Mattos Telles, David Reid, Antonio Jeronimo Pereira de Souza Junior, Riccardo Fanni, and Andy Fourie.

4.- Influence of grain size distribution on flow liquefaction a DEM study.

By Syed Uzair Us Salam Shah, Roberto Cudmani, and Andrés Alfonso Peña-Olarte.

5.- Influence of the sample reconstitution procedures on the mechanical behaviour of iron ore tailings.

By Paulo Coelho, David Camacho, Felipe Gobbi.

Session 2: Monitoring, Testing & Technology

Tuesday, October 24, 5:30pm to 6:30pm

Chair: Andrés Peña

Vice-Chair: Fredy Diaz

1.- Automatic activation systems for sirens in dams.

By Hyllttonn Bazan, Samuel Silva Mendes, Filipe Colen de Freitas Guimarães and Mauricio Baleeiro.

2.- Improvement of tailings and mine waste by means of KSI.

By Gerd Maitschke, Thomas Meier

3.- Optical Satellite imagery to monitor tailings dams.

By Christopher Galen O'Donovan, Luis Alberto Torres-Cruz and Elhadi Adam.

4.- Mechanical performance of sandy and ultrafine tailings mixtures in experimental landfills.

By W. Pirete, P. Cella, A. Freire, D. Silva, P. Andrade, T. Augusto,and A. Risoli.

5.- Stabilization of iron tailings with alkali activated binders.

By Isabela Caetano, Sara Rios, António Viana da Fonseca, and Bruno Delgado.

Session 3: Stability analysis and safety assessment

Wednesday, October 25, 9:30am to 10:30am

Chair: Ramón Verdugo

Vice-Chair: José Campaña

1.- Reliability-based analysis of tailing storage facilities. A case study Cadia NTSF embankment failure.

By Benedikt Schatz, Andrés A. Peña-Olarte, Ana Ribera, Joshua Schorr, Iason Papaioannou, and Roberto Cudmani.

2.- Influence of tailings rheological parameters on the estimation of run-out distances.

By Claudio Román, Viktor Kovács, Fernanda Kunoh, Nicolás Echeverría, and Ignacio Gutiérrez.

3.- On the interpretation of trigger analyses of upstream-raised tailings dams.

By Alejo O. Sfriso, Mauro G. Sottile, Felipe López Rivarola and Osvaldo N. Ledesma.

4.- Consulting experience in the implementation of the global industry standard on tailings management.

By Claudio Román, Fernanda Kunoh, Gabriela Barbosa, Alix Becerra and Eric Chucos.

5 - Review of the key factors that influence pseudo-static stability analyses of downstream and upstream tailings sand dams.

By Camilo Morales, Carolina Palma and Jaime Olivares.

Session 4: Undrained Behavior

Wednesday, October 25, 12:00pm to 1:00pm

Chair: Roberto Cudmani

Vice-Chair: Bruno Delgado

1.- A numerical study on the representativity of laboratory test stress paths for undrained shear strength characterization for dam reinforcement safety assessments.

By Bruno Szpigel Dzialoszynski.

2.- Calculation of Undrained Shear Strength of a Bauxite Tailings using Field and Laboratory Tests.

By Guilherme Henrique da Silva Pinto, André de Oliveira Faria, and Mauro Pio dos Santos Junior.

3.- Does the anisotropy of the collapse/instability surface play a role when assessing the stability of tailings dams?

By David Hight and Tiago Gerheim Souza Dias.

4.- Analysis of the variation of undrained shear resistance of bauxite mining tailings through Vane and CPTu tests.

By Helena Paula Nierwinski, Kymberly Ramos Martins Feltz, Marcelo Heidemann and Talita Menegaz.

Session 5: Seismic Analysis

Wednesday, October 25, 3:00pm to 4:00pm

Chair: Takemi Yamada

Vice-Chair: César Pastén

1.- Defining efficient ground motion intensity measures to estimate displacements of tailings dams.

By César Pastén, Bastián Garrido and Pablo Heresi.

2.- Influence of the foundation soil stratification on the seismic response of an earthfill tailings dam.

By Marcelo Gonzalez S.

3.- Seismic Observation and Monitoring for a Tailings Storage Facility with Soil Solidification.

By Takemine Yamada, Tomoki Hikita, Keisuke Murata and Yoshinobu Kishimoto.

4.- Validation of constitutive models for assessing the seismic response of tailing dams during strong earthquakes.

By Roberto Cudmani, Antal Csuka, Andres A. Pena-Olarte.

5.- Application of the SANISAND-SF Constitutive Model for Non-Linear Dynamic Analysis of Filtered Tailings Dams.

By Brahian Roman, Martín Villanueva and Andrés Barrero.

Session 6: Waste Piles

Wednesday, October 25, 5:30pm to 6:300pm

Chair: Rafael Jabur Bittar

Vice-Chair: Fernando Schnaid

1.- Compaction performance of iron ore tailings mixture in the iron quadrangle.

By A. Freire, P. Cella, W. Pirete, D.Silva, P.Andrade, A. Oliveira and A. Risoli.

2.- Characterisation of tailings for dry stacks.

By David Hight, Angeliki Grammatikopoulou, Tiago Dias, Felix Schroeder and Luiz Guilherme de Mello.

3.- Disposal of filtered tailings and associated waste in Brazil – the PDER Alegria Sul (Samarco) case.

By Paulo Franca, Wanderson Silvério Silva, Viviane Aparecida Rezende.

4.- Geomechanical behaviour of an iron ore tailings under high-stress levels for disposal by dry stacking.

By Bruno Guimarães Delgado, António Viana da Fonseca, Rafael Jabur Bittar, Breno de Matos Castilho and Daniela Coelho.

5.- Stability evaluation of long-standing mining waste dumps – case studies.

By Paulo Roberto Costa Cella, Flávia Augusta Padovani and Fábio Marinho da Silva.

INVITED LECTURES

Honoured Lecture

Andy Fourie, Australia

Keynote Lectures

Adrian Russell, Australia

Wlademar Świdziński, Poland

Luis Torres-Cruz, South Africa

Luis Valenzuela, Chile

Susumu Yasuda, Japan

ANDY FOURIE

ENSURING GEOTECHNICAL STABILITY OF FILTERED TAILINGS STACKS

Andy is a civil engineer, graduating with a Bachelor's Degree in Civil Engineering and a Master's Degree in Engineering from the University of the Witwatersrand in Johannesburg, South Africa. After working as a geotechnical engineer for SRK Consulting on a variety of tailings storage facilities and earth dam projects, he moved to the UK and obtained a PhD in Geotechnical Engineering from Imperial College in London. He then spent 15 years at the University of the Witwatersrand in Johannesburg, where he was appointed as Professor of Civil Engineering and led the Waste Impact Minimisation Programme research group, which investigated issues relating to tailings management and landfilling in South Africa. Andy joined the Australian Centre for Geomechanics in 2005 as a Professorial Fellow in Environmental Geotechnics and moved to the Department of Civil, Environmental & Mining Engineering at the University of Western Australia (UWA) in 2008, where he is Professor of Civil & Mining Engineering. The focus of his research work is the safe and environmentally sound management of mining, industrial and municipal solid wastes and recently had several industry-funded research projects, including TAILLIQ and Filtered Tailings Stability. He is currently the Director of Future Tails, which is funded by BHP and Rio Tinto, and through Future Tails he has established a fully online Graduate Certificate in Tailings Management at UWA. The first students are due to graduate from this programme in mid-2023. Together with Prof Ramon Verdugo, in 2022 he presented the State of the Art of Mine Tailings at the 20th International Conference on Soil Mechanics and Geotechnical Engineering, held in Sydney. Andy currently serves on a number of Independent Technical Review Boards (ITRBs) around the world and maintains strong links with industry through these and other consulting practices, thus helping to inform current and future research initiatives at UWA.

ADRIAN R. RUSSELL

PARTIAL SATURATION INFLUENCES ON THE CPT, STRENGTH AND STABILITY OF SILTY TAILINGS

Adrian Russell is a Professor in Geotechnical Engineering at UNSW Sydney. He is also an Australian Research Council Future Fellow, which requires him to devote 100% of his time to research on tailings liquefaction. His expertise is in laboratory element testing of soils and tailings, laboratory controlled CPTs and earthquake simulation, particle and pore geometry characterization, unsaturated soil mechanics and cavity expansion theory, and knowledge transfer to industry.

He is an Australian representative on TC106 and TC221, which are International Technical Committees on unsaturated soil mechanics and tailings within the ISSMGE. He does expert review work on the stability of TSFs. In 2019, he spent a 6-month (0.4FTE) secondment with Pells Sullivan Meynink Pty Ltd, providing expertise on mine waste projects.

He was awarded his PhD in 2005 and BE in 1998, each by UNSW Sydney. His first academic appointment was a lectureship at the University of Bristol in the UK (2003-2007). This was followed by a move UNSW Sydney where has been ever since.

WALDEMAR ŚWIDZIŃSKI

THE KEY ROLE OF COMPREHENSIVE MONITORING SYSTEMS IN ENSURING THE SAFE OPERATION AND DEVELOPMENT OF TSFS

Prof. Waldemar Świdziński, PhD, DSc: Permanent professor at the Institute of Hydro-Engineering, over the years Head of the Department of Geomechanics, from 2016 - Director of the Institute. Author and co-author of over 130 publications and 3 books on marine and inland civil engineering, specifically focused on: experimental mechanics laboratory element testing oriented, experimental identification and theoretical description of liquefaction of saturated and unsaturated soils, soil-water-structure interaction, modelling of groundwater flow and pollution transport, various problems of large tailings storage facilities. Rich engineering experience in an assessment of the stability of slopes, cliffs and earth dams. For 40 years an expert for Żelazny Most TSF. Recently, a member of the International Board of Experts for this facility. Member of two technical committees at the International Society of Soils Mechanics and Geotechnical Engineering: TC203 on Earthquake Geotechnical Engineering and TC221 on Tailings and Mine Wastes. At the domestic market a member of various societies and scientific committees. Currently a Secretary of the Polish Geotechnical Committee.

LUIS A. TORRES-CRUZ

TAILINGS DAM FAILURES: CAUSES AND POTENTIAL SOLUTIONS

Luis holds a PhD in Geotechnical Engineering from Wits University in Johannesburg, South Africa. He is currently a senior lecturer at Wits where his teaching contributions include postgraduate courses on tailings management and critical state soil mechanics. The main driver of his research has been the prevention of catastrophic failures of tailings dams. This has involved topics such as slope stability analysis, laboratory testing, in situ testing, and analysis of satellite imagery. Luis's achievements include best paper in South Africa's Young Geotechnical Engineer's conference, finalist of the RM Quigley Award from the Canadian Geotechnical Journal, winner of the Jennings award of the South African Institution of Civil Engineering, co-author of a 2022 state-of-the-art paper on the geotechnics of tailings dams, and winner of the Barry van Wyk award which supports emerging researchers at Wits University. Luis's research efforts have benefitted from collaborations with other academics as well as interactions with industry. Besides publications in international conferences and journals, he has presented his research findings at multiple consulting companies, mining houses, and universities, both in South Africa and abroad. Luis is a chartered engineer with the engineering council of the UK and is a member of the British and South African Institutes of Civil Engineering.

LUIS VALENZUELA

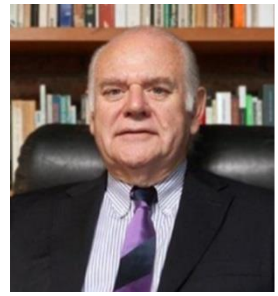

THE CHALLENGE OF LARGE WASTE ROCK DUMPS

Civil Engineer, Universidad de Chile, 1973 and MSc in Soil Mechanics, Imperial College of Science and Technology, University of London, 1975. More than 40 years of experience in large mining and infrastructure projects in several countries. After working in Brazil in earth and rockfill dams for hydroelectric projects he came back to Chile and become co-founder and partner of Geotécnica Consultores, and Arcadis Chile. Since 2016 is a fully independent geotechnical consultant. During the last 20 years he has been involved in mining projects mainly focused in tailings dams, waste rock dumps, tunnels, and mining environmental issues. He has participated in several Independent Review Boards for mining projects in Argentina, Australia, Brazil, Canada, Chile, and Peru. He has an active participation in international and Chilean learned societies as well as in several professional and business associations such as ISSMGE, Vice President for Central and South America (1994-1997); Institute of Civil Engineers of Chile (IICH) former president (2004-2005); Academy of Engineering of Chile numerary member; Argentina Academy of Engineering, correspondent member. He is also representative of the Institute of Mining Engineers of Chile in the Global Action on Tailings international task force. In 2015 he was awarded with the 2015 Gold Medal of the IICH and in the same year he delivered the Casagrande Lecture in the Pan American conference of the ISSMGE on the subject “Hydraulic Fill and Sand Tailings Dams”. Author of more than 50 publications related to soil mechanics, rock mechanics, tunnels and underground excavations, slope stability, landslides, earth dams, hydraulic fill dams, tailings dams, large waste rock dumps, and seismic analysis of earth works.

SUSUMU YASUDA

SEISMIC INSPECTION AND COUNTERMEASURES FOR EXISTING TAILINGS DAM IN JAPAN

Dr. Susumu YASUDA is professor emeritus at Tokyo Denki University. He was born in Hiroshima in 1948. He received his B.S. in civil engineering from Kyushu Institute of Technology, and his Dr. of Engineering in civil engineering from University of Tokyo in 1975. Following his Dr. of Engineering, he worked at Kiso-jiban Consultants Co. as a geotechnical consulting engineer. He joined Kyushu Institute of Technology in 1986, and then moved to Tokyo Denki University in 1994. He was the Vice President of Tokyo Denki University from 2016 to 2017. He retired in 2018 and is currently a visiting professor at Tokyo Denki University. His main research interest is in soil liquefaction during earthquakes. He visited many countries to investigate the damage due to liquefaction. He was the Vice President of the Japanese Geotechnical Society in 2006 to 2007 and the President of Japan Association for Earthquake Engineering from 2013 to 2014. In the International Society for Soil Mechanics and Geotechnical Engineering, he was the chairman of the Asian Technical Committee (ATC) No.10 on Urban Geo-informatics in 2002 to 2006 and the chairman of the ATC No.3 on Geotechnology for Natural Hazards in 2006 to 2010.

Session 1:

Soil Mechanics, Constitutive Models and Analysis

Assessment of advanced constitutive models to simulate the monotonic behaviour of mine tailings

Ana Paula Ribera, Technical University of Munich, Germany
Andrés A. Peña-Olarte, Technical University of Munich, Germany
Roberto Cudmani, Technical University of Munich, Germany
Lennon Ferreira Tomasi, Universidade Federal do Rio Grande do Sul, Brazil

Abstract

Mine tailings are granular materials with particle sizes ranging mainly from silt to sand. Tailings are often stored in large containment structures such as tailings ponds or tailings dams. They are deposited hydraulically in a very loose state, resulting in low density, high compressibility and low shear strength in comparison with natural soils with comparable grain size. In addition, depending on the source material (the ore), chemical reagents used in the extraction process and type of deposition, they can present a high degree of heterogeneity of both, solid and fluid fractions. Consequently, mine tailings might exhibit complex hydro-chemo-mechanical behaviour, including contact bonding, particle breakage, brittle material response, rate-dependence, strain softening and liquefaction, among others. Constitutive models for soils provide a valuable tool to (some extent) capture the complex stress-strain response of mine tailings, which is of utmost importance to reliably assess the stability of Tailing Storage Facilities (TFS). In this contribution, the critical features of the mechanical response of mine tailings are introduced in the framework of modern soil mechanics, and a review of the constitutive models that have been used in practice to capture the mine tailings' mechanical response is presented. A benchmark of two constitutive models (i.e. Nordsand and Hypoplasticity) with experimental results of different mine tailings is carried out. Finally, the challenges and perspectives for a more comprehensive constitutive modelling of mine tailings are discussed.

Introduction

Due to the consistent growth of the mining industry, the production and deposition of mineral waste (so-called tailings) that is left over after minerals and metals have been extracted from ore is continuously increasing. Tailings comprise granular materials mixed with chemical and processing fluids from mineral extraction. They mainly consist of sand, silt, and clay-sized particles. Tailings are usually stored as soft slurries in large containment structures known as Tailings Storage Facilities (TSFs), consisting of tailings ponds or tailings dams. Though these structures are crucial to prevent environmental contamination and minimise the release of harmful substances into the surrounding ecosystem, catastrophic failures of TSFs occur significantly more often than water retaining dams. According to (ICOLD, 2001), the likelihood of failures in tailing dams is a hundred times higher than that of water retaining dams.

Numerical methods, e.g. the finite element method and the finite difference method, in which the behaviour of the tailings is described with constitutive models, are used to investigate the hydro-mechanical response and assess the stability of tailing dams. The heterogeneous mineral composition and material properties of tailing dams, as well as the very loose state resulting from the extraction technique, hydraulic deposition, and varying mineral composition of the ore, pose a significant challenge to both the realistic modelling of the mechanical behaviour of tailings and the hydro-mechanical response of TSF.

This contribution focuses on the modelling of the mechanical behaviour of tailings using advanced constitutive models, specifically with NorSand and Hypoplasticity under drained and undrained monotonic shearing.

Properties and Mechanical Behaviour of Tailings

Tailings' characteristics vary depending on ore mineralogy and extraction processes, influencing their mechanical traits. Noteworthy properties include grain size distribution, grain shape, influenced by ore milling and grain mineralogy (Blight, 2009).

Particle relative density (G) impacts waste density and volume/mass calculations tied to host rock characteristics. Plasticity properties, defined by the Atterberg limits (plastic limit (wP) and liquid limit (wL)), are determined by the finer fraction. Tailings sands and slimes exhibit higher compressibility than natural soils due to their loose state, angularity, and gradation (Vick, 1990). Owing to their loose state, tailings can develop excess porewater pressure, leading to a significant reduction and, significantly, to a loss of effective stress and strength upon undrained monotonic and cyclic shearing. This mechanical feature of tailings confers TSF a high potential for catastrophic failure (Blight, 2009).

Hydrogeological properties depend on grain size, ore nature, pore fluid viscosity and plasticity. Hydraulic conductivity varies due to segregation and deposition, with horizontal hydraulic conductivity usually greater than vertical. Permeability parallel and normal to stratification must be measured for hydraulic deposition plans (Blight, 2009).

Shear strength of tailings depends on loading rate, permeability, and drainage conditions. Undrained or partially drained response arises from incremental embankment raises or periodic tailings deposition. If not compacted, tailings are initially deposited loosely and gradually densified through consolidation, enhancing shear strength. Most tailings lack cohesion, exhibiting zero effective cohesion intercept (c') and effective friction angle (φ') higher than similar graded natural soils due to angular particle shape (Mittal & Morgenstern, 1975).

The coefficient of consolidation affects storage construction rate, controlling drainage and strength gain. The design of TSF must ensure geotechnical stability during operation and after closure. Thereby, scenarios related to static/dynamic liquefaction are linked to catastrophic failures (e.g., Ishihara, 1984; Davies et al., 2002; Jefferies & Been, 2015).

Constitutive Models for Tailings Materials

Different advanced constitutive models have been used or have the potential to describe the mechanical behaviour of tailings under compression as well as drained and undrained shearing.

Examples of elastoplasticity models applied to the simulation of tailings are the NorSand (Morgenstern et al., 2016; Jefferies et al., 2019; Robertson et al., 2019), the UBCSand (Beaty & Byrne, 1998), the Hardening Soil Small Strain (HSS) model (Schanz et al., 1999; Benz, 2007) and the SandiSand (Manzari & Dafalias, 1997).

Despite its ability to realistically simulate the behaviour of granular materials under drained and undrained monotonic and cyclic shear (Herle, 1997; Niemunis & Herle, 1997; Gudehus, 1996; Tsegaye et al., 2010; Cudmani, 2013), Hypoplasticity has not been used to model the behaviour of tailings so far.

In the following, the performance of NorSand and Hypoplasticity are compared with experimental results from the literature to assess the suitability of these two constitutive models to capture the behaviour of tailings materials under monotonic drained and undrained shearing.

NorSand

The NorSand model was developed by Jefferies (1993) in the framework of the plasticity theory and the Critical State Soil Mechanics (CSSM). The elastoplastic model with isotropic hardening is capable of simulating static liquefaction (Li & Leao, 2018; Sternik, 2014).

The yield surface and the stress-dilatancy behaviour of the model are based on the Cam Clay model and the image state and include an internal cap to limit the maximum dilatancy at a given state. The image state is the point on the yield surface in the p-q space, where the dilatancy is zero (Sternik, 2014). This state is comparable with the apex of the ellipse in the modified cam clay model.

The constitutive model requires a set of eight parameters, of which two define the critical state line (CSL) (**Γ** and **λ**), two the elastic behaviour (**I_r** and **ν**), and four control the plastic response (**M_{tc} N** and **H**).

Further developments of the original model can also simulate cyclic mobility by incorporating kinematic hardening (Jefferies & Shuttle, 2011; Shuttle & Jefferies, 2005), whereby additional parameters are required.

Hypoplasticity

The theory of hypoplasticity was developed at the Institute of Soil and Rock Mechanics of the Karlsruhe Institute of Technology (KIT) in the nineties (Gudehus, 1996). The constitutive model consists of a nonlinear tensor equation describing the relationship between the stress rate tensor and strain rate tensor (Wolffersdorff, 1996; Niemunis, 2003). Unlike elastoplasticity, yield surfaces, plastic potential and hardening rules are not needed in hyoplasticity. Moreover, elastic and plastic deformation are not explicitly differentiated in this model. The critical state in the stress space is described by the Matsuoka-Nakai criterion, in which the critical friction angle φ_c controls the size of the cross section.

The model can realistically simulate the rate-independent, nonlinear, density-dependent (pyknotropy) and stress-dependent (barotropy) behaviour of granular materials for monotonic and cyclic loading for drained and undrained conditions.

Three pressure-dependent characteristic void ratios $\boldsymbol{e_d}(p')$, $\boldsymbol{e_c}(p')$ and $\boldsymbol{e_i}(p')$ are defined, being $e_c(p')$ the critical state line, $\boldsymbol{e_d}(p')$ the possible densest and $\boldsymbol{e_i}(p')$ loosest state. In the framework of hypoplasticity, the densest and the loosest states define the upper and lower bounds of possible states for a material. The dependence of the characteristic void ratios on pressure is controlled by the granular hardness $\mathbf{h_s}$ and the exponent **n**. Additional material parameters are the exponent $\boldsymbol{\alpha}$, controlling the material dilatancy and $\boldsymbol{\beta}$, the initial stiffness. Assuming grain permanence, the eight parameters depend on the granulometric properties and are almost state-independent. They can be determined with standard laboratory tests or estimated from index tests and empirical relationships (Wolffersdorff, 1996; Herle, 1997).

For cyclic loading, an additional tensorial state variable, the so-called intergranular strain, and five additional model parameters are needed (Niemunis & Herle, 1997)

Calibration of constitutive models

Parameter calibration is a crucial phase for model application. Material parameters can be calibrated manually (Herle & Gudehus, 1999) or automatically, e.g. using genetic algorithms (Zhao, X. et al. 2022) based on experimental results from laboratory tests. Parameter calibration aims to find an optimum set of values that capture key features of the material response, e.g. stiffness, dilatancy, strain hardening and softening, and strength at the peak and critical states.

The NorSand parameters in this contribution are taken from the literature (Morgenstern et al., 2016; Jefferies et al., 2019). The numerical integration of the constitutive equations was done with a Visual

Basic for Application (VBA) program from Jefferies and Been, 2015. The parameters of the hypoplasticity model are determined using a tool that employs genetic algorithms to automatically derive optimal parameters for constitutive models (Zhao, X. et al. 2022). The numerical integration of the constitutive equations was carried out with the program IncrementalDriver (Niemunis, 2008). Detailed summaries of the parameters used for both models can be found in the attachments section at the end of this paper.

The initial void ratio and stress for the numerical integration of the constitutive models correspond to the values in the experimental element tests. For each analysed tailing material, a unique model parameter set is used. The element test simulations with both models and the comparison with the experimental results include drained and undrained triaxial compression tests with different initial confining pressures and void ratios.

Applied Constitutive Models for Tailings materials

Tailings materials

This study examines a series of laboratory tests from two tailing dams from the literature (Morgenstern et al., 2016; Jefferies et al., 2019).

The first laboratory test series was conducted with tailings from the Cadia Tailing Dam in Australia (Jefferies et al., 2019). The Cadia tailings were divided into two materials: TC1, a predominant silt material, and TS2, corresponding to sandy silt layers. The laboratory tests were carried out to investigate the causes of the catastrophic failure of the Cadia Tailing Dam.

The second test series belongs to the experimental program to clarify the failure of the Fundão Tailings Dam in Brazil (Morgenstern et al., 2016). Also, in this case, two types of tailings, a Fundao Lower Bound (FLB) and Fundao Upper Bound (FUB), with clearly different critical state lines, were investigated.

Element tests simulations and comparison with the experiments

A series of consolidated isotropic undrained (CIU), consolidated isotropic drained (CID) and Oedometric Tests were used to calibrate the hypoplasticity model, while the parameters of NorSand were obtained from the literature mentioned above.

For the Cadia Sandy Tailings TS2, three drained and two undrained triaxial compression tests were considered for calibration. The experimental and numerical results are shown in **Figure 1**.

In the case of drained shearing, both models capture the steady-state strengths and initial stiffness for low confining stresses (Figure 1a) satisfactory, though numerical results obtained with hypoplasticity slightly deviate from experimental results for higher initial confining pressures. Experimental and simulated volumetric strains (Figure 1b) are also in good agreement for both models. Under undrained conditions (Figure 1c and 1d), both models can satisfactorily reproduce the initial stiffness, the strength at the instability state and the effective stress paths observed in the experiments. Simulations with NorSand show more significant deviations from experiments than hypoplasticity at the critical state. Up to some extent, Norsand can reproduce the quasi-steady state (QSS) observed in the experiments, while hypoplasticity cannot model quasi-steady states at all.

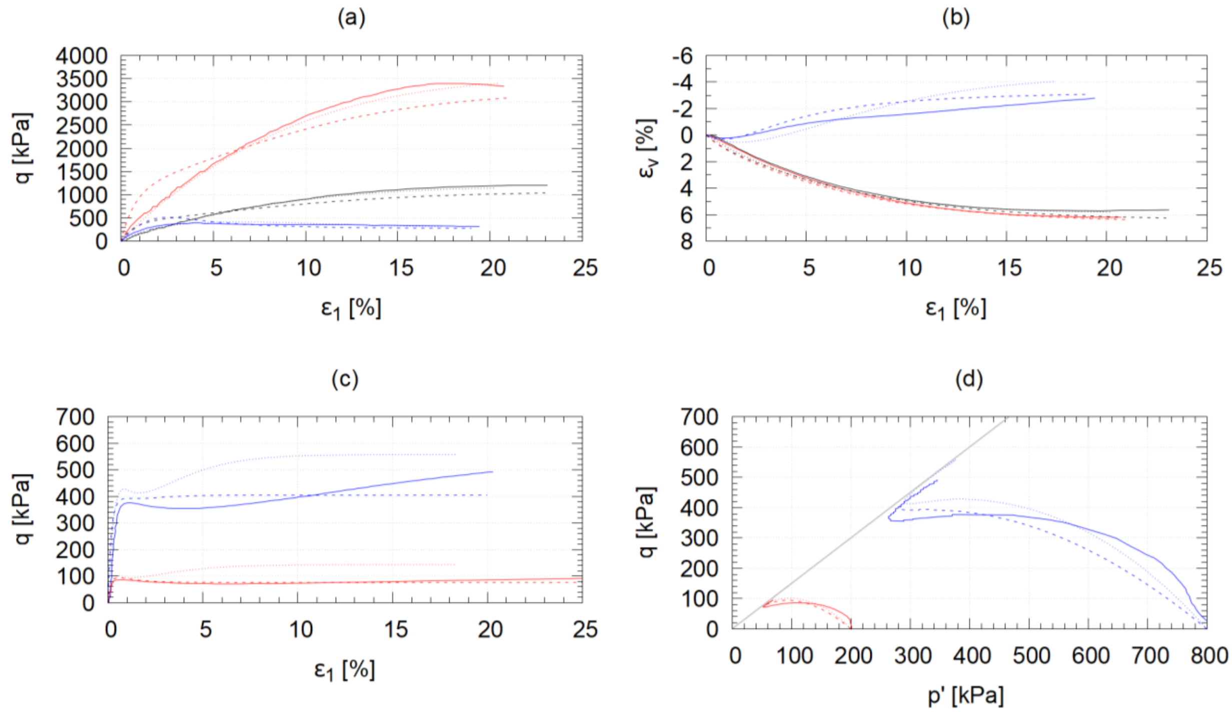

Figure 1 Triaxial test results on TS2, drained (a)-(b) and undrained (c)-(d) conditions. Experimental results are in solid lines and dashed and dotted lines correspond to hypoplastic and NorSand, respectively. Colors drained test: red p_0=1200 kPa, ψ_0=0.063, black p_0=400 kPa, ψ_0=0.065, blue p_0=100 kPa, ψ_0=-0.087. Undrained test: blue p_0=800 kPa, ψ_0=0.051, red p_0=200 kPa, ψ_0=0.049.

The Cadia Silty Tailings TC1 parameters were determined with four drained and three undrained triaxial compression tests. Results are presented in **Figure 2**.

Under drained conditions, both models can again satisfactorily reproduce the stress-strain and volumetric response observed in the experiments (Figures 2a and 2b). However, for the dense samples, the critical state is achieved much earlier in the experiments than in the simulations, and for this reason, the dilatancy is overestimated by both models. Under undrained conditions (Figure 2c), both models can realistically capture the initial stiffness but cannot accurately model the shear resistance at the instability state. In addition, NorSand predicts a QSS, which is not observed in the experiments. The softening after the instability states, the strength at the critical state and the effective stress path (Figure 2d) were realistically simulated by both models.

The trajectories of the experimental and numerical element tests in the e-p' space and the CSL considered by both models are shown in **Figure 3** for TS2 (Figure 3a) and TC1 (Figure 3b). As can be seen, experimental and numerical data are in good agreement.

For Fundao Tailings, the analysis of experimental data revealed the potential existence of two distinct critical state lines. According to the principles of critical state theory, the critical state line is unique for a given material, regardless of its state or initial condition.

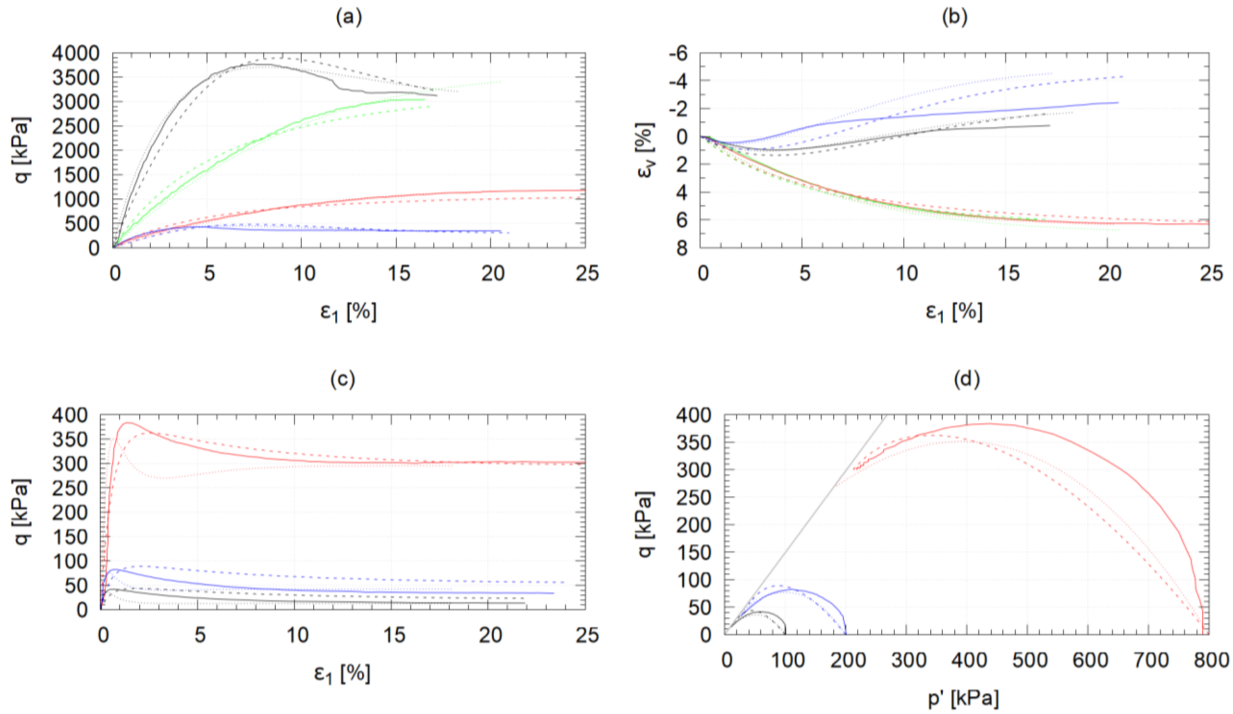

Figure 2 Triaxial test results on TC1, drained (a)-(b) and undrained (c)-(d) conditions. Experimental results are in solid lines and dashed and dotted lines correspond to hypoplastic and NorSand, respectively. Colors drained: red p_0=400 kPa, ψ_0=0.063, black p_0=1000 kPa, ψ_0=-0.069, blue p_0=100 kPa, ψ_0=-0.100, green p_0=1200 kPa, ψ_0=0.062. Undrained: blue p_0=200 kPa, ψ_0=0.092, red p_0=800 kPa, ψ_0=0.075, black p_0=100 kPa, ψ_0=0.100.

For this reason, as mentioned before, Fundao tailings were divided into two categories: Fundao Lower Bound and Fundao Upper Bound. The comparison of numerical and experimental results for each category is shown in **Figure 4** and **Figure 5**, respectively.

The observed experimental drained and undrained shearing behaviour can be capture realistically for both tailings categories by both models. For Fundao Lower Bound, the best agreement is obtained for drained shearing, particularly for lower confining pressures (Figure 4a and 4b). NorSand better reproduce experimental volumetric behavior at lower axial strains and hypoplasticity at higher ones. Both capture strain-softening and the effective stress paths observed under undrained shearing (Figures 4c and 4d).

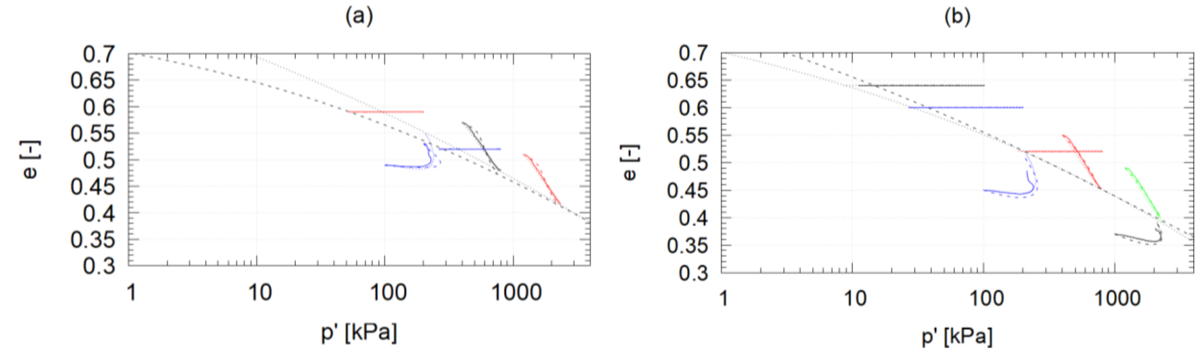

Figure 3 Critical state line from triaxial results on TS2 (a) and TC1 (b). The dashed critical state line corresponds to hypoplastic, and the dotted one to NorSand.

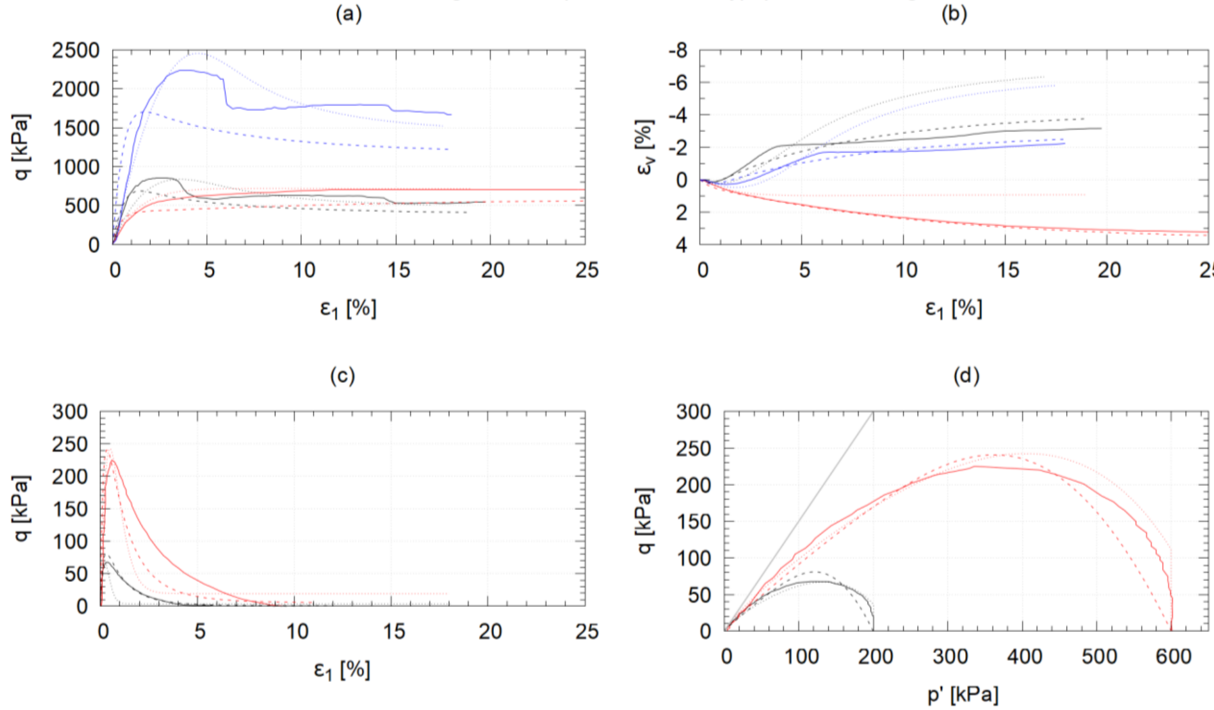

Figure 4 Triaxial test results on FLB, drained (a)-(b), and undrained (c)-(d) conditions. Experimental results are in solid lines, and dashed and dotted lines correspond to hypoplasticity and NorSand, respectively. *Colors drained: red p_0=300 kPa, ψ_0=0.01, black p_0=200 kPa, ψ_0=-0.125, blue p_0=600 kPa, ψ_0=-0.105 Undrained: red p_0=600 kPa, ψ_0=0.09, black p_0=200 kPa, ψ_0=0.105.

Under drained conditions, the experimental and numerical results for the Upper Bound Fundao Tailing (FUB) show a better agreement at higher confining pressures (Figure 5a and 5b). Under undrained conditions (Figure 5c), the initial stiffness observed in the experiments is accurately reproduced by both models for the denser samples but overestimated for the initially looser samples. As can be seen in Figure 5d, the reduction of the effective stress during undrained shearing is overestimated by both models, but overestimation is more pronounced in the Hypoplasticity element test simulation.

As shown in Figure 6a and Figure 6b, the trajectories of the experimental element tests in the e-p' space can be realistically simulated by NorSand and Hypoplasticity for the Upper Bound material. For the

Lower Bound, some discrepancies between the experimental and numerical data can be identified. This discrepancy results from the use of the same critical state line for the Upper and Lower Bound materials in the NorSand simulations. In the Expert Panel Report, at least two of the drained experimental triaxial test were excluded because axial strains were for that case considered unreliable.

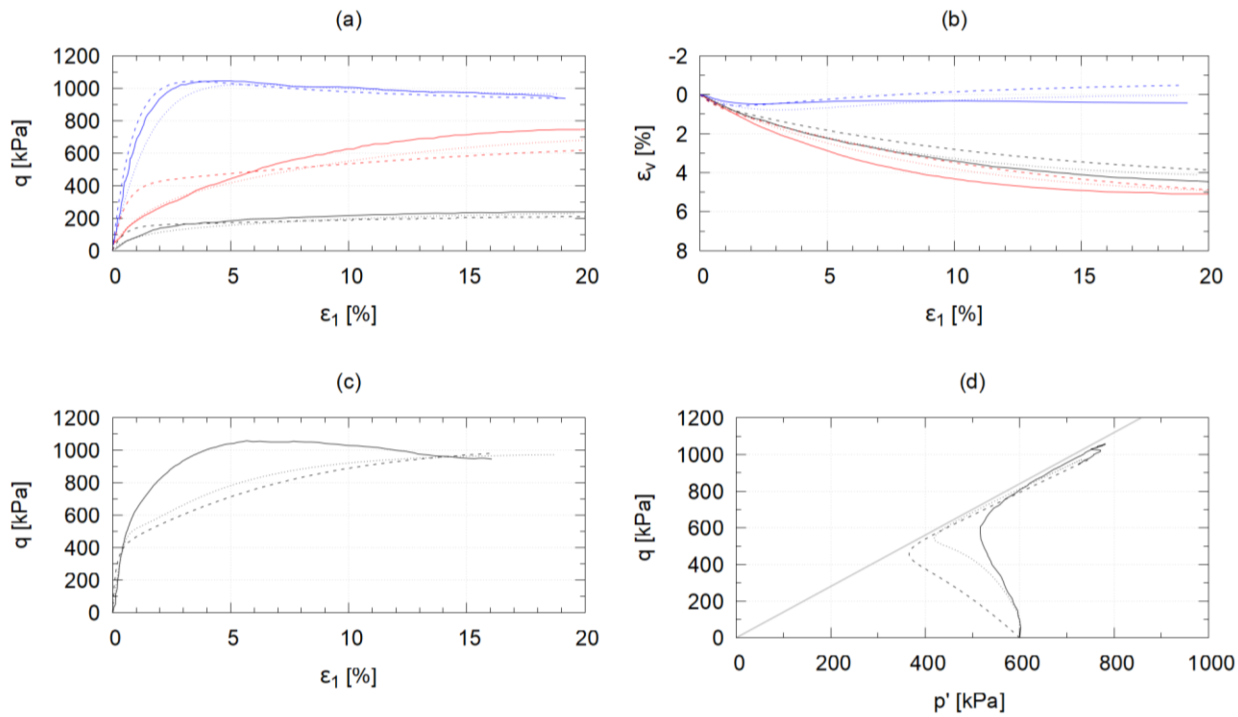

Figure 5 Triaxial test results on FUB, drained (a)-(b), and undrained (c)-(d) conditions. Experimental results are in solid lines, and dashed and dotted lines correspond to hypoplasticity and NorSand, respectively. *Colors drained: red p_0=300 kPa, ψ_0=0.08, black p_0=100 kPa, ψ_0=0.07, blue p_0=400 kPa, ψ_0=-0.015. Undrained: black p_0=600 kPa, ψ_0=-0.005.

Generally, for higher confining stresses, a steady state is not always observed in the experiments, suggesting that the critical state was not always achieved at the end of the tests. For this reason, some test trajectories do not touch the CSL. The shape of the CSL assumed in hypoplasticity enables a better fitting with experiments. As can be seen in Figure 6, the distance between the CSL adopted by NordSand and hypoplasticity increases with decreasing confining stresses.

Owing to the better fit of the CSL, hypoplasticity was able to reproduce the experimental strength at the critical state more accurately than NorSand (see **Figure 3** and **Figure 6**). The disparities between the experimental and numerical results obtained with hypoplasticity, notably the initial slope of effective stress paths from undrained shearing, could be improved by incorporating an intergranular strain tensor (Niemunis & Herle, 1997), which was not considered in the presented numerical simulations.

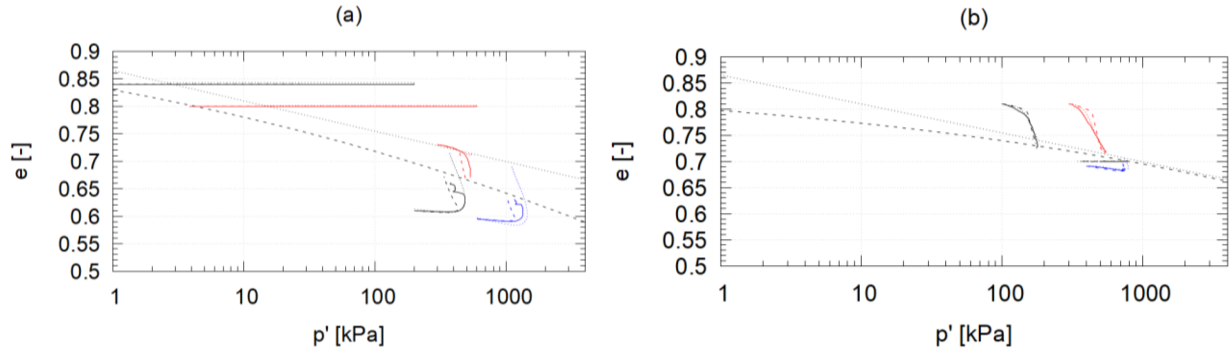

Figure 6 Critical state line from triaxial test results on FLB (a) and FUB (b). The dashed critical state line corresponds to hypoplasticity, and the dotted one to NorSand.

Conclusion

Constitutive models used to represent the behaviour of mine tailings face significant challenges due to their heterogeneity, nonlinear behaviour, undisturbed sampling and testing difficulties due to low density and fabric sensibility. The lack of a comprehensive database of laboratory test results on undisturbed samples difficult the validation of constitutive models and the determination of representative model parameters for practical applications. Constitutive models for tailings must capture the drained and, particularly, the undrained shear behaviour of very loose to medium dense silts sands and sandy silts, including liquefaction, as a function of the stress and density. Ideally, the material parameters shall be only dependent on the granulometric properties (grain size distribution, grain mineral, grain shape, grain roughness, etc.), but independent of the state.

The ability of two rate-independent advanced constitutive models, NorSand and Hypoplasticity, to capture the monotonic drained and undrained shear behavior of different tailing materials from two TSFs, which failed catastrophically, were showcased. Both models have been developed and extensively validated for coarse soils, particularly for sands, and in principle include the main features required to model tailings. The modeled tailings have different grain size distributions, grain minerals and limit void ratios, leading to different mechanical soil responses, e.g. different shear strength and stiffness upon shearing. Numerical and experimental triaxial compression tests are used to investigate the capabilities of the models.

For every investigated material, the state-dependent stress-strain and volumetric response under drained and undrained shearing, including strain softening and static liquefaction could be satisfactorily reproduced by both models using a unique set of parameters. Particularly, the critical state and the shear strengths at the instability and the steady state were realistically predicted by both models. Discrepancies between numerical and experimental results are attributed to limitations of the laboratory tests and shortcomings of the models, e.g. to reproduce the quasi-steady state. Nevertheless, further validation at the element test level for more complex stress paths as well as for simple and complex boundary value problems are recommended before using these models to assess the stability of TSFs.

It is worth mentioning that for assessing the stability of TSFs, a realistic modelling of the foundation, the macro-structure of the TSF, e.g. stratification resulting from segregation, change of minerals and processing technique, the spatial variation of the material state and the construction process, especially in the pound, are as essential as the constitutive model.

References

Beaty, M. & Byrne, P.M. (1998). An effective stress model for predicting the liquefaction behaviour of sand. In P. Dakoulas, M. Yegian, & R. D. Holtz (Eds.), Geotechnical Earthquake Engineering and Soil Dynamics III, ASCE Geotechnical Special Publication No. 75, Vol. 1, Proceedings of a Specialty Conference (pp. 766-777). Seattle: ASCE.

Blight, G. E. (2009). Geotechnical engineering for mine waste storage facilities. CRC press

Castro, G. (1969). Liquefaction of sands, PhD, Thesis, Harvard University, Cambridge, Mass, (Harvard Soil Mechanics. Series 81).

Cudmani, R. (2013, September). Soil Liquefaction: Mechanism and Assessment of Liquefaction Susceptibility. In Seismic Design of Industrial Facilities: Proceedings of the International Conference on Seismic Design of Industrial Facilities (SeDIF-Conference) (pp. 485-497). Wiesbaden: Springer Fachmedien Wiesbaden.

Davies, M. P. (2002). Tailings impoundment failures are geotechnical engineers listening. GEOTECHNICAL NEWS-VANCOUVER-, 20(3), 31–36.

Dimitrova, R. S. (2011). Geotechnique, physicochemical behaviour and a new erosion model for mine tailings under environmental loading. The University of Western Ontario (Canada).

Ferdosi, B. (2014). A numerical investigation of the seismic response of tailings impoundments reinforced with waste rock inclusions (Doctoral dissertation, École Polytechnique de Montréal).

Gudehus, G. A (1996). Comprehensive constitutive equation for granular materials. Soils and foundations 36.1 1–12.

Herle, I. (1997) Hypoplastizität und granulometrie einfacher korngerüste. Vol. 142. Inst. für Bodenmechanik und Felsmechanik.

Herle, I. & Gudehus (1999). Determination of Parameters of a Hypoplastic Constitutive Model from Properties of Grain Assemblies. Mechanics of Cohesive-frictional Materials. 4. 461 - 486.

ICOLD, U. (2001). Tailings dam–the risk of dangerous occurrences, lessons learned from practical experiences (bulletin 121). Commission Internationale des Grands Barrages, Paris, 155.

Ishihara, K. (1984). Post-earthquake failure of a tailings dam due to liquefaction of pond deposit.

Jefferies, M., et al. Report on NTSF embankment failure. Cadia Valley Operations, for Ashurst Australia (2019).

Jefferies, M., & Been, K. (2015). Soil liquefaction: a critical state approach. CRC press.

Jefferies, M. G., & Shuttle, D. A. (2005). NorSand: features, calibration, and use. In Soil constitutive models: evaluation, selection, and calibration (pp. 204–236).

Jefferies, M., & Shuttle, D. (2011, January). Understanding liquefaction through applied mechanics. In 5th international conference on earthquake geotechnical engineering, Santiago, Chile (pp. 10–13).

Jefferies, M. G. (1993). Nor-Sand: a simple critical state model for sand. Géotechnique, 43(1), 91-103.

Kolymbas, D. (1993). Hypoplasticity and critical state soil mechanics. Soils and Foundations, 33(4), 34-42

Li, J., & Leao, T. F. (2018). Application of nor sand constitutive model in a highway fill embankment slope stability failure study. Civil Eng J, 4(10), 2252-2263.

Manzari MT, Dafalias YF(1997).A critical state two-surface plasticity model for sands. Geotechnique;47(2):255–272.

Mittal, H. K., & Morgenstern, N. R. (1975). Parameters for the design of tailings dams. Canadian Geotechnical Journal, 12(2), 235-261.

Morgenstern, Norbert R., et al. Fundão Tailings Dam review panel report on the immediate causes of the failure of the Fundão dam. Cleary Gottlieb Steen & Hamilton LLP, New York (2016).

Niemunis, A. (2003). Extended hypoplastic models for soils (Vol. 34). Vienna: Inst. für Grundbau und Bodenmechanik.

Niemunis, A., & Herle, I. (1997). Hypoplastic model for cohesionless soils with elastic strain range. Mechanics of Cohesive-frictional Materials: An International Journal on Experiments, Modelling and Computation of Materials and Structures, 2(4), 279-299.

Niemunis, A. (2008). Incremental Driver, user's manual. University of Karlsruhe KIT, Germany.

Robertson, P.K., L.d. Melo, D.J. Williams, & G.W. Wilson. (2019). Report of the Expert Panel on the Technical Causes of the Failure of Feijão Dam I.

Schanz, T., Vermeer, P. A., & Bonnier, P. G. (1999). The hardening soil model: formulation and verification. Beyond 2000 in computational geotechnics, 1, 281-296.

Sternik, K. (2014). Prediction of static liquefaction by Nor Sand constitutive model. Studia Geotechnica et Mechanica, 36(3).

Tsegaye, A. B., Molenkamp, F., Brinkgreve, R. B. J., Bonnier, P. G., de Jager, R., & Galavi, V. (2010). Modelling liquefaction behaviour of sands using the hypoplastic model. 7th European Conference on Numerical Methods in Geotechnical Engineering, Trondheim, Norway, 81-87.

Wolffersdorff, P-A. A hypoplastic relation for granular materials with a predefined limit state surface. Mechanics of Cohesive-frictional Materials: An International Journal on Experiments, Modelling and Computation of Materials and Structures 1.3 (1996): 251–271.

Zhao, X., Schorr, J., Peña Olarte, A. A., & Cudmani, R. (2022, July). A step towards quantifying the uncertainty of the soil mechanical response through the use of genetic algorithms. In International Conference of the International Association for Computer Methods and Advances in Geomechanics (pp. 263-271). Cham: Springer International Publishing.

Comparing HSS and NorSand constitutive models for modeling flow liquefaction in tailings dams

Nicolas A. Rivas, SRK Consulting, Argentina

Mauro G. Sottile, SRK Consulting, Argentina

Felipe Lopez Rivarola, SRK Consulting, Argentina

Alejo O. Sfriso, SRK Consulting, Argentina

Abstract

Recent failures of tailings dams have raised the interest of the mining industry in evaluating the risk of flow liquefaction. The standard practice involves using limit equilibrium analyses to calculate factors of safety, assuming peak or residual undrained shear strength conditions. However, this procedure does not account for the post-peak softening effect commonly observed in these materials. This article applies a numerical procedure to evaluate the susceptibility of triggering flow liquefaction in a real dam; the methodology involves the use of finite element models in Plaxis 2D and the advanced constitutive models HSS and NorSand, for comparison purposes. In the example shown, the dam construction sequence is modeled in detail, and trigger analyses are carried out for various scenarios. A comparison between the two constitutive models is presented in terms of loads triggering progressive failure, kinematics of failure mechanisms, and stress paths. Results demonstrate that both constitutive models produce results that are useful for evaluating the vulnerability of dams to flow liquefaction.

Introduction

Deposition of tailings as a slurry into Tailings Storage Facilities (TSFs), along with lack of post-deposition compaction, results in a loose and saturated in-situ geotechnical body. Rapid undrained loading can thus lead to an increase of pore pressure and a sudden reduction of strength, eventually leading to flow liquefaction. Assessment of flow liquefaction in tailings has gained significant importance within the field of mine waste engineering, particularly in the wake of recent failures in upstream-raised TSFs, such as those observed in Cadia Valley, Fundâo, and Corrego deo Feijâo in Brumadinho.

Internationally recognized standards like ANCOLD (2019) promote the use of limit equilibrium methods to assess the stability of the dam, recommending the use of residual undrained shear strength for tailings that are contractive and saturated regardless the likelihood of the event that might induce the material to this state. While this approach is conservative, it does not provide information about the susceptibility of the dam to flow liquefaction. On the other hand, numerical deformation analyses are useful to evaluate the robustness of the dam by subjecting it to external disturbances, or triggers.

When dealing with materials that undergo strain-softening, the external action usually increases until progressive failure is suddenly triggered. There are several factors that affect the susceptibility of the dam to flow liquefaction, including the geometry and zoning of the dam, the brittleness of the tailings, the phreatic conditions, etc. Typical triggers are loads suddenly applied at various places, imposed deformations at the toe of the dam, raises in the phreatic surface, surface water inflow, among other factors. (Ledesma et al, 2022).

Several constitutive models exist that can reproduce the undrained strain-softening behavior of the tailings and can therefore be used in deformation analyses. In this paper, we show that the assessment of flow liquefaction can be accomplished using different constitutive models. A complete trigger analysis is performed to a hypothetical TSF using the two different constitutive models: Hardening Soil Model with Small Strain Stiffness (HSS, Brinkreve et al, 2020) and NorSand (Jefferies, 1993).

Geotechnical characterization of the tailing material

This study uses data from a laboratory testing program performed on tailings product of iron mineral extraction (Carrizo, Tasso, and Sottile, 2023). The laboratory tests entail conventional physical and mechanical tests, including: specific gravity, Atterberg limits, grain size analysis, minimum and maximum void ratios, X-ray diffraction, controlled rate of strain (CRS) oedometers, and consolidated drained and undrained triaxial test (CIDC|CIUC) with measurement of void ratio using freezing. Table 1 presents a summary of the physical properties of the tailings, and Figure 1 shows a summary of the triaxial tests data.

Table 1: Physical properties of the tailings

Property	Value
Specific gravity, G_s [-]	3.15
Plasticity Index [-]	NP
Fines content [%]	12
Minimum voids ratio, e_{min} [-]	0.56
Maximum voids ratio, e_{max} [-]	1.1

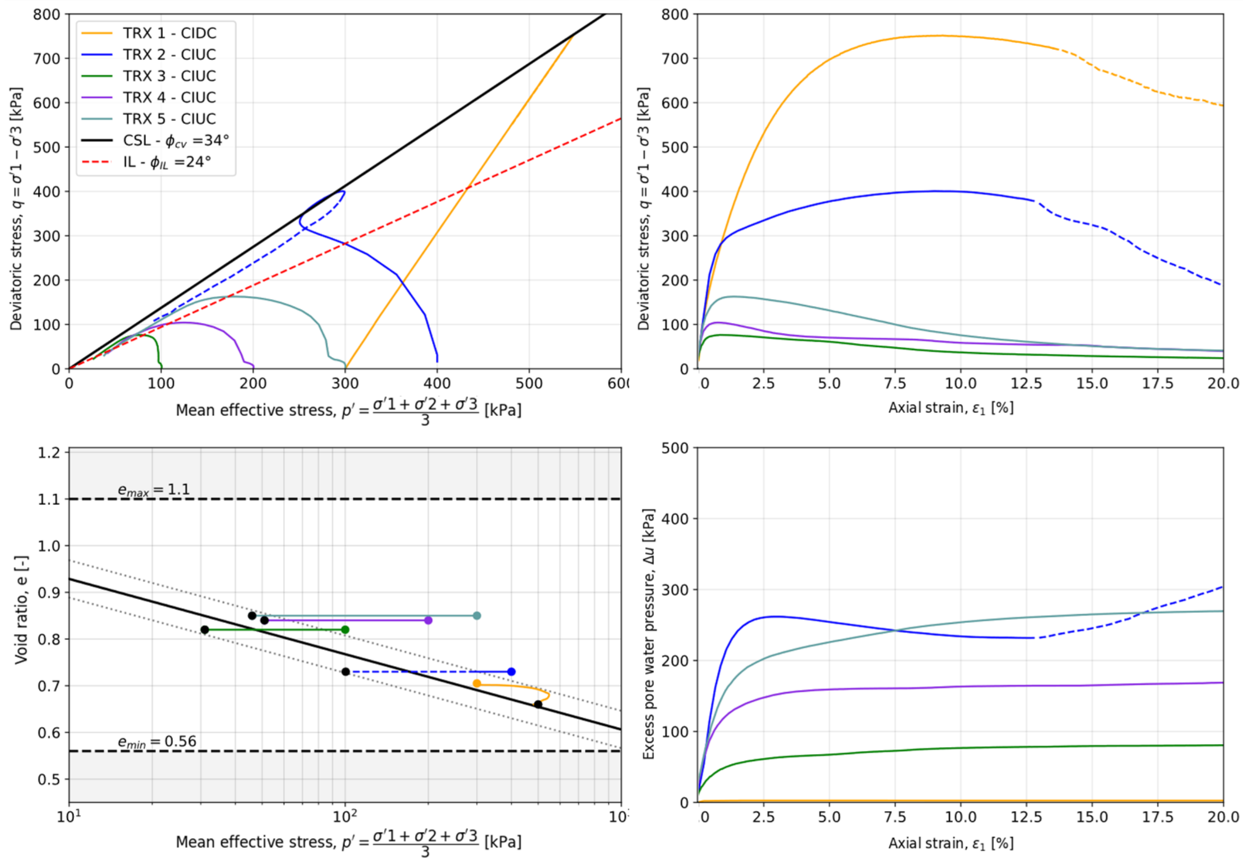

Figure 1: Summary of triaxial tests (modified from Carrizo et al, 2023).

Constitutive models

In this section, a short description of the constitutive models (HSS and NorSand) used in this study will be given, as well as the calibrated parameters for the tailing material. It is noted that the critical state line for this material was measured from laboratory testing, this includes c'-ϕ' and Γ-λ_e, being the latter relevant for the NorSand model only. The remainder of the required parameters for each model were obtained by curve fitting the laboratory test data.

Hardening Soil Model with Small Strain Stiffness

The HSS model is a non-linear elastic, effective stress, isotropic hardening plasticity constitutive model, able to represent the behavior of materials undergoing plastic compression, consolidation, and monotonic shear. HSS is not implemented in a critical state framework, and consequently the void ratio is not a state variable, i.e. stiffness and strength are independent of void ratio. This means that a critical state cannot be achieved in drained conditions, however, during undrained shearing this limitation is overcome by using a calibration methodology that focuses on the stiffness parameters that control the rate of shear-induced plastic volumetric strain, such that strain-softening during undrained shearing can be captured (Sottile et al, 2021). The HSS model was calibrated using this methodology, and a summary of the calibrated parameters are presented in Table 2.

Table 2: HSS calibrated parameters

Parameter	c'	ϕ'	G_0^{ref}	γ_{07}	p_{ref}	R_f	K_0^{NC}	m	v_{ur}	E_{ur}^{ref}	E_{oed}^{ref}	E_{50}^{ref}
Unit	kPa	°	MPa	-	kPa	-	-	-	-	MPa	MPa	MPa
Value	0	34	80	1E-4	100	0.9	0.5	0.5	0.2	100	15	7

NorSand

NorSand is a critical state constitutive model in which the state of a soil is determined by two state variables. The first one is the state parameter $\psi = e - e_c$ where e is the void ratio and e_c is the critical state void ratio at the current mean effective pressure. The second state variable is the image pressure p_{im}, the mean effective pressure at which the volumetric plastic strain rate is zero ($\dot{\varepsilon}_v^p = 0$). For more information on the model formulation and parameters the reader is referred to Jefferies (1993) and Been & Jefferies (2016).

Table 3 presents a summary of the calibrated parameters, details on the calibration for the tailing used on this study can be found in Carrizo et al (2023).

Table 3: NorSand calibrated parameters

Parameter	G_0^{ref}	p_{ref}	n_G	ν	Γ	λ_e	M_{tc}	N	χ_{tc}	H_0	H_ψ	R	S	ψ_0
Unit	MPa	kPa	-	-	-	-	-	-	-	-	-	-	-	-
Value	15	100	0.5	0.2	1.09	0.069	1.35	0.2	3	85	100	1	0	-0.1

Comparison

CIUC elemental tests were performed using the calibrated parameters. A comparison of the simulations and the CIUC triaxial data in terms of stress paths and stress-strain is shown in Figure 2.

A remarkable agreement was achieved between the two calibrated models and the test data. It is observed that: i) the stress path response closely resembles the test data; ii) the calibrated models achieve a slightly lower peak shear strength and a slightly higher residual shear strength; iii) peak and residual undrained shear strength ratios (s_u/σ'_{v0}) of 0.26 and 0.10 respectively were achieved for the test data, while the calibrated models achieve a peak undrained shear strength ratio of 0.24-0.25 and a residual undrained shear strength ratio of 0.12-0.13; iv) good agreement of the strain at peak was achieved between the simulations and the test data.

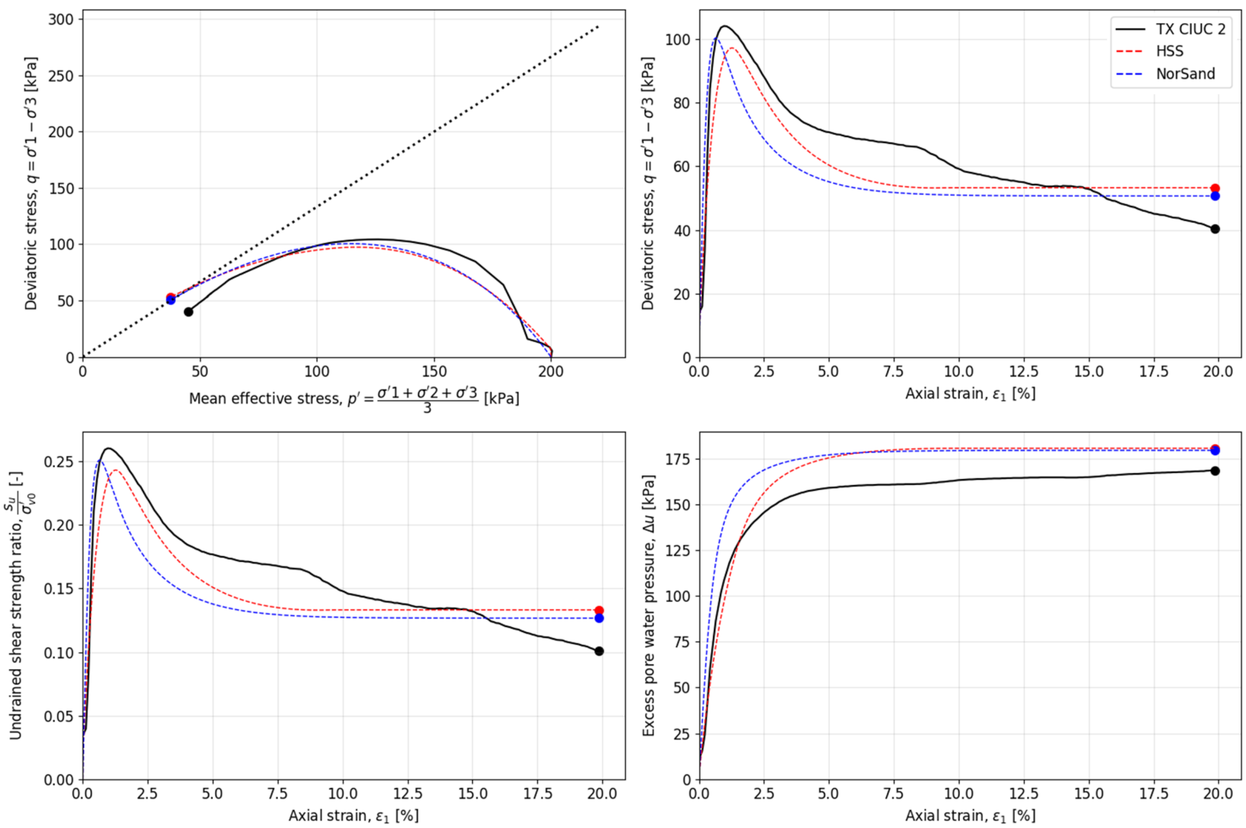

Figure 2: Constitutive models comparison for CIUC triaxial tests.

Numerical model

To demonstrate the use and comparison of these calibrations in a boundary-value problem, a hypothetical upstream-raised TSF was modelled in PLAXIS 2D® (2023) and its vulnerability against flow liquefaction was assessed employing the procedures proposed by Ledesma et al (2022). It is noted that the model, geometry, and modelling strategy is the same as in previous publications (Sottile et al., 2020; Sottile et al, 2021; Rivarola et al, 2022).

The model consists of four geotechnical units: tailings, embankment raises, foundation soil and bedrock. The embankment raises were modelled using HSS, the upper foundation using Mohr-Coulomb and the bedrock as linear elastic. For details on the material parameters and modelling strategy employed in these studies, the reader is referred to Sottile et al (2020).

Geometry and mesh

The dam has a total height of 45 m and an average slope of 1V:3.5H. The numerical model has 9145 triangular 15-node elements. The geometry and mesh are presented in Figure 3. It can be observed that the mesh is very fine in the region where flow liquefaction is expected to be initiated during trigger analyses.

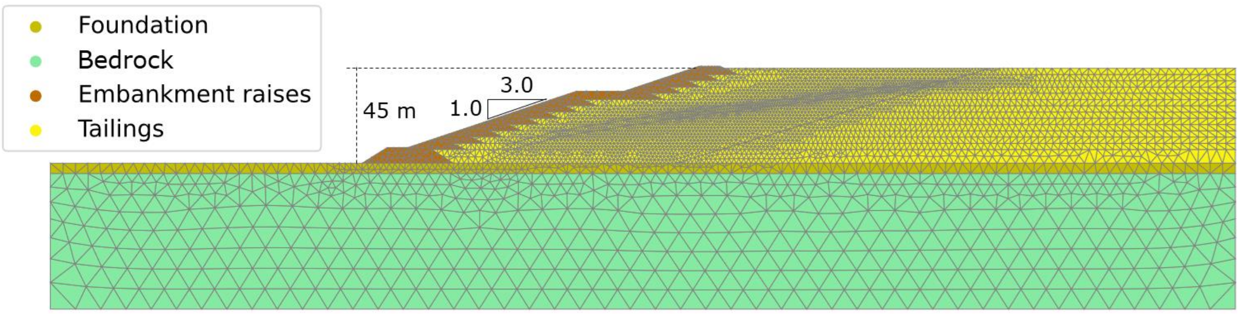

Figure 3: Geometry and mesh of the model (Rivarola et al, 2022).

Modeling strategy

The TSF was raised in several stages until its final configuration using an average embankment raise height of 3.0 m and consolidation phases with an average rate of rise of 2.0 m/year. The aim is to reasonably capture the non-linearities associated with the staged construction process, which play a critical role in determining the in-situ stress field and pore pressure distribution. A steady state groundwater flow was computed at each deposition phase. The HSS model was used for this construction sequence for both cases, once the final configuration was achieved the tailings material was switched for the NorSand case prior to the trigger analysis.

Static triggers

Once the construction was completed, flow liquefaction triggers were analyzed. In this paper, three types of load triggers were independently evaluated (Figure 4). Triggers A and B apply a load at the dam berm and the crest, respectively; this aims to represent sudden heavy traffic loads or stockpiled material during regular mining operation. Trigger C was uniformly applied across the entire tailings beach to simulate a rapid deposition of tailings.

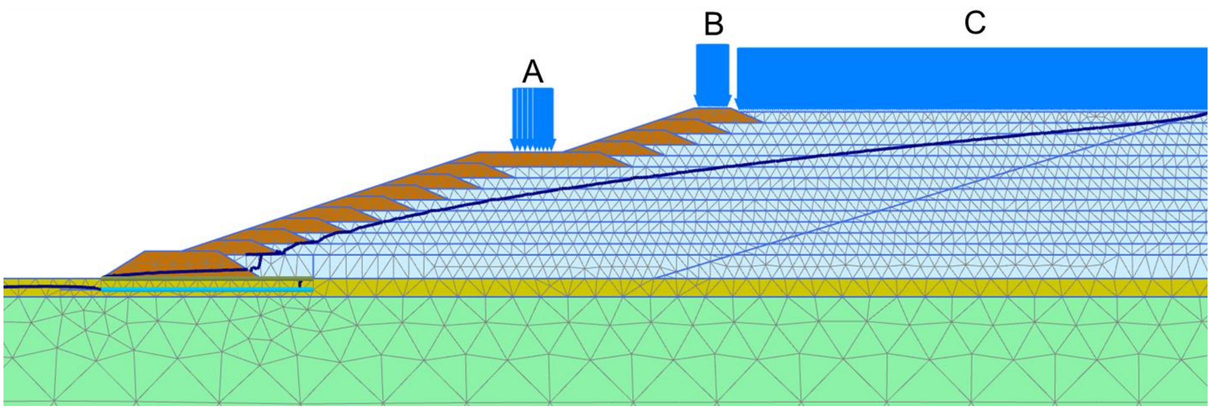

Figure 4: Analyzed triggers.

Results

A summary of the load values that trigger failure for each case is presented in Table 4. Figure 5 shows the failure surfaces in terms of total deviatoric strains, while Figure 6 presents the excess pore-pressure contours at failure. The following observations can be made,

- **Trigger A**: a good agreement was obtained between methods. The triggering load magnitude varies from 170 kPa to 220 kPa, and for both cases the failure surface starts at the berm above the started dam.
- **Trigger B**: a good agreement was obtained between methods in terms of the triggering load, with magnitudes between 280 kPa and 340 kPa. For both cases a global failure mechanism was obtained.
- **Trigger C**: a good agreement was obtained between methods in terms of the triggering load magnitude and failure mechanism. For both cases the trigger load at failure was 200 kPa, and a global failure surface is achieved for both models, starting at the tailings beach and propagating until it reaches the foundation.

Table 4: Summary of triggering loads

Trigger	HSS	NorSand
A	220 kPa	170 kPa
B	340 kPa	280 kPa
C	200 kPa	200 kPa

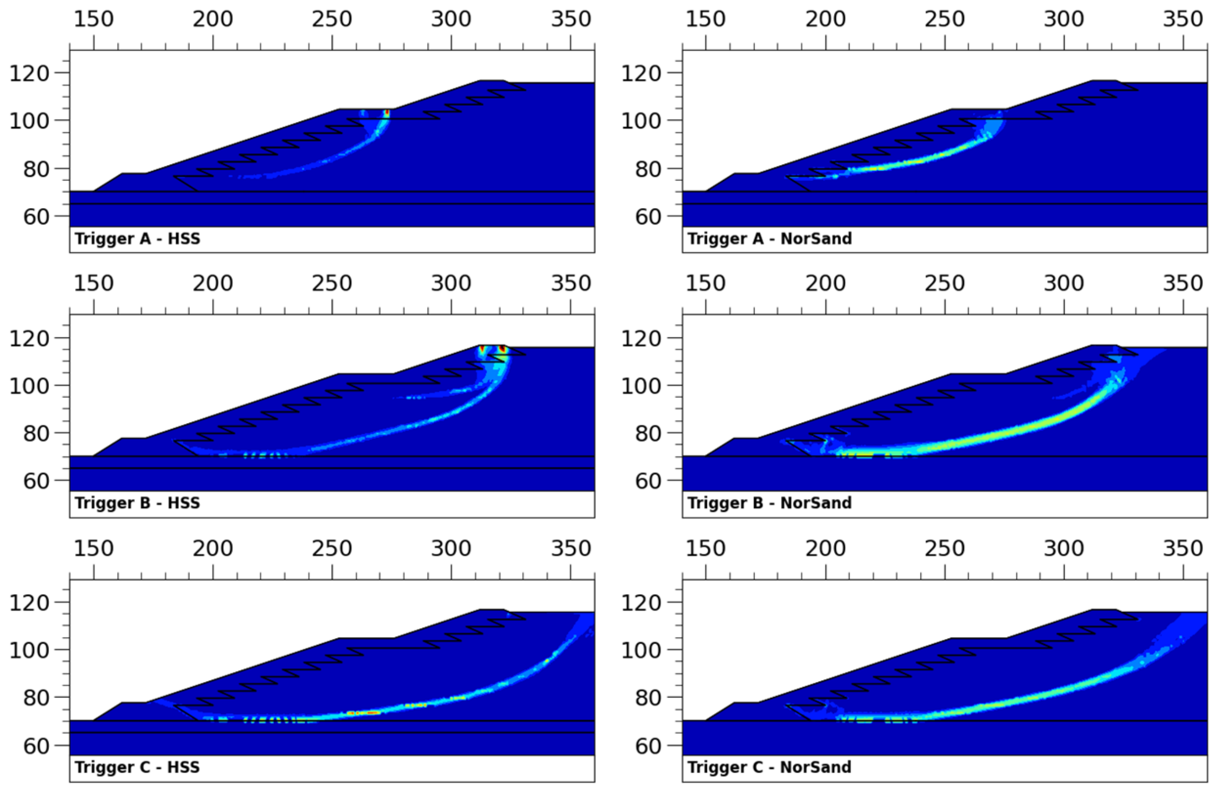

Figure 5: Incremental deviatoric strain contour maps.

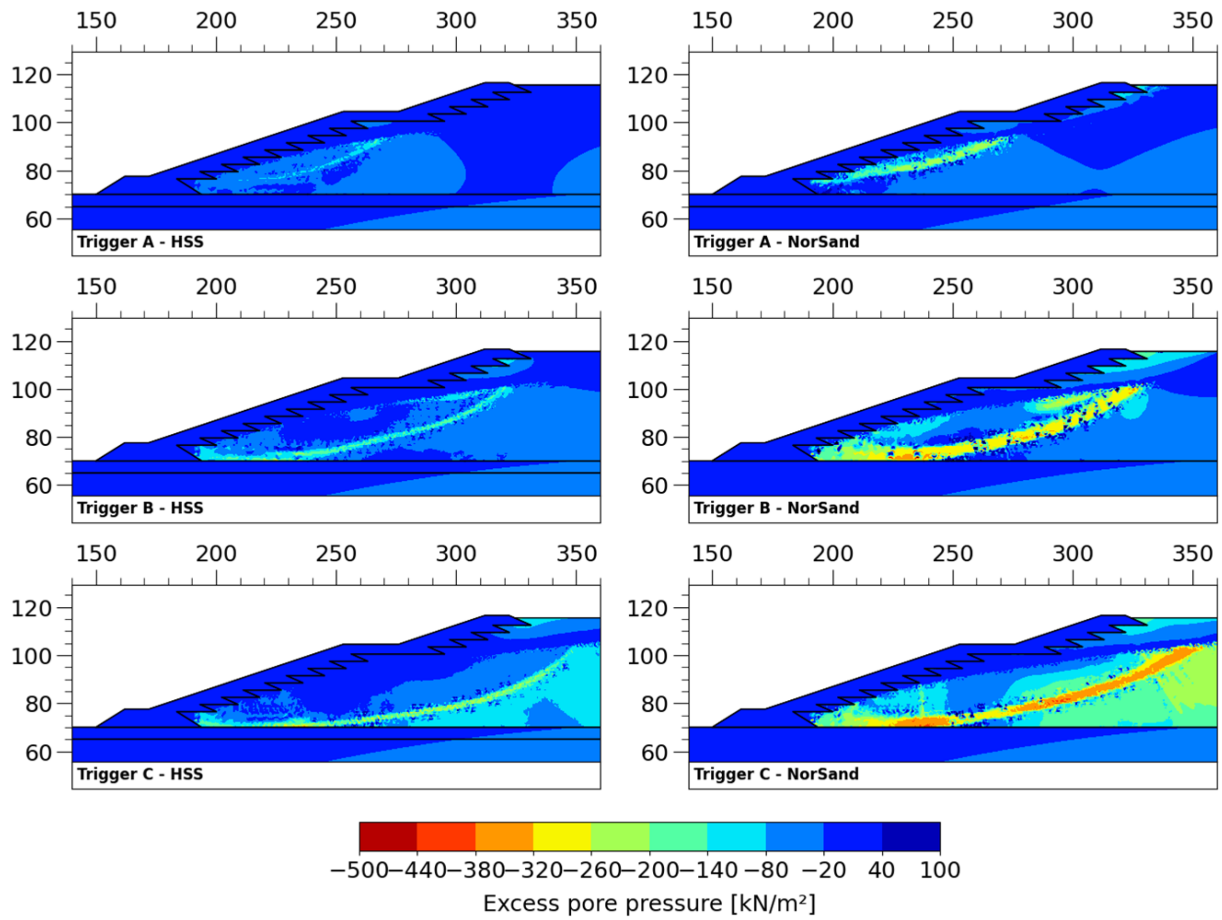

Figure 6: Excess pore pressure contour maps.

Three Gauss points were chosen to study the stress-strain-strength behavior along the failure surface for Trigger C, in order to compare the elemental tests calibrations with the full boundary value model. Results are shown in Figure 7. As failure surfaces slightly differ between HSS and Norsand models, the Gauss points chosen to produce the plots are located in slightly different positions within the mesh.

It is observed that: i) stress paths produced during flow liquefaction in the full boundary value problem are comparable to those obtained during the calibration of the constitutive models; ii) similar peak shear strength ratios, between 0.24 and 0.26, were obtained using both constitutive models; iii) a lower residual shear strength ratio of 0.10 was obtained using the NorSand model, while values closer to 0.15 were obtained when the HSS model was employed; iii) a comparable behavior between HSS and NorSand was observed at a larger scale, both in terms of strength-stress-strain and overall deformation pattern; and iv) Norsand, yielding a somewhat lower undrained residual strength, also yielded slightly lower trigger loads for two of the three triggers employed in this study, and the same load as HSS for the remaining one.

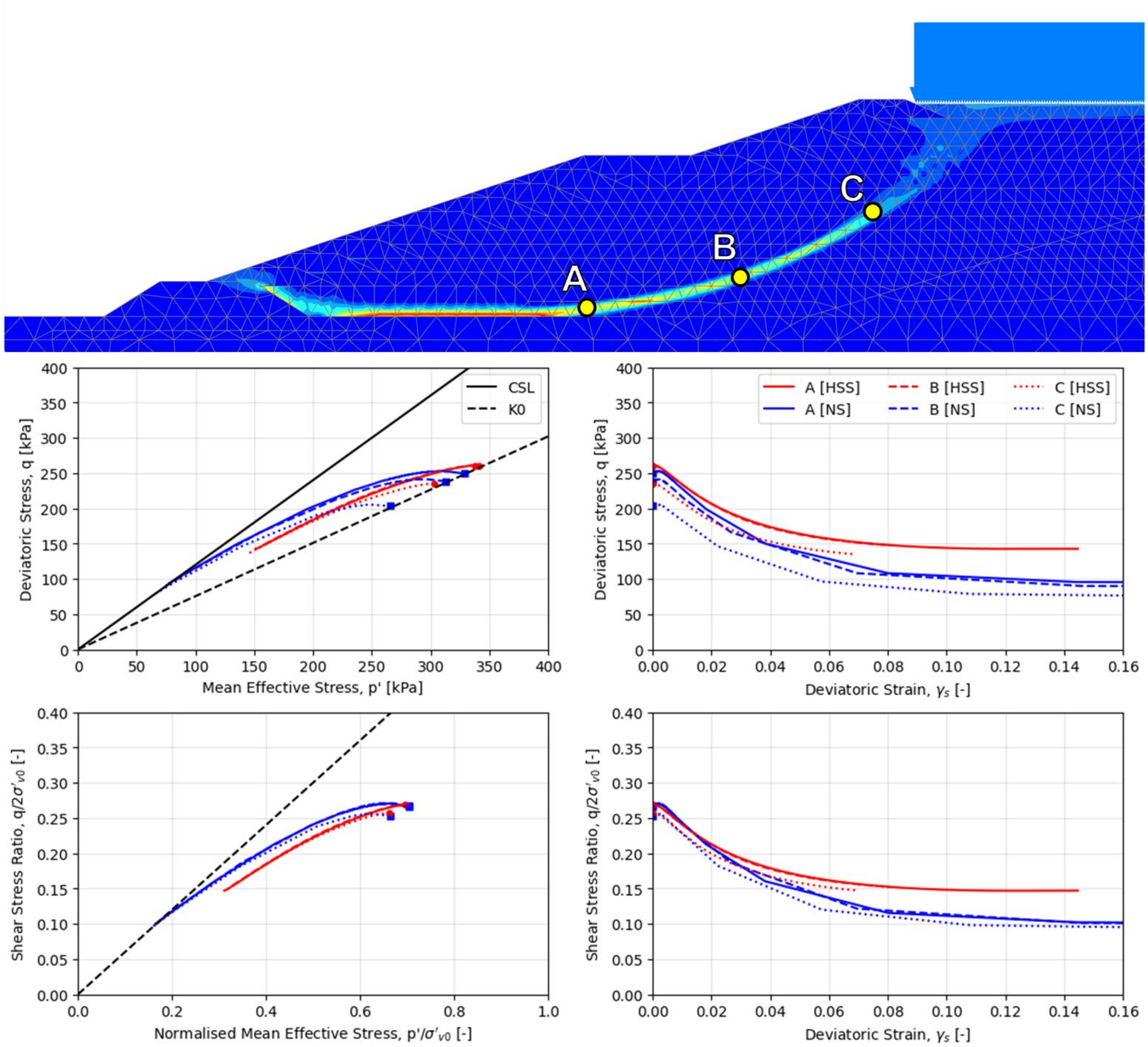

Figure 7: Example of selected gauss points and associated stress paths.

Conclusions

In this paper, two constitutive models: HSS and NorSand, were calibrated employing real tailings data and then applied in a numerical model to simulate triggers for flow liquefaction of a hypothetical, upstream-raised TSF in Plaxis. Three triggering mechanisms, consisting in undrained loads at the crest and berm, were evaluated, and the failure mechanisms, the magnitude of the trigger loads, and the excess pore-pressures were compared between constitutive models. A good agreement was found between the CIUC elemental tests simulations and the plane-strain model results. In the boundary value problem, both models were able to capture the main failure mechanisms, and comparable trigger load values were obtained, being slightly lower for Norsand than for HSS.

Acknowledgements

The authors wish to acknowledge the support of the team at SRK Consulting during the development and testing of the models presented in this paper.

References

ANCOLD, 2019. Guidelines on tailings dams - Planning, design, construction, operation and closure.

Been, K. and Jefferies, M. 2016. Soil liquefaction: a critical state approach. Taylor & Francis.

Brinkgreve R., S. Kumarswamy, W. Swolfs, E. Engin, F. Fonseca Arévalo, N. Ragi Manoj, L. Zampich and N. Zalamea. 2020. *Plaxis Manuals*. Bentley Systems.

Carrizo, L., Tasso, N. and Sottile, M. 2023. Caracterización geotécnica de un relave minero de hierro susceptible a licuar. XXVI CAMSIG. Comodoro Rivadavia, Argentina.

de Santiago, O., Mánica, M. and Ovando-Shelley, E. (2022). Simulación numérica del fenómeno de licuación de flujo. XXXI Reunión Nacional de Ingeniería Geotécnica. Guadalajara, México.

Jefferies, M. 1993. NorSand: a simple critical state model for sand. Géotechnique 43:2, 91-103.

Ledesma, O., Sfriso, A. and Manzanal, D. 2022. Procedure for assessing the liquefaction vulnerability of tailings dams. Computers and Geotechnics, vol. 144, pp.104–632.

Rivarola, F., Tasso, N., Bernardo, K., Sottile, M. and Sfriso, A. 2023. Evaluation of the triggering of static liquefaction of tailings dams considering the SWCC. Mine Waste and Tailings Conference. Brisbane, Australia.

Sottile, M., Cueto, I., and Sfriso, A. 2020. A simplified procedure to numerically evaluate triggering of static liquefaction in upstream-raised tailings storage facilities. Campinhas, COBRAMSEG.

Sottile, M., Cueto, I., Sfriso, A., Ledesma, O. and Lizcano, A. 2021. Flow liquefaction triggering analyses of a tailings storage facility by means of a simplified numerical procedure, Proceedings of the 20th International Conference on Soil Mechanics and Geotechnical Engineering.

Effect of principal stress direction on loading response of unsaturated iron ore tailings

Ana Claudia de Mattos Telles, The University of Western Australia, Australia

David Reid, The University of Western Australia, Australia

Antonio Jeronimo Pereira de Souza Junior, WSP Australia, Australia

Riccardo Fanni, WSP Australia and The University of Western Australia, Australia

Andy Fourie, The University of Western Australia, Australia

Abstract

Since the failure of the Córrego do Feijão Tailings Dam, in 2019, the mining industry has undergone considerable change. In this process, the tailings disposal using conventional slurry methods (e.g. the upstream raising method) has seen reduced in its use and the implementation of filtered tailings stacks (FTS) has increasingly become an appealing substitute. While filtered tailings are generally deposited in an unsaturated state, the design of FTS is still primarily based on results of tests performed on saturated materials. In addition, although several studies on soils and tailings demonstrate that the principal stress angle (α) and the intermediate principal stress ratio (b) affect the undrained shear strength and the shearing behaviour of these materials, design of filtered tailings stacks still often relies on results obtained from triaxial compression tests, or in some cases on direct simple shear tests. In the present work, a set of anisotropically consolidated triaxial compression and torsional shear hollow cylinder tests (TSHC) were carried out on saturated and unsaturated samples of an iron ore tailings from Western Australia. The samples were then sheared under undrained conditions (saturated) or at constant water content (unsaturated). In the TSHC tests the samples were consolidated under axisymmetric triaxial compression conditions (α=0, b=0) or at α=45°, b=0.25. The unsaturated tests were sheared with an initial degree of saturation between 34% and 36%. The results show a higher influence of α and b on the unsaturated tests than the saturated ones.

Introduction

The stress state within an earth structure, such as a tailings storage facility (TSF), cannot be fully represented by the axisymmetric condition imposed in a triaxial compression test, i.e., when the major principal stress (σ_1) is vertical and the intermediate principal stress (σ_2) is equal to the minor principal stress (σ_3). Below slope the directions of the principal stresses rotate and $\sigma_2 \neq \sigma_3$.

A common way of describing these conditions are by the intermediate principal stress ratio *b*, defined as $b=(\sigma_2-\sigma_3)/(\sigma_1-\sigma_3)$, and the principal stress angle (α), that represents the angle of the major principal stress (σ_1) plane to the horizontal. Therefore, *b* can change between 0 and 1 (although values between 0 and 0.5 are more realistic below slopes) whereas α can range from 0 to 90º (although values up to 45º are more realistic below slopes).

Tests performed on saturated soils and tailings at α and *b* different from 0 generally show a lower undrained shear strength, an increasingly contractive behaviour, a reduction in the critical state friction ratio *M*, and a lower instability stress ratio in very loose and slightly loose soils (Yang *et al*., 2008, Chu and Wanatowski, 2009, Jefferies and Been, 2015, Fotovvat and Sadrekarimi, 2022, Fanni *et al*, 2022, Reid *et al*, 2022).

Although tailings can frequently be found in a partially saturated state in TSFs (Fourie *et al*, 2001b, Robertson *et al*, 2017, Russel *et al*, 2022), studies on how changes in α and *b* affect the compressibility and shear behaviour of unsaturated tailings are still very scarce. As the appeal of filtered tailings stacks as an alternative to conventional dams grows, the relevance of understanding the behaviour of unsaturated tailings becomes increasingly important.

This study aims to assess the effect of different in situ stress conditions on the unsaturated shear behaviour of an iron ore tailings. A set of 2 triaxial compression and 4 torsional shear hollow cylinder tests were performed on saturated and unsaturated samples. The specimens were tested under two different combinations of α and *b*, with either α=0 and *b*=0, or α=45˚ and *b*=0.25. In the current research the rotation of the principal stresses was carried out during the consolidation stage to simulate the stresses below slope of a structure that was developed incrementally, as showed by Reid *et al* (2022). During shearing the values of α and *b* were maintained the same as consolidation and drainage valves were kept closed.

Torsional shear hollow cylinder (TSHC) test

The hollow cylinder apparatus (HCA) is an advanced device capable of applying different combinations of principal stress angle α and intermediate principal stress ratio *b*, thereby better reproducing stress conditions below slopes. This is accomplished by applying different pressures in the chambers outside and inside the hollow specimen, in combination with positive or negative vertical load and also application of torque. When the pressures in both chambers are equal and without application of torque, the direction of σ_1 is vertical or horizontal and therefore α=0 - *b*=0 (compression loading) or α=90˚ - *b*=1 (extension loading), respectively.

Information about the hollow cylinder device used for carrying out the tests presented in this study, as well as details about stresses and strains in a TSHC test can be found in Fanni *et al* (2022). To improve clarity of the results presented later in this paper, the definitions of octahedral deviator stress and octahedral shear strain, both used in TSHC tests are presented as follows.

Octahedral deviator stress: $q = \frac{1}{\sqrt{2}}\sqrt{(\sigma_1 - \sigma_2)^2 + (\sigma_2 - \sigma_3)^2 + (\sigma_3 - \sigma_1)^2}$

Octahedral shear strain: $\gamma_{oct} = \frac{2}{3}\sqrt{(\varepsilon_1 - \varepsilon_2)^2 + (\varepsilon_2 - \varepsilon_3)^2 + (\varepsilon_3 - \varepsilon_1)^2}$

Methods

Material and specimen preparation

Material

The material adopted in this research is a silty sand iron ore tailings from a TSF located in Western Australia. The initial preparation of the material included sieving to remove oversized material larger than 0.425 mm, increasing the moisture content, mixing and bagging of sub-samples for later use. The material then underwent characterization tests to determine its particle size distribution (PSD) curve (depicted in Figure 1) and specific gravity, as summarised in Table 1.

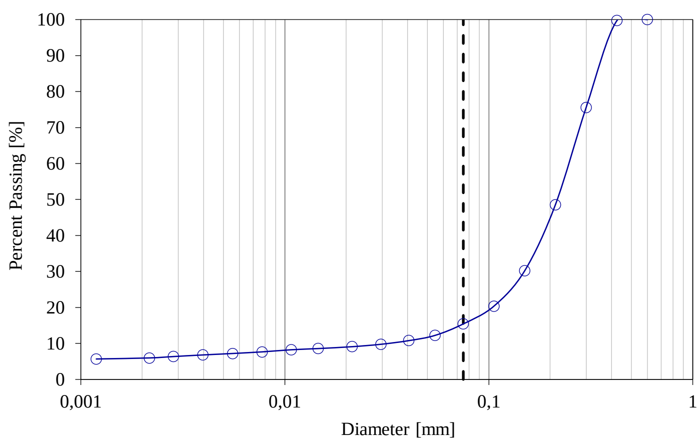

Figure 1: Particle size distribution curve

Table 1: Index property summary

Parameter	Iron ore tailings
Fines content, *FC* (<75 μm)	16%
Median particle size, D_{50} [mm]	0.22
Effective particle size, D_{10} [mm]	0.03
Specific gravity, G_S	3.86

Specimen preparation

Triaxial and hollow cylinder specimens were prepared by moist tamping the material at approximately 16%

gravimetric water content (GWC) with an undercompaction ratio of 5%. Triaxial specimens were prepared in eight layers while for hollow cylinder specimens a division of ten layers was adopted. Figure 2 illustrates some stages of the hollow cylinder specimen preparation.

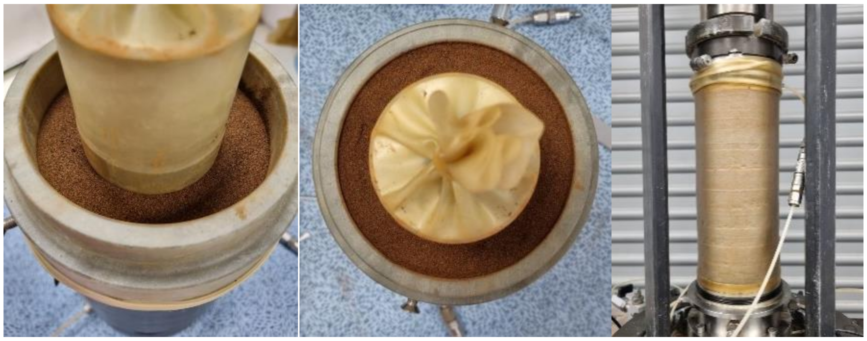

Figure 2: Stages of specimen preparation for TSHC tests

Cell calibration

Throughout a triaxial or torsional shear hollow cylinder test, the change in water volume of a pump connected to the cell is mainly due to the change of the volume of the specimen, variation in cell pressure and, in case of triaxial, also the piston displacement. The cell calibration consists of identifying the proportion of water used by the pump to pressurise the cell as needed to complete the test from the volume of water that counterbalances the changes in the specimen volume during the test. The cell calibration technique was adopted in previous studies such as Fourie *et al* (2001a) and Urbina *et al* (2023).

The calibrations were carried out employing deionized, de-aired water inside cells and pumps. In addition, steel samples were adopted, thereby eliminating any contribution of water volume associated with the sample volume variation.

Unlike the triaxial device, determining the specimen volume change during a hollow cylinder test requires the calibration of two cells, i.e., outer and inner.

Hollow cylinder testing

Four torsional shear hollow cylinder tests were conducted on saturated and unsaturated specimens. A confining stress of 40 kPa was initially applied to all samples after assembling, succeeded by either saturation procedures in the saturated tests or anisotropic consolidation in the unsaturated tests.

For saturated tests, the saturation process consisted initially of flushing the sample with deionized deaired water from the bottom to the top, until bubbles stopped coming out of the sample. Subsequently, back pressure saturation was carried out until a B value of at least 0.97 was achieved.

All specimens were anisotropically consolidated to a mean stress p of 100 kPa (effective for saturated and net for unsaturated tests) and deviator stress q of 37-38 kPa. Two different combinations of principal stress angle (α) and principal stress ratio (b) were used: α=0 and b=0 or α=45° and b=0.25. The testing conditions for the TSHC are summarised in Table 2. After consolidation the samples were sheared with drainage valves closed, keeping the undrained condition in the saturated tests and the constant water content in the unsaturated ones. Values of α and b were also kept constant during shearing.

Table 2: TSHC testing summary

Saturation	Consolidation				Shearing
	α [°]	b	p* [kPa]	q [kPa]	
SAT	0	0	100	37	Undrained
SAT	45	0.25	100	37	Undrained
UNSAT	0	0	100	38	Constant water content
UNSAT	45	0.25	100	38	Constant water content

*Values corresponding to p' for saturated tests and p_{net} for unsaturated ones

Deionised deaired water was used to fill outer and inner chambers and also the three pumps connected to the device. Void ratio determination was made in accordance with methodology developed by Fanni *et al*. (2023) for saturated tests. Conversely, for the unsaturated tests, the cell calibration method was adopted. To determine the degree of saturation in the unsaturated tests, the procedure described by Fanni *et al*. (2023) was followed in addition to the cell calibration allowing the combination of the end of test GWC to the volume tracked throughout the test with the cell calibration.

Triaxial testing

Two triaxial compression tests were undertaken, one saturated and one unsaturated, following the same procedures and same target stresses adopted in the TSHC tests. The tests were performed in a triaxial device manufactured by GDS Instruments, using enlarged and lubricated platens to increase sample uniformity at high strains. Saturated samples were then sheared under constant volume conditions while unsaturated tests were sheared under constant water content conditions. The final void ratio was determined using end-of-test freezing technique in the saturated test and by cell calibration in the unsaturated one. Similar to TSHC tests, a combination of end-of-test freezing and cell calibration technique was employed to assess the degree of saturation of the unsaturated sample.

Results and discussion

A summary of relevant conditions of the tests carried out is provided in Table 3. Figures 3 and 4 present the results of saturated and unsaturated tests, respectively, while a comparison of the stress-strain behaviour of all the six tests is showed in Figure 5.

Table 3: Testing results summary

Saturation condition	Test device	Test ID	After suction	End of consolidation					Shearing			
			e_0	α [°]	b	p_c* [kPa]	q_c** [kPa]	e_c	e_{final}	q_{peak} [kPa]	$S_{r,initial}$ [%]	$S_{r,final}$ [%]
SAT	Triaxial	TX-sat	1.77	0	0	100	37	1.65	1.65	58	≈100	≈100
	Hollow cylinder	HC-0-sat	1.77	0	0	100	37	1.66	1.66	58	≈100	≈100
		HC-45-sat	1.72	45	0.25	100	37	1.67	1.67	53	≈100	≈100
UNSAT	Triaxial	TX-unsat	1.80	0	0	101	38	1.72	1.52	214	36	40
	Hollow cylinder	HC-0-unsat	1.77	0	0	100	38	1.70	1.45	245	34	40
		HC-45-unsat	1.69	45	0.25	100	38	1.64	1.51	157	35	39

*Values corresponding to p' for saturated tests and p_{net} for unsaturated ones
**For TSHC tests q corresponds to octahedral deviator stress

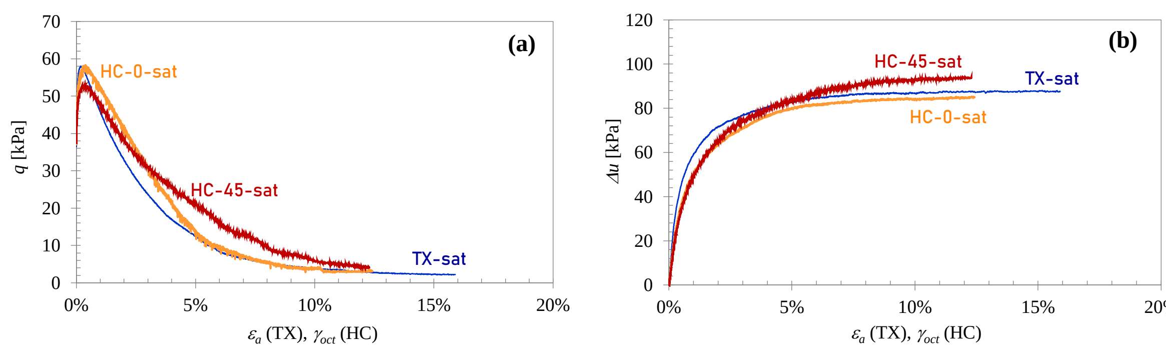

Figure 3: Results of saturated tests: (a) stress-strain curves; (b) development of pore pressure

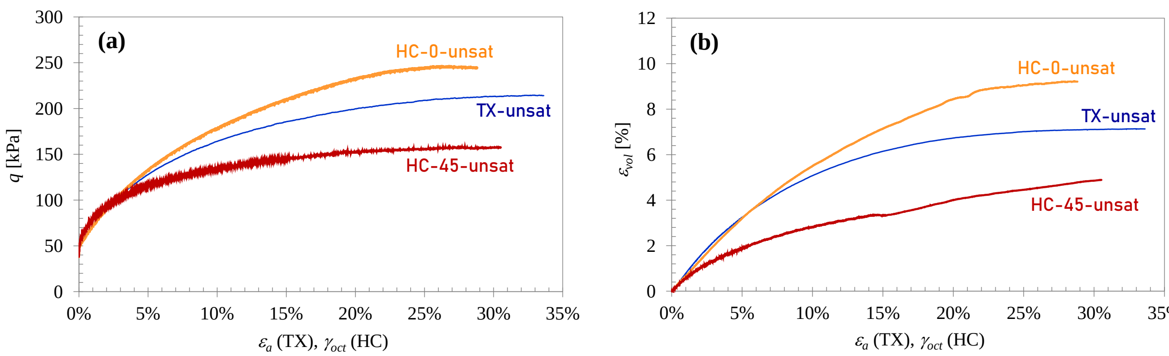

Figure 4: Results of unsaturated tests: (a) stress-strain curves; (b) volumetric strain vs. shear strain

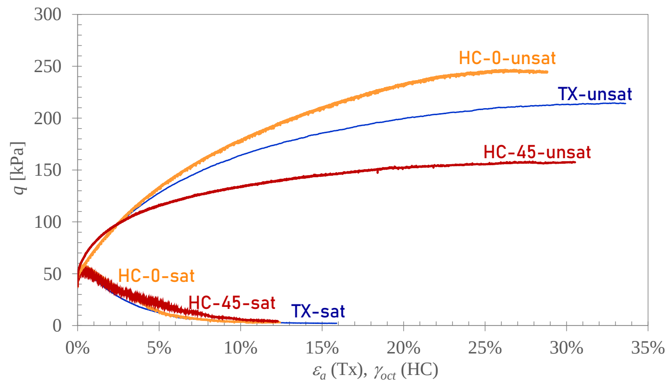

Figure 5: Comparison of the stress-strain behaviour of saturated and unsaturated tests

With respect to the saturated tests, Table 3 shows that the three tests presented almost the same values of void ratio at the beginning of shearing, despite the lower initial value of the TSHC test conducted with α=45˚, mostly due to a lower compressibility during consolidation. In terms of shearing behaviour, all saturated tests exhibited similar stress-strain curves, as demonstrated in Figure 3a, characterized by strain-softening and liquefaction of the material (p'≈0). The results also showed that whereas both tests performed under axisymmetric conditions (TX-sat and HC-0-sat) achieved identical deviator stress at peak and analogous development of excess pore pressure, test HC-45-sat displayed a slightly lower peak resistance and higher pore pressure generation.

As for the unsaturated tests, the lowest compressibility presented by HC-45-unsat during consolidation was consistent with the saturated tests. Figure 5 shows that, in contrast to the saturated tests, the unsaturated ones exhibited a steady increase in deviator stress with tendency to stabilise at larger strains, which was expected due to the lower degree of saturation. This behaviour was accompanied by an ongoing contraction of the sample (Figure 4b) due to the compression of the air contained within the voids, hence typical loose drained behaviour. It can be noted that the hollow cylinder test HC-0-unsat presented the lowest void ratio at the end of shearing and the highest shear strength among all tests. Conversely, although the unsaturated test carried out with α=45˚ (HC-45-unsat) presented virtually the same void ratio at the end of shearing than test TX-unsat, it achieved a deviator stress 27% lower than the triaxial test.

Conclusion

A set of two triaxial compression tests and four torsional shear hollow cylinder tests was carried out on saturated and unsaturated samples of an iron ore tailings. The specimens were sheared either undrained (saturated tests) or at a constant water content (unsaturated tests) under either axisymmetric conditions or with α=45˚ and b=0.25. Results showed that:

- All three saturated samples presented strain-softening behaviour followed by liquefaction during shearing, and the specimens tested under axisymmetric conditions presented virtually the same result, regardless of the device used.
- The saturated specimen tested at $\alpha = 45^\circ$ and b=0.25 presented a slightly lower peak resistance and higher pore pressure generation when compared to the tests with α and b equal to zero, which indicate a minor strength anisotropy due to the direction of loading.
- All three unsaturated samples presented the same behaviour during shearing, a strain-hardening with stabilisation at larger strains accompanied by high volumetric strains, regardless of the values of α and *b,* a typical behaviour observed in drained testing.
- In contrast to the saturated tests, the maximum deviator stress reached by the unsaturated test sheared at $\alpha = 45^\circ$ and b=0.25 was remarkably inferior to the values achieved by the tests in which α and b were zero. The value was 27% lower when compared to the triaxial test and 36% lower than the TSHC.

Acknowledgements

The first author would like to acknowledge that this research was carried out while the author was in receipt of an International Research Fees Scholarship at The University of Western Australia and a PhD scholarship funded by the Future Tails project, a partnership between the University of Western Australia, BHP and Rio Tinto.

References

Chu, J. & Wanatowski, D. 2009. Effect of Loading Mode on Strain Softening and Instability Behavior of Sand in Plane-Strain Tests. *J. Geotech. Geoenviron. Eng*. 135(1):108–120.

Fanni, R., Reid, D., and Fourie, A. 2022. Effect of principal stress direction on the instability of sand under the constant shear drained stress path. *Géotechnique*. Ahead of Print.

Fanni, R., Reid, D., and Fourie, A. 2023. A simple method to calculate the void ratio of very loose silts and silty sands in torsional shear hollow cylinder testing. *Geotechnical Testing Journal* 46(3)

Fotovvat, A. R., & Sadrekarimi, A. 2022. Instability of a Gold Mine tailings subjected to different stress paths. *Journal of Geotechnical and Geoenvironmental Engineering* 148(5).

Fourie, A. B. and Papageorgiou, G. 2001a. Defining an appropriate steady state line for Merriespruit gold tailings. *Can. Geotech. J.* 38(4): 695–706

Fourie, A. B., Hofmann, B. A., Mikula, R. J., Lord, E. R. F. and Robertson, P. K. 2001b. Partially saturated tailings sand below the phreatic surface. *Géotechnique* 51(7):577–585

Jefferies, M., and Been, K. (2015). Soil Liquefaction: A Critical State Approach, Second Edition. CRC Press.

Reid, D., Chiaro, G., Fanni, R. and Fourie, A. 2022a. Arguments for increasing the use of hollow cylinder testing in the characterisation of tailings. *Proceedings of The Tailings and Mine Waste Conference 2022*. Denver.

Reid, D., Fanni, R. and Fourie, A. 2022b. Assessing the undrained strength cross-anisotropy of three tailings types. *Géotechnique Letters* 12(1):1–7.

Robertson, P. K., da Fonseca, A. V., Ulrich, B. and Coffin, J. 2017. Characterization of unsaturated mine waste: a case history. *Canadian Geotechnical Journal* 54(12):1752–1761.

Russell, A. R., Vo, T., Ayala, J., Wang, Y., Reid, D. and Fourie, A. B. 2022. Cone penetration tests in saturated and unsaturated silty tailings. *Géotechnique*. Ahead of Print.

Urbina, F., Reid, D. and Fourie, A. 2023. Strain Softening response of loose unsaturated tailings samples in undrained triaxial tests. *Proceedings of The 8th International Conference on Unsaturated Soils*. Milos Island.

Yang, Z. X., Li, X. S. and Yang, J. 2008. Quantifying and modelling fabric anisotropy of granular soils. *Géotechnique* 58(4):237–248.

Influence of grain size distribution on flow liquefaction: a DEM study

Syed Uzair Us Salam Shah, Technical University of Munich, Germany
Roberto Cudmani, Technical University of Munich, Germany
Andrés Alfonso Peña-Olarte, Technical University of Munich, Germany

Abstract

Tailings are cost-effective materials for the construction of tailings dams. Proper segregation of coarse and fine fractions is especially crucial in upstream construction because the deposited tailings near the dam start acting as foundation as the dam is gradually raised. Results from experimental investigations on mixed compositions carry simultaneous effects from the change in gradation, grain shape and mechanical properties of grains which limits judgement about the isolated effects of change in grain size distribution on shear behavior. Discrete element modeling was employed to study the influence of grain size distribution on the mechanical behavior of idealized granular assemblies sheared at otherwise same conditions. During axisymmetric shearing under notionally undrained (or constant-volume) conditions, initial peak strength (instability state) was mobilized followed by softening until its lowest value (quasi-steady state as a transitional state) which was either sustained or led to re-hardening depending on the sample state. The steady-state lines translated downwards on the $e - p'$ (void ratio vs. mean effective stress) plane with the widening of gradation. Upon shearing, the potential of strength loss (strain-softening) decreased with the gradual densification along consolidation path which is consistent with laboratory tests. At the same initial state, stress ratio at the instability state decreased and the post-instability softening potential increased with the widening of gradation. Results show that the grain size distribution is of high relevance to the liquefaction both at its initiation and strength reduction following it. In general, results demonstrated the discrete element model to capture the complex features of soil behaviour.

Introduction

Soil liquefaction is the substantial strength loss in saturated, loose and cohesionless granular materials upon undrained shearing. Literature shows a large number of laboratory tests on the loose sand samples undergoing high strength reduction followed by large deformations (Castro et al., 1982; Been & Jefferies, 1985; Zhang & Garga, 1997). This loss of strength is induced by the increase of porewater pressure, and consequently, the reduction in effective stresses caused by the contractive potential of loose grain arrangements. The liquefaction of granular soils, particularly sands, has been systematically studied within the steady state framework (or interchangeably, the critical state framework), which is defined as the ultimate state at which a mass of particles deforms with constant stress and constant volume (Poulos, 1981). In addition to the steady state (SS), the quasi-steady state (or QSS) which is a state of local minimum resistance mobilized during the undrained shearing has also been consistently reported (Been et al., 1991; Verdugo & Ishihara, 1996; Yamamuro & Lade, 1998; Murthy et al., 2007). Occurrence of quasi-steady state follows the mobilization of instability (IS) state which marks the local peak in strength at which softening or even collapse of a loose grain skeleton starts (Lade & Yamamuro, 1998; Murthy et al., 2007). The instability state can be seen as a triggering (or yield) point which is instantaneous in its occurrence, whereas, the quasi-steady state is a transitional state which persists during a certain range of strains (depending upon the sample state) and is followed by re-strengthening towards the ultimate or steady state. The quasi-steady state is called so because it is a state of temporary standstill in strength. The typical undrained behavior of sand sample showing the instability state, quasi-steady state or temporary liquefaction is schematically presented in Figure 1a. Used stress invariants are $q = \sigma'_{\mathrm{zz}} - \sigma'_{\mathrm{xx}}$ and $p' = (\sigma'_{\mathrm{zz}} + 2\sigma'_{\mathrm{xx}})/3$. Where, σ'_{zz} and σ'_{xx} are the vertical and radial normal stresses, which are also the major and minor principal stresses, respectively. Furthermore, $\sigma'_{\mathrm{xx}} = \sigma'_{\mathrm{yy}}$ due to the considered axisymmetry. Initial state parameter, $\Psi_{o(ss)}$, is taken as the difference between void ratio (e) and e at the SS line corresponding to p'_c. As the shear behavior of contractive samples shows overshooting of state path across the steady state line towards the QSS on $e - p'$ plane, the reference state for instability state and post-instability softening should be the QSS at which the contractive potential exhausts (Fig. 1b). Therefore, $\Psi_{o(qss)}$ is the difference between e and e at QSS line corresponding to the p'_c. Moreover, the laboratory tests show that the initial states plotting underneath the SSL line also involve instability and softening. Hence, the binary classification of shear behavior on the basis of initial state with reference to the SS line in order to separate contractive/liquefiable states from the dilative/safe states can be misleading. A major challenge, however, in utilizing the QSS is that it is not a unique function of void ratio but is influenced by the consolidation pressure (Shah et al., 2023a; Shah et al., 2023b). Therefore, the association or correspondence between consolidation line and resulting QSS line is important to study the strength mechanics at instability state. In this paper, instability and the quasi-steady state will be characterized by their respective q/p' ratio and the softening index ($I_S = (q_{IS} - q_{qss})/q_{IS}$) will be presented as a measure of strength reduction after the instability. Stress ratio mobilized at the instability state is lower than that mobilized at the quasi-steady state

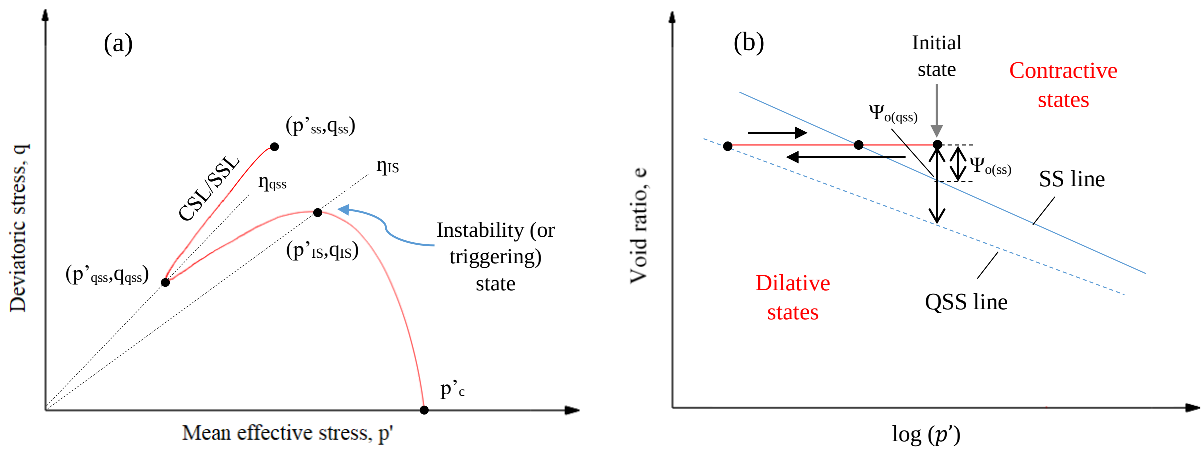

Figure 7 Schematic undrained behaviour showing temporary liquefaction (a) effective stress path & (b) state path and loci on $e - p'$ plane

and steady state and shows high state dependencies as compared to that at the latter two states (Ishihara, 1993; Yamamuro & Lade, 1998; Murthy et al., 2007). Strength reduction following the instability state can lead to catastrophic failure in loose deposits, which suggests to consider the instability as a limit state. For the utilization of the shear resistance at the limit state in stability calculations, it is of prime importance to understand its dependencies on the granulometric properties and the state of the granular skeleton. However, it is challenging to understand the influence of material properties on the stress ratio at instability from the literature as the influencing properties are difficult to be investigated separately.

In order to study the influence of gradation and grain shape, some experimental investigations involved the addition of fines in the natural sands but reached a lack of agreement regarding their influence on shear behavior not only at large strains (or SS) but also at the instability state (Been & Jefferies, 1985; Hird & Hassona, 1990; Fourie & Tashabala, 2005; Murthy et al., 2007; Rahman et al., 2014). These studies reported opposing outcomes about either the downwards translation of the SSL on the $e - p'$ plane while maintaining its obliquity or it's clockwise rotation about a pivot point with the increase in fines content. Based on these two classes of findings, some researchers judged the former case to make samples less resistant towards liquefaction, whereas the later to be yielding stronger samples, since the steady state line limits the extreme strength loss (for the void ratios above the rotational pivot of SS lines on $e - p'$ plane). Such judgement is biased since the attainable ranges of void ratios are influenced by the gradation (Cho et al., 2006). The use of the state parameter is overstated in the literature by expecting it to be giving unified relations for stress ratio mobilized at the instability even for different mixed compositions despite the simultaneous changes in gradation (grain sizes and their distribution), mechanical and geometrical characteristics of grains, etc. This research does not aim to address the complexity of such laboratory studies on mixed compositions producing simultaneous and interwoven influences from many factors but to fundamentally understand the isolated influences of grain size distribution on mechanical response. The discrete element modelling (DEM) was performed to test the assemblies with different grain size distributions at otherwise same conditions. DEM simulations were involved because of being free from implicitness unlike the laboratory tests and providing an objective basis of comparison.

Methodology

Discrete element modelling (DEM) is a technique to model the granular materials by explicitly considering the discrete (or individual) particles and their interactions. PFC3D program (Itasca Consulting Group, Inc. 2021) was used for the DEM. The different grain size distributions (GSD) were simulated by maintaining the mean particle diameter (D_{50}) as 0.22 mm and varying the coefficient of uniformity (C_u) as 1, 1.6 & 2. Figure 2a shows the simulated grain size distributions and isometric views of their initial samples. Among all these assemblies, the contact properties, inter-particle sliding friction coefficient, grain shape and the simulation setup was controlled the same in order to study isolated effects from the change in grain size distribution. Fundamentally, C_u represents the variability in grain sizes and their inertia (translational and rotational) which is expected to affect the response of assemblies (in terms of grain re-arrangement and their interactions) upon straining. The scheme of periodic boundaries after Thornton (2000) was implemented for homogeneity within the samples and to eliminate the effects induced by rigid boundaries. The initial dimensions of periodic domain were set as 4.5x4.5x4.5 mm followed by the distribution of particles within it. This distribution was performed on the basis of input grain size distribution. Deformability method with linear force-displacement formulation was used at contacts due to its computational efficiency. Details of this contact model are not provided here due to the space limitations, but can be seen in Potyondy & Cundall (2004). This formulation scales contact stiffness according to the sizes of contacting bodies which can be corroborated by the grain-level study from Sandeep et al. (2021). Notable model parameters are; effective contact modulus = 1.1×10^8 N/m^2, ratio of normal to shear contact stiffness = 1.5, inter-particle sliding friction coefficient = 0.34, critical (normal and shear/tangential) damping ratio = 0.2 and rolling friction coefficient = 0.1. Notional particle density of 3356 kg/m^3 was used and the gravity was not simulated. Density was scaled up by a factor of 10^4 in order to obtain a reasonable integration timestep which is common in numerical modelling (O'Sullivan, 2011). Density scaling does not affect the discrete force-displacement and resulting stress-strain response (Thornton, 2000). During the genesis of assemblies, the inter-particle friction coefficients were varied to obtain different initial void ratio and corresponding isotropic compression paths. The unbalanced force ratio, as defined by the ratio between the average unbalanced force to the average contact force acting on each particle, reflects the state of equilibrium. Following the constant-volume simulations from Barnett et al. (2021), the maximum unbalanced force ratio of 10^{-4} was ensured in all simulations. Notionally undrained (constant-volume) simulations were performed by prescribing the extensional principal strain increments in both minor principal strain directions to be half and opposite to the vertical (or major principal) strain increment which was compressional. The imposed vertical strain rate was 2.5 x10^{-5} % per integration timestep corresponding to the axial strain rate of $\dot{\varepsilon}_{zz} = 0.04$ which was kept same for both the consolidation and shearing phase.

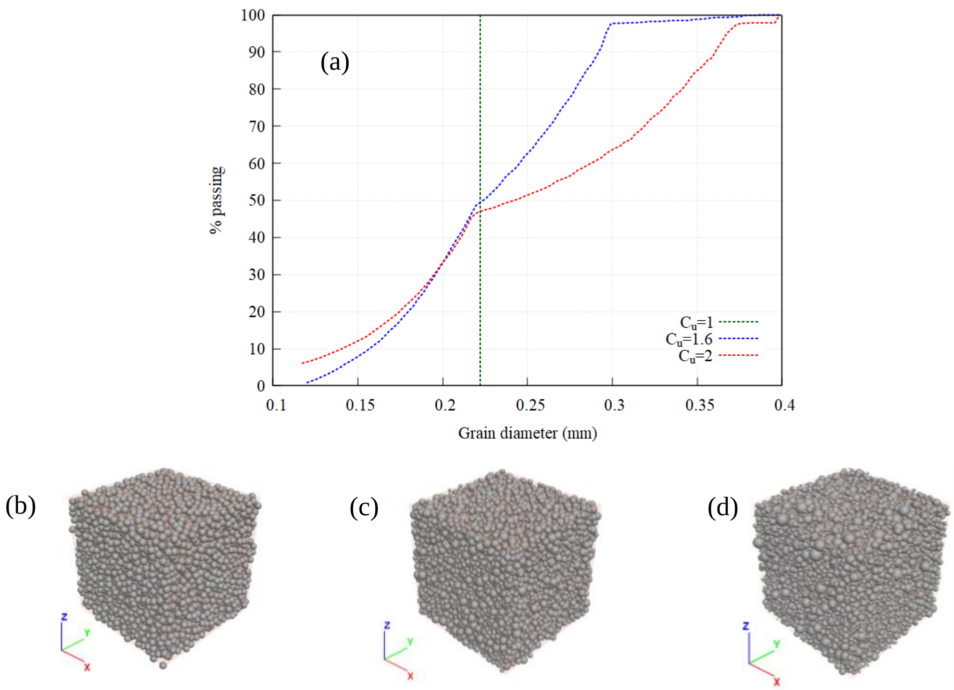

Figure 8 (a) Simulated grain size distributions and initial samples (b) C_u=1, (c) C_u=1.6 & (d) C_u=2

The stress tensor was computed according to Equation 1, as suggested by Christoffersen et al. (1981) which is commonly utilized in the DEM studies.

$$\sigma'_{ij} = \frac{1}{V}\sum_{1}^{N_c} \boldsymbol{f}_i \boldsymbol{l}_j \qquad \text{Equation 1}$$

Where N_c is the number of contacts inside the measurement region of volume V, $\boldsymbol{f}_i$ is the contact force vector and $\boldsymbol{l}_j$ is the branch vector (vector joining the centroids of two contacting pieces). i and j cycle from 1-3 (3-dimensions). Equation 1 takes outer product between the contact force vector and the branch vector. $\sigma'_{xx} = \sigma'_{yy}$ due to the considered axisymmetry. The Coordination number (CN) is defined as the average number of contacts per particle. As each contact is being shared between two particles, the number of particles is halved as following:

$$Coordination\ number\ (CN) = {}^{2N_c}\!/_{N_p} \qquad \text{Equation 2}$$

Where N_p is the number of particles. Fabric is defined in the form of a second rank tensor as proposed by Satake (1978) in Equation 3**¡Error! No se encuentra el origen de la referencia.**. This definition of fabric is extensively used in DEM research.

$$Fabric\ tensor\ = \varphi_{ij} = \frac{1}{N_c}\sum_{1}^{N_c}\boldsymbol{n}_i\boldsymbol{n}_j \qquad \text{Equation 3}$$

Where $\boldsymbol{n}$ is the contact normal unit vector with $\boldsymbol{n}_i$ and $\boldsymbol{n}_j$ being the corresponding column and row vectors, respectively. Based on the axisymmetric conditions, $\varphi_{\mathrm{xx}} = \varphi_{\mathrm{yy}}$ due to the transverse-isotropy.

Results and discussion

As shown in Figure 3, the SS lines for assemblies with different C_u are nearly parallel to each other but translated downwards on $e - p'$ plane with the increase in C_u or the widening of gradation. At the same void ratio, the availability of differently sized grains resulted the assemblies to flow at the SS ($\delta q = \delta p' = 0$) with the mobilization of lower stresses as the grains with various sizes can rearrange into denser configuration. Also, in order to mobilize a certain magnitude of the mean stress at the SS (at vanishing stress increment), the widening of gradation requires lower void ratio or denser grain matrix. The SS lines are can be approximated with the power-law function as following

$$e_{ss} = \Gamma - \lambda.({p'_{ss}}/{p'_a})^{\xi} \qquad \text{Equation 4}$$

where p'_a is the atmospheric pressure, and Γ, λ and ξ are the fitting parameters. Γ is the intercept of SS line with void ratio axis upon vanishing stresses and λ shows its slope on $e - (p'/p'_a)^{\xi}$ plane. Reasonability of such fitting can be seen in Li & Wang, 1998; Murthy et al., 2007; Yang & Lou, 2015. Downwards translation of SS lines with increase in C_u is consistent with the experimental results presented by Murthy et al., 2007; Carrera et al., 2011; Rahman & Lo, 2014; Barnett et al., 2021.

Comparison of the isotropic consolidation lines for samples with two different C_u = 1.6 & 2 but from coinciding initial states is presented in Figure 4. Data points along the consolidation lines correspond to the initial states upon constant-volume shearing. The resulting transitional (quasi-steady state) and ultimate (steady) state lines are also provided. Due to the higher void ratio and upwards plotting of their states on $e - p'$ plane, mono-disperse assemblies could not be placed in this comparison but their mechanics will be discussed in comparison with respect to the state parameter. The compressibility or $||\, \delta e/\delta p'_c \,||$ increased with the widening of gradation which indicates higher rearrangement potential due to a variety of grain sizes.

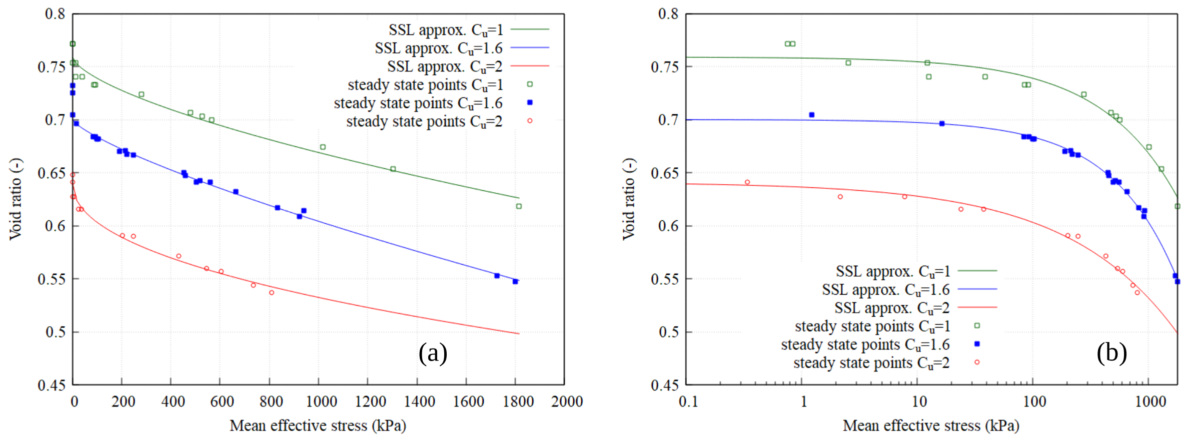

Figure 9 ***Steady state lines for assemblies with different C_u (a) arithmetic plot & (b) semi-logarithmic plot***

Increase in compressibility with C_u is consistent with the experimental observation, e.g. Rahman & Lo (2014). Upon shearing at the same void ratio, assemblies with wider gradations showed higher contractive potential which can be seen through the greater horizontal shift between their consolidation and quasi-steady state lines. Moreover, the dilation potential followed by strength softening was also insignificant in assemblies with wider gradation. Such behaviour is also evident from the test results by Yang & Wei (2012) as the presence of fines or increase in their percentage (widening of gradation) enhanced the softening potential and countered the re-strengthening. For shearing from the initially coinciding consolidation lines, a comparative bias is present due to the downwards movement of steady state line with the widening of gradation and increasing flow potential with the upwards movement of consolidation line on $e - p'$ plane. This comparative bias was shown through the analysis of laboratory test results from Yamamuro & Lade (1998). Therefore, the strength behaviour will also be compared on the basis of state parameter.

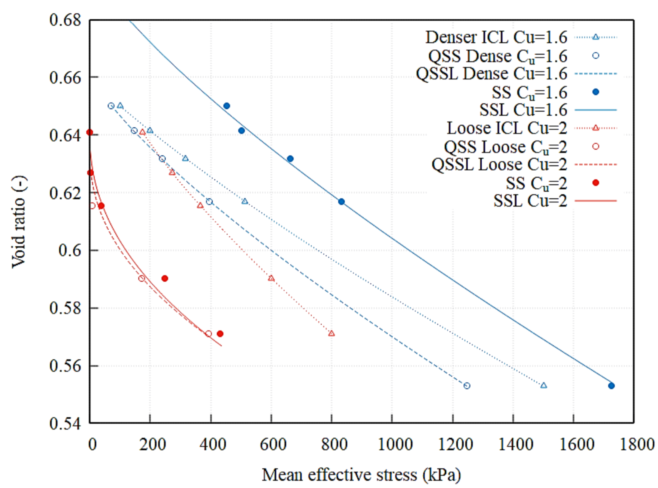

Figure 10 ***Initially coinciding consolidation lines and state lines for assemblies with C_u = 1.6 & 2***

Figure 5a shows the deviator stress vs. axial strain and effective stress paths for the samples with different C_u but sheared from almost the same consolidation pressure. Upon the application of shearing, the sample with C_u=1.6 showed relatively higher strength evolution and very insignificant softening. Whereas, the sample with wider gradation (C_u=2) mobilized lower strength at the instability state after which it was softened to a lower strength at the quasi-steady state despite its lower void ratio. For shearing beyond the quasi-steady state, sample with wider gradation (C_u=2) showed lower re-hardening as compared to that with C_u=1.6. As shown in Figure 5b, the q/p' stress obliquity mobilized at instability was higher for the sample with lower C_u.

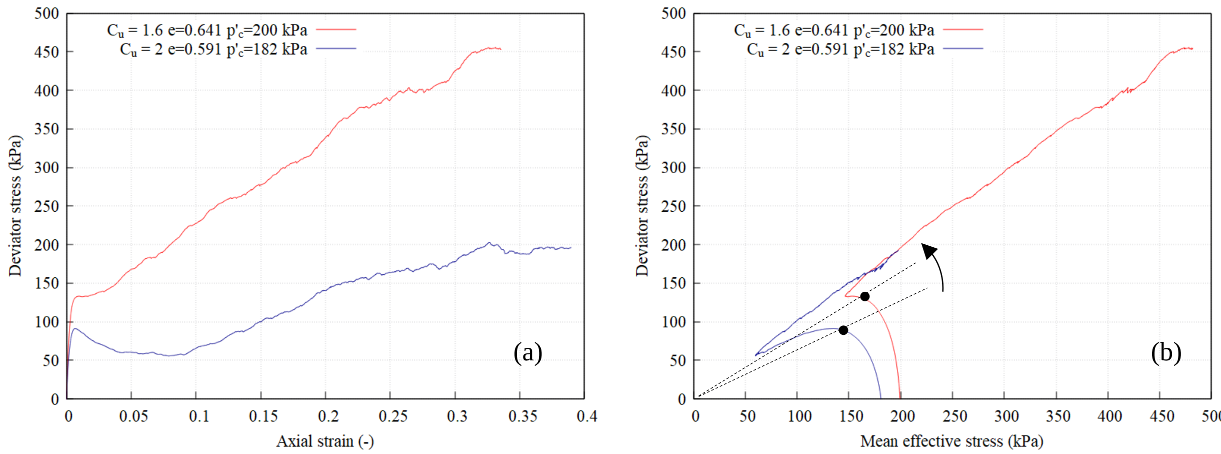

Figure 11 (a) Stress-strain curves & (b) effective stress paths for simulated samples with different C_u but proximate initial states

Figure 6a shows the micro-mechanical (coordination number and fabric deviator) evolutions for the sample pair in discussion. The initial coordination number was higher for the sample with lower C_u which shows relatively higher contact density despite its higher void ratio. Upon shearing, the coordination number decreased untill the respective quasi-steady state which was followed by an increase. Throughout the shearing, coordination number for sample with C_u=1.6 remained higher than that for the sample with C_u=2. Upon shearing, sample with C_u=2 moved from the initial state to the instability state after a smaller reduction in average coordination number which shows its potential to reach the state of softening relatively rapidly. The evolution of fabric deviator ($\varphi_d = \varphi_{zz} - \varphi_{xx}$) is shown in Figure 6b. Due to the isotropic start, the fabric deviator (φ_d) was initially 0. Upon the reduction in p' (contractive potential), relatively less contact re-orientation was required for the sample with C_u=2 to mobilize its instability state followed by softening towards the quasi-steady state. Further shearing through the quasi-steady state incurred higher increase in fabric deviator for the sample with wider gradation. This indicates higher granular rearrangement and contact re-orientation in sample with the wider gradation. Both the coordination number and the fabric deviator were approaching constant values towards the steady state.

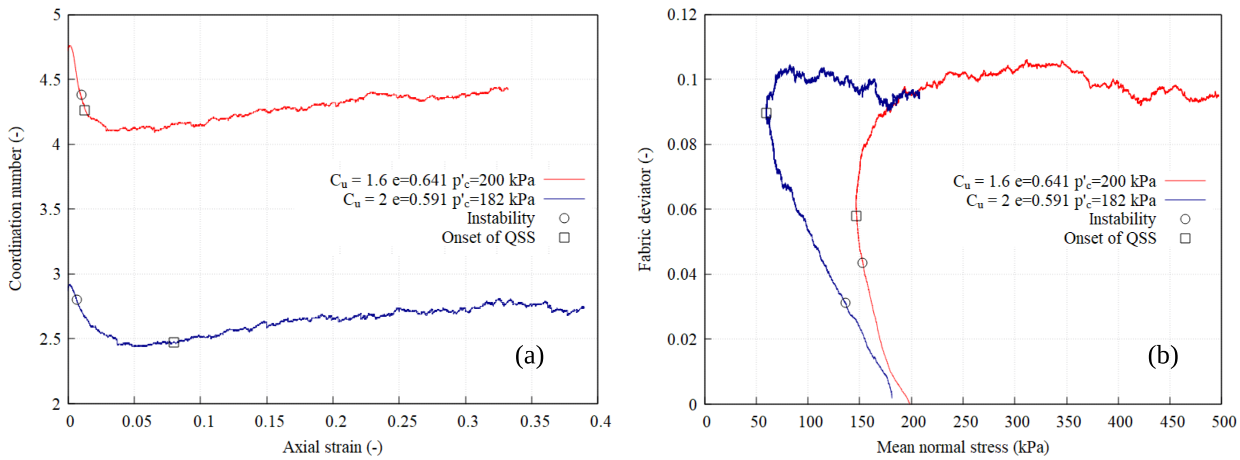

Figure 12 (a) Coordination number vs. axial strain & (b) fabric deviator vs. p' for simulated samples with different C_u but proximate initial states

Figure 7a shows the $q_{IS}/p'_{IS} - e$ relations for simulated gradations. For samples sheared from each consolidation line, the q_{IS}/p'_{IS} increased with the decrease in void ratio (or gradual consolidation). For simplicity, only the behaviour of samples sheared from loose consolidation lines will be discussed here. The $q_{IS}/p'_{IS} - e$ relations moved downwards with the increase in C_u. In other words, at the same void ratio upon shearing, the q_{IS}/p'_{IS} ratio decreased with the increase in C_u. This means that keeping everything else the same, presence of a variety of grain sizes promotes grain rearrangement and counters grain interlocking. This can also be linked with the higher compressibility of wider grain size distribution as discussed above. The leftwards movement of the $q_{IS}/p'_{IS} - e$ relations with the increase in C_u is due to the lower attainable void ratio of wide-graded materials. Therefore, the behavioural comparison among different gradations against the void ratio is not objective and suggests to study the relations between state parameter and q_{IS}/p'_{IS}. Figure 7b shows the stress ratio at the instability state of samples sheared from loose consolidation lines against their initial state parameter $\Psi_{o(qss)}$. For each material, q_{IS}/p'_{IS} increased with the decreasing $\Psi_{o(qss)}$ or with increasing proximity between the initial state and the QSS, at which the softening potential terminates. At the same $\Psi_{o(qss)}$, the q_{IS}/p'_{IS} decreases with increasing C_u which indicates correspondingly increasing tendency to reduce pore volume upon shearing.

Both the softening index, $I_s = [(q_{IS} - q_{qss})/q_{IS}]$, and the flow potential, $u_f = [(p'_c - p'_{qss})/p'_c] * 100$, decreased with the decrease in $\Psi_{o(qss)}$ or with the following of consolidation lines (Fig. 7c-d). In other words, the densification of grain skeleton along the consolidation lines countered softening and contractive potential. For very loose conditions, full strength loss ($I_s = 1$) and flow ($u_f = 100\%$ or loss of effective stress), i.e. flow liquefaction occurred. To the denser extreme, the softening (post-peak behaviour) was insignificant ($I_s \approx 0$) but the contractive potential was present. At the same $\Psi_{o(qss)}$, both the softening index and flow potential increased with the increase in C_u which shows that the presence of a variety of grain sizes promotes grain mechanics which favours strength reduction. These results are in agreement with the results from laboratory tests (Ishihara, 1993; Yang & Wei, 2012; Schnaid et al., 2013, etc.).

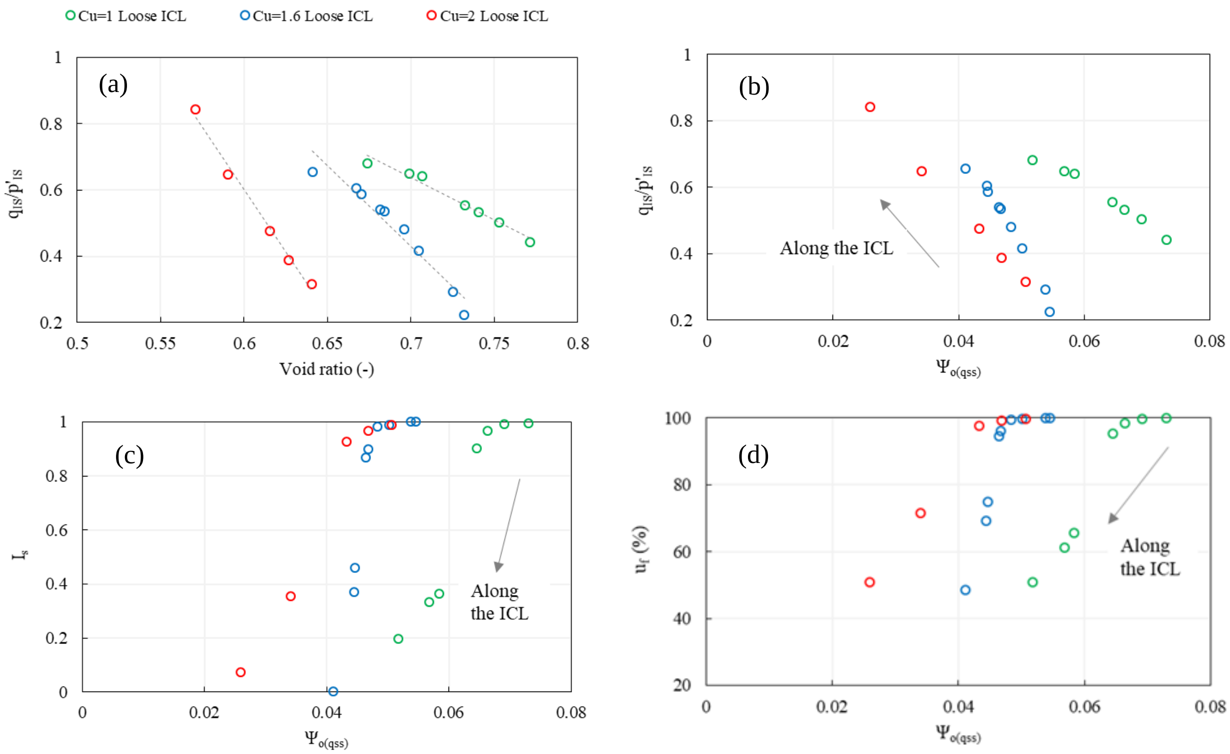

Figure 13 Influence of C_u on instability and post-instability mechanics (a) Stress ratio at instability against void ratio (b) Stress ratio at instability against $\Psi_{o(qss)}$ (c) Softening index against $\Psi_{o(qss)}$ & (d) flow potential against $\Psi_{o(qss)}$

Conclusion

Tailing dams are mainly composed of sands extracted from the tailing materials with a variety of grain size distributions and non-plastic fines content (Branch, 1994). Therefore, understanding the influence of the gradation characteristics on the undrained shear behaviour, particularly on the initiation of liquefaction is crucial to assess the stability of such structures. In order to investigate this influence, numerical simulations with the discrete element method were carried out in this contribution. In accordance with the experiments, results from simulations show that the gradual densification with the increase in p'_c along an isotropic compression line strengthens the grain skeleton and the shear response transits from flow liquefaction to the occurrence of quasi-steady state and then to the phase transformation (contractive behaviour without the strength reduction). This is due to the gradually increasing proximity and coordination between grains as the consolidation is advanced. The SSLs translated downwards on the $e - p'$ plane with the widening of gradation. At the same void ratio, decreasing uniformity or the availability of differently sized grains caused the assemblies to flow at the steady state with the mobilization of lower p'_{ss}. For initially coinciding ICLs, the compressibility increased with the widening of gradation which was due to the correspondingly higher grain rearrangement. At the same initial state, stress ratio mobilized at the instability state decreased and the post-instability softening (brittleness) increased with the widening of gradation. We conclude that the widening of gradation favours grain rearrangement and promotes contractive behaviour causing a decrease in strength at both the instability and the quasi-steady state.

References

Barnett, N., M.M. Rahman, M.R. Karim, H.K. Nguyen and J.A.H. Carraro. 2021. Equivalent state theory for mixtures of sand with non-plastic fines: a DEM investigation. *Géotechnique*. 71(5):423–440.

Been, K. and M.G. Jefferies. 1985. A state parameter for sands. *Géotechnique*. 35(2):99–112.

Been, K., M.G. Jefferies and J. Hachey. 1991. The critical state of sands. *Geotechnique*. 41(3):365–381.

Branch, S.W. 1994. *Design and evaluation of tailings dams*. USA

Carrera, A., M.R. Coop and R. Lancellotta. 2011. Influence of grading on the mechanical behaviour of Stava tailings. *Géotechnique*. 61(11):935–946.

Castro, G., J.L. Enos, J.W. France and S.J. Poulos. 1982. Liquefaction induced by cyclic loading. *NASA STI/Recon Technical Report N. 83*.

Cho, G. C., J. Dodds and J.C. Santamarina. 2006. Particle shape effects on packing density, stiffness, and strength: Natural and crushed sands. *Journal of geotechnical and geoenvironmental engineering*. 132(5):591–602.

Christoffersen, J., M.M. Mehrabadi and S. Nemat-Nasser. 1981. A Micromechanical Description of Granular Material Behavior. *J. of Applied Mechanics*. 48(2):339–344.

Fourie, A. B. and L. Tshabalala. 2005. Initiation of static liquefaction and the role of K 0 consolidation. *Canadian geotechnical journal*. 42(3):892–906.

Hird, C. C. and F. A. K. Hassona. 1990. Some factors affecting the liquefaction and flow of saturated sands in laboratory tests. *Engineering Geology*. 28(1-2):149–170.

Ishihara, K. 1993. Liquefaction and flow failure during earthquakes. *Geotechnique*. 43(3):351–451.

Itasca Consulting Group, Inc. 2021. *PFC — Particle Flow Code, Ver. 7.0*. Minneapolis: Itasca.

Jefferies, M. and K. Been. 2015. *Soil liquefaction: a critical state approach*. CRC press.

Li, X.S. and Y. Wang. 1998. Linear representation of steady-state line for sand. *Journal of geotechnical and geoenvironmental engineering*. 124(12):1215–1217.

Murthy, T.G., D. Loukidis, J.A.H. Carraro, M. Prezzi and R. Salgado. 2007. Undrained monotonic response of clean and silty sands. *Géotechnique*. 57(3):273–288.

O'Sullivan, C. 2011. *Particulate discrete element modelling: a geomechanics perspective*. CRC Press.

Potyondy, D.O. and P.A. Cundall. 2004. A bonded-particle model for rock. *International journal of rock mechanics and mining sciences*. 41(8):1329–1364.

Rahman, M. M. and S.R. Lo. 2014. Undrained behavior of sand-fines mixtures and their state parameter. *Journal of geotechnical and geoenvironmental engineering*: 140(7):401–406.

Sandeep, C.S., S. Li and K. Senetakis. 2021. Scale and surface morphology effects on the micromechanical contact behavior of granular materials. *Tribology International*. 159:106929.

Satake, M. 1978. Constitution of mechanics of granular materials through the graph theory. *In Proc. US-Japan Seminar on Continuum Mech. Stat. Appr. Mech. Granul. Mater.* Sendai :203–215.

Schnaid, F., J. Bedin, A. J. P. Viana da Fonseca and L. de Moura Costa Filho. 2013. Stiffness and strength governing the static liquefaction of tailings. *Journal of Geotechnical and Geoenvironmental Engineering*. 139(12):2136–2144.

Shah, S. U. U. S., R. Cudmani and A.A. Peña-Olarte. 2023a. Micromechanics of the quasi-steady state: a DEM study. *Proceedings of the 17th Danube European Conference on Geotechnical Engineering (17DECGE) June 7–9, 2023*, Bucharest, România, *ISSMGE.*

Shah, S. U. U. S., R. Cudmani and A.A. Peña-Olarte. 2023b. Influence of initial confining stress on the quasi-steady state. *Proceedings of 10th European Conference on Numerical Methods in Geotechnical Engineering June 26–28, 2023.* ICL, London, *ISSMGE*.

Thornton, C. 2000. Numerical simulations of deviatoric shear deformation of granular media. *Géotechnique*. 50(1):43–53.

Verdugo, R. and K. Ishihara. 1996. The steady state of sandy soils. *Soils and foundations*. 36(2):81–91.

Yamamuro, J.A. and P.V. Lade. 1998. Steady-state concepts and static liquefaction of silty sands. *J. of geotechnical and geoenvironmental engineering*. 124(9):868–877.

Yang, J. and X.D. Luo. 2015. Exploring the relationship between critical state and particle shape for granular materials. *J. of the Mech. and Physics of Solids*. 84:196–213.

Zhang, H. and V.K. Garga. 1997. Quasi-steady state: a real behaviour?. *Can. Geot. Journal*. 34(5):749–76.

Influence of the sample reconstitution procedures on the mechanical behaviour of iron ore tailings

PAULO A.L.F. COELHO, University of Coimbra, Portugal
DAVID L.D. CAMACHO, University of Coimbra, Portugal
FELIPE GOBBI, FGS Geotecnia, Brazil

Abstract

Tailings dams built around the world can pose serious threats to the environment and to those living nearby, as several dramatic failures that occurred in the past show. The global growing demand for minerals and metals imposed by the desire to achieve a more sustainable economic growth and development based on a decarbonised economy may aggravate this problem and reinforce the need to improve our current understanding on the behaviour of tailings under different loading conditions. Because intact samples of tailings dams are seldom available, proper geotechnical testing requires suitable reconstitution procedures.

This paper considers the important problem of sample reconstitution, namely with respect to the case of iron ore tailings, discussing the implications of variations of the reconstitution procedures and comparing the behaviour of intact and reconstituted samples. The reconstituted samples are prepared through a slurry-based procedure using water contents representing possible but variable depositional conditions found in tailings dams in the field. This enlightens the effect of the water content of the slurry used in the sample reconstitution on the index properties and on the mechanical behaviour of the samples under undrained loading. In addition, the behaviour of the reconstituted samples prepared with different values of water content of the slurry is compared to the behaviour of undisturbed samples when loaded under comparable loading conditions. The reconstituted and the undisturbed samples were collected from an experimental site located in the North of Portugal. The experimental results suggest that the water content of the slurry used in the reconstitution process influences both the index properties and the mechanical behaviour under undrained triaxial compression. In fact, the higher the water content used in the reconstitution using the slurry-based method, the higher the resulting values of void ratio and the softer is the sample response to triaxial compression. In addition, samples prepared with higher water contents seem less representative of the behaviour observed in undisturbed samples and show more signs of particle segregation during reconstitution.

Introduction

The world demand for minerals and metals requiring mining activities has been increasing massively during the recent decades in order to satisfy the needs of modern society for its development. This growth can be exacerbated by the additional requirements imposed by the transition to a so-called low carbon economy, which is expected to support an even stronger demand for minerals and metals in the short and long-term. As a result, mining activities have been expanding around the world, a movement that is expected to continue as long as the current political trends are in place. Unfortunately, the surge of the mining activities results in an inevitable increase in the amount of mining waste produced, which often represents a major proportion of the rock material excavated. In fact, the amount of final product resulting from some mining activities can be residual in comparison to amount of ore mined from the earth, the resultant waste being termed “tailings”. Table 1 illustrates this problem for some commonly mined minerals and metals, representing the average proportions of tailings and final product obtained from several different Brazilian mines, giving an idea about how much waste can be generated by some type of mining activities.

Table 1: Average proportions of tailings and final product obtained for different minerals and metals in different Brazilian mines (Abrão, 1987, mentioned by Galvão Sobrinho, 2014)

Mineral/metal	% of waste resulting from mining activities	% of product resulting from mining activities
Iron	33.33	66.67
Coal	75.00	25.00
Phosphate	83.33	16.67
Copper	96.77	3.23
Gold	99.99	0.01

The amount of tailings deposits generated creates serious problems, some of which are fairly obvious, including the different environmental impacts imposed by these massive structures, even when they perform according to planned. Unfortunately, these structures fail more often than desired, often causing massive environmental, economic and social consequences and, in some cases, dramatic human deaths. Figure 1 represents the data collected by the watchdog World Mine Tailings Failures (WMTF, 2023), representing the number of severe and very severe tailings dams failures per decade and also the accumulated distance travelled by the tailings after failure. Assuming that the linear trends derived from the past data are valid, more than 30 severe and very severe tailings dams failures can be expected for the current decade, the accumulated distance travelled by the tailings after failure exceeding 700 km.

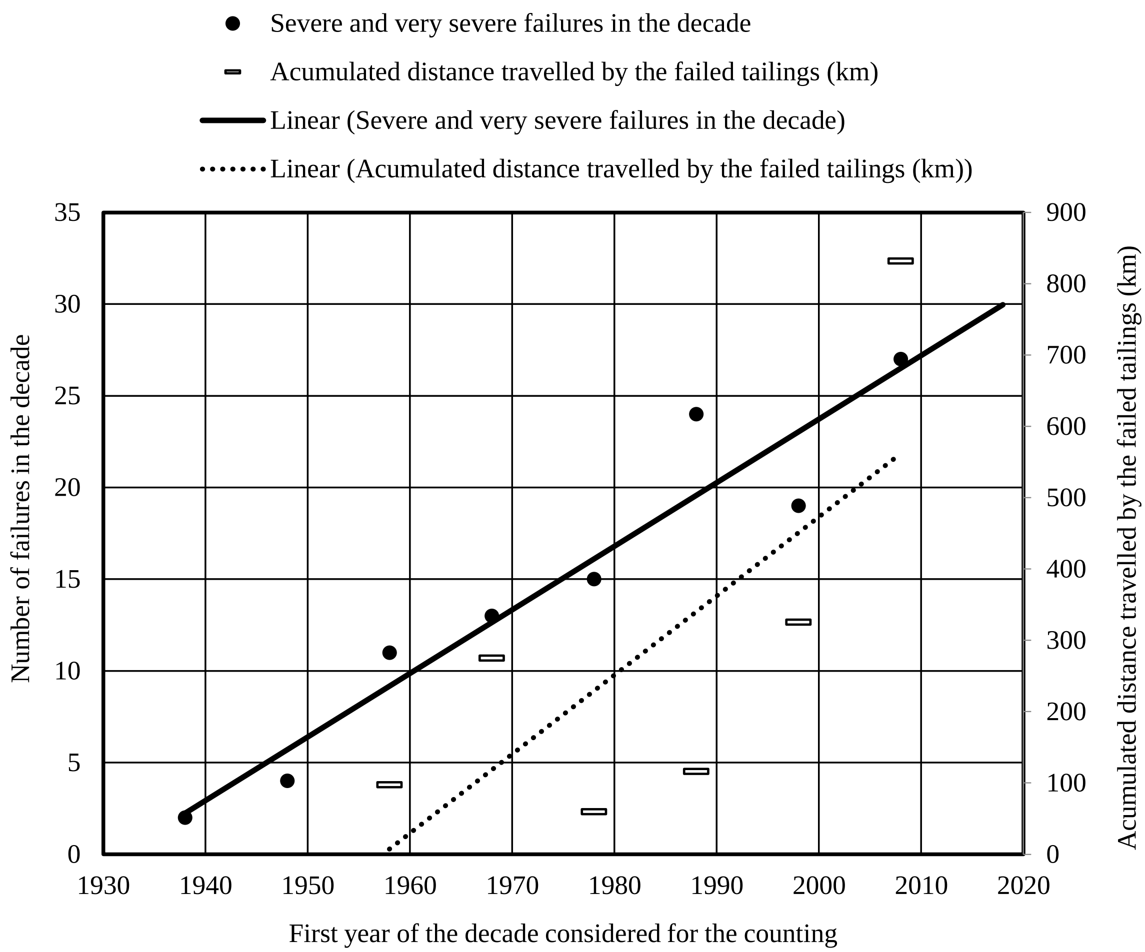

Figure 1: Number of failures and accumulated distance travelled by the tailings after failure in severe and very severe tailings dams per decade (data from WMTF, 2023)

Because of the dramatic consequences of these failures and the society demand for increasing the safety and sustainability of mining activities, proper understanding of the behaviour of tailings has been attracting researchers from different fields, particularly geotechnical engineers. In fact, tailings tend to act like geomaterials even if they are not produced by processes usually found in nature and responsible for the formation of natural deposits. Thus, tailings show some particular features of behaviour that favour their inclusion in the category of unconventional geomaterials. In order to characterize the behaviour of tailings through a geotechnical approach and including all the different types of consolidation and loading conditions that can possibly be observed in the field, suitable samples representing the field behaviour are required. Because undisturbed samples are seldom available and the effects of variability can be extremely large in these materials, sample reconstitution is often required to obtain the necessary number of identical samples for experimental testing. As discussed in the next section, this is not a trivial matter, namely but not only in the case of iron ore tailings, irrespective of the reconstitution method selected.

Particular characteristics of iron ore tailings

Iron ore tailings, like other ore tailings, are usually composed of irregular particles, resulting from the industrial processes involved in the iron ore processing, namely crushing and grinding. Iron ore tailings also have particles with different mineralogical compositions, including iron particles with a density that significantly exceeds that normally found in natural soils. Because it is expected that both the shape and the density of the particles influence the index properties and the mechanical behaviour of this unconventional geomaterial, it is important to assess the properties of relevant tailings deposits in the field to serve as a guide for the evaluation of the reconstitution procedure. In fact, irrespective of the reconstitution procedure selected, if the samples do not, at least qualitatively, replicate the physical conditions and the behaviour of undisturbed samples, the experimental results may be misleading.

The Brumadinho iron ore tailings

The failure of the Córrego do Feijão (Brumadinho) Tailings Dam, in 2019, marked a turning point in the society's perception of the risks posed by these massive structures, mostly because of the death toll resulting from the failure. Table 2 compiles some of the physical and index properties of the dam, formed by iron ore tailings, which were obtained previously to the failure (data from Silva, 2010) and after the failure (data from Robertson et al, 2019). The grain size distributions determined for various samples collected from the Brumadinho Tailings Dam before the failure are also presented in Figure 2 (Silva, 2010). The data obtained, both before and after the failure, suggests that the variability observed in the Brumadinho Tailings Dam is very high and tends to exceed the variability that is usually observed in many natural deposits. The variability is particularly important in the case of the index properties, notably in the void ratio, but it is also is clear in the grain size composition, even if sand and silt are the dominant fractions.

Table 2: Physical and index properties of Brumadinho dam measure before and after the failure

Physical and identification properties	Measured values before the failure (Silva, 2010)	Measured values after the failure (Robertson et al, 2019)
Density of solid particles- G [-]	3.8~4.9	3.6~5.0
Dry unit weight- γd [kN/m^3]	18.1~30.9	12.0~23.7
Water content- w [%]	16~20	6~37
Void ratio- e [-]	0.43~1.45	-
Liquid limit- w_L [%]	18~33	18~30
Plastic limit- w_P [%]	18~23	14~23

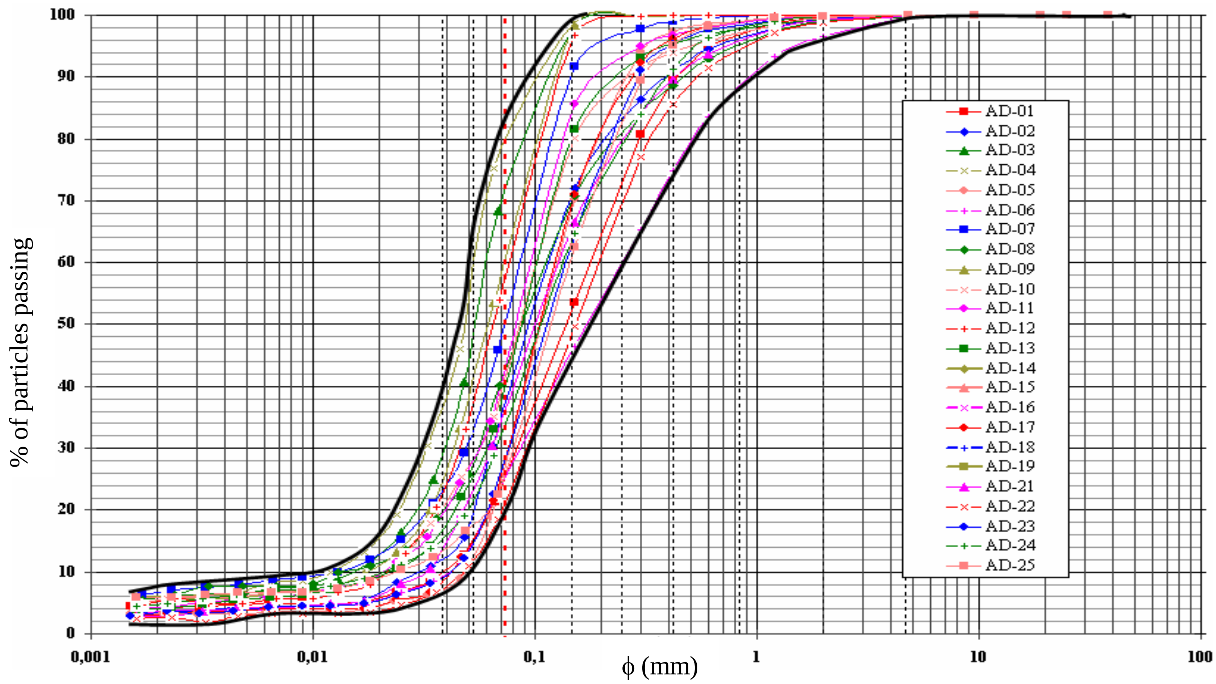

Figure 2: Grain size distributions of 25 samples collected from Brumadinho dam before the failure (Silva, 2010)

Two additional relevant aspects of the properties listed must be highlighted. Firstly, the remarkably high values of the density of solid particles (G), whose values vary between 3.6 and 5.0, showing not only a significant variability but also average values that notably exceed those found in common soils (G≈ 2.65). The results obtained are due to the presence of iron particles, whose density (G_{iron}≈ 7.9) considerable exceeds that of silica and feldspar. This increases the average values of the density of iron ore tailings, which contain iron in variable proportions depending on the conditions of the extraction, production and deposition phases. Secondly, the values of the void ratio measured in the field (before the failure) are extremely variable, ranging from relatively low values (0.43), which would be typical of a dense soil, to significantly high values (1.45), which could hardly be found in natural granular soils.

The Torre de Moncorvo iron ore tailings

The recent increased interest in mining activities led to the reopening of an old iron mine in Torre de Moncorvo, located in the North of Portugal (Fig. 3), near Douro river and the border with Spain. This mine formed the largest industry in the region until its closure in the 80’s, a significant amount of iron ore tailings being stacked in particular locations during the long period of duration of the mining activities in the area. Samples were collected from one particular site of the tailings deposit, produced decades ago in a poorly controlled manner, in order to obtain some physical and index properties of the local iron ore tailings.

Figure 3: Torre de Moncorvo iron ore waste site

The values of the physical and index properties measured at a particular site of Torre de Moncorvo tailings are, in average, similar to those observed in Brumadinho Tailings Dam, although the level of variability observed is considerably smaller. However, this may simply result from the fact that the samples were collected only from a specific site of the tailings deposit in the Torre de Moncorvo mine. With respect to the values measured, the extremely high values of the density of solid particles measured must be again highlighted, the range observed (4.4~5.1) being in line with the values found in Brumadinho and reflecting the presence of iron particles in the tailings. Once again, the silt and sand fractions are dominant and the plasticity is relatively limited, the Plasticity Index being just around 5 %. The void ratio measured in situ (0.65~0.7) is comparable to the range measured in Brumadinho, with a tendency to be, on average, somewhat lower than the average values observed in the failed Brazilian tailings dam.

Table 3: Physical and index properties of Torre de Moncorvo tailings at a specific site

Physical and identification properties	Measured values
Density of solid particles- G [-]	4.4~5.1
Water content- w [%]	≈ 0
Void ratio- e [-]	0.65~0.70
Sand fraction [%]	50~54
Silt fraction [%]	44~48
Clay fraction [%]	0~2
Liquid limit- w_L [%]	19~21
Plastic limit- w_P [%]	14~16

Sample reconstitution of iron ore tailings

Considering the particular features of iron ore tailings described above, it is important that the reconstitution process limits the risk of particle segregation during preparation, which can be encouraged by the difference in the sizes and density of iron ore tailings particles. But, at the same time, it is crucial that the usual requirements of sample reconstitution are guaranteed.

Importance and requirements of sample reconstitution

Reconstituted samples are usually required to prepare suitable samples for extensive laboratory testing. These samples should qualitatively represent the field behaviour of the geomaterial, while being uniform and being based on replicable procedures. This usually involves using the same particles of the natural geomaterial and, when possible, using reconstitution procedures matching natural depositional conditions.

The most common approaches to prepare reconstituted samples of tailings are the moist-tamping and the slurry-based methods, the first deriving from a method commonly used in non-uniform granular geomaterials and the second used more often to reconstitute samples of more or less plastic geomaterials. Considering that the formation of tailings dams involves deposition of liquid slurries, this paper discusses the impact of the particular procedures used in the slurry-based reconstitution method on the characteristics of the resulting samples, namely the water content of the slurry. In fact, the impact of the reconstitution procedures on the samples physical and mechanical properties has been considered for sandy-silty soils (e.g., Carraro & Prezzi, 2008) and for tailings with no iron (e.g., Chang et al, 2011, or Bhanbhro, 2017).

Slurry-based sample reconstitution of iron ore tailings

Taking into consideration that iron ore tailings are very prone to segregation during reconstitution, slurry-based preparation methods that take advantage of the fact that the materials exhibit some plasticity present a good alternative for samples reconstitution. In fact, these methods tend to better replicate the field depositional conditions while achieving the common reconstitution goals, in particular by reducing the segregation potential in the preparation of samples of iron ore tailings. The reconstitution procedure, illustrated in Figure 4, usually involves the selection of a representative mass of tailings (Fig. 4.a) and adding water to prepare a slurry with a liquidity index reasonably above unity, so that the mixture can be fully homogenised, while avoiding particle segregation (Fig. 4.b). The homogenization tends to be facilitated when using larger amounts of water, while the segregation potential increases with the amount of water, which requires a suitable balance of the water content of the slurry used in the sample reconstitution procedures. The slurry is then deposited in a mould selected in accordance with the testing requirements (Fig. 4.c). The method has been proven effective in the preparation of element tests for testing different loading conditions (Coelho et al, 2021) and in the preparation of physical models (Coelho, 2022).

Figure 4: Reconstitution procedures: a) selection of tailings particles; b) slurry mixing at high water content; c) deposition of the slurry in the container.

Slurry-based sample reconstitution of Torre de Moncorvo iron ore tailings

This section discusses the slurry-based sample reconstitution method when applied to the Torre de Moncorvo iron ore tailings, namely when the water content is varied within a range of about 23 to 28 %, which exceeds the liquid limit of the material ($w_L \approx$ 20 %). The range was established in order to satisfy the requirements relative to the minimum water content that would ensure the ability to homogenize the slurry ($w \approx$ 23 %) and the maximum water content above which particle segregation was evident ($w =$ 28 %). However, it should be noted that some level of segregation seemed to occur for water contents above 26 %.

Effect of water content on the void ratio

The different void ratios of the resulting reconstituted samples were measured for different water contents used in the slurries in the reconstitution process. The void ratio was calculated using 2 different approaches and considering, in both cases, the average G value measured for the tailings selected ($G \approx$ 4.69): (i) using the final dry unit weight (γ_d) of the reconstituted samples, after drying the samples in the oven for 24 hours at 110 ºc and ignoring possible sample shrinking during drying; (ii) assuming that the tailings particles would settle with no water loss from the voids in the mould, with a saturation degree of 80 to 100 %.

Figure 5 presents the values of void ratio estimated for the reconstituted samples prepared with slurries having different values of water content and using different calculation approaches. The first conclusion is that increasing the water content of the slurry tends to increase the void ratio of the reconstituted sample. However, the results also suggest that increasing the water content may decrease the saturation of the slurry and/or that the calculations based on the final dry unit weight may be affected by an error, namely for higher water contents of the slurry. Visual inspection of the samples prepared with water content values above about 26 % showed increasing particle segregation, finer particles migrating to the top on a foamy paste and causing artificially low values of the final dry unit weight and, as a result, surprisingly high values of void ratio. In fact, even if the slurries were not saturated, the tendency of the void ratio to increase with the slurry water content is surprising when compared to the values calculated based on reasonable assumptions to calculate the void ratio from the water content of the slurry. The values presented are relative to near-zero effective consolidation stresses, which suggests that further reduction of the void ratio would be expected after sample consolidation that would precede subsequent shear testing.

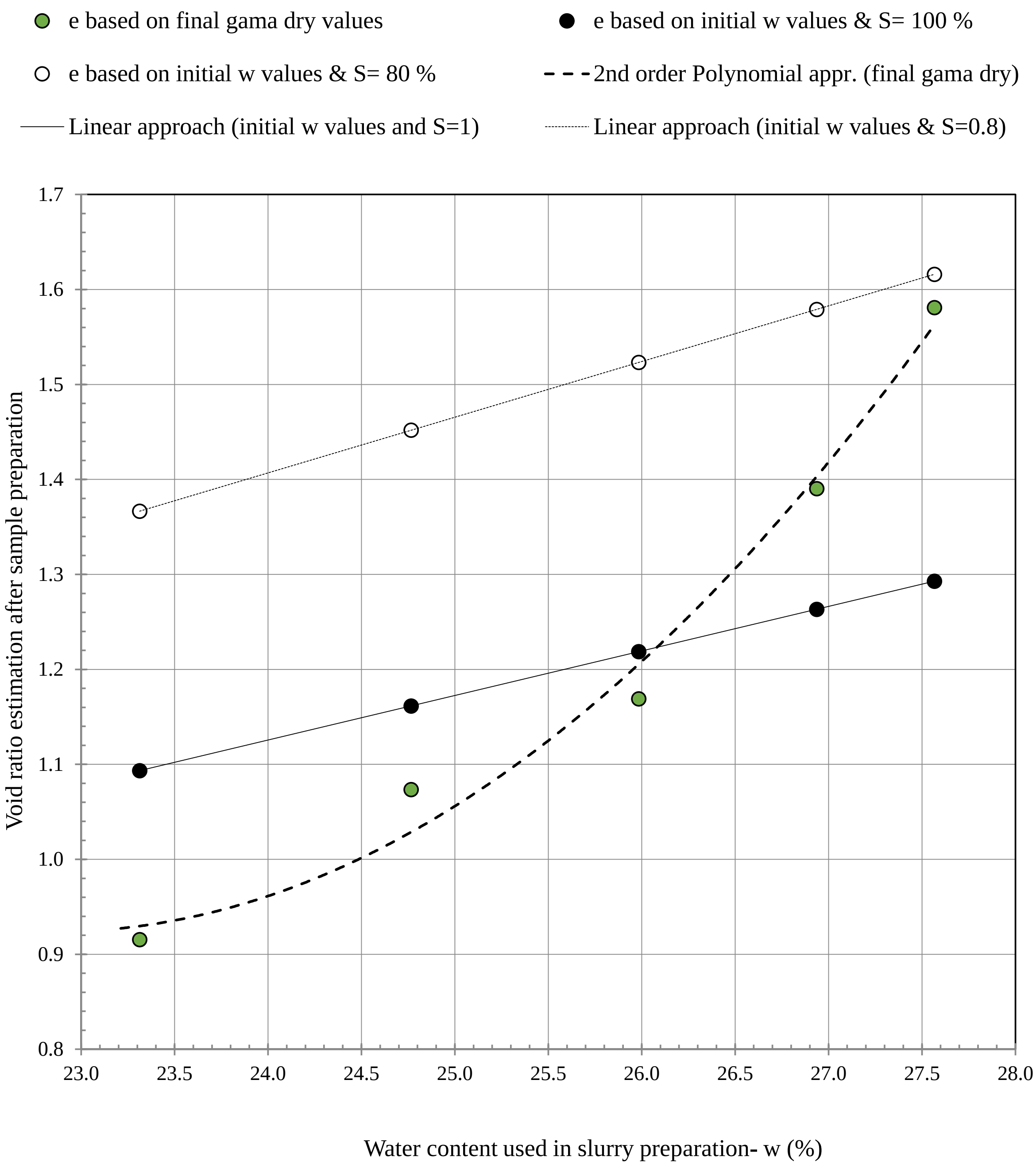

Figure 5: Values of void ratio estimated for the reconstituted samples prepared with slurries with different water contents and using different calculation approaches.

Effect of water content on the mechanical behaviour under triaxial compression

In order to assess the implications of the different characteristics of the reconstituted samples, namely the void ratio, 3 undrained triaxial compression tests were carried out on one undisturbed sample and on two samples reconstituted based on the slurry method. One of the reconstituted samples was prepared with a water content of 23 % and the other was prepared with a water content of 27 %, which are close to the limits of the range discussed in the previous section. The triaxial tests results are shown in Figure 6.

The stress-paths and the variations of the excess-pore-pressure with the deviatoric stress exhibited by the two reconstituted samples are different (Figs 6a-b), the sample prepared with a more liquid slurry having a response that reflects the larger void ratio of the sample, as previously discussed (Fig. 5). On the other hand, the behaviour of the sample prepared with a more consistent slurry replicates better the behaviour observed in the undisturbed sample using the same perspectives of analysis (Figs 6a-b). This probably reflects the fact that the void ratio of this reconstituted sample after consolidation ($e \approx 0.7$) was closer to the value of the void ratio measured in situ (Table 3). In contrast, the other reconstituted sample had a void ratio after isotropic consolidation to 200 kPa close to 0.85. These values were estimated based on the fact that the sample was saturated at the end of the tests, as the measured values of B close to 1 confirm. With respect to the stress-strain response of the reconstituted samples, whether assessed in terms of the variation of q or σ'_1/σ'_3 with ε_a, no significant differences were observed between the two samples. However, both reconstituted samples are less rigid than the undisturbed sample when tested in undrained compression, maybe due to possible time-related effects (cementation, yielding, etc) that may occur in the field but cannot be replicated by reconstituted samples.

Conclusions

The accumulation of tailings around the world requires geotechnical-based solutions based on reconstituted samples combining homogeneity and realistic behaviour under different loading conditions. This can be a significant challenge in the case of iron ore tailings, as the different particle sizes and densities seriously promote particle segregation during reconstitution. This paper discusses the characteristics of samples reconstituted through the slurry-based method, namely by assessing the effects of the water content of the slurry during the reconstitution procedures, using tailings from Torre de Moncorvo iron mine. The results suggest that adding more water to the slurry than strictly required for producing uniform samples increases particle segregation and air incorporation in the mixture during reconstitution, which affects the accuracy of the calculations of the void ratio. Because of the importance of this property, more research effort should exist on assessing void ratio values in situ in order to guide reconstitution procedures.

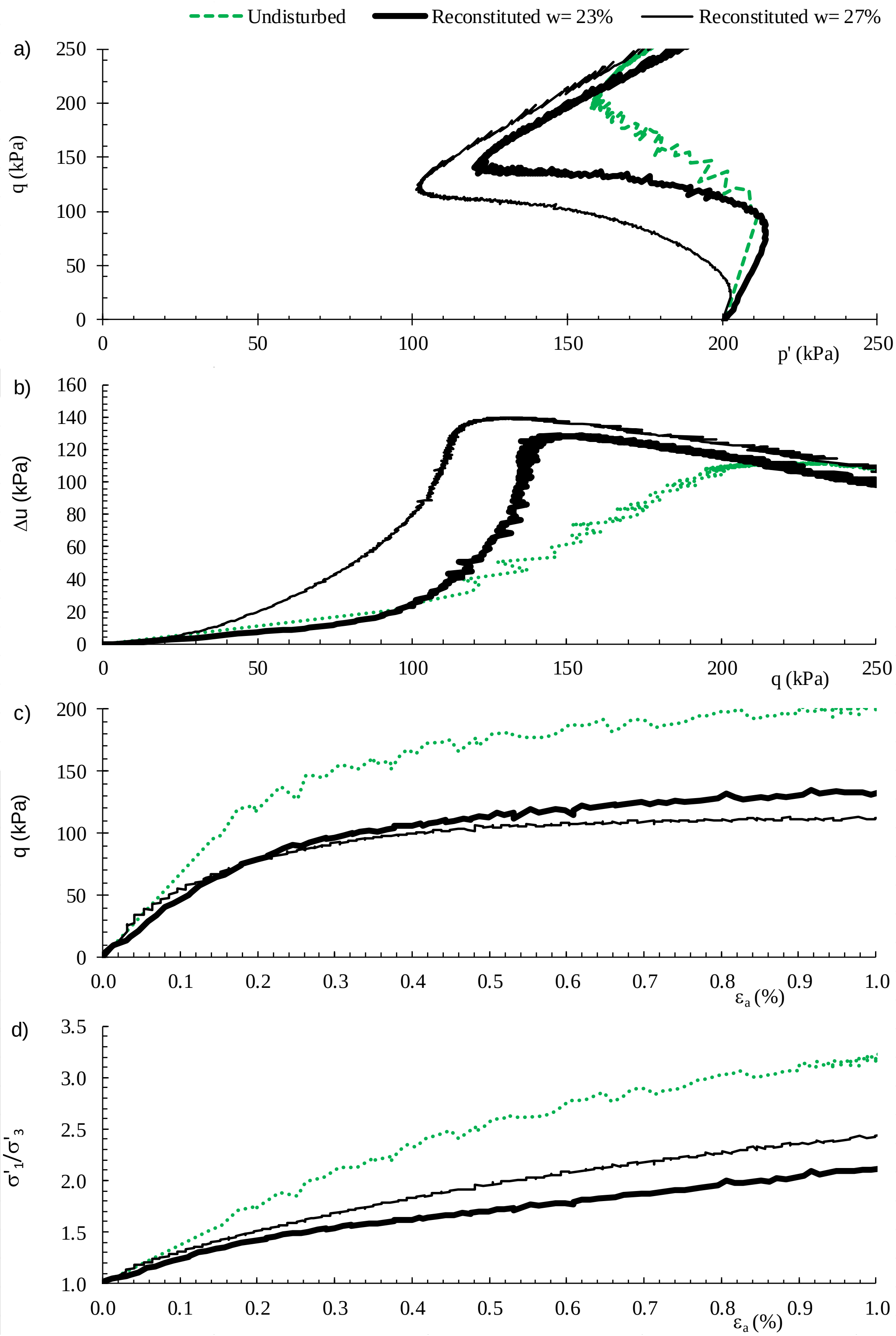

Figure 6: Response in undrained triaxial compression of undisturbed and reconstituted samples prepared with slurries at different water contents (23 and 27 %): a) stress-paths; b) variation of Δu with q; c) stress-strain response; d) variation of the principal stress ratio with ε_a

Overall, in the tailings tested, the void ratio and the mechanical behaviour of the sample reconstituted with a more consistent slurry better replicates the undisturbed sample behaviour.

Acknowledgements

This research is funded by FCT- Foundation for Science and Technology, through the research grant PTDC/ECI-EGC/4147/2021. The author also acknowledges the contribution to this research by the company responsible for Torre de Moncorvo's Iron Mine, Aethel Mining, Ltd.

References

Abrão, P.C. 1987. On the deposition of mine tailings in Brazil. Symposium on tailings dams and deposition of industrial and mining wastes- REGEO'87, Rio de Janeiro, RJ, 1987, I: 1-10 (*in Portuguese*)

Bhanbhro, R. (2017) Mechanical Behavior of Tailings- Laboratory Tests from a Swedish Tailings Dam, PhD Thesis, Luleå University of Technology, Sweden, 2008

Carraro, JAH, & Prezzi, M (2008) A new slurry-based method of preparation of specimens of sand containing fines. ASTM geotechnical testing journal 31 (1), 1-11

Chang, N., Heymann, G. & Clayton, C. (2011) The effect of fabric on the behaviour of gold tailings, Géotechnique 61, No. 3, 187–197

Coelho, P.A.L.F. 2022. An alternative model preparation method for assessing the behaviour of iron ore tailings through physical modelling. Keynote lecture at the 10th International Conference on Physical Modelling in Geotechnics 2022- ICPMG2022, Daejeon- South Korea

Coelho, P.A.L.F., Camacho, D., Gobbi, F. & Santos L. 2021. Sample reconstitution for evaluating the cyclic liquefaction resistance of iron ore tailings. 20th International Conference on Soil Mechanics and Geotechnical Engineering, Sydney, Australia

Galvão Sobrinho, A. 2014. Methodology for the implementation of a depositional system for iron ore tailings in the semiarid region: a case study. MSc Thesis. UFRG do Norte, Natal, 2014 (*in Portuguese*)

Robertson, P. K., Melo, L., Williams, D. & Wilson, G. W. 2019. Report of the Expert Panel on the Technical Causes of the Failure of Feijão Dam I. (http://www.b1technicalinvestigation.com/pt, assessed in August 2023)

Silva, W. P. 2010. Study of the static liquefaction potential of an upstream tailings dam applying the 2001 Olson's methodology. MSc Thesis, UFOP, Ouro Preto, MG, Brazil. (*in Portuguese*)

WMTF. 2023. Estimate of World Tailings Portfolio, Data from the Organization World Mine Tailings Failures (https://worldminetailingsfailures.org/ accessed in August 2023)

Session 2:

Monitoring, Testing and Technology

Automatic activation systems for sirens in dams

Hyllttonn W. D . Bazan, Vale S.A., Brazil
Samuel Silva Mendes, Vale S.A, Brazil
Filipe Colen de Freitas Guimarães, Vale S.A, Brazil
Mauricio Baleeiro, Vale S.A, Brazil

Abstract

This article addresses the current context of automatic siren triggering projects in mining dams, driven by the tragic Brumadinho accident in 2019. Brazilian legislation currently requires companies to implement automatic siren triggering systems in their mining dams, aiming to increase safety and prevent possible accidents.

In this sense, the article presents case studies in dams with the application of two distinct technologies: tiltmeters and Doppler radars. Both technologies aim to detect the movement of the dam's mass, allowing for automatic siren triggering in case of imminent risk of rupture. The results obtained in these studies indicate that these technologies are efficient in detecting possible dam ruptures and triggering sirens automatically, significantly reducing response time in case of emergency.

In addition, the article discusses other technologies being evaluated, such as triggering sirens through the rupture of fiber optics installed in the dam's mass or downstream in case of a rupture. This technology is still experimental and has the potential to improve the efficiency and safety of automatic siren triggering in dams.

In summary, the article highlights the importance of automatic siren triggering systems in mining dams to ensure safety and prevent accidents, as well as addressing the reliability and main characteristics and logic associated with the technologies. The technologies presented in the study are promising and can help reduce risks associated with dam operation.

Introduction

In recent years, safety in mining operations has become a priority due to significant events that have highlighted the urgency of preventing disasters. The Brumadinho disaster in 2019 highlighted the dangers associated with mining dams, leading Brazilian legislation to require stringent measures, including automatic siren activation systems to quickly alert communities and teams in the event of a collapse threat.

This article focuses on automatic siren activation projects in dams, emphasizing the importance of sensing for safety. The main objective is to analyze case studies that investigate the effectiveness of two technologies: tiltmeters and Doppler radars. These technologies have the ability to detect changes in the movement patterns of dams, allowing for early activation of sirens and significantly reducing response time in emergency situations. Additionally, the article explores future perspectives, such as the experimental use of optical fibers for rupture detection, with the aim of further improving the safety of mining dams.

Literature Review

Brazilian Legislation

Resolution ANM No. 95/2022 plays an essential role in the regulation of mining dams in Brazil, notably through Article 8. This article imposes stringent requirements for dams with high or medium DPA, requiring the implementation of automated siren and alert systems in the Zone of Self-Salvation (ZAS), as well as manual and remote activation mechanisms, all with safeguards in case of failures. Paragraph 2 highlights the customization of these systems according to the characteristics of each dam, incorporating deformation and displacement criteria defined by the designer, thus solidifying the legislative approach to safety and risk mitigation in mining dams.

Siren Alerts

The use of sirens is crucial to alert and save lives in a variety of emergency situations. Here are some important examples in which the use of sirens played a key role in safeguarding people:

- Tsunami alerts: In coastal areas vulnerable to tsunamis, tsunami warning sirens are used to warn communities about the imminence of a tsunami, allowing people to move away from risk areas and seek higher ground.
- Natural disaster alerts: Sirens are often used to warn of natural disasters such as hurricanes, tornadoes, earthquakes, and floods. They give people advance warning so they can take safety measures, such as evacuating risk areas or taking shelter in safe locations.
- Industrial emergencies: In the event of chemical leaks, explosions, or other industrial accidents, sirens are used to warn neighboring communities about the need to take protective measures, such as closing doors and windows, or even evacuating the area.

- Urban fires: Fire sirens are used to alert people about fires in urban areas. They help to direct firefighting efforts and also to ensure that residents are evacuated safely.
- Mass evacuations: In situations of mass evacuations due to threats such as landslides, dam collapses, or other emergencies, sirens are used to inform people about the need to leave their homes quickly.

Following the 2011 Japan earthquake and tsunami, the role of tsunami warning sirens in safeguarding lives became evident, as their activation in coastal cities provided essential alerts, enabling residents to seek higher ground. Japan Meteorological Agency (2013) noted room for improvement in the Japanese warning system's alert agility, reliability, and community training.

False Alerts

Inappropriate activation, known as a false positive, in emergency alert systems can result in significant adverse consequences for individuals, the trust in alert systems, and the effectiveness of response authorities. The repercussions of false positives are varied:

- Loss of Trust in Alert Systems: False positives raise questions about the effectiveness and reliability of alert systems, undermining trust in future information. This undermines readiness and response to emergency situations.
- Emotional and Psychological Strain: Erroneous activations generate fear, anxiety, and stress, whose intense emotions can have long-lasting consequences for mental health, even after the situation is clarified.
- Unpreparedness for Future Emergencies: The frequency of improper alarms can lead to complacency and reduced response to real alerts, compromising effective response to imminent risks.
- Congestion on Evacuation Routes: Excessive responses to false positives can lead to congestion on evacuation routes, impairing mobility and increasing accident risks.
- Loss of Productivity: Routine disruptions resulting from false positives cause abrupt exits from daily activities, resulting in loss of productivity and impacting operations.
- Impact on Authorities and Response Agencies: The recurrence of false positives affects the credibility of the authorities responsible for the alerts, impairing communication with response agencies and the public, making coordination in emergencies difficult.

Regarding the loss of trust in alert systems caused by false alarms, a study conducted by Lim et al. (2019) suggests that apprehensions regarding false alarms leading to public complacency might be overstated, especially in the context of tornado alerts in the southeastern United States. The study did not uncover clear evidence that false alarms lead to public complacency. On the contrary, it was found that the more people perceive the rate of false alarms and the accuracy of tornado alerts, the more likely they are to report taking protective measures. Furthermore, it was discovered that people's perception of the false alarm rate is lower than the actual false alarm rate in their counties. These contradictory findings are intriguing and warrant further research.

However, to mitigate adverse effects, it is essential to invest in robust systems, implement pre-activation verification protocols, and educate the public about the interpretation and response to alerts. Transparency is crucial for communicating false positives and minimizing emotional impacts.

Radar Doppler

Doppler radar technology has played a significant role in identifying avalanches and landslides in various real-world scenarios, contributing to the prevention of tragedies and the preservation of lives.

A notable example of the use of Doppler radar technology is the avalanche monitoring system implemented in the mountainous regions of Switzerland. In this context, Doppler radars are employed to detect minor movements in the snow, which could indicate the imminent threat of an avalanche. This detection capability allows for the prompt alerting of local authorities and rescue teams, facilitating the proactive evacuation of high-risk areas and the implementation of safety measures. Meier et al.'s (2019) article discusses a real-time avalanche detection system that utilizes long-range, wide-angle Doppler radars for road safety in Zermatt, Switzerland. The system employs two Doppler radars to monitor two nearby avalanche-prone ravines along the sole access road to Zermatt. When an avalanche is detected, the system immediately triggers warning signals and deploys barriers to block access to the endangered road sections. Local authorities are promptly alerted and can monitor the avalanche's location and distance traveled on a password-protected website. The system successfully detected 27 avalanches between December 2015 and April 2016, without any false alarms.

Tiltmeters

Tiltmeters have demonstrated their effectiveness in disaster prevention and the protection of human lives in various contexts. Notable cases underscore their role in providing timely alerts to avert catastrophic events.

According to Garcia (2010), tiltmeters are monitoring instruments that deliver high-resolution and precise ground inclination data. They are particularly valuable for landslide monitoring, as they enable the detection of subtle and continuous movements over time.

Perez et al. (2022) discusses the application of long-range, battery-operated wireless tiltmeters for the rapid detection of slope failures. These tiltmeters are part of a wireless monitoring system that utilizes LoRa technology for long-distance communication. The tiltmeter-based event detection solution offers swift detection, minimal installation requirements, easy deployment, and operation in adverse weather conditions. Furthermore, it is compatible with ground sensors connected via wireless data loggers, allowing for real-time monitoring and immediate event detection. The solution has been installed at various tailings dams in

Brazil for early detection of deformations that could affect dam stability. Different installation methods were employed, considering the specific conditions of each site and the expected rupture mechanisms.

These studies reveal the real-time monitoring capabilities of tiltmeters in slopes and tailings dams, triggering alerts when critical tilt thresholds are exceeded and facilitating evacuations in the event of landslides and ruptures. Collectively, these findings underscore the pivotal role of tiltmeters in enhancing safety through risk detection and timely intervention.

Fiber Optics

Fiber optic technology has demonstrated its efficacy as a sensor for the early identification of natural disasters, such as avalanches and landslides. It plays a significant role in issuing timely alerts and enabling preventive actions, thereby safeguarding lives and mitigating material damage. This approach has been successfully implemented in the Swiss Alps.

Edme et al (2023) discusses the application of fiber optics for snow avalanche detection. The study shows that it is possible to detect snow avalanches using the Distributed Acoustic Sensing (DAS) system with existing fiber optic cables. During the winter of 2021/2022, researchers employed a roughly 10 km long fiber optic cable along an avalanche-prone road in the Swiss Alps. The DAS data clearly recorded multiple snow avalanches, including those that did not reach the cable. The study's results open new perspectives for real-time, long-distance snow avalanche monitoring using pre-installed fiber optic infrastructure. This can prove to be a more cost-effective solution for monitoring and alerting regarding avalanches, particularly in critical areas like roads, railways, dams, and tunnels. Additionally, DAS provides information about traffic, which can be valuable for estimating potential damage caused by mass movements and assisting rescue teams.

The successes in the Swiss Alps exemplify the technology's significance in disaster prevention, providing advanced warnings and facilitating precautionary measures. These achievements also underscore the growing relevance of this technique in the pursuit of enhanced safety against potentially catastrophic natural events.

Materials and Methods

The detection of dam failure is a critical issue for ensuring the safety of nearby communities and preventing tragedies. There are several possible methods for detecting a dam failure, many of which can be used in combination to improve accuracy and effectiveness. These methods fall into two groups:

- Pressure and Water Level Measurement: Sensors installed in the dam can monitor changes in water levels and pressure. A rapid and abnormal drop in water levels may indicate a possible failure.

- Motion and Vibration Sensors: Detect abnormal movements or vibrations in the dam that may indicate impending collapses.

In this study, our focus is on the analysis of motion sensors, specifically tiltmeters, Doppler radars, and fiber optic technology.

Tiltmeters

The use of tiltmeters plays an important role in the prevention and identification of displacements and dam failure. These sensitive devices that measure the movement and tilt of the terrain provide accurate data on variations in the tilt angle of slopes and embankments. By constantly monitoring these changes, tiltmeters can detect the first signs of instability, such as subtle ground displacements. This early detection allows mitigation measures to be taken in time, such as the evacuation of vulnerable areas, the implementation of structural reinforcements, or the activation of early warning systems for the population. Ultimately, the use of tiltmeters as part of geotechnical monitoring systems contributes to the safety of communities in regions prone to dam failures, minimizing the risks and potential impacts of these events.

A tiltmeter that uses accelerometers to operate works by detecting gravitational acceleration along different axes. Accelerometers are sensitive to acceleration, allowing the measurement of the tilt or tilt angle of an object relative to the Earth's gravity. By monitoring changes in gravitational forces along the X, Y, and Z axes, accelerometers provide information about how an object is oriented relative to the horizontal plane. Based on these acceleration data, the tiltmeter calculates the tilt angles relative to the desired axes and converts them into information that is understandable for users.

Doppler Radar

The use of Doppler radar plays a key role in the detection and identification of displacements and dam failure. Using radar principles and Doppler technology, these systems are capable of monitoring the movement and speed of moving particles, allowing the early identification of potential landslides or failures. By emitting microwave pulses towards the surfaces of interest and analyzing the return of these pulses, Doppler radars can accurately determine whether there is significant mass movement, alerting authorities and local communities so that preventive measures can be taken in time, minimizing the risks associated with these destructive events.

A Doppler radar used for displacement monitoring operates based on the principle of the Doppler effect, which involves the change in the frequency of electromagnetic waves reflected by an object in motion relative to the observer. When the radar emits microwave pulses towards the target object, these pulses reflect off of it and return to the radar. If the object is approaching, the frequency of the reflected waves increases, while if the object is moving away, the frequency decreases. By measuring this frequency difference, the Doppler radar determines the radial velocity of the object relative to the radar. With continuous information on radial velocities over time, it is possible to calculate the displacements of the object and monitor its movement with accuracy, making it valuable for applications such as structure movement detection.

Fiber Optics

The use of fiber optics has proven to be a critical innovation in the detection and identification of displacements and dam failure. By being carefully installed along slopes or geotechnical structures, fiber optics act as sensitive sensors, capable of monitoring the most subtle variations in the environment. Changes in soil tension, meticulous movements, and even small vibrations are detected by the fiber, allowing for continuous analysis of the stability of the area. This technology offers an early warning system, providing valuable information that can be used to activate preventive measures and ensure the safety of the affected regions, minimizing risks and impacts associated with these destructive events.

A fiber optic system for the monitoring of displacements or dam failure works by strategically placing fiber optic cables along the slope. The fiber optic acts as a distributed sensor, taking advantage of the principle of total internal reflection. As the slope moves or undergoes changes, the tension exerted on the fiber optic also changes, affecting the propagation of light through it. These changes are detected and analyzed to identify displacements or potential failures in the slope. As fiber optics can cover long distances, the system offers a wide area of continuous and real-time monitoring, making it effective in the early detection of ground movements.

Processing Time

The processing time of information collected by sensing technologies plays a critical role in ensuring the safety and effectiveness of siren activation in emergencies, such as potential dam failures. A prompt and efficient response is essential to protect lives and property in the affected areas. Here is the importance of the processing time of information for the rapid activation of sirens:

- Minimizing Response Time: The rapid processing time of information collected by instruments allows for early detection of abnormal changes or imminent threats to the dam. The faster the data is processed and interpreted, the shorter the time between the detection of a problem and the activation of emergency measures.
- Opportunity for Evacuation: The anticipation and early detection of a possible dam failure are crucial to give enough time for the authorities to coordinate orderly evacuations of the risk areas. A rapid processing of information allows the sirens to be activated promptly, alerting people to evacuate the region before the situation worsens.

- Mitigation of Damage: In an emergency, such as the potential collapse of a dam, every minute counts. Sirens activated quickly give people the opportunity to move away from danger areas, significantly reducing the risk of loss of life and property damage.
- Credibility of Warning Systems: An efficient and prompt response warning system gains credibility among the population. Confidence in sirens and emergency communication systems increases when people see that these systems are activated and work in a timely manner.
- Coordination of Emergency Resources: In addition to alerting the population, the information processed quickly allows emergency response teams to prepare for action. This includes mobilizing resources, such as rescue teams, hospitals, shelters, and other essential services, to deal with the consequences of the emergency.

The processing time of information collected by sensors is a key piece in the puzzle of dam safety and related emergencies. Sensors through tiltmeters, Doppler radar, and fiber optic meet this processing requirement.

Ensuring that information is analyzed and transmitted quickly and accurately is essential to protect lives and property, as well as to maintain confidence in the safety measures adopted.

Modes of Failure, Technology Selection, and Design

The consideration of failure modes plays a key role in the selection of technologies and the development of designs for automatic siren activation systems for dams. By identifying and understanding the possible failure scenarios in geotechnical structures such as these, it is possible to design appropriate countermeasures to mitigate the associated risks. This not only ensures the reliability and effectiveness of sirens in critical situations, but also contributes to public safety and the protection of lives. By incorporating failure mode analysis from the early stages of development, design teams can create more resilient systems, capable of facing a variety of adverse situations and providing quick and accurate responses when needed.

Failures in earthen dams can be grouped into three general categories: overtopping failures, seepage failures, and structural failures. Each of these categories represents a mechanism by which an earthen dam can collapse.

Overtopping Failures

When the amount of water flowing into a dam exceeds the capacity of the spillway, the dam may experience an overtopping failure. This can happen during intense precipitation events, when the volume of water reaching the dam is greater than its storage or drainage capacity. The excess water may flow over the top of the dam, eroding the soil and undermining its integrity. Over time, this can lead to dam collapse.

Seepage Failures

Seepage failures occur when water penetrates the body of the dam and weakens the soil, resulting in a possible collapse. Earthen dams are typically built with impervious layers, such as compacted clay, to prevent water infiltration. If these layers are compromised due to erosion or other factors, water can pass through the dam, creating internal flow channels. This undermines the stability of the dam, eventually leading to collapse.

Structural Failures

Structural failures occur due to design problems, improper construction, low-quality materials, or other defects in the structural integrity of the dam. This may include the collapse of segments of the dam, ruptures in support structures, or deformations that affect the overall stability. Structural failures can be caused by a combination of factors, including overload, poor soil quality, or failures in drainage systems.

Liquefaction

Liquefaction is another failure mode that can affect dams, especially those built in areas with saturated and sandy soils. Liquefaction is a phenomenon in which a saturated soil temporarily loses its strength due to the application of stresses caused by earthquakes or other dynamic loads. This can cause the soil to behave temporarily as a liquid, leading to settlements, landslides, and even structural collapses.

Breach Openings

In the context of dams subjected to overtopping, seepage, and structural failure modes, a breach opening forms during the dam collapse process. These breaches constitute relevant data for the development of siren activation systems, especially with regard to the application of tiltmeters.

There are several formulations and approaches that can be used to estimate breach openings. Some of them include Empirical Equations. Some empirical equations can be used to estimate the dimensions of the breach based on the height and volume of the reservoir. These equations are typically developed from statistical analyses of previous cases and can vary depending on the characteristics of the dam.

Froelich (2008) presents a methodology for estimating the parameters of the rupture of earthen dams, including the width, height, and time of formation of the breach. The methodology is based on an empirical model that was developed from data from 74 cases of dam ruptures.

The theory of probable breaches, such as that of Froelich (2008), assumes an increased importance, together with the critical consideration of the precise positioning of tiltmeters, when we confront the prospect of a breach occurring in the interval between the tilt devices themselves. In this scenario, it is of paramount importance to recognize how an inadequate placement of these sensors can lead to unidentified risks.

Results

In this section, we will discuss the results obtained through the installation of a total of 69 tiltmeter systems and 12 Doppler radars in iron ore dams, as well as important insights from fiber optic projects.

Comparison among Tiltmeters, Doppler Radars, and Fiber Optics for Dam Failure Detection

The high data acquisition rate represents a substantial advantage for tiltmeters, Doppler radars, and fiber optics in the context of dam failure detection. These systems demonstrate the ability to collect data at extremely short time intervals, on the order of seconds or milliseconds, enabling a swift response to critical events.

Tiltmeters, in particular, offer notable advantages, such as easy installation, which involves positioning these devices along the dam. Furthermore, wireless communication constitutes another significant advantage, eliminating the need for excavations or cable routing through the dam structures. However, it is important to highlight that in dams with long crests, a considerable number of tiltmeters are required for effective breach detection. Additionally, regular maintenance, including the periodic replacement of batteries and calibrations, is a disadvantage associated with these devices.

As for Doppler radar, its primary advantage lies in rapid deployment, requiring only the configuration of appropriate parameters and filters, such as areas and velocities, for the detection of mass displacement-related events. Moreover, there is no need for excavations or sensor placement on the dam, as the radar is installed to provide comprehensive coverage of the structure. However, it is worth noting that the costs associated with the acquisition and installation of Doppler radars are substantially higher compared to alternatives like fiber optics and tiltmeters. Additionally, there is limited documented use of Doppler radar specifically for dam failure detection, even though it was originally developed for identifying avalanches on natural slopes, which share similarities with dam breaches. Furthermore, Doppler radar's sensitivity to vehicle movements, such as trucks, helicopters, and drones, can result in the generation of false alarms if not properly configured and adjusted.

Regarding fiber optics, its primary advantage lies in minimal maintenance required after installation along the dam, as the sensor element does not require regular replacements. However, the main drawback of this technology is the need for excavations to pass the fiber optic through specific areas of the dams. Fiber optics, nevertheless, stand out as an ideal choice for large dams, where the application of tiltmeters and Doppler radars may be impractical.

It is crucial to emphasize that regardless of the chosen technology, the implementation of siren activation logic is necessary to ensure the effectiveness of the alert system. For tiltmeters, the logic must take into account the number of sensors activated during breach detection, for instance. In the case of fiber optics, it is imperative to configure the logic to monitor and count the number of broken fibers during a breach occurrence. Finally, for Doppler radars, the activation logic must consider mass movement in specific dam areas, ensuring precise siren activation.

Challenges and Solutions in Detecting Multiple Failure Mechanisms in Dams

All dams equipped with automatic siren activation systems rely on geotechnical monitoring instruments, such as piezometers and deformation monitoring by total stations. However, tiltmeters, Doppler radars, and fiber optics have been and continue to be implemented to provide a rapid response for siren activation in the event of dam failure. All three mentioned technologies demonstrate the capability to identify breaches and liquefaction-induced ruptures as they occur. In the case of failure modes such as overtopping, piping, and structural failures, these technologies are also capable of detecting these failure modes when they lead to the opening of a breach in the dam.

It is of paramount importance to emphasize that these technologies are not intended to replace traditional geotechnical monitoring, such as that carried out through open-tube piezometers and deformation monitoring by total stations. Instead, they play a complementary role since traditional geotechnical monitoring often fails to provide an effective and timely response. This is due, for example, to the fact that open-tube piezometers often exhibit slow response times, while robotic total station systems may require processing times on the order of minutes.

Experience with Doppler Radar

An experience based on an actual event occurred at a dam during the overflight of a helicopter. The Doppler radar detected the helicopter; however, during this event, the duration and characteristics of the flight exceeded the pre-established parameters concerning the capture of events related to the helicopter's area and speed. This resulted in an inappropriate activation of the siren. This incident is of significant relevance as it clearly illustrates the importance and seriousness associated with the design and implementation of automatic siren activation systems.

Conclusion

In summary, this article addressed the importance of safety in mining operations, highlighting the need for rigorous measures following the Brumadinho disaster in 2019. The main focus was on automatic siren activation projects in dams, emphasizing the relevance of detection for safety. Case studies were analyzed to investigate the effectiveness of two technologies, including tiltmeters and Doppler radars, in detecting changes in dam movement patterns. Furthermore, the article explored future perspectives, such as the experimental use of optical fibers for rupture detection, with the aim of further enhancing the safety of mining dams. The literature review highlighted the significance of Brazilian legislation, the role of sirens in natural and industrial disaster alerts, as well as the challenges associated with false alarms. To mitigate these adverse effects, the need to invest in robust systems, pre-activation verification protocols, and public education was emphasized. Additionally, the article provided a detailed discussion of the three detection technologies - tiltmeters, Doppler radars, and fiber optics - highlighting their advantages and disadvantages in relation to dam failure detection. Finally, topics related to rapid information processing, the importance of considering different failure modes when selecting technologies, and the pivotal role of siren activation logic to ensure system effectiveness were addressed.

Acknowledgments

We thank all the collaborators who contributed to the realization of this article, including the authors of the case studies analyzed. We also thank all the members of the Technology Directorate and Geotechnical Directorates of Vale S.A. who made these studies and applications possible.

We hope that this article contributes to the advancement of safety in mining operations and, consequently, to the protection of communities and the environment.

References

Brazilian National Mining Agency. ANM Resolution No. 95, dated April 27, 2022.

Edme, P. & Paitz, P. & Walter, F. & van Herwijnen, A. & Fichtner, A. (2023). Fiber-optic detection of snow avalanches using telecommunication infrastructure. arXiv. 10.48550/arXiv.2302.12649.

Froehlich, E. M. (2008). Embankment dam breach parameters and their uncertainties. *Journal of Hydrology*, 354(1), 120-134.

Garcia, A. & Hördt, A. & Fabian, M. (2010). Landslide monitoring with high-resolution tilt measurements at the Dollendorfer Hardt landslide, Germany. Geomorphology, 120, 16-25. 10.1016/j.geomorph.2009.09.011.

Japan Meteorological Agency (2013), Lessons learned from the tsunami disaster caused by the 2011 Great East Japan Earthquake and improvements in JMA's tsunami warning system, October 2013.

Juan Perez Arcas; Victor Salinas; Francesc Figueras; Claudia Abanco (2022). Rapid detection of landslide events using battery-operated long-range wireless tiltmeters. Proceedings of 11th International Symposium on Field Monitoring in Geomechanics (ISFMG2022). Session 3a – Landslides.

Lim, J. R. & Liu, B. & Egnoto, M. (2019). Cry Wolf Effect? Evaluating the Impact of False Alarms on Public Responses to Tornado Alerts in the Southeastern United States. Weather, Climate, and Society. 10.1175/WCAS-D-18-0080.1.

Meier, L. & Jacquemart, M. & Blattmann, B. & Arnold, B. (2016). Real-Time Avalanche Detection with Long-Range, Wide-Angle Radars for Road Safety in Zermatt, Switzerland. Proceedings, International Snow Science Workshop, Breckenridge, Colorado, 2016

Improvement of Tailings and Mine Waste by means of KSI.

Dipl.-Ing. Gerd Maitschke, KEMROC Spezialmaschinen GmbH, Germany
Dr.-Ing. Thomas Meier, BAUGRUND DRESDEN Ingenieurgesellschaft mbH, Germany

Abstract

This paper describes a mixed-in-place soil improvement method called KSI and its potential regarding the application in the framework of the treatment of tailings and mine waste materials. After a general description of the method its projected application for a tailing pond of Europe's largest copper mine in Bulgaria is shown. The effectiveness of the method is shown in terms of a short feasibility study by means of 3-dimensional finite element analyses regarding reduction of settlements and increase of bearing capacity. An outlook is given on how a FE model, such as the KSI model presented in this paper in conjunction with advanced validated constitutive models can be used to investigate even most complex problems such as the mitigation of the liquefaction potential of tailings enclosed by an KSI grid under seismic excitation.

Introduction to the Soil Mixing Method

One of the main challenges in construction projects is often the subsoil. If the subsoil's bearing capacity and stiffness are too low, this can lead to damage to buildings, dams, dikes or waterproofing. This holds especially true in case of dam heightening measures on very soft tailings. In such cases, soil improvement is necessary. One way to improve the subsoil is to use soil mixing techniques.

Soil mixing is a process in which the existing soil is mixed with aggregates to improve its properties. The aggregates can be different materials such as sand, gravel, cement, or other binders as required. The mixture (slurry) is prepared in situ on site and mixed directly into the ground using a KSI. The KSI is an excavator-mounted device for vertical mixing of soil (cf. below).

The soil mixing process is usually performed with special machines that loosen the soil and mix in the aggregates. There are two main types of soil mixing processes: deep mixing and surface mixing.
Here we will deal exclusively with the deep mixing process using a KSI from KEMSOLID.

In this process, the soil is loosened to depths of up to 13m below the ground surface and mixed vertically with the aggregates. A mixing blade (KSI) with an injection lance is inserted into the soil while milling. This loosens the soil and mixes in the aggregates at the same time. This process is used to improve the soil for foundation construction mainly regarding strength and stiffness.

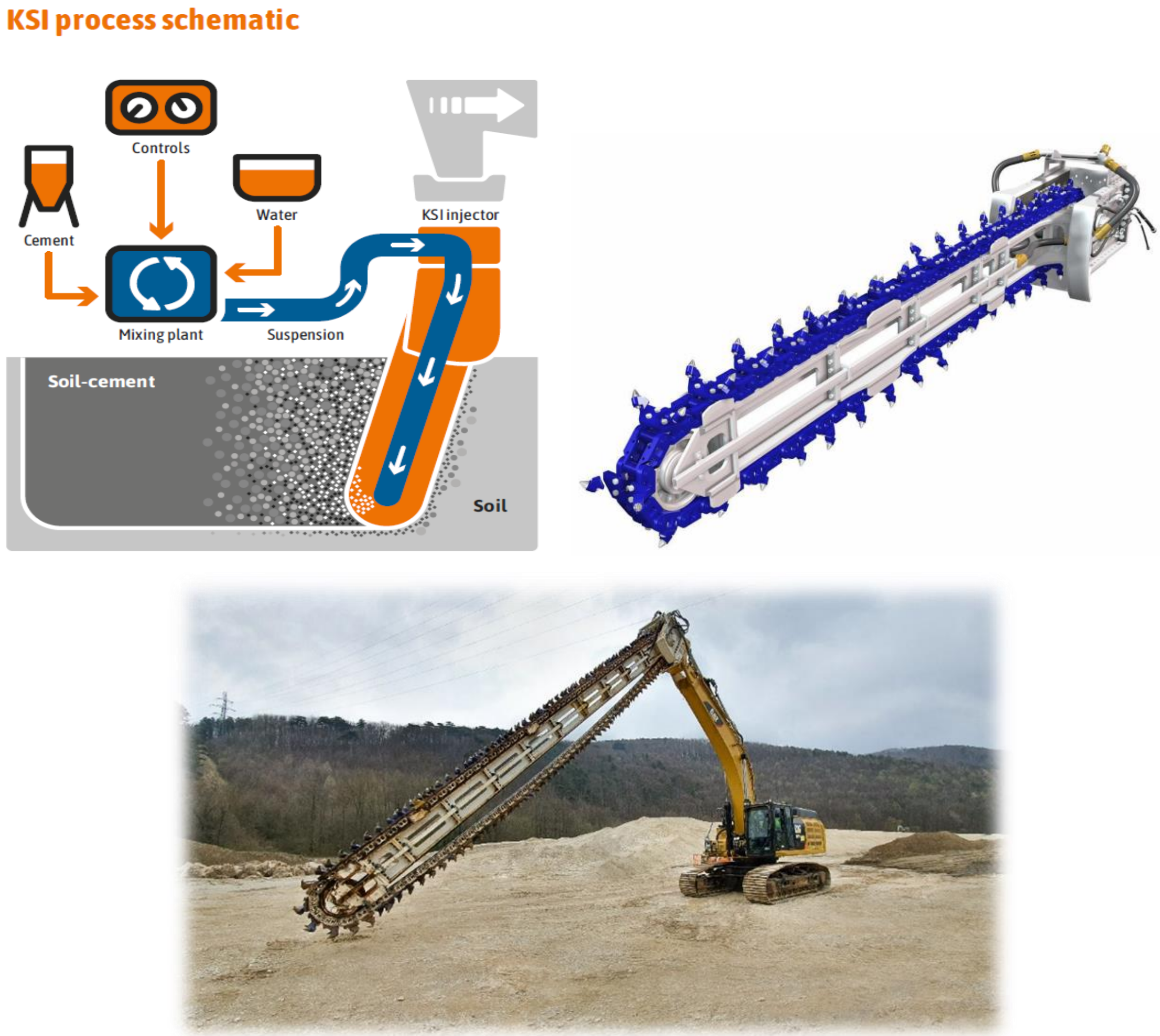

Figure 1: KSI process schematic and mixing Sword

The method can be used very effectively in the rehabilitation of dams and dikes through an earth concrete wall milled into the core or in sealing off flowing water for excavations, etc. It can also be used to contain contamination, minimize vibration, or create excavation shoring.

The milling-mix injection method is a proven method of subsoil improvement that is used in many construction projects. This method is particularly suitable for soils that have a low bearing capacity or that have become unstable due to changes in the groundwater level. We will explain in more detail the operation, advantages, and applications of the mill-mix injection process.

The mill-mix injection process is a multi-stage process consisting of three phases. First, the soil is loosened by milling. Then, a binder is injected into the soil, which is mixed with the soil. In the third phase, the soil-binder mixture sets, resulting in much higher strength and stiffness.

The binder injected into the soil profile can consist of different materials, depending on the requirements of the construction project and the properties of the soil. Commonly used binders are, for example, cement or ready-made diaphragm wall mix consisting of lime, cement, and bentonite. The addition of binders changes the soil properties and significantly improves the bearing capacity and impermeability of the soil.

The mill-mix injection method has many advantages over other methods of soil improvement. First, it is a cost-efficient method because it can be done quickly and efficiently and requires very little material. Second, it is very precise and allows for targeted treatment of specific areas of the soil, which is especially advantageous for complex construction projects.

Overall, the mill-mix injection process is a proven and efficient method of soil improvement that is suitable for a wide range of applications. It is a particularly effective method for stabilizing of soft soils with low bearing capacity and allows contractors to implement more efficient and safer construction projects.

Soil mixing offers several advantages over other soil improvement methods. Here are some of the most important advantages:

- Cost savings: The use of soil mixing methods often has a lower cost than other methods such as replacing the soil or using diaphragm walls, narrow walls, MIB walls or jet grouting.
- Time savings: The soil mixing process can often be performed quickly and reduces the time required for soil improvement.
- Flexibility: The soil mixing process can be adapted to different soil conditions to meet the needs of a particular construction project.
- Environmental friendliness: The soil mixing process reduces the need for landfill space by utilizing existing soil and eliminating the need for additional materials.
- Therewith, it is a sustainable soil improvement method.

Conclusion: The soil mixing process is an effective method for improving the subsoil. By the company KEMROC a flexible device was produced as an excavator attachment. The KSI is sold by KEMROC under the KEMSOLID range. The FMI method using KSI has now been used on a wide variety of construction sites and for different purposes.

Dams on the Danube have been rehabilitated by means of internal earth concrete walls using the method described here, and newly constructed dams have been stabilized to stop water passing through.

For the improvement of the subsoil under future buildings, earth concrete walls have been produced using KSI in the soil mixing process.

Another possible application is the isolation of groundwater or the containment of contaminants. Tests have already been successfully carried out in the USA in San Diego, Corpus Christi and for Mobile Alabama.

The rehabilitation of old flood control dams or retention basins is another field of application for the method using KSI, since the dam widths are often less than 3m, the KSI is very well suited as an excavator attachment to perform these services.

Due to the lower loads of the excavator compared to large special foundation engineering equipment, a fast operation is possible even on soft soils. Depths of 5-13m can be reached with widths of the earth concrete walls of 400 mm to 650 mm.

Technical details Costs

The KSI is an excavator attachment for the mill-mix injection process.

As an excavator attachment, the production of mixed earth concrete walls is possible from 5m over 7m with an excavator 40 to, depending on the excavator size and KSI size. The wall width of the KSI 7.000 can vary from 350mm to 470mm.

Or with a KSI 12.000 length of 10m - 13m with an excavator 55-70to.

Walls from 470mm - 650mm can be produced.

It is also possible with a KSI 16.000 to produce widths from 650 to 950mm, this requires at least a 120to excavator. Or a machine with a mast.

Depending on the width, length and customization, the price ranges from 180.000€ for the KSI 7.000 to 480.000€ for the KSI 16.000.

The production time after order is 2 - 3 months without transport time.

The time needed to adapt the KSI to the excavator is about 2-3 hours.

The following equipment is needed for the production:

1. binding agent silo, binding agent
2. mixing plant
3. pump for suspension
4. hoses 2-3 inch
5. water

The construction of the site equipment should not take more than one day.

Production depending on the ground

The KSI is designed for rock and concrete excavation.

The soil strength in which the KSI can be used ranges from very fluid to strengths of 20 - 25MPA.

It is basically dependent on the ground and the static technical requirements which wall width and which strength is to be produced.

The wall widths from 350mm to 950mm can reach strengths up to 10MPA depending on the soil.

It is possible to pass through rock layers with stone sizes up to 30cm diameter, but this is very wear intensive.

The homogeneity of the walls is very good because this process involves a vertical mixing of all soil layers, and no joints are created.

In sandy-gravelly soils, outputs of up to 1200m² per day can be achieved. In cohesive material and organic material can be produced up to 1000m ² per day.

In very coarse and stony material, outputs of up to 800m² are possible.

An important factor for the performance is the chain speed which should be approx. 2.5m/s and the feed rate of approx. 15cm/minute.

In addition, the amount of suspension is a decisive factor for the performance and wear.

The mixture of the suspension must be adjusted and tested for each type of soil to achieve the desired parameters.

Feasibility Study

Motivation & Objective

A field of application of the soil mixing method that has received little attention so far is the rehabilitation and stabilization of dams and dam heightening of tailings and mining waste ponds in the largest European open pit copper mine in Bulgaria there is a need to raise the dam of a tailing pond.

An existing dam, which has already been raised several times and which seals off a valley, must be heightened further. Due to the space available, tailings must be built over in some areas. The situation is aggravated by the fact that the dam is in an earthquake-prone region.

For this reason, a simple feasibility study based on numerical investigations is carried out by BAUGRUND DRESDEN prior to the construction work, which is presented briefly below based on results available so far.

The objective of this simple study is to show how the soil mixing method described above can be used to improve the bearing capacity and serviceability of tailings in the dam raise area.

Basics of the Numerical Investigations

To investigate the effect of a grid of walls produced using the KSI method regarding bearing capacity of the improved tailings and the increase in stiffness, i.e., the reduction of settlements due to the heightening of the dam of the tailing pond in a first step 3-dimensional effective stress-strain analyses were performed using the FE software “Plaxis”.

A plane section of the projected dam was modelled in 3D to allow for the spatial bearing behaviour of the 3-dimensional soil improvement grid consisting of KSI soil mixing walls.

Model description

The finite element model is based on the cross-section of the projected dam as depicted in Figure 2. A soil improvement grid resulting in boxes of 5 m x 5 m with a thickness of 40 cm the 3D-slice of the full model has a width of 10 m to use existing symmetries.

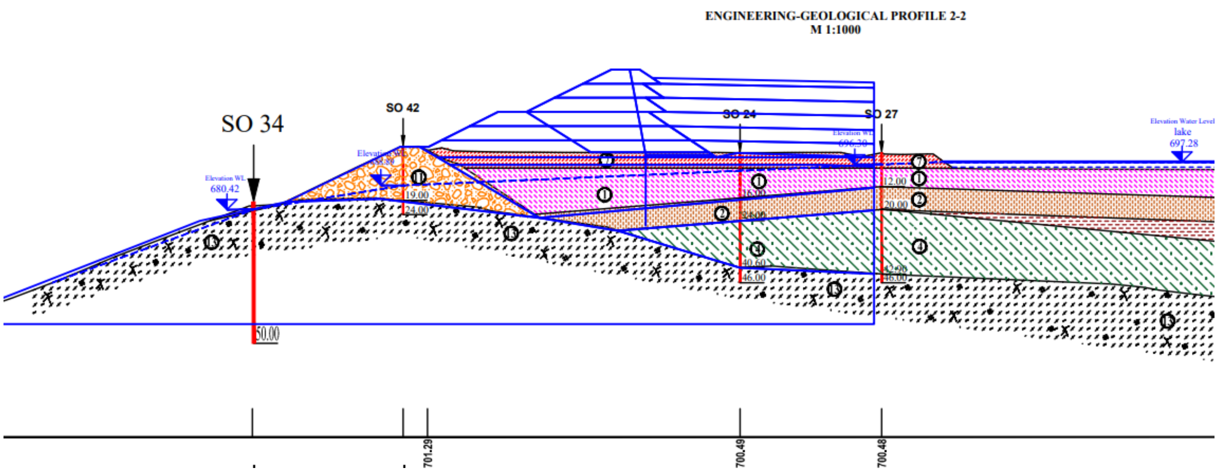

Figure 2: Investigated cross-section of the existing and projected dam.

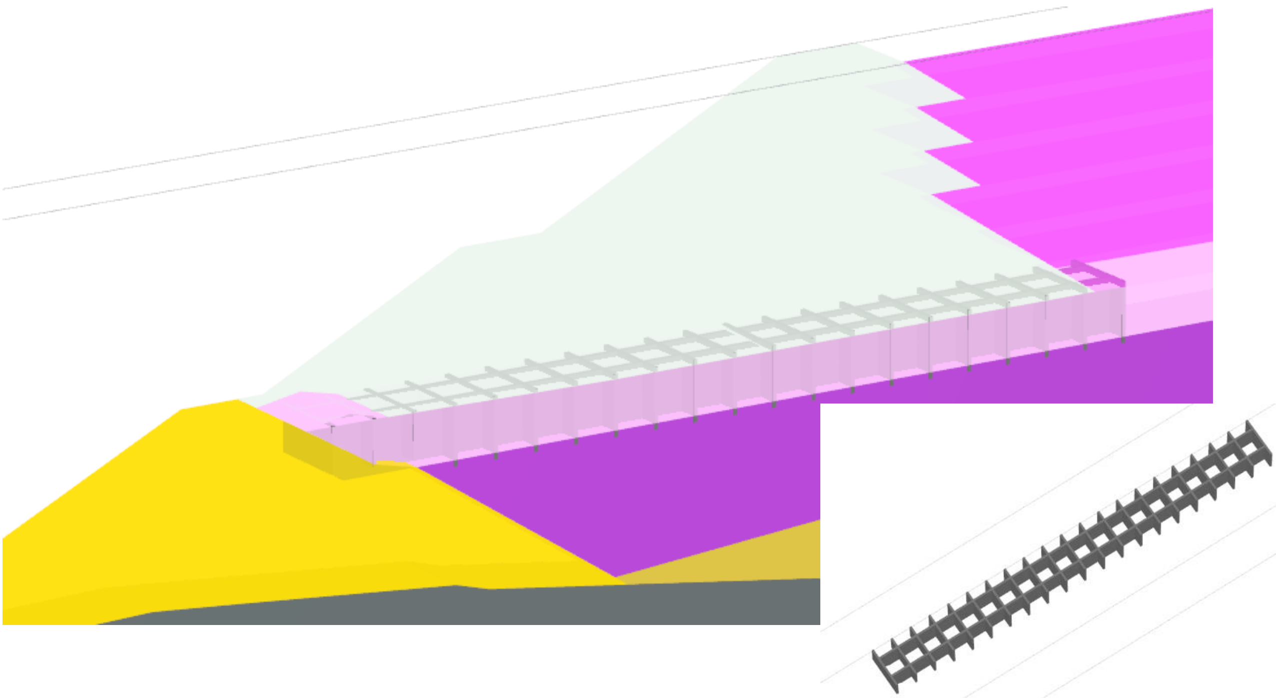

Figure 3: Part of the FE model and detailed depiction of the soil improvement grid

The lower boundary of the model is fixed in all directions, the lateral boundaries in normal direction.

One idea of the grid pattern of the improved soil (Fig. 3) is to reduce shear deformation during earthquake and thus mitigate the liquefaction potential.

First Results

The positive effect of the soil improvement grid on settlements is shown for the first construction stage of the new dam (Fig. 4). The resulting vertical displacements are reduced by approx. 20%. That this effect is not much more pronounced is due to the fact, that the improvement grid is installed floating in the already existing tailings.

The effect on the potential failure mechanisms because of numerical stability analyses (shear strength reduction method or phi-c-reduction respectively) is shown in Figure 5. Whereas without the improvement a classical slip circle mechanism develops, with the improvement grid no failure of the new dam can be observed.

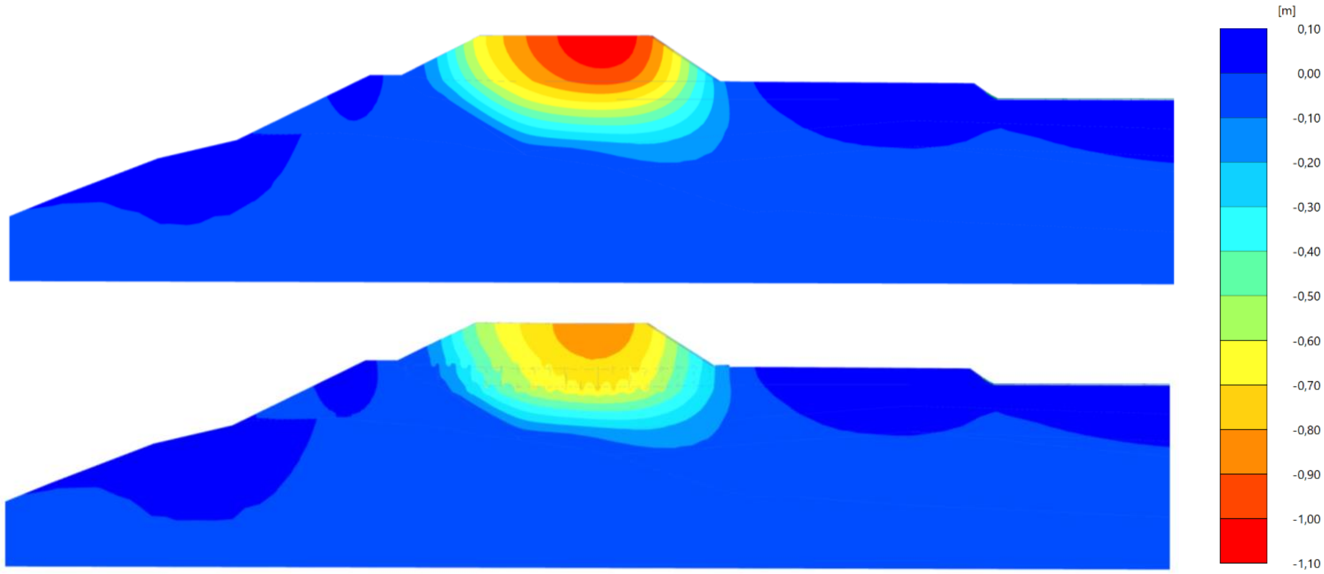

Figure 4: Settlements of the newly constructed dam (stage 1) without (top) and with (bottom) improvement.

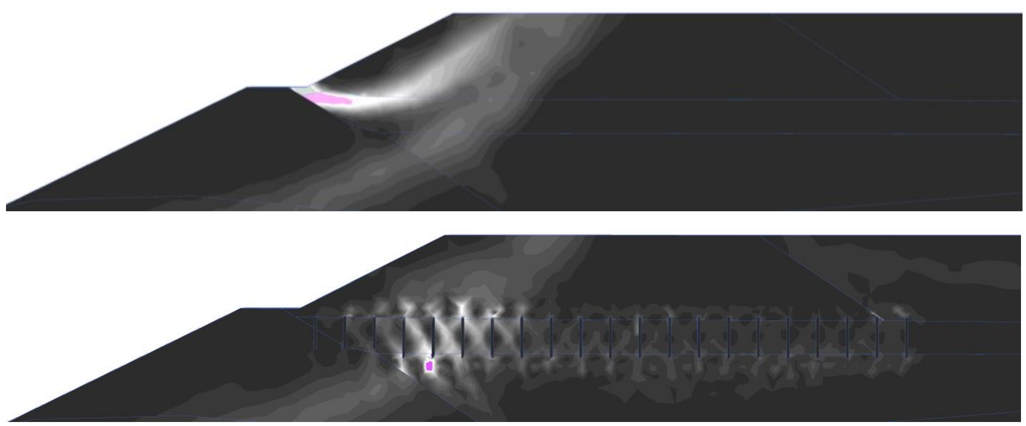

Figure 5: Failure mechanisms of the newly constructed dam without (top) and with (bottom) improvement visualized by shear strain invariant.

Outlook

In the further course of the feasibility study or the realization of the project, it is planned to numerically investigate the further essential aspects of the design, i.e.:

- Fully coupled analyses using advanced e.g., hypoplastic soil models to allow for a realistic prediction of pore water pressure development and consolidation processes taking real construction times into account.

- Seismic analyses to investigate the effect of the foreseen improvement grid regarding the mitigation of liquefaction of the improved tails underneath the new dam (also only possible with advanced soil models)

Summary

In this paper the KSI soil mixing method is described. Based on the current status of a feasibility study based on 3-diemnsional finite element analysis, the applicability in the field of tailings is shown. Furthermore, it is shown that besides the improvement of serviceability and bearing capacity or slope stability, respectively, there is another important possibility of the presented construction method in combination with modern numerical methods, namely the reduction of the liquefaction potential of fully saturated tailings.

Optical satellite imagery to monitor tailings dams

Mr. Christopher Galen O'Donovan, University of the Witwatersrand, Johannesburg, South Africa.
Dr. Luis Alberto Torres-Cruz, University of the Witwatersrand, Johannesburg, South Africa
Prof. Elhadi Adam, University of the Witwatersrand, Johannesburg, South Africa

Abstract

The last few decades have seen an increase in the number of optical earth observation satellites capturing multispectral imagery. Indeed, it is now accurate to say that virtually all dry land on the planet is imaged on a daily basis by at least one satellite. The characteristics of some of these satellites make them suitable to contribute to monitoring tailings dams. The current paper aims at familiarising tailings dam engineers with some of the most important features of these satellites and explaining how such satellite imagery can contribute to monitoring tailings dams. We present a brief summary of the role that multispectral satellite imagery has played in the investigation of some high-profile tailings dam failures. We investigate the different public and private satellite missions that may be of interest to tailings engineers. In particular, we define spatial, temporal, spectral and radiometric resolutions and explain how they affect the capabilities and limitations of the imagery. Attention is also brought to the different options available to access, download, and process satellite imagery. Lastly, we present some insights, enabled by multispectral satellite imagery, into two prominent tailings dam failures that occurred on the African continent in 2022.

Introduction

The last few decades have seen a significant increase in the number of optical earth observation satellites. The characteristics of some of these satellites make them suitable to contribute to the monitoring of tailings dams and this paper provides a brief introduction to this topic. Monitoring is a central aspect of tailings dam management and it is explicitly addressed in the Global Industry Standard on Tailings Management (ICMM et al. 2020).

The contributions that optical satellite imagery can make to the monitoring of tailings dams have been illustrated by the investigations of recent catastrophic tailings dam failures. For instance, optical satellite images contributed to the development of a computer model of the Fundão Tailings Dam which failed in Brazil in 2015 (Morgenstern et al. 2016). In particular, the satellite images contributed to the reconstruction of the topography, the tailings deposition history and the evolution of the extent and elevation of the decant pond. To this end, the Fundão Dam investigation considered commercial satellite images as well as images freely available from Google Earth (www.google.com/earth/download).

The investigation into the failure of Dam I in Brumadinho, Brazil in 2019 also made use of satellite imagery to investigate the behaviour of the dam during the year prior to its failure (Robertson et al. 2019). In particular, satellite images aided the identification of wet spots, decant water, vegetation, and human activity. The Brumadinho investigation analysed publicly available images from the Sentinel-2 satellite mission (ESA 2015) and from Google Earth as well as commercial satellite images.

Another satellite-based technology that has been widely applied to the monitoring of tailings dams is interferometric synthetic aperture radar (InSAR) (Vulpe et al. 2022). However, this technology falls beyond the scope of this paper because, as its name suggests, it relies on radar and not optical information (see section "Active vs. passive remote sensing").

The remainder of the paper is divided into three main parts. The first part provides a brief conceptual framework. The second part summarises satellite missions that are relevant to the monitoring of tailings dams with particular emphasis on missions whose data is publicly available or can be accessed for free by researchers. Lastly, we present satellite-based insights regarding the failure of two African tailings dams in 2022.

A Brief Conceptual Framework

Types of Orbit

Most satellite orbits fall into one of three categories: geostationary orbit (GEO), low Earth orbit (LEO), and medium Earth orbit (MEO) (ESA 2020). A GEO has a height of ~36,000 km and is located directly above the equator. Satellites on this orbit move at the same pace as the Earth's rotation meaning that they remain above a fixed point on Earth. Because they are relatively faraway from Earth, GEO satellites can observe a large portion of Earth simultaneously although not in great detail. Accordingly, GEO satellites are useful for communication and weather tracking purposes, but not for monitoring tailings dams.

Conversely, a LEO has a height between 400 and 1,000 km. This greater proximity to Earth implies that LEO satellites capture images in greater detail albeit with a narrower area in view. The level of detail in the images of LEO satellites makes them suitable to monitor tailings dams. When observing changes in time, it is useful to use images from satellites that are in a specific type of LEO called a sun-synchronous orbit (SSO). An SSO passes approximately over the poles of Earth and ensures that images are always acquired at the same local solar time which enhances consistency in solar illumination between images, barring seasonal fluctuation (Jensen, 2015).

A medium Earth orbit MEO falls in between the height of a LEO and a GEO. That is, between 1,000 and ~36,000 km. MEO is used by navigation satellites such as those that power the Global Positioning System (GPS) (ESA 2020).

Active vs. Passive Remote Sensing

Active remote sensing refers to taking measurements of an object by transmitting a signal and measuring its return, or backscatter (Lillesand et al., 2015). The Sentinel-1 mission, which employs the Synthetic Aperture Radar (SAR) technique, is an example of active remote sensing. SAR readings enable the InSAR technique which, as noted above, is being frequently used to monitor displacements in tailings dams. Active remote sensing is not considered further herein.

Passive remote sensing refers to systems that do not transmit energy but rather measure the reflectance or emission of naturally occurring energy (Lillesand et al., 2015). Optical satellites, which are the focus of this paper, are passive as they measure the visible and near infrared radiation from the sun that is reflected off the Earth. It follows that optical satellites can only collect information during the day and when their view is not obstructed by clouds.

Satellite Image Resolutions

Spatial Resolution

The spatial resolution of an imaging system is a measure of the smallest identifiable object or distance (Lillesand et al., 2015). Finer pixel spacing in the imaging sensor provides higher spatial resolution which in turn enables the definition of objects and distances with a greater degree of certainty. Figure 1 depicts the decant pond of a tailings dam at different spatial resolutions.

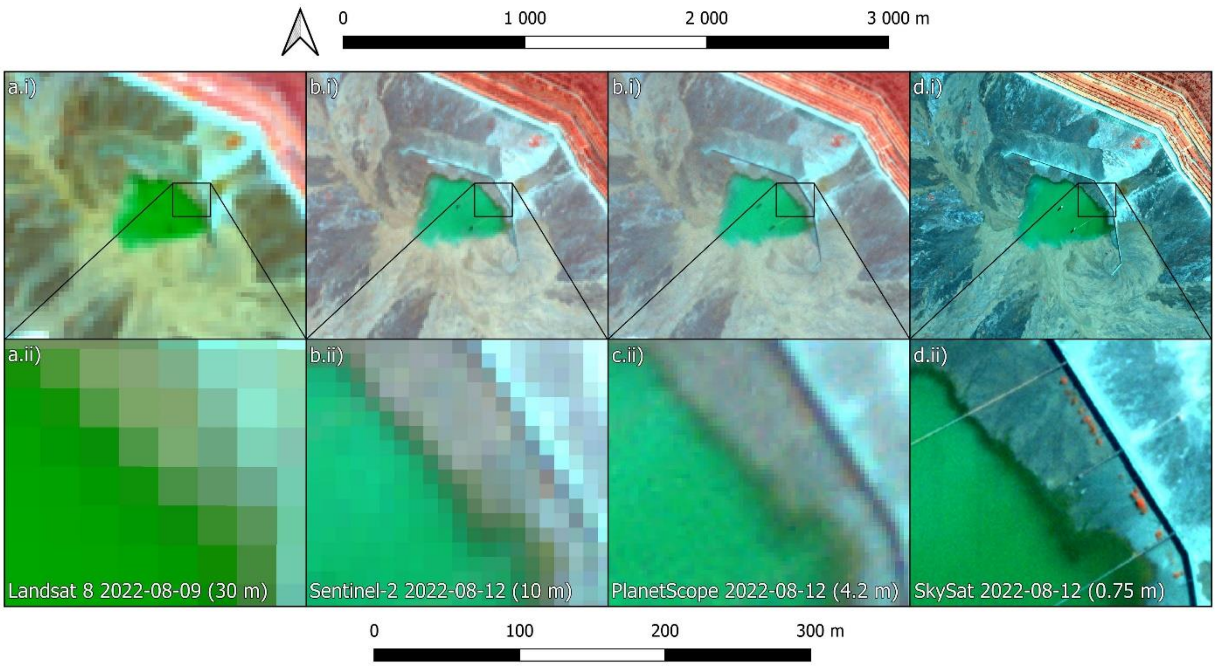

Figure 1: False colour imagery of a tailings dam decant pond. a) Landsat 8, b) Sentinel-2, c) PlanetScope, and d) SkySat. Note: Pixel size indicated in brackets in lower images.

Spectral and Radiometric Resolution

Electromagnetic energy may be separated into spectral domains. This is apparent when a prism separates white light into its constituent wavelengths (i.e. colours). In satellite imaging, the discretely sensed spectral domains of light sensed by an imaging system are referred to as bands (Figure 2). The intensity of an individual band can be measured independently of the intensity of other bands. Sensing a higher number of narrow bands provides increased classification abilities (e.g. identification of supernatant water) compared to a fewer number of wider bands. This type of resolving power is referred to as spectral resolution (Lillesand et al., 2015; Jensen, 2015). Satellites able to make measurements of multiple bands of the electromagnetic spectrum are called 'multispectral'. Some satellites make measurements from a large number of narrow bands and are called 'hyperspectral' (Figure 2).

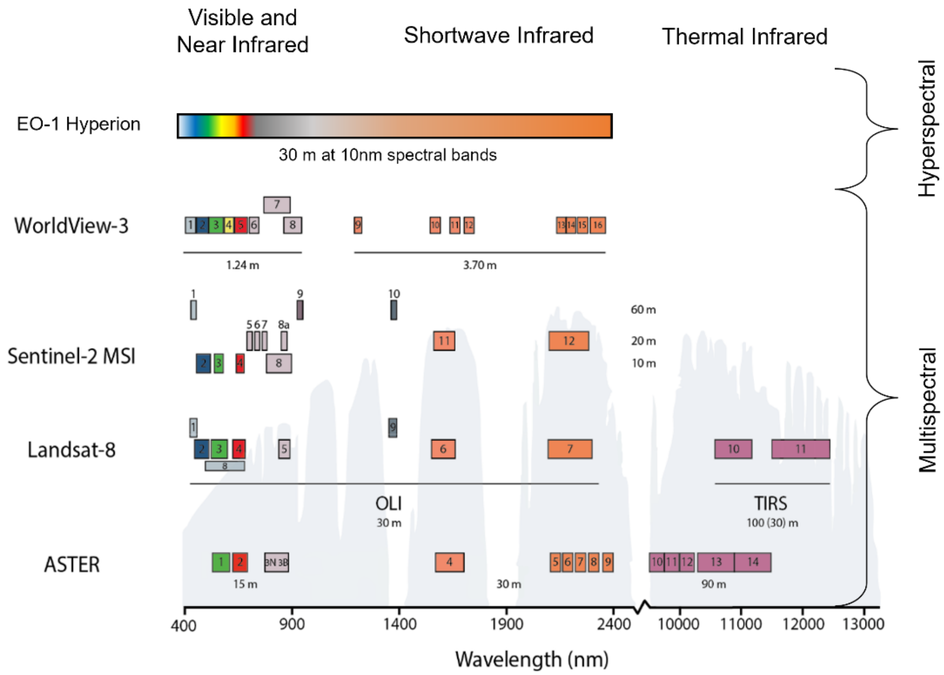

Figure 2: Important multispectral and hyperspectral satellite missions (after Cardoso-Fernandes et al., 2020, modified)

Radiometric resolution refers to the ability to differentiate between fine changes in the intensity of light within a particular band (Figure 3). The bit depth of each band characterises its radiometric resolution (Lillesand et al., 2015; Jensen, 2015). Namely, the number of intensities that a band can detect is equal to 2 to the power of the bit number. For instance, a 12-bit band can identify 4096 levels of light intensity.

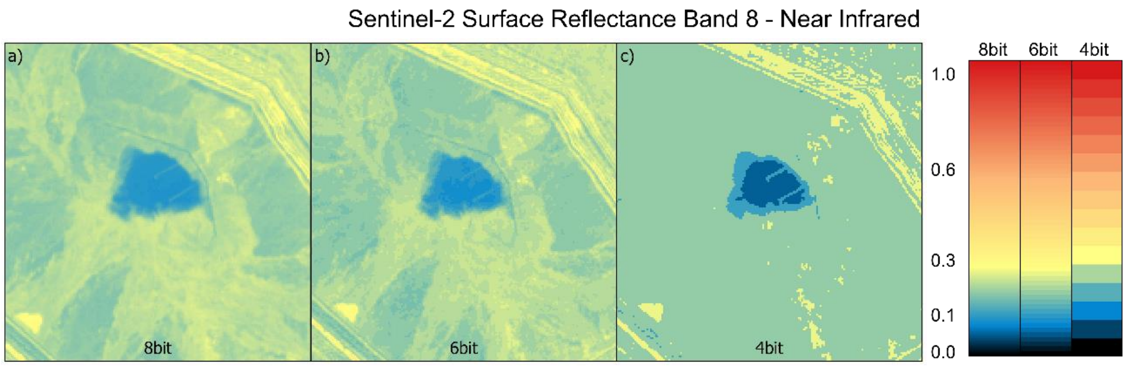

Figure 3: Tailings decant pond in Sentinel-2, band 8, near infrared surface reflectance at simulated a) 8bit, b) 6bit and c) 4bit radiometric resolutions.

Temporal Resolution

Temporal resolution, or revisit time, refers to the time between two successive images of the same point taken by the same satellite or by different satellites of the same satellite constellation (Lillesand et al., 2015).

A satellite constellation refers to a group of satellites of similar or identical characteristics traveling along the same path. Shorter revisit times result in a higher temporal resolution which enables the monitoring of changes that occur at a faster rate.

Tradeoffs between resolutions

There are generally tradeoffs between the different types of resolution of satellite images. For instance, better temporal resolution can be achieved by regularly covering wider swaths of ground using a wider field of view or higher orbit altitude. But this improvement in temporal resolution comes at the expense of spatial resolution. Furthermore, given that the smaller ground sensing distance associated with greater spatial resolution reduces the area of ground from which radiation is measured, a higher spatial resolution requires light to be sensed from a wider bandwidth which reduces spectral resolution. (Lillesand et al., 2015).

Imagery Pre-Processing

Georeferencing, Orthorectification and Conversion to Reflectance

Georeferencing refers to assigning real world coordinates to an image. Orthorectification refers to removing distortions in an image caused by the tilt of the sensor (camera) and the topography of the terrain (Lillesand et al., 2015).

Satellites measure the amount of radiation, within a particular band, coming from Earth's surface. However, quantitative analyses on satellite imagery generally requires converting the radiation, or irradiance, measurements into reflectance values. Reflectance, or more specifically spectral reflectance, is a measurement of the proportion of the radiation reaching Earth's surface that is reflected back to space, usually measured over a specific wavelength (Lillesand et al., 2015).

Many public satellite datasets are available in pre-processed orthorectified and georeferenced products that provide calibrated measurements of reflectance. As such, these are aspects of remote sensing that tailings engineers do not generally have to deal with.

Atmospheric Correction

Satellite data is usually used in one of two product levels, top-of-atmosphere and surface reflectance. As the names suggest, top-of-atmosphere reflectance is the reflectance as measured by the satellite including the light scattering effects of the atmosphere. This type of data provides some useful information for aerosol and dust monitoring. However, for temporal change monitoring, the effects of atmospheric scattering and changing weather conditions can introduce uncertainty. This is where atmospheric transmission and scattering models (Vermote et al., 1997) come into play and can be used to remove atmospheric effects (Figure 4). The removal of atmospheric effects is known as atmospheric correction and its purpose is to estimate the reflectance values that would have been measured if the atmosphere were not there. That is, surface reflectance values.

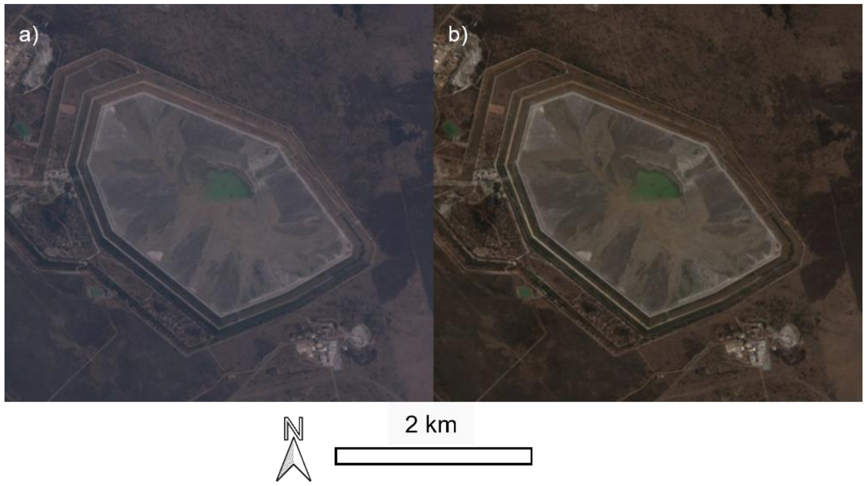

Figure 4: Atmospheric Correction of Sentinel-2. a) Level 1C, Top of Atmosphere Reflectance product before atmospheric correction, b) Level 2A, Surface Reflectance, product after atmospheric correction.

Relevant Satellite Missions and Data Access Platforms

Figure 5 summarises the temporal availability and temporal and spatial resolutions of several public and commercial satellite missions relevant to the tailings engineer. Satellite imagery can be viewed, analysed and downloaded using a suite of web and cloud-based platforms. Public satellite data from the Sentinel and Landsat missions (USGS 2019, 2022) can be accessed via Sentinel-Hub (www.sentinel-hub.com). ASTER, Landsat, National Agriculture Imagery Program (NAIP) and other data managed by the United State Geological Survey (USGS) can be accessed with the EarthExplorer portal (https://earthexplorer.usgs.gov). Google Earth Engine (https://earthengine.google.com/) is a cloud-based analysis engine where a large amount of public satellite data is available for analysis (Gorelick et al. 2017). The Sentinel-Hub and Google Earth Engine platforms allow users to render, analyse and aggregate satellite imagery via cloud-based computer infrastructure, facilitating analyses that are usually too computationally resource intensive for a typical personal computer. The China-Brazil Earth Resources Satellites (CBERS) are a family of high-resolution optical imaging satellites jointly designed and operated by Brazil and China (Sausen 2001). CBERS imagery is accessible via the INPE catalogue available at www.dgi.inpe.br/catalogo/explore. Archival timeseries of natural colour satellite data are available on Google Earth Pro for Desktop. This imagery is down sampled to spatial resolutions of ~1 m from a variety of very high resolution commercial satellites. The PlanetScope and SkySat constellations are managed by Planet Labs and can be accessed via PlanetExplorer (www.planet.com/explorer). Table 1 summarises platforms where satellite data can be accessed for non-commercial and research work.

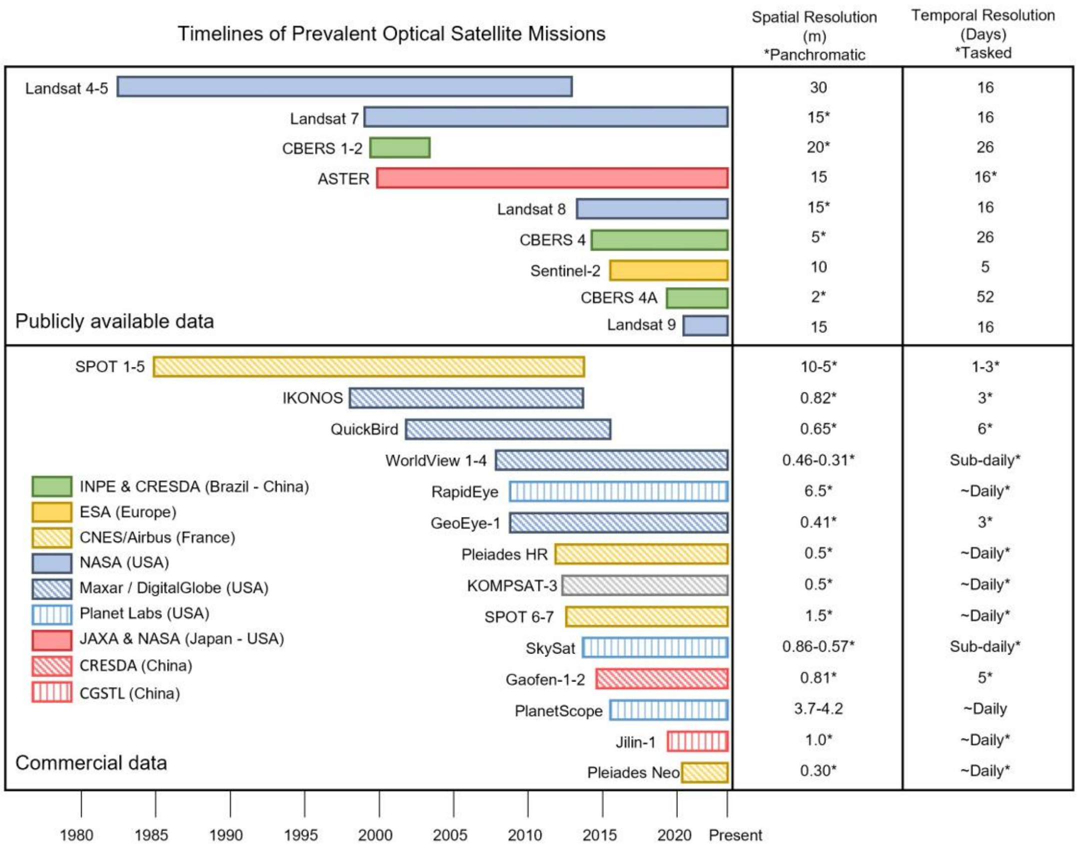

Figure 5: Public and commercial satellite platforms open for civilian use (adapted from Turner et al., 2021)

Table 1: A few platforms where public and research-access satellite imagery is available

Platform	**Notable Public / Research Datasets**	**Access**
Sentinel-Hub	Landsat, Sentinel-1and 2.	Public*
EarthExplorer	ASTER, Landsat, NAIP.	Public*
INPE	CBERS.	Public
Google Earth Engine	ASTER, Landsat, Sentinel-1 and 2, NAIP	Research - Commercial subscriptions available.
Google Earth Pro (Desktop)	Resampled very high-resolution satellite imagery.	Public
Planet Explorer	PlanetScope, Landsat, Sentinel-2.	Commercial - Research access available.

*Note: While the platforms are accessible to the public, some features may be reserved for commercial use.

Case Studies

Jagersfontein

The South African town of Jagersfontein was subject to a devastating tailings dam failure on the morning of 11 September 2022. The tailings dam failure flooded the town and killed at least one person. Analysis of multispectral images from multiple sources has been useful in identifying possible precursors of failure (Torres-Cruz & O'Donovan, 2023; Cacciuttolo & Cano, 2023). Figure 6 shows natural colour and NDWI renders of Sentinel-2 imagery which suggest a large decant pond on the Jagersfontein dam. Similarly, satellite imagery has also been useful to assess some of the immediate consequences of failure such as the 56 km distance travelled by the tailings spill until reaching the Kalkfontein dam (Torres-Cruz & O'Donovan, 2023).

Williamson Mine

A tailings dam servicing the Williamson Diamond mine in Tanzania failed on 7 November 2022 (Slater, 2022), causing a large runout of material into the surrounding area and water courses (Petley, 2022). The condition of the decant pond prior to failure has been assessed using Sentinel-2 imagery (Cacciuttolo & Cano, 2023). Furthermore, satellite imagery has also been used to assess the extent of the tailings spill (Petley, 2022). Figure 7 illustrates the capability of a high resolution optical satellite acquisition and stereographic model reconstructing the post-failure tailings dam geometry at Williamson Daimond mine. Such data may be useful to those interested in the failure and tailings engineers calibrating dam breach runout models.

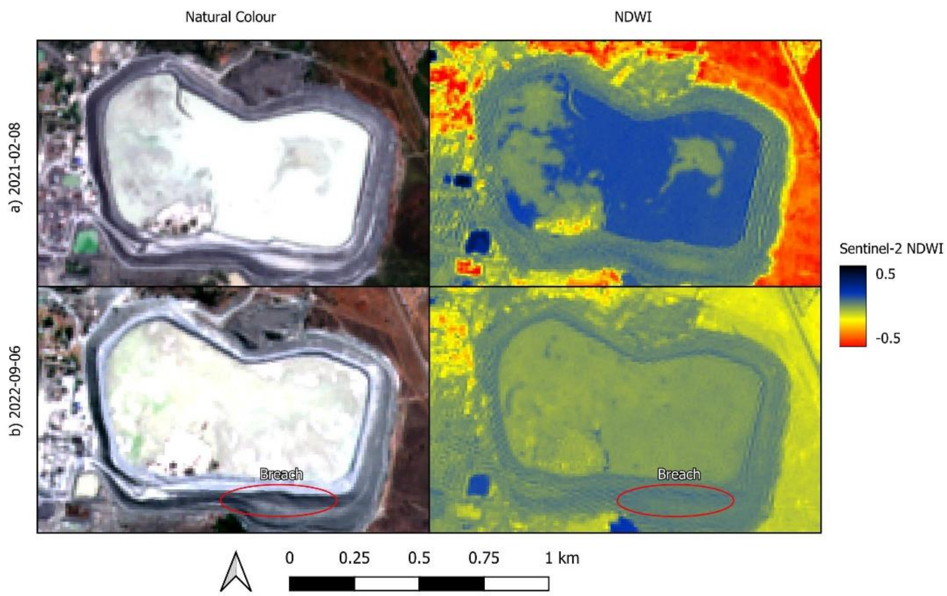

Figure 6: Natural colour and NDWI Sentinel-2 imagery of the Jagersfontein dam prior to failure. Adapted from Torres-Cruz & O'Donovan (2023).

Figure 7: Williamson mine tailings dam breach. Note: Contour lines indicate meters above sea level and are based on interpretation of a stereo pair image.

Conclusion

Optical satellite imagery provides a rich archive of data of the surface of the Earth. Never before have the public satellite data offerings been more applicable to the monitoring of tailings dams. This paper aimed at providing a brief introduction to optical satellite imagery that is relevant to the monitoring of tailings dams. The paper defined key concepts, summarised public and commercial satellite missions that are adequate to monitor tailings dams, mentioned platforms that can be used to access and process satellite images, and illustrated some of the capabilities of optical satellite imagery using two African case histories of tailings dam failures in 2022. We hope to have shown that optical satellite imagery is worthy of a space in the monitoring toolkit of all tailings dams.

References

Cacciuttolo, C. & Cano, D. (2023) Spatial and Temporal Study of Supernatant Process Water Pond in Tailings Storage Facilities: Use of Remote Sensing Techniques for Preventing Mine Tailings Dam Failures. Sustainability. 15 (6), 4984. doi:10.3390/su15064984.

Cardoso-Fernandes, J., Teodoro, A., Lima, A., Perrotta, M. & Roda-Robles, E. (2020) Detecting Lithium (Li) Mineralizations from Space: Current Research and Future Perspectives. Applied Sciences. 10, 1785. doi:10.3390/app10051785.

ESA (2015) Sentinel User Handbook and Exploitation Tools (SUHET): Sentinel-2 User Handbook. European Commission. (Issue 1, Rev 2). https://sentinel.esa.int/documents/247904/685211/Sentinel-2_User_Handbook.

ESA (2020) Types of Orbits.

https://www.esa.int/Enabling_Support/Space_Transportation/Types_of_orbits [Accessed: 14 Sept. 2023].

Gorelick, N., Hancher, M., Dixon, M., Ilyushchenko, S., Thau, D., & Moore, R. (2017) Google Earth Engine: Planetary-scale geospatial analysis for everyone. Remote Sensing of Environment. Vol. 202.

ICMM, UNEP and PRI (2020) Global Industry Standard on Tailings Management.

Jensen, J.R. (2015) Introductory Digital Image Processing: A Remote Sensing Perspective. Pearson series in geographic information science. 4th edition. Illinois, USA, Pearson Education, Inc.

Lillesand, T., Kiefer, R.W. & Chipman, J. (2015) Remote Sensing and Image Interpretation. 7th edition. John Wiley & Sons.

Morgenstern, N. R., Vick, S. G., Viotti, C. B. & Watts, B. D. (2016) Report on the immediate causes of the failure of the Fundão Dam - Appendix A. (Commissioned by BHP Billiton Brasil Ltda., Vale S.A., and Samarco Mineração S.A.).

Petley, D. (2022) Another tailings dam failure: the Williamson Mine in Tanzania. The Landslide Blog. https://blogs.agu.org/landslideblog/2022/11/08/williamson-mine-1/.

QGIS.org (2022) QGIS Geographic Information System. 2022. QGIS Association. https://www.qgis.org/ [Accessed: 1 February 2022].

Robertson, P.K., de Melo, L., Williams, D.J. & Wilson, G.W. (2019) Report of the expert panel on the technical causes of the failure of Feijao Dam I (commissioned by Vale S.A.).

Sausen, T.M. (2001) The China-Brazil Earth Resources Satellite (CBERS). ISPRS Soc., 6(2).

Slater, D. (2022) Petra says eastern wall of Williamson tailings dam breaches, teams on site. Mining Weekly. https://www.miningweekly.com/article/petra-says-eastern-wall-of-williamson-tailings-dam-breaches-teams-on-site-2022-11-07.

Torres-Cruz, L.A. & O'Donovan, C. (2023) Public remotely sensed data raise concerns about history of failed Jagersfontein dam. Scientific Reports. 13 (1), 4953. doi:10.1038/s41598-023-31633-5.

Turner, I.L., Harley, M.D., Almar, R. & Bergsma, E.W.J. (2021) Satellite optical imagery in Coastal Engineering. Coastal Engineering. 167, 103919. doi:10.1016/j.coastaleng.2021.103919.

USGS (2019) Landsat 8 (L8) Data Users Handbook. Version 5.0 (LSDS-1574).

USGS (2022) Landsat 9 Data Users Handbook. Version 1.0 (LSDS-2082).

Vermote, E.F., Tanre, D., Deuze, J.L., Herman, M. & Morcette, J.-J. (1997) Second Simulation of the Satellite Signal in the Solar Spectrum, 6S: an overview. IEEE Transactions on Geoscience and Remote Sensing. 35 (3), 675–686. doi:10.1109/36.581987.

Vulpe, C., Magnall N., Larkin H., Fourie, A., Boshoff, J., McNab, L., Thomas, A. (2022) On the importance of proactive collaboration between mining operators and InSAR monitoring specialists. 11th International Symposium on Field Monitoring in Geomechanics.

Mechanical Behavior of the Compaction of the Mixture of Sandy and Ultrafine Tailings in Experimental Landfills.

W. Pirete, BVP Engenharia, Brasil

P.Cella, BVP Engenharia, Brasil

A. Rissoli, Vale S.A, Brasil

A. Freire, BVP Engenharia, Brasil

D.Silva, BVP Engenharia, Brasil

P.Andrade, BVP Engenharia, Brasil

T.Augusto, BVP Engenharia, Brasil

Abstract

The Studies on alternative methods of disposal of filtered tailings have been growing substantially in mining, especially in iron ore mines located in the Iron Quadrangle. The main information about the different types of filtered tailings is obtained through tests in experimental landfills to evaluate compaction performance, considering variations in moisture and energy, as well as knowledge and understanding of variations in tailings from ore extraction, through the beneficiation/filtration process to disposal in the test area.

In the experimental landfills, layers with different thicknesses, energies, and variations in moisture were tested. In these layers, undisturbed samples were collected to evaluate mechanical behavior. In this context, this work presents the results of drained and undrained triaxial tests performed on samples collected from compacted layers within a target moisture range, with satisfactory compaction results.

The results of layers with moisture below and above the target compaction range, with moderate compaction performances, are also presented. The evaluation of compaction performance is related to the mechanical behavior observed in triaxial tests, with a good performance analysis understood by the response of dilatant behavior, with positive volumetric variation (volume increase) in the drained test and a significant reduction in pore pressure in the undrained loading for confinement stresses up to 3,200 KPa. Regarding the analysis of moderate compaction performance, the behavior begins with a low rate of pore pressure, followed by a reduction during loading, and in the drained test, there is a reduction in volume for confinement stresses above 1,600 KPa. The study also compares the strength envelopes of compacted layers within the target moisture range with layers compacted below and above the target moisture range.

Introduction

This study presents the mechanical behavior through drained and undrained triaxial tests of undisturbed samples taken from experimental landfills of a filtered tailings mixture conducted in an iron ore mine, involving mixtures of sandy and ultrafine tailings. These proportions largely represent the variations in fines and sandy tailings generated from the processing plants in the Iron Quadrangle Mines.

In the tests of the experimental landfills with mixtures filtered tailings, referred to in this work as partial tailings (represented by a proportion of approximately 90% sandy and 10% ultrafine, by mass) and total tailings (represented by a proportion of approximately 80% sandy and 10% ultrafine, by mass), variations in moisture content were tested to simulate operations during dry and wet seasons, as well as variations in compaction energy (roller passes) and layer thickness.

The results of the compaction performance tests of the experimental landfills with both partial and total filtered tailings mixtures were compiled and interpreted for an integrated analysis of the mixtures, considering behaviors related to the reduction of void ratios and variation of degree of saturation after compaction, with moisture content varying inside the target range (close to optimal moisture) and below and above the target moisture range. After the compaction tests, undisturbed samples were collected to evaluate the mechanical performance of the compacted layers inside the target range, under wet and dry conditions.

Methodology applied in the experimental landfills

The evaluation of the mechanical behavior of sandy tailings and mixtures (sandy and ultrafine) was carried out through compaction tests in experimental landfills, where different layer thicknesses, moisture contents, and compaction energies (variation of passes and vibration conditions) were tested.

In the experimental landfill tests, compacting was performed with variations in moisture content to identify the best compaction performance based on moisture ranges. The following ranges were programmed: near optimum (target range), range in the wet branch, and range in the dry branch. These tests were intensified in the total tailing tests (sandy + ultrafine mixture) to assess the compaction performance indices in compacted layers near the optimum, in the wet branch, and in the dry branch. After the layers were compacted, undisturbed samples were collected for drained and undrained triaxial tests to evaluate the mechanical behavior of the compacted layers within the target range (near optimum) and outside the target range (wet branch and dry branch).

The experimental tests were conducted using three types of tailings: partial tailings, total tailings, and sandy tailings, produced by Industrial Scale Filtration Plants, namely:

- Partial Tailings: Mass mixture proportion of 90% sandy tailings + 10% ultrafine tailings (slime), nominally referred to as the 90 x 10 proportion;

- Total Tailings: Mass mixture proportion of 80% sandy tailings + 20% ultrafine tailings (slime), nominally referred to as the 80 x 20 proportion;
- Sandy Tailings: 100% of sandy tailings.

The mixtures of tailings (sandy and ultrafine), referred to as partial and total, are generated through pulp mixing in a conditioning tank, with the feed of thickened slurry from the thickener's underflow and the feed of the sandy tailings through the cyclone battery (sandy tailings). Subsequently, after conditioning in the tank and adjusting the pulp density with reagents, the feed to the disk filters (filtration plant) takes place, resulting in the generation of filtered cake, which is consequently destined for the experimental landfill area.

The layers were compacted with a smooth roller weighing 20 (twenty) tons, with variations in energy based on the number of passes, both with and without vibration, in addition to variations in layer thicknesses. In these energy variations, variations in moisture content were also considered to understand the compaction performance. Figure 2 presents images of compacted tracks in the experimental landfills with compacted layers, considering different tested thicknesses (30cm, 50cm, 70cm, and 100cm), with different moisture ranges (near optimum, wet branch, and dry branch).

Figure 1: Compaction with a smooth roller of 20 tons of tailings mixtures and sandy tailings.

During the tests of the experimental landfills, controls were carried out regarding the physical characteristics of the tailings, with particle size distribution tests using sieving and sedimentation methods, according to NBR 7181 (ABNT, 2018), grain densities according to NBR 6458 (ABNT, 2016), and Proctor Normal compaction tests as per NBR 7182 (ABNT, 2016). To assess the mechanical behavior of the compacted layers of the experimental landfill tracks, undisturbed samples were collected for drained triaxial tests according to ASTM D 7181 (2020) and undrained tests according to ASTM D 4767 (2011). This work will present the results of the mixed tailings (partial and total).

Physical Characteristics and Compaction Curves of Filtered Tailings Mixture

Based on the interpretation of the tests conducted on the tailings in the experimental landfills, it was observed for both partial and total tailings a variability in the particle size distribution and compaction curves, which reflect the influence of tailings variations within an operational context. It is not feasible to conduct a single specific curve test that would represent the exact proportion of a mixture. This observed variability may be linked to various operational factors, varying based on the type of ore processed in the plant or the influence in the filtration process, such as flocculant dosages, control of the mass proportion of ultrafine in the mixture, as well as controlling the pulp density in the conditioning tank prior to feeding the disk filters.

In this context, following an assessment of the variations in particle size distribution curves between the partial and total tailings, a geotechnical evaluation was proposed within the limits of variation, encompassing a range that includes all particle size distribution curves tested in the experimental landfills. Compaction tests were also conducted on all tested tailings to assess compaction performance, evaluating variations in dry densities and optimal moisture content. Thus, in a scenario where controlling a specific type of mixture is challenging, an approach was taken to address the variations in tailings mixtures, seeking to represent the material generated by the Plant. Incorporating mass mixture proportions from 90/10 to 80/20, a "Base Case" was proposed, as shown in Figure 2 and Table 1.

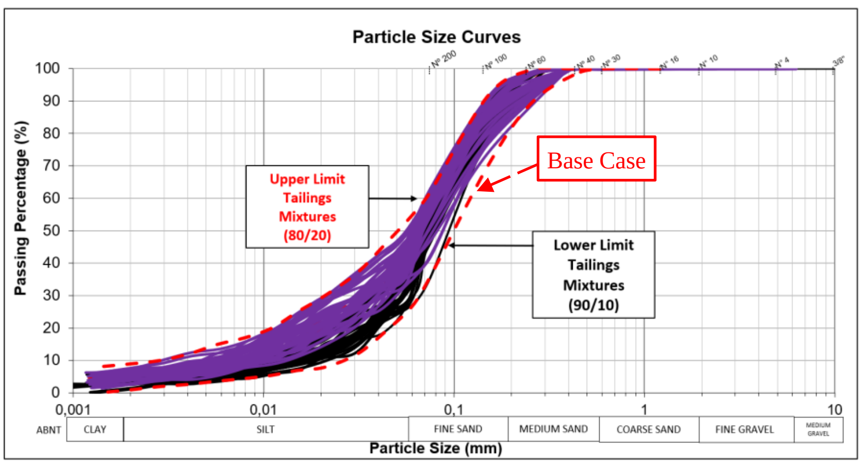

Figure 2: Limits of Particle Size Distribution Curves of Tailings Mixtures - Base Case

Table 1: Lower and Upper Limits of Tailings Mixtures Curves - Base Case

Sieve Opening (mm)	Upper Limit (% Passing)	Lower Limit (% Passing)
0,42	100	98
0,25	100	89
0,15	94	70
0,075	67	36
0,045	48	19
0,03	38	12
0,01	20	5,5
0,005	14	3,7

Similarly, the compaction curves were interpreted and analyzed for all the unified particle size distribution curves of the tested tailings in the "base case," assessing the compaction performance within moisture ranges for compaction performance interpretation. Figure 3 displays the compaction curves of the tailings tested in the "base case.

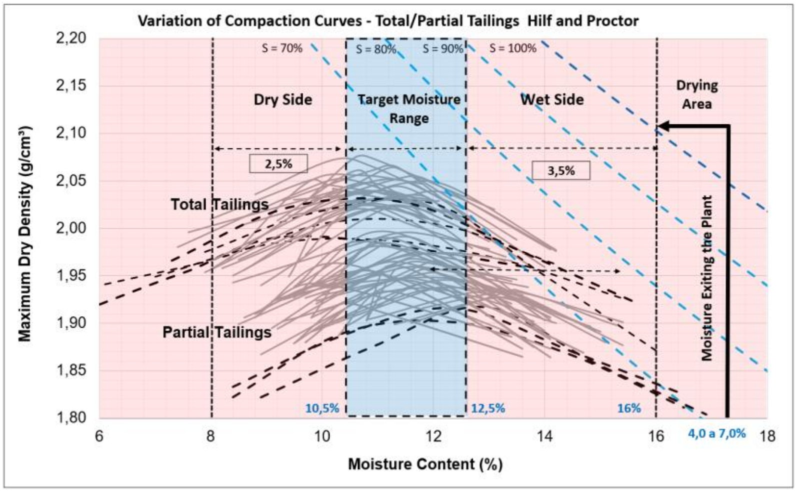

Figure 3: Target Moisture Content Ranges for Compaction

As can be observed in Figure 3, several crucial pieces of information should be interpreted and established as construction controls for effective compaction performance, yielding suitable void ratio and degree of saturation outcomes for satisfactory geotechnical behavior. Some moisture variation controls were tested in the landfills, following the limits below:

- Target moisture range: Moisture variation between 10.5% and 12.5%, interpreted as good compaction performance for both partial and total tailings (base case);
- Moisture range in the wet branch: Moisture variation between 12.5% and 16%, interpreted as moderate compaction performance for both partial and total tailings (base case), with the presence of sticky material;
- Moisture range in the dry branch: Moisture variation between 8% and 10.5%, interpreted as moderate compaction performance for both partial and total tailings (base case), requiring vibration for improved performance;

The study presents a subsequent analysis of mechanical performance in terms of the strength of the compacted layers within the target moisture range (good performance), compared to the analysis of results from the compacted layers in the wet and dry branches. This analysis examines the primary results of compaction performance versus mechanical behavior in terms of strength through triaxial tests.

Compaction Performance vs. Void Ratios

The compaction performance of the "base case" tailings, as presented in Figure 2, was analyzed considering moisture variations shown in Figure 3, to comprehend the compaction results and the void ratio outcomes of the compacted layers inside and outside the target moisture range. Figures 4a, b depicts the compaction performance and dry densities of the compacted layers inside the target moisture range.

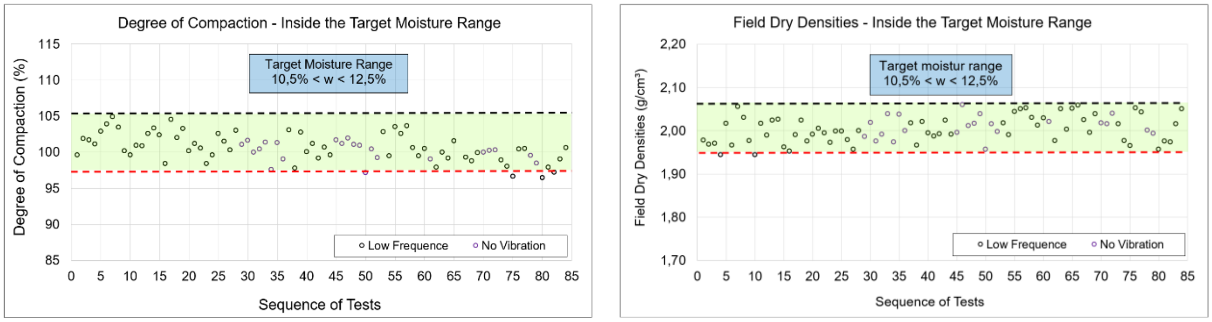

Figure 4: Compaction Performance (a) and Field Dry Densities of Compacted Layers inside the Target Moisture Range (b).

It is observed that the degrees of compaction inside the target moisture range, compacted with a smooth roller weighing 20 (twenty) tons, at different energies (number of passes), showed a compaction degree variation from 97% to 105% and field dry densities ranging between 1.95 t/m³ and 2.07 t/m³.

To assess the compaction performance under moisture conditions outside the target range, compacting was performed in the wet branch and dry branch, simulating compaction conditions during the rainy season and extreme dry season. Figures 5a, b presents the results of the compaction performance and field dry densities of compacted layers outside the target moisture range.

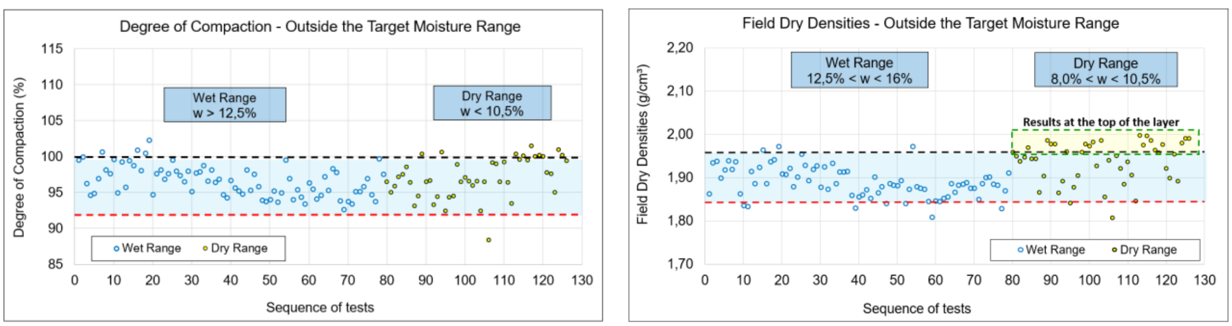

Figures 5: Compaction Performance (a) and Field Dry Densities (b) of Compacted Layers within the Target Moisture Range.

In the compaction tests with moisture levels outside the target range, the degrees of compaction exhibited poorer performance compared to the layers compacted inside the target moisture range, with compaction degrees ranging from 92% to 100% and field dry densities varying between 1.82 and 1.96 t/m³.

It's worth noting that the degrees of compaction play an important role as references to understand compaction performance. However, to comprehend the mechanical behavior of sandy-silty tailings, the analysis of variations in void ratios in the compacted layers within and outside the target moisture range must be evaluated and interpreted alongside the responses from drained and undrained triaxial tests, with special emphasis on the analysis of pore pressure generation (Δu) and volumetric variations (Ɛv). Figure 6 illustrates the relationship between compaction performance and void ratio outcomes to aid in understanding the guidelines of drained and undrained triaxial tests, among others (compressibility and permeability).

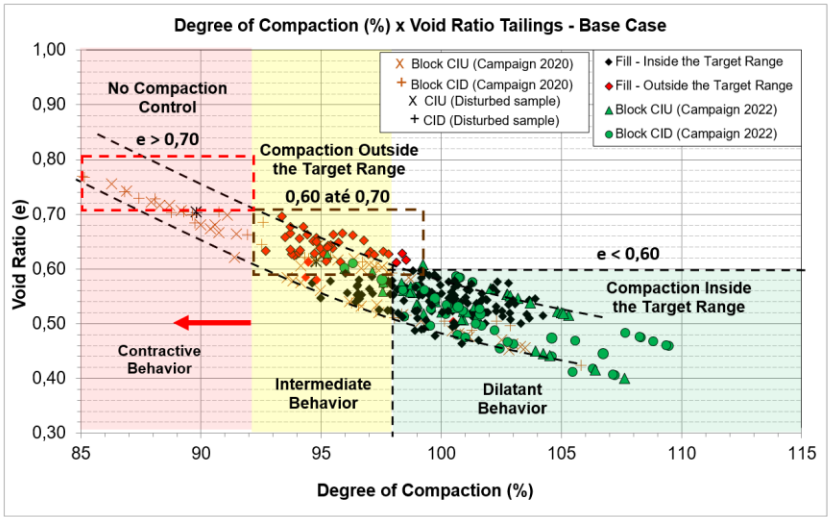

Figures 6: Analysis of compaction degrees vs. void ratio of compacted layers.

The results of compaction performance in relation to the void ratio of compacted layers with a smooth roller weighing 20 tons, 50 cm thick layers, at moisture levels within and outside the target range, and in samples with low compaction representing a spread condition, directed the types of compaction controls:

- Type I: Compaction inside the target range: GC above 98% and void ratio below 0.60;
- Type II: Compaction outside the target range: 92% < GC < 98% and void ratio 0.60 < e < 0.70;
- Type III: Low compaction - spread with a crawler tractor: GC < 92% and void ratio > 0.70.

After understanding the compaction performance behavior and variations in the void ratios of the compacted layers within and outside the moisture range, a condition was also considered where a layer above 50cm was spread with a crawler tractor, simulating low compaction at the base of the layer, with a void ratio exceeding 0.70. Subsequently, samples represented by the three types of control were collected for the analysis of undrained and drained triaxial test behaviors, aiming to support the design criteria for a Filtered Tailings Disposal Stack.

Mechanical Performance of Compacted Layers Inside and Outside the Target Moisture Range and with Low Compaction

The analysis of mechanical behavior will be carried out through undrained and drained triaxial tests, using properly saturated samples, analyzing three types of graphs: pore pressure vs. deformation curves, volumetric variation vs. deformation curves, and the effective stress paths p' and q, of the undisturbed samples with void ratios below 0.60 (target range), between 0.60 and 0.70 (outside the target range), and of the samples with void ratios above 0.70.

First, the results of tests on the compacted layers within the target moisture range (Type I), exhibiting better compaction performance and void ratio below 0.60.

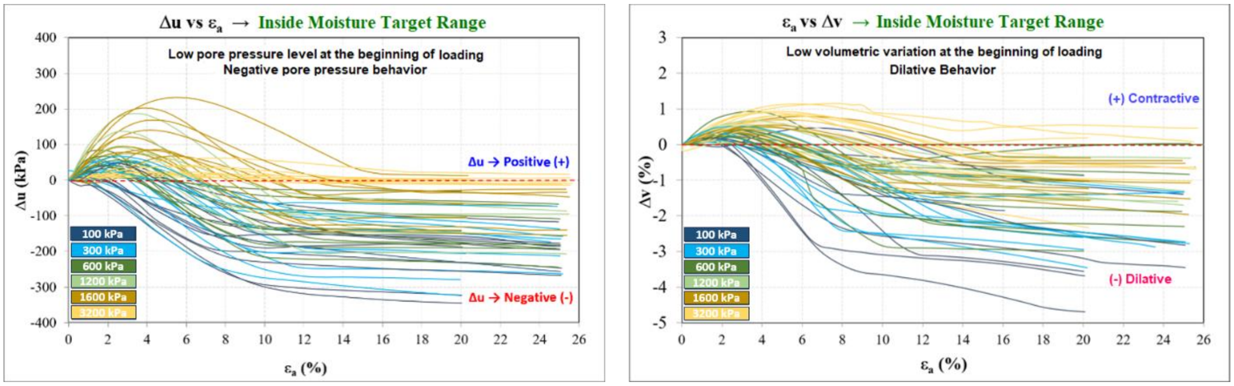

Figures 7: Results of CIU and CID triaxial tests - Pore pressure variations (a) and volumetric variations (b) - Compaction Control Type I.

Figures 7a, b exhibited satisfactory behaviors of the samples collected from the compacted layers within the target moisture range, displaying, after initial contraction, increments of negative pore pressure or volume increase during loading (dilation), for confinement stresses ranging from 100 kPa to 3,200 kPa, with the exception of some samples that showed a contractive regime throughout the entire test under higher stresses.

Intermediate behavior, Type II, illustrated in Figures 8a, b with void ratio variations between 0.60 and 0.70 (compaction outside the target moisture range), presented an excess of positive pore pressure up to deformations of 5-10%, mainly for stresses above 600 kPa, followed by a variable reduction in deformations beyond 10%, and the opposite occurred for low confinement stresses, as demonstrated in the Figures below. This rather erratic pattern of compacted reject outside the target moisture range draws attention to sectorization in the conception of the tailings stack design (confined zone).

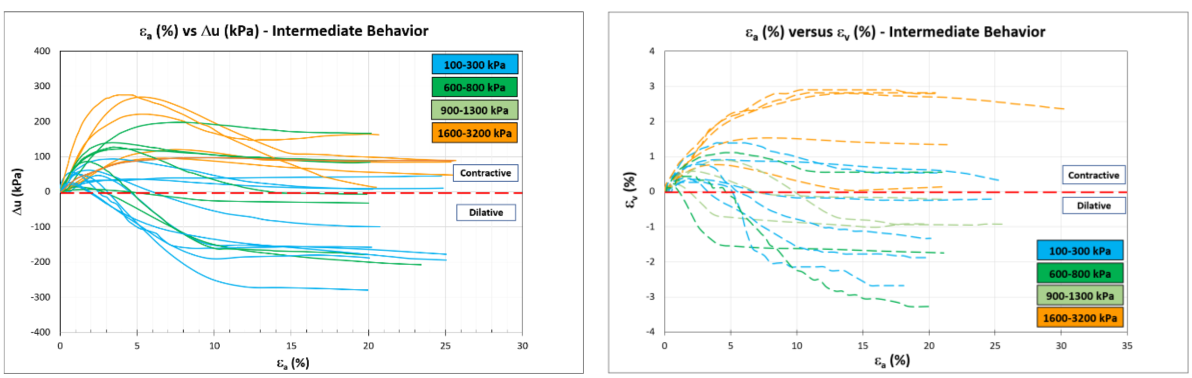

Figures 8: Results of CIU and CID triaxial tests - Pore pressure variations (a) and volumetric variations (b) - Compaction Control Type II.

Lastly, the behavior of a layer spread over 50cm - Type III was not effective, as expected, and is not recommended to constitute the structural zone of a filtered tailings stack. This condition simulates layers with low compaction, resulting in a significant loss of strength associated with high rates of pore pressure generation and high volumetric variation (contraction), as shown in the figures below.

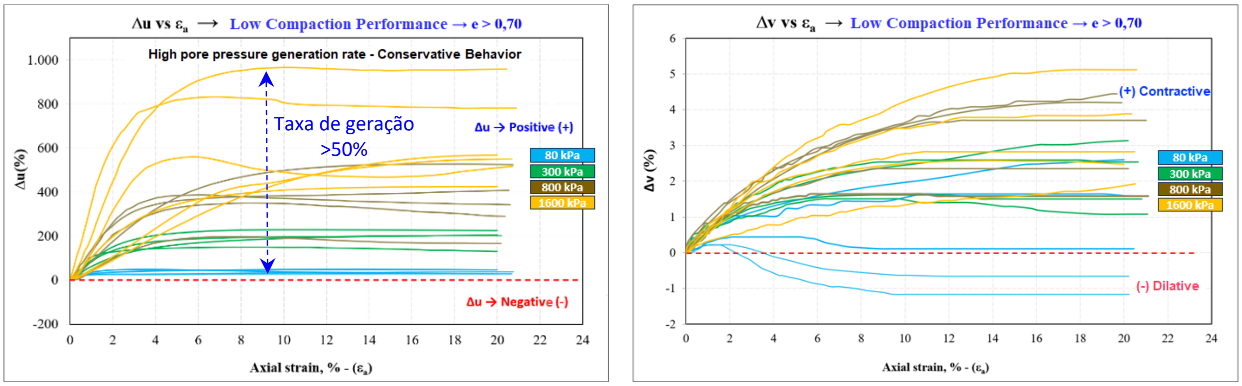

Figures 9: Results of CIU and CID triaxial tests - Pore pressure variations (a) and volumetric variations (b) - Type III Compaction Control (low compaction).

The stress paths of the undrained triaxial tests were interpreted according to the MIT definition, where p' is the mean effective stress, $p'=(\sigma'1+\sigma'3)/2$, and q is the shear stress, $q=(\sigma'1-\sigma'3)/2$. This interpretation illustrates a comparative analysis between the compacted samples within the target moisture range and the compacted samples outside this target range (Fig. 10a) and also a comparison between the compacted samples within the target moisture range and the samples with void ratios above 0.7 (Fig. 10b).

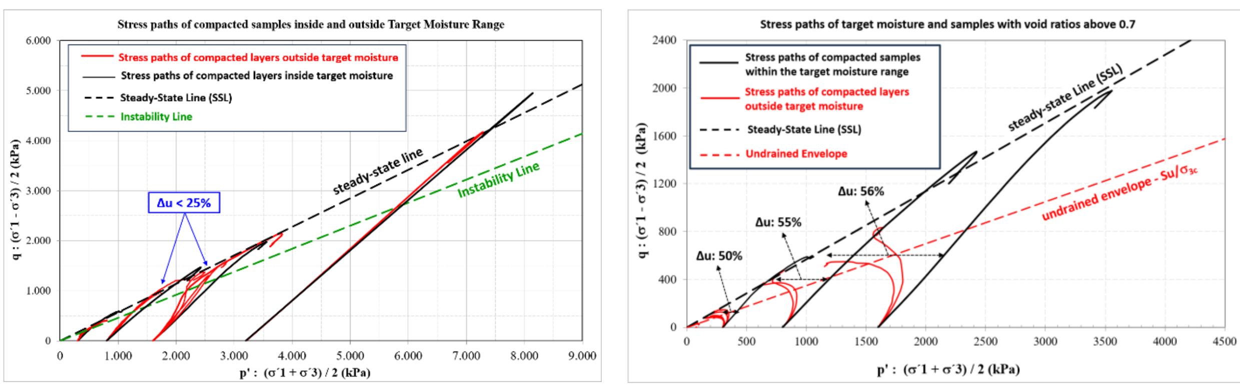

Figures 10: Comparison of stress paths from CIU tests of compacted samples within the target moisture range with compacted samples outside the target moisture range (a), and also with samples that have void ratios above 0.7 (b)

Figure 10a presents the envelope that delimits a narrow zone of potential instability, observed through the stress paths of samples compacted outside the target moisture range, and determined by q and p' at the maximum pore pressure between 4% and 6% deformation, close to the steady-state Line (SSL). It is worth mentioning that in this case, the samples compacted outside the target moisture range did not show indications of instability under stress states above the instability line.

Figure 10b presents a comparison between stress paths of samples with void ratios above 0.7 (low compaction) and samples within the target range, void ratios lower 0.60. Notably, a high pore pressure rate above 50% is observed. In this case, the undrained strength envelope is determined by q_{max} e σ_{3c}, deviating from the Steady State Line (SSL) due to significant losses in effective stresses. This represents an undesirable behavior for structural zone areas (strict compaction control) of a Filtered Tailings Stack.

Cruz (1996) and Maiolino (1985) present the main behaviors of compacted soils (deviator stress vs. strain, pore pressure vs. strain, and stress paths) in undrained triaxial tests. The figures below depict some types of behavior similar to the behaviors identified in the compaction controls of the tailings.

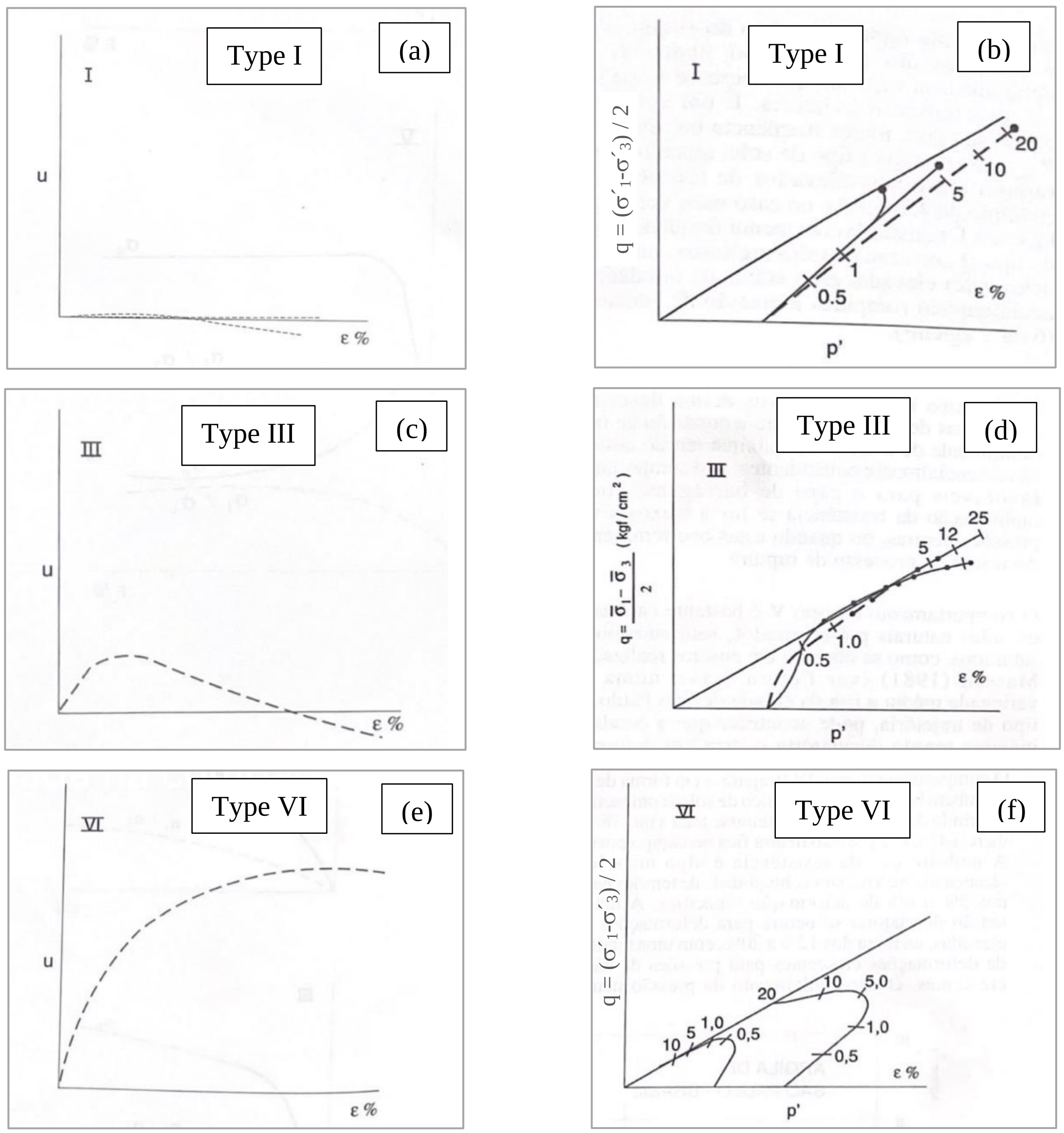

Figures 11: Present the behaviors of undrained triaxial tests of compacted soils Type I (a and b), Type III (c and d) and Type VI (e and f).

In the mentioned behaviors above, the similarity of type I (Cruz, op. cit.) is observed with the type I of compacted tailings within the target moisture range, exhibiting a trajectory similar to drained tests. The type III (Cruz, op. cit.) behavior is similar to the intermediate behavior, type II, of the tailings. Lastly, the type VI, resembling the tailings with low compaction (type III), exhibits high rates of pore pressure. This latter mechanical behavior is considered entirely unfavorable for an engineered landfill.

Another important technical aspect in the analysis of mechanical behavior is the determination of construction controls for the tailings stack through the interpretation of the critical state line or range (CSL). In relation to this aspect, the tests that reached the critical state condition (constant pore pressure and constant volumetric variation) were considered.

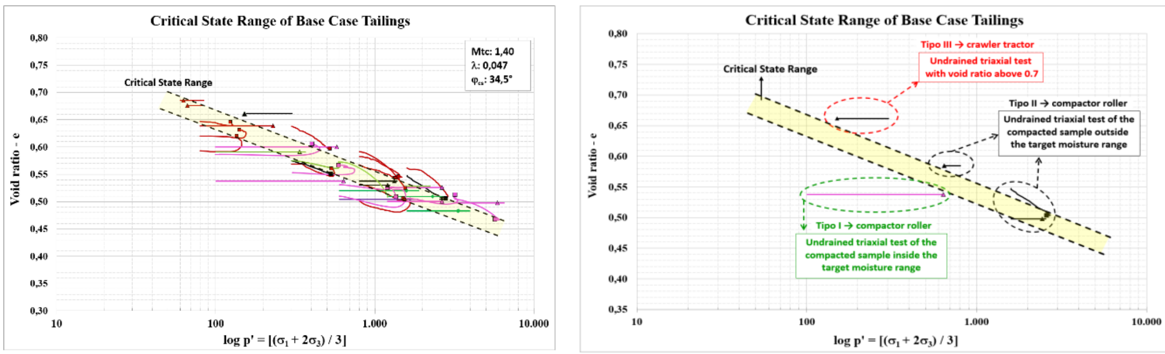

Figures 12: Range that delimits the 'locus' of the critical state (a) and behaviors of tests for the three types of compaction control relative to the critical state (b).

In Figure 12a, it's possible to interpret the maximum void ratios for the effective mean stresses of the waste stack design (base case) and determine the critical state parameters. Figure 12b illustrates the three types of behaviors studied: Type I illustrates how the compacted layers within the target moisture range are far from the critical state range on the dense side. In Type II behavior, the achieved densification state was adequate, but it exhibits a slight decrease in effective stress or is situated within the CSL range or very close to the CSL.

On the other hand, Type III exhibits high positive pore pressure or significant volumetric contraction, with a notable loss of effective stress in the undrained condition and contraction in the drained test.

Conclusion

The mechanical behavior of the mixtures of sandy and ultrafine tailings (base case) was analyzed through an extensive campaign of undrained and drained triaxial tests on undisturbed samples collected from compacted layers in the experimental landfill and laboratory-molded samples representing an uncompacted layer.

The study highlights the importance of conducting tests on experimental landfills to understand the variations in tailings within the operational context of the mine and Filtration Plant, as well as to gain insights into the performance of the compaction processes carried out under different compaction control methods (moisture ranges and energy variations). The main behaviors interpreted from the results of the triaxial tests were classified according to compaction types for the "baseline case" tailings, as below:

Type I Behavior - void ratio < 0.60: Behavior with negative pore pressures in undrained tests that essentially replicate the stress paths of drained tests for confinement stresses up to 3,200 kPa. A few samples from this group exhibited volumetric reduction under higher stresses, potentially due to micro-mechanism effects, which remain undetermined in strength tests. This is an aspect that deserves specific study. The strength envelope is determined by the permanent state line, and the indicated compaction control for a structural zone in a filtered tailings stack;

Type II Behavior - void ratios - 0.60 < e < 0.70: Behavior with low excess pore pressure generation at the beginning of loading, followed by reduction, with an increase in the mean effective stress. Stress paths are characterized by an "S"-shaped behavior, and their effective strength envelope, at the apex of the effective stress path (p' vs q), occurs between 4 and 6% deformation. This compaction control can be accepted during rainy or extremely dry seasons, as long as the typical cross-section of the project determines a structural "shell" with sufficient thickness to accommodate this condition in a confined, internal area of the Filtered Tailings Stack.

Type III Behavior – Low compaction - void ratio > 0,70: Behavior with excessive positive pore pressure throughout the entire undrained loading, while in drained tests, volume reduction occurs for all confinement stresses up to 3,200 kPa. Such behavior is characteristic of undrained strength, always lower than drained strength, representing an unfavorable and not recommended condition for a structural zone in a filtered tailings stack.

Finally, the study reinforces that the compaction of tailings in the "base case," with compaction controls both within and outside the target moisture range, the latter under special conditions, can be applied in Filtered Tailings Stacks, considering the zoning between the structural zone (void ratio < 0.60), with width provenly sufficient for all stability analysis scenarios, with the confined zone (void ratio between 0.60 and 0.70). On the other hand, compaction control with a crawler tractor (low compaction) should be avoided as a construction control for an engineering landfill and may be eventually considered, as long as it is restricted to an area with no structural function.

Acknowledgements

I would like to thank the technical teams of BVP Geotechnics and Hydrogeotechnics (both office and field) for their dedicated efforts in interpreting and assessing the results of field and laboratory tests, along with the technical team from Vale's experimental landfill area.

References

BVP Engenharia e Hidrotecnia, 2023, Relatório Final Aterros Experimentais. P.429.

CRUZ, Paulo Teixeira da. 1996. 100 barragens brasileiras: casos históricos, materiais de construção, projeto. Tipologia de solos compactados. São Paulo, ed. 2004. pp. 206-235.

Maiolino, A. L. G. (1985). Resistência ao cisalhamento de solos compactados: Uma proposta de tipificação. Thesis research, Federal University of Rio de Janeiro, COPPE.

Stabilization of iron tailings with alkali activated binders.

Isabela Caetano, Construct-GEO, Faculdade de Engenharia, Universidade do Porto - FEUP, Portugal
Sara Rios, Construct-GEO, Faculdade de Engenharia, Universidade do Porto - FEUP, Portugal
António Viana da Fonseca, Construct-GEO, Faculdade de Engenharia, Universidade do Porto - FEUP, Portugal
Bruno Delgado, Construct-GEO, FEUP. Corporate Geotechnics Department, Vale S/A, Brazil

Abstract

Mine tailings are a challenge for the mine activity as they need to be managed and disposed safely. One common solution is the disposal in upstream tailing dams, which have been discouraged and even prohibited in Brazil due to recent accidents with environmental and human loses. Alternatively, dry stack of filtered tailings is gaining market, and many studies are being developed on this subject. Although this solution seems to assure higher safety factors due to the lower water content of the filtered tailings in comparison to the slurry disposed in dams, failures have also occurred on these structures. The dry stack stabilisation can be ensured with a berm of cemented filtered tailings, typically with Portland cement. To reduce the environmental impact, in this work Portland cement (whose production releases a large amount of CO_2) has been replaced by an alkali activated binder (AAB), using fly ash and a sodium hydroxide solution. The use of sodium silicate, very common in AAB, was not considered due to its higher carbon footprint. This work presents an optimisation study to obtain the best mixture of an iron tailings and the AAB. For this purpose, a statistical approach based on the design of experiments was used considering three main variables: the liquid content, the fly ash content, and the sodium hydroxide concentration. Uniaxial Compression Strength (UCS) tests at 7 days of curing time were performed in specimens moulded in different conditions and the mixture with a higher strength was selected for further analysis. This in-depth study includes the evaluation of UCS and elastic stiffness evolution with curing time. This later was assessed by measuring the shear waves propagation time with ultrasonic piezoelectric transducers. The curing temperature was found to have a significant influence on strength and stiffness evolution.

Introduction

The tailing deposition

An alternative to the disposal in tailing dams is the deposition in dry stacks, where filtered tailings are placed in embankments with much lower water contents than the slurry deposited in dams. In dry stacks, compaction is possible which is an advantage in comparison to the dam, where tailings are deposited in a hydraulic fill. However, these stacks also have their limitations, since the filtered tailings water content is usually higher than the optimum water content of Proctor compaction curve (Davies, 2011). Considering the usual need to achieve very large embankment heights, high effective stresses can be mobilized at the base of the dam and the material is often on the wet side of the critical state line being, therefore, contractile upon shear. Therefore, the undrained instability observed in liquefaction phenomena is also a concern in these structures. A possible solution under study is the stabilization with cemented berms, made by the mixing the filtered tailings with a binder such as Portland cement (Carvalho *et al.* 2023).

The environmental impact of Cement Portland

The most common binder used for this purpose is the Portland cement. However, its use is currently discouraged due to its carbon footprint. According to data from WBCSD (2002) about 3% of global greenhouse gas emissions and approximately 5% of CO_2 emissions were cement industry responsibility. In addition to the high amount of CO_2 released in the clinker production (40%), there is still a significant amount generated by the production process (50%), by transport (5%) and using electricity (5%). Consequently, this industry has a high polluting potential. Taking this into account, it is our responsibility to seek for more eco-friendly alternatives and economically viable.

The alternative: alkali activated binders

Considering the need to reduce the environmental impact, an alternative binder has been studied made by the alkali activation of industrial wastes (called herein AAB). AAB are obtained by a chemical reaction between aluminosilicate materials – precursors – with alkali or alkali-based earth – activators – generating polymeric bonds Si – O – Al (Pinheiro *et al*., 2020). The precursors must be rich in silicon and aluminium, so the fly ash fits. Activators originate from alkaline soluble metals, most often based on sodium and potassium (Wallah & Rangan, 2006). This reaction leads to the formation of a gel, which is called C-A-S-H (2D structure) when the calcium content is significant, and N-A-S-H (3D structure) when this content is low (Davidovits, 2005). This gel allows the system reorganization due to increased network connectivity, resulting in a three-dimensional network of aluminosilicate associated with the geopolymer (Duxson *et al*., 2007).

Some studies have been published regarding the application of AAB to soils (Glendinning *et al*., 2011; Sukmak *et al*., 2013; Rios *et al.*, 2017; Rios *et al*., 2019; Pinheiro *et al*., 2020) and mine tailings (Xu, 2013; Manjarrez & Zhang, 2018; Obenaus-Emler *et al*., 2020; and Cristelo *et al*., 2020).

Statistical model

In order to minimize the amount of laboratory experiments, a statistical plan was carried out known as Response Surface Method (RSM) (Rivera *et al.*, 2019; Pinheiro *et al*., 2020). The conventional way to obtain the optimized mixture would be to change the amount of each constituent at a time (complete factorial plan), which leads to a high number of specimens to be made and tested. In addition, this method does not allow the identification of interactions between variables. In this work, a composite plan of centered face was used, that is, the axial points are at the center of each face of the factorial space (Anderson & Whitcomb, 2016). This approach has been used not only for the optimized mixture identification, but also for the main variables and outliers' values identification. Three input variables were considered – ash content (A); liquid content (B); and activator concentration (C). The ash content is the ash weight divided by the dry soil weight; the liquid content is obtained by the ratio of liquids divided by the solids of the mixture; and the activator concentration, being, in this case, the concentration of the sodium hydroxide (SH) solution. The range defined for each input variable was 0.1 to 0.3 for (A); 0.14 to 0.17 for (B); and 5 to 11.76 mol/kg for (C). Although a wide research plan is ongoing, in this paper the first phase of the testing plan, comprising 11 specimens, is presented which already shows significant differences between treated and untreated specimens. The main output variable considered for analysis was unconfined compressive strength (UCS).

Methodology

Materials

Iron tailings from Minas Gerais (Brazil) was used in this work, whose grain size distribution curve can be seen in **Figure 14**. The particles unit weight (γ_S) is quite high (29.5 kN/m^3) when compared to natural soils due to the iron content. The tailings did not present plasticity and liquidity limits, being classified as non-plastic (NP). The precursor used in this work is type F ash, i.e., with low lime content (< 5 %). It has in its composition: SiO_2 (54.84 %), Al_2O_3 (19.46 %), Na_2O (1.65 %) and CaO (4.68 %). Typically, activators are composed by the combination of sodium hydroxide (SH) and sodium silicate (SS). In this study, the use of SS was eliminated since its fabrication process also has a great environmental impact. The SH solution consists of 32 % NaOH and 68 % water, with a concentration of 11.76 mol/kg, which was diluted for the lower concentrations.

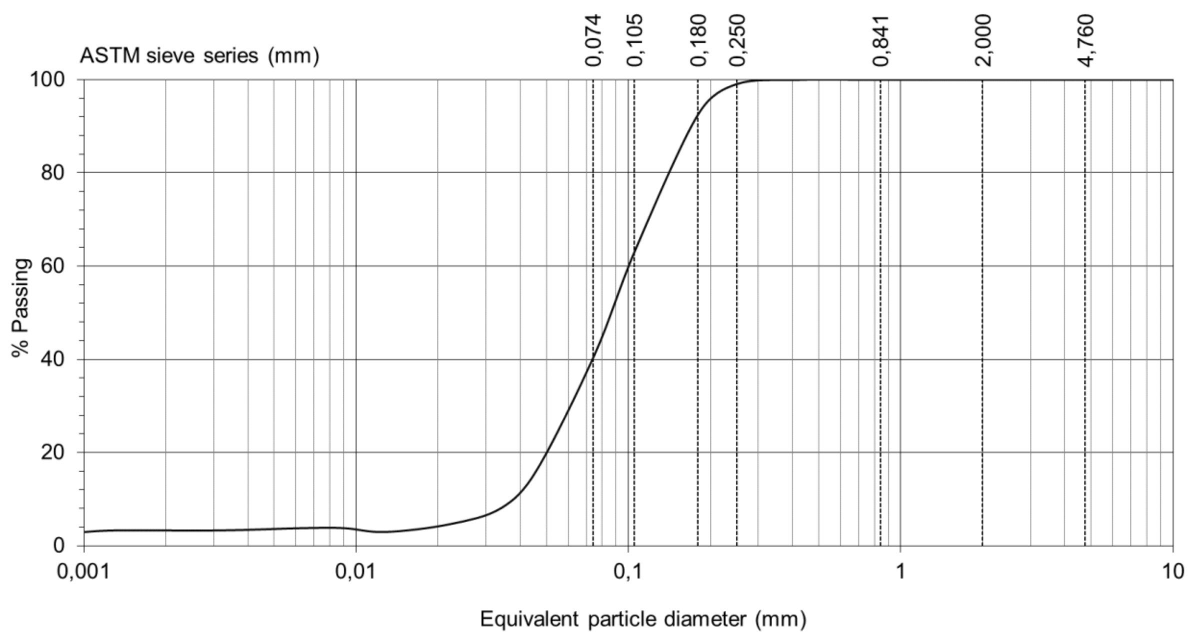

Figure 14: Iron tailing grain size distribution curve

Sample preparation

Molds of 38 mm in diameter and 65 mm in height were used for the specimen preparation. The tailings were initially oven dried to allow the moisture control. However, as filtered tailings still have a significant water content a fixed quantity of water was added to the soil. In this case this amount was fixed to 15 ml, which corresponds to a water content between 14 % and 17 % depending on the ash content. Thus, alkali activation was tested for different soil moistures. Because of this water addition, the SH concentration was eventually diluted.

Initially, 15 ml of water was added to the dry tailings to make them homogeneous. Then, the ash was incorporated, and, after homogenization, the SH was added. Once all the components were incorporated, the mixture was transferred into a sealed plastic container to avoid moisture loss. Compaction was performed in three equal layers to obtain the target dry unit weight (γ_d) equal 17.2 kN/m^3. The specimen extraction was carried out on the same day, being then stored for 7 days.

To study the influence of curing temperature on the specimen's strength and stiffness, some specimens were placed in a low temperature oven for 24 hours. After this time, they were stored at room temperature until the seventh day. At that time the specimens were removed from the box and wrapped in plastic film for better handling and to keep the specimen moisture.

Testing procedures

Unconfined compression strength tests were performed following ASTM D2166-06 (2006) standard for the untreated tests and the Portuguese specification (LNEC E 264, 1972) for the treated specimens, using a load cell of 20 kN of capacity and a constant rate of 0.02 mm/min, using the test setup indicated in **Figure 15**.a.

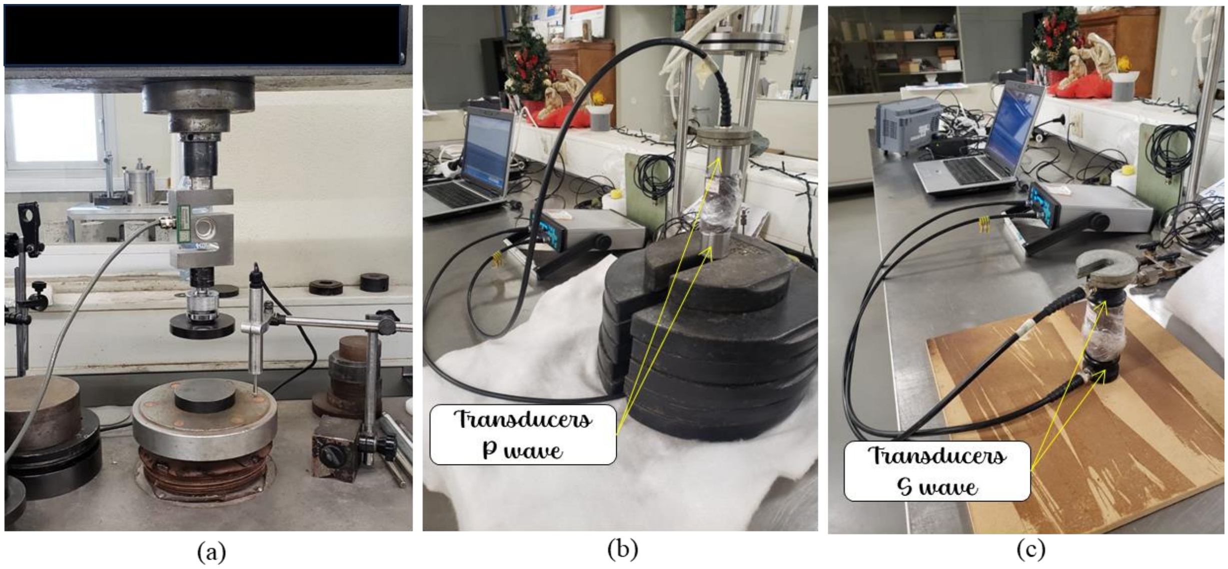

Figure 15: Performed tests configuration: a) UCS test; b) P waves reading; c) S waves reading.

Seismic wave velocities measurements were performed following EN 12504-4 (CEN, 2003), to obtain the propagation time of compression (P) and shear (S) waves towards the calculation of elastic parameters. These measurements were performed with piezoelectric ultrasonic transducers as described by Rios *et al.* (2017) and different input frequencies were used depending on the specimen type and curing time (Viana da Fonseca, Ferreira, e Fahey 2009; Ferreira *et al.*, 2021). Readings were performed at 7, 14, 21 and 28 days. The great advantage of this test is to be non-destructive, allowing to do measurements in the same specimen over the 28 days of curing time and at the end the specimen is still suitable for other tests such as a UCS test, for example. The configuration of this test can be seen in **Figure 15**.b for P waves and **Figure 15**.c for S waves.

Data and discussion

The selected mixture

After executing the statistical plan, UCS tests were performed at 7 days in the 11 mixtures. The mixtures input variables are shown in **Table 1**, where the parameter A is the fly ash content; B is the liquid content, C is the SH concentration, η is the porosity and e_0 is the initial void ratio the specimen in the moulding day. The value of the porosity in the compression day is difficult to be calculated because the liquid content varies, and it is not possible to be estimated precisely. However, all initial porosity are very close (minimum

= 0.390 and maximum = 0.430), with a differential equal 0.04. The same can be seen for the initial void ratios, with a difference equal 0.12 (minimum = 0.639 and maximum = 0.755). The UCS result of all mixtures is shown in **Figure 16**. The mixture that presented the highest strength (ID-8) was selected as optimized mixture. Its input variables are: (A) 0.30; (B) 0.17; and (C) 11.76 mol/kg. The temperature influence on strength and stiffness will be studied only in this mixture.

UCS tests were also performed on the untreated tailings according to the following compaction degrees based on Normal Proctor test – 90 %, 95 % and 100 % that comprises the void ratio 0.811; 0.716 and 0.630 respectively – and the obtained results are presented in **Figure 16** (by the horizontal lines). As there is no chemical reaction the strength does not evolve in time and so the specimens were sheared on the moulding day. It is noted that the maximum strength (40 kPa) was obtained for the highest compaction degree but is much lower than the strength obtained with the optimum treated mixture (182 kPa). Although the compaction degree of the treated specimens ranged from 90 % to 95 % of Normal Proctor, all these specimens had higher strength than the untreated soil at 100 % of Normal Proctor (with exception of mixture 1 which has slightly smaller values).

Table 1: Input parameters mixtures.

ID	1	2	3	4	5	6	7	8	15	16	21
A	0.10	0.30	0.10	0.30	0.10	0.30	0.10	0.30	0.20	0.20	0.20
B	0.14	0.14	0.17	0.17	0.14	0.14	0.17	0.17	0.16	0.16	0.16
C	5.00	5.00	5.00	5.00	11.76	11.76	11.76	11.76	8.50	8.50	8.50
η	0.430	0.412	0.410	0.394	0.424	0.391	0.395	0.390	0.394	0.411	0.403
e_0	0.755	0.700	0.696	0.649	0.737	0.642	0.652	0.639	0.651	0.699	0.675

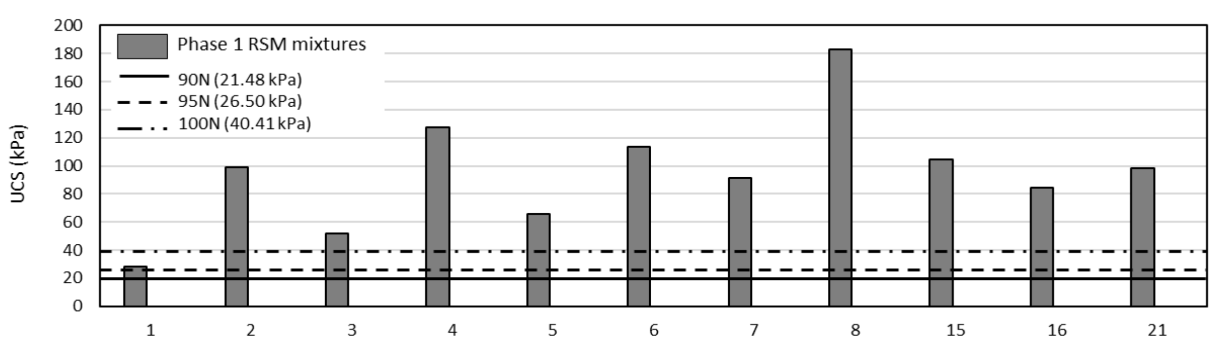

Figure 16: UCS Results.

Effect of curing temperature

Stiffness evolution

Readings of the propagation time for compression (P) and shear (S) waves were performed at 7, 14, 21 and 28 days for the specimens that were 24 hours in the low temperature oven after molding (Group 1) and for the specimens cured at room temperature (Group 2). The distance between the transducers divided by the wave propagation time gives the wave propagation velocity. From the shear wave velocity (V_S) the maximum shear modulus (G_0) can be determined by equation 1:

$$G_0 = \rho_m \times V_S^2 \quad (1)$$

where ρ_m is the mixture density obtained by the ratio between the specimen weight and its volume. The results of the stiffness evolution over 28 days of groups 1 and 2 is observed in **Figure 17**.a. The stiffness of the specimen belongs to Group 1 is already much higher at 7 days than the stiffness at 28 days of the specimen belong to Group 2. However, in percentage, the sample of Group 2 had a stiffness increase of more than 200 % (140 to 432 MPa) while the other sample (Group 1) had a stiffness increase of around 50 % (832 to 1245 MPa). It is also interesting to notice that the evolution shows a tendency to continue increasing over time.

Strength evolution

Unconfined compression strength evolution with curing time was evaluated also for the two groups of specimens (Groups 1 and 2) for 7, 14, 21 and 28 days. In mixture of Group 2 the strength increases gradually over time, totaling an increase at 28 days of 27 % compared to the value obtained at 7 days. The mixture of Group 1 showed a dubious trend. It has a high strength increase from 7 to 14 days, and then it reduces having the value of 28 days lower than that obtained at 21 days, but still higher than the initial and that all the specimens that belong to Group 2. These curves can be seen in **Figure 17**.b. A possible explanation for this observed characteristic is associated with a possible temperature variation in the oven, since the 7 and 28 days were molded in one day and those of 14 and 21 was molded in another day when the oven temperature was higher. Further studies are being conducted with greater temperature control to better understand this trend.

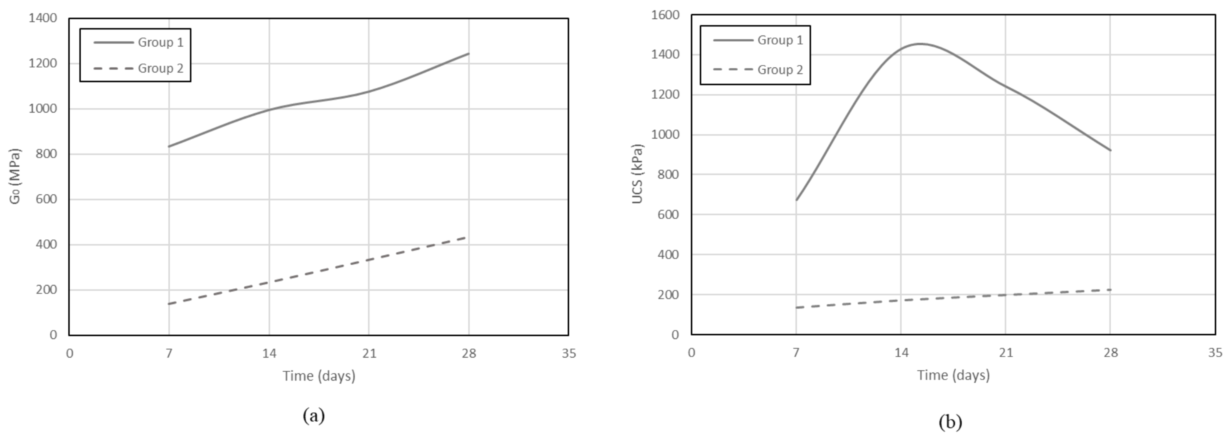

Figure 17: Evolution over 28 days: (a) Stiffness evolution; (b) Strength evolution.

Conclusion

The statistical model (RSM) facilitated the identification of the optimal mixture, since from only 11 specimens it was possible to reach a mixture with satisfactory strength well above the UCS strength obtained in the soil without treatment. Elastic stiffness evolution was almost linear for both cases cured with and without temperature, but the values cured with temperature are much higher indicating that this method is suitable for applications in hot climates. Strength also increased with temperature, although further studies are being conducted with greater temperature control to better define the UCS trend with time.

Acknowledgements

This work was financially supported by: Base Funding - UIDB/04708/2020 of the CONSTRUCT - Instituto de I&D em Estruturas e Construções, by the project INPROVE-2022.02638.PTDC, and by scholarship 2022.13858.BD, all funded by national funds through the FCT/MCTES (PIDDAC).

References

Anderson, Mark J., e Patrick J. Whitcomb. 2016. RSM Simplified: Optimizing Processes Using Response Surface Methods for Design of Experiments, Second Edition. 2o ed. New York: Productivity Press. https://doi.org/10.1201/9781315382326.

ASTM D2166-06. 2006. "ASTM D2166-06: Standard Test Method for Unconfined Compressive Strength of Cohesive Soil". https://www.astm.org/d2166-06.html.

Carvalho, João Vítor de Azambuja, A. C. Wagner, H. C. Scheuermann Filho, H. M. Chaves, J. P. S. Silva, B. G. Delgado, e N. C. Consoli. 2023. "Evaluation of Strength Parameters for Application in Cemented Iron Ore Tailings Stacks". Indian Geotechnical Journal, fevereiro. https://doi.org/10.1007/s40098-023-00712-9.

CEN. 2003. "EN 12504-4: Testing Concrete - Part 4: Determination of Ultrasonic Pulse Velocity.h". Brussels, Belgium.

Cristelo, Nuno, João Coelho, Mafalda Oliveira, Nilo Cesar Consoli, Ángel Palomo, e Ana Fernández-Jiménez. 2020. "Recycling and Application of Mine Tailings in Alkali-Activated Cements and Mortars—Strength Development and Environmental Assessment". Applied Sciences 10 (6): 2084. https://doi.org/10.3390/app10062084.

Davidovits, J. 2005. "Geopolymers: Inorganic Polymeric New Materials". Journal of Thermal Analysis and Calorimetry 37 (8): 1633–56. https://doi.org/10.1007/bf01912193.

Davies, Michael. 2011. "Filtered Dry Stacked Tailings : The Fundamentals". Em Proceedings Tailings and Mine Waste 2011. Vancouver, BC, Canadá. https://doi.org/10.14288/1.0107683.

Duxson, P., A. Fernández-Jiménez, J. L. Provis, G. C. Lukey, A. Palomo, e J. S. J. van Deventer. 2007. "Geopolymer Technology: The Current State of the Art". Journal of Materials Science 42 (9): 2917–33. https://doi.org/10.1007/s10853-006-0637-z.

E 264, Especificação LNEC. 1972. "E - 264-1972 - Solo- Cimento Ensaio de Compressão". Portugal.

Ferreira, C., S. Rios, N. Cristelo, e A. Viana da Fonseca. 2021. "Evolution of the optimum ultrasonic testing frequency of alkali-activated soil–ash". Géotechnique Letters 11 (3): 158–63. https://doi.org/10.1680/jgele.21.00041.

Glendinning, Stephanie, Amândio Pinto, e Nuno Cristelo. 2011. "Deep soft soil improvement by alkaline activation". Proceedings of the ICE - Ground Improvement 164 (maio): 73–82. https://doi.org/10.1680/grim.900032.

Manjarrez, Lino, e Lianyang Zhang. 2018. "Utilization of Copper Mine Tailings as Road Base Construction Material through Geopolymerization". Journal of Materials in Civil Engineering 30 (9): 04018201. https://doi.org/10.1061/(ASCE)MT.1943-5533.0002397.

Obenaus-Emler, R., M. Falah, e M. Illikainen. 2020. "Assessment of Mine Tailings as Precursors for Alkali-Activated Materials for on-Site Applications". Construction and Building Materials 246 (junho): 118470. https://doi.org/10.1016/j.conbuildmat.2020.118470.

Pinheiro, Claver, Sara Rios, António Viana da Fonseca, Ana Fernández-Jiménez, e Nuno Cristelo. 2020. "Application of the Response Surface Method to Optimize Alkali Activated Cements Based on Low-Reactivity Ladle Furnace Slag". Construction and Building Materials 264 (dezembro): 120271. https://doi.org/10.1016/j.conbuildmat.2020.120271.

Rios, Sara, Nuno Cristelo, António Viana da Fonseca, e Cristiana Ferreira. 2017. "Stiffness Behavior of Soil Stabilized with Alkali-Activated Fly Ash from Small to Large Strains". International Journal of Geomechanics 17 (3): 04016087. https://doi.org/10.1061/(ASCE)GM.1943-5622.0000783.

Rios, Sara, Catarina Ramos, António Viana da Fonseca, Nuno Cruz, e Carlos Rodrigues. 2019. “Mechanical and durability properties of a soil stabilised with an alkali-activated cement”. European Journal of Environmental and Civil Engineering 23 (2): 245–67. https://doi.org/10.1080/19648189.2016.1275987.

Rivera, Jhonathan F., Nuno Cristelo, Ana Fernández-Jiménez, e Ruby Mejía de Gutiérrez. 2019. “Synthesis of Alkaline Cements Based on Fly Ash and Metallurgic Slag: Optimisation of the SiO2/Al2O3 and Na2O/SiO2 Molar Ratios Using the Response Surface Methodology”. Construction and Building Materials 213 (julho): 424–33. https://doi.org/10.1016/j.conbuildmat.2019.04.097.

Sukmak, Patimapon, Suksun Horpibulsuk, e Shui-Long Shen. 2013. “Strength Development in Clay–Fly Ash Geopolymer”. Construction and Building Materials, Special Section on Recycling Wastes for Use as Construction Materials, 40 (março): 566–74. https://doi.org/10.1016/j.conbuildmat.2012.11.015.

Viana da Fonseca, António, Cristiana Ferreira, e Martin Fahey. 2009. “A Framework Interpreting Bender Element Tests, Combining Time-Domain and Frequency-Domain Methods”. Geotechnical Testing Journal 32 (2): 91–107. https://doi.org/10.1520/GTJ100974.

Wallah, Steenie, e B. Rangan. 2006. “Low-Calcium Fly Ash-Based Geopolymer Concrete: Long Term Properties”. Curtin - University of Technology.

WBCSD, World Business Council for Sustainable Development. 2002. “Battelle Scoping Study: Toward a Sustainable Cement Industry”. Geneva, Switzerland. https://www.wbcsd.org/rl0uf.

Xu, Shuai. 2013. “Research on Application of Iron Tailings on Road Base”. Advanced Materials Research 743: 54–57. https://doi.org/10.4028/www.scientific.net/AMR.743.54.

Session 3:

Stability analysis and safety assessment

Reliability-Based Analysis Of Tailings Storage Facilities. A Case Study: Cadia NTSF Embankment Failure

Benedikt Schatz, Vulcan Energie Ressourcen GmbH, Germany
Previously at Center for Geotechnics, Technical University of Munich, Germany
Andrés A. Peña-Olarte, Center for Geotechnics, Technical University of Munich, Germany
Ana Ribera, Center for Geotechnics, Technical University of Munich, Germany
Joshua Schorr, Center for Geotechnics, Technical University of Munich, Germany
Iason Papaioannou, Engineering Risk Analysis Group, Technical University of Munich, Germany
Roberto Cudmani, Technical University of Munich, Germany

Abstract

The frequent catastrophic failures of tailings storage facilities (TSFs) have raised concerns about the adequacy of current design methods and guidelines, highlighting the need for a more comprehensive approach to assessing TSF stability. Integrating reliability-based approaches with conventional deterministic analyses can contribute to a more thorough examination of the inherent uncertainty in geotechnical problems and the assessment of the reliability of a system. This study introduces basic concepts of probabilistic stability analysis and showcases their application in investigating the Cadia Northern TSF embankment failure that occurred on March 9, 2018. The joint probability distribution of the shear strength parameters is employed to select their characteristic values in a deterministic Factor of Safety (FoS) calculation, as well as to conduct a full probabilistic stability analysis. The probabilistic analysis was conducted using the First-Order Reliability Method (FORM) and the Model-Correction-Factor Method. In the latter approach the results of the simplified Limit Equilibrium Method (LEM) used in FORM are corrected based on a validated Finite Element Method analysis. Both drained and undrained conditions are examined. Under drained conditions the required FoS using the deterministic LEM analysis was achieved with the characteristic strength parameters, however the reliability analysis revealed an insufficient reliability or a high probability of failure. Under undrained conditions, the post-liquefaction FoS drops below 1.0 and the probability of failure is equal or greater than 0.5.

Introduction

Tailings Storage Facilities (TSFs), essential for waste containment in mining, frequently suffer catastrophic failures, such as the notable Cadia Northern TSF (NTSF) failure in 2018. These incidents highlight the well-known challenges and to some extent, the inadequacy of existing design methods and guidelines for the stability assessment of TSFs (Franks et al., 2021). The Cadia Valley Operations failure in 2018, resulted in a massive slump of about 280 m width and the immediate release of 720,000 m^3 of tailings. The geological complexity, characterized by Ordovician Forest Reef Volcanics (FRV) and Tertiary Basalt, contributed to the intricate factors behind the failure (Jefferies et al., 2019). Current design methods rely on deterministic analyses that overlook uncertainties inherent in geotechnical systems due to factors like spatial variability and incomplete knowledge. Complex soil behaviour and parameter uncertainties make advanced numerical analysis and reliability-based approaches essential (Baecher & Christian, 2003), (Wiley & Mah, 2004).

This study addresses these limitations using the Cadia NTSF failure as a case study. It involves a re-evaluation of existing shear strength data, and the derivation of bivariate probability distributions through Maximum Likelihood Estimate (MLE) and Method of Moments (MOM). The probabilistic reliability analysis is performed using the First-Order Reliability Method (FORM) on an idealized Limit Equilibrium Method (LEM) model. A Finite Element Method (FEM) model is then introduced, and the LEM and FEM models are combined through the Model-Correction Factor Method (MCFM). More details are available in Schatz (2023).

Overview of Cadia NTSF Failure

Cadia Valley Operations is a gold and copper mining and processing facility in New South Wales, Australia. On March 9, 2018, a 280 m long section of the NTSF slumped, resulting in a displaced volume of 720 000 m^3. The regional geology is complex and dominated by the FRV and Tertiary Basalt. These rocks have locally developed strong weathering to an extent where they are characterized as “soil-like” materials.

Figure 1 shows a cross-section through the dam at the location of failure. The geometry was simplified for the current analysis so that only foundation (purple), rockfill (yellow) and tailings (green) remain. This simplification did not have a significant influence on the factor of safety (FoS) based on the comparison with the report of the Independent Technical Review Board (ITRB) commissioned to investigate the NTSF failure (Jefferies et al., 2019). The ITRB found a strain-weakening layer, Unit A, in the FRV at the location of failure. This layer yielded during the stagewise construction of the dam. Shortly before failure, ongoing construction works included the construction of a buttress supporting the upstream raises and the stripping at the dam’s toe. This led to increased displacements of the dam, which in turn triggered a static liquefaction of the tailings, leading to a rapid collapse.

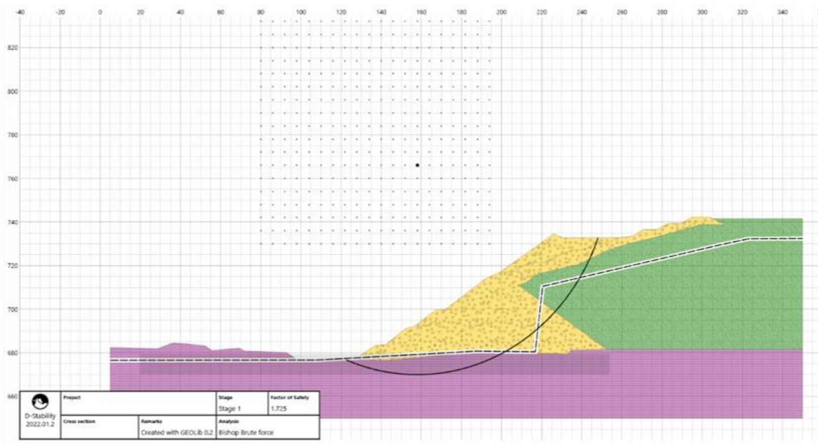

Figure 18 : Cross-section at failure location from LEM software Deltares D-Stability

From the ITRB's report and previous investigations, the publicly available geotechnical data is presented in Table 1.

Table 2 : Available test results and literature values used in this study

Stratigraphy	Pre-Failure	Post-Failure	Literature
Foundation	10x CIU	17x CIU, 13x DSS	-
Rockfill	-	-	25x φ'_{peak} (CID)
Tailings	13x CPTu	-	-

Fundamental Concepts of Probabilistic Stability Analysis

Uncertainty In Slope Stability Analysis

Uncertainty in the context of geotechnics can be grouped in (i) natural variability, such as spatially varying extent of weathering, (ii) knowledge uncertainty, for example from site characterization and selection of parameters; and (iii) decision model uncertainty, which includes uncertainties from operation, and decisions (Baecher & Christian, 2003). This study focuses on knowledge uncertainty about soil strength parameters.

Any model input parameter can be represented by a fixed value or a probability distribution. Typically, values are chosen sufficiently far on the conservative side so that worse values are unlikely. Probability distributions allow insights into the entire range of parameters, the likelihood of exceeding or falling below certain values, and enable modelling correlations between parameters. For example, friction angle and cohesion are typically negatively correlated (Lumb, 1970). Neglecting the joint probability is on the conservative side leading to uneconomical designs and a waste of resources.

Fitting Probability Distributions

The MLE method (Fisher & Russell, 1922) is a standard approach for parameter estimation of a chosen distribution model. The basic idea of MLE is to estimate the parameters $\boldsymbol{\theta}$ that are most likely to have generated the data under the chosen model $f_X(x|\boldsymbol{\theta})$. The likelihood function is defined as the probability density of the data conditional on the parameters. Assuming that the data are independent observations of the underlying soil property X, the likelihood function is given by:

$$L(\boldsymbol{\theta}) = \prod_{i=1}^{n} f_X(x_i|\boldsymbol{\theta})$$

Finding the best estimate $\widehat{\boldsymbol{\theta}}$ of the parameters $\boldsymbol{\theta}$ is now solved by maximizing $L(\boldsymbol{\theta})$.The value of the likelihood allows to choose the best parameter estimate of the probability distribution and to compare the fit of different distribution types. Among several models, the one with the largest likelihood is chosen.

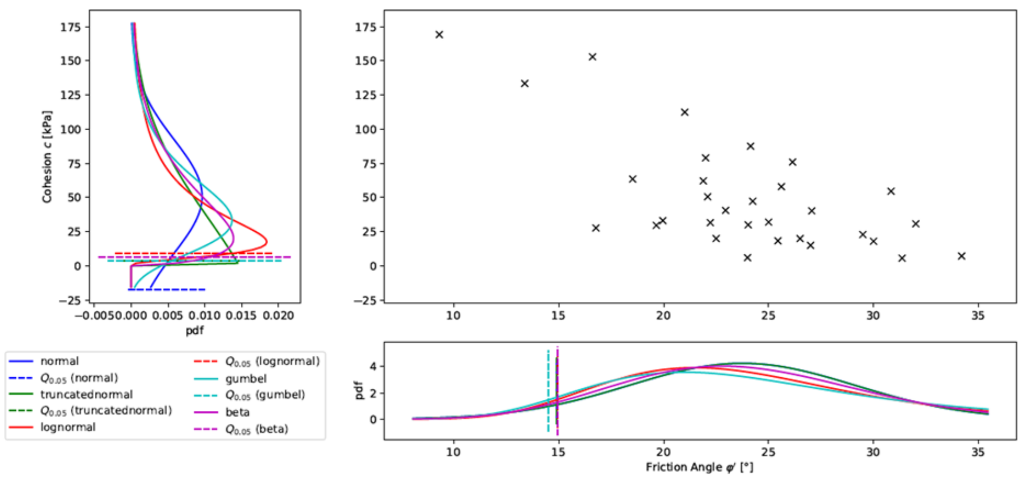

Figure 19 : MLE for all data drained peak shear strength

While the MLE also applies to multivariate random variables, a simplified approach is used in this study for bivariate random variables. In the first step, the marginal distributions are fitted using the MLE method. The correlation is approximated using MOM. Then the joint distribution is defined by a Gaussian copula through a Nataf iso-probabilistic transformation (Nataf, 1962). The described procedure is depicted in Figure 2, which shows the scattered data and the marginal MLEs together with marginal 5%-quantiles for different choices of the marginal distribution models. The data shows a clear negative correlation.

Probability of Failure

The limit state is defined as the hyperplane that separates the parameter space in a safe region (stable structure), and an unsafe region, where the analysis suggests failure. The probability that a randomly selected set of parameters lies within the unsafe region is the probability of failure. In most geotechnical applications, the stability analysis cannot be represented by an analytical model, hence the probability of failure must be approximated numerically.

The Monte-Carlo method, first introduced by Metropolis and Ulam (1949), approximates the entire parameter space by many randomly generated discrete samples, which follow the distributions of the underlying random variables. The stability analysis is solved for each sample, and the probability of failure is estimated as the proportion of samples leading to failure. This approach requires a large number of samples and corresponding solutions of the stability analysis.

Repeated evaluation for hundreds of samples is not feasible for computationally expensive models, such as FEM. In these cases, FORM allows a good approximation of the problem's reliability with a significantly smaller number of evaluations. The method was first introduced by Hasofer and Lind (1974) and generalized by Rackwitz and Flessler (1978). They applied an iso-probabilistic transformation of non-normal random variables to an equivalent standard normal space so that the original method can be used for general problems. In the standard-normal space the limit state is approximate by a first-order Taylor expansion at the most-probable failure point. The most-probable failure point is found iteratively, as the point with the shortest distance β to the origin. β is the FORM reliability index and is used to obtain an approximate probability of failure.

Model-Correction-Factor Method

The MCFM, as presented by Ditlevsen and Arnbjerg-Nielsen (1994), is used for reliability analysis of computationally expensive models. As a full probabilistic analysis using a more realistic and complex model g_r, such as FEM, might not be feasible due to the great computational effort (Ureel and Momayez 2014), an idealized model g_i is used to perform the probabilistic analysis. The elaborate model is evaluated only at a few deterministic points to determine the effectivity factor $\nu(\boldsymbol{x})$.

In this study, the more realistic model $g_r(\boldsymbol{x}_S, \boldsymbol{x}_R, \boldsymbol{x}_D) = SRF(\boldsymbol{x}_S, \boldsymbol{x}_R, \boldsymbol{x}_D) - 1 = 0$ is represented by a FEM model, using the shear strength reduction method (SSR), which results in the shear strength reduction factor (SRF). The idealized model $g_i(\boldsymbol{x}_S, \boldsymbol{x}_R, \boldsymbol{x}_D) = FoS(\boldsymbol{x}_S, \boldsymbol{x}_R, \boldsymbol{x}_D) - 1 = 0$ is given using the FoS from an LEM analysis. The effectivity factor is defined as:

$$\nu(\boldsymbol{x}) = \frac{\mathrm{SRF}(\boldsymbol{x}_S, \boldsymbol{x}_R, \boldsymbol{x}_D)}{\mathrm{FoS}(\boldsymbol{x}_S, \boldsymbol{x}_R, \boldsymbol{x}_D)}$$

where $\boldsymbol{x}_S$ and $\boldsymbol{x}_R$ are all parameters that contain the unit of force, of which $\boldsymbol{x}_R$ are the random variables in the calculation of FoS and SRF, e.g. shear strength. This deviates from the traditional definition of x_S, loads, and x_R, resistance, because in slope stability analysis the shear strength appears in both, the acting and the resisting, stresses. $\boldsymbol{x}_D$ denotes all remaining parameters, e.g., dimensions.

The effectivity factor corrects the idealized model's strength parameters so that it is equivalent to the more realistic model in the probability of failure (Ditlevsen & Arnbjerg-Nielsen, 1994). It can be determined by an iterative approach using a starting value for the effectivity factor ν_0:

1. Perform the reliability analysis using FORM on the idealized LEM model, with $g_{\mathrm{i}}(\boldsymbol{x}_S, \boldsymbol{\nu}_{\boldsymbol{k}}\boldsymbol{x}_R, \boldsymbol{x}_D) = 0$ as the limit state function, where k denotes the iteration step. This results in the most-probable failure point x_{k+1} and the probability of failure p_{k+1}
2. Solve the SSR for $\mathrm{SRF}_{\mathrm{k+1}}$ using the FEM model at the most-probable failure point $\boldsymbol{x}_{k+1}$ $g_r\left(\mathrm{SRF}_{\mathrm{k+1}}\boldsymbol{x}_{S,k+1}, \boldsymbol{x}_{R,k+1}, \boldsymbol{x}_D\right) = 0$
3. Update the effectivity factor $\nu_{k+1} = \nu_k \mathrm{SRF}_{\mathrm{k+1}}$
4. Check convergence $\mathrm{SRF}_1, \mathrm{SRF}_2, \ldots \rightarrow 1$ and $p_1,\ p_2, \ldots \rightarrow p$, if not yet achieved repeat at 1.

Quantiles and Characteristic Values

Eurocode 0 (DIN-Normenausschuss Bauwesen, 2021) and 7 (DIN-Normenausschuss Bauwesen, 2014) require that the probability of more unfavourable values than the characteristic value of resistance parameters is not larger than 5%. This is fulfilled if the 5%-quantile of the respective parameter is selected. The k%-quantile $Q_{X,k}$ of a random variable X is defined as:

$$\Pr\left(X \leq Q_{X,k}\right) = k \ \leftrightarrow \ Q_{X,k} = {F_X}^{-1}(k)$$

This concept can be directly applied to bivariate random variables, such as the Mohr-Coulomb parameters which show a negative correlation and should be modelled as a bivariate random variable.

Figure 3 depicts the contour lines of the CDF of the foundation's residual drained shear strength. Every pair of parameters lying on the 5%-contour of the CDF denotes a 5%-quantile of the bivariate random variable. Among these pairs a critical combination must be selected. The most rigorous approach would be to use this contour line in a constrained minima search, which minimizes the FoS in a stability analysis.

Usually, characteristic values are defined in a project stage where the models involved in the stability analysis are not yet available. Thus, two approaches are introduced that are not based on the final model. Firstly, the parameters with the largest probability of occurrence can be found by solving:

$$\hat{\varphi}'_{0.05}, \hat{c}'_{0.05} = \underset{\varphi', c'}{\arg\max} f_X(\varphi', c') \mid F_X(\varphi', c') = 0.05$$

This is depicted as the full triangle in Figure 3. Alternatively, a shear-strength criterium can be selected and the pair leading to the minimum shear strength can be searched:

$$\hat{\varphi}'_{0.05}, \hat{c}'_{0.05} = \underset{\varphi', c'}{\arg\min}\ \tau(\varphi', c', x) \mid F_X(\varphi', c') = 0.05$$

In most cases this will depend on additional parameters x. In the case of the Mohr-Coulomb criterium the effective normal stress σ must be defined, which can often be estimated in an early project stage. Figure 3 shows the resulting quantile for $\sigma = 500\ \mathrm{kN/m^2}$ as a square.

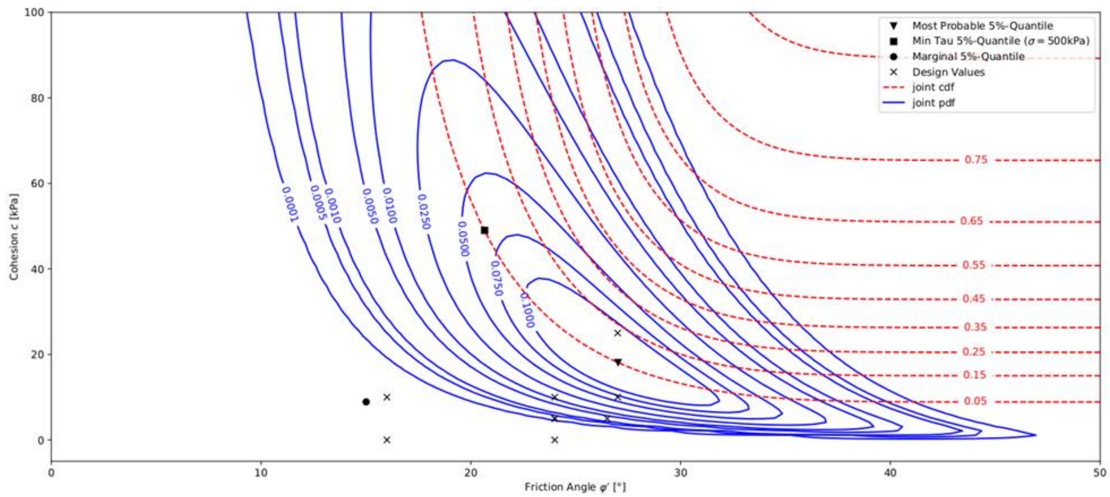

Figure 20: CDF and quantiles of bivariate random variables

Model Description

Standard Model

Geometry

All models share a common geometry which is derived from Light Detection and Ranging (LiDAR) measurements and the as-built model at the location of failure, CH 1950. The detailed geometry is presented in the ITRB report, from which the simplified geometry was derived as shown in Figure 1.

Geotechnical Parameters

The above described distribution fitting approach was applied to two data sets of foundation shear strength, literature values of rockfill strength and CPTu data for the tailings shear strength. The first data set of foundation shear strength is the data available before failure, for which the stratigraphy was not reported. From this investigation period, only drained peak shear strength values were reported. The second group of foundation data was collected after failure. 21 peak and 12 residual drained shear strengths, as well as 17 peak and 10 residual undrained shear strengths were obtained from CIU and DSS tests on samples retrieved in the vicinity of the slump. The rockfill's shear strength was derived from literature values on rockfill strength of fine-grained igneous rocks provided by Leps (1970). For the tailings shear strength, a CPTu campaign from 2017 comprising 13 CPTu tests was reevaluated by the ITRB. The report provides the logs of the derived peak and post-liquefaction shear strength ratio, which were binned, and mean values were calculated. Based on these values a probability distribution was fitted with the MLE while spatial trends in the data were neglected. The relevant marginal and joint shear strength distributions and quantiles are summarized in Table 2. Cohesion is given in kPa and the friction angle in radians for the distributions and in degrees for the quantiles.

Failure Surface

Before failure, several cracks were observed on the crests of stages 5, 6, 7, and 8, the upstream buttress and at the dam’s toe. Together with the information found in two drill holes placed on the slump, the failure surface is constrained in the outcrop location and depth.

The crack development showed mostly lateral displacements indicating a planar failure surface at its base. The ITRB incorporated this information by applying a block search algorithm. In this study, the failure surfaces are circular and show a similar shape and FoS as the results from the ITRB.

Phreatic Surface

The phreatic surface was well monitored up to failure. From these readings and other information, the ITRB created a 3D hydrogeological model and derived the phreatic surface at the failure cross-section. This surface is also used within this study and shown as a dashed line in Figure 1.

LEM Modelling Approach

The LEM analysis was carried out using Bishop’s simplified method and a grid search. Bishop´s method makes gross assumptions about the equilibrium of forces. It showed similar results for the studied problem, when compared with the more rigorous Spencers method. The Deltares D-Stability (Deltares, 2022a) was used to carry out the LEM calculations, which were automated using Python and geolib (Deltares, 2022b).

Modelling Strain-Weakening and Liquefaction in LEM

LEM cannot model the strain-weakening behaviour of the foundation, accumulating deformations, time-dependencies, or static liquefaction of tailings. Therefore, these events must be examined with separate LEM models, each representing the conditions prevailing at a certain point in time. This is carried out using models at three time steps: Model A, B, and C.

Model A (drained peak) represents the onset of deformations, before yielding occurred. At this point, the system response is drained, and the soils have not yet been loaded beyond their peak strength. Model B (drained residual) aims to model the scenario right before collapse. It is assumed, that the entire failure surface yields. The system response is still drained, as deformations accumulate slowly, and the residual strength is mobilized. The post-liquefaction stability is associated with Model C. The tailings are at the

Table 3 : Parameters of Relevant Shear Strength Distributions and Quantiles

Soil	Property	Distribution	5%-Quantiles Marginal	5%-Quantiles Most-Probable	5%-Quantiles Min. Shear Strength	Stage 10 Stability Analysis
Foundation Pre-Failure Drained Peak	φ'	Gumbel ($a_n = 0.05,\ b_n = 0.44$)	22.1	24.2	23.5	27
	c'	Log – Normal ($\mu_{ln\,X} = 2.95,\ \sigma_{ln\,X} = 0.70$)	6.0	18.2	24.1	10
	ρ	-0.41	-	-	-	-
Foundation Post-Failure Drained Peak	φ'	Trunc. Normal ($\mu = 0.39,\ \sigma = 0.09,\ a = 0,\ b = \infty$)	13.9	24.5	19.2	-
	c'	Beta ($r = 2.09,\ s = 30.86,\ a = 0,\ b = 1000$)	12.4	27.8	59.2	-
	ρ	-0.66	-	-	-	-
Foundation Post-Failure Drained Residual	φ'	Trunc. Normal ($\mu = 0.40,\ \sigma = 0.12,\ a = 0,\ b = \infty$)	11.7	22.4	18.9	-
	c'	Beta ($r = 0.45,\ s = 8.62,\ a = 0,\ b = 1000$	0	0	0	-
	ρ	-0.61	-	-	-	-
Foundation Post-Failure Undrained Residual	ssr	Gumbel ($a_n = 0.06,\ b_n = 0.28$)	0.21	-	-	0.51
Tailings Undrained Residual	ssr	Beta ($r = 13.99,\ s = 37.73,\ a = 0,\ b = 0.41$)	0.07	-	-	0.05
Rockfill Drained Peak	φ'	Beta ($r = 105.78,\ s = 132.69,\ a = 0,\ b = 100$)	39.1	-	-	40

residual undrained strength and due to the sudden loss of strength the tailings act as an additional load on the dam and foundation. Standard LEM software cannot model this. Schatz (2023) presents three approaches using equivalent loads and adjusted shear strengths.

FEM Modelling Approach

FEM was used to compare the results from LEM with a more realistic model that incorporates stress and strain analysis. In order to accurately represent the in-situ stress conditions, the construction stages of the dam were modelled. The model was built in Rocscience RS2 (Rocscience, 2023) with 6-noded triangles and mesh refinement. More details on the model can be found in Schatz (2023).

An elastoplastic model with Mohr-Coulomb failure criterion is used. FEM Model A applies the derived peak shear strength, while FEM Model B uses both the peak and the residual shear strength. FEM undrained analysis for Model C was performed but numerical convergence was not achieved. The SSR is used to define the SRF, which can be interpreted in a similar way as the FoS. SRF is calculated by iteratively reducing the shear strength of the selected layers until the analysis does not longer converge. A contour plot of the maximum shear strain and displacement vectors for Model B are depicted in Figure 4. Green lines represent the layer and stage boundaries. The localization of high shear strain is similar to the slip surface resulting from a grid search in LEM (see Figure 1).

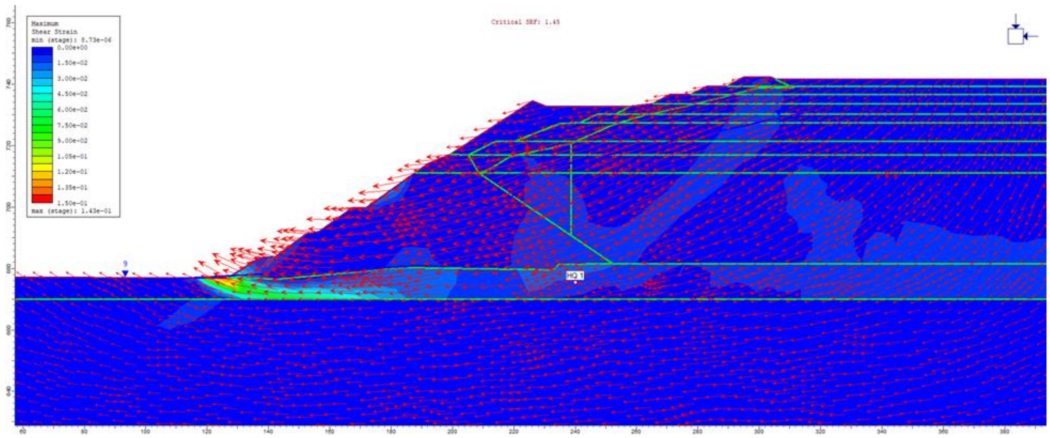

Figure 21 : Model B maximum shear strain and displacement vectors in RS2

Stability Analysis of Cadia NTSF embankment failure

The results of the LEM for Models A and B are presented in Table 3. The derived characteristic values vary significantly depending on the selected data set and method. While both approaches, which consider the joint distribution of friction angle and cohesion, lead to satisfactory FoS for Model A (drained peak), the results from Model B (drained residual) indicate non-compliant FoS with the International Commission on Large Dams - Australian National Committee (2019) regulations. Selecting the marginal 5%-quantiles predicts non-compliance and failure. For Model C the FoS is smaller than 1.

Table 4 : FoS for different choice of characteristic foundation shear strength

Model and Data Set	Marginal			Most-Probable			Min. Shear Strength		
	φ'	c	FoS	φ'	c	FoS	φ'	c	FoS
A – Pre-Failure	22.1	6.0	1.43	24.2	18.2	1.57	23.5	24.1	1.58
A – Post-Failure	13.9	12.4	1.20	24.5	27.8	1.63	19.2	59.2	1.59
B – Post-Failure	11.7	0	0.93	22.4	8.5	1.32	18.9	28.2	1.32

The results of the probabilistic analysis (reliability index β and probability of failure p) are presented in Table 4. When using FORM, only Model A predicts accordance with the reliability class RC3 defined in Eurocode 0, which requires $\beta \geq 5.2$ (DIN-Normenausschuss Bauwesen, 2021). However, by applying MCFM the reliability of the system for Model A decreases and moves towards the non-compliant range. For Model B none of the results are acceptable. If the post-liquefaction stability (Model C) is studied, FORM results in a probability of failure of 0.5 and the FEM model does not converge, indicating failure.

Table 5 : Results of probabilistic analysis

	β (FORM-LEM)	p (FORM-LEM)	β (MCFM)	p (MCFM)
Model A	5.60	1.07×10^{-8}	4.33	7.26×10^{-6}
Model B	2.88	1.98×10^{-3}	3.83	6.47×10^{-5}

Summary

Full probabilistic analysis of geotechnical problems using FEM is often not feasible due to the great computational effort. In this study, the MCFM combines the ease of performing a probabilistic analysis with FORM and LEM and a more realistic modelling of stress-strain response using FEM. The FEM model is used to correct the strength parameters of the idealized LEM model so that the models are equal in the probability of failure.

Furthermore, two methods for choosing characteristic shear strength parameters from a quantile of bivariate distributions, such as the Mohr-Coulomb parameters, are introduced. The quantile must lie on the 5% contour line of the CDF. The first approach selects the set of parameters with the largest probability of occurrence. The second approach minimizes the shear strength for a characteristic effective normal stress level. Within this case study, both approaches delivered similar FoS. Due to its simplicity, choosing the most-probable 5%-quantile is preferred if the choice of a characteristic effective normal stress is not straightforward.

Studying the stability of the Cadia NTSF dam showed that a deterministic LEM analysis at the drained peak shear strength indicates a safe dam (Model A). By applying a probabilistic analysis using LEM and FORM only regulation compliance for Model A is obtained. Combining the idealized LEM model with FEM through MCFM shows that the dam does not meet the demanded FoS or reliability even for Model B. Future work will focus on the further applicability of reliability analysis to assess the stability of TSF.

Literature

Baecher, G.B. and J.T. Christian. 2003. *Reliability and Statistics in Geotechnical Engineering*. Chichester: John Wiley & Sons Ltd.

Deltares. 2022a. *D-Stability Version 2022.01.2.* Accessed 08/242023 at: https://www.deltares.nl/en/software-and-data/products/d-stability#demo-screenshots

Deltares. 2022b. *geolib.* Accessed 08/24/2023 at: https://github.com/Deltares/GEOLib

DIN-Normenausschuss Bauwesen. 2021. *DIN EN 1990:2021-10 Eurocode: Grundlagen der Tragwerksplanung; Deutsche Fassung EN 1990:2002 + A1:2005 + A1:2005/AC:2010*. Berlin: Beuth Verlag GmbH

DIN-Normenausschuss Bauwesen. 2014. *DIN EN 1997:2014 Eurocode 7: Entwurf, Berechnung und Bemessung in der Geotechnik Deutsche Fassung EN 1997-1:2004 + AC:2009 + A1:2013*. Berlin: Beuth Verlag GmbH

Ditlevsen, O. and T. Arnbjerg-Nielsen. 1994. Model-Correction-Factor Method in Structural Reliability. *J. Eng. Mech.* 120(1):1–10.

Fisher, R.A. and E.J. Russell. 1922. On the mathematical foundations of theoretical statistics. *Philos. Trans. Royal Soc. A* 222:309–368.

Franks, D.M., M: Stringer, L.A. Torres-Cruz, E. Baker, R. Valenta, K. Thygesen, A. Matthews, J. Howchin and S. Barrie. 2021. Tailings facility disclosures reveal stability risks. *Sci Rep* 11, 5353

Hasofer, A.M. and N.C. Lind. 1974. An Exact and Invariant First Order Reliability Format. *J. Eng. Mech.* 100:111–121.

International Commission on Large Dams - Australian National Committee (2019). *Guidelines on tailings dams: Planning, design, construction, operation and closure.*

Jefferies, M., N.R. Morgenstern, D. Van Zyl and J. Wates. 2019. *Report on NTSF Embankment Failure - Cadia Valley Operations for Ashurst Australia*

Leps, T.M. 1970. Review of Shearing Strength of Rockfill. *J. Soil Mech. Found. Div*. 96(4):1159–1170.

Lumb, P. 1970. Safety factors and the probability distribution of soil strength. *Can. Geotech. J.* 7(3):225-242.

Metropolis, N. and S. Ulam. 1949. The Monte Carlo Method. *J. Am. Stat. Assoc*. 44(247):335–341.

Nataf, A. 1962. Determination des distributions dont les marges sont donnees. *Comptes rendus de l’Académie des Sciences* 225:42–43.

Rackwitz, R. and B. Flessler. 1978. Structural reliability under combined random load sequences. *Comput. Struct.* 9(5):489–494.

Rocscience. 2023. *RS2 Version 11.0.8.1.* Accessed 08/24/2023 at: https://www.rocscience.com/software/rs2

Schatz, B. 2023. *Reliability Analysis of Slopes in Tailings Storage Facilities using a Combination of the Limit Equilibrium and Finite Element Methods. Master Thesis.* Munich: Technical University of Munich

Ureel, S. and M. Momayez. 2014. An Investigation of the Limit Equilibrium Method and Numerical Modeling for Rock Slope Stability Analysis. In: L. Zhang and E.L.N.Y. Wong (editors), GSP 237. 2014. *Rock Mechanics and Its Applications in Civil, Mining, and Petroleum Engineering*. American Society of Civil Engineers:218-227

Wiley, D.C. and C.W. Mah. 2004. *Rock Slope Engineering.* Abingdon: The Institute of Mining and Metallurgy and E. Hoek and J. W. Bray.

Influence of tailings rheological parameters on the estimation of runout distances

Claudio Román, Ausenco, Chile

Viktor Kovács, Ausenco, Chile

Fernanda Kunoh, Ausenco, Brazil

Nicolás Echeverría, Ausenco, Chile

Ignacio Gutiérrez, Ausenco, Chile

Abstract

Tailings rheology is one of the most influential parameters, and one of the least understood and studied in a Tailings Dam Breach Analysis (TDBA). In contrast to other important aspects such as hydrology and topography, rheological parameters are not usually discussed or questioned, and are often obtained from references that are not representative of the failure conditions of the analyzed tailings storage facility (TSF).

Experience from some of the last TSF failures has shown that the rheological parameters are significantly lower than what is expected for consolidated tailings in a sunny day scenario, comparable even to water, which could be related to the susceptibility to flow liquefaction phenomena.

This paper presents the results obtained from a TDBA model of a hypothetical TSF catastrophic failure. Two cases were modeled in a sunny day scenario, considering two different interpretations of the same tailings rheological tests in order to illustrate the influence of rheological tests and their interpretation – or misinterpretation – in TDBA results, particularly in the estimation of the downstream effects and in the Consequence Classification of the TSF. Rheological tests on copper tailings samples were carried out especially for this purpose.

Introduction: What is a Tailings Dam Breach Analysis?

According to the Technical Bulletin: Tailings Dam Breach Analysis (CDA, 2021), a tailings dam failure is *"a physical breach of the dam followed by uncontrolled and typically sudden and catastrophic release of any or all stored materials (e.g., fluids, tailings, sludge, etc.)"*. It implies *"the inability of the dam to meet its design intent, whether in terms of management, operational, structural, or environmental function, resulting in potential loss of life, loss to the stakeholders, or adverse environmental effects"*. Therefore, a Tailings Dam Breach Analysis (TDBA) *"evaluates hypothetical dam failure scenarios and involves a series of analyses to assess tailings flow characteristics for downstream impact assessment"*.

In addition, the Global Industry Standard on Tailings Management, GISTM (ICMM, UNEP, & PRI, 2020), defines a TDBA as *"a study that assumes a failure of the tailings facility and estimates its impact. Breach Analyses must be based on credible failure modes. The results should determine the physical area impacted by a potential failure, flow arrival times, depth and velocities, duration of flooding, and depth of material deposition. The Breach Analysis is based on scenarios which are not connected to probability of occurrence. It is primarily used to inform emergency preparedness and response planning and the consequence of failure classification. The classification is then used to inform the external loading component of the design criteria"*.

Behavior of tailings during failures

Figure 1 shows some of the best-known catastrophic cases of TSF failures over the last 30 years. In all of them, it is observed that the tailings behave as a fluid in the failure zone, regardless of whether there was no excess of free water, or whether it was a sunny day condition. Because of this, the tailings rheological parameters are of great importance on the estimation of runout distances and downstream consequences. Some failure cases show that the rheology does not seem to correspond to consolidated tailings, having significantly lower values instead, showing even a water-alike behavior (Kovacs et al, 2019).

As indicated in the CDA Technical Bulletin (CDA, 2021), TDBA are recent and must address an important gap related to the hydrodynamic, rheological, and geotechnical processes of tailings flows.

Figure 1: Examples of some historic TSF catastrophic failures (Roman et al, 2022)

Multiple factors are determinant in the results to be obtained from a TDBA: topography, hydrology, rheology, duration and mobilized volume of the flooding, among others (Figure 2). In general, all of them have known methodologies for their estimation and calculation. In contrast, rheology is one of the least understood and studied for this kind of analyses. Even more, rheological parameters are not usually discussed or questioned, and are often obtained from out-of-date references or acquired erroneously from the thickeners and pipelines design criteria, impacting the modelling results directly.

Measurement of the yield stress at the point of deposition after undergoing the shear thinning process is rarely a part of a tailings facility operation. Yield stress measurements (if taken at all) are usually obtained by sampling from the thickener or thickener underflow and analyzing the material with a rheometer in a lab setting. These yield stress measurements are inevitably higher than the actual yield stress at the point of deposition (Drozdiak and Salfate, 2019), due to the shear thinning process during tailings transport described above which creates a dynamic condition that differs from the initial static condition (Figure 3). The same thing happens, but on a much larger scale, when a tailings dam breaks.

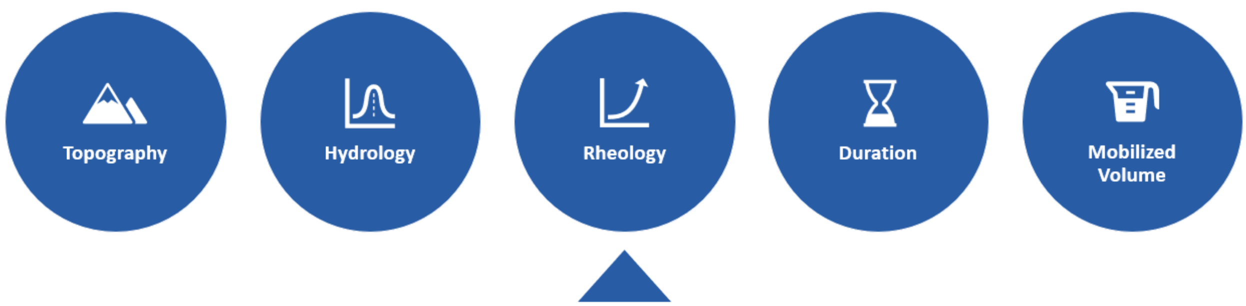

Figure 2: Typical most influential factors on a TDBA

A better rheological characterization demands for additional studies and field programs to collect required information, or make reasonable assumptions based on the expert judgement of experienced consultants, where possible. The following sections present relevant aspects for a better characterization of the tailings in terms of rheology, and the effects of an inadequate election of the rheological parameters when performing a TDBA.

Tailings rheological characterization

The tailings characterization has been obtained from rheological tests carried out on Chilean copper tailings samples at Ausenco's Tailings Laboratory, focusing on the dynamic behavior and the influence of shearing on the yield stress parameter at high concentrations.

Figure 3 presents the results of these tests. The higher the solids concentration, the higher the peak value observed for the yield stress. However, as the tests progress in time, the yield stress tends to decrease due to shearing applied by the vane. Shearing or cycling causes a strong decrease in yield stress to reach a residual value for highly concentrated tailings (consolidated tailings).

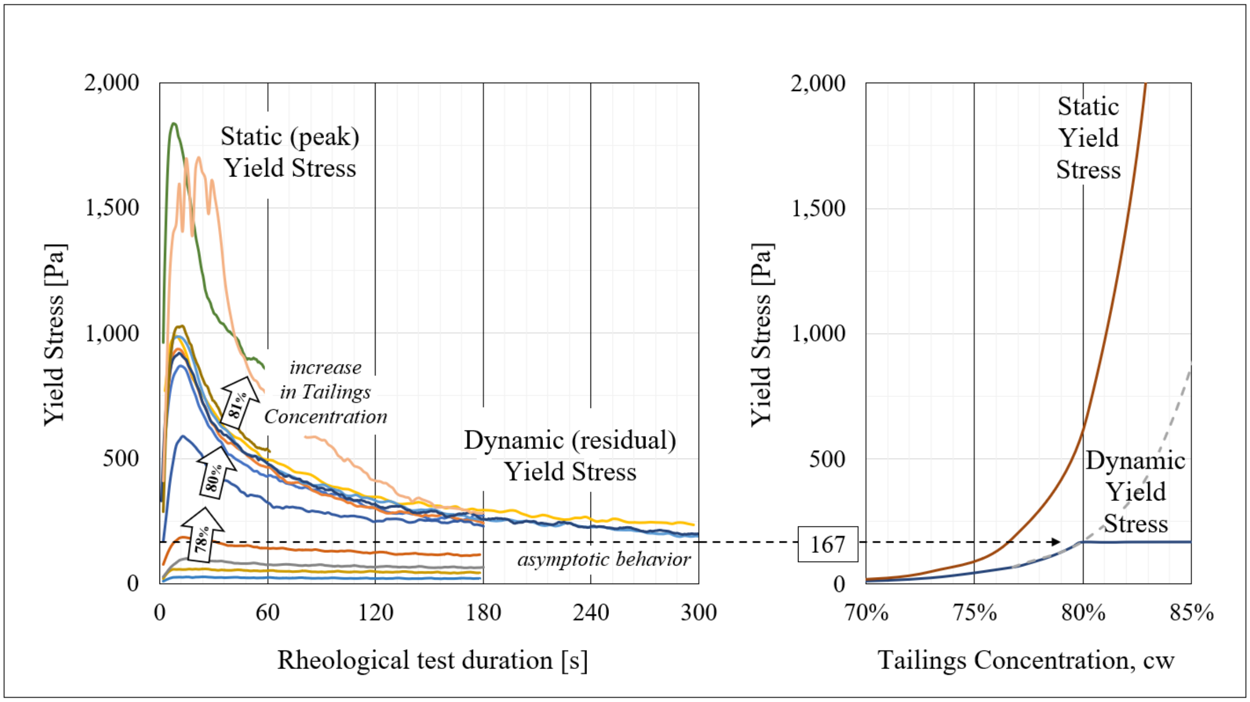

Figure 3: Residual yield stress concept for high concentrations

The peak (static) and residual (dynamic) yield stress values can be interpreted as different operation or design conditions, while the first value (peak) is typically used in the design of thickeners, pipelines, or structures subjected to blockage, the second one (residual) should be used in analysis focused on runouts or flows, resulting more representative of the liquefaction phenomena, and thus more suitable for its use in TDBAs. The cases shown in Figure 1 provide examples of this fluid behaviour (Roman et al, 2022).

Tailings viscosity is the other important parameter in a TDBA. In this case, data are typically available for tailings solids concentrations (concentration indicated by weight, cw) between 50% and 65% (Figure 4). For this article, viscosity parameters were obtained for the same tailings sample as above, in this range of concentrations. For higher concentrations, Figure 4 shows two potential curves considering a higher or a lower tailings flowability, within a typical range of possible values of viscosity for TDBA.

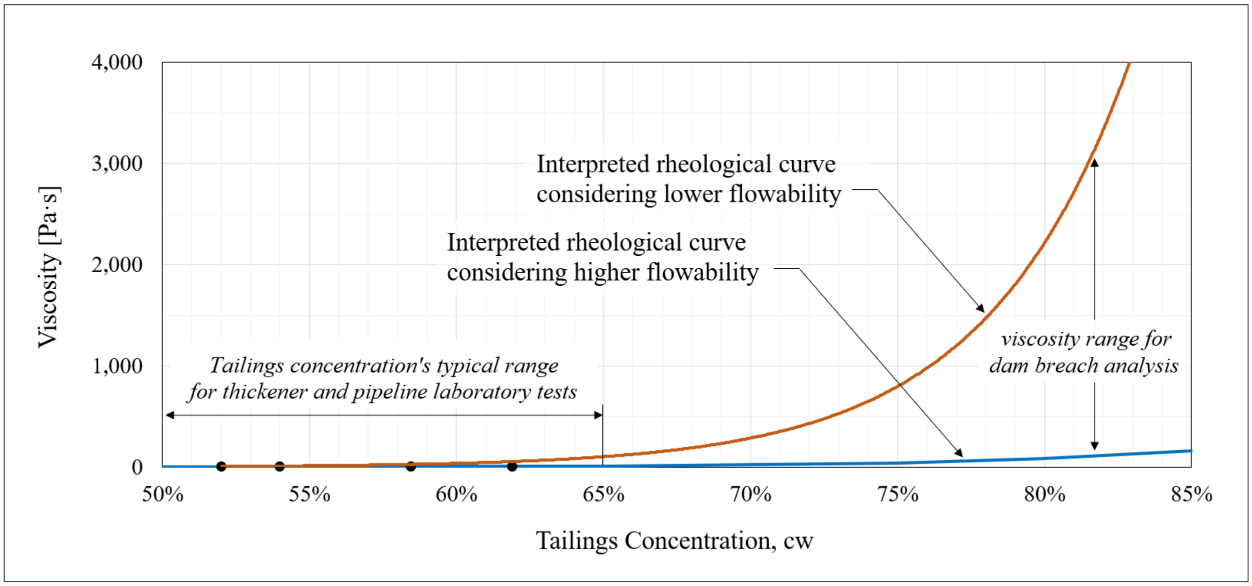

Figure 4: Differences in the interpretation of the viscosity parameter

Implications of using the incorrect rheology in a TDBA

As already noted, the interpretation of the tailings rheological parameters can lead to large differences in the results of a TDBA. Figure 5 presents the effects of two potential rheological scenarios, depending on the tailings rheological data interpretation, for a TSF catastrophic failure example.

The example considers a fictitious TSF that stores 5.25 Mm^3 of consolidated conventional tailings. It has the rheological properties shown in Figures 3 and 4, with a solids concentration cw near to 82%. A fictitious town of 8,000 inhabitants is located 9 km downstream of this fictitious TSF.

As a result of a catastrophic failure, 1.6 Mm^3 of tailings are released from the TSF (30% of the volume), consistent with the formulas based on statistics of failures (Rico et al, 2007; Concha & Lall, 2018).

The effects of the two scenarios are shown in Figure 5. Case (a) shows the results obtained considering the interpretation of the rheological curves towards a low flowability of the tailings. Case (b), the interpretation towards a high flowability of them instead.

The model was carried out using the Flo-2D software and high-resolution topography data for a sunny day condition.

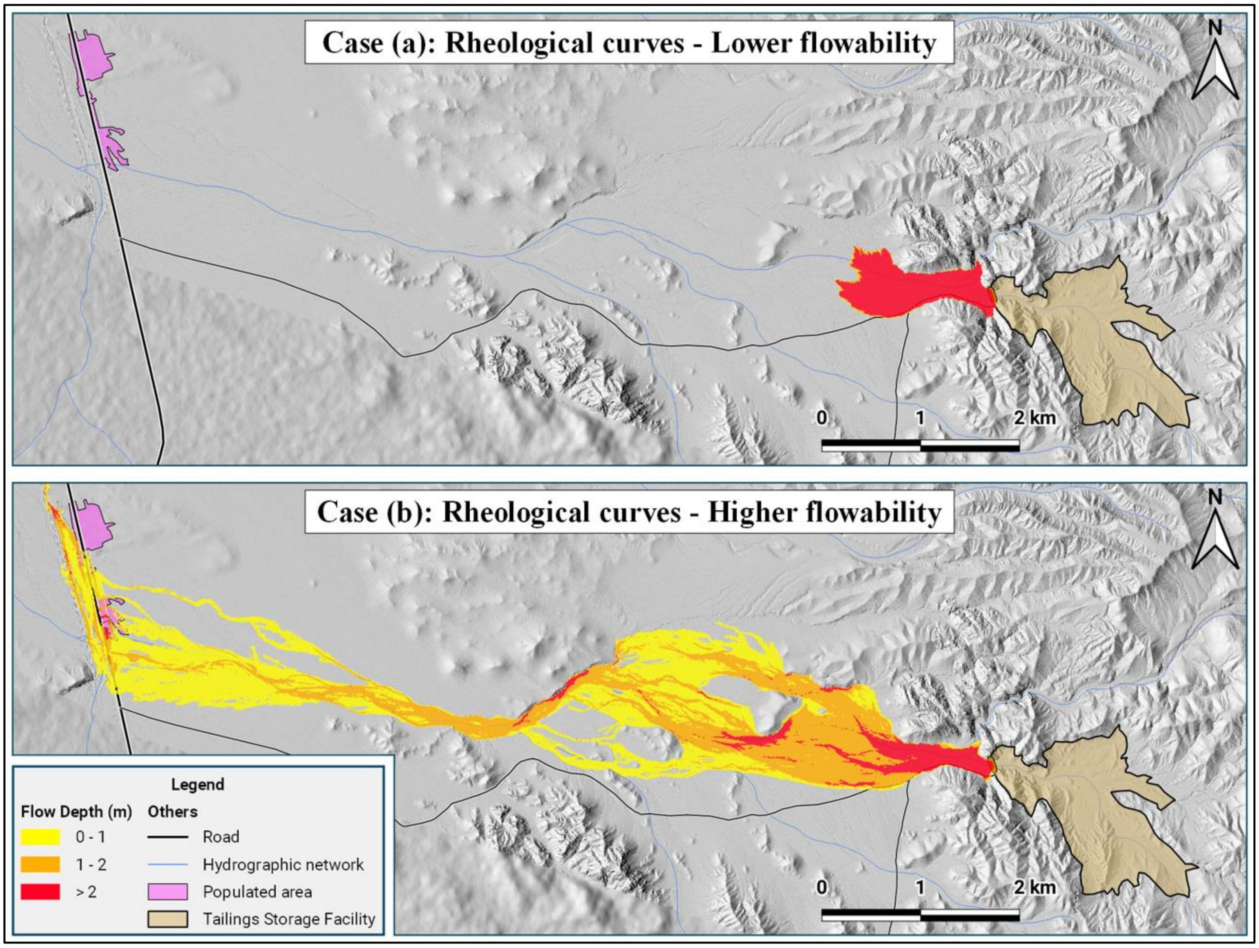

Figure 5: Results of TDBA simulations considering different criteria for tailings parameters

According to the GISTM´s Dam Failure Consequence Classification categories established (GISTM, 2020), the downstream consequences vary considerably when comparing these two scenarios. For Case (a), the Consequence Classification (Figure 6) could reach the category of *"Low"*, with "none" potential population at risk. Meanwhile, for Case (b), the category could be increased to *"Extreme"*, with ">1,000" potential persons at risk, and some eventual fatalities depending on the emergency plans.

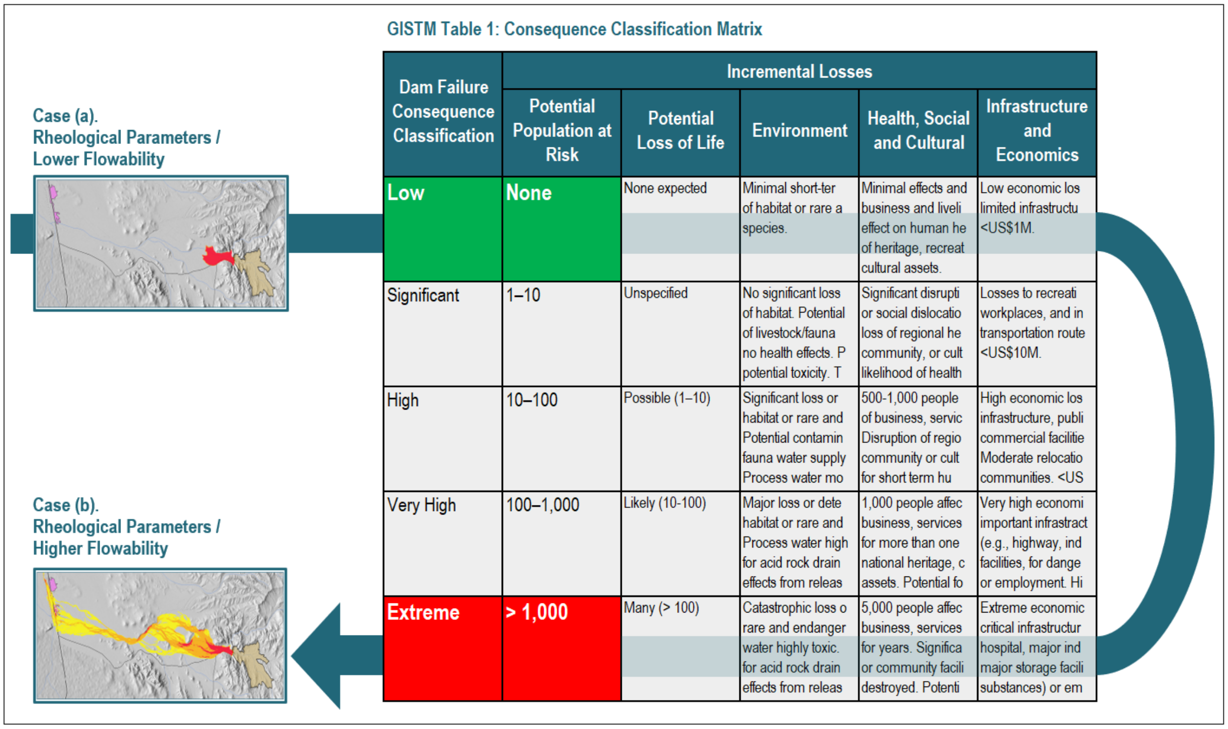

Figure 6: Example of the potential impact of the rheological parameters in dam classification

Conclusion

It is evident that special care must be taken in the selection of the rheological parameters when performing a TDBA, since in the occurrence of a failure phenomenon, yield stress parameters would reach much lower values than those commonly obtained under normal test conditions, while viscosity parameters can have interpretation problems due to limitations in laboratory testing ranges.

If the rheology parameters are well interpreted and well selected, the results to be obtained in a TDBA could represent the real situation in a more accurate manner, and allow to better contribute to the main objective, which is to safeguard the *"Population at risk"*; prevent the *"Loss of life"*; protect the state of the *"Environmental and cultural values"* and preserve the *"Infrastructure and economics"* aspects (Figure 6). Otherwise, the results could be less conservative in terms of the potential downstream effects.

This research confirms that the rheological parameters depend strongly on how the laboratory tests are carried out and how the results of these tests are interpreted. The above may imply:

- An overestimation (or underestimation) of the rheological properties when the origin of the tests is uncertain or methodologies for the design of thickeners and tailings transport systems are used in dam breach analyses.

- This could lead to an underestimation (or overestimation) of the downstream consequences and the Dam Consequence Classification of the TSF.
- Emergency preparedness and response plans could not be able to address a potential TSF failure.
- Utilization of inadequate (seismic and flood) design criteria. Due to the use of an underestimated probability of exceedance, according to the international recommendations of the CDA and/or GISTM.

When conducting new TDBAs in the future, the following is recommended:

- Pay special attention on how the tailings rheology parameters have been calculated. It is mandatory to be involved in the testing process to ensure the representativeness of the tests according to the desired objective. The way the samples are obtained along with the condition in which the tailings will be disposed in the future are relevant factors to take into consideration.
- Dimension the amount of water that will potentially be stored in the tailings dam, as accurately as possible, in terms of operational, hydrological or water table levels. The presence of water directly affects the tailings rheology parameters.
- Include sensitivity analyses in upcoming TDBAs for those parameters with greater uncertainty, such as rheology, hydrological conditions, discharged volumes, and/or downstream conditions. Small changes in these parameters can lead to large changes in the consequence classification of some TSFs (for better or worse).
- Always consider the credibility of the scenarios being analyzed. If non-credible cases, parameters, and/or sensitivities are included, they should be clearly identified.
-

The bow-tie chart presented in Figure 7 shows the main causes and consequences listed above, and their recommended controls.

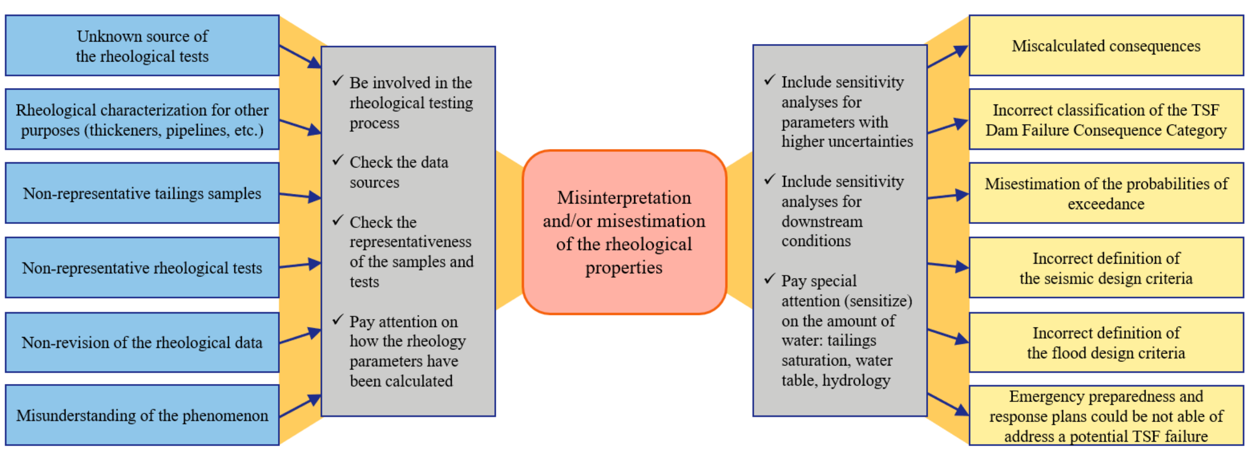

Figure 7: Possible causes and consequences of rheological parameters misinterpretation

Acknowledgements

Special thanks to the Ausenco´s laboratory located in Santiago, Chile, for allowing the execution of the rheological tests whose results have been presented in this article.

References

CDA (Canadian Dam Association). 2021. *Technical Bulletin: Tailings Dam Breach Analysis.*

Concha, P. and U. Lall. 2018. *Tailings dam failures: Updated statistical model for discharge volume and runout.*

Drozdiak, J. and E. Salfate. 2019. *Management of Geotechnical and Rheological Behaviour of Tailings to Produce Engineered Fill*. Proceedings of Tailings and Mine Waste 2019. Vancouver, Canada. November 17-20, 2019.

Hunter, G. and R. Fell. 2003. *Travel distance angle for "rapid" landslides in constructed and natural soil slopes.* Can. Geotech J. 40: 1123-1141.

ICMM (International Council on Mining & Metals), UNEP (United Nations Environment Program), PRI (Principles for Responsible Investment). 2020. *Global Industry Standard on Tailings Management.*

Jeyapalan, J., J. Duncan and H. Seed. 1983. *Investigation of flow failures of tailings dams.* Journal of Geotechnical Engineering, 109(2), 172-189. Doi:10.1061/(asce)0733-9410(1983)109:2(172).

Jeyapalan, J., J. Duncan and H. Seed. 1980. *Summary of research on analyses of flow failures of mine tailings impoundments.*

Kovacs, V., C. Roman, P. Galdeano and M. Mussé. 2019. *A Different View of Run-Out Distance after Tailings Impoundment Failure*. Proceedings of the Sixth International Conference on Tailings Management Tailings 2019. Santiago, Chile.

McPhail, G., R. Ugaz and F. García. 2023. *Rheological testing for dam break modelling*. Paste 2023, doi:10.36487/ACG_repo/2355_45.

O'Brien, J. and P. Julien. 1988. *Laboratory analysis of mudflow properties*. Journal of Hydraulic Engineering, ASCE, 114(8), 877-887.

Pirouz, B., Z. Lu and S. Javadi. 2023. *Estimating rheological properties of liquefied tailings for dam break simulation using site-specific parameters and laboratory testing*. Paste 2023, doi:10.36487/ACG_repo/2355_48.

Rico, M., G. Benito and A. Díez-Herrero. 2007. *Floods from tailings dam failures*. Journal Hazardous Materials 154 (2008), p. 79–87.

Roman, C., G. Barbosa, M. Lombardo and C. Cortés. 2022. *Importance of Tailings Rheology in Dam Failure Consequence Classification*. Proceedings of the CDA Annual Conference 2022. St. Johns, Canada.

Si, C., M. Mergili, N. Rana, S. Zhang, B. Dai and Y. Han. 2023. *Failure analysis and flow dynamic modeling using a new slow-flow functionality: the 2022 Jiaokou tailings dam breach*. Doi:10.1007/s10346-023-02145-z.

On the interpretation of trigger analyses of upstream-raised tailings dams

Alejo O. Sfriso, SRK Consulting and University of Buenos Aires, Argentina
Mauro G. Sottile, SRK Consulting and University of Buenos Aires, Argentina
Felipe López Rivarola, SRK Consulting and University of Buenos Aires, Argentina
Osvaldo N. Ledesma, SRK Consulting, Canada

Abstract

Current practice for evaluating the vulnerability of upstream-raised tailings dams involves the computation of factors of safety by the limit equilibrium method assuming drained and undrained shear strength and, in the case of brittle tailings, also assuming softening to residual strength. In this latter case, a FoS = 1.0 may be accepted, in the rationale that if such FoS is attained, the dam would be stable even in the event of a full liquefaction of the tailings body. This method has drawbacks: i) it is deterministic, and its result depends on the choice of the liquefied strength, dragging uncertainty into the process and outcome; ii) it provides no information about which actions could lead to such massive liquefaction; and iii) it does not address the deformations that the dam might undergo in the event of a limited liquefaction.

To circumvent these drawbacks, the evaluation is complemented with trigger analyses, which can be broadly grouped in two types: i) simulating credible modes of failure by applying external actions that are relevant for a particular dam, e.g. a rise in the phreatic level in the dam´s body; and ii) external actions that are known to be deleterious are applied to the dam, regardless of their plausibility, and these actions are increased in value until the dam fails. In this paper, recent experiences with trigger analyses of upstream-raised tailings dams are commented and some discussions on the uncertainty in the interpretation of the results are provided.

Introduction

Motivated by recent dam failures, the industry developed a guide for managing tailings (GISTM, ICMM 2020) in which design and operation principles were established, including the obligation to carry out deformation analyses in all dams whose risk category was greater than a certain threshold. At the same time, the Australian National Committee on Large Dams produced a revision of its guidelines that incorporates two disruptive concepts in the analysis methods (ANCOLD 2019): i) “a conservative approach for materials susceptible to flow liquefaction would be to assume that liquefaction will occur regardless of the trigger mechanism that produces it”; and ii) "analyze stability (refers to determining safety factors) and estimate deformations using finite element methods or simplified methods".

Before this update in the industry guidelines, and largely to date, industry practice for Tailings Storage Facility (TSF) design consists on the calculation of Factors of Safety by limit equilibrium analyses. These analyses usually fall short as they are unable to take strain-softening into account: shear strength remains constant through the analyses, so progressive failure cannot be captured. Numerical modelling, on the other hand, can account for material complexities, namely: i) complex material behaviour including strain-softening, unsaturated materials and arbitrary stress-paths; ii) complex hydraulic conditions including transient seepage, generation and dissipation of pore pressures, de-saturation and re-saturation; iii) complex failure mechanisms involving materials with widely different behaviours, automatically accounting for strain-compatibility; iv) the mechanisms of progressive failure, including the propagation of pore-pressure waves triggered by contained liquefaction.

While deformation modelling can also be employed for the computation of factors of safety, its real value lies in the so-called trigger analyses, where events that might induce flow liquefaction of the TSF are simulated and credible paths to failure are investigated. In “pushover” trigger analyses, external actions are imposed to the final dam configuration and are increased until flow liquefaction is triggered. The max value of each action is then interpreted as an engineering estimate of the liquefaction vulnerability of the dam. Relevant actions must be included but, as the objective is to address the resilience of the dam, it is not required that all the external actions be relevant or realistic for a given dam. For instance, it is correct to apply a sudden rise of the water table to a dam located in a desert (Ledesma et al, 2022, Ledesma, 2023).

The industry is still building a consensus on how to interpret trigger analyses. Discussions often span into which aspects of the material behaviour should be included, whether there is value in analysing failure modes that are not plausible for a particular facility, and what is the engineering meaning of a particular quantitative result. This paper summarizes recent experience with trigger analyses of TSF facilities and presents some opinions intended to contribute to the aforementioned discussion.

Strategies in deformation modelling of tailings dams

Static vs dynamic analyses

In static analyses, inertia forces are neglected. Applied stresses must be balanced by the available strength of the various materials, and lack of numerical convergence is an indication of the onset of failure. Numerical convergence is also affected by tolerances and integration strategies, and both expertise and experience are required to determine whether the shape of the failure surface is an indication of real failure or a numerical issue (Rivarola et al, 2022).

In dynamic analyses, on the other hand, inertia forces are taken into account. Applied stresses are balanced by a combination of strength of the various materials and acceleration of parts of the dam. In these analysis, lack of numerical convergence is not observed, and attention must be focused on the appearance of post-convergence residual accelerations within the mesh. While both strategies are correct and are widely used by the industry, comparison of results coming from static and dynamic analyses is not direct, as results will be similar but not identical due to the different termination criteria employed for computing them.

Plastic vs fully coupled flow-deformation analyses

The typical modelling sequence includes modelling a realistic initial condition and construction sequence aimed at obtaining a credible stress field both in the solid and the fluid components of the model. In most cases, “drained construction” suffices, as it is assumed that excess pore pressure due to the rate of construction or raises have fully dissipated. When required, “consolidation-type” modelling or fully coupled deformation-flow is employed, more so if the transient pore-pressure distribution is of importance for the objectives of the study, like in Rate of Raise optimization.

TSFs are complex hydraulic structures. Water is provided to the structure through wet deposition, climate, and sub-surface ingress from the basin, and removed through pumping and flow through drains, foundation and lateral closure structures. Flow is transient in nature and includes storage components, saturation and de-saturation of tailings, and excess flow due to the consolidation of the tailings mass.

From the perspective of estimating the performance of TSFs, modelling of the full transient hydraulic problem is rarely required, a snapshot of the pore pressure field is usually enough: the analysis starts from a steady-state flow net which reasonably reproduces the phreatic surface and pore pressure gradient, and an “excess pore-pressure” field (including changes in suction, when applicable) is computed as the result of shear-induced volume change, in the so-called “undrained analysis”. When compression and consolidation behaviours are relevant to the performance and must be considered, their contribution to excess pore pressure can be computed either by a staged deformation-flow strategy or by a fully coupled analyses. Which of the two is used in each case depends on the nature and complexity of the problem, and on the weight of consolidation-induced flow on the overall performance of the TSF (Rivarola et al, 2023).

Factors of safety for strain-softening materials

In safety analyses performed by the limit equilibrium method, materials are assumed to reach a strength plateau, either for drained, undrained (peak) or undrained (residual) shear strength. A Factor of Safety (FOS) is computed in each case and is compared with minimum requirements provided by guidelines, e.g. ANCOLD (2019) recommend $FoS_{peak} = 1.5$ and $FoS_{res} = 1.0$.

When employing deformation modelling, the outcome is denoted as Shear Strength Reduction (SSR) and is not entirely comparable to FoS. As deformation modelling allows for the consideration of strain-softening and produces results that are “strain-compatible” by definition, an approach is proposed that – at least conceptually - complies with both $FoS_{peak} = 1.5$ and $FoS_{res} = 1.0$ at the same time. The procedure gradually reduces the material parameters used on an appropriate constitutive model to produce the stress-strain curves shown in Figure 1b, where peak strength is reduced but residual strength is kept, as opposed to the more common approach shown in Figure 1a (Sottile et al, 2020a).

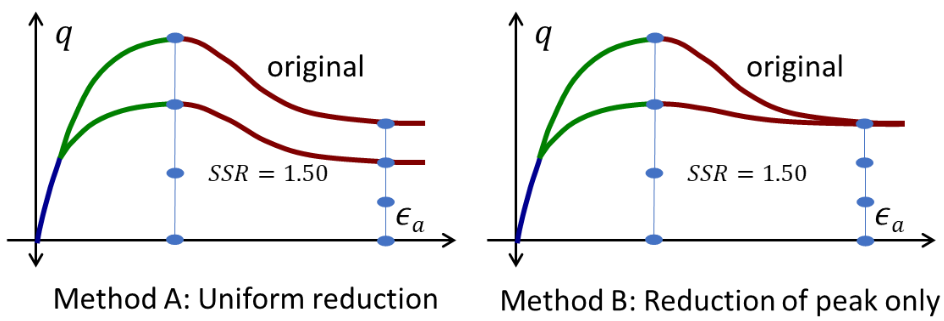

Figure 1. a) Classical Method A for strength reduction, and b) proposed Method B for more informative results accounting for strain-softening (Sottile et al, 2020a).

Trigger analyses

Trigger analyses investigate two sources of concern: i) whether a credible change in the configuration of a TSF can start an uncontrolled process of progressive failure leading to loss of containment; and ii) which are the salient vulnerabilities of an existing dam, including its foundations, drainage systems, etcetera. In the first approach, triggers selected should be relevant to a specific dam, e.g. sudden changes in the phreatic surface are not required to be studied for closed dams located in desert zones. In the second approach, such trigger would be considered, as it would be considered interesting to learn that, for instance, a rise of one or two meters in the phreatic surface would suffice to bring the dam to failure, and that such vulnerability could be eliminated by building a toe drain.

From the numerical modelling perspective, trigger analyses are numerical excursions around a stable configuration to check the stability of equilibrium and the resilience of the system. The model simulating such stable configuration is built by staged construction and calibrated to whatever data may exist with respect to foundation materials, coarse and fine tailings distribution, phreatic surface and perched water, hydraulic gradient, and other similar features of the dam (Ledesma et al, 2022, Ledesma, 2023).

Typical triggers, which induce different stress paths that might start progressive failure, are shown in Figure 3 (Ledesma et al, 2022): 1) raise in the phreatic surface, or surface water inflow; 2) deformations at the foundation or starter embankment; 3) instant loads at various places in the crest; and 4) (not shown in the picture) the spontaneous liquefaction of a small cluster within the tailings body.

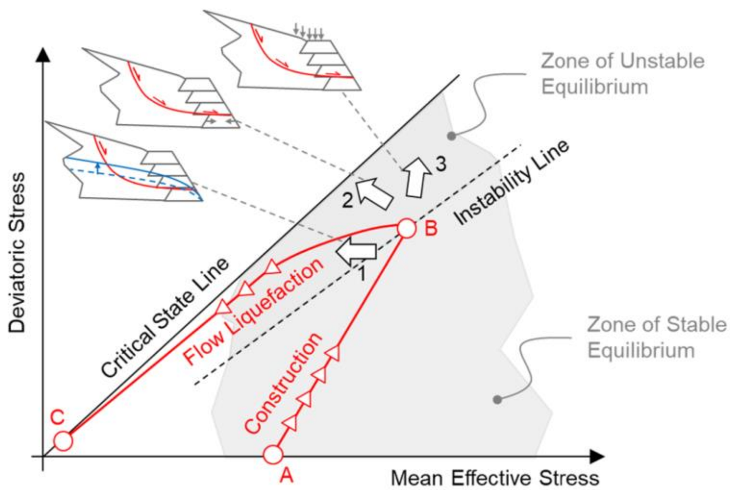

Figure 2. Typical trigger actions leading to flow liquefaction of a TSF (Ledesma et al, 2022).

Use of a SWCC in the trigger analyses

In trigger analyses, a soil water characteristic curve (SWCC) can be employed to take into account the distinct behaviours of the tailings in their various states: submerged, saturated (capillary zone), nearly saturated (relevant effects of suction) and near dry. A realistic SWCC should be used, as it has been proven that the associated suction plays a marginal impact on the trigger values for most dams (Rivarola et al, 2023). However, there is a strong preference in the industry to neglect the "beneficial" effect of suction, so a workaround is proposed as follows (Rivarola et al, 2023): a step-like SWCC is employed to compute the effective degree of saturation S_e, making the transition from "fully saturated-undrained" and "fully dry-drained" as narrow as desired. Figure 3 shows an example of such step-like SWCC, where $S_e = (S_{sat} - S_w)/(S_{sat} - S_{res})$ changes from 100% to 0% as the degree of saturation S_w drops from the upper bounding value $S_{sat} = 80\%$ to the residual saturation $S_{res} = 75\%$. By employing this modelling strategy and calibration, a unique set of material parameters suffices to describe the behaviour of all tailings (submerged, saturated but not submerged, partially saturated and near dry). Changes in the phreatic surface, the effect of transient flow and several other scenarios can be analysed without the need to modify the meshes or model calibrations, a feature that is considered a relevant sign of robustness of the model.

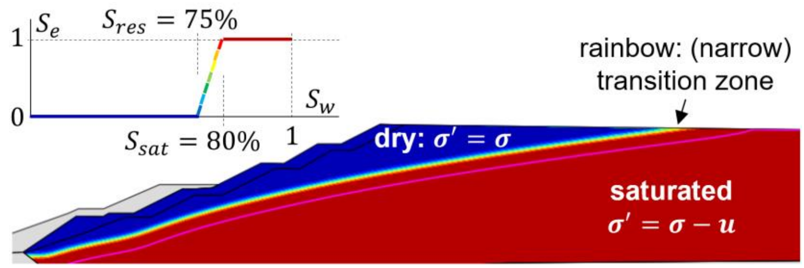

Figure 3. Effective degree of saturation obtained with a step-like SWCC (Rivarola et al, 2023).

Modelling of undrained strain softening

Modelling of strain softening of tailings in undrained shear would normally require a constitutive model based on CSSM, like Norsand (Jefferies, 1993, Jefferies & Been, 2016), CASM (Yu, 1998), MPZ (Ledesma et al, 2021), Arena (Sfriso & Weber, 2010). However, HS-Small (Benz, 2006), the flagship constitutive model available in Plaxis (Brinkgreve et al, 2020) and one of the most popular constitutive models in hardening plasticity for soils, is also able to reproduce strain softening in undrained shear, despite the fact that it is not implemented in a critical state framework (Sottile et al, 2020, Rivarola et al, 2023).

This extended capacity of the HS-Small model compared to the HSM model (Schanz & Vermeer, 1999) is due to the incorporation of the Li-Dafalias stress-dilatancy theory (Li & Dafalias, 2000) in partial replacement of the Vermeer-de Borst stress-dilatancy theory implemented in HSM model. However, the choice of material parameters required to reproduce strain-softening is strongly different to what would be a reasonable calibration for staged construction and drained loading, and therefore trigger analyses employing HS-Small usually require two sets of material parameters, one for building the model and a different one for performing the numerical excursions. Figure 4 shows an example of the simulation of CK0UC tests employing HS-Small, and exhibiting undrained strain-softening (Sottile et al, 2022).

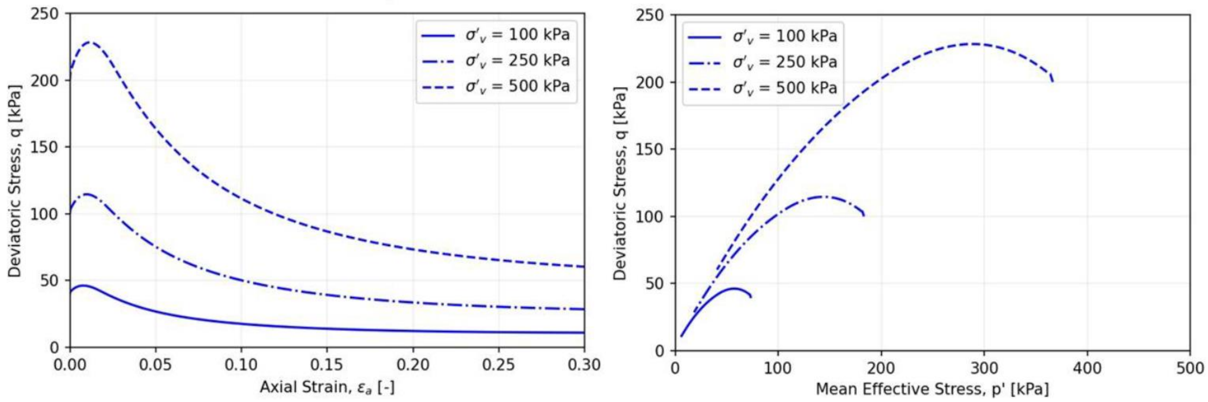

Figure 4. Simulations of CK0UC tests employing HS-Small and exhibiting undrained strain-softening (see model parameters in Sottile et al, 2022).

Uncertainties in trigger analyses

Input data

There are multiple uncertainties that accumulate throughout the analysis process. The first one is related to the reliability and quality of the input data, which is often based on CPTu soundings. As an example of the challenges found in practice, Figure 5 shows the state parameter ψ (Jefferies & Been, 2016) calculated according to two methods and for four CPTu logs obtained from (Sottile et al, 2022). It can be seen that the dispersion is very large and that the adoption of a reasonable design value can be very difficult.

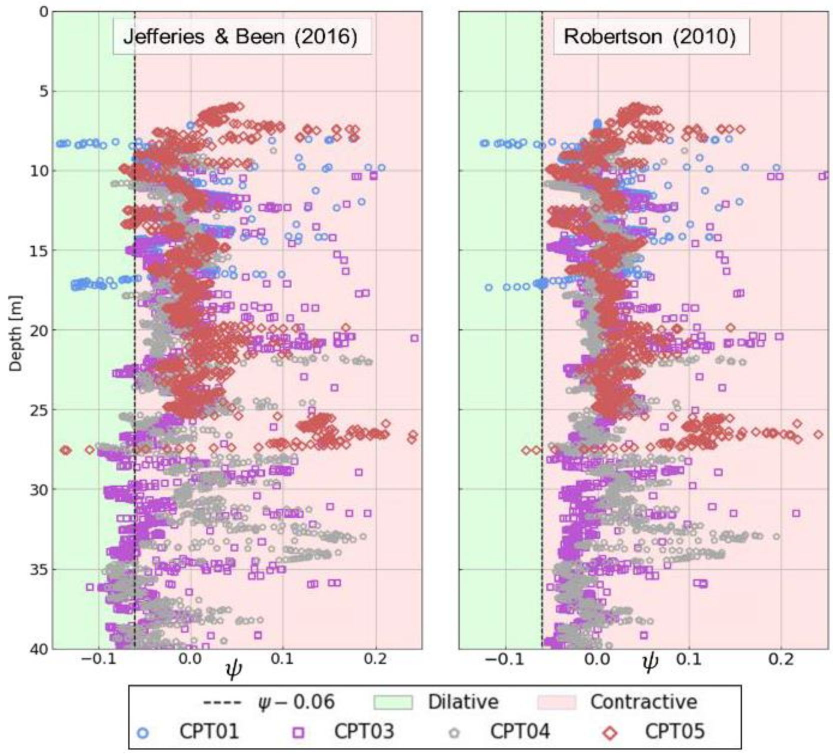

Figure 5. Example of estimation of the state parameter of a tailings dam employing four CPTu soundings and two procedures (Sottile et al, 2022).

One of the most popular tests for calibrating constitutive models for undrained strain-softening is the direct simple shear test (DSS). In this test, the stress state is not fully defined (only two of six component of the stress tensor are known). Two assumptions are employed in determining the undrained shear strength for design: equation 1 (total stress analysis, Ladd 1991); and equation 2 (undrained stress analysis, Ladd 1991). Equation 1 applies to total stress constitutive models, while equation 2 is physically correct (Ladd & DeGroot, 2003) and can be employed in practice to calibrate constitutive models based on effective stress:

$$\tau_{max} = s_u = (\sigma_1' - \sigma_3')/2 \quad (1)$$

$$\tau_{max} = s_u \cdot cos[\phi_{cv}] \quad (2)$$

In the above equations, $\tau_{\max}$ is the shear stress at failure, s_u is the undrained shear strength, σ_1' and σ_3' are the major and minor principal stresses, and ϕ_{cv} is the constant volume friction angle. When interpreting DSS tests in the light of numerical modelling, it must be reminded that effective stress constitutive models do not reach failure at the highest shear stress in Mohr´s circle (defined by equation 1) but at the highest obliquity (defined by equation 2). For additional discussions on challenges in interpreting the DSS test see Fanni et al, (2022).

Interpretation of results

The biggest uncertainty and the open issue for discussion consists in reading and interpreting the results. As flow liquefaction trigger analyzes are relatively recent, there is yet no consensus on how to apply and interpret them, let alone regulated "allowable values" for typical cases (Sfriso & Ledesma, 2023).

From a scientific point of view, liquefaction is a physical process in which a pore pressure pulse is generated, which propagates in all directions at the propagation speed of sound in water, about 1600 m/s. This propagation cannot be modelled with the numerical techniques available in commercial geotechnical software packages, so what is actually being simulated is not the pressure pulse but rather an elastoplastic, quasi-static, strain-softening deformation including localization (Andrade et al, 2013), a problem that does not correspond to experimental observations of flow liquefaction, (e.g. Lade & Pradel, 1990). To illustrate the point, a plane strain compression test is simulated with a standard Mohr-Coulomb model and two modelling strategies: i) a undrained "plastic analysis", the usual engineering practice where no flow within the model is allowed; and ii) a fully coupled flow-deformation analysis, where boundaries are closed but flow is allowed within the sample (closer to the physics of the problem). Results are shown in Figure 6.

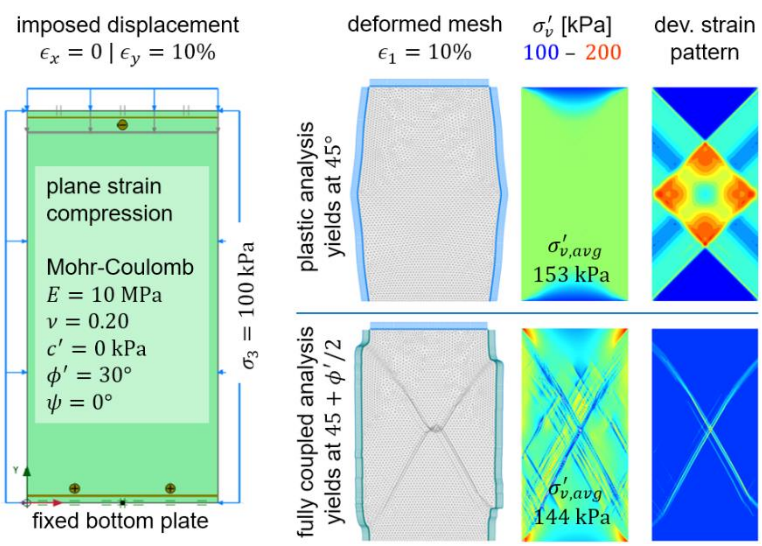

Figure 6. Undrained plane strain compression using plastic and fully-coupled strategies.

Very different deviatoric strain patterns, but similar stresses at failure, are obtained: "plastic analysis" produces a rather uniform deformation, while fully coupled flow-deformation analyses produces a highly localized deformation. It is not yet clear to what extent the use of "plastic analysis" affects the results and conclusions of the study. Further research is required to address this open question.

Use of trigger analyses as a decision-making tool

The geomechanical problem of upstream-raised tailings dams is created by the fact that tailings are artificial soils that are stored in dams, their stability depending on the strength of the tailings themselves. The real problem requiring a decision from stakeholders is different: identify the multiple sources of data, evaluate their reliability and uncertainty, and somehow quantify the risk that a tailings dam, if it starts a deformation process, will develop a progressive failure leading to loss of containment and spillage of tailings.

In pushover trigger analyses, in which a monotonic increasing load or strain is applied, failure of the dam is almost always achieved, because there is always an action strong enough to fail the dam. Therefore, failure is not an indication of vulnerability. The failure shape, the value of the trigger action (load, displacement, etcetera) and the deformation from onset of failure to loss of containment, on the other hand, are valuable sources of information for decision-makers. As an example of typical outcomes, see Figure 7: a) a load at the crest creates an inconsequential superficial slope instability; b) the liquefaction of a cluster creates a global failure surface but no apparent loss of containment; and c) a rise of only 2.0 m in the phreatic surface at the right end of the model triggers global failure.

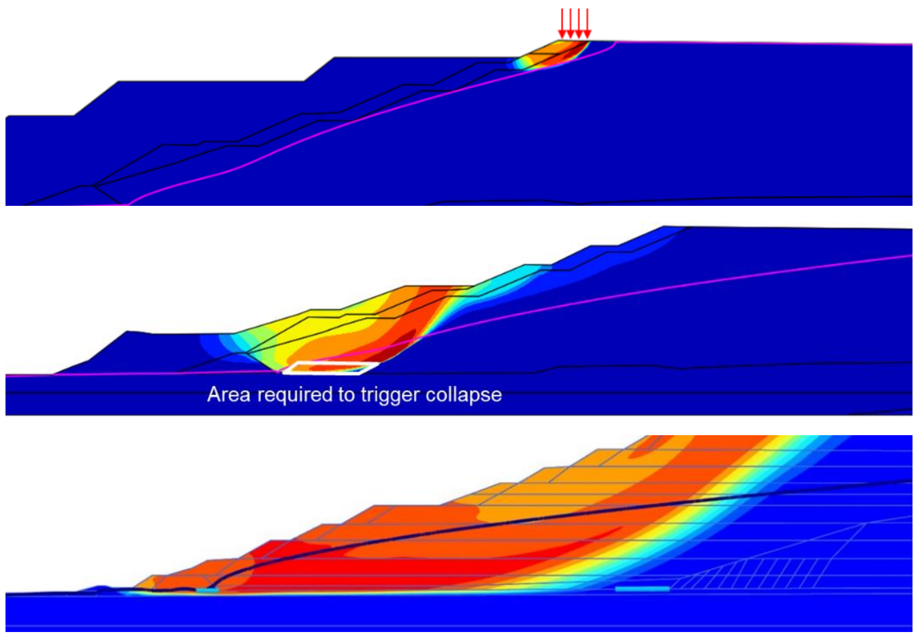

Figure 7. Examples of trigger analyses a) a load at the crest; b) liquefaction of a cluster; c) rise in the phreatic surface.

Conclusions

This paper summarizes recent experiences with trigger analyses of upstream-raised tailings dams, resulting from the enforcement of ICMM/GISTM and ANCOLD guidelines. Trigger analyses complement and, in some cases, replace traditional stability analyses employing limit equilibrium procedures, as they can provide engineering estimates of the liquefaction vulnerability of a given dam as a system.

The industry is building consensus on how to interpret trigger analyses. In this paper, some comments are provided with respect to the choice of static vs dynamic analyses, plastic vs fully coupled flow-deformation analyses, the use of deformation models to address an extended version of SSR stability analyses, and approaches to trigger analyses. It is claimed that trigger analyses can be understood as numerical excursions around a stable configuration to check the stability of equilibrium and the resilience of the system, and as such it is not very important if a particular trigger is a credible action on a given dam.

Being one, if not the most important trigger, a change in the phreatic surface is always employed in trigger analyses. In this paper, the use of a step-like SWCC is revisited to show that it can be a convenient and robust numerical tool to account for the distinct behaviour of saturated and unsaturated tailings, albeit avoiding the need for remeshing or other manual updates to models.

Trigger analyses, however, have proven to be valuable sources of information for decision makers. Outcomes like the failure shape, the value of the trigger action, and the deformation from onset of failure to loss of containment, aid in deciding whether a TSF requires reinforcement, buttressing, drainage or other works, decisions that are not easy to do with the limited information provided by limit equilibrium analyses.

Multiple uncertainties remain, related to input data, the modelling as such, and the interpretation of results. Liquefaction is a physical process in which a pore pressure pulse propagates within the dam, but modelling practice in fact simulates a shear-induced strain softening and localization, in essence a different mathematical and physical problem. It is not yet clear to what extent this simplification affects the results and conclusions of the analyses, and therefore further research is required to address this open question.

Acknowledgements

This paper is the result of the team work of a large numerical modelling group sitting in various parts of the world, and working together to service the pressing demands of the mining industry. The names of the members of this group can be found in the author´s list of the many references cited in this text. A special acknowledgement is owed to the many clients and reviewers that support our work with their opinions and advice.

References

ANCOLD. 2019. Guidelines on tailings dams– planning, design, construction, operation and closure, revision 1. www.ancold.org.au.

Andrade J., A. Ramos and A. Lizcano. 2013. Criterion for flow liquefaction instability. Acta Geotechnica, 8(5), 525-535.

Benz, T. 2006. Small-Strain Stiffness of Soils and its Numerical Consequences. Ph.D. thesis, Universität Stuttgart.

Brinkgreve, R., S. Kumarswamy, W. Swolfs, E. Engin, F. Fonseca Arévalo, N. Ragi Manoj, L. Zampich and N. Zalamea. 2020. Plaxis Manuals. Bentley Systems.

Fanni, R., D. Reid and A. Fourie. 2022. On reliability of inferring liquefied shear strengths from simple shear testing. Soils and Foundations 62(3), doi.org/10.1016/j.sandf.2022.101151.

International Council on Mining and Metals. 2020. Global Industry Standard on Tailings Management. GlobalTailingsReview.org.

Jefferies, M. 1993. Nor-Sand: A simple critical state model for sand. Géotechnique 43(1), 91-103.

Jefferies, M. and K. Been. 2016. Soil Liquefaction - A critical state approach. 2nd ed., CRC Press, London.

Ladd, C. 1991. Stability evaluation during staged construction. The XXII Karl Terzaghi Lecture. Journal of Geotechnical Engineering, 117(5), 540-615.

Ladd, C. and J. DeGroot. 2003. Recommended practice for soft ground site characterisation: Arthur Casagrande Lecture. Proceedings 12th PCSMGE, Boston.

Lade P. and D. Pradel. 1990. Instability and plastic flow of soils. I: Experimental Observations. Journal of Engineering Mechanics, ASCE, 116 (11): 2532–2550.

Ledesma O., D. Manzanal, and A. Sfriso. 2021. Formulation and numerical implementation of a state parameter-based generalized plasticity model for mine tailings. Computers and Geotechnics, 135 (2021) 104158.

Ledesma O., A. Sfriso and D. Manzanal. 2022. Procedure for assessing the liquefaction vulnerability of tailings dams. Computers and Geotechnics, doi.org/10.1016/j.compgeo.2022.104632.

Ledesma, O. (2023). Modelación numérica de licuación de presas de relaves. Tesis Doctoral: Universidad de Buenos Aires.

Li, X. and Y. Dafalias. 2000. Dilatancy for cohesionless soils. Géotechnique. 50(4), 449–460.

Rivarola F., N. Tasso, K. Bernardo and A. Sfriso. 2022. Numerical aspects in the evaluation of triggering of static liquefaction using the HSS model. XXXIX MECOM, Bahía Blanca.

Rivarola F., N. Tasso, K. Bernardo, M. Sottile and A. Sfriso. 2023. Evaluation of the triggering of static liquefaction of tailings dams considering the SWCC. Mine Waste and Tailings 2023, Brisbane.

Schanz T. and P. Vermeer. 1999. The Hardening soil model: Formulation and verification. Beyond 2000 in Computational Geotechnics, Rotterdam, p. 281-290.

Sfriso A. and G. Weber. 2010. Formulation and validation of a constitutive model for sands in monotonic shear. Acta Geotechnica, doi 10.1007/s11440-010-0127-y.

Sfriso A and N. Ledesma. 2023. The contribution of numerical modelling to the engineering of tailings storage facilities. Eduardo Núñez Lecture, XXVI CAMSIG, Comodoro Rivadavia.

Sottile M., N. Labanda, A. Kerguelén, I. Cueto and A. Sfriso. 2020a. Stability assessment of a tailings storage facility using a non-local constitutive model accounting for anisotropic strain softening. IACMAG 2020, Torino.

Sottile M., I. Cueto and A. Sfriso. (2020). A simplified procedure to numerically evaluate triggering of static liquefaction in upstream-raised tailings storage facilities. Proceedings XX COBRAMSEG, Brazil.

Sottile M., I. Cueto, A. Sfriso, O. Ledesma and A. Lizcano. 2022. Flow liquefaction triggering analyses of a tailings storage facility by means of a simplified numerical procedure. Proceedings XX ICSMGE, Sydney.

Yu H. (1998). CASM: a unified state parameter model for clay and sand. International Journal for Numerical and Analytical Methods in Geomechanics, 22, 621–653.

Consulting Experience in the Implementation of the Global Industry Standard on Tailings Management

Claudio Román, Ausenco, Chile
Fernanda Kunoh, Ausenco, Brazil
Gabriela Barbosa, Ausenco, Chile
Alix Becerra, Ausenco, Chile
Eric Chucos, Ausenco, Peru

Abstract

The launch of the Global Industry Standard for Tailings Management, GISTM, in 2020 has undoubtedly helped to gain a better understanding on how to develop safe and responsible management of tailings storage facilities (TSF) by incorporating social and environmental aspects into tailings management systems. The Standard has led mining stakeholders to rethink how TSF are being designed, built, operated, monitored, and closed nowadays; and even more important, how they are managed, reviewed, maintained, and governed.

This paper aims to show Ausenco's experience in implementing GISTM and assessing its conformance in different mining companies, focusing on the key concepts and approaches taken to address the 6 Topics, 15 Principles, and 77 Requirements covered by the Standard. This covers guidelines for initiating implementation of the Standard considering the context in which the TSF is situated, how the mining company should be involved, the importance of understanding the credibility of failure scenarios and associated risks, and finally, what happens after implementation.

Introduction

In response to increasing TSF catastrophic failures, tailings management has taken on a more prominent role in responding to growing public concerns about the negative social and environmental impacts of the mining industry.

Recent iconic failures of Mount Polley (Canada, 2014), Fundão (Brazil, 2015), and Córrego do Feijão (Brazil, 2019) have raised doubts about the high risk levels involved in the mining industry, generating an atmosphere of uncertainty in which the social license to operate is being called into question.

Motivated by the above described, the International Council on Mining & Metals (ICMM), the United States Environment Programme (UNEP), and the Principles for Responsible Investment (PRI) decided to elaborate a guide as a tool to help preventing the occurrence of more tailings catastrophes, and jointly released the Global Industry Standard for Tailings Management, hoping it will be a major step towards recovering society's reliance in mining. The Standard rises as a comprehensive response to current international challenges and concerns, integrating the social aspect as one of the fundamental pillars.

The GISTM was elaborated through an independent process, including the support of a multidisciplinary expert panel, input from a stakeholder advisory group and an expanded public consultation that incorporated affected communities, government representatives, investors, multilateral organizations, and mining industry representatives. It was based on a comprehensive review of the international standards and guidelines, including the Towards Sustainable Mining's Mining Waste Protocol, Initiative for Responsible Mining Assurance's Standard for Responsible Mining, and ICMM's Tailings Governances Position Statements, among others (Global Tailings Review, 2020).

This Standard stands out by connecting technical tailings management with social performance, providing a more holistic and responsible approach to safe management. By incorporating the best available practices (BAP) of sustainable mining, the GISTM recognizes the need of involving local communities and indigenous groups, as well as to promote transparency and accountability, in decision making.

Traditionally, tailings management has been centered on operational continuity of mineral processing and mine waste disposal. The current scenario calls for a change in the course of action towards sustainable development through BAP and BAT (best available technologies), strengthening tailings management systems and the way in which the mining industry conducts its business.

This paper explores the most important aspects of GISTM implementation based on Ausenco's experience, providing recommendations for preliminary steps, and undertaking application of the Standard.

Key Aspects on GISTM Implementation

Since before 2020, Ausenco was already participating as a consulting firm in specialized studies, which were later formalized in the GISTM, such as Dam Breach Analyses (DBA), risks assessments under the FMEA (Failure Modes and Effect Analysis) methodology, Dam Safety Reviews (DSR) and Operation, Maintenance and Surveillance (OMS) manuals updates, among others.

Furthermore, Ausenco has developed a methodology for progressive evaluation of compliance in the implementation of the Standard in different TSF, based on the Conformance Protocols of ICMM, which has allowed to identify gaps, elaborate plans to cover them and finally, assist in the development of follow-up mechanisms for proper functioning of tailings management systems.

Based on this experience, 8 key aspects to consider during the GISTM implementation have been identified (Figure 1).

Figure 1: Key aspects on GISTM implementation

Where to Start

The GISTM convers 6 main topics, divided into 15 principles from which 77 requirements are derived, as shown in Figure 2. The implementation of the Standard is supported by three documents: the Conformance Protocols (ICMM, 2021), used to apply and verify the compliance of the 77 requirements; the Good Practices Guide (ICMM, 2021), which supports the use of BAP and BAT for tailings management; and the Tailings Governance Framework (ICMM, 2021), which states the context and management responsibilities in the governances of the TSF.

At first glance, the idea of verifying compliance with the 77 requirements may sound overwhelming. Although Topic I "Affected Communities" is the core of the Standard – which is not in doubt –, it is convenient to start from what is more familiar to the Operator: Topic III "Design, Construction, Operation and Monitoring of the Tailings Facility". The application and verification of conformance with this topic allows to quickly understand the magnitude of the potential impacts associated with the TSF risks, based on the utilized design criteria. Identifying potential failure modes of a facility and their potential consequences is fundamental when developing a tailings management system based on risk management.

From Topic III results natural to move on to Topics II and IV, identifying the affected area by the facility through the development of an interdisciplinary "Integrated Knowledge Base", and review of the governance structure that supports the management system.

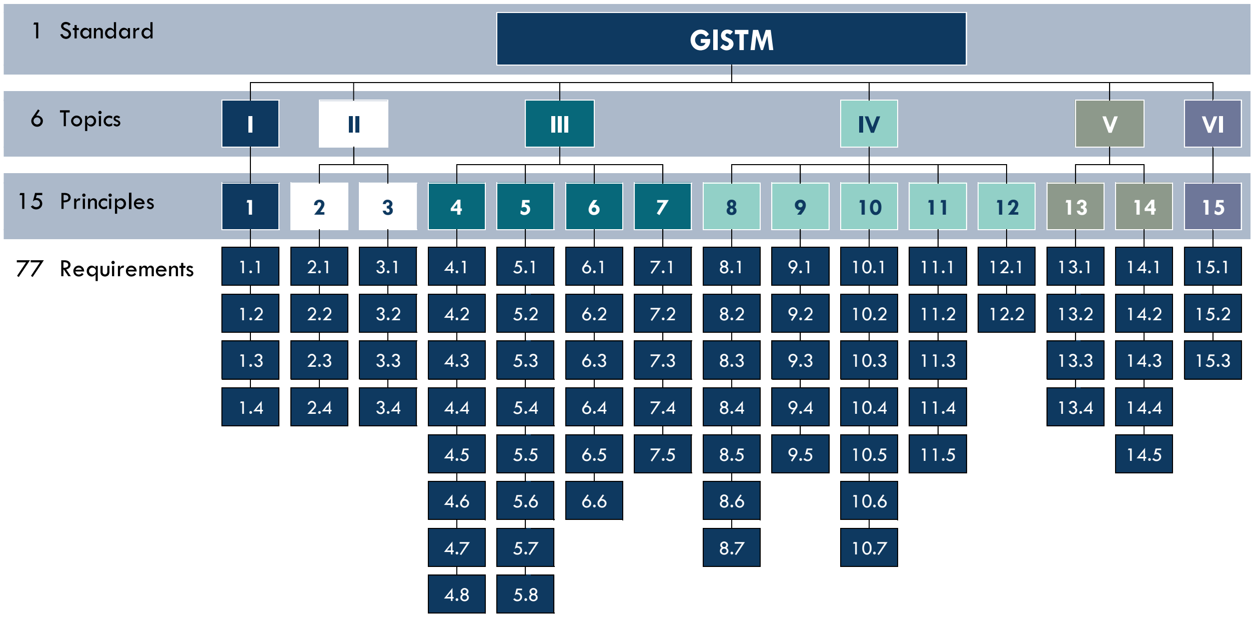

Figure 2: Distribution of GISTM Topics, Principles and Requirements

Having accomplished the development of the above topics, it is possible to move on to Topic I "Affected Communities" and Topic V "Emergency Response and Long-Term Recovery", which are connected as they are directly related to the "meaningful engagement" of affected communities in the co-development of plans. Regarding these topics, it should be pointed out that "meaningful engagement" is to be interpreted as the achievement of effective understanding between both parties (communities and mining company) for joint decision making. The mining company must characterize their respective communities, understand, and actively listen their requests and propositions in order to build long-lasting rapport in time.

Last but not least, is the public disclosure of the information to support public accountability, as stated in Topic VI "Public Disclosure and Access to Information", which primary objective is to report the most important evaluated aspects and their support in a clear and simple manner for all stakeholders.

Local and International Context

On the other hand, when starting the implementation of the Standard, it is necessary to consider the local and global context in which the TSF and the mining company are immersed.

With respect to local regulations, one might ask: are they aligned with the best practices and requirements of the GISTM? How? In general, countries with characteristics as high seismicity require regulatory compliance with stringent seismic design criteria. Also, global mining companies tend to have corporate standards that comply with the best practices in tailings management.

Consideration should also be given to the maturity of the mining industry in the location of the TSF, since it is not the same to implement the Standard in one country or another. In this case, some helpful questions may be: How developed is the mining industry in this location? What is the social perception of the company? Have there been any conflicts with nearby communities? How is the social license and stakeholders' confidence supported?

An understanding of this context will help to adapt and interpretate the GISTM requirements from a local point of view, and find the better way to implement these principles in any TSF.

Mining Company Vision

GISTM implementation is not just about developing reports and standards and tracking them to display a badge indicating that the company complies with the Standard. The long-term vision, commitment and empowerment of the Operator are key elements.

The mining company must immerse in the philosophy behind the Standard, its pillars, and guiding principles. The motivation of the stakeholders involved in the Standard and social, environmental, and economic benefits must be comprehended, as well as that the ultimate goal is for society to regain confidence in the mining industry and become part of it, in order to embark on the path towards sustainable development through responsible investment, which will also enhance the recovery of the mining industry's reputation.

Besides the above, it should not be forgotten that this joint process must be monitored and controlled for continuous improvement. A strong governance system, which can ensure continuity of roles, should support this monitoring and handover of information. This may be particularly relevant for older TSF which may not have up-to-date and/or supported data.

Establishing a Company Coordinator

This aspect is strongly connected with the previous one. When contracting a third party to assist in the implementation of the Standard, the mining company must not lose sight of the scope that the consultant will cover in this role, which is generally focused on providing guidelines, conducting independent revisions, and developing specific studies for successful implementation and follow-up continuity.

Even if the implementation of the Standard is developed with or without the advice of a consultant, the assignment of a GISTM company coordinator – or team –, with a high level of dedication to this process has been proven to be key. The coordinator should have direct contact with the operators, responsible entities and key roles identified by the GISTM, such as the Engineer of Record (EoR) and the Responsible Tailings Facility Engineer (RTFE). In case of working with a third party, this coordinator should also have direct contact with the consultant.

Figure 3 shows an example of evolution tracking of GISTM compliance for a single TSF (and how complex it can result), according to the criteria described in the Conformance Protocols (ICMM, 2020) and the staged assessment methodology used by Ausenco in its evaluations. As presented in the diagram, this process may require several (more than one) evaluations, and a specific follow-up on each requirement and its associated criteria, without forgetting the overall vision.

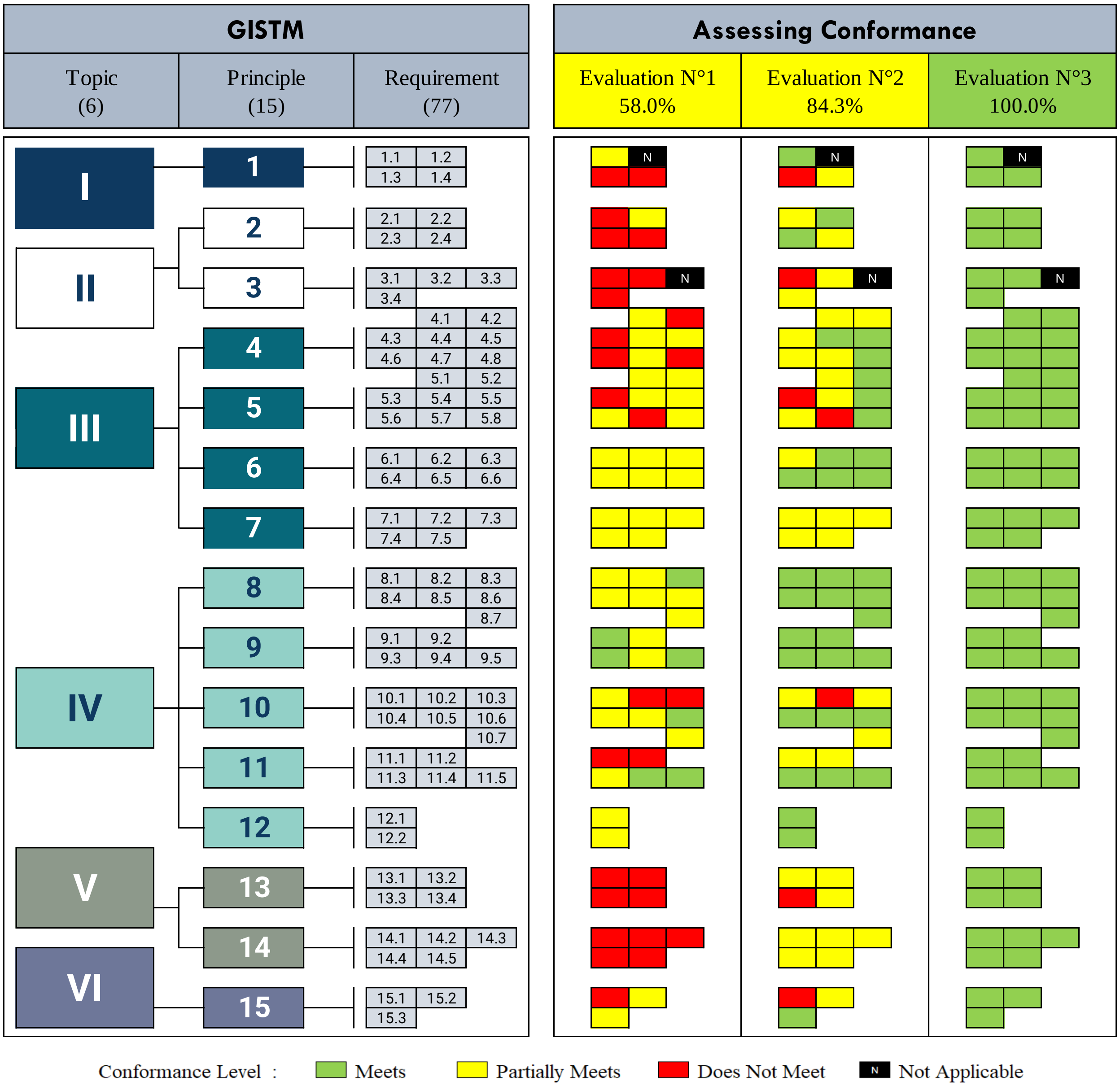

Figure 3: Example of follow-up on the GISTM implementation

Without any doubt, the assignment of this role contributes to unify and align criteria in different areas of the mining company such as operation, construction, environment and legal, in addition to facilitate the implementation process.

Different People, Different Results

People play a fundamental role in the implementation of the Standard. Not only because communities are at the center, but also because people are in charge of the implementation, evaluations, and updates in line with the Global Tailings Review guidelines.

Although GISTM aims to standardize the way things are being done, it is inevitable that the results may vary depending on who executes them. Since the implementation has a great influence of the vision, motivation, and experience of those participating, it is quite likely that different people (companies and/or consultants) will arrive to different results, with a common base of tailings management knowledge.

Moreover, it is probable that all stakeholders have different particular goals based on their needs. While mining companies may be interested in achieving higher productivities, affected communities may want to eliminate their negative externalities, authorities may want safer and environmentally friendly operations, and investors may be concerned about risk control and profits. Because of the above, and given that the implementation requires the interpretation of conformance criteria, it is important for all participants to be aware of biases that may arise, and to stay open-minded in order to reach agreements in which none of the parties is left behind and the interests of all are safeguarded.

Credibility of Failure Scenarios

Understanding the credibility of the TSF failure scenarios is a key aspect to establish the design intent and compliance with all requirements associated with the facility. This requires the analysis of the credibility of failure modes and consequences. Conducting risk assessments through the Failure Modes & Effects Analysis (FMEA) methodology contributes significantly to this purpose.

According to Section 2.7.2 of the Good Practice Guide (ICMM, 2021), a credible failure scenario requires both failure mode and consequences to be credible, and when consequences – evaluated in a dam breach analysis (DBA) – are catastrophic, so is the scenario, as illustrated in Figure 4.

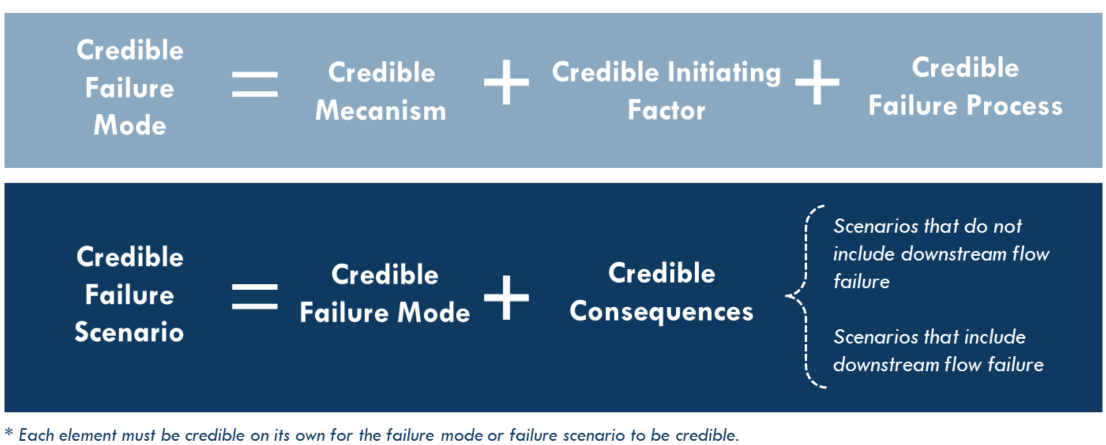

Figure 4: Credibility of Failure Scenarios

These potential catastrophic scenarios require controls to prevent the occurrence of failures, rigorous monitoring over time, and a stricter implementation of the GISTM principles. According to Hopkins & Kemp (2021), the risk-based approach requires decision making to be primarily based on the severity of consequences, rather than probability of occurrence. If the consequences of a risk are sufficiently serious, no matter how low the probability, actions must be taken to prevent the risk from occurring.

Therefore, having a good understanding for application of these concepts is key to establish the Consequence Classification of the TSF, which will imply certain effects on the implementation of the Standard depending on the level of consequence. Whilst the Standard recommends different design criteria according to the TSF Consequence Classification, the use of the criteria associated with the highest consequence categories, if possible, allows for a better management of the facility's risks.

ALARP

As stated by the GISTM, "As Low As Reasonably Practicable" (ALARP) "*requires that all reasonable measures be taken with respect to 'tolerable' or acceptable risks to reduce them even further until the cost and other impacts of additional risk reduction are grossly disproportionate to the benefit*".

This concept is mentioned 12 times throughout the Standard, and is explicitly incorporated into 4 of the requirements. ALARP can be applied using different semi-quantitative, qualitative or experimental methods, depending on the project conditions (e.g. geographical location, social constraints, environmental aspects, etc.) and its complexity. Regardless of the used method, the process itself is a powerful tool to document the approaches taken to reduce risks during the life cycle of the TSF to a level tolerable by society and in line with good practices.

Figure 5 illustrates the understanding according to some authors (Hartford, 2022) of the ALARP concept on how regulations and good practices relate to the tolerance ranges that society would have in relation to risk. It also shows that it is a dynamic concept that sets increasingly demanding limits over time.

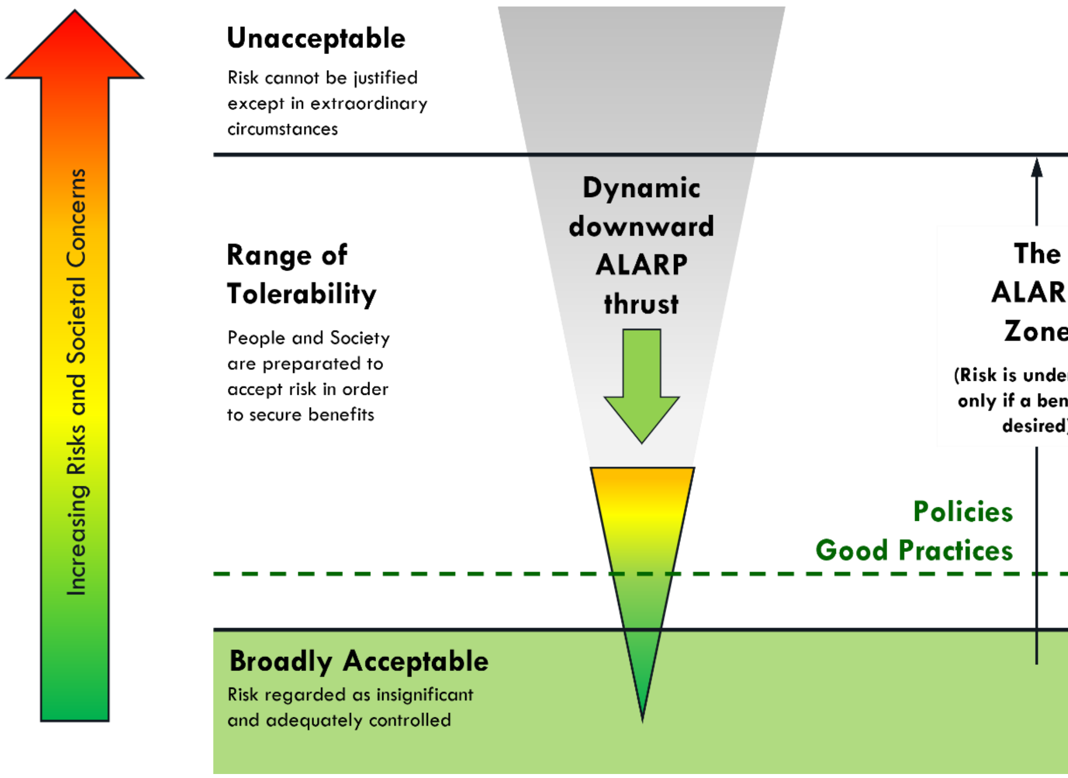

Figure 5: Understanding the ALARP Concept (adapted from Hartford, 2022)

Nevertheless, as it has been seen in recent years, putting this concept into practice is not easy. Considering that there are different points of view on how to implement it, it is difficult to reach a consensus. In fact, in the current scenario, there are groups with divergent positions regarding the ALARP approach. Adding independent lines of review to this process could be helpful in developing a deeper and more complete understanding.

This concept has definitely generated reflection and discussion in the mining industry, since the interpretation and application of this approach may vary according to the regulations dictated by the competent authorities in each jurisdiction, and the internal policies of each mining company.

Beyond Implementation

The process initiated by the launch of the GISTM does not end with the declaration of conformance in its implementation. Mining companies adopting the Standard should develop robust and understandable follow-up mechanisms, similar to the diagram shown in Figure 3.

The GISTM has stressed the importance of having robust governance systems in place (Topic IV "Management and Governance"), ensuring the recording and disclosure of the TSF information (Topic VI: "Public Disclosure and Access to Information"), and emphasizing the need to adopt a continuous improvement approach over time with clearly designated roles. In the other hand, technical causes of TSF failures have been extensively studied, but the same has not necessarily happened for organizational causes

(Hopkins & Kemp, 2021). Therefore, having an integral tailings management system, which is periodically reviewed and updated to keep the knowledge base up to date with the current state of art, is essential for safe operation.

The Standard and Mining Regulations in Brazil

Brazil has different organizations that supervise and/or deliberate on mining activities. Among these, it is CONAMA (*Conselho Nacional do Meio Ambiente* or National Environmental Council), which establishes the rules and criteria for the granting of licenses for effective or potentially polluting activities, as is the case of mining. The CNRH (*Conselho Nacional de Recursos Hídricos* or National Council of Water Resources) develops the mediation rules between the different water users, being one of the main actors in charge of implementing water resources management in the country. Additionally, it is the ANM (*Agência Nacional de Mineração* or National Mining Agency), which supervises research and extraction activities for the use of minerals, and the safety of TSF for the disposal of tailings resulting from these activities.

It should be noted that there is a broad legal framework when referring to the mining industry in Brazil. More specifically, in February 2022 the ANM issued a resolution regarding safety of TSF: Resolution N°95. In terms of governance, Resolution N°95 relates to the GISTM by legally establishing the necessity to incorporate the role of the Engineer of Record, and a risk management system for TSF with high damage potential.

The Emergency Preparedness and Response Plan (EPRP), noted in Resolution N°95 as a requirement for every TSF, regardless of the accumulated potential damage, is related to Topic V of the Standard. In this sense, it is important for mining companies to be prepared in case of failure of TSF. The issue is so relevant that Resolution N°95 additionally introduced the requirement to evaluate the compliance of the EPRP: it is necessary that another company verifies that this plan is effectively operational.

Conclusion

The publication of the Global Industry Standard on Tailings Management, GISTM, is a milestone for the evolution of responsible practices in mining, adding the pillars of meaningful participation of affected communities and environmental preservation as a basis for tailings management systems. This has brought significant advances in moving from a prescriptive design to a performance and risk-based approach.

This paper has identified 8 key aspects to consider in the process of implementation of the Standard, from a consultant's point of view, based on Ausenco's experience in implementation and conformance assessment of the GISTM. Stakeholders' engagement – including affected communities-, continuous development of knowledge bases, disclosure of operational information and deeper understanding of tailings facilities risks have been recognised as essential elements for safe and transparent management.

Considering that the deadline for publication of progress on GISTM implementation for tailings storage facilities with “very high” and “extreme” consequences has already expired, several mining companies have disclosed information on the status at their operations, which has led us to reflect… Does the publication of this information imply that communities are better informed or more involved today? Does this mean that companies are committed to adopt continuous improvement in the implementation of these principles? Have these efforts been focused on involving society or on winning back investors?

Although this first step of implementation has been completed for a number of larger facilities, the task is far from complete. Tailings management is a dynamic field, and therefore it is expected that new knowledge and technologies will continue to emerge. Given the above, it is vital that all stakeholders take a more proactive stance to maintain this process of continuous improvement, truly placing communities at the center, and not wait for another catastrophe to happen before taking action.

Mining companies must develop comprehensive tailings management systems, with clear action plans and robust governance, in collaboration with all stakeholders – communities, governments representatives, consultants, investors, and even other companies – to keep up to date with best practices for safe and sustainable operation. Let’s not forget that the causes of tailings storage facilities failures can also be related to organizational deficiencies, so periodic internal and reviews are vastly valuable and enriching.

In the end, multidisciplinary work and research, innovation, cooperation with a critical view, and a clear long-term vision, are essential to move forward on addressing the current global challenges on the tailings field.

References

Hartford, DND. 2022. *Reframing Risk-Informed Safety Assessment of Dams.* CDA Annual Conference, 17th – 19th October, St. John’s, Newfoundland & Labrador, p. 33-43.

Hopkins A., Kemp. D. 2021. *Credibility Crisis. Brumadinho and the Politics of Mining Industry Reform*.

Initiative for Responsible Mining Assurance. 2018. *Irma Standard for Responsible Mining.* IRMA-STD-001.

International Council on Mining & Metals, United Nations Environment Programme, Principles for Responsible Investment. 2020. *Global Industry Standard on Tailings Management.*

International Council on Mining & Metals, United Nations Environment Programme, Principles for Responsible Investment. 2020. *Towards Zero Harm.*

International Council on Mining & Metals. 2021. *Conformance Protocols: Global Industry Standard on Tailings Management.*

International Council on Mining & Metals. 2021. *Tailings Management: Good Practice Guide.*

Jarvie-Eggart, M. E. (Ed.). 2015. *Responsible mining: case studies in managing social & environmental risks in the developed world.* SME.

World Gold Council. 2019. Responsible Gold Mining Principles

A review of the key factors that influence pseudo-static stability analyses of downstream and upstream tailings sand dams

Camilo Morales, SRK Consulting, Chile
Carolina Palma, SRK Consulting, Chile
Jaime Olivares, Universidad de Chile, Chile

Abstract

Limit equilibrium analyses under pseudo-static conditions are compulsory by most international standards, which establish a minimum factor of safety (FoS) typically ranging from 1.0 to 1.2 for stability analysis. The limitations of this type of analysis are acknowledged, particularly regarding the fact that the stress-strain response of the materials is not considered, and the seismic load is represented by the addition of an inertial force. However, insights about the seismic response of the structure may still be obtained through a quick and simplified analysis. This paper presents a review of the parameters influencing the pseudo-static analysis results of downstream and upstream tailings sand dams. During the modeling stage, generic downstream and upstream dams are analyzed using steady-state analysis in Slide2, by which the water table is determined, and a subsequent limit equilibrium analysis (LEA) is performed to assess dam stability. From this analysis, various dam heights, drainage conditions, and beach lengths are evaluated, allowing the degree of influence of these parameters on the FoS for both construction methodologies to be compared.

Introduction

Tailings, the primary waste generated from mining exploitation, consist of the chemicals utilized for ore extraction, uneconomic metals, minerals, organisms, and typically a substantial quantity of water (Heidarian, 2012). As the demand for commodities experiences an annual increase, the discovery of high-mining-grade ore bodies is observed to be becoming increasingly complex, leading to the generation of more mining waste. This, in turn, necessitates an expansion in the size of tailings storage facilities (TSFs) (Blight, 2010). In the context of current ore grades, it can be noted that more than 99% of the rocks extracted are categorized as mining waste.

Given the presence of water containing toxic chemical compounds in tailings dams, the design of these facilities is faced with significant challenges to prevent adverse effects on the environment and the nearby populations. Regrettably, numerous failures of tailings dams have been documented in the literature during the latter half of the 20th century (Rico et al., 2008). In the past decade, particular attention has been drawn to catastrophic dam disasters that have transpired in upstream tailings facilities, such as those at Mount Polley (2014), Fundão (2015), Feijão (2019), and, more recently, Jagersfontein (2022). These incidents resulted in severe environmental damage and loss of life (Morgenstern et al., 2015; Morgenstern et al., 2016; Robertson et al., 2019; Mail & Guardian, 2022).

Worldwide, many of these structures are found in highly seismic regions such as Chile, Peru, or Mexico, where the occurrence of earthquakes with magnitudes above Mw 7.5 is not uncommon. Consequently, the seismic design of these structures is recognized as playing a crucial role in stability analysis. Indeed, numerous failures in Chile and Peru during the past century have led both countries to forbid the construction of upstream tailings dams. Following the Feijão dam failure in 2019, this construction methodology was also banned in Brazil (CIM Magazine, 2019). However, most abandoned TSFs were constructed using this methodology and were subject to low engineering standards. Therefore, understanding the key parameters influencing these structures' geomechanical response is critical.

The stability of a dam may be influenced by several factors, including - but not limited to - the construction methodology, the dam's geometry and material, the position of the pond (or beach length), and the tailings discharge rate (Sarsby, 2013; Vick, 1980). When multiple critical factors coincide, the dam's stability might be compromised due to inadequacies in the design, construction that lacks quality control, or improper operation. Furthermore, partial, or total collapses can occur in many instances when seismic effects are considered.

This research focuses on identifying the key factors that influence the stability of downstream and upstream tailings dams in LEA under pseudo-static conditions, specifically regarding the FoS results. Consequently, multiple factors are examined to ascertain their relative importance in the seismic stability of both types of facilities. This includes consideration of variations in dam heights, beach lengths, drainage conditions, and different seismic horizontal coefficients.

Pseudo-static analysis in tailings dams

Kramer (1996) identified the assessment of seismic slope stability as one of the most frequent and challenging tasks in geotechnical earthquake engineering practice. Analytical methods, from pseudo-static LEA to finite element analysis, have been widely integrated into various commercial software tools. These tools can be utilized to compute and evaluate the performance of slopes rapidly.

In general terms, the pseudo-static approach is essentially analogous to the static method but incorporates a horizontal force (F_h) to represent the earthquake load (Vick, 1983). This force is commonly expressed by the horizontal seismic coefficient (k_h) multiplied by the weight of the potential sliding mass (W). Figure 1 presents the typical generalized pseudo-static analysis setting, in which both horizontal and vertical forces (F_v) are considered.

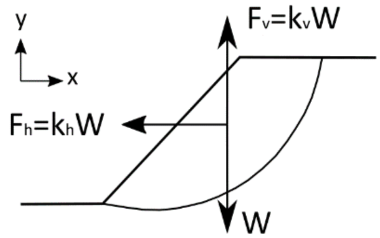

Figure 1: Pseudo-static analysis approach (from Morales, Bard and Palma, 2021)

Notwithstanding, certain limitations are inherent in pseudo-static analysis, as it does not consider compatibility or displacement boundary conditions, and, therefore, it fails to indicate the induced deformation caused by ground shaking. Owing to this limitation, properly incorporating brittle material behaviour and pore water pressure generation into the analysis cannot be achieved. Consequently, these analyses are typically conducted during the initial engineering stages of the design process.

In countries characterized by low seismicity, the value of k_h is typically lower than 0.1. In contrast, in highly seismic regions such as Chile, Peru, Mexico, and Japan, this value may range from 0.1 to 0.25, depending on the area and the type of structure (Melo & Sharma, 2004; Towatha, 2008; Campaña, 2019). Within the geotechnical practice on tailings dams, the kh value is still determined as a function of the peak ground acceleration (PGA), which is usually derived from the site-specific probabilistic seismic hazard assessment (PSHA) (Kramer, 1996; Towatha, 2008; Campaña, 2019).

From the regulatory perspective, most international standards and regulations commonly mandate a LEA under pseudo-static conditions for assessing seismic slope stability performance. In this analysis, attaining a minimum factor of safety (FoS) that ranges from 1.0 to 1.2 is typically necessitated to continue the design process. More advanced analyses are performed during subsequent engineering stages (Sernageomin, 2007; ANCOLD, 2012; CDA, 2014).

However, the FoS is not only dependent on the engineering design but also influenced by construction and operation; consideration of these aspects should also be incorporated in the analyses. Several authors have studied tailings dam stability, and it has been established that water management issues are among the main reasons for tailings dam failures (Saad, 2008; Rico, 2008; Morales & Taborda, 2022).

In addition, studies have shown that most failures occur in upstream tailings dam facilities (UTSFs). The most critical triggers, identified as static and seismic liquefaction, piping, and beach overtopping, are cited respectively (Morales & Taborda, 2022). These factors are directly or indirectly linked to saturated soil undergoing high pore-water pressures, hydraulic gradients, or elevated phreatic surfaces (Brisson, 2006). Consequently, it must be understood that the behaviour of saturated tailings and poorly compacted sand tailings can transition from a drained to an undrained response, dramatically reducing their shear strength. Such occurrences are commonly attributed to a high construction rate (short drying time in tailings of upstream dams) and seismic events.

Sarsby (2013) establishes, through a steady-state analysis, that a ratio between the beach length (measured horizontally from the toe of the dam, L) and the height of the dam (H) of less than five may be critical for the TSF stability. Conversely, L/H ratios over ten have been proven to be safe. This conclusion was drawn under the consideration of a static scenario (k_h=0) and a basal drain (located below the dam) operating in accordance with its design, that is, with a zero-pore water pressure BC at its boundary. Unfortunately, the literature provides limited information regarding how these findings might be altered if seismic effects are considered or how they might influence various construction methodologies.

Geotechnical Model

Geometry

Figures 2a, and b show the generic models implemented in Slide2 to simulate downstream and upstream dams, respectively. Based on this, five geotechnical units can be identified in both models: the foundation soil, basal drain, starter dam, tailings, and sand dam. For the upstream dam case, sand dyke rises of 5 m height have been considered. The overall downstream slope of both dam models is 4:1 (H:V), or 14° of inclination, with a crest width of 10 m and a freeboard of 3 m. Additionally, a 1% slope has been assumed for the tailings on the impoundment, representing an average condition for conventional tailings (Blight, 2010).

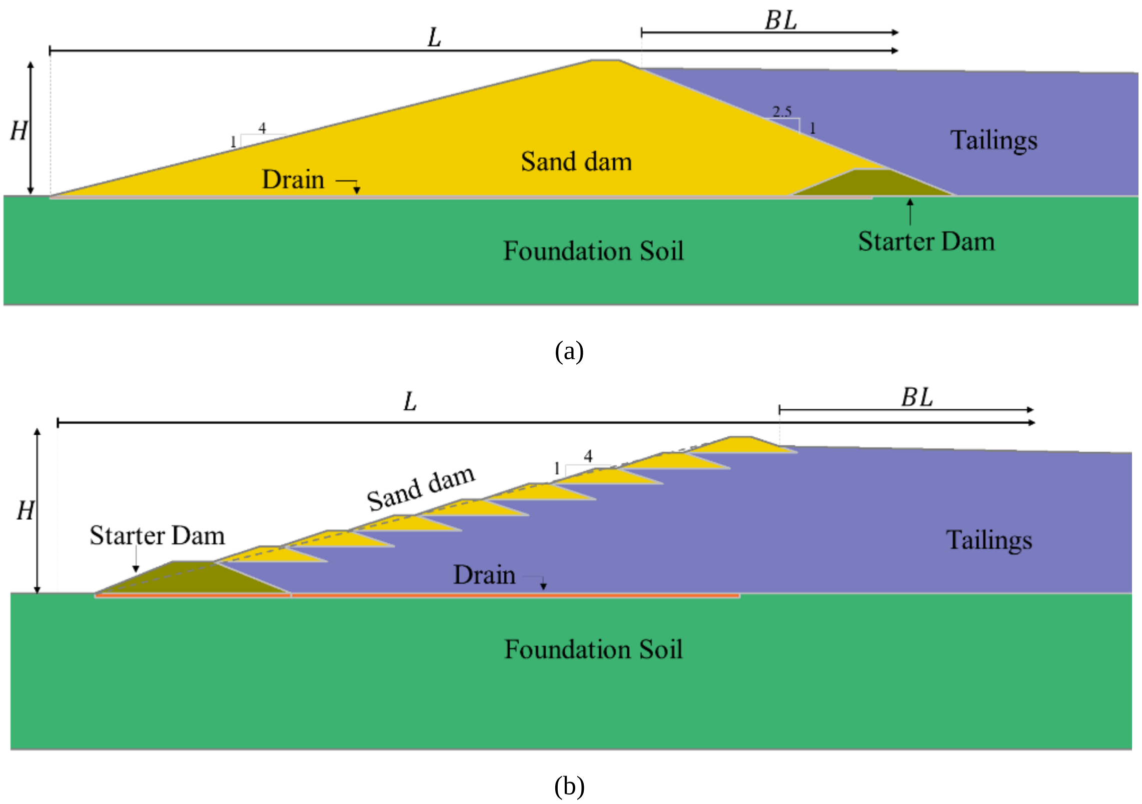

Figure 2: (a) Downstream and (b) upstream dam generic models implemented in Slide2

Material properties

Table 1 presents the saturated permeabilities in both the vertical and horizontal directions for the steady-state analysis. According to Table 1, foundation soil was excluded because it was considered impervious for simplicity (i.e., with kv=$1\cdot10^{-20}$ m/s in the model). Regarding material's anisotropy, an increase of 10 and 5 times in the horizontal direction was considered for tailings and tailings sands permeabilities, respectively, following similar procedures available in the literature for steady-state analyses (Valenzuela, 2015; Sarsby, 2013). For the starter dam and drainage material, constant saturated permeabilities of k_v^{sat} $=1\cdot10^{-5}$ m/s and k_v^{sat} $=1\cdot10^{-4}$ m/s were considered, respectively (Blight, 2010; Kulhawy & Mayne, 1990).

Regarding mechanical properties, Table 1 presents the Mohr-Coulomb parameters considered for each geotechnical unit. Again, to isolate the effect of the foundation, this material has been considered with infinite strength. According to Blight (2010) and Sarsby (2013), tailings and tailings sands were considered cohesionless. Regarding the friction angle, the average parameters provided by Vick (1983) were adopted. For the total stress parameters used to represent the undrained behaviour of tailings and sand tailings, the average values provided by Jefferies & Been (2016) were adopted. Finally, coarse materials such as the drain and the starter dam were considered using the guidelines of Kulhawy and Mayne (1990) for medium-dense gravel. In addition, these materials are considered to behave under drained conditions in the static and pseudo-static analyses; hence, the undrained parameters are not reported in Table 1.

Table 1: Hydromechanical properties considered for each geotechnical unit

Material	$\gamma_{dry}\left(\frac{kN}{m^3}\right)$	$\gamma_{sat}\left(\frac{kN}{m^3}\right)$	$k_v^{sat}(m/s)$	$k_h^{sat}(m/s)$	$\phi'(°)$	$c'(kPa)$	S_u/σ'_{v0}
Tailings	14	18	$1\cdot10^{-7}$	$1.5\cdot10^{-6}$	30	0	0.1
Sand dam	16	18	$3\cdot10^{-6}$	$1.5\cdot10^{-4}$	35	0	0.2
Starter dam	20	21	$1\cdot10^{-5}$	$1\cdot10^{-5}$	40	0	-
Drain	20	21	$1\cdot10^{-4}$	$1\cdot10^{-4}$	40	0	-

Cases of analysis

Three dam heights (H) were analyzed: 20, 50, and 80 m, along with five beach length ratios (L/H) for upstream dams (for downstream dams, only H/L ratios of 5, 7, and 9 were considered). A basal drain was considered for the upstream and downstream dam setting, extending from the toe of the dam up to half the crest width. Regarding the drainage conditions, two scenarios were considered: the first involved a fully operational drain, implying a zero-pressure boundary condition (BC) application. In contrast, the second scenario simulated a clogged drain (with no zero-pressure BC applied and reducing its permeability by a factor of ten). All these combinations of cases were analyzed for k_h values of 0.05, 0.10, and 0.15. For simplicity, the vertical seismic coefficient was neglected. All these combinations resulted in 2160 cases of analysis.

Modeling considerations

The geotechnical models were discretized for the steady-state analyses using 6-node triangular elements, with an average element size of 1 m on the tailings. Based on this, a steady-state analysis was conducted to estimate the position of the phreatic surface. For this analysis, a base case scenario was considered, with a beach length ratio (H/L) corresponding to a 50 m dam's height for both construction methodologies. For both types of dams, using a geomembrane on the upstream face was not considered, which, in the long term, is similar to considering a leaky geomembrane.

The calculated phreatic surface in the steady-state analysis is used as an input for the LEA. The FoS is then calculated using Morgenstern and Price's (1967) methodology for non-linear potential slipping surfaces. Based on this, only global failures are analyzed, with the requirement that the slipping surface must compromise at least half of the dam's crest, and the toe must be involved in the failure. Additionally, the depth of the potential slipping surfaces is set to be at least 20% of the dam's height.

Regarding the behavior of the soil, tailings and sand tailings below the water table are considered to behave undrained for pseudo-static analysis. In contrast, geotechnical units above the water table are considered to behave as drained. Finally, the starter dam and drain material are assumed to behave as drained for static and pseudo-static analyses.

Results

The FoS for the base case scenario, with beach length ratios (L/H) ranging from 5 to 13 for downstream and upstream dams of a 50 m height, is presented in Figure 3a, b. The continuous line shows an operative drain ("OP"), while the dashed lines show a clogged drain scenario ("CL") with the permeability reduced by a factor of 10. Additionally, the analyses are presented for horizontal seismic coefficients ranging from 0.05 to 0.15. For the static scenario (k_h=0), two cases were considered: (i) all materials exhibiting drained behavior ("dr"), and (ii) all materials displaying undrained behavior ("und").

Based on Figure 3, when the drain is fully operative, the FoS does not vary with the beach length or L/H ratio, regardless of the construction methodology when applying a seismic load (kh). However, it can be observed that the higher the k_h applied, the lower the FoS becomes. These results indicate that assuming pwp=0 to be zero at the drain boundary could be too optimistic in terms of the stability analysis since this situation leads to a lowering of the phreatic level to the level of the foundation soil, resulting in minimal soil saturation. It is also important to mention that even when considering a beach length of 50m, the water table does not influence potential slip surfaces.

Additionally, in the static case (kh=0), the FoS for downstream dams (see Fig 3a) and clogged drain is influenced by the beach length only for L/H<9 for drained behavior and L/H<11 for undrained behavior, respectively. Indeed, for larger beach lengths, the FoS reaches the same value as the fully operative drain case.

For downstream dams with k_h=0 and a clogged drain (see Fig 3b), the FoS is influenced by the beach length up to L/H<9 for drained behavior. However, for undrained behavior, the FoS decreased dramatically compared to the drained behavior. Beach lengths ratios below 9 are not safe according to most international standards.

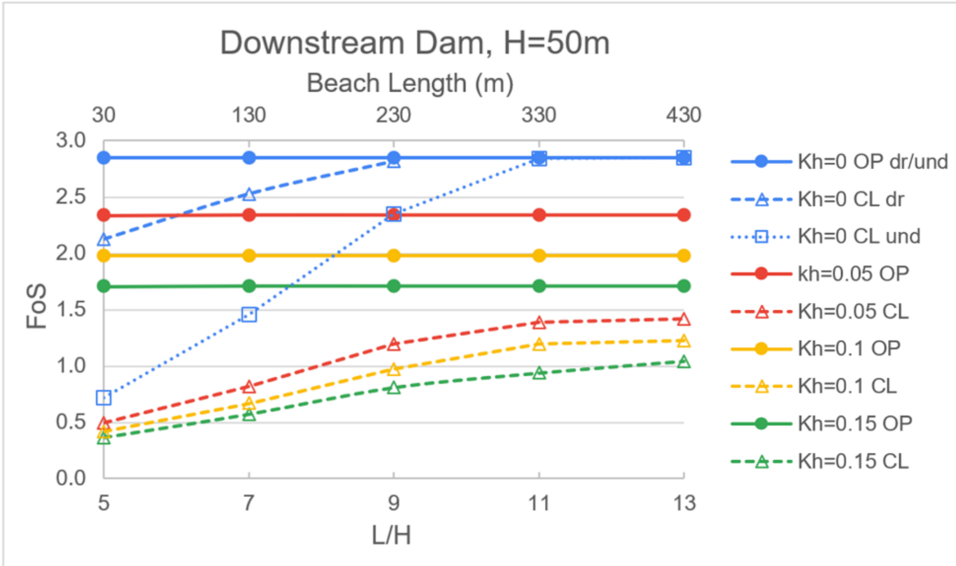

(a)

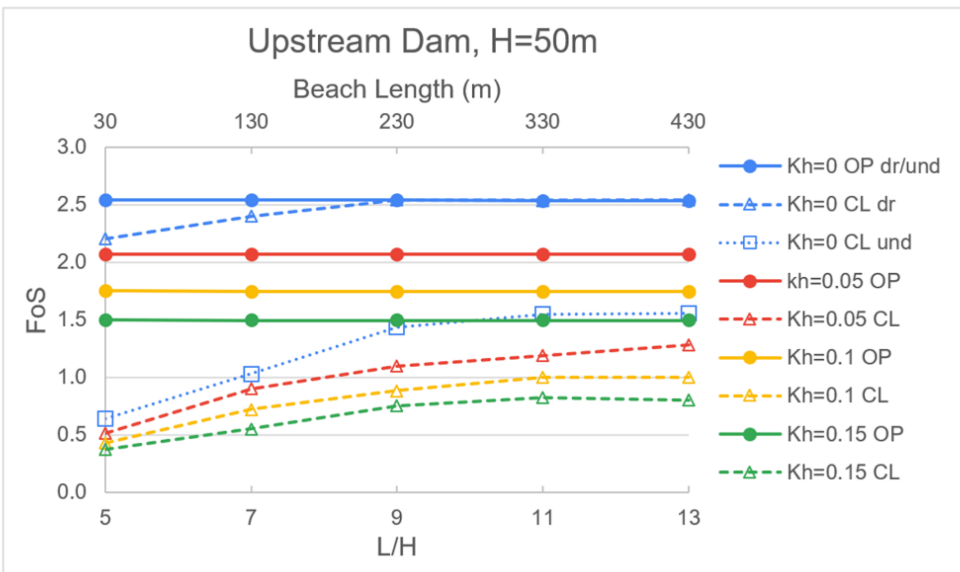

(b)

Figure 3: (a) Downstream and (b) upstream dam generic models implemented in Slide2

Simultaneously, considering a clogged drain and inertial forces (kh>0) results in a significantly lower FoS since the phreatic level rises above the foundation level, saturating the dam's core. In fact, for downstream dams, the results indicate that if the drain is clogged, a minimum beach length ratio of 11 must be ensured for kh=0.1, while for kh=0.15, stability is not guaranteed even for L/H=13. For upstream dams, when dealing with clogged drains, the stability is slightly achieved when kh=0.05 and L/H≥ 10, but seriously compromised when $k_h \geq 0.1$ regardless of the beach length ratio.

Figures 4a and 4b present the effect of dam height on the FoS for L/H= 9, considering (a) an operative drain and (b) a clogged drain. According to the results, a taller dam leads to a lower FoS regardless of the construction methodology and drainage condition. However, the decrease in the FoS is significantly smaller in the operative drain scenario compared to the clogged drain scenario. In fact, if an operative drain is considered (Fig 4a) for all the analyzed heights of the dam and kh values, the FoS remains above 1.5. On the other hand, when analyzing the clogged drain scenario (Fig 4b), the reduction in the FoS is more pronounced as the dam's height increases. In addition, upstream dams tend to experience a slightly greater decrease in their FoS as their height increases compared to downstream dams.

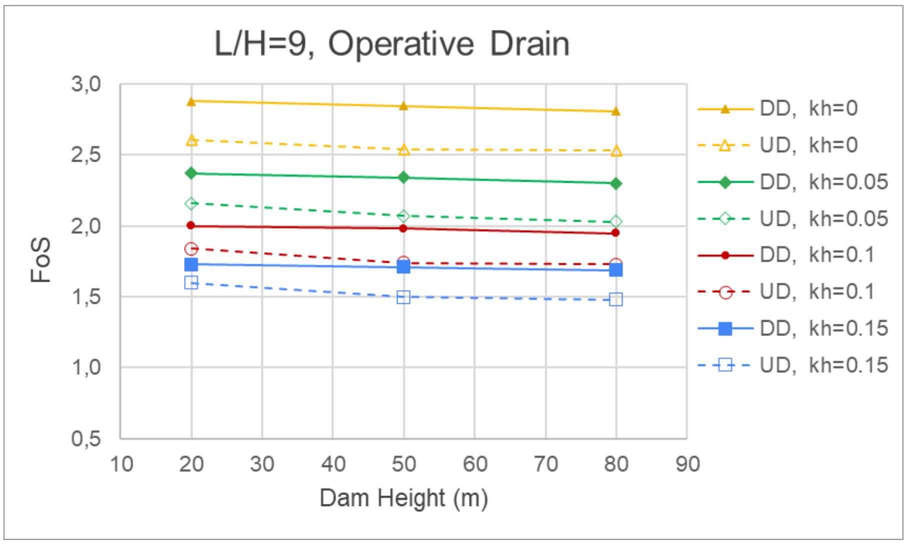

(a)

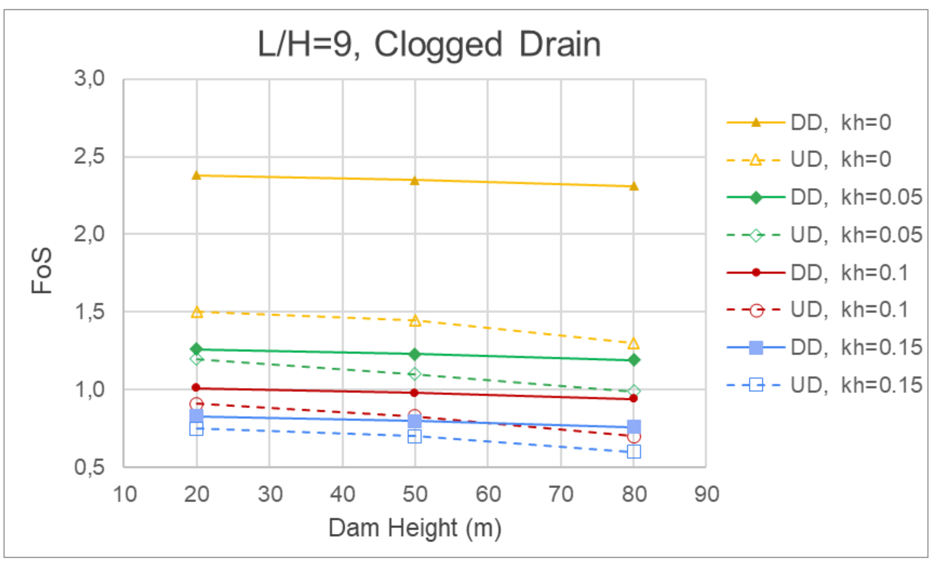

(b)

Figure 4: (a) Downstream and (b) upstream dam generic models implemented in Slide2

Conclusions

The factor that most influences the pseudo-static dam's stability analysis is the drainage condition, followed by the pond's position in the impoundment (or the beach length). The results demonstrate that assuming pwp=0 at the drain leads to high hydraulic gradients, causing a sharp reduction of the phreatic surface in the tailings. Therefore, the geotechnical models analyzed indicate a greater soil volume in an unsaturated state, exhibiting drained behavior and higher shear strength parameters. However, when a clogged drain is considered, the water table rises above the drain, reducing the Factor of Safety (FoS). This is primarily caused by the presence of more soil in a saturated state, exhibiting undrained behavior under pseudo-static conditions. This shows a significant change compared to the scenario where a pwp=0 is assumed as a boundary condition in the drainage system.

Indeed, if the drainage system is well-designed (pwp=0), extending properly through the base of the TSF (in this research, it was assumed to extend from the toe to halfway up the dam's crest), and is adequately covered to prevent clogging, both types of dams show a satisfactory response (FoS ≥1.5). Additionally, downstream dams exhibit higher FoS than upstream dams, consistent with the findings of previous studies. However, if the drainage system does not meet a pwp=0 condition (mainly caused by fines migration or clogging), upstream dams dramatically decrease their FoS under pseudo-static conditions, while downstream dams are more resilient.

Furthermore, the dam's height is the factor that has the least impact on stability when compared to the drainage condition, beach length, and soil behavior (in terms of the drained or undrained shear strength). In general, the results indicate that the FoS reduction due to dam height is marginal and is significantly influenced by the assumed boundary condition of the drain.

Based on the results, it is also crucial to assess the drained and undrained behavior of the dams under static conditions since their stability performance can change significantly if the beach length is small and drainage conditions are poor. In accordance with this, the efficiency and robust design of the drainage system is key to preventing the phreatic surface from rising at the base of the dam and triggering an undrained response in the tailings.

Consequently, if poor drainage conditions are considered, along with kh≥0.1, the pseudo-static FoS for upstream dams becomes very low (FoS≤1.0) for a dam height exceeding 50 m, even with extensive beach lengths. Finally, the results indicate that the lower the dam's height, the higher the FoS obtained for both construction methodologies. Again, the dam's height seems to have a more significant impact on upstream dams compared to downstream dams.

Future work

This study was conducted considering a kh of 0.15 or less, a maximum dam height of 80 m, and beach length ratios up to 13. Future research should include kh values up to 0.25 to account for regions with higher seismicity, such as Chile and Perú, as well as larger beach lengths to establish trends of safe beach length regardless of drainage condition. Moreover, the dam heights for downstream tailings dams have been observed to reach more than 200 m. Consequently, an analysis of dam heights up to 200 m, using advanced numerical tools for comparison, would be beneficial to the industry.

Finally, this is a bi-dimensional simplified analysis. For complex geometries, it would be useful to consider 3D models which could predict in a more realistic way the FoS assessment, usually obtaining higher FoS (Huang, 2014).

References

ANCOLD (2012) Guidelines on Tailings Dams: Planning, Design, Construction, Operation and Closure.

Jefferies & Been (2016) Soil Liquefaction: A Critical State Approach, 2nd edition.

Blight, G. E. (2010). Geotechnical Engineering for Mine Waste Storage Facilities. Taylor & Francis.

Bray, J. & Travasarau, T. (2011). "Pseudostatic slope stability procedure," 5th International Conference on Earthquake Geotechnical Engineering.

Campaña, J. (2019), Charla Técnica – ICOLD Chile: Reflexiones sobre el coeficiente sísmico para análisis seudoestáticos en el diseño de presas, 7 de octubre 2019 (in spa-nish).

CDA (2014) Application of Dam Safety Guidelines to Mining Dams.

CIM Magazine, https://magazine.cim.org/en/news/2019/brazil-bans-upstream-tailings-dams-after-corrego-de-feijao-collapse, last accessed 2022/02/17.

Huang. Y. H. (2014) Slope stability analysis by the limit equilibrium method. Fundamentals and methods. Asce press.

Sernageomin (2007). DS 248 Aprueba Reglamento para la aprobación de proyectos de diseño, construcción, operación y cierre de los depósitos de relave. Santiago, Chile: Biblioteca del Congreso Nacional (in Spanish).

Kramer, S. L. (1996). Geotechnical earthquake engineering. New Jersey. Prentice-Hall.

Mail & Guardian, https://mg.co.za/environment/2022-10-13-jagersfontein-dam-collapse-to-cost-hundreds-of-millions-of-rands/, last accessed 2022/02/17.

Morales, Bard & Palma (2021). The impact of considering the vertical seismic coefficient (kv) on the pseudo-static slope stability analysis of downstream cohesionless tailings sand dams. Proceedings of the XI Chilean Geotechnical Conference, 22 -24 November 2021, Talca, Chile.

Morales & Taborda (2022) A review of the hydro-mechanical behaviour of tailings and its importance to the stability of tailings dams. Proceedings of the 7th International Young Geotechnical Engineers Conference, 29 April - 1 May 2022, Sydney, Australia

Morgenstern, N, & Price V, (1965) "The analysis of stability of general slip surfaces", Géotechnique 15. pp, 79-93.

Morgenstern, N. R., Vick, S. G., & Van Zyl, D. (2015). Independent Expert Engineering Investigation and Review Panel: Report on Mount Polley Tailings Storage Facility Breach.

Morgenstern, N. R., Vick, S. G., Viotti, C. B., & Watts, B. D. (2016). Fundão Tailings Dam Review Panel: Report on the Immediate Causes of the Failure of the Fundão Dam.

Rico, M., Benito, G., Salgueiro, A. R., Díez-Herrero, A., & Pereira, H. G. (2008). Re-ported tailings dam failures A review of the European incidents worldwide. Journal of Hazardous Materials, 846–852.

Robertson, P. K., de Melo, L., Williams, J. D., & Wilson, G. W. (2019). Report of the Expert Panel on the Technical Causes of the Failure of Feijão Dam I.

Sarsby, R. W. (2013). Chapter 15: Tailings dams. In R. W. Sarsby, Environmental Geotechnics (pp. 365-391). ICE Publishing

Sarma, SK (1975). Seismic stability of earth dams and embankments. Geotech-nique;25(4):743–61.

Valenzuela, L. (2015). Tailings Dams and Hydraulic Fills – The 2015 Casagrande Lecture. Geotechnical Synergy in Buenos Aires 2015, 5, pp. 5-49.

Vick, S. G. (1983). Planning, Design and Analysis of Tailings Dams. John Wiley & Sons.

Session 4:

Stability analysis and safety assessment

A numerical study on the representativity of laboratory test stress paths for undrained shear strength characterization for dam reinforcement safety assessments

Bruno Szpigel Dzialoszynski, Vecttor Projetos, Brazil

Abstract

It is well known that undrained shear strength is not an intrinsic soil property, but rather a convenient quantification of soil behaviour. For many projects, said undrained shear strength is characterized through isotopically consolidated undrained triaxial tests (CIU) which may not yield the same anisotropic initial stress states and complex loading stress paths which generally occur *in situ*.

Focusing on these variables, this paper proposes a simplified conceptual study through numerical simulations to evaluate the representativity of undrained shear strengths measured in triaxial CIU tests for the assessment of the construction of dam reinforcement berms. The Hardening Soils constitutive model was applied to simulate undrained behaviour during triaxial tests and slope failure during construction of a reinforcement berm, in order to compare characterized undrained shear strengths and stress paths under these distinct conditions, for a set of hypothetical geomaterials.

Introduction

Following a series of catastrophic tailings dam failures (e.g. Morgenstern et al., 2015, Morgenstern et al., 2016; Robertson et al., 2019, Morgenstern et. al., 2019), Brazilian dam safety legislation has seen substantial change in recent years, generally with more restrictive criteria to be met by the structures. In some instances, reinforcements were required either as a permanent measure, or as a temporary measure, to increase safety for the decharacterization works. For the reinforcement works, a solution that has been applied to some dams consists of a stabilizing berm with granular material on the downstream slope.

Said reinforcement may have to be raised at rates that lead to excess porepressure accumulation within the existing dam and/or its foundations. In this cases, commonly undrained shear strengths are assumed in "end of construction" limit equilibrium slope stability analyses for design.

For many of projects, said undrained shear strengths are characterized through isotopically consolidated undrained triaxial tests (CIU), or direct simple shear (DSS) tests, for example as illustrated by France et. al (2015). As undrained shear strength is not an intrinsic soil property, when applying undrained shear strength measured on soil tests, one implicitly assumes not only that the sample itself is representative of in situ conditions (accounting for variability, state, etc.) but also that the initial stress state and loading path of the test is analogous or similar to those foreseen in situ.

This paper proposes a simplified conceptual study through numerical simulations to evaluate the representativity of undrained shear strength characterization techniques based on triaxial CIU tests for the assessment of the dam reinforcement berms previously described, focusing on initial stress state and loading path.

Relevant features of undrained behaviour and undrained behaviour modelling

Lambe and Whitman (1969) define an "undrained load"' as loading that induces porepressure variation, and possibly effective stress variation, but with no water flow entering or exiting the loaded soil. The restrictions to water flow lead to excess porepressure generation.

From a modelling perspective, the most direct way of representing undrained behaviour is to consider soils responds mechanically with regards to effective stresses, and directly estimate the excess porepressures. However, said estimation generally requires elastoplastic equilibrium calculations, which often require numerical solving. Also, excess poreprepressures may be considerably sensitive to soil constitutive behaviour and parameters, among other features that must be inputted to the calculations.

For these reasons, many times, instead of directly modelling undrained behaviour under an effective stresses approach, a total stresses approach is adopted. Porepressure generation complexity and uncertainties are implicitly / indirectly considered / covered by directly measuring the relevant undrained behaviour, such as shear strength, and directly applying it as a parameter (Lambe and Whitman, 1969).

However, when applying this methodology, one implicitly assumes that the aforementioned features that influence undrained behaviour in the considered measuring method / test are representative of the in situ / actual loading conditions.

Indeed, the undrained behaviour of soils and its associated quantifications - such as undrained shear strength - are not intrinsic soil properties, but convenient quantifications of soil behaviour for specific conditions. The undrained response and shear strength depends not only on the soil's intrinsic parameters, but also on many features, such as initial soil state - compacity, stresses, fabric - as well as on the load and loading path itself (Jefferies and Been, 2016).

Undrained shear strength characterization

Under these discussions, the method of measurement and characterization of undrained shear strength should be considered in the light of the expected initial and loading conditions. Winckler (2018) describes various methods and techniques for undrained shear strength characterization. The study proposed in this paper shall consider 3 approaches briefly described hereafter, all based on results of triaxial CIU tests.

Approach 1: Mohr-Coulomb Total Stresses CIU envelope

This approach is fairly traditional in the geotechnical engineering practice, and is commonly referenced in basic textbooks, such as Pinto (2000). It consist of adjusting a Mohr Coulomb envelope with regards to total stresses, defining undrained shear strength s as follows:

$$s = c_{CIU} + \sigma * tan\varphi_{CIU}$$

Where σ is the normal total stress at the shear plane, c_{CIU} and φ_{CIU} are the envelope parameters. This approach has conceptual limitations associated to s being correlated to total stresses after undrained loading.

Approach 2: Undrained shear strength as a function of effective stresses prior to loading

In this approach the maximum shear strength s_u (generally not the shear stress at the failure plane) at each triaxial test is correlated to the consolidation stress of the test. The consolidation stress is assumed to be analogous to effective in situ stresses prior to undrained loading. For the present study, the reference stress is assumed as the octaedric stress, p'_0, yielding:

$$s_u = \kappa + \lambda * p'_0$$

Where κ and λ are parameters of the derived correlation. This approach may be seen as a simplified analogy of SHANSEP (Ladd and Foot, 1974), as it does not account for over-consolidation.

Approach 3: Failure shear stress at failure plane as a function of effective stresses at failure plane prior to undrained loading

This approach was originally proposed by Duncan et al (2014) for rapid drawdown analysis. Winckler (2018) applies the methodology with a more general perspective, by substituting effective stresses prior to drawdown by effective stresses prior to undrained loading.

The method involves deriving correlations between the shear stress at the failure plane at failure τ_{ff} and the effective normal stress at the failure plane prior to undrained loading σ'_{fc}. Correlations are derived for the isotropic consolidation case $K_c = 1$ and the case with maximum anisotropy (which would lead to shear failure) in consolidation $K_c = K_f$ as follows:

$$\tau_{ff(K_c=1)} = d_{K_c=1} + \sigma'_{fc} * tan\Psi_{K_c=1}$$

$$\tau_{ff(K_c=K_f)} = d_{K_c=K_f} + \sigma'_{fc} * tan\Psi_{K_c=K_f}$$

Where d and Ψ are the parameters to be adjusted. Note that all parameters may be derived based on triaxial CIU tests. Strength for the actual value of K_c is obtained by interpolating the 2 envelopes.

The original method applies stages of limit equilibrium analyses and some simplifying assumptions to derive the values of σ'_{fc} and K_c. In the present study, however, the effective stresses prior do undrained loading were directly taken from the numerical elastoplastic equilibrium simulations.

Scope and methodology of the numerical study

When limit equilibrium analyses consider a total stress approach for modelling undrained shear strengths, it is implicitly assumed that:

- The samples are representative of field conditions with regards to intrinsic soil properties and state (compacity, fabric, etc.), including variability and scale effects.
- The test procedure is representative of the foreseen field conditions, including initial stress state and loading stress path.

Direct verification of the aforementioned assumed representativity during actual construction is generally impractical as actual stress paths during undrained loading generally are not / cannot be measured.

The present conceptual study aims at eliminating said limitations, with the "trade-off" of being fully conceptual / hypothetical. The study proposes the mathematical simulation of soils tests, and of the failure of a hypothetical dam during the construction of a reinforcement berm. The modelled geomaterials are also hypothetical, with controlled constitutive models and parameters.

One the one hand, the study does not represent any particular dam or case history, neither is based on actual monitoring data. On the other hand, as a "trade-off", the failure mechanism may be fully mapped, and during the simulation, stress paths along the whole domain may be monitored.

Likewise, the modelled geomaterials are also hypothetical, which, on the one hand means they do not represent any sampled material in particular, and complex soil behaviour not contemplated in the selected constitutive model is neglected. On the other hand, there is no uncertainty with regards of sample representativity, and uncertainties related to soil behaviour are eliminated.

Thus, the methodology seeks to isolate the uncertainty related to initial stress and loading path when evaluating the representativity of the undrained shear strength characterization techniques.

Hypotheses of the numerical study

The numerical study was performed as a sequence of plane strain elastoplastic equilibrium analyses solved thought the finite elements method with the *software* Plaxis 2D (Bentley, 2023a).

Geometry, finite elements mesh and boundary conditions

Figure 1 illustrates the applied finite elements mesh. The soil was modelled with triangular 15-nodded elements. The filter/drain was modelled simply as an “internal boundary condition”.

The geometry of the model was defined so that it is representative of a dam that would require reinforcement. The hypothetical dam, prior to reinforcement, has a static factor of safety of ~1,3 (obtained from a shear strength reduction factor analysis) assuming drained behaviour for all materials. If the reinforcement works were completed, the dam would have a static factor of safety of ~1,5 assuming drained behaviour for all materials. However, assuming undrained behaviour of the embankment and Clayey Foundation (Figure 1) during reinforcement construction, the structure fails when the raising is ~20m high.

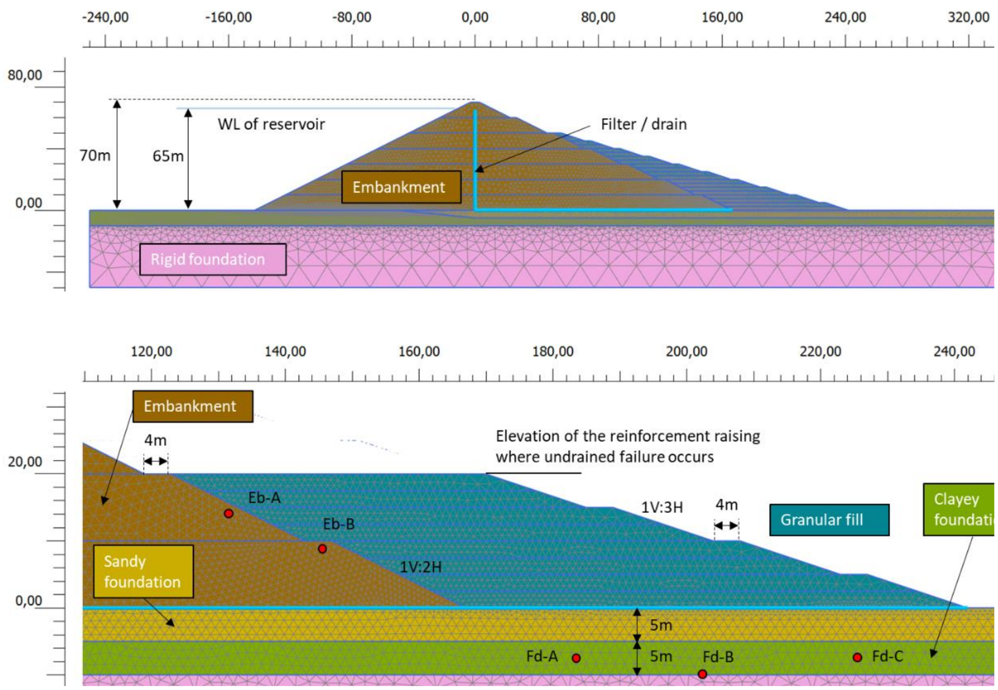

Figure 1: Geometry and finite elements mesh. At the top, finite elements mesh general view. At the bottom, detail in the region of interest.

As stored tailings generally have complex, plastic behaviour, which would practically not affect the downstream slope where the analysis is focused, they were omitted from the model. A boundary condition of fixed horizontal displacement and open flow was assigned to the lateral boundaries. The inferior boundary was assigned with fixed displacements, and closed to flow.

Calculation sequence

The calculation sequence was performed as follows:

- Stress initialization through the K_0 procedure (Bentley, 2023a), for the natural ground.

- Construction of the dam, discretized in 10m high raisings. Fully drained behavior was considered for all materials, assuming concomitant dissipation of any excess porepressure.
- Filling of the reservoir. Steady state seepage was assumed, for typical parameters of the materials. Due to the internal drainage considered, influence on the area of interest is negligible.
- Construction of the reinforcement berm, discretized in 2,5m high raisings. Fully undrained behavior was assumed for the Embankment and for the Clayey Foundation. Other materials were assumed with drained behavior.

There may be criticism to considering fully undrained behaviour, as at least part of the excess porepressure would be expected to dissipate during construction, especially close to draining boundaries (e.g. slope of the Embankment adjacent to granular berm, top of the Clayey Foundation, adjacent to drain, etc.). Also, the Embankment is not fully saturated / above the water level. Nonetheless, for the sake of the present study, fully undrained behaviour was assumed, and suctions associated to the steady state flow were fully neglected as a simplification.

Geomaterial modelling and parameters

The Embankment and the Clayey Foundation, where undrained behaviour during berm raising is assumed, are the focus of the study. Undrained behaviour was explicitly modelled, i.e. mechanical behaviour was assumed with regards to effective stresses and excess porepressure was estimated within the calculations.

The Hardening Soils constitutive model (Bentley, 2023b and Schanz et al, 1999) was applied for these materials. Table 1 summarizes the assumed parameters. As illustrated by the parameters, the Embankment was assumed to be poorly compacted. Considering the scope of the study, for simplicity, both materials were considered as normally consolidated.

Table 1: Parameters considered for the Embankment and Clayey Foundation

Parameter	Symb.	Unit	Embankment	Clayey Fdt.
Specific weight	γ	kN/m3	18,0	19,0
Ref. secant stiffness in CID triaxial test	E50ref	kPa	4.50E+04	6.00E+04
Ref. tangent stiff. for primary oed. loading	Eoedref	kPa	3.00E+04	4.00E+04
Unloading / reloading stiffness	Eurref	kPa	1.35E+05	1.80E+05
Power for stress-level dependency	m	-	0.50	0.7
Effective cohesion	c'	kPa	5	20
Effective friction angle	φ'	o	28	30
Angle of dilatancy	Ψ	o	0	0
Tension cut-off	σt	kPa	1	1
Poisson's ratio for unloading-reloading	νur	-	0.2	0.2
Reference stress for stiffnesses	pref	kPa	100	100
K0 -value norm. consolid., stress initiali.	K0nc	-	0.5305	0.5

Failure ratio	Rf	-	0.9	0.9

Despite its limitations, this constitutive model reasonably represents many key soil behaviours, such as stress dependent stiffness, shear and compression hardening, etc. Figure 2 present results of numerically simulated laboratory tests on the materials, illustrating some of the represented behaviours.

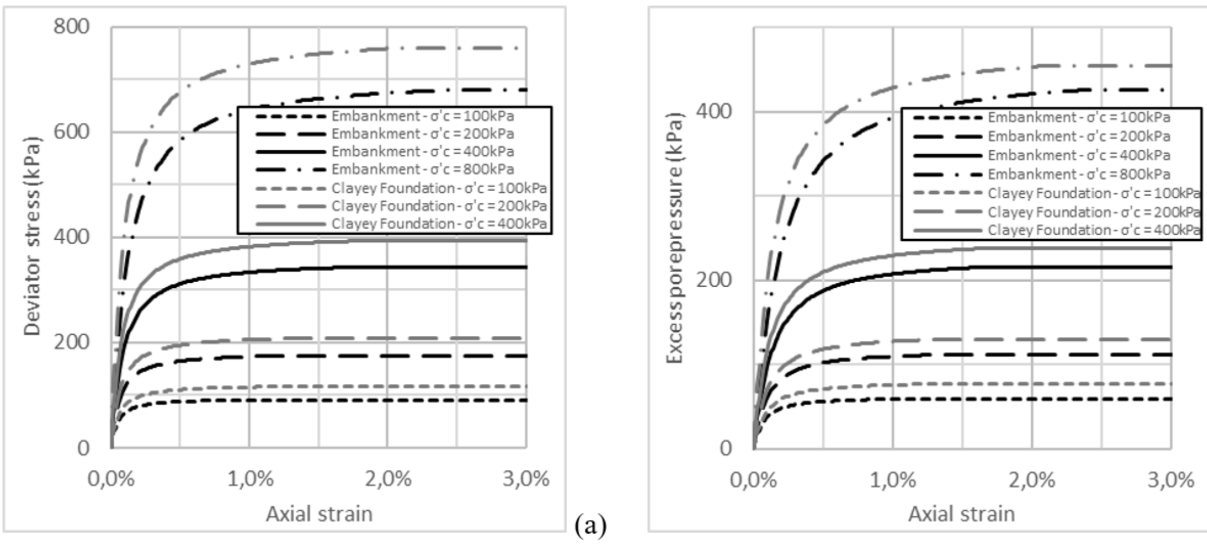

Figure 2: Numerically simulated laboratory test results. (a) Stress-Strain for triaxial CIUs. (b) Excess porepressure for triaxial CIUs.

It is relevant to note, however, that phenomena such brittleness, liquefaction, critical state mechanics in general are not contemplated, so the study's results should be considered under this disclaimer.

The other materials, which are not the focus of the study, were modelled as linear-elastic, perfectly plastic, with a Mohr-Coulomb yielding criterion. Table 2 summarizes the considered parameters.

Table 2: Parameters considered for Sandy Foundation, Granular Fill and Rigid Foundation

Parameter	Symb.	Unit	Granular Fill	Sandy Fdt.	Rigid Fdt.
Specific weight	γ	kN/m3	19	19	20
Eff. Modulus of Elasticity	E'f	kPa	7.00E+04	7.50E+04	4.00E+05
Eff. Poisson's Ratio	υ'	kPa	0.25	0.25	0.25
Effective cohesion	c'	kPa	0.25	10	60
Effective friction angle	φ'	o	38	32	37
Angle of dilatancy	Ψ	o	0	0	0
Tension cut-off	σt	kPa	0	1	0
K0 -value stress initializ.	K0nc	-	-	0.4701	0.3982

Simulated laboratory tests

Triaxial CIU tests were numerically simulated for the Embankment and Clayey Foundation for consolidations tresses of 100kPa, 200kPa, 400kPa and 800kPa. Basic results are presented in Figure 2, where general soil behaviour was reasonably represented. Stress paths were interpreted to derive parameters for the undrained strength characterization approaches previously outlined, as illustrated in Figure 3 and 4.

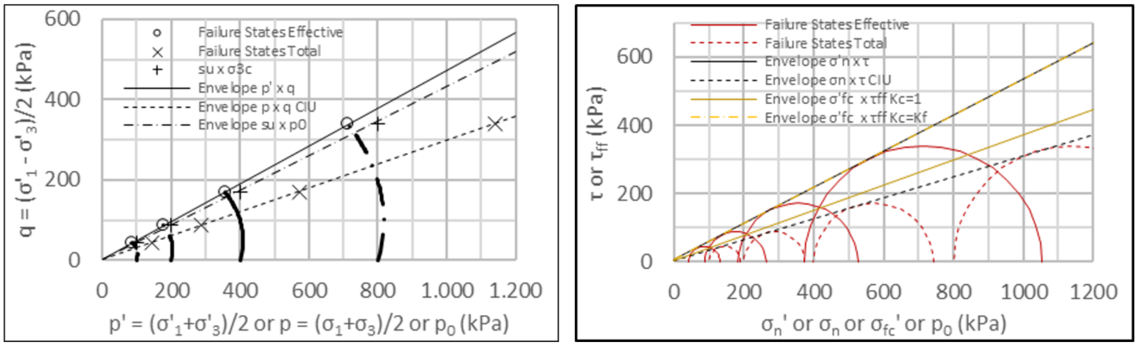

Figure 3: Embankment – Simulated CIU test interpretation.

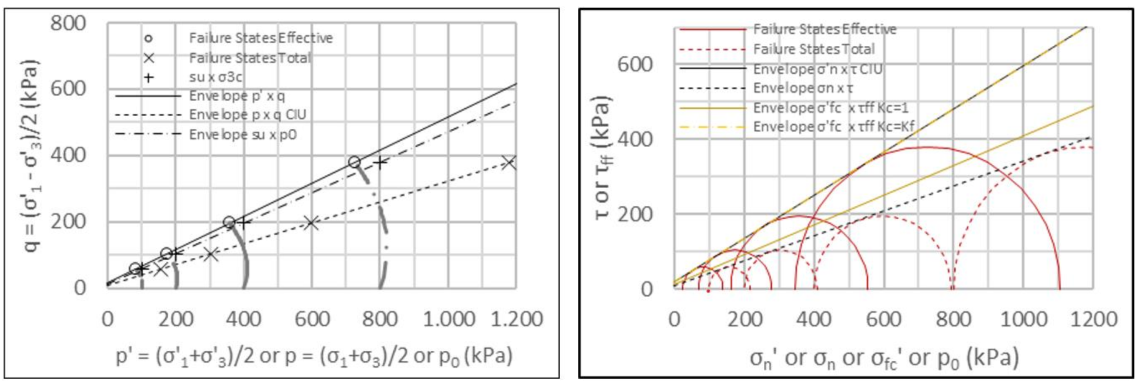

Figure 4: Clayey Foundation – Simulated CIU test interpretation.

Table 3 presents the resulting undrained shear strength characterization parameters.

Table 3: Undrained shear strength characterization parameters derived from simulated tests

Material	Approach 1		Approach 2		Approach 3			
	c_{CIU} (kPa)	ϕ_{CIU} (o)	κ (kPa)	λ	$d_{Kc=1}$ (kPa)	$\psi_{Kc=1}$ (o)	$d_{Kc=Kf}$ (kPa)	$\psi_{Kc=Kf}$ (o)
Embankment	2.30	17.20	3.10	0.43	2.75	28.57	5.00	20.00
Clayey Fdt.	8.90	18.40	12.30	0.46	10.69	21.77	28.00	30.00

Failure Mechanism

As the reinforcement berm raising approaches the height of 20m, the model estimates that slope failure occurs (i.e. failure to converge, with shear mobilization and displacements characterizing a failure mechanism). The mechanism passes though the Embankment, near its contact with the granular fill, and then through the Clayey Foundation, and is conditioned by the undrained behaviour, as illustrated in Figure 5.

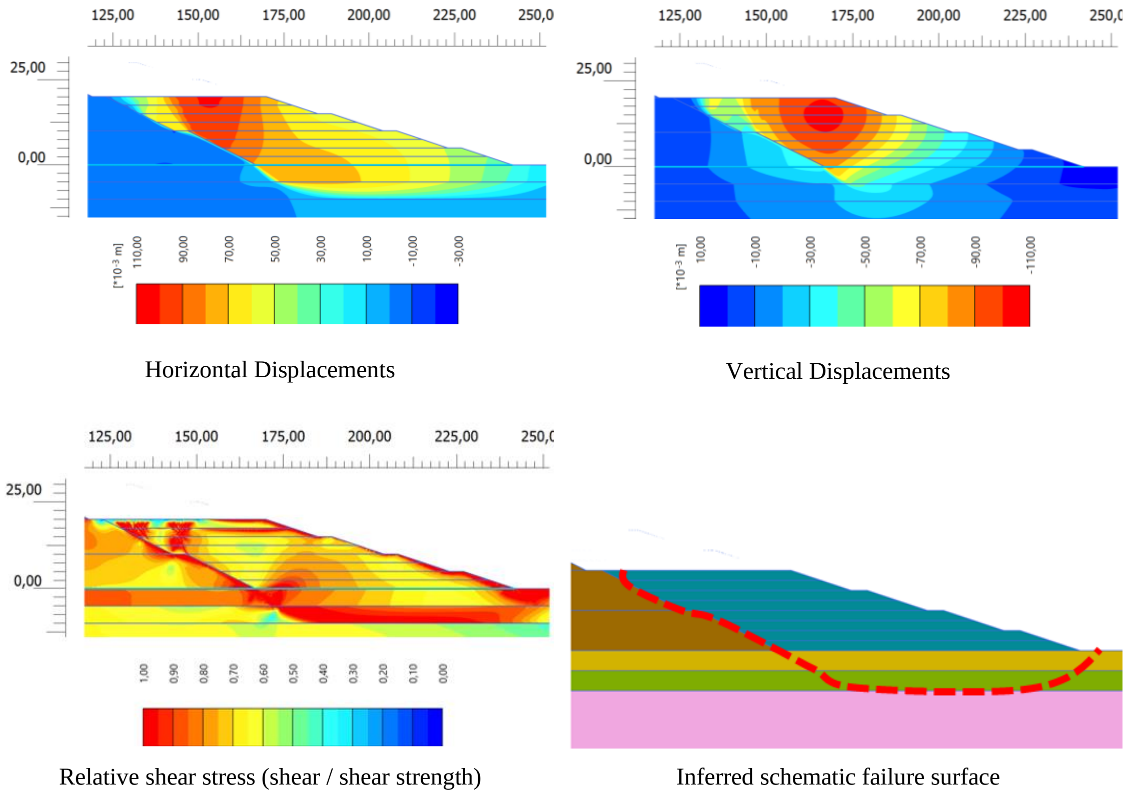

Figure 5: Model results at the onset of failure illustrating failure mechanism.

Low effective stresses tend to govern the shear strength at the portion of the failure mechanism within the Embankment, as it is close to the surface prior to the construction of the berm / undrained loading.

Stress paths and undrained shear strength

Stress paths in some points of the model, indicated with red dots in Figure 1, were "monitored" during the raising of the reinforcement berm / undrained loading for comparison with the simulated laboratory tests.

Figure 6 presents the effective stress paths of the monitoring points for each material, in comparison to the stress paths of a simulated triaxial CIU test at a similar stress level. For assessment of the representativity of Approach 2 of undrained shear strength characterization, the corresponding "envelope" is also plotted, along with the corresponding points (as "Xs") for each stress path.

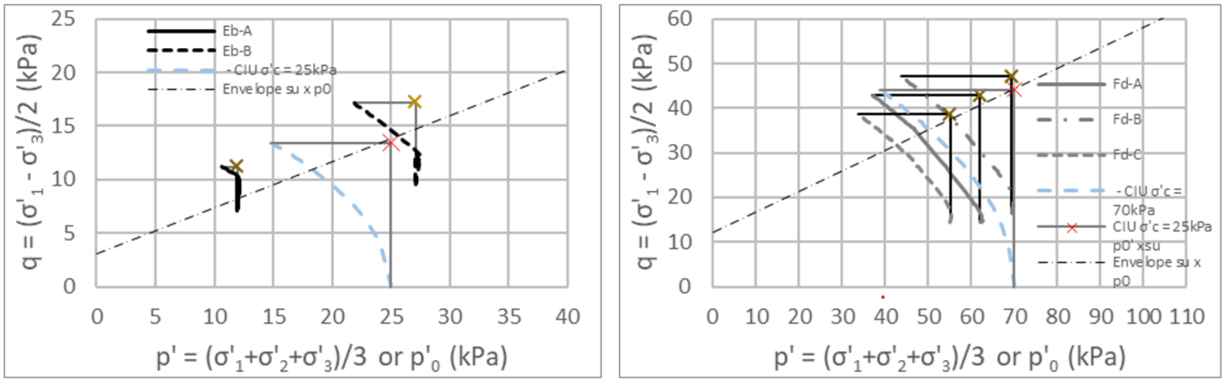

Embankment

Clayey Foundation

Figure 6: Effective stress paths until dam failure in comparison to stress path in triaxial CIU test and Approach 2 "envelope".

As it may be seen, initial stresses vary significantly in relation to the CIU tests, as the *in situ* condition is not isotropic. The stress paths general aspects are similar for the Clayey Foundation, and reasonably similar for the Embankment. The undrained shear strengths obtained with Approach 2 were slightly overestimated in relation to those computed in the model, especially for the Embankment. However, it is considered that the order of magnitude is still similar, and reasonable values could be characterized.

For assessment of the representativity of Approach 1, Figure 7 plots the characterized envelope along with the monitored total stress paths until dam failure in the model (indicated by "Xs").

As it may be seen, initial total stresses and total stress paths do not resemble those of the triaxial CIU tests. Likewise, undrained shear strengths characterized by Approach 1 are significantly overestimated.

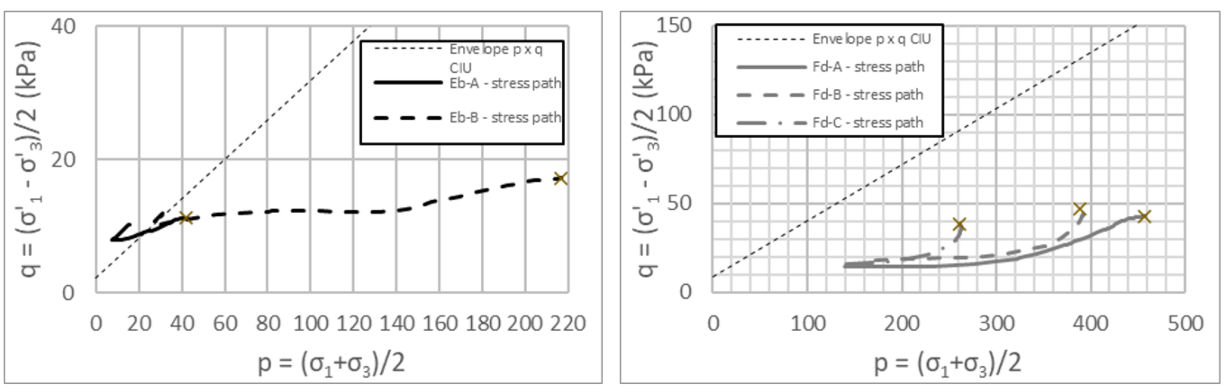

Embankment

Clayey Foundation

Figure 7 – Total stress paths until dam failure in comparison to Approach 1 envelope.

Lastly, Figure 8 compares shear stress at the failure plane at failure estimated with Approach 3 compared to the values estimated with the numerical model. Consolidation stresses for input in Approach 3 were taken from the corresponding calculation stage of the model.

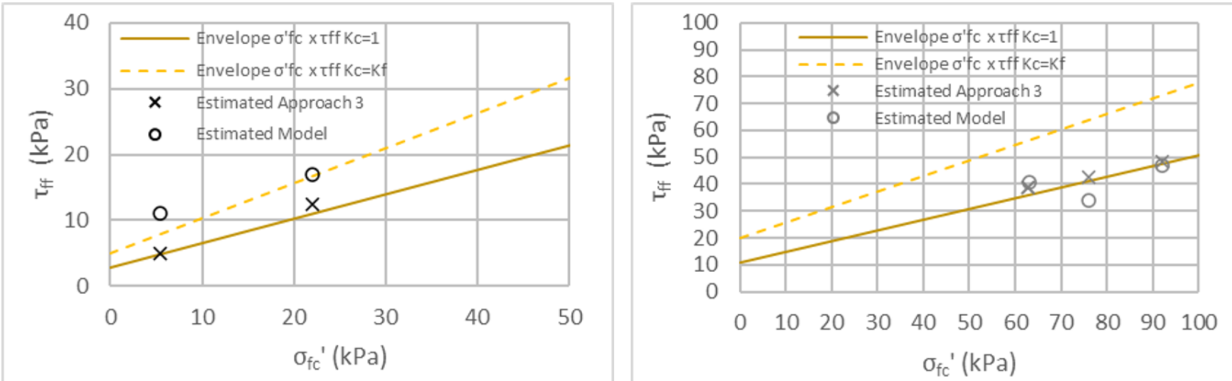

Embankment Clayey Foundation

Figure 8 – Comparison of shear at failure estimated with Approach 3 and numerical model.

As it may be seen, Approach 3 generally slightly underestimated the undrained shear strength, or led to similar values in relation to the model, and in one case slightly overestimated the value. It is considered that the order of magnitude was always similar, and reasonable values could be characterized.

Conclusions

The numerical study simulated a hypothetical dam failure and hypothetical geomaterials to conceptually evaluate the representativity of stress paths and undrained shear strength characterization techniques based on triaxial CIU test results for the analysis of the construction of reinforcement berms in the downstream slope of dams. As the simulated geomaterials are fully hypothetical, common uncertainties during soil testing and sampling were eliminated, allowing for an isolated, conceptual assessment of the physical behaviors of interest.

For the simulated conditions, the study indicated, on the one hand, that anisotropy led to differences in the initial stresses when comparing the *in situ* and triaxial CIU conditions. On the other hand, when considering stress variation (i.e. despite the differing initial states), the loading stress paths along the failure surface were at least reasonably / qualitatively similar to those of triaxial CIU tests.

For the simulated materials and loading conditions, results have shown that, despite differences in initial stresses and stress paths, the evaluated shear strength characterization approaches which correlate to consolidation stresses prior to undrained loading – i.e. Approach 2 and 3 - yielded reasonable approximations / estimations, in relation to the numerical simulations. However, results suggest caution when applying Approach 1, i.e., when characterizing undrained shear strength in relation to normal total stress along the failure surface after loading, which generally led to significant overestimation of undrained shear strengths.

It is relevant to note, however, that phenomena such brittleness, liquefaction, critical state soil mechanics in general are not contemplated in the applied constitutive model, so the study's results should be considered under this disclaimer. This is especially relevant under the conclusion that initial stress anisotropy leads to differences in the conditions observed *in situ* and for triaxial CIU tests.

References

Bentley (corporate author). 2023a. *Plaxis 2D Reference Manual*. [s.l]: Bentley.

Bentley (corporate author). 2023b. *Plaxis 2D Material Models Manual*. [s.l]: Bentley.

Duncan, J.M., Wright, S.G. and Brandon, T.L. 2014. Analyses for Rapid Drawdown. In *Soil Strength and Slope Stability*. Hoboken: John Wiley & Sons, pp. 169–178.

France, J.W., Williams, J.L., Winckler, C.J.C., Adams, T.E.. 2015. Soil Shear Strength Selection for Stability Analysis – Practical Guidance. In: *Proceedings of Dam Safety 2015*. New Orleand (LA): Association of State Dam Safety Officials: 1-36.

Jefferies, J. and Been, K. 2016. Dilatancy and the state parameter. In *Soil Liquefaction: A Critical State Approach. 2nd Edition*. Boca Raton: CRCD Press, pp. 35-100.

Ladd, C. C., and Foott, R. 1974. New design procedures for stability of soft clays, *ASCE, Journal of Geotechnical Engineering*, 100(7): 763-786.

Lambe, T.W. and Whitman, R.V. 1969. *Soil Mechanics*. New York: John Wiley & Sons.

Morgenstern, N.R., Jefferies, M., Zyl, D.V. and Wates, J. 2019. *Report on NTSF Embankment Failure Cadia Valley Operations for Ashurst Australia. Newcrest*. [s.l.]: Expert Panel.

Morgenstern, N.R., Vick, S.G., Viotti, C.B. and Watts, B.D. 2016. *Fundão Tailings Dam Review Panel - Report on the Immediate Causes of the Failure of the Fundão Dam*. [s.l.]: Fundão Tailings Dam Review Panel.

Morgenstern, N.R. Vick, S.G. and Zyl, D.V. 2015. *Independent Expert Engineering Investigation and Review Panel - Report on Mount Polley Tailings Storage Facility Breach*. Victoria: Government of British Columbia.

Pinto, C.S. 2000. *Curso Básico de Mecânica dos Solos*. São Paulo: Oficina de Textos.

Robertson, P.K., de Melo, L., Williams, D.J. and Wilson, G.W. 2019. *Report of the expert panel on the technical causes of the failure of Feijão Dam I*. [s.l.]: Expert Panel.

Schanz, T., Vermeer, P.A. and Bonnier, P.G. 1999. The hardening-soil model: Formulation and verification. In *R.B.J. Brinkgreve, Beyond 2000 in Computational Geotechnics*. Rotterdam: Balkema, pp: 281–290.

Winckler, C. 2018. *Undrained Shear Strength Selection*. Workshop Presentation for ABMS-MG, 28 June 2018. Belo Horizonte: ABMS-MG.

Calculation of Undrained Shear Strength of a Bauxite Tailings using Field and Laboratory Tests

Guilherme Henrique da Silva Pinto Geotechnical Engineer, Pimenta de Ávila Consultoria, Nova Lima, Brazil,
André de Oliveira Faria Geotechnical Engineer, Pimenta de Ávila Consultoria, Nova Lima, Brazil,
Mauro Pio dos Santos Junior Geotechnical Coordinator, Pimenta de Ávila Consultoria, Nova Lima, Brazil.

Abstract

Determining the undrained shear strength of contractive materials is of fundamental importance to evaluate the stability condition of geotechnical structures. Commonly, this evaluation is performed using laboratory tests, such as the isotropically consolidated undrained triaxial compression test (CIUC), or field tests, such as the Field Vane Shear Test (FVST) and the Cone Penetration Test (CPTu). Based on the CPTu, different methodologies (empirical and/or analytical) were developed in the literature to assess the undrained shear strength. This paper aims to evaluate the yield and remolded undrained shear strength of a bauxite tailings, using field and laboratory tests. The yield undrained shear strength was calculated based on the CPTu test using the classical equations based on bearing capacity factors (N_{kt}, N_{ke} and $N_{\Delta u}$), considering three methodologies: i) Mantaras *et al.* (2014); ii) Mayne & Peuchen (2018) and iii) Mayne *et al.* (2023). The remolded undrained shear strength was determined based on the sleeve friction of the CPTu, following the classical equation developed by Robertson *et al.* (1986). The values obtained were compared with the CIUC tests (with and without correction to account for anisotropic consolidation) and the FVST. The results have shown that: i) if accounted for anisotropic consolidation, the laboratory results are similar to the values determined using N_{kt} and $N_{\Delta u}$ ii) possibly due to the inaccuracy of the measurement of the sleeve friction (f_s), the remolded undrained shear strength measured using the CPTu showed lower results than the FVST.

Introduction

The correct measurement of tailings properties such as its strength and stiffness are highly important in geotechnical engineering since they are used to evaluate the stability condition of a Tailings Storage Facility (TSF). If the geotechnical parameters are not adequately determined, the TSF may either be over-dimensioned or, in the worst situation, it may not present the necessary resilience to the expected loads it will face throughout its life cycle.

To evaluate the tailings characteristics and its behavior, geotechnical engineers usually perform laboratory and field tests to assess proprieties such as grain-size distribution, Atterberg limits, stiffness, drainage conditions and shear strength. Among the commercially available field tests, the Field Vane Shear Test (FVST) and the Cone Penetration Test (CPTu) are the most often used.

The undrained shear strength (S_u) can be defined as the geomaterial shear resistance in a saturated or nearly saturated condition, mobilized under a fast loading without allowing time for volumetric change (Lunne *et al.*, 1997). In contractile materials, the generated porewater pressure is positive, which reduces the effective stress and, therefore, its shear strength. The undrained shear strength can be calculated by the CPTu using equations based on the bearing capacity factors (N_{kt}, $N_{\Delta u}$ and N_{ke}) as described by Lunne *et al.* (1997), or directly measured by the FVST and the laboratory tests (such as triaxial compression, and direct simple shear).

To determine the bearing capacity factors, several methodologies (analytical and/or empirical) have been published in the literature based on CPTu data, such as Mantaras *et al.* (2014), Mayne & Peuchen (2018), Mayne *et al.* (2023), and others. Most of these methodologies were developed for natural soils. The reliability of these proposes must be evaluated when applied in tailings, since they present certain unique characteristics, such as geochemistry, angular particles, and potentially high compressibility.

This paper aims to present the evaluation of the undrained shear strength profile of a bauxite tailings using laboratory and field tests (CPTu and FVST). To perform the N_{kt}, $N_{\Delta u}$ and N_{ke} calibration three methodologies were applied: i) Mantaras *et al.* (2014); ii) Mayne & Peuchen (2018) and iii) Mayne *et al.* (2023). The remolded undrained shear strength was determined based on the sleeve friction of the CPTu as suggested by Robertson *et al.* (1986). Additionally, the results obtained were compared with the FVST (yield and remolded conditions) and the triaxial compression test (CIUC), with and without the correction to account for anisotropic consolidation.

Grain-Size Distribution and Atterberg Limits

The bauxite tailings evaluated in this study is the by-product of washing a bauxite ore at a mine in the state of Pará/Brazil. No chemicals were used in the ore processing. As indicated in Figure 22, the average particle-size distribution, using the American standard D422-63 criteria (ASTM, 2007) is: 2% sand; 28% silt; and

70% of clay size particles, with the mean value of the specific gravity (G_s) equal to 2.9. On average, the Atterberg Limits, determined according to the standard D4318-17 (ASTM, 2018), indicated a Liquid Limit (LL) of 55%, a Plastic Limit (LP) of 29% and Plasticity Index (PI) of 26%, classifying as a high plasticity clayey soil, just above the A-Line. These results were obtained as mean of 70 samples.

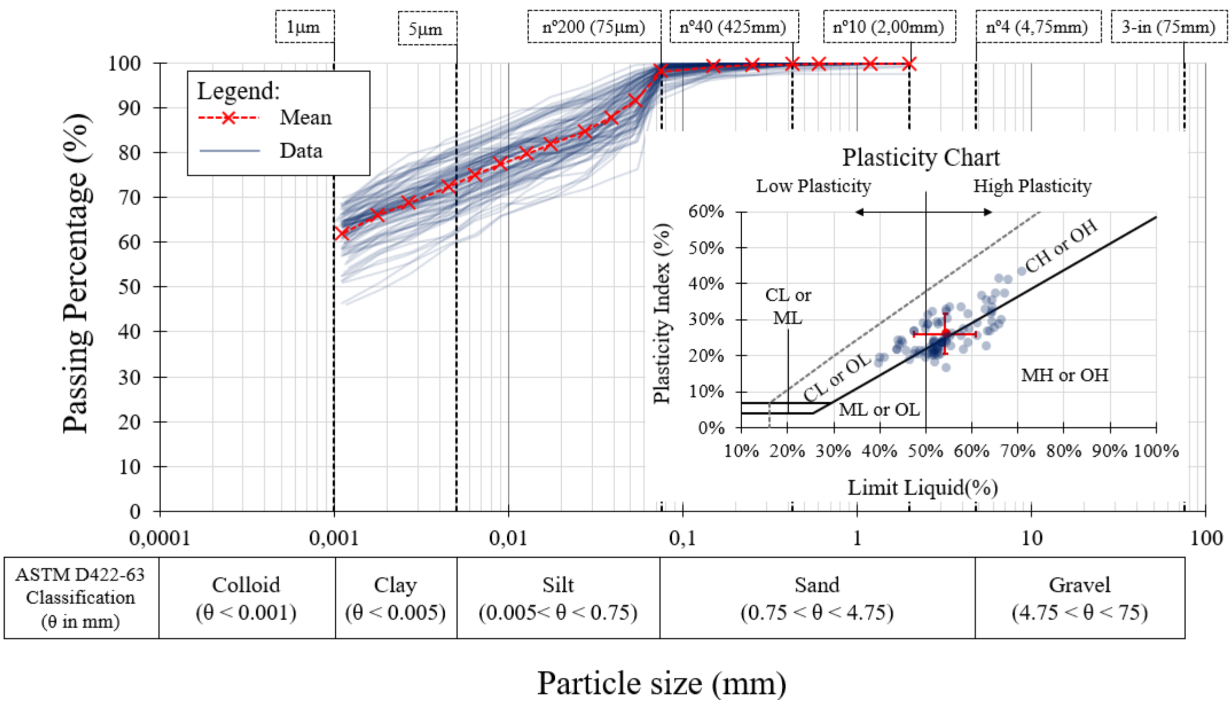

Figure 22: Particle size distribution and Plasticity Chart – Bauxite Tailings

In-situ Behavior

To evaluate the tailings *in-situ* behavior a Cone Penetration Test with Pore pressure measurement (CPTu) and 5 dissipation tests (DDP) was performed. The CPTu was performed as described by the international standard 22476-1 (ISO, 2022). The cone used has a cross-sectional area of 10 cm², and the penetration was carried out at a rate of 2.0 ± 0.5 cm/s with readings taken every 5 cm. The CPTu performed with DDP provides four independent parameters: (i) the cone tip resistance (q_c), which characterizes the soil resistance to cone penetration; (ii) the sleeve friction (f_s), which represents the soil adhesion to the friction sleeve; (iii) the porewater pressure (u), commonly measured behind the cone tip (u_2 location); and iv) the equilibrium *in-situ* porewater pressure (u_0) obtained by the full stop of the cone penetration and the dissipation of the excess porewater pressure.

As described by Lunne *et al.* (1997), the total cone resistance q_t can be calculated as $q_t = q_c + u_2 (1\text{-}a)$, where "a" is the cone area ratio, to account for the unequal end area effect. In this paper, the parameter "a" is equal to 0.82 as provided by the cone calibration certificate.

To evaluate the *in-situ* tailings behavior, the soil behavior type index proposed by Jefferies & Davies (1991) was applied using the normalized parameters presented by Equations 1 to 3, which are: Normalized Friction Ratio (F_R), the Normalized Cone Resistance (Q_t or Q) and pore pressure ratio (B_q), respectively. The classification system proposed by the authors should be understood as a behavior-based classification, since it does not measure physical characteristics, such as grain size or plasticity.

$$F_R = \frac{f_s}{q_t - \sigma_{v0}} \text{ x } 100\% \tag{1}$$

$$Q = Q_t = \frac{q_t - \sigma_{v0}}{\sigma'_{v0}} \tag{2}$$

$$B_q = \frac{u_2 - u_0}{q_t - \sigma_{v0}} \tag{3}$$

To evaluate the dilatancy, the analytical equation proposed by Dos Santos Junior (2021) to represent the contractive/dilative boundary suggested by Shuttle & Cunning (2008) was applied, as shown in Equation 4. Values plotted above the boundary are classified as dilative and values plotted below the boundary are classified as contractive.

$$\left[Q\left(1 - B_q\right) + 1\right] = 2{,}35 + \frac{93{,}15}{\left[1 + \left(\frac{F_R}{25{,}40}\right)^{0{,}634}\right]^{9{,}93}} \tag{4}$$

As a screening tool, the B_q was used to evaluate the tailings drainage condition. It was assumed that B_q values higher than 0.40 ($B_q \geq 0.40$) represented an undrained response to the cone penetration. This criteria agrees with the range of values suggested by Schnaid (2009). An additional criterial was used in this paper to further evaluate the drainage condition during penetration. The I_q-B_q index (Equation 5, valid only to $B_q > 0$) proposed by Mayne *et al.* (2023). Using this criteria, the undrained penetration is assumed for values below 4.

$$I_{Q-B_q} = Q.\,10^{(-1.9B_q)} \tag{5}$$

Figure 23 shows the CPTu primary data (q_t, f_s, u_2 and B_q) for the test performed in the bauxite tailings, as well as the results of the dissipation tests. In the same figure is presented the equilibrium porewater pressure profile obtained by the interpolation of the dissipation tests (u_0) and a 100% hydrostatic profile. Using the data from the CPTu, it was possible to distinguish three different materials: i) the unsaturated tailings, with the mean value of q_t = 1 MPa and B_q < 0.40; ii) the saturated tailings, with the q_t value around 0.50 MPa, showing a linear increase of q_t and u_2 over depth (normally consolidated behavior as detailed by Mayne *et al.*, 2023), and values of $B_q \geq 0.40$; and iii) the foundation soil with q_t > 1.5 MPa and B_q approximately equal to 0.

Figure 23 also shows the five dissipation test curves obtained from the saturated tailings (the porepressure data and the normalized data). As can be seen, the bauxite tailings show a monotonic behavior with the porepressure reducing over time (dissipation of a positive excess of porewater pressure), characterizing a normally consolidated clay. Also, it is possible to note that the time for 50% consolidation (t_{50}) is over 1000 seconds, which suggests an undrained condition according to Robertson (2010).

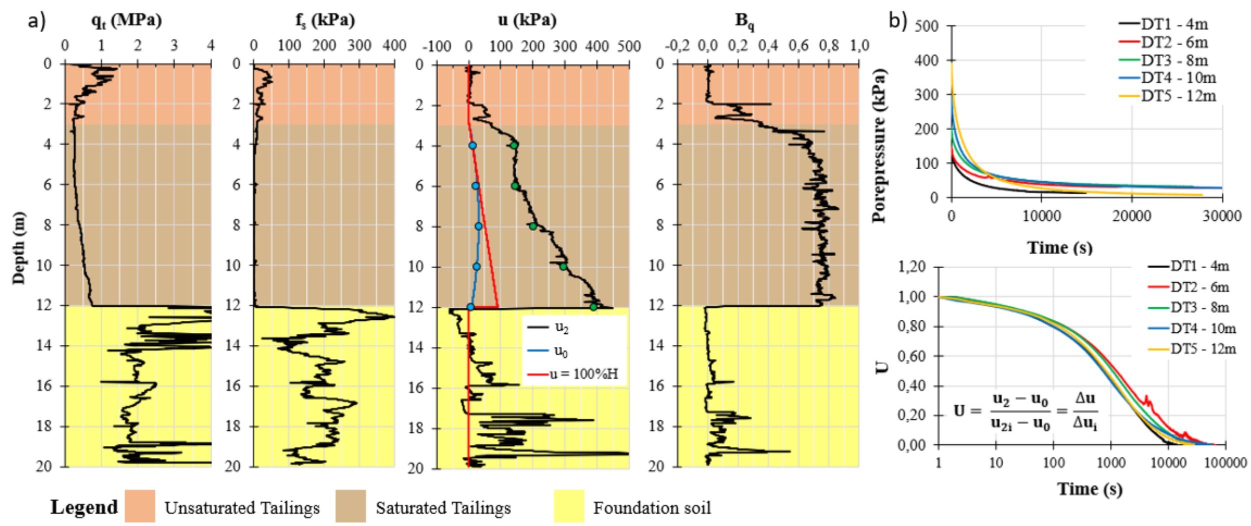

Figure 23: Results of: a) the CPTu; and b) Dissipation tests.

Figure 24a shows the data of the CPTu performed in the bauxite tailings plotted in the soil-behavior type chart proposed by Jefferies & Davies (1991) using the boundary proposed by Dos Santos Junior (2021) to distinguish contractive and dilative behavior. Also, Figure 24b shows the contour of the I_Q-B_q index prosed by Mayne *et al.* (2023) to evaluate the drainage condition of the penetration.

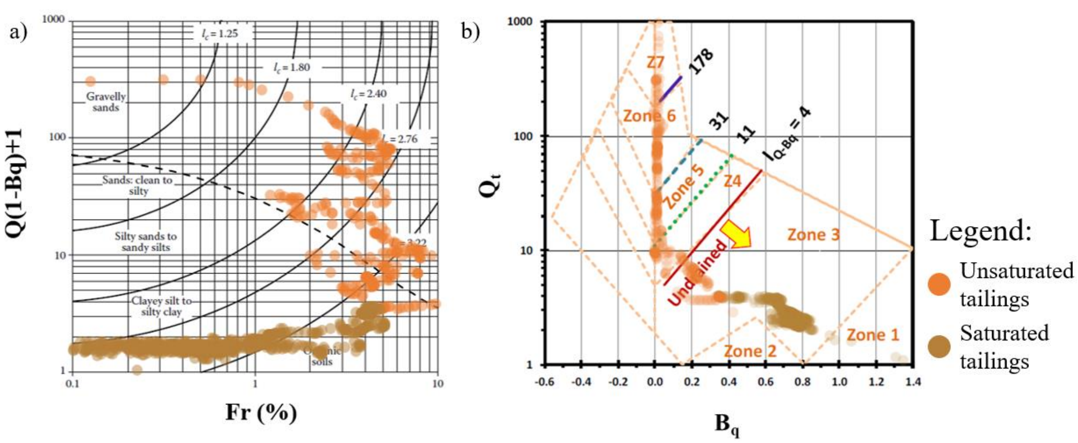

Figure 24: a) SBTn with Dos Santos Junior (2021) CD boundary; and b) I_Q-Bq index proposed by Mayne *et al.* (2023)

As can be noted in Figure 24a, the saturated tailing ($B_q \geq 0.40$) shows a contractive and clay-like behavior plotting below the boundary proposed by the author whereas the unsaturated tailing ($B_q < 0.40$) shows a dilative behavior ranging in terms of soil classification from clay to silty clay. This same behavior can be seen in Figure 24b, showing that the values of I_Q-B_q index are lower than 4 for the saturated tailings and predominantly above 4 for the unsaturated tailings.

Undrained Shear Strength

To perform the calculation of the undrained shear strength using the CPTu data, three methodologies were used to determine the cone bearing factors N_{kt}, N_{ke} and $N_{\Delta u}$: i) Mantaras *et al.* (2014); ii) Mayne & Peuchen (2018) and iii) Mayne *et al.* (2023). The remolded undrained shear strength was also evaluated based on the sleeve friction measurement as suggested by Robertson *et al.* (1986). The results were compared with the FVST measurements and with a series of undrained triaxial compression tests (CIUC) with and without correction to account for anisotropic consolidation.

To predict the S_u of contractive saturated (or nearly saturated) clayey materials, Lunne *et al.* (1997) present three different equations based on the bearing capacity factors. Equation 6 is based on net cone resistance ($q_{net} = q_t - \sigma_{v0}$), Equation 7 is based on the excess porewater pressure ($\Delta u = u_2 - u_0$), and Equation 8 is based on the effective cone resistance ($q_{eff.} = q_t - u_2$).

$$S_u = \frac{q_t - \sigma_{v0}}{N_{kt}} \tag{6}$$

$$S_u = \frac{u_2 - u_0}{N_{\Delta u}} \tag{7}$$

$$S_u = \frac{q_t - u_2}{N_{ke}} \tag{8}$$

Mantaras *et al.* (2014)

Based on an analytical approach, Mantaras *et al.* (2014) prosed Equation 9 to calculate $N_{\Delta u}$ from the dissipation test, as a function of the Rigidity Index (I_R) and the maximum excess of porewater pressure.

$$N_{\Delta u} = \frac{u_2 - u_o}{4.2 \log I_R} \tag{9}$$

The Rigidity Index (I_R) was calculated herein using the proposed equation by Agaiby & Mayne (2018) as indicated by Equation 10. The equation proposed by the authors is based on the hybrid formulation of Spherical Cavity Expansion and Critical State Soil Mechanics (SCE-CSSM). The slope of the critical state line (M_{tc}) was obtained from the triaxial compression tests and the parameter a_q, proposed by the authors, is taken as the slope of the chart composed by $u_2 - \sigma_{v0}$ (vertical axis) and $q_t - \sigma_{v0}$ (horizontal axis).

$$I_R = \exp\left[\frac{1.5 + 2.925\ M\ a_q}{M\ (1 - a_q)}\right] \tag{10}$$

Mayne & Peuchen (2018)

Based on a database of high-quality triaxial compression tests with anisotropic consolidation (CAUC), for 62 different clays categorized into five groups based on their stress–history (ranging from fissured to sensitive clays), as well as for different test conditions (onshore and offshore), Mayne & Peuchen (2018) developed a relationship between B_q and the N_{kt} as expressed by the Equation 11.

$$N_{kt} = 10.5 - 4.6\ln(B_q + 0.1) \tag{11}$$

Mayne et al. (2023)

Based on the same database of Mayne & Peuchen (2018), Mayne *et al.* (2023) proposed two different independent equations to evaluate the bearing capacity factors $N_{\Delta u}$ and N_{ke} as indicated by Equations 12 and 13, respectively.

$$N_{\Delta u} = 7.9 + 6.5\ln(B_q + 0.3) \tag{12}$$

$$N_{ke} = 4.5 - 10.66\ln(B_q + 0.2) \tag{13}$$

Remolded undrained shear strength

As described by Robertson *et al.* (1986), the remolded shear strength of clays is approximately equal to the CPTu sleeve friction. Based on this, the estimation of this parameter can be performed by Equation 14.

$$f_s = \text{Su remolded} \tag{14}$$

Field Vane Shear Test (FVST)

The Field Vane Shear Test consists of a set of cruciform rectangular blades pushed to pre-defined depths with a rotation rate equal to 6.0±0.6º/min (ASTM D2573-08, 2008). The yield undrained shear strength is measured when the vane is pushed in the soil/tailings and the remolded condition after 10 complete rotations. Furthermore, the standard presents Equation 15 to evaluate the materials' sensitivity, defined as the ratio of the yield undrained shear strength to the remolded undrained shear strength.

$$S_t = \frac{Su_{yield}}{Su_{remolded}} \tag{15}$$

Triaxial Compression Test with Isotropic Consolidation (CIUC)

For this study, three undisturbed samples of the bauxite tailings were collected and nine CIUC tests were performed with the consolidation pressures of 50kPa, 100kPa, and 200kPa. Based on the test data, the following parameters were calculated: i) the normally consolidated undrained shear strength ratio ($S_u/\sigma'_c = \sigma_d/2\sigma'_c$), as described by Olson & Mattson (2008), based on the maximum deviator stress ($\sigma_d = \sigma_1 - \sigma_3$) criteria; ii) the effective friction angle (φ'), assuming an effective cohesion equal to 0, as expected to a normally consolidated clay; and iii) the slope of the CSL in the q – p' plane (M).

To correct the isotropic stress state from the CIUC (S_u/σ'_c) to the anisotropic *in-situ* condition (S_u/σ'_{v0}) and perform the correct comparison of the CIUC data with the field assessment, Equation 16 proposed by Jaky (1948) *apud* Mayne *et al.* (2023) and Equation 17 were used.

$$k_0 = 1 - \text{sen}(\varphi') \tag{16}$$

$$\frac{S_u}{\sigma'_{v0}} = \left(\frac{1+2k_0}{3}\right)\frac{S_u}{\sigma'_c} \tag{17}$$

Undrained Shear Strength Profile

Figure 25 shows the results obtained from the CIUC tests. As can be seen, the samples generated a high shear–induced excess porewater pressure, even higher than the deviator stress. Also, it is noted that the bauxite tailings have a very ductile behavior, with no strength loss during shear, what is expected of high plastic tailings. The main results obtained were: i) $Su/\sigma'_c = 0.32$; ii) $\varphi' = 27°$ with $c' = 0$; and iii) $M_{tc} = 1.72$. Based on this data, the k_0 value obtained was 0.55 and Su/σ'_{v0} equal to 0.22.

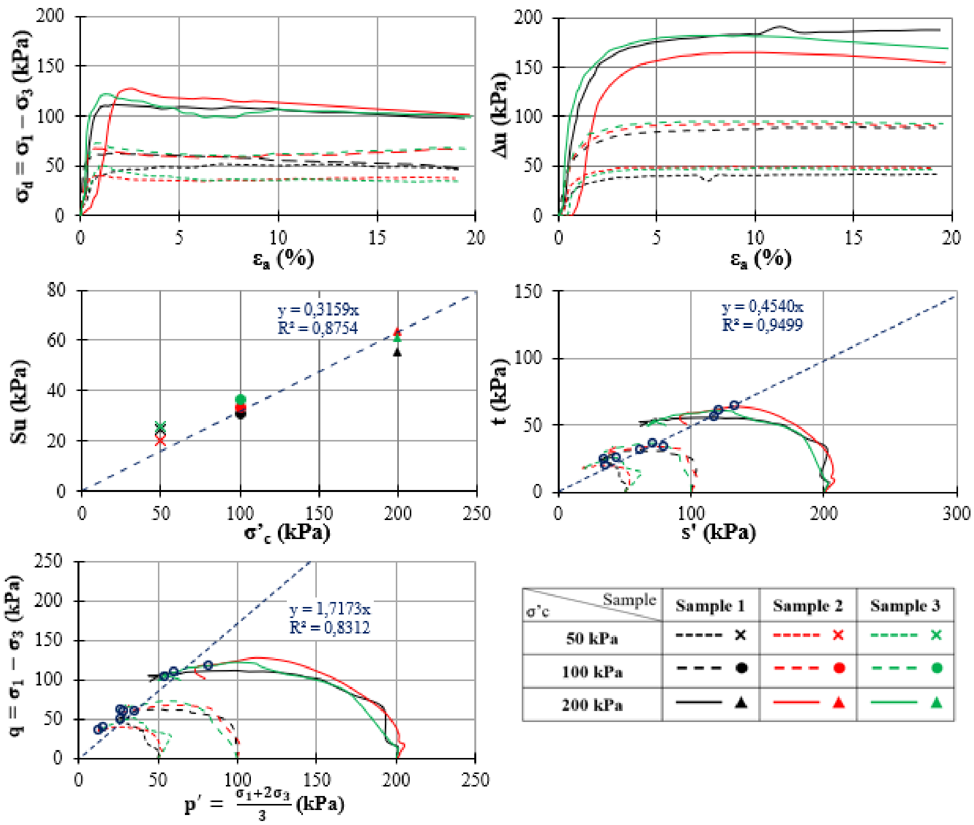

Figure 25: Isotropically consolidated undrained triaxial compression tests – Main Results

Equation 10 was used to calculate the I_R for the bauxite tailings, in order to apply the methodology proposed by Mantaras *et al.* (2014). The a_q parameter was obtained as shown in **Figure 26**, considering only the saturated portion of the tailings (undrained behavior). By using M_{tc} equal to 1.72 (**Figure 25**) and the a_q value equal to 0.37 the I_R value obtained was equal to 22.

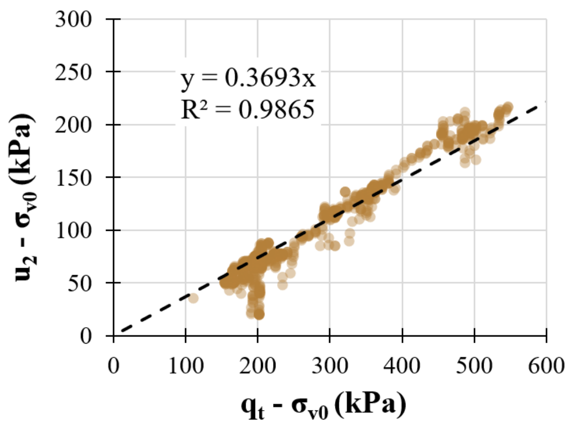

M	1.72
$\mathbf{a_q}$	0.3693
$\mathbf{I_R}$	22.17

Figure 26: Calculation of the I_R based on the a_q parameter.

Figure 27 shows the comparison of the yield and remolded undrained shear strength considering all the field tests (CPTu and FVST) and laboratory tests (CIUC) available. In the evaluation presented herein it was only considered the tailings below 3,0 m of depth, since this is the region where undrained penetration of the cone was observed, as mentioned earlier in this paper. The surface of the tailings is subjected to weathering and high temperatures in the north of Brazil, creating an unsaturated crust (which is also observed in the field).

Figure 27, shows two different patterns of S_u profile. The first one is obtained by the i) CIUC considering the undrained shear strength normalized by the consolidation pressure (S_u/σ'_c); ii) $N_{\Delta u}$ from Mantaras *et al.* (2014); and iii) N_{ke} from Mayne *et al.* (2023).

The second pattern shows a convergence of the values from the i) CIUC test with correction to account for anisotropic consolidation (S_u/σ'_{v0}); ii) N_{kt} from Mayne & Peuchen (2018); and iii) $N_{\Delta u}$ from Mayne *et al.* (2023). Also, it can be noted that the FVST shows similar results with these methods below the depth of 6m.

The remolded undrained shear strength is also presented in **Figure 27**, based on the sleeve friction measurement of the cone (f_s) which shows a tendency to decrease over depth, reaching almost zero below 4 m of depth. **Figure 27** also shows the results of the remolded undrained shear strength measured by the FVST, which indicates higher values. This difference is probably associated with the inaccuracy of the sleeve load cell used to measure the sleeve friction of the cone penetration, a common issue related to soft soils as already reported by Lunne *et al.* (1997), McConnell & Wassenaar (2022) and Buò *et al.* (2022).

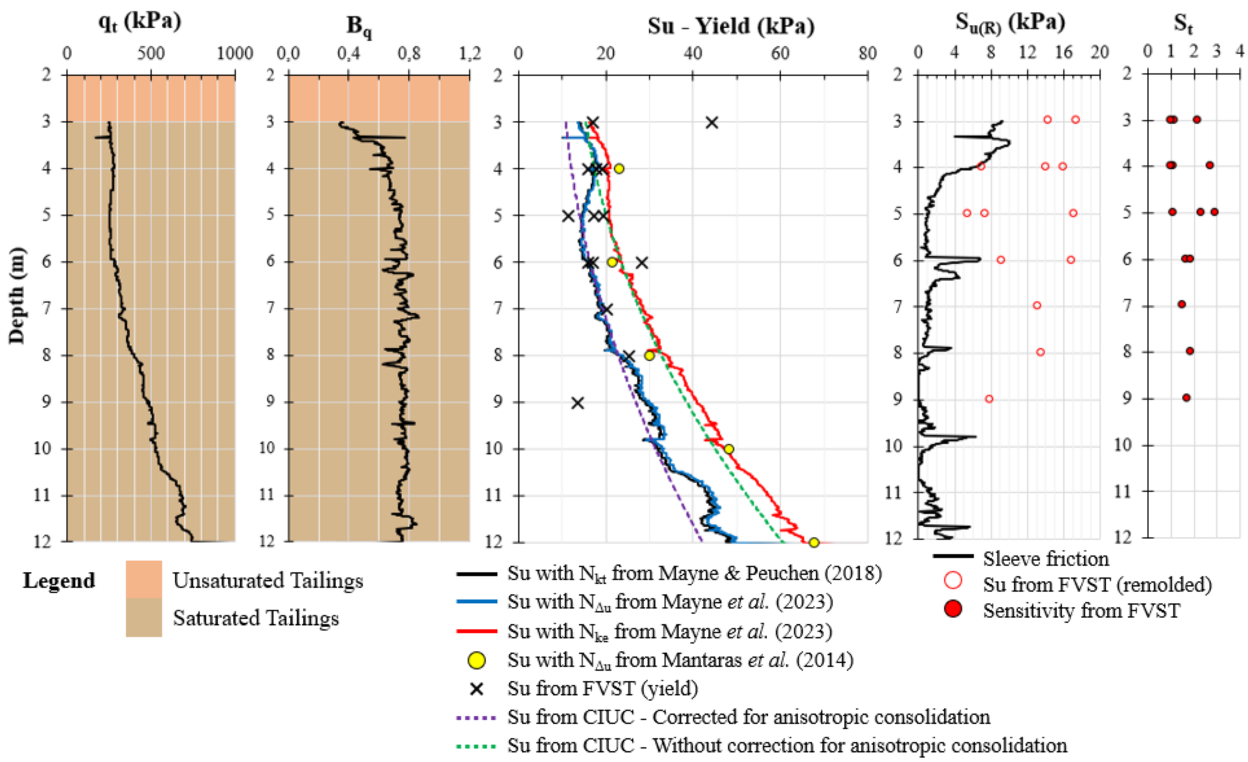

Figure 27: Undrained shear strength profile (yield and remolded) of the Bauxite Tailings

Figure 27 shows the yield and the remolded undrained shear strength from the FVST as well the sensitivity ($S_t = S_{u\ yield} / S_{u\ remolded}$) calculated based on Equation 15, over depth. The results indicate that the sensitivity of the bauxite tailings ranges from 1 to 3 ($1 \leq S_t \leq 3$), which is classified as a low to medium sensitivity, according to Skempton & Northey (1952). This behavior is in accordance with the observed behavior in the triaxial compression test (CIUC) since no significant strength loss is noted at large strains (ductile behavior).

Conclusion

This paper presents a case study focusing on the evaluation of the undrained shear strength of a bauxite tailing using laboratory and field tests. Also, geotechnical characterization was conducted by laboratory tests (grain-size distribution, Atterberg Limits, and specific gravity). The soil behavior-type classification system proposed by Jefferies & Davies (1991) was used along with the equation proposed by Dos Santos Junior (2021) to represent the boundary suggested by Shuttle & Cunning (2008) to distinguish contractive and dilative behavior. The behavior-based classification shows that the tailings evaluated is a predominantly contractive clay-like geomaterial, which is consistent with the physical classification and the stress-strain behavior shown in the triaxial compression test.

The calculation of the undrained shear strength was performed in the regions where undrained penetration was observed. The criteria used to characterize undrained penetration was based on the pore pressure ratio, as suggested by Schnaid (2009) and the I_Q-B_q index suggested by Mayne *et al.* (2023). Both criteria proved useful to distinguish drained and undrained penetration, but the I_Q-B_q index, presented by Mayne *et al.* (2023) seems to better capture the behavior of the soil, since it incorporates pore pressure (B_q) and the resistance of the soil (Q_t).

The comparison of different methodologies using field and laboratory tests to calculate the undrained shear strength of a bauxite tailings was performed. The results have shown that the undrained shear strength determined based on N_{kt} (Mayne & Peuchen, 2018) and $N_{\Delta u}$ (Mayne *et al.*, 2023), presented similar values with the CIUC test with the k_0 correction to account for anisotropic consolidation and the FVST. The methodology based on the N_{ke} (Mayne *et al.*, 2023) and on $N_{\Delta u}$ (Mantaras *et al.*, 2014) yielded the S_u profile higher than the other bearing capacity factors, in agreement with the profile from the CIUC test without stress correction. This difference highlights the uncertainty in the determination of the undrained shear strength due to the usually unknown horizontal stress. In the tailings examined herein, the authors believe that the lower profile (based on the anisotropic correction of the CIUC), would be the most appropriate, since it agrees well with the FVST and the most often used bearing capacity factors (N_{kt} and $N_{\Delta u}$).

Regarding the remolded undrained shear strength calculated based on the sleeve friction, the results indicated lower values when compared to those measured by the FVST, which highlights the inaccuracy of the sleeve friction measured in very soft soils, as pointed out by McConnell & Wassenaar (2022) and Buò *et al.* (2022). To deal with this issue, the international standard 22476-1 (ISO, 2022) recommends using friction load cell with accuracy of 5 kPa or 10% when dealing with very soft soils, to obtain reliable results.

The results of the undrained shear strength show the importance of comparing different methodologies based on the CPTu test and with direct measurement of undrained shear strength, such as using CIUC test and the FVST, to define the best methodology to evaluate the stability condition of a TSF. Finally, it is important to highlight that the conclusions obtained in this paper are specific to the bauxite tailings evaluated and the authors do not recommend a direct replication of the results presented herein.

Acknowledgments

The authors would like to acknowledge the support received by Pimenta de Ávila during the develop of this paper.

References

Agaiby, S.S. & Mayne, P.W. 2018. Evaluating undrained rigidity index of clays from piezocone data. Proceedings of the 4th International Symposium on Cone Penetration Testing (CPT'18).

American Society for Testing and Materials – ASTM. 2020. D792-20: Standard Test Methods for Density and Specific Gravity (Relative Density) of Plastics by Displacement.

American Society for Testing and Materials – ASTM. 2008. D2573: Standard Test Method for Field Vane Shear Test in Cohesive Soil.

American Society for Testing and Materials – ASTM. 2007. D422-63: Standard Test Method for Particle-Size Analysis of Soils.

American Society for Testing and Materials – ASTM. 2018. D4318-17e1: Standard Test Methods for Liquid Limit, Plastic Limit, and Plasticity Index of Soils.

Dos Santos Junior, Mauro. 2021. Avaliação da susceptibilidade à liquefação de um rejeito silto-arenoso com base em ensaio CPTu. Dissertação. Universidade Federal de Ouro Preto - UFOP. Núcleo de Geotecnia.

International Organization for Standardization - ISO 22476-1. 2022: Geotechnical investigation and testing — Field testing — Part 1: Electrical cone and piezocone penetration test.

Jefferies, M.G. and Davies, M.P. 1991. Soil classification by the cone penetration test: Discussion. Canadian Geotechnical Journal, 28(1), 173–468

Lunne, T.; Robertson, P.K. & Powell, J.J.M. 1997. Cone Penetration Testing in Geotechnical Practice. First Edition. Abingdon: E & FNSpon Press.

McConnell, A. J. & Wassenaar, J.C. 2022. An innovative new 3MPa CPT – to detect and measure very small fs values. Cone Penetration Testing 2022 (CPT 2022). ISBN 978-1-032-31259-0

B. Di Buò, M. D'Ignazio, T. Länsivaara & M. Haikola. 2022. Issues related to piezocone sleeve friction measurement accuracy in soft sensitive clays. Cone Penetration Testing 2022 (CPT 2022). ISBN 978-1-032-31259-0

Mayne P. W., Ethan, C., James, G. 2023. A CPT Design Parameter Manual.

Mayne, P.W. & Peuchen, J. 2018. Evaluation of CPTU N_{kt} cone factor for undrained strength of clays. In Proceedings of the 4th International Symposium on Cone Penetration Testing (CPT'18).

Olson, S. M., & Mattson, B. B. 2008. Mode of shear effects on yield and liquefied strength ratios. Canadian geotechnical journal, 45(4), 574-587.

Robertson, P. K., Campanella, R. G., Gillespie, D., & Greig, J. 1986. Use of piezometer cone data. In Use of in situ tests in geotechnical engineering (pp. 1263-1280). ASCE.

Robertson, Peter K. 2010. Estimating in-situ soil permeability from CPT & CPTu. 2nd International Symposium on Cone Penetration Testing, California State Polytechnic University Pomona, CA.

Shuttle, Dawn & Cunning, John. (2007). Liquefaction potential of silts from CPTu. Canadian Geotechnical Journal.

Skempton, A. W., and Northey, R. D. 1952. The Sensitivity of Clays, Géotechnique, 3 (1), pp. 30-53.

Does the anisotropy of the collapse/instability surface play a role when assessing the stability of tailings dams?

David Hight, Geotechnical Consulting Group LLP, UK
Tiago Gerheim Souza Dias, Geotechnical Consulting Group LLP, UK

Abstract

The paper considers the factors known to determine the existence and shape of the collapse/instability surface in sedimented samples of a number of sub-angular sands, based on the results of published data from triaxial, plane strain and hollow cylinder apparatus tests. Stress paths which cross the collapse surface, including those involving increasing pore pressure or rotation of principal stress directions, both at constant deviator stress, can cause runaway failure under load-maintained conditions or strain softening under strain-controlled conditions. The presence of fines in tailings sands will modify the shape, including anisotropy, of the collapse surface seen in clean sands.

Successful back analyses of failures of tailings dams often rely on parameters from tests run on tailings specimens reconstituted using moist tamping sample preparation methods. The fabric in these reconstituted samples is unlikely to match that of hydraulically placed tailings and the shape and anisotropy of the collapse surface may not be correctly represented. Does this need to be considered when predicting the response of tailings dams, particularly during their deconstruction, when different stress paths to those applying in past failures may be involved?

Introduction

Before embarking on the deconstruction/dismantling of existing upstream tailings dams that retain hydraulically placed silty sand tailings, it is perhaps timely to recall published findings on instability and anisotropy in loose sands, and on the shortcomings in the use of moist tamping as a reconstitution method. Extrapolation of these findings on clean sands to tailings requires careful consideration of the potential impact of the fines content.

Collapse surface and instability lines in loose sands

To assist in the explanation of the collapse of a hydraulically placed subsea sand berm, which occurred at Nerlerk in the Canadian Beaufort Sea, Sladen et al (1985 a and b) introduced the concept of a 'collapse surface' in loose sedimented sands. The 'collapse surface'[1] or more correctly a 'collapse line', was found by drawing a line through the peak points on effective stress paths from isotropically consolidated undrained, CIU, triaxial compression tests on specimens prepared at the same post consolidation void ratio by a form of moist tamping, and connecting this to the steady state or critical state point. An example of a 'collapse line' is presented in Figure 1, this time based on CIU tests on loose Leighton Buzzard sand samples prepared by moist tamping. Experiments show that the peak strengths fall on a straight line in stress space.

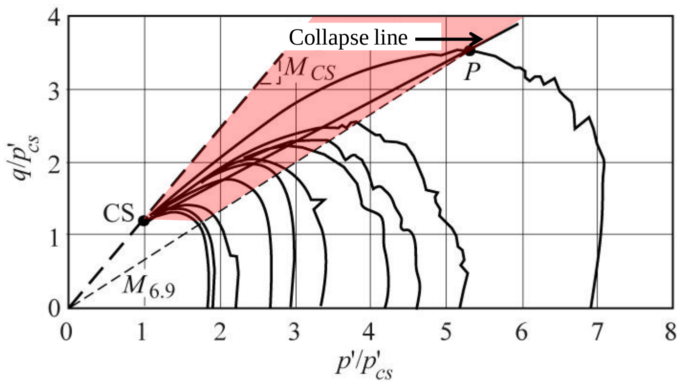

Figure 1: Undrained triaxial compression tests on isotropically consolidated loose Leighton Buzzard sand showing the collapse or instability line, the critical state (CS) and the zone of potential instability (shaded pink). (Modified from Leroueil et al, 2009 and Sladen et al, 1985b).

Lade (1993) explored these ideas, and the cause of the Nerlerk failure, referring instead to static instability and to instability lines, IL, which had been identified in CIU triaxial compression tests on Valgrinde sand samples prepared by moist tamping (Bjerrum et al, 1961). Lade (1993) argued that '*Since it goes through the top points of the yield surfaces, which evolve from the origin, the instability line also intersects the stress origin. This location of the instability line is different from that used previously by Sladen et al.(1985a) and Lade (1992)…recent realization of the true origin and nature of the instability line indicates that it goes through the origin of the stress diagram rather than through the ultimate state.*'

Chu et al (2003) and Chu and Wanatowski (2008) carried out a comprehensive investigation of instability lines, running CIU triaxial and plane strain compression tests on moist tamped samples of Changi sand. Their tests illustrated how the slope of the instability line varies with void ratio (Figure 2a). Interestingly, Chu and Wanatowski (2008) found that the relationship between the slope of the instability

[1] Vaid and Chern (1985) used the term 'the Flow Liquefaction Surface (FLS)' to refer to a similar surface to the collapse surface.

line and void ratio was not affected by whether the specimen was isotropically or k_0 consolidated or whether tested in triaxial or plane strain compression (Figure 2b).

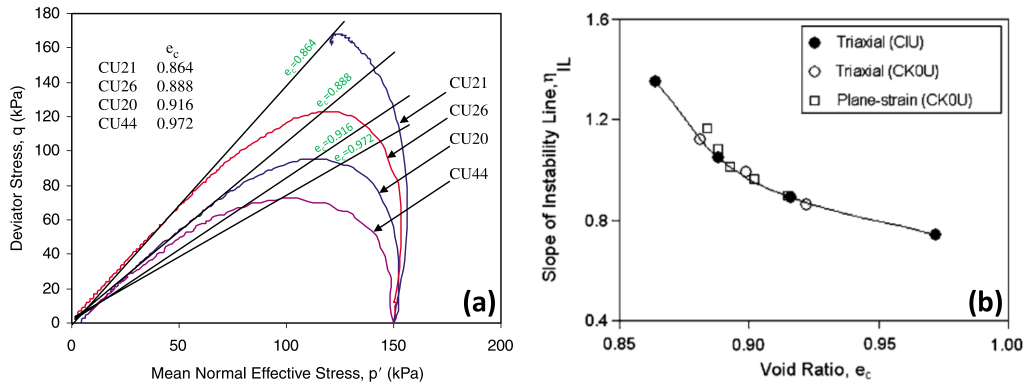

Figure 2: (a) Undrained triaxial compression tests on isotropically consolidated loose Changi sand showing the variation of the instability line with void ratio, from Chu et al 2003; (b) Relationship between the slope of the instability line and the void ratio established for CIU and CK_0U triaxial and plane strain tests on loose Changi sand, from Chu and Wanatowski, 2008.

Taking into account the dependence of the shape of the effective stress path in CIU triaxial compression on particle shape (Figure 3), and on fabric, i.e. on different methods of sample reconstitution (Figure 4), it is reasonable to expect both particle shape and fabric to have an important effect on the instability and the post-peak behaviour

Chu et al (2003) and Leroueil et al (2009) introduced a framework which made use of instability lines and critical state to anticipate the response of loose and dense sands to drained and undrained perturbations in slopes. This included the response to reducing mean effective stress at constant shear stress (CSD test), a common situation in slopes undergoing infiltration or rising groundwater level. The framework for loose sand, our interest here, is illustrated in Figure 5.

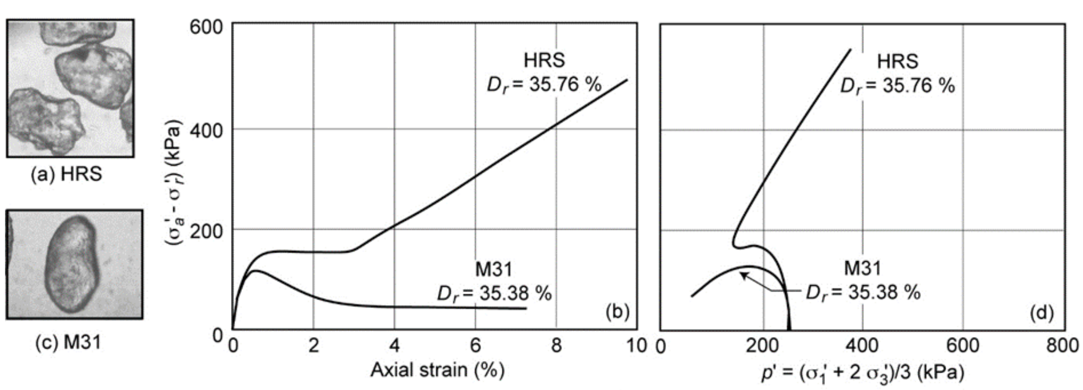

Figure 3: Effect of particle shape on behaviour in undrained triaxial compression (after Tsomokos and Georgiannou, 2010).

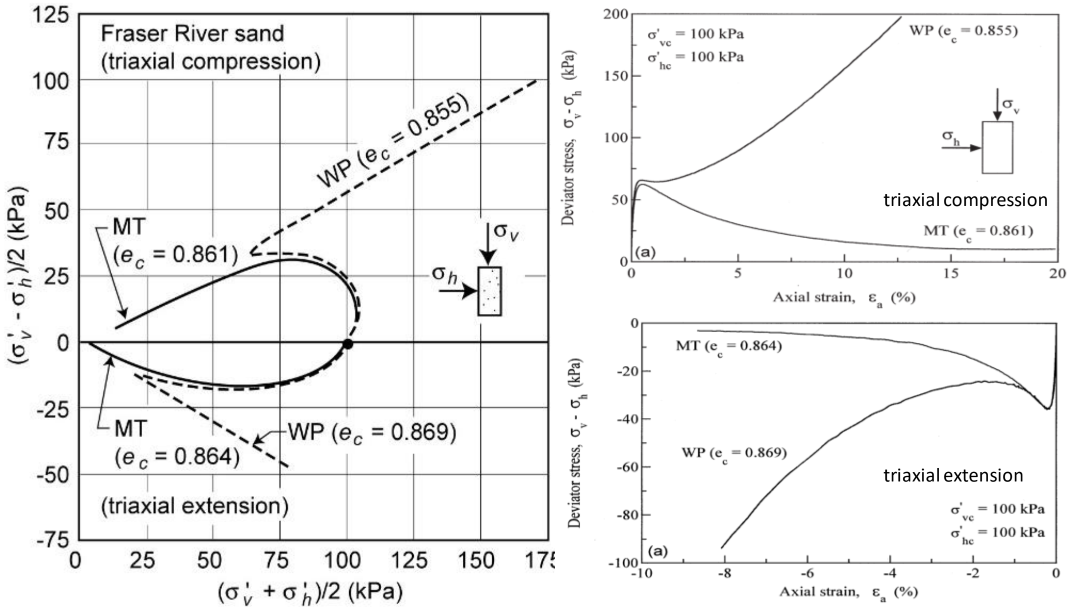

Figure 4: Undrained triaxial compression and extension stress paths and stress-strain curves obtained on loose Fraser River sand specimens reconstituted by water pluviation (WP) and moist tamping (MT) (after Vaid et al, 1999)

Features of soil behaviour that emerge from these findings are summarised below. Herein, instability is taken to be soil behaviour in which large plastic strains are generated before general failure because the soil cannot sustain the applied load or stress; collapse or static liquefaction are used when the drop from peak to ultimate strength is large and occurs rapidly, usually under load-controlled conditions.

- '*Instability occurs inside the failure surface and so is not synonymous with failure, although both lead to catastrophic events*', Lade (1993).
- For a granular material to become unstable, the state of stress must be located on or above the instability line, in a zone bounded by the IL and the critical state line, CSL, and referred to as the zone of potential instability or instability zone (Figure 1).
- Instability can occur under drained, undrained and partially drained conditions.
- Under undrained conditions, only very loose[2] sand can become unstable and this can lead to static liquefaction or collapse if the driving shear stress is and remains significantly higher than the ultimate or critical state strength.
- Drained instability in both loose and dense[3] sands only occurs when there is a reduction in the mean effective stress that may result from a decrease in total mean stress (e.g. an excavation) or from an increase in pore pressure (e.g. rising groundwater level).

[2] Loose enough under the consolidation stress to be contractant and strain softening.
[3] Dense enough under the consolidation stress to be dilatant.

- The difference between undrained and drained conditions is illustrated using the framework in Figure 5. When a loose sand is sheared along a constant deviator stress path, starting from point I, instability occurs at point Y, on the IL. If the pore water pressure can dissipate freely (i.e. under drained conditions), the stress path will eventually reach the failure state at point C1, on the critical state line which is also the failure line for loose sands. During this process, large axial and volumetric strains will develop and the void ratio of the soil will decrease. If the pore water pressure cannot dissipate, the stress path will move towards the critical state associated with its current water content, i.e. C2, under undrained conditions.
- A triggering mechanism for collapse is one that causes the pore pressure to increase faster than it can dissipate when the stress state is in the instability zone or has been brought to the instability line. Once initiated, collapse can propagate progressively and rapidly, particularly into areas where the stress state lies in the instability zone.
- Load-controlled conditions, which are more appropriate to field conditions, are more likely than deformation-controlled conditions to result in undrained instability on crossing the collapse surface. Tests reported by Chu and Wanatowski (2009) and shown in Figure 6 illustrate the much shorter time to reach ultimate conditions under load-control. In Figure 6, the ultimate strength reached under load-control is shown to be lower than that reached under deformation-control. Although difficult to measure, it is reasonable to expect this based on the lack of time for local equilibration of varying local positive excess pore pressures during collapse under load-control.

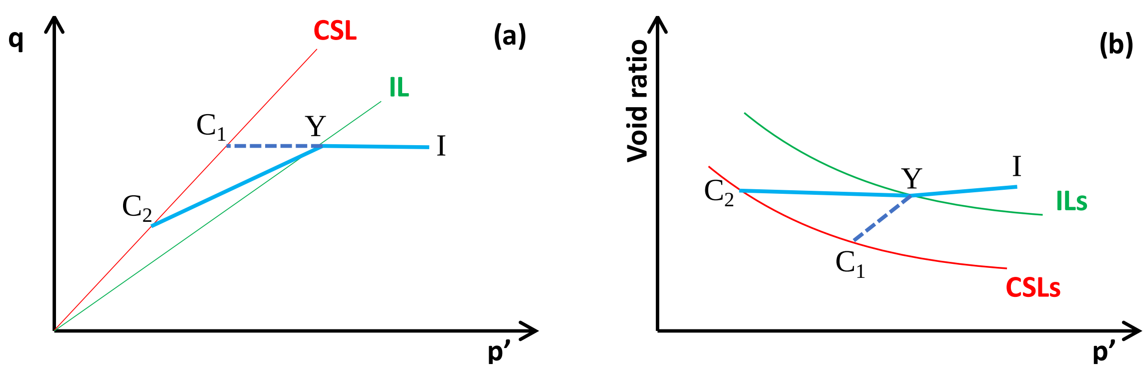

Figure 5: Schematic illustration of instability conditions for loose sand along a CSD path (modified after Chu et al, 2003 and Leroueil et al, 2009).

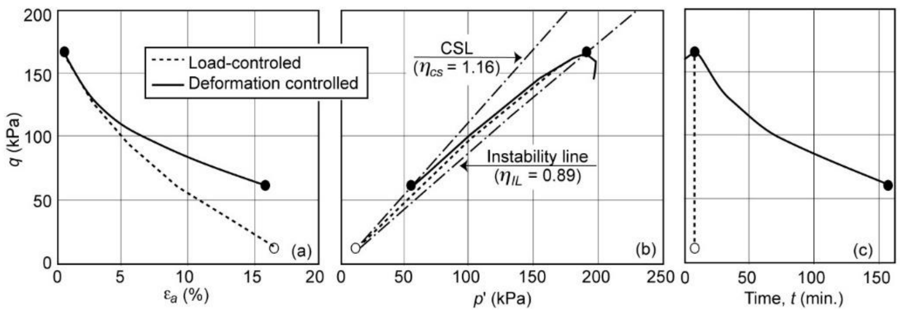

Figure 6: Comparison of undrained plane strain tests on very loose Changi sand under deformation and load-controlled shear: (a) stress-strain; (b) effective stress paths; (c) deviator versus time (data from Chu and Wanatowski, 2009).

- Strains to reach the instability line are very small, making it difficult to use displacement monitoring to predict incipient instability. The small strains probably explain the insensitivity to the value of b[4] when comparing triaxial and plane strain compression tests (Figure 2b).

Anisotropy of undrained shear behaviour of sedimented loose sands

The response seen in Figure 4 for the moist tamped and water pluviated samples tested in undrained triaxial compression and extension, reveals the impact of the combined differences of b and major principal stress direction, alpha[5], on the instability of clean sands. Many practical geotechnical problems involve varying size rotations of principal stresses, rather than step changes of 90 degrees, and varying values of b.

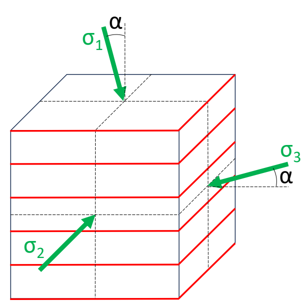

Figure 7: Definition of alpha, the angle of the major principal stress relative to the vertical.

The work reviewed in the preceding section did not consider the potential effect of anisotropy and principal stress rotation on instability or collapse behaviour, yet investigations in the hollow cylinder apparatus, HCA, at around that time, showed important anisotropy of undrained shear behaviour in sedimented sub-angular sands. Published results of HCA tests on isotropically consolidated undrained HCA

[4] b is a measure of the relative magnitude of the intermediate principal stress, and is defined as $b=(\sigma_2-\sigma_3)/(\sigma_1-\sigma_3)$

[5] in triaxial compression b=0 and alpha=0 whereas in triaxial extension, b=1 and alpha=90 degrees. Alpha is defined in Figure 7 as the rotation away from vertical in a vertical plane.

tests on sedimented Fraser River Sand and Toyoura Sand are presented in Figures 8 and 9 as a reminder of the findings.

The similarity between the observed undrained behaviours in different clean and sub-angular sands and different testing equipment is striking:

- Sedimented sands are non-brittle when the major principal stress is vertical (alpha = 0 degrees). This is consistent with the findings in triaxial compression tests on sedimented sands and contrasts with the extreme brittleness that is found in the same sand at the same global void ratio when prepared by moist tamping (Figure 4).
- Sedimented sands become brittle when sheared with the major principal stress rotated away from the vertical, i.e. from the direction of deposition (alpha>15 to 30 degrees). This is perfectly logical when considering the fabric that develops during sedimentation (e.g. Oda, 1972) and the anisotropic load transfer framework that develops in sands[6].
- Peak undrained strengths reduce with increasing values of alpha and brittleness increases.
- Strains to peak are small for all values of alpha.
- Adding instability lines to the data shown in Figures 8 and 9, and taking these lines through the origin in stress space for simplicity, shows that the IL inclinations reduce as alpha increases. The fan of instability lines for different alpha values is similar to the fan for different void ratios in triaxial compression (Figure 2a).

The anisotropy observed in these HCA tests is that existing after sedimentation and so before any subsequent stress or strain history. It could be indicative of the anisotropy of relatively recently sedimented silty sand tailings but one must consider the potential impact of fines.

Stacking the effective stress paths from CIU HCA tests on sedimented Ham River Sand in q-p'-e space (Figure 10), the initial anisotropy of the sand can be portrayed and the resulting surface can be used to identify when collapse could occur under rotation of principal stresses at constant deviator stress. Slices through this surface at constant alpha, can, with the addition of the relevant instability line and critical state line, be used to define the instability zone and to anticipate when instability could develop, for example as in a CSD test at different or constant alpha values (Figure 11a).

[6] The difference in response to undrained triaxial compression and extension in sedimented sands seen in Figure 4 is to be expected, because in triaxial extension there has been a step change in alpha of 90 degrees away from the direction of deposition.

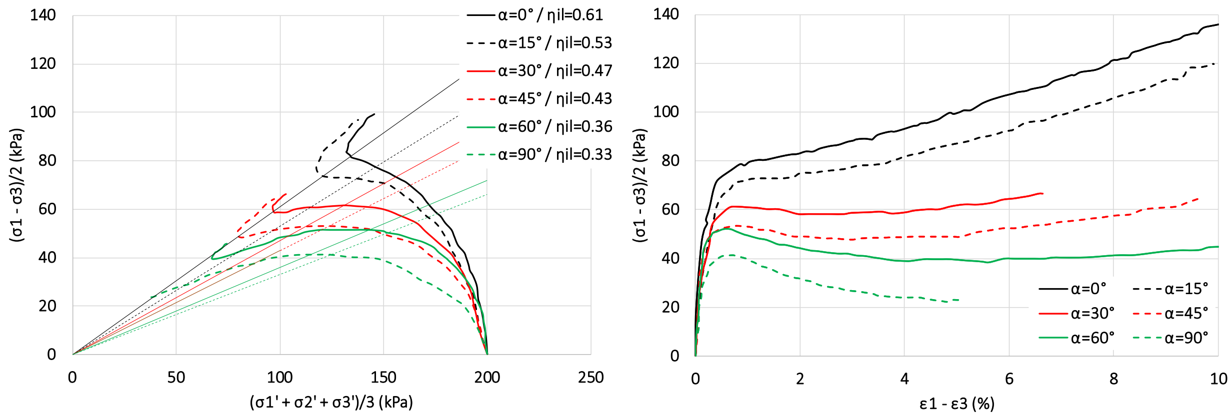

Figure 8: Undrained HCA tests on water pluviated Fraser River sand. Isotropic consolidation, b=0, Dr=30%. (Redrawn from Uthayakumar and Vaid, 1998).

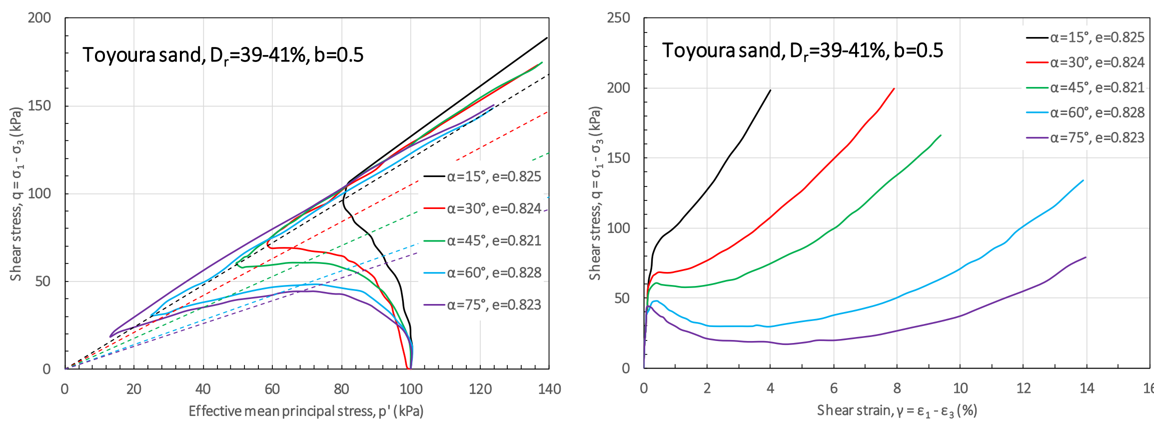

Figure 9: Undrained HCA tests on water pluviated Toyoura sand. Isotropic consolidation, b=0.5, Dr=39-41%. (From Yoshimine et al, 1998)

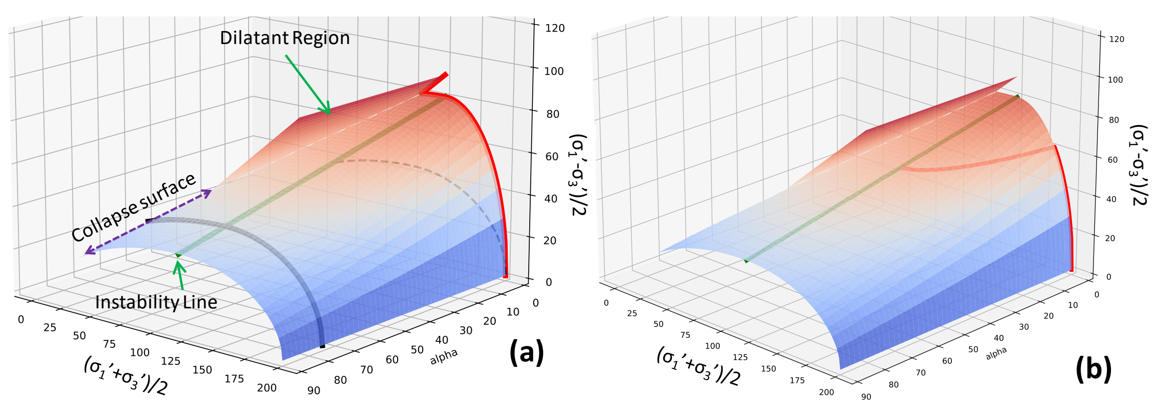

Figure 10: (a) Extent of collapse surface in relation to complete local bounding surface for water pluviated Ham river sand. (b) Undrained principal stress rotation at constant t leading to failure. Refer Shibuya and Hight (1987) and Leroueil and Hight (2003)

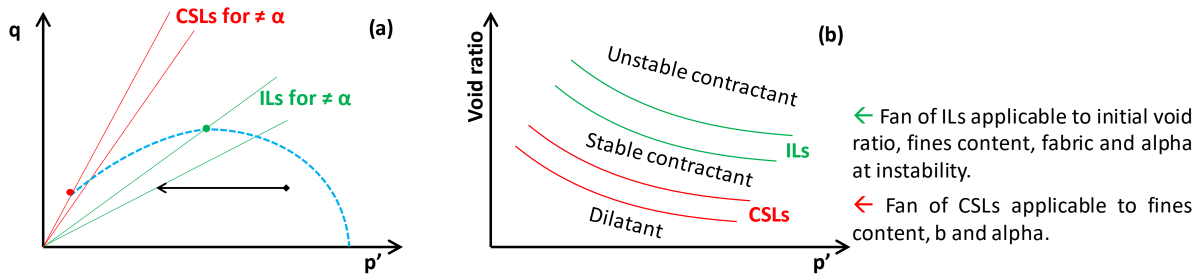

Figure 11: (a) Fans of CSLs and ILs for different values of alpha, and CSD path at constant or changing alpha; (b) Fan of ILs and CSLs showing regions of stable and unstable contractant, and dilatant response.

The impact of fines

The applicability of these findings on instability and anisotropy in clean sub-angular sands to silty sand tailings needs to consider the potential effects of the addition of fines. These effects depend on their quantity[7], size range, shape and plasticity, if any, and include:

- Reducing permeability and increasing compressibility with increasing fines content. The combined effect is to increase the time for dissipation of excess pore pressures that may be generated and may result in instability becoming an undrained rather than a drained event.
- Changes in maximum and minimum void ratios (Lade et al, 1998) and the existence of a transitional fines content above which behaviour changes from sand-dominated to fines-dominated.
- Lowering of the critical state line with increasing fines contents up to the transitional fines content.
- Difficulties of reconstitution of samples because of segregation of fines and the host sand.

In terms of the impact of a given fines content on instability, and the anisotropy of instability, it depends on the location of the fines within, and the part they play in, the load-carrying framework. When the fines merely occupy some of the void space between the host sand, i.e. with fines contents less than the transitional fines content, the coarse material will continue to dominate the load-carrying framework and the instability and anisotropy seen in the laboratory tests on sedimented clean sands is likely to persist. It is possible that there is a reduction in instability and an increased tendency to dilate.

When fine sand is sedimented into silt in suspension, which must occur in parts of a tailings pond, a fabric similar to that sketched by Monkul and Yamamaro (2010) (Figure 12a) could develop, with the fines

[7] The fines content in hydraulically placed tailings will vary with distance from the discharge points. Identifying which fines content and which fabric create the highest instability becomes the challenge, together with the challenge of modelling the varying behaviour with changing psd.

separating to some extent the sand particles and so increasing compressibility and instability[8]. With densification by removal of the meta-stable contacts, for example under increasing overburden, the fines are pushed into the voids (Figure 12b), restoring the dominance of the coarse particles.

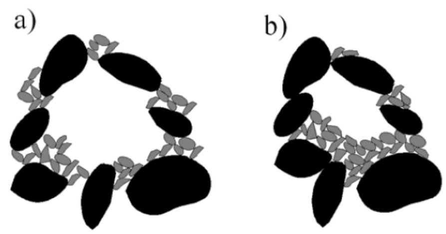

Figure 12: Evolution of soil fabric in the silty sand laboratory specimens a) after deposition, b) after densification. (From Monkul and Yamamuro, 2010).

The ability of fines to increase instability in undrained triaxial compression, i.e. to reduce the resistance to collapse, has been demonstrated by Chu and Leong (2002) (Figure 13), and by Lade and Yamamuro (1997), testing samples at particularly low stress levels. To reconstitute their specimens with different fines content, Chu and Leong used moist tamping and Lade and Yamamuro used dry funnel deposition. The fact that two different reconstitution methods with different shape fines lead to similar conclusions has to be significant. Whether either method produces a fabric similar to any of the fabrics in the tailings pond is not known, nor is the level of anisotropy of the collapse surface that each method produces. What their work did demonstrate was that neither void ratio nor relative density can be used to identify a potential to collapse in sands with fines. However, Chu and Leong found that the instability condition established for clean sand is the same as that for silty sand if the intergranular void ratio[9] is used and the fines content is less than the transitional value. As with void ratio (Figure 2a) and major principal stress direction (Figure 11a), a fan of instability lines is found for different fines contents (Figure 13).

Moist tamping

Specimens used by Sladen et al (1985b), Lade (1992), and Chu et al (2003) to investigate instability in loose sands were reconstituted by moist tamping or a variant of that method. As a sample reconstitution method, moist tamping has the advantage of producing extremely loose samples that will, unlike sedimented samples, show contractant and strain softening behaviour in undrained triaxial and plane strain compression. This, in turn, enables critical state parameters to be determined more easily than in dense samples, and has allowed the concept of collapse/instability to be explored under these restricted forms of loading.

[8] The sedimentation of sand into a silt suspension is quite different to the procedure followed when determining maximum void ratio, e_{max}, and different fabrics will result, possibly with yet higher void ratios than e_{max} being achieved. Moist tamping can also lead to void ratios higher than e_{max}.

[9] Intergranular void ratio (or skeleton void ratio) is the void ratio of the host sand with the fines excluded.

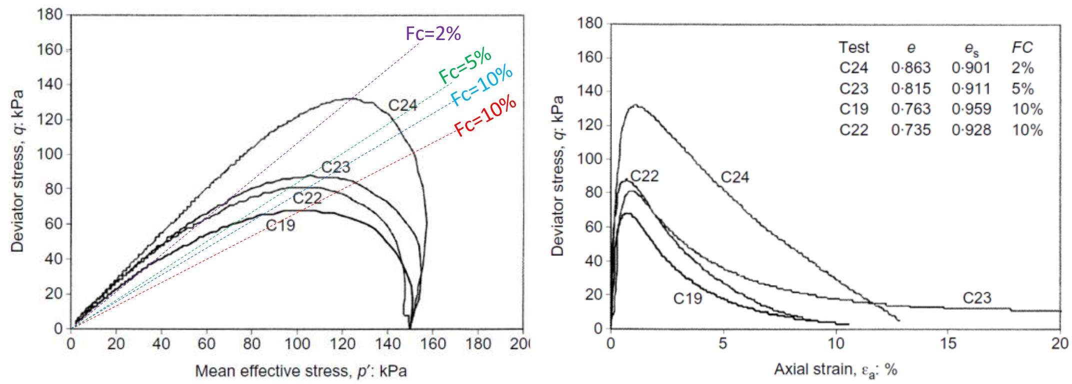

Figure 13: Results of CIU triaxial compression tests on sands with different fines contents of kaolin powder. (From Chu and Leong, 2002).

However, in clean sands, moist tamping results in a specimen with widely varying local void ratios (Jang and Frost, 1998), and a fabric (Quinteros and Carrero, 2023) and a behaviour (Figure 4) that does not match that of sedimented sand. Figure 14, from Chang et al (2011), compares the fabrics of in situ gold tailings in the pond area, with the same material reconstituted by moist tamping. Clustering of fines in the moist tamped specimen makes it unsuitable for investigating the anisotropy and instability of these particular tailings.

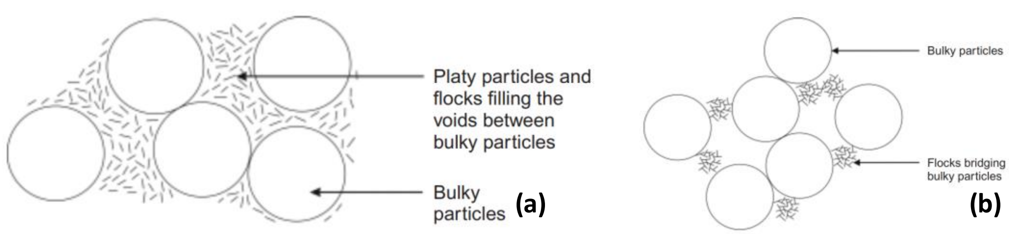

Figure 14: Sketches of fabric of tailings samples: (a) Beach undisturbed and (b) Beach reconstituted with MT method (after Chang et al. 2011).

It is vitally important that the fabrics in hydraulically placed silty sand tailings are studied, so that, firstly, an assessment can be made as to whether the fines are acting as separators, increasing instability, or stabilisers, reducing instability, refer to Leroueil and Hight (2002). Secondly, whether a reconstitution method can be found that produces a match to the in situ fabric and can be used to prepare samples for hollow cylinder testing. Thirdly, whether moist tamping can play any part in this.

Analyses of tailings dams

There are reports/papers describing back analyses of tailings dams that have failed in the recent past. These back analyses have successfully matched the extent and form of the failure, without the need to model the anisotropy of the tailings or to consider the implications of collapse or instability surfaces. It is, perhaps, noteworthy that the laboratory tests on which these analyses relied were undrained triaxial compression tests on reconstituted samples prepared by moist tamping.

Tests run on moist tamped samples for these back analyses are unlikely to have reflected the true behaviour of the in situ tailings, and may have overestimated the undrained brittleness in triaxial compression. The use of a global/isotropic brittleness in these analyses appears to have compensated for any effects of anisotropy and pre-failure instability. It is also possible that, in these cases, anisotropy of the tailings was not important in terms of their placement and in the particular stress path of the triggering mechanism.

Deconstruction of existing tailings dams will involve quite different stress paths to those involved in the construction and perturbation of the dams that have been back analysed. Unloading stress paths will dominate with principal stress rotation so that anisotropy of collapse surfaces will be relevant. To determine whether the dam can become unstable, it will be necessary:

- to predict the states of stress in the dam relative to the local collapse surface, and,
- to identify where that state of stress lies within the instability zone or whether it could be brought to the collapse surface by potential triggering mechanisms that could then initiate instability under drained or undrained conditions.

It seems appropriate to quote again from Lade (1993): '*Initiation of static instability occurs at very low amounts of strain. Once the static instability has been triggered, the instability leads to liquefaction at large strains and steady state (or ultimate state) conditions. However, steady state conditions are not relevant to considerations dealing with initiation of the instability. Analyses based on steady state conditions describe the sand behavior at large strains after initiation and during flow of the liquified sand.*'

The alternative of considering collapse surfaces and their anisotropy is obviously not straightforward because of the impact of so many variables discussed above: particle shapes, void ratio, fines content, fabric, stress level, perturbing stress path including the effects of b and alpha (Figure 11b). However, can the existence of collapse surfaces in hydraulically placed tailings be ignored? Is it not more important to identify the instability line as a turning point for stability, the point at which brittleness is introduced, and design to avoid crossing this line rather than concentrating on determining the post collapse strengths?

Acknowledgements

The first author is grateful to Professor Serge Leroueil for the use of some of his unpublished figures and to him and Professor Chu Jian for many helpful discussions on the topic over the years.

References

Bjerrum, L., Kringstad, S. and Kummeneje, O. 1961. The shear strength of a fine sand. Norwegian Geotechnical Institute Publication 45.

Chang, N., Heymann, G. and Clayton, C. 2011. The effect of fabric on the behaviour of gold tailings. Géotechnique 61 (3): 187-197.

Chu, J., and Leong, W. K. 2002. Effect of fines on instability behaviour of loose sand. Geotechnique. 52(10): 751-755

Chu, J., Leroueil, S. and Leong, W.K. 2003. Unstable behaviour of sand and its implication for slope stability. Canadian Geotech. J., 40: 873-885.

Chu, J. and Wanatowski, D. 2008. Instability conditions of loose sand in plane-strain. J. Geotech. Geoenviron. Eng. 134(1): 136–142.

Chu, J. and Wanatowski, D. 2009. Effect of loading mode on strain softening and instability behavior of sand in plane-strain tests. J. Geotech. Geoenviron. Eng. 135(1): 108–120.

Jang, D-J. and Frost, J.D. 1998. Sand structure differences resulting from specimen preparation procedures. Proc. ASCE Specialty Conf. on Geotechnical Earthquake Engineering and Soil Dynamics Seattle, USA. V1: 234-245

Lade, P.V. 1992. Static instability and liquefaction of loose fine sandy slopes. ASCE Journal of Geotech. Eng. 118(1): 51-71.

Lade, P.V. 1993. Initiation of static instability in the submarine Nerlerk Berm. Canadian Geotech. J. 30(6): 895-904.

Lade, P.V. and Yamamuro, J.A. 1997. Effects of nonplastic fines on static liquefaction of sands. Canadian Geotech. J. 34: 918–928.

Lade, P.V., Liggio Jr., C.D. and Yamamuro, J.A. 1998.Effects of non-plastic fines on minimum and maximum void ratios of sand. Geotech.Test. J. ASTM. 21(4):336–347.

Leroueil, S. and Hight, D.W. 2003. Behaviour and properties of natural soils and soft rocks. Proc. Int. Workshop on Characterisation and Engineering Properties of Natural Soils. Singapore, Vol. 1: 29-254. Balkema.

Leroueil, S., Chu, J. and Wanatowski, D. 2009. Slope instability due to pore water pressure increase. First Italian Workshop on Landslides: Rainfall-Induced Landslides. Naples, Vol. 1: 81-90.

Monkul, M.M. and Yamamuro, J.A. 2010. Influence of densification method on some aspects of undrained silty sand behaviour. 5th International Conference on Recent Advances in Geotechnical Earthquake Engineering and Soil Dynamics and Symposium in Honour of Professor I.M. Idriss. San Diego, California.

Oda M. 1972. Initial fabrics and their relations to mechanical properties of granular material. Soils and Foundations. 12(1): 17-36.

Quinteros, V. S. and Carraro, J. A. H. 2023. The initial fabric of undisturbed and reconstituted fluvial sand. Géotechnique. 73(1): 1-15.

Shibuya, S. and Hight, D.W. 1987. A bounding surface for granular materials. Soils & Foundations. 27(4): 123-136.

Sladen, J.A., D'Hollander, R.D., Krahn, J. and Mitchell, D.E. 1985a. Back analysis of the Nerlerk berm liquefaction slides. Canadian Geotech. J. 22(4): 579-588.

Sladen, J.A., D'Hollander, R.D. and Krahn, J. 1985b. The liquefaction of sands, a collapse surface approach. Canadian Geotech.l J. 22(4): 564-578.

Tsomokos, A. and Georgiannou, V.N. 2010. Effect of grain shape and angularity on the undrained response of fine sands. Canadian Geotech. J.:47, 539-551.

Uthayakumar, M. and Vaid, Y.P. 1998. Static liquefaction of sands under multiaxial loading. Canadian Geotech. J., 35(2): 273-283.

Vaid, Y. P. and Chern, J. C. 1985. Cyclic and monotonic undrained response of saturated sands. Advances in the Art of Testing Soils under Cyclic Conditions. ASCE. 120–147.

Vaid, Y.P., Sivathayalan, S. and Stedman, D. 1999. Influence of specimen reconstitution method on the undrained response of sand. Geotech. Testing J. ASTM. 22(3): 187-195.

Yoshimine, M., Ishihara, K. and Vargas, V. 1998. Effects of principal stress direction and intermediate principal stress on undrained shear behaviour of sand. Soils & Foundations. 38(3): 179-188.

Analysis of the variation of undrained shear resistance of bauxite mining tailings through vane and CPTu tests

Helena Paula Nierwinski, Federal University of Santa Catarina, Brazil
Kymberly Ramos Martins Feltz, Federal University of Santa Catarina, Brazil
Marcelo Heidemann, Federal University of Santa Catarina, Brazil
Talita Menegaz, University of State of Santa Catarina, Brazil

Abstract

The bauxite mining tailing is a material without commercial value and, the most economical way to store this product is deposition through dams. For the development of safe designs for these structures, one of the frequently evaluated geotechnical properties is the tailings' undrained resistance, considering that such materials are saturated and often subjected to rapid loading (undrained response). The undrained resistance (*Su*) can be obtained through field tests such as the vane test and the CPTu. The vane test provides the value of *Su* directly through the rotation of a cruciform vane inside the massif. However, the vane test is performed punctually, not returning a continuous profile of *Su*, which can make it costly if more detailed information is required. In this sense, the CPTu test can provide the value of *Su* through empirical correlations with the tip resistance throughout the entire depth. Therefore, this paper aims to compare the undrained resistance obtained through the vane test with the calibrated undrained resistance through the *Nkt* factor, estimated by the CPTu. Analysis of the results demonstrated that the *Nkt* values that provide the closest *Su* values to those obtained by the vane test vary significantly from test to test and site to site, even when dealing with the same type of material. Thus, it is concluded that, especially in deposits of bauxite mining tailings, evaluating *Su* based on CPTu tests and adopting *Nkt* values typically indicated in the literature must be carried out judiciously for use in engineering designs.

Introduction

Aluminum is widely used worldwide due to its properties: low specific weight, high ductility, and great possibility of recycling. According to the U.S. Geological Survey (2020), the annual world production of bauxite (aluminum precursor mineral) is over 350 million tons. Brazil is the third country with the most significant production worldwide, with about 29 thousand tons in 2018.

In the bauxite refining process, prior to electrolysis, it must undergo a beneficiation process to obtain alumina (Al_2O_3). Miura (2016) affirms that the bauxite refining process is called the Bayer method, in which caustic soda is used to obtain alumina. According to Nierwinski (2019), this bauxite beneficiation process promotes an increase in alumina productivity. However, at the same time, it generates a large amount of tailings. Based on IBRAM (2016) and Edraki *et al*. (2014), this tailing is formed by fine particles in a saturated condition, with dissolved metals and reagents used in processing.

Rodrigues (2017) comments that the substantial increase in the generation of tailings from mining requires the adoption of safe and stable storage methodologies capable of storing all the quantity produced. According to Nierwinski (2019), the disposition of tailings is commonly used through raising dams, which can be built up to even with the tailing. The method is attractive due to its economy and ease of execution.

On the other hand, tragedies associated with the rupture of a tailings dam, such as happened in the state of Minas Gerais, Brazil, in 2015 with the Fundão dam (Morgenstern *et al*., 2016) and in 2019 with the Córrego de Feijão dam (Robertson *et al*., 2020), has drawn the attention of the community technique for a better understanding of the behavior of tailings and stability of these structures. Pereira (2005) lights an alert for the need to implement systematic studies related to the characterization technology of the tailings to establish, judiciously, the design premises of its containment structures.

According to Vick (1983), mining tailings are disposed of in dams by aqueous route, thus being saturated. Due to their fine granulometry, they also present intermediate permeability (Nierwinski, 2019). In this way, in many design situations, the material may receive requests that its behavior be undrained. According to Klahold (2013), undrained strength (*Su*) is a crucial parameter for stability analysis under undrained loading conditions. Undrained strength reflects the greatest shear stress that a saturated soil can withstand without showing tearing or excessive deformation in undrained conditions.

According to Almeida and Marques (2010), the most recommended field trials for obtaining the undrained shear strength are the vane and piezocone tests (through empirical correlations), considering the excellent cost-benefit. As the vane test becomes costly to be carried out at all depths of interest, using the CPTu test to obtain *Su* becomes attractive, allowing an evaluation along the depth. However, using empirical formulations developed based on a database of tests carried out in natural soils, the value of *Su* obtained through the CPTu test in mining tailings can generate uncertainties. Thus, this research intends to evaluate the Su values obtained through vane tests, compared to values estimated through the CPTu test, with the aid of the load capacity factor, *Nkt*. Schnaid and Odebrecht (2012) states that values between 10 and 20 are acceptable for *Nkt* in Brazil and that 12 is a typical value for Brazilian soft soils. However, Randolph *et al*. (1998) reiterate that the error when estimating the *Nkt* is about 20% to 40%. In this way, it is intended to compare and evaluate the possible divergences between the *Su* values obtained in the different tests and verify if *Nkt* values typically indicated by the literature for defining *Su* from the CPTu in natural soils apply to the study of the behavior of a bauxite mining tailings.

Methodology

The test data analyzed in this research come from three different Brazilian reservoirs for storing bauxite mining tailings. In this work, the reservoirs will be named Site 1, Site 2, and Site 3. CPTu (ASTM D5778, 1995) and vane (ASTM D2573, 2008) tests were carried out in these reservoirs. The CPTu assay provided readings every 2 cm of q_t, f_s, and *u* parameters. The reed tests were carried out at specific depths. Table 1 presents the summary of the studied tests.

Table 1: Summary from the test data analysed

Site	CPTu Test Number	CPTu total depth (m)	Vane Depths (m)
Site 1	1	20.0	2.0; 4.0; 6.0; 8.0; 10.0; 12.0; 14.0; 16.0; 18.0
	2	7.0	3.0; 4.0; 5.0; 6.0; 7.0
	3	12.0	2.0; 4.0; 6.0; 8.0; 10.0; 12.0
	4	9.3	2.0; 3.0; 4.0; 6.0; 7.0; 8.0
	5	15.0	2.0; 4.0; 6.0; 8.0; 10.0; 12.0; 14.0
	6	6.0	2.0; 3.0; 4.0; 5.0; 6.0
Site 2	1	5.0	2.0; 4.0
	2	8.78	1.0; 3.0; 5.0; 7.0
	3	5.0	3.0; 4.0; 6.0; 8.0
	4	9.0	1.0; 3.0; 5.0; 7.0
	5	8.0	2.0; 5.8
Site 3	1	7.1	1.0; 2.0; 3.0; 4.0; 5.0; 6.0; 7.0
	2	12.6	1.0; 2.0; 3.0; 4.0; 5.0; 6.0; 7.0; 8.0; 9.0; 10.0; 11.0
	3	12.0	1.0; 2.0; 3.0; 4.0; 5.0; 6.0; 7.0; 8.0; 9.0; 10.0; 11.0; 12.0

For the interpretation of the results of the vane tests, the value of the friction of the soil with the rods of the used machinery was discounted (when necessary), and from the graphically plotted values of the undrained shear strength, the maximum value of undisturbed *Su* was defined.

If the material presented plasticity, it would be necessary to correct the resistance value obtained in the test using the factor of Bjerrum. However, as the bauxite tailings have zero or very low real plasticity due to the lack of natural clay minerals, the Bjerrum factor will be considered equal to 1.

In order to estimate the undrained shear strength through the CPTu's tests, it was necessary to estimate the value of the *Nkt* factor for each site test and arrive at an average for each site since it was the same material. The *Nkt* value for the mining tailings studied in this work was evaluated in two different ways. The first followed the assumptions that Schnaid and Odebrecht (2012) presented, using the *Su* value obtained by the vane test to calibrate the value estimated by the cone test (Equations 1 and 2). In this case, the load capacity factor will be called *Nkt1*. The other alternative comes from the study by Robertson (2012), which suggests estimating *Nkt* from the friction ratio (*Fr*) obtained through CPTu. This estimate is presented by Equation 3, and in this case, the factor will be called *Nkt2* in the present study.

$$Nkt = \frac{(q_t - \sigma_{v0})}{Su_{palheta}} \qquad \text{Eq.1}$$

$$(Nkt_1)$$

$$Su_{CPTu} = \frac{(q_t - \sigma_{v0})}{Nkt} \qquad \text{Eq. 2}$$

$$Nkt = 10.5 + 7.\log Fr \qquad (Nkt_2) \qquad \text{Eq. 3}$$

where: q_t is the cone tip resistance and σ_{vo} is the total initial vertical stress.

The estimation of *Su* from the CPTu test allows the definition of a profile of the parameter variation along depth. The *Su* values obtained through the vane tests will be plotted along with this profile for comparative purposes.

Results

The results will be discussed for each of the sites studied. Initially, the values of *Nkt1* and *Nkt2* defined for the site will be presented, and later, the *Su* values of the vane and those estimated by the CPTu with the different *Nkt* values will be compared for each test vertical.

Site 1

Site 1's mean *Nkt1* and *Nkt2* values found were 16 and 12, respectively. These values were used to determine the *Su* values in depth for each of the test verticals, as shown in Figure 1. Table 2 presents the average error (Eq. 4) of the *Su* values measured in the vane test and estimated by CPTu, for the values of *Nkt1* and *Nkt2*.

$$Error\ (\%) = \frac{|Su_{palheta} - Su_{CPTu}|}{Su_{palheta}} \qquad \text{Eq.4}$$

It is observed that, except for vertical 3, the values of *Su* measured in the vane test are closer to those estimated by CPTu using *Nkt1*. However, even so, there is an average error of 27% for *Su* from *Nkt1* on this site. It is also worth mentioning that the average *Nkt1* value obtained on this site was 16, a value above that typically indicated for Brazilian natural soils.

The *Su* values estimated from *Nkt2*, for the most part, showed greater divergences in relation to the *Su* values measured by the vane. The mean value of the estimated *Su* error in this case was 36%.

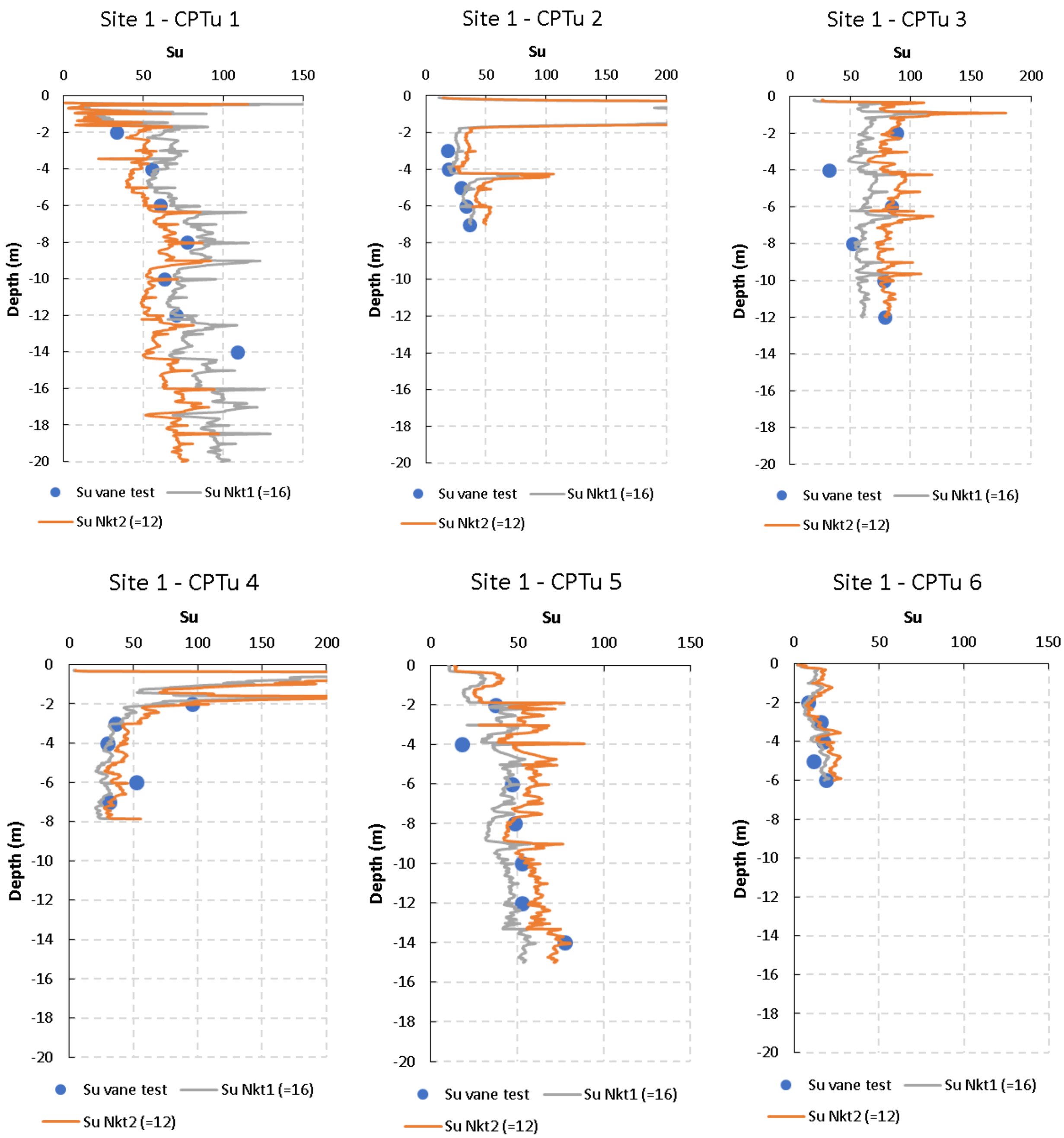

Figure 1: Comparison between *Su* values from site 1

Table 2: Mean absolute errors for *Su* estimated from CPTu tests on site 1

Site	CPTu test number	Error *Su Nkt1* (%)	Error *Su Nkt2* (%)
Site 1	1	25.87	24.64
	2	13.48	53.63
	3	31.53	19.76
	4	25.37	26.51
	5	36.95	48.42
	6	28.77	42.95
Mean (%)		**26.99**	**35.98**

Site 2

Site 2's mean *Nkt1* and *Nkt2* values found were 17 and 11, respectively. These values were used to determine the *Su* values in depth for each of the test verticals, as shown in Figure 2. The average errors of the *Su* estimates from the CPTu tests are shown in Table 3.

For site 2, it was found that the *Su* values estimated from *Nkt1* were also closer to the values measured by the vane. The average error for *Su* values from *Nkt1* was 23%. It can be seen from the CPTu 1 and 2 tests that the vane tests were carried out in a more superficial layer, and it seems that the material changes its behavior in depth, a fact that may contribute to more significant divergences between the measured and estimated *Su* values.

The value of *Nkt1* for site 2 was even higher than for site 1, moving further away from the typical values reported in the literature for Brazilian soils. The *Nkt2* was closer to the typical values. However, it resulted in *Su* values with an average error greater than 40%.

Table 3: Mean absolute errors for *Su* estimated from CPTu tests on site 2

Site	CPTu test number	Error *Su Nkt1* (%)	Error *Su Nkt2* (%)
Site 2	1	27.22	18.94
	2	19.72	26.94
	3	24.98	16.20
	4	9.94	40.64
	5	33.13	105.74
Mean (%)		**22.99**	**41.69**

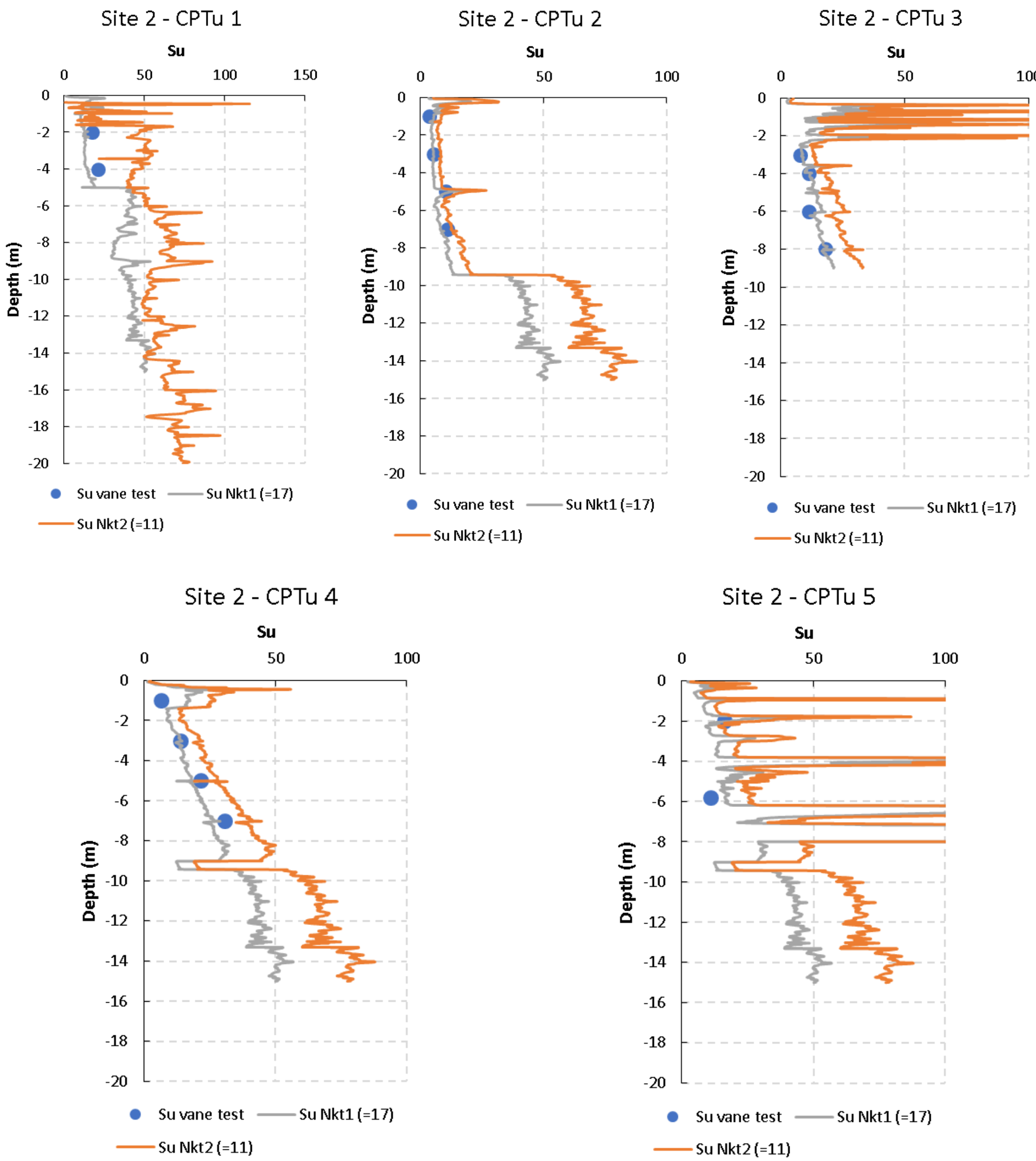

Figure 2: Comparation between *Su* values from site 2

Site 3

The analysis of the tests carried out on site 3 showed a very discrepant behavior in relation to the other two sites studied in this work. The average values of *Nkt1* and *Nkt2* found for this site were greater than 20, the maximum value defined in the literature. This situation probably resulted from a more resistant surface layer observed in the CPTu 1 and CPTu 2 tests.

Given this atypical behavior on this site, it was decided to compare the *Su* results measured with the vane with the *Su* values estimated from the CPTu, using *Nkt* values of 10 and 20, minimum and maximum indicated in the literature. The measured and estimated *Su* values are shown in Figure 3, and the mean errors are shown in Table 4.

The *Su* values estimated from the lower and upper limits showed 32% and 41% errors, respectively. Intermediate *Nkt* values were also tested, resulting in errors never below 32%. For example, one can observe CPTu 3 *Su* values estimated from a *Nkt* of 14.

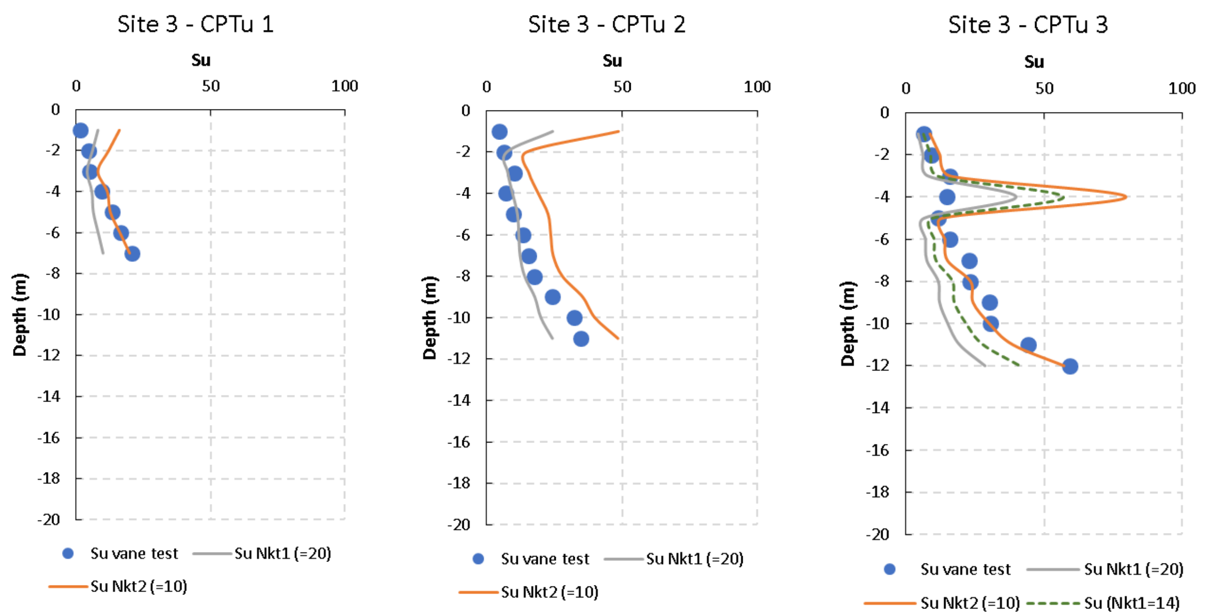

Figure 3: Comparation between *Su* values from site 3

Table 4: Mean absolute errors for *Su* estimated from CPTu tests on site 3

Site	CPTu test number	Error *Su Nkt1* (%)	Error *Su Nkt2* (%)
Site 3	1	48.43	8.75
	2	24.52	73.79
	3	50.16	14.70
Mean (%)		**41.04**	**32.41**

Conclusion

Regarding the analyses carried out to evaluate the values of *Su*, it can be concluded that the great challenge in obtaining *Su* from the results of the CPTu test is in the correct definition of the *Nkt* factor values. In the present work, correlations provided by the literature were used for calculating *Nkt*, and the limits and values typically indicated for natural soils were analysed. When comparing the values of *Su* obtained from the CPTu test with the *Su* values obtained in the vane test, it was verified that the *Nkt* values that defined the best fit showed significant variability. Furthermore, even observing the best fit, the average errors between the values of *Su* estimated by the CPTu and those measured in the vane test showed considerable values, even more significant than the errors already indicated by the literature for natural soils.

Interestingly, there was a more significant influence on the cone tip resistance in deposits where greater heterogeneity was identified along the depth. This condition greatly influenced the definition of *Nkt* through correlations of literature. Still, in the case of site 3, there was a possible existence of resistant layers on the surface, which caused resistance cone tip peaks, a fact that may also have considerably affected the definition of *Nkt* values and, in many cases, resulted in values outside the range typically indicated in the literature for the variation of this factor. Variations in the values of q_t and f_s caused by the heterogeneity of the waste layers inside the deposits directly affect the estimate of the value of *Nkt* and *Su* based on empirical equations (Eq. 1 to Eq. 3). Increases in q_t and f_s values are directly proportional to increases in Nkt values.

In estimating the *Nkt* values through correlations, it was found that in most cases, the value defined based on the friction ratio (*Fr*) provided more discrepant values of *Su* in relation to that measured by the vane test. Thus, it can be concluded that this correlation would not be the most suitable for evaluations carried out in bauxite mining tailings deposits based on the results of the CPTu assay. The study also allowed us to conclude that even if the CPTu test is used to estimate Su values, vane tests are still necessary for the most suitable calibration of *Nkt* values for the deposit in question. This need for calibration proves to be very important in mining tailings deposits due to the atypical behavior of the material and variables depending on the processing process and extracted ore.

Finally, it is recommended that the use of results from the CPTu assay for the estimation of *Su* in bauxite mining tailings is carried out very sparingly in design cases, paying attention to all the specificities of the warehouse and material.

References

Almeida, M. S. S.; Marques, M. E. S.; 2014. Landfills on soft soils: design and performance. 2nd ed. São Paulo: Oficina de Textos.

Brazilian Mining Institute - IBRAM. 2021. Mineral Economy 2021. In: https://ibram.org.br/ 05/07/2021.

Edraki, M; Baumgartl, T; Manlapig, E; Bradshaw, D; Franks, D.M; Moran, C. J. 2014. Designing mine tailings for better environmental, social and economic outcomes: A review of alternative approaches. Journal of Cleaner Production, 84 (1), pp. 411-420.

Klahold, P. A. 2013. Interpretation of field tests in soils with permeability intermediary. Master's thesis presented to the Graduate Program in Civil Engineering, UFRGS.

Miura, Y. S. 2016. Revegetation of the bauxite residue deposit: an analysis of promising techniques for the hydro Alunorte case. Master Thesis, Course on Sustainable Use of Natural Resources in Tropical Regions, Vale Sustainable Development Technological Institute, Belém.

Morgenstern, N.R., Vick, S.G., Viotti, C.B, Watts, B.D. 2016. Fundão Tailings Dam Review Panel. Report on the Immediate Causes of the Failure of the Fundão Dam. Available from http://fundaoinvestigation.com/the-report/.

Nierwinski, H.P. 2019. Characterization and geomechanical behavior of mining tailings. Doctoral thesis, Graduate Course in Civil Engineering, Federal University of Rio Grande do Sul, Porto Alegre.

Pereira, E. L. 2005. Study of the liquefaction potential of ore tailings fromiron under static loading. 2005. Master thesis, Graduate Course in Civil Engineering, Federal University of Ouro Preto.

Robertson, P. K. 2012. The James K. Mitchell Lecture: Interpretation of in situ tests-some insights. Geotechnical and Geophysical Site Characterization 4, ISC 4, Brasil, p. 3-24.

Robertson, P. K.; Melo, L.; Willians, D. J.; Wilson, G. W. 2019. Report of the Expert Panel on the Technical Causes of the Failure of Feijão Dam I. December.

Rodrigues, A. B. 2017. Mining tailings disposal risks and techniques disposition alternatives. TCC (Graduation) - Mining Engineering Course, Federal University of Ouro Preto, Ouro Preto.

Schnaid, F.; Odebrecht, E. 2012. Field Test and aplications. 2o ed. São Paulo: Oficina de Textos.

U.S. Geological Survey. 2020. Mineral Commodity Summaries. Lime. Report. United States of America.

Vick, S.G. 1983. Planning, Design and Analysis of Tailings Dams. John Wiley & Sons, Inc., 369p.

Session 5:

Seismic Analysis

Defining Efficient Ground Motion Intensity Measures to Estimate Engineering Demand Parameters of Tailings Dams

César Pastén, University of Chile, Chile
Bastián Garrido, University of Chile, Chile
Pablo Heresi, Federico Santa María Technical University, Chile

Abstract

The design of tailings dams in Chile requires pseudo-static limit equilibrium and dynamic analyses to verify the stability of the dam when subjected to earthquake loadings. The dynamic analyses verify that the seismically-induced dam deformation does not compromise the safe containment of tailings. The displacement of the dam at specific locations, such as the crest settlement, can be considered as an engineering demand parameter (EDP) in the framework of performance-based earthquake engineering. The input ground motions adopted in these analyses, either synthetic or instrumental records compatible with site-specific seismic hazard, can be characterized by their intensity measures IM, such as peak ground acceleration (PGA), Destructiveness Potential (Pd), Arias Intensity (AI), and peak ground velocity (PGV). In this paper, archetypes of Chilean dam cross-sections of 50, 100, and 150 m height were subjected to 80 ground motions each using the PLAXIS2D software to determine the correlation between a series of EDPs in the dams and ground motion IMs in the free field. The numerical results show that the PGA is among the less efficient IMs to determine the crest displacements of the analyzed dams, whereas Pd, PGV and $Sa(T_0)$ are more efficient, depending on the dam height.

Introduction

The design of tailings dams in Chile is prescribed by the Supreme Decree Nº248 (MMC 2007) and the Decree 50 (MOP 2015), both of which require pseudo-static limit equilibrium and dynamic analyses to verify the seismic stability of the dam when subjected to earthquake loadings. The dynamic analyses verify that the seismically-induced dam deformation does not compromise the safe containment of tailings. The input ground motions adopted in these analyses, either synthetic or instrumental records, are selected to be compatible with results from site-specific seismic hazard analyses. These ground motions can be characterized by intensity measures (IM), such as peak ground acceleration (PGA), peak ground velocity (PGV), Arias Intensity (AI), Destructiveness Potential (Pd), Cumulative Absolute Velocity (CAV), and pseudo-spectral accelerations at a given period [PSa(T)].

The performance-based earthquake engineering (PBEE) framework aims to determine the probability of observing structural damage given an IM at the site where the structure is emplaced. Our long-term project seeks to adopt the PBEE framework for tailings dams in Chile, given the main characteristics of the dams and the seismotectonic framework. One of the steps in the adoption process is to find an engineering demand parameter (EDP), defined as a structural response quantity that can be used to estimate the failure or damage state of a component. Depending on the analysed structure, there may be a set of several EDPs that can be correlated with damage. The EDP is selected such that it can be easily estimated from a known IM, which is usually determined from site-specific seismic hazard analyses. The deformation of the dam at specific locations, such as crest settlement and downstream slope lateral displacement, can be considered as EDPs. Efficiency is the ability of a given IM to estimate the EDP with low uncertainty.

Several studies have determined the most efficient IMs for predictions of EDPs with the aid of nonlinear dynamic finite element analyses and have found that the most efficient IMs were neither PGA nor the PSa(T), the most used in practice. Armstrong et al. (2020) modeled two earthfill dams and executed 342 simulations to find that the most efficient IM that predicts accumulated vertical and horizontal crest displacements was the AI. Lavanda et al. (2021) built a representative tailings dam model following the upstream method (currently banned in Chile), including materials susceptible to liquefaction, and executed 25 simulations, finding that the most efficient IM was the spectral power of the seismic record in a frequency band related to the predominant frequency of the analyzed dam. Cho and Rathje (2022) analyzed 49 uniform material slope models of 15 and 30 m height and performed 1051 simulations for each model, to find that the PGV was the most efficient IM. Boada et al. (2023) analyzed abandoned tailings dams, consisting of a uniform material slope of 15 m height, subjected to 169 strong ground motions and found that the most efficient IM was AI.

This paper focuses in analyzing the efficiency of various combinations of IMs and EDPs for three archetypes of Chilean tailings dams, 50, 100, and 150 m height, through numerical simulations.

Numerical Models

The geometry of the three archetypes of Chilean tailings dams analyzed in this paper is schematically depicted in Figure 1 and the main geometric parameters are summarized in Table 1. The dams are 50, 100, and 150 m height and represent the typical geometry of dams constructed with borrowed materials in Chile, unlike sand tailings dams, which have gentler downstream slopes (H:V > 3.5:1).

Based on the geometries, finite-element method (FEM) models were developed with the PLAXIS2D software (Plaxis, 2022). The numerical models consist of three materials: the embankment dam, the stored tailings, and the foundation soil (Figure 1). The constitutive models adopted for each material were the Hardening Soil with Small Strain (HSS), the Mohr Coulomb (MC), and the Linear Elastic (LE) models. The HSS model is the simplest elastoplastic nonlinear model implemented in the PLAXIS2D software that can account for stiffness degradation and hysteretic damping of granular materials. However, the model only estimates plastic shear strain under cyclic loading (i.e., it does not consider volumetric plastic strain). Although the elastoplastic MC model is not recommended for cyclic loading, it was chosen for simplicity given the large number of simulations, as well as the selection of the LE model for the foundation. The constitutive model parameters of each material are shown in Tables 2 to 4. The parameters adopted for the dam materials result in a shear modulus increasing with depth from the dam crest. Given the dam material properties, the average shear wave velocity (Vs*) in the dams' central axes can be calculated (values shown in Table 5). The yield seismic coefficient (Ky) obtained from limit equilibrium (LEM) analyses for each archetype dam is shown in Table 5.

The model foundation material was chosen with a high stiffness (Vs= 1200 m/s) since many of the tailings dams constructed in northern Chile are founded on stiff soils. The finite element sizes were defined such that the maximum transmitted shear wave frequency in the three archetype models is 25 Hz, according to recommendations from Kuhlemeyer and Lysmer (1973). It is worth noting that Chile does not have a standard for dynamic analyses of tailings dams and that numerical procedures adopted in the engineering practice depend on the experience of consulting firms and specific standards of mining companies.

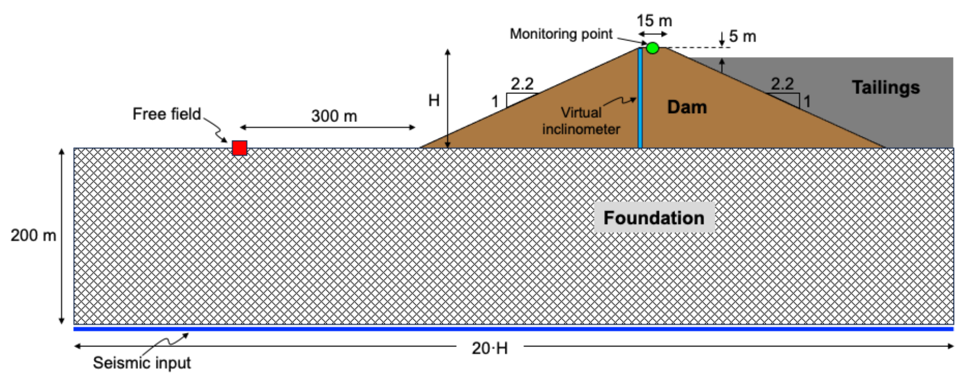

Figure 1: Dam model geometry. Figure is not to scale.

Table 1: Models geometric features

Parameter	Symbol	Value
Height (m)	H	50-100-150
Crest Width (m)	W	15

Freeboard (m)	R	5
Upstream slope (—)	$H{:}V_u$	1:2.2
Downstream slope (—)	$H{:}V_d$	1:2.2
Foundation height (m)	H_f	200
Foundation width (m)	W_f	20·H

Table 2: Embankment dam parameters - Hardening Soil with Small Strain model

Parameter	Symbol	Value
Total unsaturated unit weight (kN/m3)	γ_{unsat}	20
Secant stiffness in standard drained triaxial test (MPa)	E_{ref50}	30
Tangent stiffness for primary oedometer loading (MPa)	E_{ref_eod}	30
Unloading/reloading stiffness from drained triaxial test (MPa)	E_{ref_ur}	90
Power for stress-level dependency of stiffness (-)	m	0.46
Cohesion (kPa)	c'	10
Friction angle (°)	ϕ'	39
Dilatancy angle (°)	ψ'	0
Poisson's ratio for unloading-reloading (-)	ν_{ur}	0.2
Failure ratio (-)	R_f	0.9
Reference stress for stiffnesses (kPa)	p_{ref}	100
Reference shear modulus at very small strains (MPa)	G_0	165
Threshold shear strain at which Gs=0.722·G0 (-)	$\gamma_{0.7}$	0.00013

Table 3: Tailings parameters - Mohr Coulomb model

Parameter	Symbol	Value
Total unsaturated unit weight (kN/m3)	γ_{unsat}	17
Young's modulus (kN/m2)	E	7800
Cohesion (kPa)	c'	20
Increase of cohesion with depth (kPa)	c'_{inc}	1.7
Altura de cohesión mínima (m)	y'_{ref}	(H – R)
Friction angle (°)	ϕ'	0
Dilatancy angle (°)	ψ'	0
Poisson's ratio (-)	ν	0.4

Table 4: Foundation Parameters - Linear Elastic model

Parameters	Symbol	Value
Total unsaturated unit weight (kN/m3)	γ_{unsat}	24
Young's modulus (MPa)	E	8450
Poisson's ratio, ν (-)	ν	0.2

Table 5: Models characteristics

Height (m)	Yield seismic coefficient Ky (-)	Average shear wave velocity Vs* (m/s)	T= 2.6H/Vs* (s)	Fundamental period T_0 (s)
50	0.361	305	0.43	0.55
100	0.312	350	0.74	0.90
150	0.306	381	1.02	1.11

Input Ground Motions

Forty ground motion recorded in Chilean seismic stations were selected from the SIBER RISK database (Castro et al. 2021) to define the input ground motions in the numerical models. The selected ground motions (Table 6) simultaneously satisfy 2 conditions: 1) the average shear-wave velocity from the surface to a depth of 30 m (Vs_{30}) of the station is larger than 750 m/s and 2) the recorded peak ground acceleration (PGA) is larger than 0.12 g. The selected ground motions are associated to 11 earthquakes, 8 of which are interface earthquakes and 3 intraplate ones that occurred in the Northern Chile subduction zone.

Numerical Results

Dynamic numerical simulations of the seismic response of each of the three archetype dams were performed considering 80 input ground motions, corresponding to the selected set of records in Table 6 and the same set scaled twice. Due to wave amplification in the foundation material, the ground motions calculated at the model free field monitoring point (see Figure 1) amplified from 2 to 4 times the PGA of the original records. Then, ten ground motions were eliminated from the analysis due to excessive PGAs at the model surface and high energy content in the horizontal direction at low frequencies. Figure 2 shows examples of permanent shear strain fields calculated inside the dams when the models are subjected to the 2014-04-03 Mw 7.6 earthquake recorded at the T05A station in the NS direction. The zones in the dams that reach shear strains of about 2% coincide with the critical surfaces calculated with LEM analysis (surfaces with factors of safety FoS=1.0).

The numerical simulations allowed computing the fundamental period (T_0) of the dams from standard spectral ratios (SSR) calculated by dividing the smoothed amplitude Fourier spectrum of the acceleration time history at the dam crest (see location of the monitoring point in Figure 1) and that of the free field monitoring point. The values of T_0 tend to increase with the ground motion intensity, so the lowest calculated periods are reported in Table 5.

Table 6: Selected seismic records.

Date	Magnitude	Depth	Station	Component	PGA [g] NS – EW
2005-06-13	7.9	111	ACC	NS - EW	0.163 – 0.191
2006-10-12	6.2	37	PA	EO	0.141
2013-01-30	6.7	52	GO03	NS	0.194
2014-04-03	7.6	27	PB11	NS - EW	0.196 – 0.216
2014-04-03	7.6	27	GO01	NS - EW	0.239 – 0.197
2014-04-03	7.6	27	T09A	NS - EW	0.185 – 0.142
2014-04-03	7.6	27	T06A	NS - EW	0.202 – 0.139
2014-04-03	7.6	27	T08A	NS - EW	0.299 – 0.408
2014-04-03	7.6	27	T05A	NS - EW	0.180 – 0.168
2014-07-13	5.6	40	T08A	EO	0.128
2014-08-14	5.6	50	T04A	NS - EW	0.446 – 0.230
2014-08-23	6.4	40	VA01	NS	0.432
2018-04-10	6.2	74	C08O	EO	0.250
2018-11-01	6.3	101	T15A	NS	0.121
2019-01-20	6.7	50	C10O	NS - EW	0.522 – 0.479
2019-01-20	6.7	50	CO05	NS - EW	0.301 – 0.254
2019-01-20	6.7	50	C19O	NS - EW	0.238 – 0.258
2019-01-20	6.7	50	C09O	NS - EW	0.480 – 0.473
2019-01-20	6.7	50	C22O	NS - EW	0.203 – 0.207
2019-01-20	6.7	50	C08O	NS - EW	0.208 – 0.203
2019-01-20	6.7	50	C29O	NS - EW	0.275 – 0.295
2019-01-20	6.7	50	C27O	NS	0.136
2019-01-20	6.7	50	C23O	EO	0.121
2020-09-06	6.3	29	CO06	NS - EW	0.124 – 0.185

The accumulated vertical and horizontal displacements in the center of the dam crest were retrieved from the monitoring point in Figure 1 at the end of each simulation. Likewise, the accumulated maximum shear strain was calculated along the virtual inclinometer located at the intersection between the crest and the downstream slope of the models (see location in Figure 1). The displacements and shear strains were selected as engineering demand parameters (EDPs).

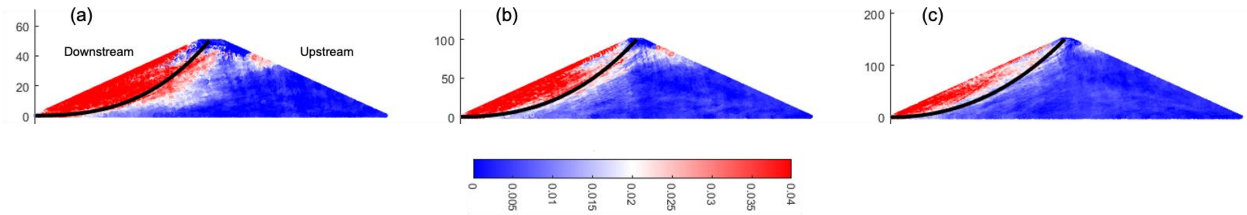

Figure 2: Shear strain in the (a) 50 m, (b) 100 m, and (c) 150 m height dams subjected to the 2014-04-03 Mw 7.6 earthquake recorded at the T05A station in the NS direction. The tick black lines are the critical surfaces from pseudo-static LEM analyses

The calculated IMs at the free field monitoring point (see Figure 1) were PGA [g], PGV [cm/s], CAV [g·s], AI [cm/s], Pd [cm·s], and Sa(T) [g]. The following function was proposed to capture the trend between an IM and an EDP

$$Ln(EDP_p) = a_o + a_1 Ln(IM) \quad (1)$$

Where a_0 and a_1 are dimensionless constants, the displacements EDPs are in meters, and the shear strain EDP is dimensionless.

For each IM, the root mean square error RMS was determined from the predicted EDP (EDP_p calculated with Equation 1) and the calculated EDP from the n numerical simulations (EDP_c)

$$RMS = \sqrt{\frac{1}{n}\sum_1^n\left[Ln\left(EDP_p\right) - Ln\left(EDP_c\right)\right]^2} \quad (2)$$

Figure 3 shows the accumulated vertical displacements at the center of the dams crests correlated with the calculated IMs. The vertical displacements do not exceed 2 m in any of the simulations although the PGA in the free field can be as high as 1.5 g. In general, the accumulated vertical displacements of the 50 m dam are lower than the displacements of the taller dams for a given IM.

Figure 4 summarizes the RMS for all IM, including Sa(T) at various periods, for accumulated vertical and horizontal displacement at the center of the dams crests and the maximum shear strain along the virtual inclinometer. The IM with the lowest RMS is assumed as the most efficient with respect to the EDP. Pd, PGV, and Sa(T_0) are among the most efficient IMs for the three heights. In contrast, the PGA has almost the lowest efficiency from the analyzed set of IMs (larger RMS). The efficiency of the PGA decreases with the dam height.

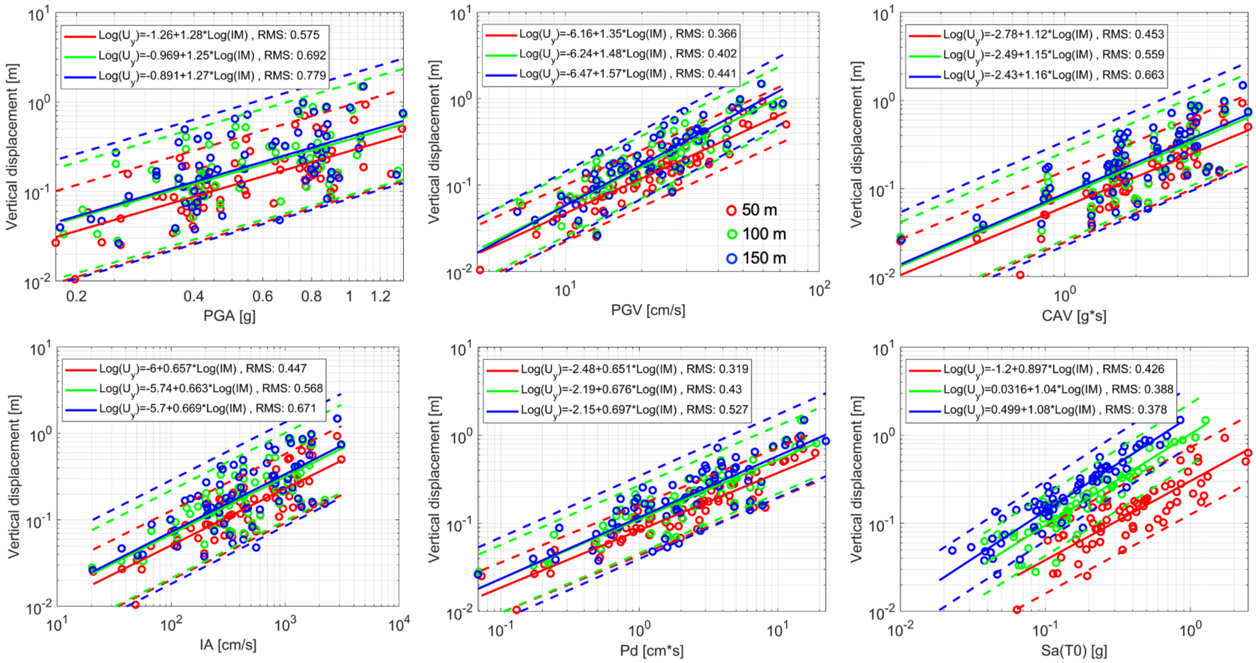

Figure 3: Correlation between the accumulated vertical displacement at the dams' crest and various IMs in the free field for 70 ground motions.

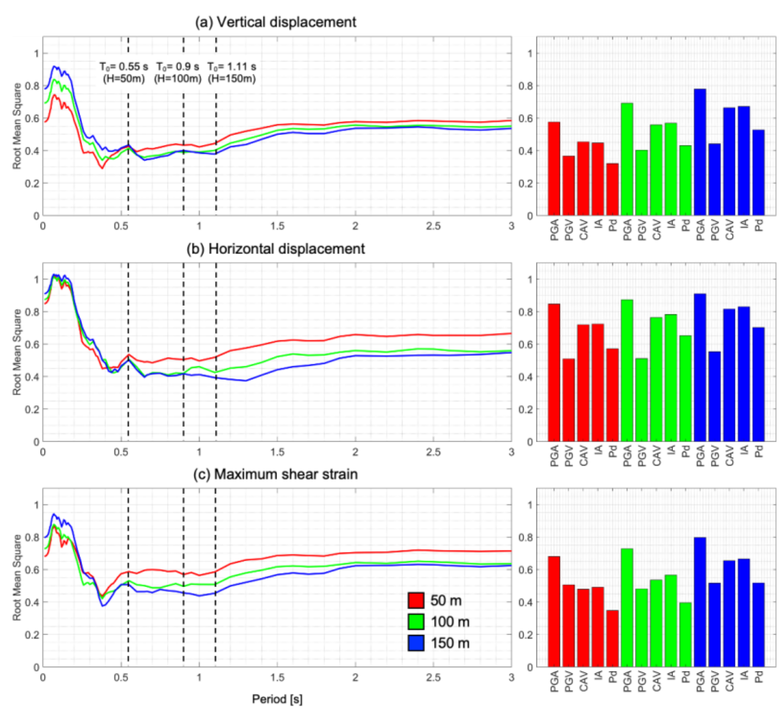

Figure 4: Summary of RMS for different IMs correlated with accumulated vertical and horizontal displacements at the center of the dams' crest as well as the maximum shear strain in the virtual inclinometer

Figure 5 shows the RMSs of the correlation between the accumulated vertical displacements at different points in the dams (H= 50, 100, and 150 m) and PGV, Pd, and Sa(T_0). The RMSs of these IMs are similar in the dams, except near the base of the upstream slopes where the efficiency decreases, most likely due to the lower displacements obtained in these areas.

The relative efficiency of an IM at a given point in the dam can be estimated by dividing the RMS by the minimum RMS (RMS_{min}) among the analyzed IMs. Figure 6 shows RMS/RMS_{min} of the accumulated vertical displacements and the IMs shown in Figure 5. Pd tend to be the most efficient IM (lower RMS/RMS_{min} in blue) for the 50 m dam whereas PGV and Sa(T_0) are more efficient in the tallest dams.

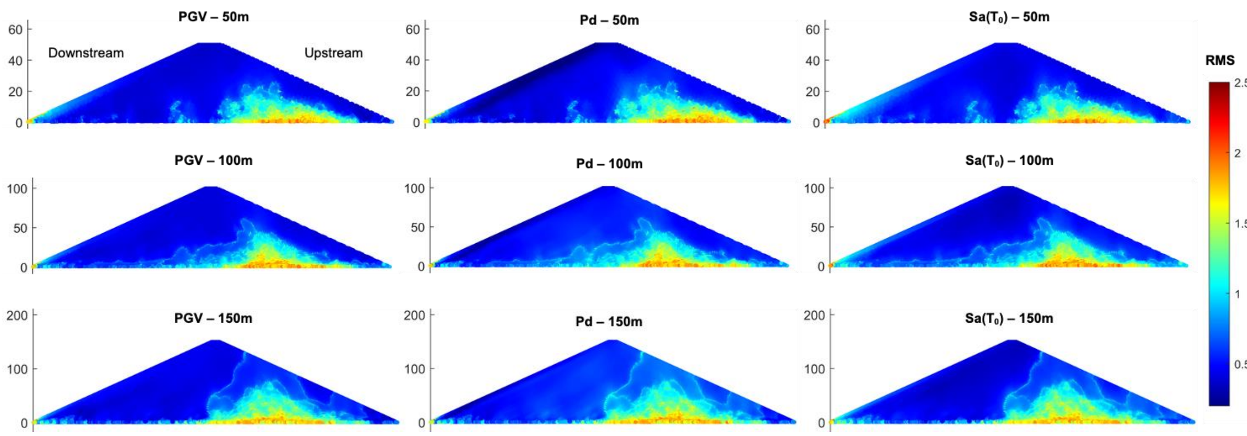

Figure 5: RMS of the correlation between vertical displacements at different points in the dams (H= 50, 100, and 150 m) and various IMs (PGV, Pd, and Sa(T_0))

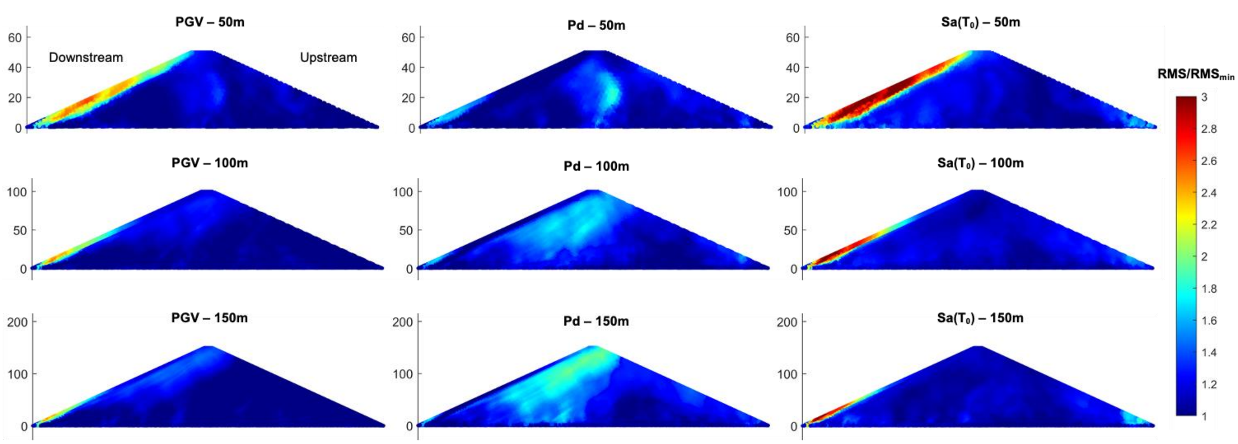

Figure 6: RMS/RMS_{min} of the correlation between vertical displacements at different points in the dams (H= 50, 100, and 150 m) for various IMs (PGV, Pd, and Sa(T_0))

Discussion

The accumulated vertical displacements obtained with numerical simulations are the result of the plastic shear strain predicted by the HSS model, which does not account for volumetric plastic strain in cyclic loading. This model feature may limit the predicted deformations of the dams compared to deformations obtained with more complete constitutive models.

The RMSs of the correlations between the accumulated horizontal displacement of the dam crests and the considered IMs are the largest of the analyzed EDPs whereas the RMSs for the accumulated vertical displacement of the dams crests are similar to those for the maximum shear strain along the virtual inclinometer. This means that vertical displacements and maximum shear strain can be determined from IMs with lower uncertainties. The advantage of using maximum shear strain as an EDP is that it could be directly related to a damage measure of the downstream slope of a dam.

The high impedance contrast between the underlying foundation material and the dams may exacerbate their deformations. The use of softer foundation materials decreases the impedance contrast, but increases the site amplification, so the net effect in the efficiency reported in this article must be revised in such cases.

Since the lifecycle of a tailings dam can span several decades since the beginning to the end of construction, the change in efficiency of the IMs that predict displacements should be considered.

Conclusions

The numerical simulations performed in this study provides important information about the seismic performance of tailings dams subjected to subduction seismic records. The results presented allow supporting the following conclusions:

1. The use of the accumulated horizontal displacements of dam crest as an EDP may not be convenient due to the large RMSs of the correlation with the analyzed IMs.
2. The use of the maximum shear strain along the virtual inclinometer defined in this study as an EDP seems convenient given the low RMSs obtained and the direct relationship with the damage of the models in the downstream slopes.
3. PGA is one of the least efficient IMs to predict accumulated vertical and horizontal displacements of dam crest as well as maximum shear strains along the virtual inclinometer. Using PGA may result in large errors, particularly for the tallest analyzed dams.
4. Pd is an efficient IM to predict accumulated vertical displacements and maximum shear strains in the analyzed dams. However, the use of Pd in real applications may be cumbersome since there are few ground motion models available to predict it.
5. PGV and Sa(T_0) are efficient IMs that are also easier to predict in real applications with available ground motion models.

Acknowledgements

This work was funded by the Advanced Mining Technology Center (AMTC PIA ANID grant AFB180004), Piensa Minería 2023-CODELCO (National Corporation of the Copper, Chile), and the National Agency for Research and Development (ANID) scholarship for PhD studies in Chile.

References

Armstrong, R., T. Kishida, and D. Park. 2020. Efficiency of ground motion intensity measures with earthquake-induced earth dam deformations. *Earthquake Spectra*. 37(1): 5-25.

Boada, G., C. Pastén, and P. Heresi. 2023. Analytical fragility curves for abandoned tailings dams in North-Central Chile. *Soil Dynamics and Earthquake Engineering.* 164, 107637.

Castro, S., R. Benavente, J.G. Crempien, G. Candia, and J.C. de la Llera. 2022. A Consistently Processed Strong-Motion Database for Chilean Earthquakes. *Seismological Society of America*. 93(5): 2700-2718.

Cho, Y. and E.M. Rathje. 2022. Generic Predictive Model of Earthquake-Induced Slope Displacements Derived from Finite-Element Analysis. *Journal of Geotechnical and Geoenvironmental Engineering*, 148(4): 04022010.

Kuhlemeyer, R. and J. Lysmer. 1973. Finite element method accuracy for wave propagation problems. *Journal of the Soil Mechanics and Foundations Division*, 99(5): 421-427.

Labanda, N., M. Sottile, I. Cueto, and A. Sfriso. 2021. Screening of seismic records for performing time-history dynamic analyses of tailings dams: a power-spectral based approach’, *Soil Dynamics and Earthquake Engineering*. 146, 106750.

MMC. 2007. Decreto Supremo N°248: Reglamento para la aprobación de Proyectos de Diseño, Construcción, Operación y Cierre de los Depósitos de Relaves. Ministerio de Minería, Chile.

MOP. 2015. Decreto 50: Aprueba reglamento a que se refiere el artículo 295 inciso 2º, del código de aguas, estableciendo las condiciones técnicas que deberán cumplirse en el proyecto, construcción y operación de las obras hidráulicas identificadas en el artículo 294 del referido texto legal. Ministerio de Obras Públicas, Chile.

Plaxis. 2022. PLAXIS 2D Reference Manual. Dublin: Bentley Systems International Limited.

Influence of the foundation soil stratification on the seismic response of an earthfill tailings dam

Marcelo Gonzalez S., Independent consultant, Chile

Abstract

The current study numerically analyzes the response of a typical configuration of an earthfill tailings dam subjected to inter-slab thrust earthquakes with moment magnitudes greater than Mw > 8.0. The study analyzed two-foundation soil configuration: (1) a 200m soil deposit with its shear stiffness increasing with depth and (2) A 20m soil deposit placed on soft rock with an impedance value of 0.38. It was noted that the response of the dam in terms of accelerations and deformations strongly depends on the proposed stratification of the foundation soil. The results show that the peak accelerations, the vertical relative displacement at the dam crest and the seismic acceleration amplification respect to the dam base were greater for case two.

Introduction

In countries that frequently suffer from earthquakes, the use of rockfill or earthfill material for tailings dams is recommended, mainly due to the better performance that they have shown in comparison to the cyclone sand tailing dams. Unfortunately, the rockfill or earthfill geotechnical design is still a challenge. Obtaining in-situ and laboratory geotechnical parameters for numerical analyses is complex mainly due to the reduced capacity of conventional equipment to test large particles. On the other hand, the access to the instrumentation information is limited, in many cases due to the private nature of the data and/or the concern of environmental and social implications that such data publication could imply. Despite the previous difficulties, any effort to perform numerical models with geotechnical parameters obtained from field and laboratory tests and validated with real dam behavior measured from the instrumentation would be well rewarded. Once these well-calibrated models are available, their use in sensitivity analysis constitutes a tool for design optimization and performance evaluation under different site conditions.

Various numerical studies have shown that the seismic response of earthfill tailing dams depends on innumerable factors, including among the most relevant those such as: dam geometry, dam material, foundation soils stratigraphy, soil foundation stiffness and earthquake frequency, intensity and duration.

This study analyses the influence of the soil layer configuration with different stiffness on the seismic response of a homogeneous earthfill tailings dam. Two types of foundation stratifications were analysed: (1) A unique soil deposit that its shear stiffness modulus increasing with depth as a power function and (2) A soil deposits of 20m thickness placed on a softrock with an impedance value of approximately 0.35 (defining the impedance value as $I = \rho_s v_s / \rho_r v_r$, where the ρ and v are the mass density and the shear wave velocity for the soil deposit (s) and the softrock(r)),

For the two foundation soil configurations, the numerical model for the dam was subjected to a series of interplate thrust earthquakes recorded in the Maule and Iquique earthquakes occurred on February 27, 2010 and April 01, 2014, respectively.

Dam geometry and geotechnical properties

Geometry of the numerical model and finite element mesh

The Chilean experience in the seismic design of high earthfill tailings dams (heights between 90m to 150 meters) has resulted in the use of upstream and downstream slopes of the order of 2:1 [H:V]. Considering the previous knowledge, the current study considers a dam with a high of 100m with slopes 2:1 [H:V] (upstream & downstream slopes), 12m crest width and a freeboard of 1m respect to the slimes. The phreatic level was considered at the level of basal drains, assuming soil dry condition above the phreatic level.

To simulate an infinite foundation layer in horizontal and vertical directions, a relationship between the length and depth of the model was adopted equal to L/H=20, following the recommendation of Dey A. (2011). The foundation depth was established in 200m and its length in 4000m.

Fixed conditions at the model base and allowed vertical displacements at the lateral boundaries were established. Viscos dampers were used to absorb shear waves and prevent their reflection at the boundaries.

The current study considers two foundation soil conditions (hereinafter referred to in this article as cases (1) and (2)):

- An homogeneous soil layer with its shear stiffness increasing monotonically with depth and
- A two layers system (20m superficial soil stratum over a soft rock) with high shear wave velocities contrast.

The first case aims to represents those old alluvial deposits whose properties improve with depth, such as those located in the North of Chile, while the second case aims to evaluate the response of a tailings dam placed on fluvial deposits of reduced thickness over a soft rock.

A fine grid dimension was considered below the dam, for the dam and tailings (elements size 2.5 m by 2.5 m). Away from the dam, a coarse finite element mesh was used to reduce computation time. The dimensions of the finite elements under the dam follow the recommendation of Kuhlemeyer & Lysmer

(1973), where the length of the elements should be less than the ratio between the shear wave velocity of the soil and eight times the predominant frequency of the earthquake signal.

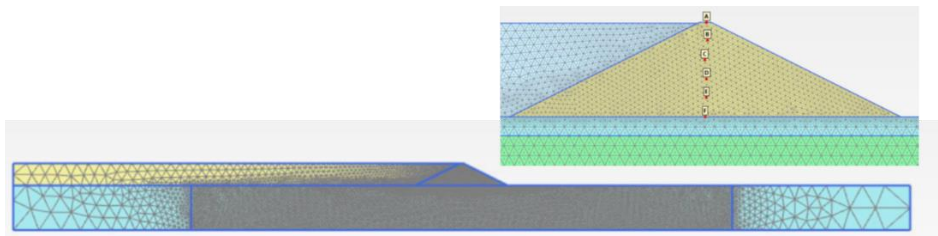

Figure 1: Numerical model mesh of the dam & soil foundation and ground motion control points

Constitutive soil & rock model and geotechnical properties

The soil foundation and the dam were analyzed by using the constitutive model HS Small. This constitutive model is a modification of the hardening soil model (Schanz 1998 & Shanz et. al. 2000) that accounts for the increased stiffness of soils at small strains and its variation non-linearly with strain. The model parameters are characterized by standard laboratory test, such as triaxial and oedometer tests. Its formulation incorporates different aspects, such as dependency of elastic modulus on the confining pressure, hyperbolic elastoplastic behavior, two yield surfaces with non-associated and associated plasticity and friction and dilatancy angles of the material. An elastic model for the soft rock stratum was considered.

For both foundation layouts, the dam material and the foundation soils considered a shear stiffness increasing monotonically with depth. In the model case with an impedance contrast, an average shear wave velocities of Vs=450 m/s was considered for the superficial soil stratum and a constant value of Vr=1200 m/s for the soft rock stratum, resulting in an average impedance value of approximately 0.35 (ρsVs/ρrVr). The main geotechnical properties assumed in the present study are described in Table 1.

Table 1: Soil model properties

Dam material property	Unit	Dam	Soil Foundation		
			One layer	Upper layer	Bottom layer
Total unit weight, γ	kN/m3	22.0	22.0	22.0	24.0
Internal friction angle, Φ	Degrees	42	40	40	-
Cohesion, c	kPa	0	10	10	-
Reference secant stiffness modulus at 50% of ultimate deviatory stress, E_{ref50}	MPa	120	150	25	-
Reference oedometric modulus, E_{refeod}	MPa	112	148	24	-
Reference unloading / reloading modulus, E_{refur}	MPa	240	420	50	-
Reference shear Modulus for very small strains, G_{0ref}	MPa	200	350	45	3,500
Reference shear strain at 70% of the ratio G/ G0ref, $\gamma_{0.7}$	%	0.020	0.020	0,024	-
Model parameter, m		0.47	0.50	0.50	-
Poisson ratio		0.20	0.20	0.20	0.23

The degradation curves of the shear modulus and damping ratio versus the shear strain were calibrated by using curves determined for coarse granular soils for confining pressure of 300kPa (Kokusho, 1981). In the case of the damping curves, it was considered a maximum material damping of D= 7.5% for shear strain greater than 0.03%.

Input seismic records

The current study used seven megathrust earthquakes acceleration records measured at outcrop rock. The seismic events correspond to: (1) Maule´s earthquake Mw=8.8, occurred on February 27, 2010 and (2) Iquique´s earthquake Mw=8.3, occurred on April 1, 2014. The main characteristics of the seismic records are described in Table 2.

Table 2: Main properties for the Maule 2010 and Iquique 2014´s earthquakes stations

Seismic Event	Location	Directional component	PGA [g]	Arias Intensity [m/s]	Duration [s]	Predominant frequency [Hz]
El Maule 2010 Mw=8,8	C. Viejo (CV)	E-W	0.15	1.74	65.16	4.44
	Melado (ME)	N-S	0.14	0.81	57.32	1.51
	Rapel (RA)	N-S	0.20	1.88	34.03	2.23
	El Roble (RA)	N-S	0.18	1.54	32.96	1.59
	Santa Lucía (STL)	E-W	0.22	2.11	41.38	4.21
	Tórtolas (T)	N-S	0.18	1.47	39.99	1.06

	Valparaíso (V)	E-W	0.30	0.49	21.78	1.83
Iquique 2014 Mw=8,3	T05A	N-S	0.28	2.76	36.48	3.62
	T06A	E-W	0.26	1.90	34.33	1.45

According to Table 2, the peak ground accelerations (PGA) and Arias intensity (Ia) values are in a narrow range (excepting Valparaiso station). The PGA and Ia varies between 0.14g to 0.18g and 0.81 to 2.11, respectively. The minor observed differences between the recorded values of Ia and PGA may mainly associated to hypocentre – focus distance and rock stratigraphy, type and weathering condition. The significant duration of the earthquakes was estimated by considering the time intervals between the 5% and 95% of the Arias intensity as the initiation and ending of the earthquake, respectively (Kempton, 2006).

The acceleration signal applied at the bottom of the numerical models is determined through deconvolution of the acceleration records measured at the outcrop rock through the methodology proposed by Mejias and Dawson (2006).

Numerical results

Accelerations

Control points (Figure 1) to measure time histories of: acceleration, velocity, displacement, shear stresses and strains were established at the dam central axis and free field location. All the time histories were determined for the two soil foundation stratifications cases and all inputs earthquakes. Figure 2 shows an example of the accelerations time histories obtained for the Iquique´s earthquake subjected to the TA(05) station. The accelerations were measured at the dam central axis in six different depths from the dam crest (y/H=0) to the dam base (y/H=1).

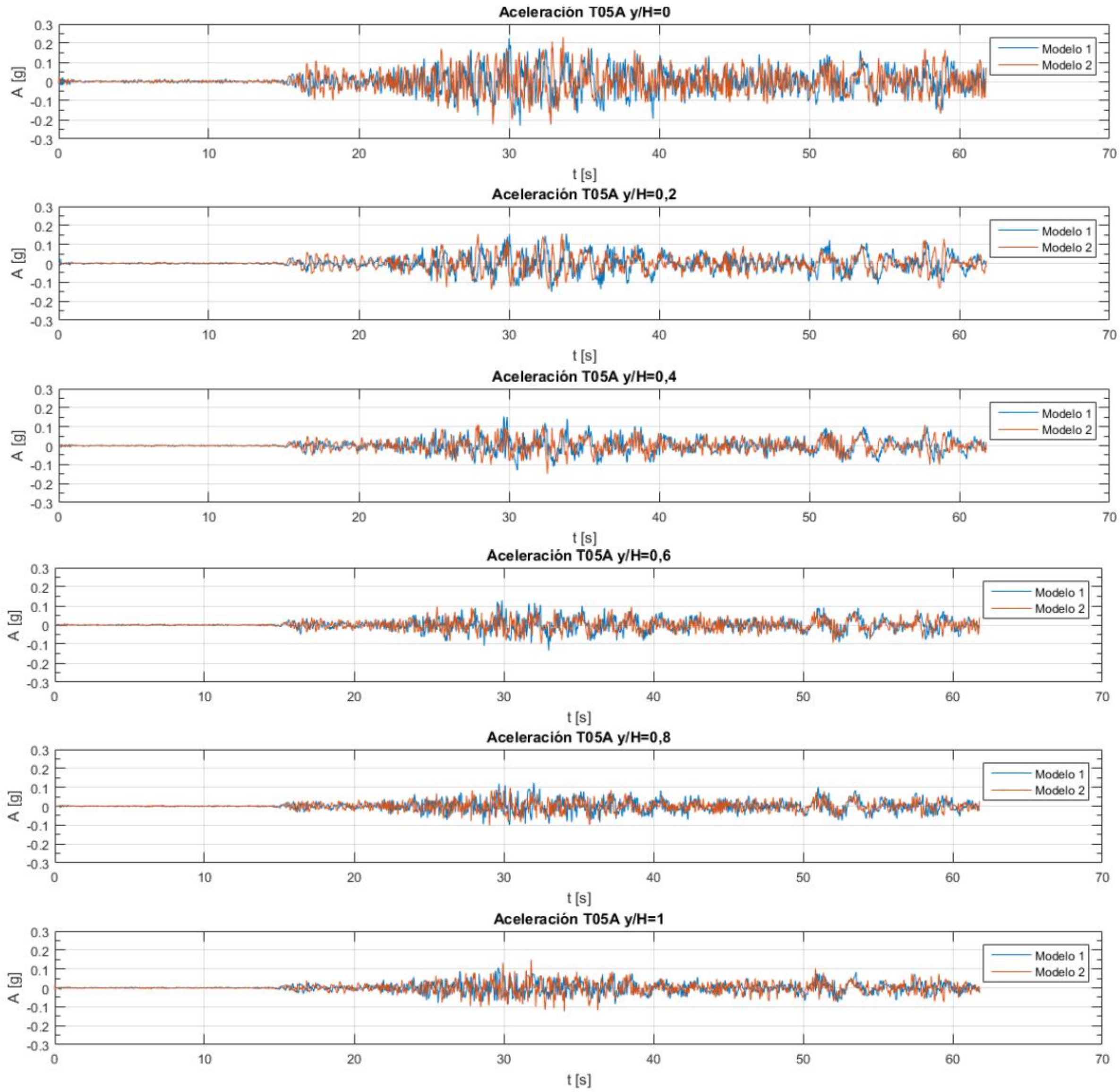

Figure 2: Acceleration time histories in depth at the dam central axis

For the different input earthquakes, the maximum accelerations for the two cases of foundation strata is shown in Figure 3. Figure 3(a) shows the relationship between the maximum acceleration measured at the base of the model and the maximum acceleration measured at the surface in the free field. Figure 3(b) shows the latter and the acceleration at the crest of the dam. The yellow and red dots indicate the relationship values for the foundation soil cases (1) and (2), respectively. The abbreviations of the seismographic stations shown in the figures can be observed in Table 2.

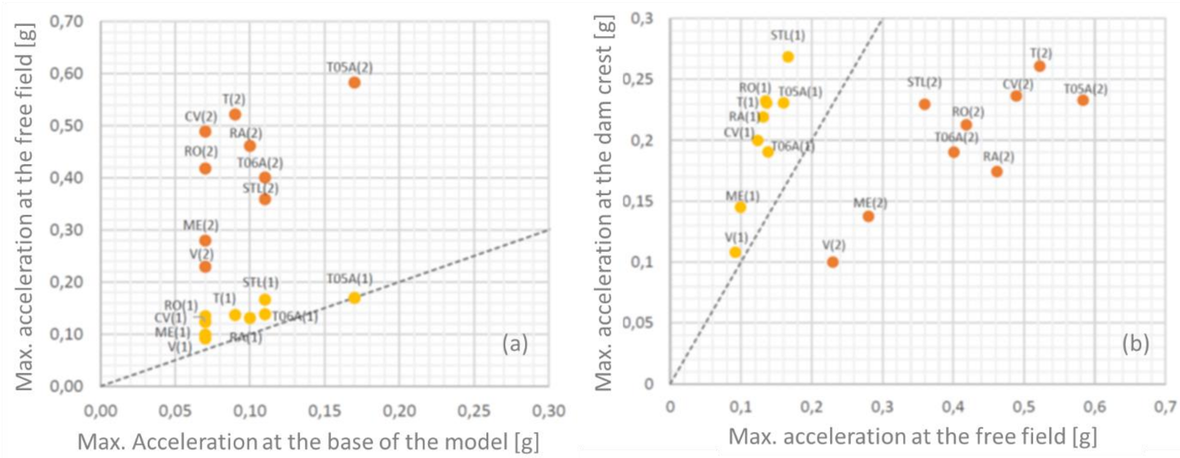

Figure 3: Maximum acceleration measured at (a) the soil foundation and (b) the dam. Red and yellow dots correspond to the foundation soil conditions (2) and (1), respectively

Although the maximum accelerations in Figure 3 do not occur simultaneously, the relationships can still be used to conclude in general terms about the acceleration amplification in the foundation soil and dam.

Considering the above, both foundation soil cases amplify the input acceleration at the free field (see Figure 3(a)) but the greatest acceleration amplifications occurs for the case (2). Figure 3(a) shows an average amplification of 3 for the foundation soil case (2), while for the foundation soil case (1) an average amplification value of 1.5 is observed.

In the case of the dam amplification, the tendency for the foundation soil case (2) is to de-amplify the maximum acceleration at the free field in an average value of 0.5. For foundation soil case (1), the dam amplifies the acceleration by an average value of 1.6 times the value recorded at the free field.

Horizontal dam displacement

The profiles of the relative maximum horizontal displacements for a given time with respect to the displacements measured at the base of the dam are shown in Figure 4. Figures 4(a) and (b), show the displacement profile for the foundation soil case (1) and case (2), respectively.

In both cases, it is possible to approximate the displacement profile through an exponential function but for the case (2) the exponential shape of the displacement profile is more pronounced, assimilating to a "whiplash effect" with great shear strain occurring near the crest of the dam.

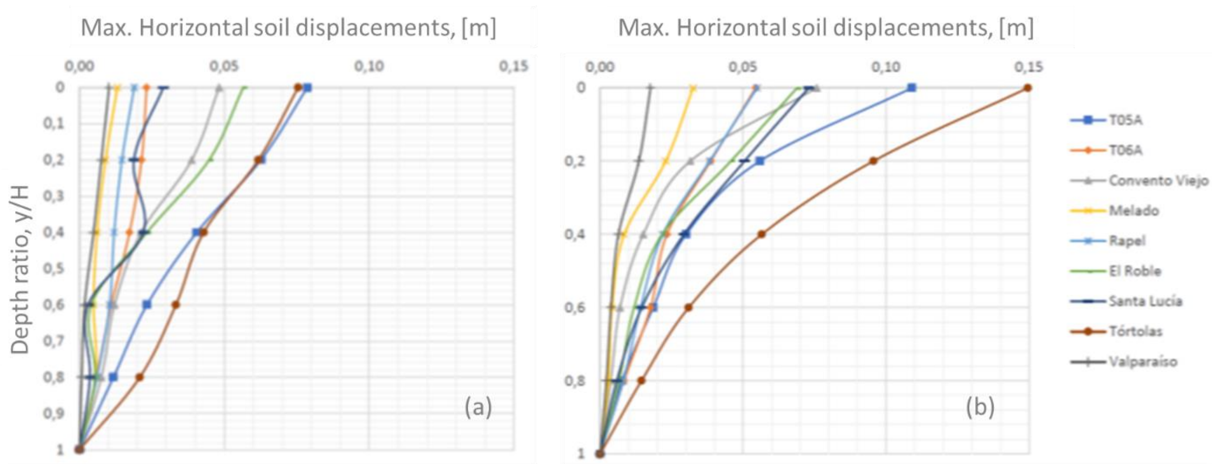

Figure 4: Relative horizontal maximum displacement profile for: (a) foundation soil case (1) and (b) foundation soil case (2)

Gazetas (1987) used the simplified method "shear beam" to show that increasing the exponent m, which increases the shear stiffness distribution with depth in the dam, $G = G_b(z/H)^m$, the dam increases its "whiplash effect", characterized by large shear strain and high acceleration near the crest of the dam in the second and higher modes. Gazetas also showed that under stronger shaking, nonlinear behavior of the materials in the actual earth dam might prevent the development of the high acceleration at the dam crest.

Pseudo spectral acceleration

Figure 5 shows the pseudo spectral accelerations at the free field for the two foundation soil cases. For the foundation soil case (1) three pseudo-acceleration peaks can be identified, which occur approximately at periods of 0.2s, 0.6s and 2s. In the case of the foundation system (2), a single pseudo acceleration peak at approximately 0.6s is clearly observed.

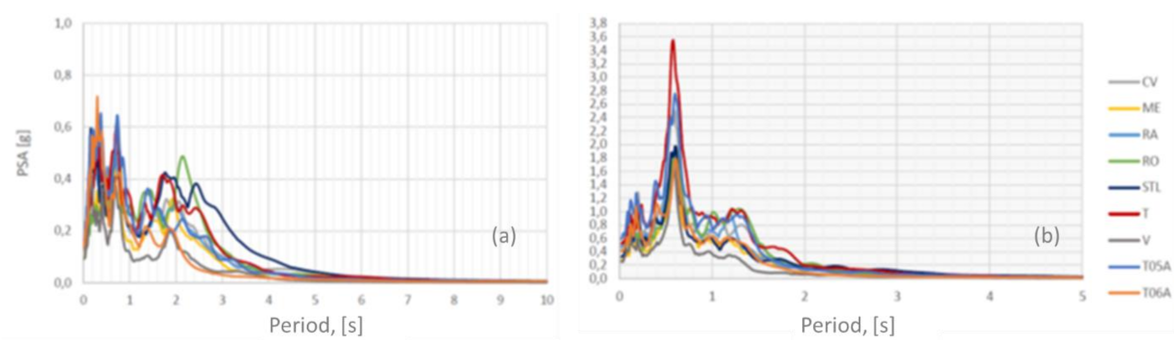

Figure 5: Pseudo – spectral acceleration at the free field for the foundation soil: (a) case 1 and (b) case 2

Based on the formulation initiated by Ambraseys and Sarma (1967) and developed later by Dakoulas (1985) for a nonlinear shear- strain relationship and shear stiffness depending on the confining pressure, the fundamental period of a dam can be determined by the expression:

$$T_n = \frac{16\pi}{(4+m)(2-m)\beta_n}\frac{H}{V_s} \quad (1)$$

where, m is the exponential value for the shear stiffness distribution in the dam $G = G_b(z/H)^m$, G_b the average shear modulus of the dam foundation, H the dam height, V_s the average dam shear wave velocity, and β_n the nth root of a period relation for the modes of vibration of an earth dam (Dakoulas and Gazetas, 1985).

By using expression (1), the first three natural periods of the dam can be estimated to be: $T_1 = 0{,}73s$, $T_2 = 0{,}35s$ and $T_3 = 0{,}23s$. According to the previous values, in the case of the foundation soil (2), the predominant period of the earthquake at the free field becomes close to the fundamental period of the dam, causing the dam to oscillate mainly in its fundamental mode. In the case of the foundation soil strata (1), the predominant periods of earthquake at the free field are more associated with the first and third vibration mode periods of the dam.

Vertical deformations at the dam crest

Figure 6 shows the relationship between the relative vertical deformations at the dam crest (respect to the deformations measured at the base of the dam) and Arias intensity of the input earthquakes measured at the free field. In Figure 6, the yellow and red dots indicate the relationship values for the foundation soil cases (1) and (2), respectively. As shown, the largest relative vertical deformations occur for the foundation soil configuration (2), reaching approximately a relative vertical deformation values of 0.10 m for Arias intensities of 1.6 m/s. In the case of a foundation soil case (1), relative vertical deformations no greater than 0.06m are observed for Arias intensity of 0.2 m/s.

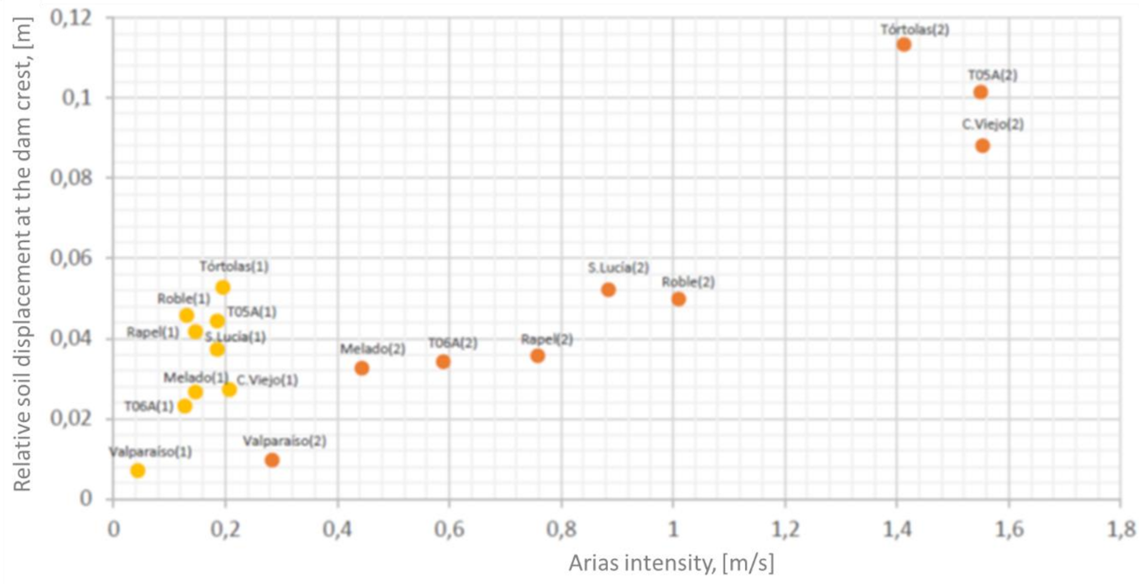

Figure 6: Relative vertical displacement at the dam crest for foundation soil cases 1 and 2

Conclusions

The current study numerically analyzes the response of a typical configuration of an earthfill tailings dam subjected to inter-slab thrust earthquakes with moment magnitudes greater than Mw > 8.0. The study analyzed two-foundation soil configuration: (1) a 200m soil deposit with its shear stiffness increasing with depth and (2) A 20m soil deposit placed on soft rock with an impedance value of 0.38.

The results shown in the present study for the cases: (1) uniform soil layer with shear stiffness increasing with depth and (2) soil layer over a soft rock, showed the following differences in their seismic responses subjected to large-magnitude subductive earthquakes (Mw>=8.0):

- For both cases of foundation soil, there is a free field amplification of the maximum input acceleration applied to the models
- There is an amplification and de-amplification at the crest of the dam of the maximum acceleration measured in the free field for case (1) and case (2), respectively.
- The largest vertical displacements relative to the base of the dam occur for case (2).
- The configuration of the foundation soil (site effect) can clearly modify the seismic response of an earthfill tailings dam, which is consistent with the conclusions of multiple related investigations

Acknowledgments

This research could not have been carried out without the results of the thesis work of the undergraduate student from the University of Chile, Daniela Barrios C., and the financial support of the national corporation of copper CODELCO, Chile.

References

Ambraseys, N. N. and Sarma, S. K. 1967. The response of earth dams to strong earthquakes, Geotechnique, 17(2), 181-213

Dakoulas, P. 1985. Contributions to seismic analysis of earth dams, PhD Thesis, Rensselaer Polytechnic Institute

Dey, A. 2011. Calibration of a PLAXIS Finite Element Dynamic Model: Effect of Domain Width and Meshing Schemes/AES, Third Indian Young Geotechnical Engineers Conference, Indian Geotechnical Society, New Delhi.

G. Gazetas, 1987. Seismic response of earth dams: some recent developments. Soil Dynamic Earthquake Engineering

Kempton J., Stewart JP. 2006. Prediction equations for significant duration of earthquake ground motions considering site and near-source effects. Earthquake Spectra, 22, pp 985–1013

Kuhlemeyer, R.L. and Lysmer. J. 1973. Finite Element Method Accuracy for Wave Propagation Problems. Journal of the Soil Dynamics Division, 99, 421-427

Mejias, L.,Dawson, E. (2006). Earthquake deconvolution for FLAC.4th International FLAC Symposium on Numerical Modeling in Geomechanics.Minneapolis.

Schanz, T. 1998. Zur Modellierung des mechanischen Verhaltens von Reibungsmaterialien. Mitt. Inst. für Geotechnik 45. University ofStuttgart. Stuttgart, Germany.

Schanz, T., Vermeer, P. A. & Bonnier, P. G. 2000. The Hardening Soil Model: Formulation and Verification. Beyond 2000 in Computational Geotechnics. pp.: 281-290. Rotter dam: Balkema.

T. Kokusho, Y. Esashi. 1981. Cyclic triaxial test on sands and coarse materials Proc. 10th ICSMFE (Quoted by Ishihara 1986), Stockholm, Sweden

Seismic Observation and Monitoring for a Tailings Storage Facility with Soil Solidification

Takemine Yamada, Kajima Technical Research Institute, Japan
Tomoki Hikita, Kajima Technical Research Institute, Japan
Keisuke Murata, Sumitomo Metal Mining, Japan
Yoshinobu Kishimoto, Sumitomo Metal Mining, Japan

Abstract

In response to recent collapses of tailings storage facilities (TSFs) worldwide, the International Council on Metals and Mining advises affiliated operators to design and operate monitoring systems for risk management during all phases of TSF life cycles, including the closure stage.

In the study reported here, slope stabilization for a tailings storage facility in Japan was applied using cement-based lattice-pattern ground solidification with a replacement rate of 20% to prevent ground liquefaction and TSF collapse during large earthquakes. Seismic observation at the site since March 2017 indicates no change in the acceleration transfer function of the slope, thereby demonstrating the maintenance of seismic performance. Excess pore water pressure in the ground within the lattice area also exhibited response to minor earthquakes (observed as seismic waveforms). Accordingly, monitoring of such pressure in addition to water levels in improved ground (in addition to the use of optical fibers for sensing and measurement of strain in improved walls) can be seen as a practical approach to long-term evaluation of seismic performance in tandem with acceleration measurement. The implementation of results from such observations is expected to support effective real-time monitoring of the seismic and static stability of TSFs.

Introduction

The 2011 Great East Japan Earthquake caused accidental spillages at three tailings storage facilities (TSFs, or closed mines) in the country's Tohoku and Kanto regions (Ishihara et al., 2015). In November 2012, Japan's Ministry of Economy, Trade and Industry (METI) revised design codes (Yasuda, 2020) to ensure stability against maximum expected earthquake motion (i.e., level 2 large-scale) for: 1) upstream-type TSFs stacked higher than foundation embankments; 2) TSFs on high-infiltration water tables (shallower than 10 m); and 3) TFSs with a sediment volume of 50,000 m^3 or more (except where major structures are present downstream). Stabilization measures against earthquakes are currently underway for such TSFs.

Following a series of tailings dam breaches, the International Council on Mining & Metal (ICMM), the United Nations Environmental Programme (UNEP) and the Principles Responsible Investment (RPI) organizations collaborated on the Global Industry Standard on Tailings Management (GISTM) in 2020 (ICMM, UN, RPI, 2020). Major participating mining companies worldwide are obligated to implement its management practices.

In this context, liquefaction countermeasures were implemented in 2016 at a TSF managed by Sumitomo Metal Mining (SMM) with slope improvement featuring large-scale grid soil solidification based on cement-based stabilization. Seismic observation to monitor ground acceleration and pore water pressure in the ground were subsequently conducted (Yamada et al., 2019). As a GISTM measure, groundwater level observation wells have been augmented and comprehensive investigation has been initiated, including steps to address facility aging.

This paper gives an overview of stabilization measures and GISTM responses at the TSF, where seismic observations remain ongoing. The discussion includes post-stabilization performance examination, analysis of seismic observation records, and consideration of a future earthquake damage monitoring system for TSFs.

Recent TSF initiatives

Stabilization and seismic observation for level-2 earthquake ground motion (Yamada et al., 2019)

The upstream-type TSF in question (Fig. 1, Table 1) is in Kagoshima Prefecture in Japan's southern Kyushu region, and underwent liquefaction remediation work in 2016. Based on revised technical standards (METI Technical Committee, 2012), finite element seismic response analysis of the facility was conducted in consideration of a Level-2 earthquake (Fig. 2) that might typically happen at the site. The results suggested that tailings spillage due to liquefaction and lateral slope flow may occur.

For stabilization, the entire slope was improved with wide 20% replacement-rate lattice-type solidification in 2016. Seismic observation with three seismographs and two hydrometers has since been conducted to analyze the effects of the improvement and establish an earthquake damage monitoring system.

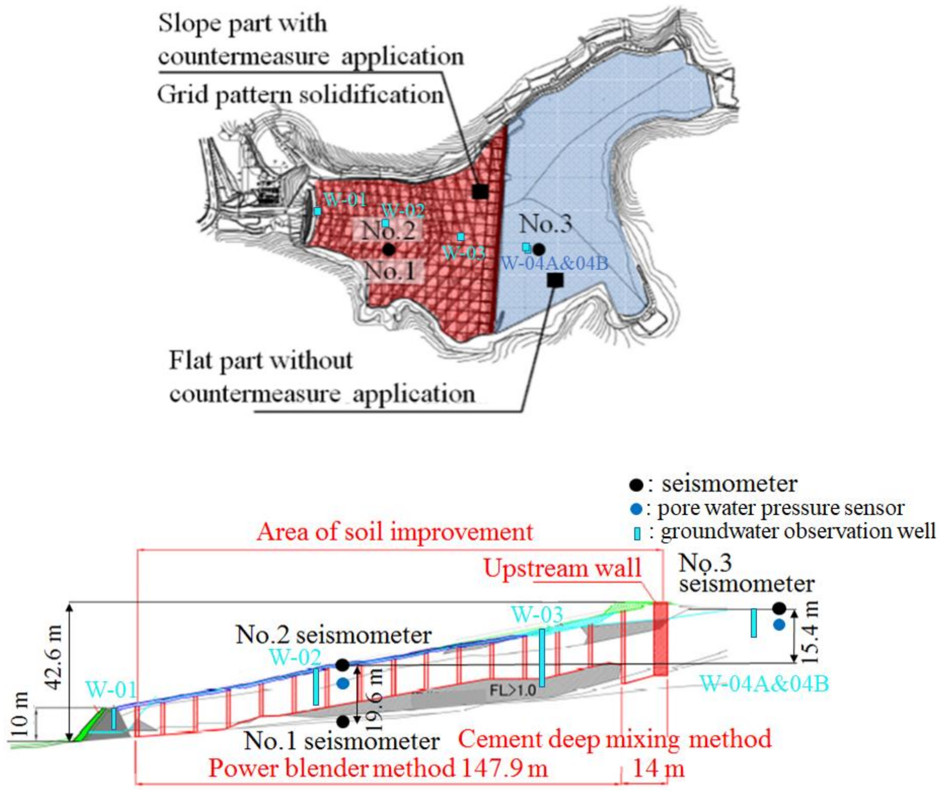

Figure 1: Target TSF, with implementation of lattice pattern wall-type soil solidification for the whole slope and a related monitoring system

Table 1: TSF overview

Item	Description
Location	Okuchi, Isa, Kagoshima, Japan; facility No. 2
Tailings disposal period	1937 – 1977, with a long intermission midway
Disposal method	Upstream raised-embankment type
Tailings volumes	350,000 m^2; 270,000 m^3
Slope portion	Length: 150 m; average gradient: 20%
Liquefaction countermeasures	Improvement between April 2014 and March 2015 with cement deep mixing (CDM; 20,296 m^3) for the upstream wall and power blending (32,800 m^3) for the wide-pitch lattice pattern wall-type soil solidification part (average replacement ratio: 20%; wall width: 1.0 m; wall pitch: 10 m)
Seismic observation	Ongoing since March 2017

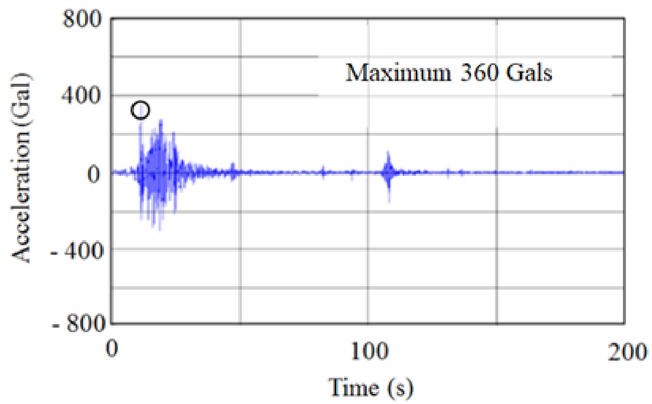

Figure 2: Input wave used in seismic design for TSF stability under Level-2 earthquake conditions

Enhancement of groundwater-level monitoring wells and comprehensive facility evaluation

GISTM applies to mining waste based on social, environmental and technical perspectives, and requires independent third-party oversight as well as transparency and information disclosure. ICMM places such management as a membership requirement.

In response to GISTM requirements, SMM implements ICMM to strengthen groundwater-level observations, and conducts comprehensive evaluation of aging facilities toward the compilation of a dam safety assessment report (DSR) by 2024 and the release of related information thereafter (Fig. 3). Two extra groundwater observation wells were installed at the TSF in 2022 (Fig. 1; total of five wells including three installed in 2013), and water-level observations were started in 2022 to evaluate the total water head of the tailings aquifer. SMM plans to report the survey results to METI as a third-party review and provide a summary of the outcomes.

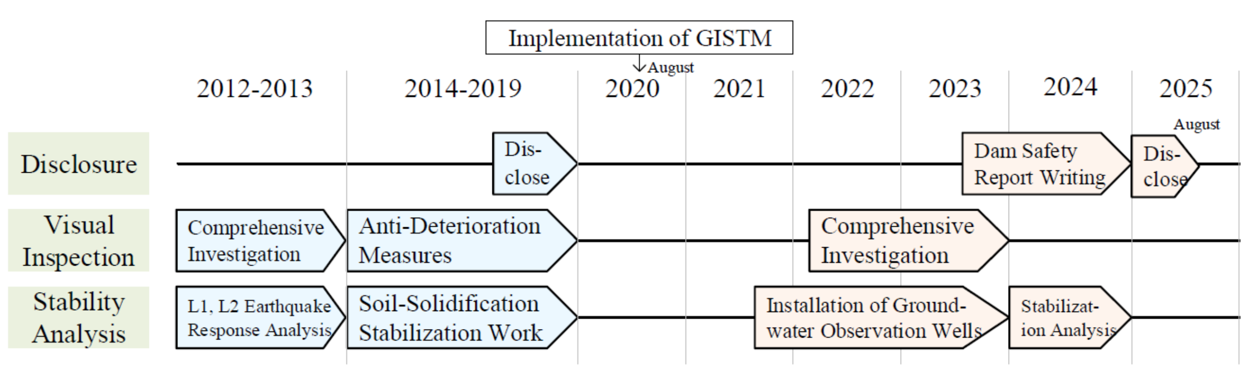

Figure 3: SMM roadmap for GISTM requirements

Observation results and discussion

Earthquake observations between March 2017 and March 2021 provided 86 acceleration records with a source distance within 200 km from epicenters exhibiting a JMA magnitude of 3.5 or greater and a maximum acceleration (the maximum of the three components) of 0.1 cm/s^2 or greater for the No. 1 slope underground part (Fig. 4). The acceleration response of the ground surface where mineral waste is deposited was greater than that of No. 1 in both the horizontal and vertical components for both slope and flat areas due to ground response amplification. The acceleration response of the improved slope section was smaller than that of the unimproved flat part. This is because the equivalent stiffness of the improved ground is four to five times greater than that of the unimproved ground. It has been confirmed that slope-section acceleration response is lower as a result of improvement (Yamada et al., 2019).

Noting the water pressure response in Fig. 4, no response in excess pore water pressure is observed in the unimproved flat part when earthquake acceleration is a maximum of 4 gal at base location No. 1. In the improved section, excess pore water pressure response is clearly observed in the improved ground with seismic waveforms. This may be attributable to the fact that, in seismic response analysis for ground with lattice-type solidification, the total stress of the improved soil generally changes repeatedly during earthquakes because the improvement wall constrains soil response. This change in total stress is converted to excess pore water pressure due to the undrained condition of the soil pore water. Thus, analysis of excess pore water pressure in ground with lattice-type solidification indicates the effectiveness of improvement even in earthquakes with low acceleration levels.

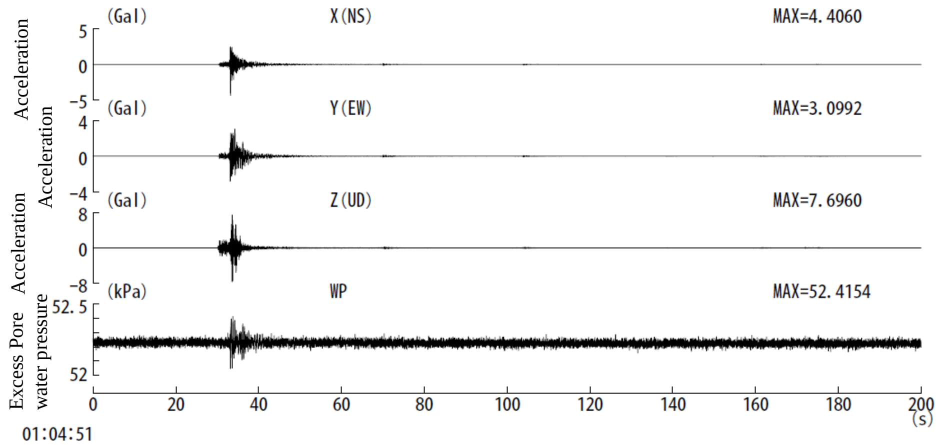

No.2 Acceleration and No.4 Excess pore water pressure

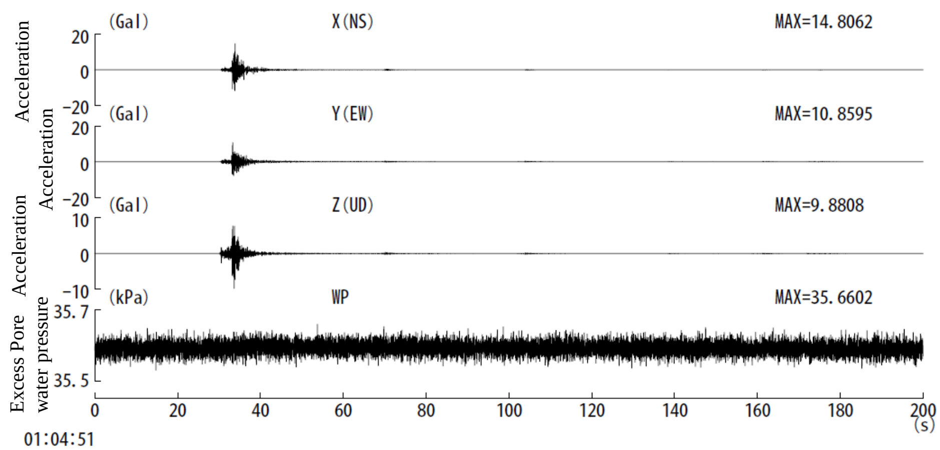

No.3 Acceleration and No.5 Excess pore water pressure

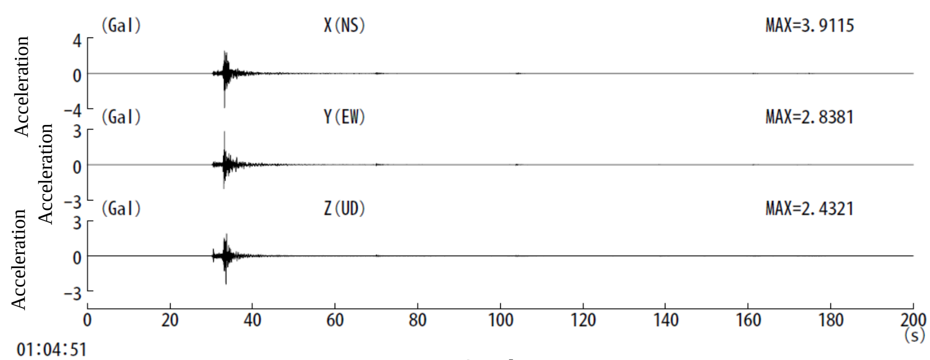

No.1 Acceleration

Figure 4: Seismic observation waveforms, Dec. 11 2018. Ebino region, S Kyushu. M = 3.4, H = 6.2 km, X = 20.1 km, Δ = 19.2 km, φ = 102.4°, tp = 30.07 s, ts = 32.59 s

Comparison of amplitudes of the average transfer functions of No. 2/No. 1 for each observation period showed an average function of 20.48 seconds after the S-wave rise time for three periods divided into roughly equal numbers of records. The two horizontal components (NS, EW) were treated as independent data, and the average transfer function of all recordings was evaluated (Fig. 5). Here, the first-order natural frequency of the ground changed from 2 Hz before improvement to approximately 5 Hz afterward. Figure 5 shows no clear difference in the transfer function depending on the observation period. The maximum acceleration of the No. 1 record was divided into three categories of less than 1 cm/s^2, 1 – 10 cm/s^2, and greater than 10 cm/s^2. Comparison of amplitudes for the average transfer function in each category (Fig. 6) showed no clear difference in maximum acceleration.

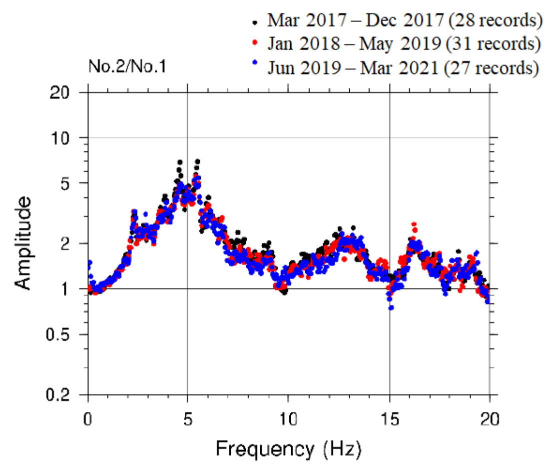

Figure 5: Transfer functions of No. 2/No. 1 acceleration categorized by period

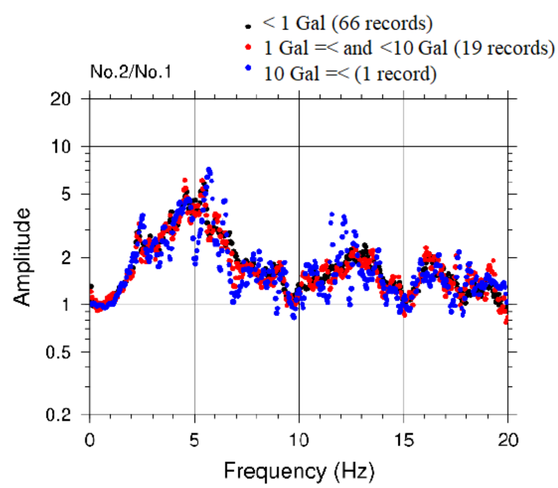

Figure 6: Transfer functions of No. 2/No. 1 acceleration categorized by magnitude of seismic acceleration in No. 1

In summary, the amplification characteristics of the acceleration response over the period of countermeasure application from 2016 to 2021 exhibited little temporal change for small earthquakes. The results indicate that the seismic performance of ground improved with soil cement solidification in a wide grid pattern for the slope of tailings on highly acidic soil did not decrease over the period, and that changes in TSF performance can be monitored via similar ongoing observations and analysis.

As an example of the response of pore water pressure to precipitation, Fig. 7 shows the results of a four-month observation conducted in 2021. Although the maximum water level differs for pore water pressure in the improved and unimproved sections due to differing sensor depths, both show that the groundwater level increases or decreases in response to precipitation, that the groundwater level reaches the ground surface, and that water pressure peaks when precipitation is high. During the design of the remedial measures, it was assumed that the improved ground would be surrounded by a solidification wall, which would block the supply of groundwater from upstream, thereby preventing the groundwater level from rising. However, observations showed that the groundwater level actually did rise. This may be attributable to the weathered stratum near the top of the basement (where the solidification wall had not been rooted in) being in an aquifer, supplying groundwater to the improved ground.

Water-level observation wells were also augmented to support monitoring of ground water levels across the whole TSF, and observations remain ongoing. Continuous monitoring of these levels is expected to be useful in TSF stability research and appropriate facility maintenance work (such as drainage planning) against the effects of climate change and seismic hazards.

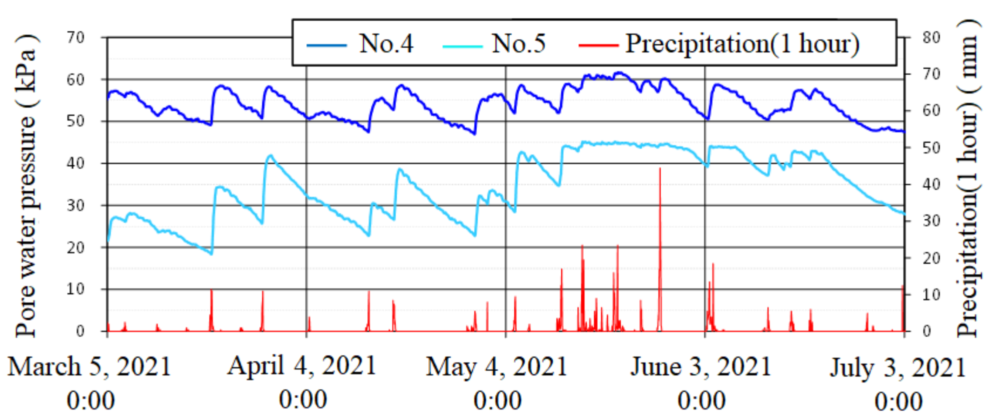

- Water pressure (groundwater level) is high in both sloped/improved and flat/unimproved areas.
- Water pressure is sensitive to precipitation. However, the amount of fluctuation in water pressure is larger in the flat and unimproved areas.
- When precipitation is heavy, the water pressure rises to a level equivalent to that of the ground surface.

Figure 7: Time histories of pore water pressure and hourly rainfall for March 2021 – July 2021

Considerations for future earthquake disaster monitoring systems

Based on the results, Fig. 8 illustrates the basic concept of long-term monitoring for the TSF subjected to soil cement stabilization at the site. Analysis to identify any changes in site properties is conducted via continuous monitoring of ground acceleration amplification characteristics and water pressure/water levels as described above. Research on TSF stability may be adapted in response to any changes in site characteristics.

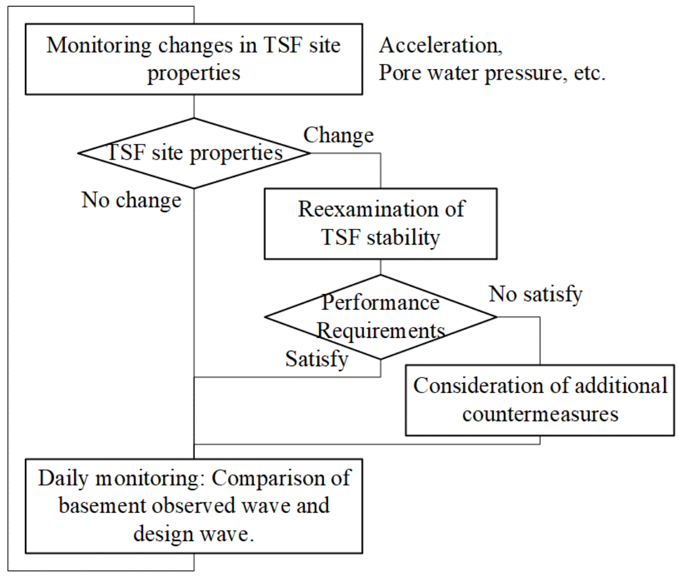

Figure 8: TSF monitoring and management for earthquakes

Earthquake damage can be assessed in real time by comparing observed and design waves. Figure 9 shows input seismic motion at the TSF as estimated using records from the Hitoyoshi KiK-net observation station 16 km away and comparison with design waves (Yamada et al., 2021). The level of the estimated seismic waves was much lower than that of the design waves, indicating TSF stability against earthquakes. This type of evaluation allows assessment of TSF stability immediately after tremors based on input seismic motion estimated from the correlation of cumulative observation records for two sites since 2017 (Yamada et al., 2021). In the area of damage assessment, periodic strain monitoring for solidification walls using embedded optical fibers is promising, as it enables direct evaluation of the status before and after major earthquakes.

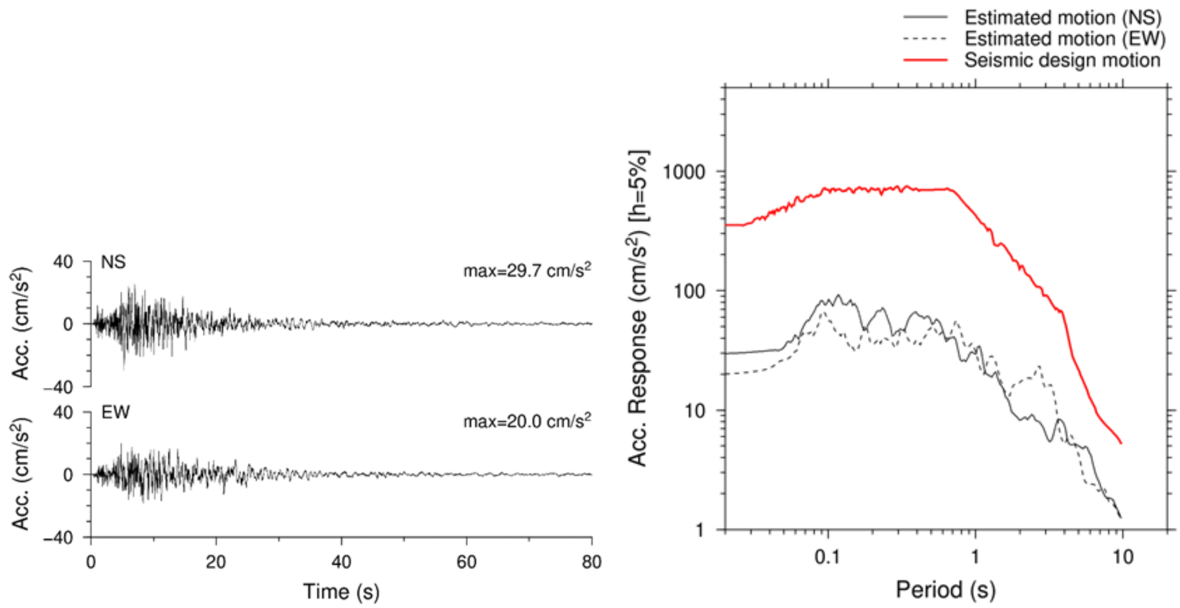

Figure 9: Acceleration waveforms from the Okuchi site during the 2016 Kumamoto Earthquake (April 16, Mj 7.3) as estimated from Hitoyoshi KiK-net observation records, and comparison of the acceleration response spectrums of estimated wave and seismic design ground motion (Yamada et al., 2021)

Conclusions

This paper presents an overview of stabilization measures and GISTM response at a tailings storage facility where seismic monitoring remains ongoing, an analysis of four years of seismic observation records to evaluate countermeasure performance, and a discussion of future monitoring systems for seismic events. The study can be summarized as follows:

- Seismic observations were conducted on the slope of a tailings storage facility with highly acidic fine ore, which was improved with cementitious solidification in a wide grid pattern, and related seismic response characteristics were evaluated. The results indicated no change in seismic performance by around five years after the solidification.
- Excess pore water pressure in the improved ground showed a clear response to seismic waveforms with acceleration levels as low as 4 gal at maximum at the base location. In this context, analysis of excess pore water pressure in ground improved with lattice solidification may support evaluation of the improvement effect even for earthquakes with low acceleration levels.

- Groundwater levels in improved ground surrounded by lattice walls fluctuated with rainfall, indicating the importance of long-term monitoring of water pressure and water levels for the whole TSF.
- Continuous monitoring of ground acceleration and water pressure allows evaluation of site characteristics and TSF seismic resistance. The TSF monitoring proposed here is important in evaluating stability when site characteristics change, judging safety immediately after earthquakes, and gauging static stability.

Focus on GISTM compliance requires enhanced water-level monitoring and measures to prevent aging at tailings facilities. Against such a background, a dam safety assessment report (DSR) will be compiled and the major results will be disclosed to the public by August 2025.

References

International Council on Mining and Metals, UN environment programme and Principle Responsible Investment:. 2020.. Global Industry Standard on Tailings Management, GlobalTailingsReview.org.

Ishihara, K., Ueno, K., Yamada, S., Yasuda, S. and Yoneoka, T. 2015. Breach of a tailings dam in the 2011 earthquake in Japan, Soil Dynamics and Earthquake Engineering, Volume 68, 3-22.

METI's Technical Committee for Administration of Reservoir of Waste Soils and Tailings. 2012. Report on the administration of reservoirs for waste soils and tailings, Ministry of Economy, Trade and Industry: a ministry of the Government of Japan. (in Japanese)

Yamada, T., Hikita, T., Ichimura, T., Fujita, K., Umedera, M. and Seo, T. 2019. Seismic response of tailings storage facility applied liquefaction mitigation, Earthquake Geotechnical Engineering for Protection and Development of Environment and Constructions – Silvestri & Moraci (Eds), 5697-5704, Associazione Geotecnica Italiana, Rome, Italy, ISBN 978-0-367-14328-2.

Yamada, T., Hikita, T., Ichimura, T., Fujita, K., Umedera, M., Nakamura, T. and Seo, T. 2021. Evaluation of seismic behavior of upstream tailings storage facility applied liquefaction mitigation by wide-pitch lattice-pattern-walls type soil solidification, 17th World Conference On Earthquake Engineering.

Yasuda, S. 2020. Soil investigations and soil tests required for seismic inspection of abandoned tailings dams in Japan, 6th International Conference on Geotechnical and Geophysical Site Characterization.

Validation of constitutive models for assessing the seismic response of tailing dams during strong earthquakes

Roberto Cudmani, Technical University of Munich, Germany
Antal Csuka, Technical University of Munich, Germany
Andrés A. Peña-Olarte, Technical University of Munich, Germany

Abstract

Modelling the seismic response of tailing dams is particularly challenging due to the complex behavior of the involved material and interacting system components, i.e., the dam, the foundation, and the stored slimes. Due to their versatility for the solution of complex boundary-value problems, numerical analysis, particularly the finite element and finite difference method (FEM and FDM), in combination with advanced constitutive models, are being increasingly applied in practice to assess the stability and safety of Tailing Storage Facilities (TSF). This contribution proposes different benchmark tests to validate constitutive models that intend to capture the response of tailing dam materials under seismic loading. Exemplarily, the proposed benchmarks are simulated with a hypoplastic constitutive model. The validation includes a plausibility assessment and a comparison of the numerical results with experimental data from laminar shake box tests and actual seismic records from a well-documented site during strong earthquakes. The imperious necessity for a comprehensive validation of constitutive models to detect and improve model weaknesses and ensure numerical robustness before they are applied to predict the seismic response of tailing dams is demonstrated.

Introduction

During an earthquake, the induced shear strain in a slope or a dam is a function of both time and space. The degree of effective pressure reduction at a particular location depends not only on the soil layers, the material properties, and the state of the soil in the slope but also on the characteristics of the bedrock motion (amplitude, frequency content, and duration) and the slope geometry (inclination, height). Despite their complex behavior, the analysis of potentially liquefiable slopes and dams under earthquake loading is often based on empirical methods such as the “cyclic stress approach” (Seed & Idriss, 1970) and simplified methods as the Limit Equilibrium Method (LEM) analysis. However, as indicated by (Cudmani et al. 2003), the cyclic stress approach cannot capture the complex behavior of liquefiable soils under dynamic loading. In addition, the accuracy of the LEM relies on an undrained shear strength, which can be ambiguously estimated neither in the field nor the laboratory.

Alternatively, more advanced methods like the Finite Element Method (FEM) or the Finite Difference Method (FDM) can be used to study the seismic response of tailing dams. However, the quality of the predictions strongly depends on the constitutive model describing the mechanical behavior of the tailings. The models must simulate the pore pressure build-up, the evolution of the undrained shear resistance, and the accumulation of shear strains during alternating loading in a realistic manner. Several constitutive models differing in complexity, abilities, and number of model parameters have been proposed in the literature. The more advanced constitutive models are based on elastoplasticity and hypoplasticity. In elastoplasticity, the relationship between the stress rate and the strain rate is derived from the elasticity and plasticity theory, in which yield surfaces, hardening, and flow rules are required to define the plastic strain rate. As distinct from elastoplasticity, the description of the plastic strain in hypoplasticity models does need neither the introduction of yield surfaces, hardening, and flow rules nor the explicit decomposition of the strains into elastic and plastic parts. Developing a constitutive model is time-consuming and includes not only the development of the constitutive equations but also different validation phases and the assessment of the numerical robustness. For this reason, only a few models have been implemented in commercial codes and are available for the numerical solution of boundary-value problems in practice. Besides availability, the precise physical meaning of the parameters and the feasibility of their determination are essential conditions for the applicability of advanced constitutive models. In addition, since the state of the soil, density, and stress changes spatially and during loading, models with state-independent parameters are advantageous.

In this contribution, different numerical benchmarks are proposed to validate and select suitable constitutive models for the numerical analysis of the seismic response of TSFs. With this aim, the capabilities of constitutive models to capture the behavior of tailings in dynamic boundary-value problems, including large multi-directional alternating shearing, can be assessed. The proposed benchmarks are the motion of a rigid block on a 1) thin dry and 2) saturated soil layer, in-plane, and anti-plane shaking of 3) homogeneous dry and 4) saturated soil layer, 5) horizontally layered soil deposit and 6) inclined homogeneous saturated soil layer. Benchmark 6) considers the effect of initial static shear stress and loading direction on liquefaction and is particularly relevant for tailing dams.

In a further validation step, the results of the numerical simulations must be compared with experimental data. Experimental benchmarks can be conducted at 1-g level (shake-box) or n-g level (centrifuge test) for this validation step. Examples of 1-g testing are shake box tests with horizontal layers (Gudehus et al. 2004) and with inclined layers, simulating the "infinite" slope conditions (Dobry et al. 2011).

A series of n-g benchmarks considering different geotechnical structures have been conducted in the VELACS (Arulanandan and Scott 1993) and LEAP (Kutter et al. 2017) projects.

The proposed framework is exemplarily applied to the hypoplastic constitutive model with intergranular strain (Niemunis & Herle, 1998).

First validation phase: BVP with homogenous stress and strain fields

The first benchmark consists of a block with a mass m_a resting on a horizontal plane that undergoes harmonic shaking (Gudehus et al. 2004); see Fig. 1. There is a thin granular layer between the block and the plane, whose response is modeled with a hypoplastic constitutive law as given in (Niemunis & Herle, 1998). The base is excited with a harmonic acceleration $a = a_0 \cos(\omega t)$, whereby a_0 is the amplitude of the acceleration and $u_0 = -a_0/\omega^2$ is the amplitude of the displacement of the base. The constitutive model should be able to predict the non-linear behavior of the granular layer under homogeneous shear conditions. The granular layer can be 1) dry (drained conditions) or 2) saturated (undrained conditions). At this validation level, either the stress or strain rates in the vertical direction can be controlled. It is worth noting that the shearing of a soil element during an earthquake is neither stress-rate or strain-rate controlled in vertical direction. The shear stress and shear strain rates in horizontal directions result from the solution of the boundary-value problem.

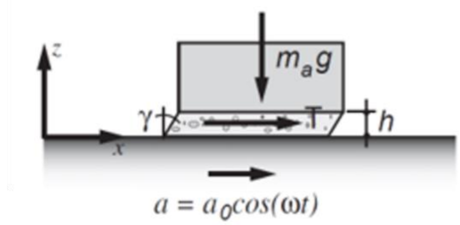

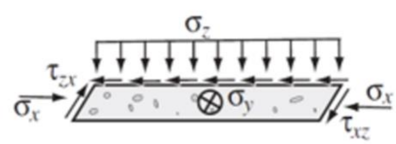

Figure 1: Block resting on a laterally confined thin granular layer on a horizontal plane, according to (Gudehus et al. 2004)

1st Benchmark: Block on a thin, dry granular layer

Simple shear conditions of the dry granular layer are enforced. In the vertical direction z, the initial pressure σ_z = 100 kPa is constant and given by the weight $m_a g$ of the block. The horizontal pressures are $\sigma_y = \sigma_x = K\sigma_z$ with an earth pressure coefficient K = 0.5, and the initial density is loose (I_d = 0.25). During shaking, the shear force T_x and normal force T_z acting on the block are proportional to the shear stress τ_{xz} and the vertical stress σ_z in the granular layer, respectively (Fig. 1b). In Fig. 2a, the mass displacements for harmonic shaking of the horizontal base are presented. The horizontal block motion $|u_X|$ is amplified and thus larger than the amplitude of the displacement of the base $|u_0|$. Additionally, u_X exhibits a time lag to the base displacement and is not harmonic. The block presents a stepwise downward movement due to densification, as seen in Fig. 2b. The frequency of this downward movement is twice as high as that of the base. For one complete shearing cycle (two reversals of γ), the layer undergoes two densification cycles (without pressure change). The rate of accumulation of permanent vertical displacements u_Z diminishes with the number of cycles as the material densifies. Fig. 2 c-d shows the evolution of shear stress and void ratio as functions of shear strain. Compared to the second cycle, the granular layer for the thirtieth cycle is stiffer and denser, and as such, the hysteresis is smaller. It is of utmost importance that constitutive models can capture the shear stiffness degradation and damping ratio dependency with shear strain.

2nd Block on a thin saturated granular layer

A block rests on a saturated and undrained granular thin soil layer. Both the layer height h and the total vertical pressure σ_Z are constant. The effective pressure σ' and the pore water pressure p_w change according to $\sigma = \sigma' + p_w$. The system response under harmonic shaking on a horizontal plane is shown in Fig. 3. As can be seen in Fig. 3b, the mean effective pressure p' decreases during shearing with the number of cycles due to the tendency of the granular layer to reduce its volume. The mean effective pressure p' oscillates with twice the frequency of that of the base and reaches a nearly fully liquefied state. Following an initial amplification, the block oscillates at a much lower amplitude than the base excitation. This is due to the loss of shear stiffness in the liquefied state that impedes further shear waves from the base to the mass. The ancient Japanese seismic isolation technique, Hanchiku, uses this effect, whereby saturated loose sand layers were embedded in fat clay (Pralle & Gudehus 2000). The isolation effect of a liquefying layer was also demonstrated experimentally using shaking table tests with the system of Fig. 3, in which the saturated sand layer was contained in a cushion.

Second validation phase: BVP with inhomogeneous stress and strain fields

The next step for validating a constitutive model is to extend the homogeneous deformation conditions of the first benchmark to non-homogeneous conditions. This is achieved by simply increasing the thickness of the thin layer so that a non-homogeneous deformation is enforced along the height of a 1) dry and 2) saturated column of granular material. The benchmarks presented in this section can be investigated in the laboratory, e.g. in a shake box, or based on back-calculated events of case histories.

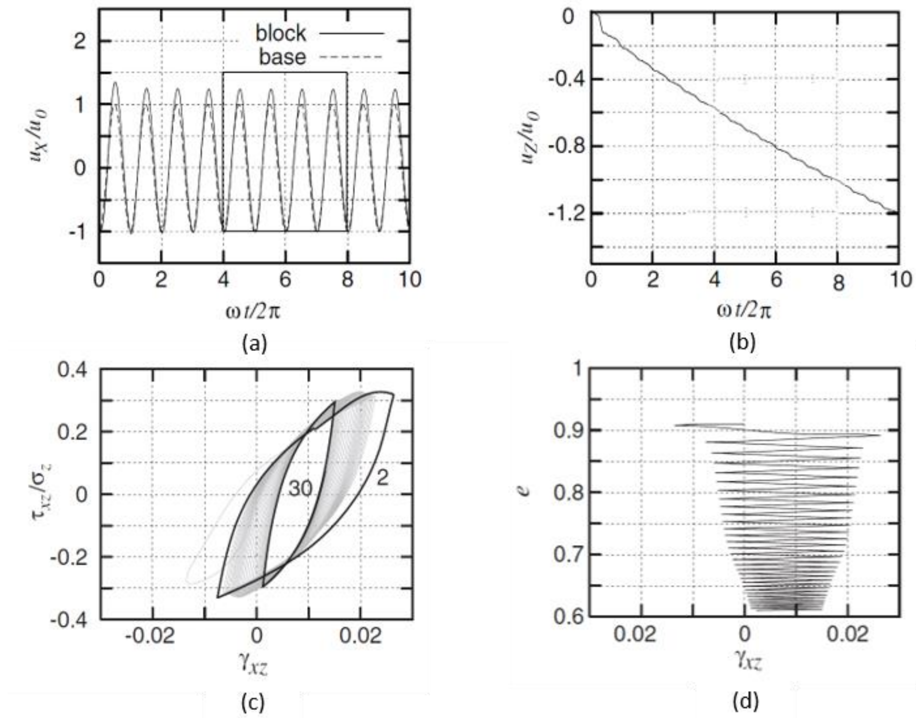

Figure 2: Response of system resting on a dry granular layer, (a) horizontal displacements of the base and the block, (b) vertical displacement of the block versus the number of shaking cycles, and (c) normalized shear stress and (d) void ratio versus shear strain γ_{xz}. Calculations are performed with a_0 = 0.3g and f = 3Hz, according to (Gudehus et.al. 2004)

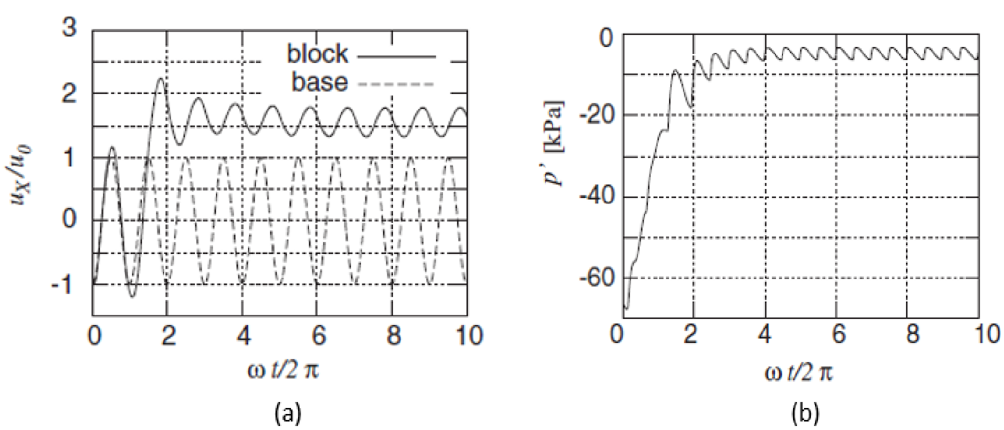

Figure 3: Response of system resting on a saturated undrained granular layer, (a) horizontal displacements of the base and the block, (b) mean effective pressure versus number of cycles. Calculations are performed with a_0 = 0.3g and f = 3Hz, according to (Gudehus et.al. 2004)

Propagating plane waves lead to changes in the soil state, and if the material exhibits permanent deformations, they can change the wave propagation dynamics. Numerical investigations for harmonic base shaking of a dry soil deposit using the hypoplastic constitutive relation reveal several non-linear effects

(Osinov, 2000; Osinov & Gudehus, 2003). Three of these effects can be used to assess the performance of the constitutive model. The first two effects relate to the changes in shape and amplitude of the induced shaking that is no longer sinusoidal. The third significant effect is that the dilatant-contractive response of granular materials during cyclic shear causes longitudinal waves with double excitation frequency.

3rd and 4th Benchmark: Plane shear waves in dry and saturated sand with horizontal surface

We now consider the results of a 1-g laminar shake box (length 400 mm, width 300 mm, height 500 mm) from (Gudehus et al. 2004). The dynamic base excitation is generated using a series of springs attached at the base of the box. An initial displacement of the box activates the spring forces, which induce a dynamic excitation at the bottom upon release. The horizontal and vertical displacements of the soil surface are recorded. A comparison of experimental results and numerical simulations with the hypoplastic model is shown in Fig. 4. First, the horizontal motion undergoes a strong oscillation followed by the other three smaller ones. Afterwards, the movements are damped out. During the first two large oscillations, the densification is the largest and decreases further during the lower amplitude oscillations. The vertical oscillation has twice the frequency compared to the horizontal one. A comparison of the results of laminar box tests and numerical simulations for a saturated sand layer can also be found in (Gudehus et al. 2004).

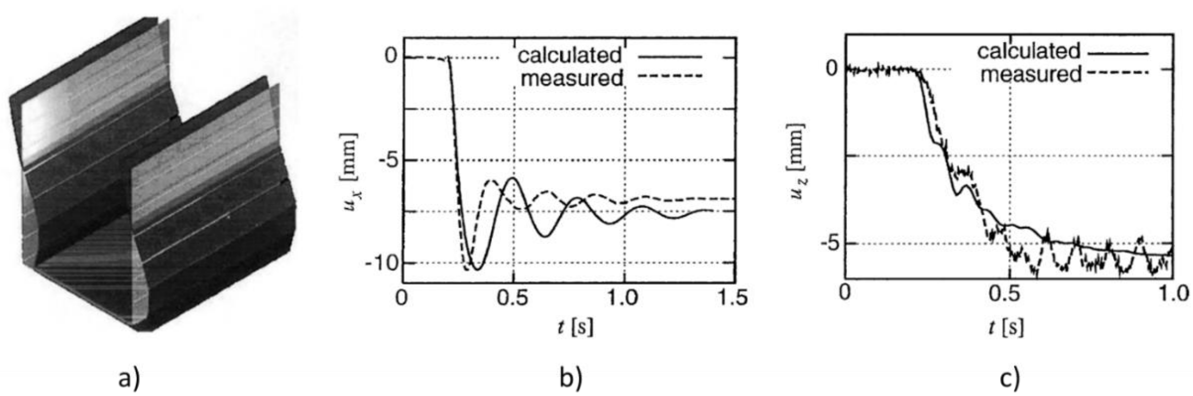

Figure 4: a) Deformation mode of laminate walls and observed and calculated (b) horizontal and (c) vertical displacements at the free surface of initially loose dry sand in the shake box, according to (Gudehus et al. 2004)

5th Benchmark: Plane shear waves in saturated sand with a horizontal surface

A well-documented strong earthquake at Kobe Port Island is used to assess the ability of the constitutive model to predict the one-dimensional propagation of seismic waves under undrained conditions. Based on the geological profile found in the literature, the sand layers were simulated in our numerical model using the hypo-plastic model and the clay layers using the visco-hypoplastic model (Niemunis, 2003) (Fig. 5a). The visco-hypoplastic model can simulate the phenomena of creep, relaxation, and rate-dependency. The strain rate is decomposed into an elastic and a viscous part, with the viscous portion being a stress and void ratio function. The intergranular strain concept is also used for enhancing the cyclic behavior of the visco-hypoplastic constitutive law. The model parameters were estimated from the granulometric properties of the layers and can be found in (Gudehus et al. 2004). The initial void ratios in the cohesionless layers were determined using SPT data found in the literature. The initial void ratio in the cohesive soil layers is derived from the constitutive equation assuming OCR = 1. The conducted site response analysis assumes one-dimensional wave propagation. We use for the validation the borehole recordings at different depths from the 1995 Hyagoken-Nanbu earthquake. At the model's base, we apply the acceleration record from the 83 m depth. The calculated and measured horizontal velocities at the other two recording locations show a good agreement (Fig. 5b). In addition, a pronounced reduction of the effective stress is observed in the sand layers at the end of the earthquake. This result agrees with the extensive soil liquefaction observed at Kobe Port Island during the 1995 earthquake.

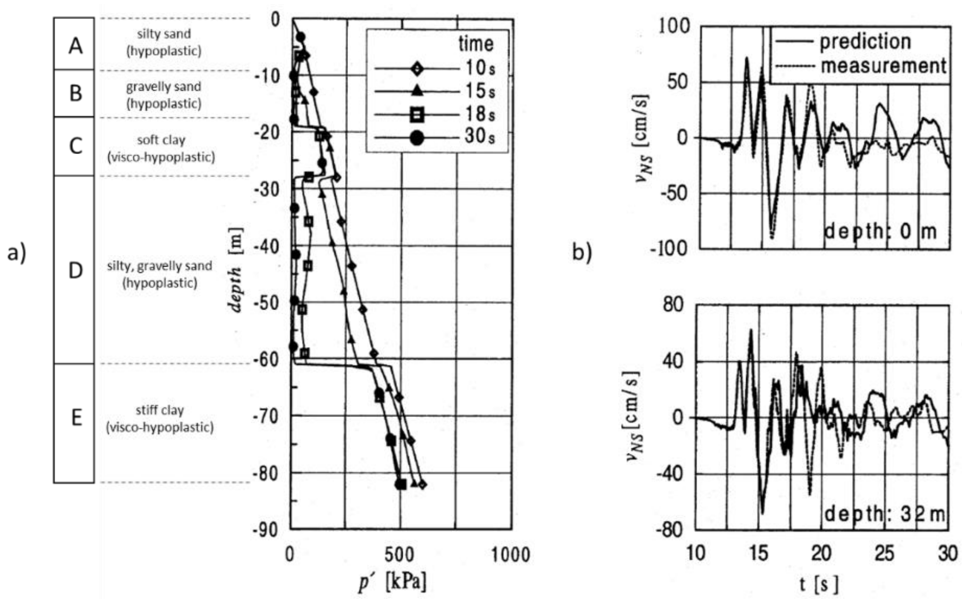

Figure 5: a) Simplified profile for back analysis of the Kobe Port Island ground profile and calculated effective pressure vs. depth after 10, 15, 18, and 30 s, respectively, and b) numerical and measured horizontal shaking during the 1995 earthquake at the surface and in a depth of 32 m, according to (Gudehus et al. 2004)

Third validation phase: Insights into considering anisotropic stress states and multi-directional loading conditions in BVP

Since the non-zero initial static shear stress and the multi-directional shearing induced by the earthquake can influence the undrained behavior of tailings, the ability of the constitutive model to capture both effects must also be checked. It is worth mentioning that most constitutive models found in the literature needed to be validated for multi-directional simple shear loading. Moreover, due to the technical difficulties of conducting multi-directional cyclic shear tests, the experimental database available for validating constitutive models for multi-directional loading paths is scarce.

Using the hypoplastic model and the parameters of Karlsruhe Sand given in (Csuka et al. 2023), we investigate the liquefaction resistance for in-plane and anti-plane undrained cyclic shearing. In the element test simulations (simple shear), the initial relative density and the vertical stress are I_d = 0.85 and 100 kPa, respectively. K_0 conditions are assumed to estimate the initial horizontal stress. The simulations are conducted for different initial shear stresses, defined by the factor $\alpha = \tau_{xz} / \sigma_{v,0}'$. As can be seen in Fig. 6a, higher initial shearing leads to a higher liquefaction resistance for in-plane shearing. However, for the anti-plane case, CSR reduces with increasing initial shear stress (see Fig. 6b).

In Fig. 7a, the K_α factor for dense sand, defined as $K_\alpha = CRR_\alpha / CRR_0$, where CRR is the CSR (Cyclic Stress Ratio) for N = 10 cycles, is compared with the experimental range of K_α for sands proposed by (Harder & Boulanger, 1997). As can be seen, the calculated values of K_α lie in the range of the experimental ones for both in-plane and anti-plane. The ratio between the CRR for the in-plane and anti-plane loading also shows a good agreement with experiments (Fig. 7b).

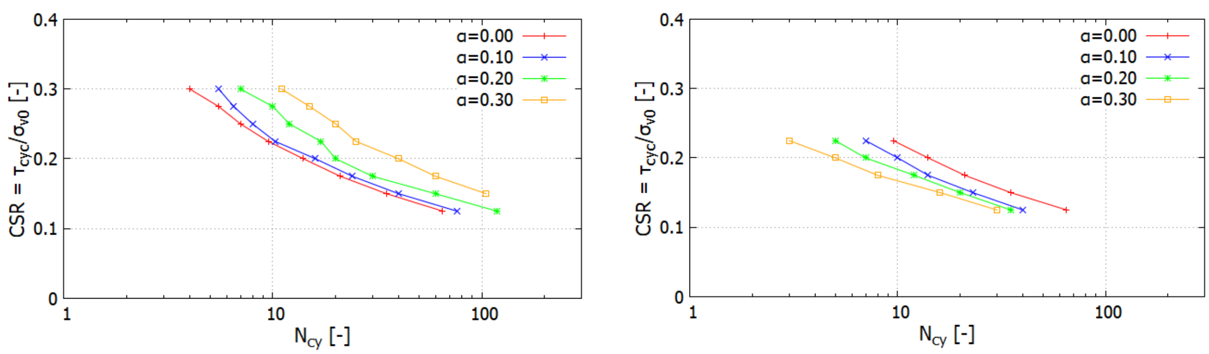

Figure 6: Cyclic shear ratio dependence on initial static shear stress in cyclic shear test for a) in-plane and b) anti-plane loading

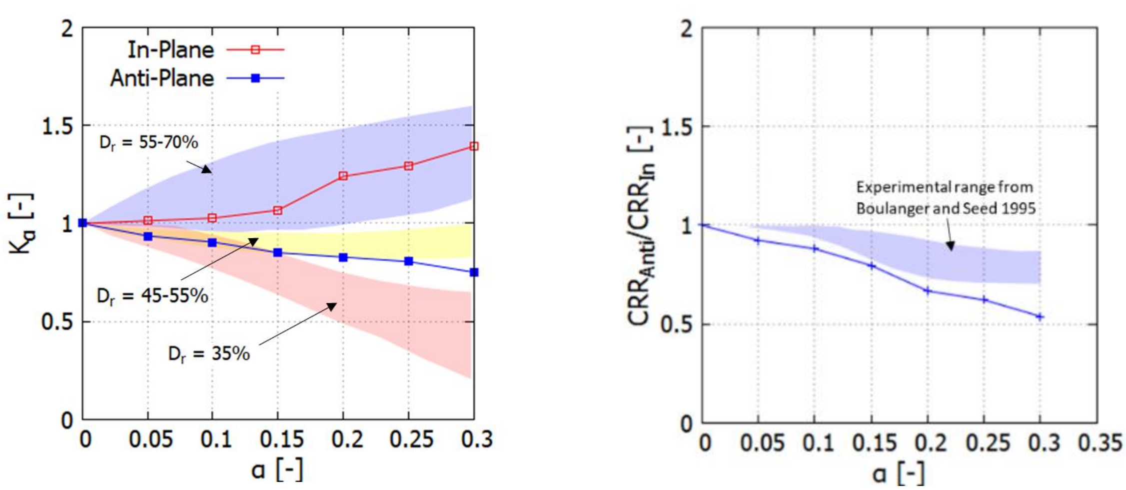

Figure 7: Influence of initial shear stress on a) K_α factor and b) In-Plane / Anti-Plane liquefaction ratio, from (Csuka et al. 2023)

6th Benchmark: Inclined homogeneous saturated soil layer

To assess the implications of the results presented in the last paragraph, we consider the shaking of an infinite slope under undrained conditions (Fig. 8). Infinite slope conditions are imposed by constraining the nodes at the same level to undergo the same displacement. Different slope inclinations were set by activating the gravity in the xz-plane at different inclination angles. The base excitation is harmonic with f = 2 Hz and an amplitude of 0.2 m/s. The simulations consider two initial densities of Id = 0.15 and 0.85. The evolution of the displacements at the slope's surface over the shaking time is shown in Fig. 9. As can be seen, the displacements increase exponentially for the loose soil layer and are independent of the shaking direction. This response results from soil liquefaction at the base of the column and slope sliding downward as a rigid block. The comparison with the free fall solution, which is shown exemplarily for the 10° slope inclination, confirms the significant decay of the shear resistance due to liquefaction (Fig. 9a). For the dense soil layer, the results for a given slope inclination show that the in-plane displacements induced by anti-plane shaking are much larger than those generated by in-plane shaking. Several results found in the literature support these results. (Gudehus et.al. 2004) showed that a rigid block on an inclined plane with frictional contact of the Coulomb type undergoes more significant in-plane deformations due to anti-plane than in-plane loading. Infinite slope conditions simulations using a coupled lattice Boltzmann discrete element method (El Shamy and Abdelhamid, 2016) showed that anti-plane shaking led to slightly larger deformations than the in-plane loading. As can also be seen in Figure 9b, the displacements increase by increasing the inclination angle for the anti-plane case. In contrast, the largest displacements occur in the in-plane case for the 5 ° inclination and the lower at 15° inclination. Although these results may seem counterintuitive, the larger accumulation at lower inclination levels can be attributed to the effect of initial static shear stress, as shown by the results of triaxial tests from the literature (Yang and Sze 2011a,b). However, to the authors' knowledge, 1-g or n-g model test results are missing in the literature to validate these results.

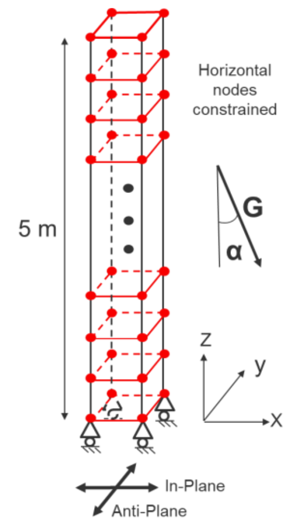

Figure 8: Numerical model of the infinite slope used for the simulations

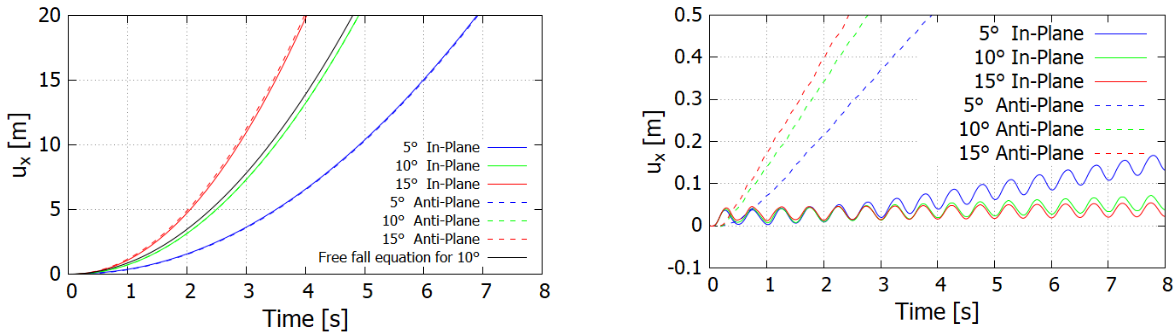

Figure 9: Influence of inclination angle on the displacements for in-plane and anti-plane shaking for a) loose sand layer and b) dense sand layer

Conclusion

The high failure rate of tailings storage facilities and the foreseen increment in the number and the size of new facilities highlight the need for more comprehensive guidelines and the use of advanced tools to address the several challenges arising during the design, construction, operation, and closure of TSFs.

For the seismic performance of TSF, simplified quasi-static approaches with inertial forces and 'cyclic shear strength' can be used in a preliminary design phase. However, advanced numerical models calibrated and validated using laboratory, in-situ experiments, and monitoring data are required for realistic predictions of the behavior of TSFs in the serviceability and limit states.

The constitutive model used to model the behavior of the tailing material has to go through a comprehensive validation process with different degrees of complexity. In the first step, the model should be able to capture the response of the tailing at an element level. After that, the plausibility of the model response and the numerical robustness shall be further assessed using numerical and experimental benchmarks, including homogeneous, layered, and sloped ground under dynamic shaking. Particularly, the capability of the constitutive models to capture the influence of multidirectional shearing and the initial static shear stress on liquefaction susceptibility shall be assessed, as multi-directional simple shear devices are seldom used in the development of constitutive models.

After validating the hypoplasticity model with the proposed approach, we conclude that the model contains the features required to realistically predict the seismic response of TSFs. Nevertheless, the validation of the model response could not be completed for sloped ground due to a lack of appropriate experimental data. Therefore, we plan centrifuge tests with sloped ground to generate the required database.

References

Arulanandan K, Scott RF (1993): Verification of numerical procedures for the analysis of soil liquefaction problems. In: Proceedings of the international conference on the verification of numerical procedures for the analysis of soil liquefaction problems. Vols. 1 and 2. Rotterdam (The Netherlands): A. A. Balkema; 1993–1994

Azam, S., & Li, Q. (2010). Tailings dam failures: a review of the last one hundred years. Geotechnical news, 28(4), 50-54.

Boulanger R, Seed R (1995) Liquefaction Of Sand under Bidirectional Monotonic and Cyclic Loading. Journal of Geotechnical Engineering 121(12):870–878

Csuka, A.; Grandas-Tavera, C.E.; & Cudmani,R. (2023). Numerical investigations on the influence of initial static shear stress in bi-directional loading of dense sand. 10th European Conference on Numerical Methods in Geotechnical Engineering. https://doi.org/10.53243/NUMGE2023-45

Cudmani,R.,Osinov,V.,Bühler,M.M.,Libreros,A.-B.,Gudehus,G.(2003): A model for evaluation of liquefaction susceptibility in layered soils due to earthquakes. Proceedings of the 12th Panamerican Conference on SMGE, Cambridge USA, vol.II: 969–976

Dobry, R., Thevanayagam, S., Medina, C., Bethapudi, R., Elgamal, A., Bennett, V. (2011). Mechanics of lateral spreading observed in a full-scale shake test. Journal of Geotechnical and Geoenvironmental Engineering, 137(2): 115–129. https://doi.org/10.1061/(ASCE)GT.1943-5606.0000409

El Shamy U, Abdelhamid Y. Some aspects of the impact of multidirectional shaking on liquefaction of level and sloping granular deposits. J Eng Mech 2016;143(1):C4016003.

Gudehus G, Cudmani RO, Libreros-Bertini AB (2004) In-plane and anti-plane strong shaking of soil systems and structures. Soil Dynamics and Earthquake Engineering 24:319–342

Harder LF, Boulanger RW (1997) Application of Kσ and Kα correction factors. In: Technical Report NCEER-97-0022, National Center for Earthquake Engineering Research, pp 167–190

ICOLD. (2001). Tailings dams: risk of dangerous occurrences: lessons learnt from practical experiences (Vol. 121)

Kramer SL (1996) Geotechnical Earthquake Engineering. Prentice-Hall

Kutter, B., Carey, T., Hashimoto, T., Zeghal, M., Abdoun, T., Kokalli, P., Madabhushi, G., Haigh, S., Hung, W.-Y., Lee, C.-J., Iai, S., Tobita, T., Zhou, Y. G., Chen, Y., & Manzari, M. T. (2017). LEAP-GWU-2015 experiment specifications, results, and comparisons. International Journal of Soil Dynamics and Earthquake Engineering. https://doi.org/10.1016/j.soildyn.2017.05.018

Niemunis A, Herle I (1998) Hypoplastic model for cohesionless soils with elastic strain range. Mechanics of Cohesion-Frictional Materials 4:279–299

Niemunis A. (2003) Extended Hypoplastic Models for Soils. No. 34, Habilitation Thesis at the Institute of Soil and Rock Mechanics, University of Bochum; 2003

Osinov VA (2000). Wave-induced liquefaction of a saturated sand layer. Continuum Mech Thermodyn 2000;12(5):325–39

Osinov VA, Gudehus G. (2003) Dynamics of hypoplastic materials: theory and numerical implementation. In: Hutter K, Kirchner N, editors. Dynamic response of granular and porous materials under large and catastrophic deformations. Berlin: Springer; 2003. p. 265–84.

Pralle N, Gudehus G. (2000) Compaction of loose flooded granular masses using air pulses. In: Kolymbas D, Fellin W, editors. Compaction of soils, granulates, and powders. Advances in geotechnical engineering and tunneling, Balkema, vol. 3.; 2000. p. 207–31

Seed HB, Idriss IM (1970) Simplified procedure for evaluating soil liquefaction potential. Journal of the Soil Mechanics and Foundations Division 107:1249–1274

Suazo, G., A. Fourie, J. Doherty, and A. Hasan. (2016) "Effects of confining stress, density and initial static shear stress on the cyclic shear response of fine-grained unclassified tailings." Géotechnique66 (5): 401–412. https://doi.org/10.1680/jgeot.15.P.032

Villavicencio, Gabriel; Espinace, Raúl; Palma, Juan; Fourie, Andy; and Valenzuela, Pamela. (2013). Failures of sand tailings dams in a highly seismic country. Canadian Geotechnical Journal. 51(4): 449-464. https://doi.org/10.1139/cgj-2013-0142

Vucetic M, Dobry R (1991) Effect of soil plasticity on cyclic response. Journal of Geotechnical Engineering 117:89–107

Yang J, Sze HY (2011a). Cyclic behavior and resistance of saturated sand under non-symmetrical loading conditions. Géotechnique 61 (1): 59-73.

Yang J, Sze HY (2011b). Cyclic Strength of sand under sustained shear stress. Journal of Geotechnical and Geoenvironmental Engineering 137 (12): 1275-1285

Application of the SANISAND-SF Constitutive Model for Non-Linear Dynamic Analysis of Filtered Tailings Dams

Brahian Roman, SRK Consulting, Peru
Martín Villanueva, SRK Consulting, Peru
Andrés Barrero, SRK Consulting, Canada

Abstract

In the last decade, the use of filtered tailings has steadily increase in the mining industry in South America as it is an innovative solution for the construction of tailings storage facilities (TSF). This technology allows increasing the safety of tailings dams since it eliminates the slurry pond from the impoundment. Moreover, filtered tailings enhances the recovery of water for mining processes and enables the application of co-disposal schemes. Many TSFs are located in zones where major earthquakes may occur such as the countries located within the fire belt. Thus, the behavior of filtered tailings when subjected to large dynamic shear stresses must be assessed. The state-of-practice recommends the application of numerical modelling with advanced constitutive models capable of reproduce the behavior of tailings to assess the performance of TSFs against large earthquakes. There are many models already implemented in commercial software; nevertheless, these constitutive models have disadvantages when dealing with dynamic loading. For instance, the widely used PM4Sand model can only model boundary problems in 2D conditions. The HS Small model does not take into account explicitly the theory of critical state soil mechanics. The NorSand model is not suited for dynamic problems. Hence, there is a need for another constitutive model that cover these gaps. In this regard, the family of SANISAND constitutive models is a new option to be applied in mining. SANISAND-Sf was implemented in a finite difference software and applied in a real project located in zones where peak ground accelerations of 0.60g and higher are expected. This constitutive model is an improvement of the original SANISAND. The SANISAND-Sf includes a new set of parameters that allows reproducing the undrained cyclic behavior of granular soils when the effective confining stress is low and the material behaves in a semi-liquid state or semi-fluidized (SF).

Introduction

Filtered tailings are obtained through the mechanically dewatering of conventional tailings to reduce the water content and separate the solids from the liquids. The process of filtering the tailings involves passing them through a series of filters, such as a filter press or a belt filter, to remove the excess water. The resulting material is a dry, solid mass that can be transported and stored more easily than traditional slurry-like tailings called filtered dry stacked tailings facilities (Davies, 2018). These facilities are generally considered to be a safer and more environmentally friendly option for tailings management, as they reduce the risk of dam failures, runout distances and can minimize the amount of water and chemicals needed to treat the tailings. They also have the potential of co-disposal schemes by mixing tailings and waste rock.

However, despite the many advantages of this technology. There are still failure mechanisms that shall be addressed during the design stage. A failure mechanism is the earthquake-induced displacements and settlements specially in zones susceptible large earthquakes. Conventional pseudostatic analysis are not capable of modelling the effects of earthquakes in embankments and therefore the state of practice is moving toward Non-linear dynamic analysis using finite element or finite difference programs.

A set of non-linear dynamic analysis (NDA) of a filtered dry stacked tailings facility was carried out as part of a detailed engineering project for a mine expansion in a country where megathrust earthquake events are expected. This type of analysis is of great importance for ensuring the safety and stability of critical mining infrastructure assets. Two advanced state-of-the-art constitutive models based on critical state soil mechanics and bounding surface plasticity were used: the SANISAND-Sf (Barrero, 2020) and the PM4Sand (Boulanger and Ziotopoulou, 2017). The main objectives of the NDA were:

- Understanding the TSF behavior under extreme loading conditions: The probabilistic horizontal PGA range from 0.70g (2475 years of return period) to 0.80g (5000 years of return period). The NDA helps to understand how these extreme loading conditions affect the behavior of the TSF and its foundation.
- Identification of potential failure modes: Non-linear dynamic analysis can identify potential failure modes of the dam, such as slope instability, foundation failure, and earthquake-induced liquefaction. Identifying these potential failure modes help to design appropriate safety measures to prevent dam failure such as confirming that the proposed design of the overall downstream slope is adequate. Furthermore, seismic displacements (total and differential) can be estimated which could impact the underdrainage system.
- Optimizing design: NDA can be used to optimize the design. This analysis can help to identify the most suitable location, height, and other design parameters to ensure the safety and stability of the TSF under different loading conditions.

The analysis was performed using the software FLAC 2D (v.8.10). It considered a two-dimensional effective stress model in the time domain. Plane strain conditions were deemed suitable since the length of the filtered fry stacked tailings is much higher than the cross-section dimensions as seen in Figure 1.

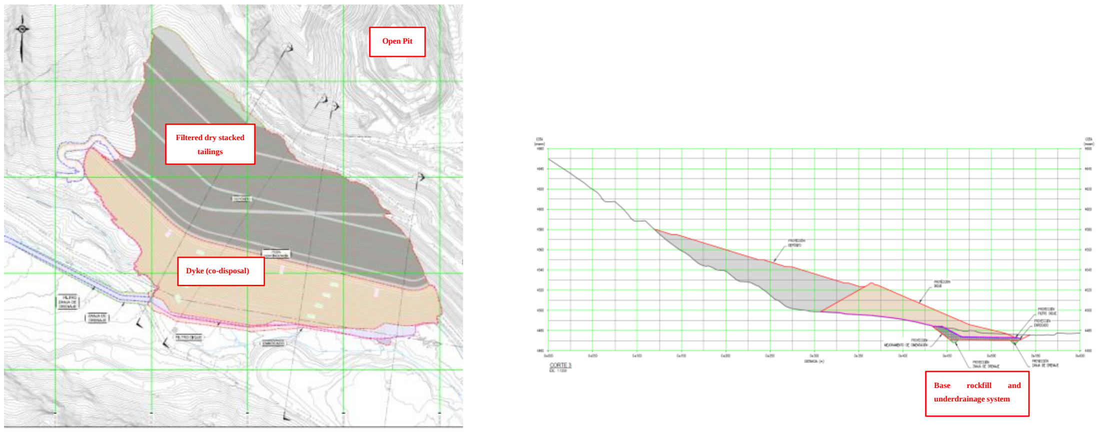

Figure 1: Plant view and cross-section number 3 of filtered dry stacked tailings

Model Setup

Model Geometry and Construction Sequency

The results of the NDA of only one cross-section are shown in this paper. Four main geotechnical units stand out: the filtered dry stacked tailings, the dyke made of co-disposal between filtered tailings and waste rock (ratio 3 to 1 respectively) and the base rockfill and underdrainage system. The mesh size selected was 2.5 m x 2.5 m to comply with accurate wave propagation criteria by Kuhlemeyer and Lysmer (1973). The modelling sequency follows the construction planning and is shown in Figure 2.

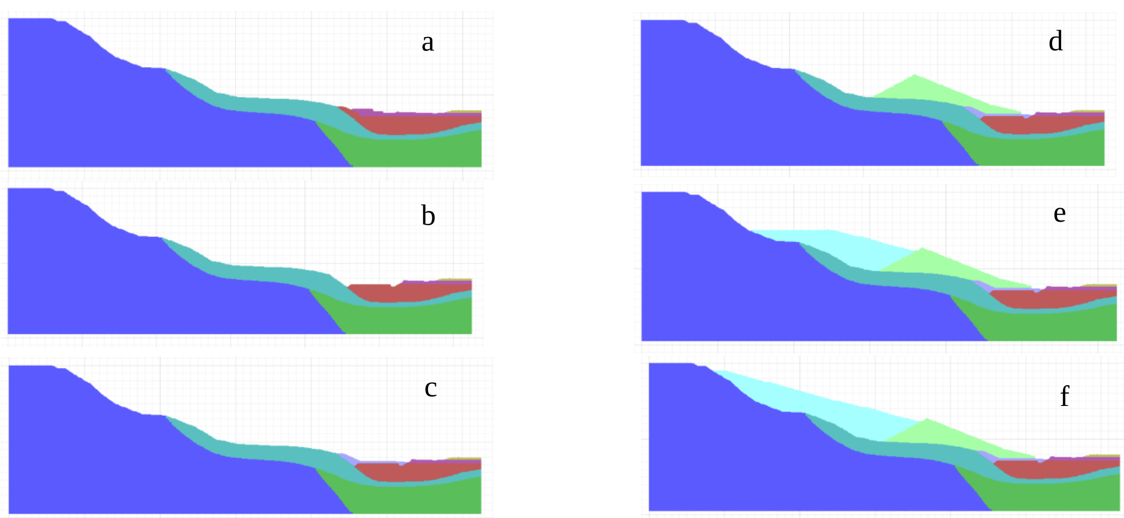

Figure 2: Modelling sequency: a) initial condition, b) foundation preparation, c) base rockfill placement, d) co-disposal placement for dyke construction, e) filtered tailings placement, f) final raise

Geotechnical Characterization

The geotechnical characterization of two geotechnical units were selected due to its relevance in the analysis: the filtered tailings (RF), the mix or co-disposal between filtered tailings and waste rock (MR). Moreover, an additional unit will be shown to be used as baseline: the whole tailings (RT) before undergoing cycloning, thickening and filtering processes. The three units have a great amount of non-plastic fines (IP<5) ranging from 55% for the mix or co-disposal, 70% for the filtered tailings and 60% for the whole tailings.

Table 1: Summary of standard properties of geotechnical units

Unit	Gravel	Sand	Fines	USCS	D50	LL	IP
	(%)	(%)	(%)	-	mm	(%)	-
MR	20.9	26.8	52.3	CL-ML	0.07	18	6
RF	0	29.8	70.2	CL-ML	0.032	19	7
RT	0	42.6	57.4	CL-ML	0.046	18	6

Constitutive Modelling and Associated Parameters

There are many advantages of using advanced constitutive models in geotechnical engineering since they enable more accurate predictions of soil behaviour under various loading conditions. These models can incorporate factors such as soil structure, nonlinearity, and anisotropy, which may not be accounted for in simpler models. In this chapter, the two constitutive models used for the NDA are briefly described.

SANISAND-Sf Constitutive Model (Barrero and Taiebat, 2020)

The SANISAND family is a widely used soil constitutive models that was first introduced by Dafalias and Manzari (2004). It is a modified version of the classical plasticity theory that incorporates the effects of fabric dilation and degradation of the soil matrix due to plastic straining. The model assumes that the soil matrix consists of a set of interconnected ellipsoidal particles, which are subject to anisotropic stress states. The deformation behaviour of the soil is described by three key parameters: the stress ratio, the fabric tensor, and the plastic potential. The stress ratio is defined as the ratio of the deviatoric stress to the mean stress. The fabric tensor describes the orientation and distribution of the ellipsoidal particles in the soil matrix, and is updated during plastic straining. The plastic potential represents the energy dissipation during plastic deformation. The SANISAND family model has been used to simulate the behaviour of a wide range of soils under various loading conditions, including cyclic loading and liquefaction. Barrero (2020) incorporated the effects of very low effective confining stress conditions in the model: the so-called “semi-fluidized” (SANISAND-Sf) part which upgraded the model to better simulate the cyclic undrained behaviour of granular soils when approaching the phase transformation surface. Although this model was developed originally for clean sands, it can be applied to the three aforementioned units (filtered tailings, co-disposal and whole tailings) given its low plasticity and granular condition the three unites are expected to have a sand-like behaviour. Nevertheless, caution and conservatism are necessary to avoid unrealistic results. Undrained monotonic triaxial compression tests were used to calibrate the model for static conditions as seen in Figures 3 and 4 (stress-strain and effective stress path diagrams). As can be seen, the model better represents plastic deformations for high confining stresses in all units. Moreover, all simulations reach the experimental critical state envelope at large deformations.

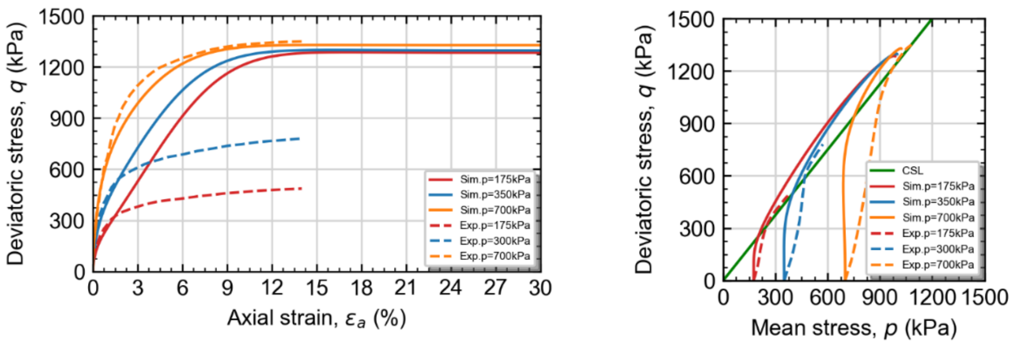

Figure 3: Undrained Monotonic Triaxial Compression Calibration for Co-disposal (CD)

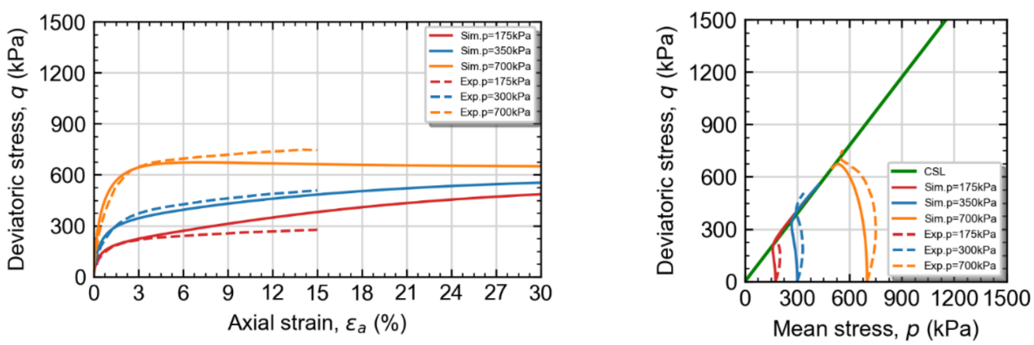

Figure 4: Undrained Monotonic Triaxial Compression Calibration for Filtered Tailings (FT)

For the undrained cyclic condition, a sensitive analysis was performed considering the liquefaction criteria as 3% of strain in single amplitude in CDSS condition (CDSS results were available only for filtered tailings). Figures 5 and 6 show the cyclic stress-strain behavior as well as the liquefaction triggering curves for the three units being studied.

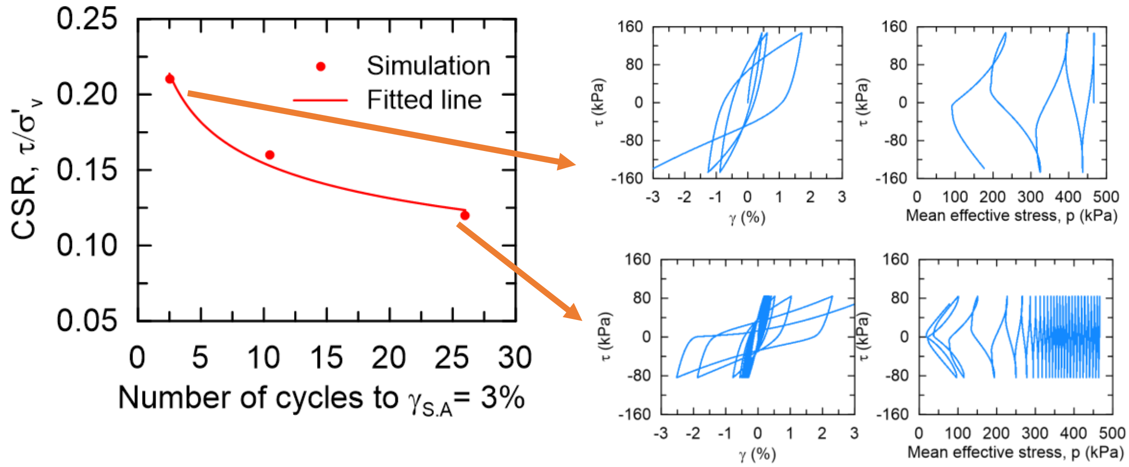

Figure 5: Undrained Cyclic CDSS Showcase for Co-disposal (CD)

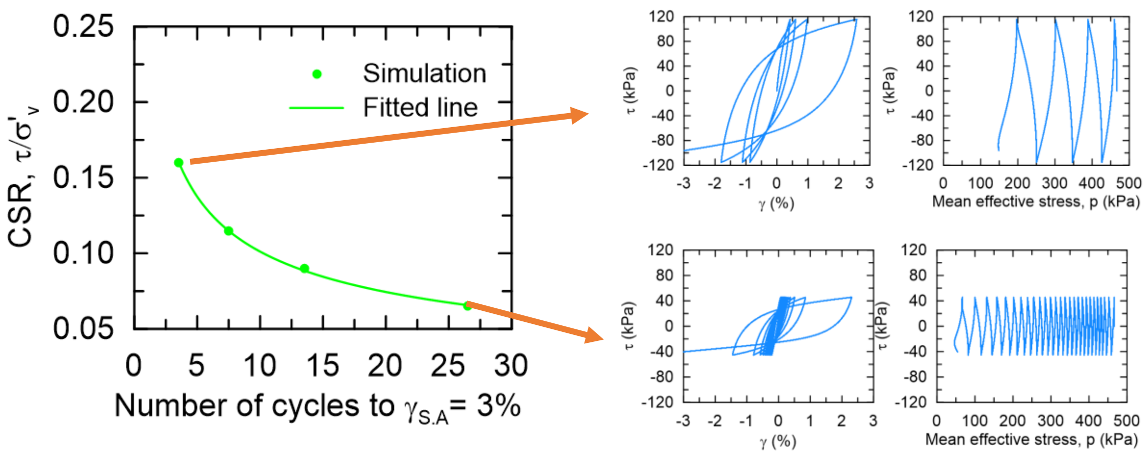

Figure 6: Undrained Cyclic CDSS Showcase for Filtered Tailings (FT)

Table 2 shows the parameters used for the generation of the soil response of a weightless' single-element model. The parameters are divided in 7 categories: Elasticity, Critical State, Yield Surface, Semi-fluidized Zone, Plastic Modulus, Dilatancy and Fabric Tensor. The parameters obtained for the calibration of experimental results on clean Toyoura Sand (Ishihara, 1993) by Dafalias and Manzari (2004) are presented as a reference. Differences of orders of magnitude in the range of values between Toyoura sand and the geotechnical units being studied are indicative of possible numerical instability. For instance, the co-disposal material requires parameters of the Semi-fluidized Zone and Fabric Tensor that are 5 times and 10 times bigger than those used for Toyoura sand respectively. These large differences also highlight potential limitations in the application of the model to the co-disposal unit.

Table 2: Summary of SANISAND-Sf parameters for single element soil response

Parameter	Variable	Co-disposal (CD)	Filtered Tailings (FT)	Whole Tailings (WT)	Toyoura Sand (*)
Elasticity	G_0	70	70	70	125
	ν	0.05	0.05	0.05	0.05
Critical State	M	1.3	1.3	1.33	1.25
	c	0.8	0.8	0.8	0.712
	λ_c	0.06	0.06	0.06	0.019
	e_c	1.05	0.9	0.99	0.934
	ξ	1.0	1.0	1.0	0.7
Yield Surface	m	0.03	0.03	0.02	0.01
Semi-fluidized Zone	x	20.0	3.0	3.0	4
	c_l	300	100	100	50
Plastic Modulus	h_0	5.0	5.0	9.0	7.05
	c_h	0.968	0.968	0.968	0.968

	n^b	0.5	0.5	0.5	1.1
Dilatancy	A_0	0.2	0.2	0.2	0.704
	n^d	2.5	0.7	0.7	3.5
Fabric Tensor	z_{max}	35	4.0	4.0	4.0
	c_z	9000	600	600	600

(*) Calibration of the model for experimental results on Toyoura sand by Dafalias and Manzari (2004)

Input Ground Motions

Both deterministic (DSHA) and probabilistic seismic hazard analysis (PSHA) were developed using recent ground motion prediction equations (GMMPE) like the Next-Generation Attenuation for subduction zone regions project (NGA-Sub). Figure 7 shows the response spectra in type B soil (IBC, 2021) comparing results for deterministic scenarios (intraplate Mw=8, plate interface Mw=9 and three faulting systems with 84th percentile), and probabilistic scenarios (return period of 2475 and 5000 years).

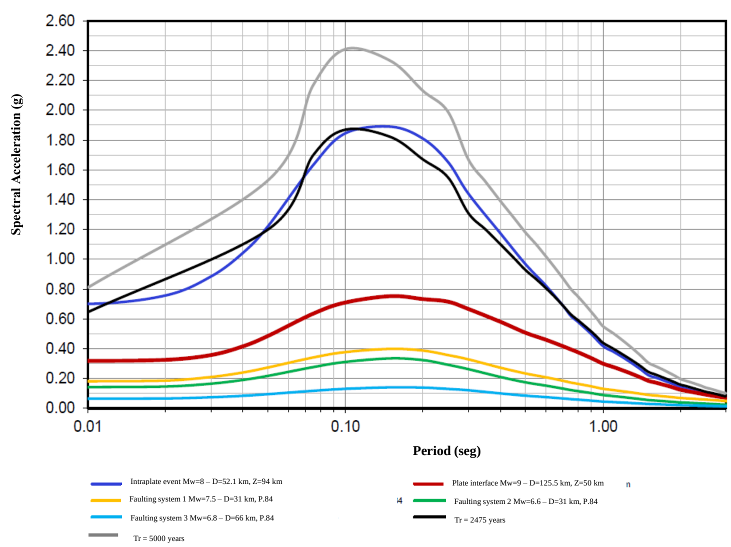

Figure 7: Deterministic and probabilistic response spectra in B type soil

The consequence classification of the filtered dry stacked tailings facility was defined as "very high" using the guidelines of the Global Standard on Tailings Management – GISTM (ICMM, 2020). Thus, the controlling earthquake must be either the Maximum Credible Earthquake (MCE) or the earthquake with a period of return of 5000 years. According to Martinez and Hull (2019), tailings storage facilities of high and above classification of consequence located in subduction zones shall be designed using the Maximum Credible Earthquake (MCE) to account for the important difference on peak ground accelerations (PGA) of both DSHA and PSHA. Therefore, the intraplate event was selected as the MCE with a PGA of 0.704g and a peak spectral acceleration of 1.90g at approximately 0.15 seg of period. The artificial ground motions for the NDA were performed by using the Spectral Matching technique from seed earthquakes of similar tectonic settings. Seven spectrally matched artificial ground motions were used for the NDA to assess the effects of different earthquake characteristics (duration, Arias intensity, frequency content, among others). This paper shows the results of the artificial ground motion which gave the highest value of displacements and shear stress patterns which correspond to the Maule earthquake that took place at Chile in 2010. It is worth mentioning that the earthquake-induced shear stresses are applied to the model as velocities after being deconvoluted following the recommendations of Mejia and Dawson (2006).

Result of Boundary Value Problem Simulation with the SANISAND-Sf model

Figure 8 “a” and “b” show the contours of vertical and horizontal displacements induced by the spectrally matched Maule earthquake (Chile, 2010). The filtered dry stacked tailings and the co-disposal dyke do not have a clear water table and their behavior require the application of partially saturated soil mechanics. Hence, no excess pore water pressures were obtained. Shear strains contours (Figure 8 “c”) are shown instead. The SANISAND-Sf model gives a maximum 2 m of vertical settlement in the crest of the co-disposal dyke and 3.5 m of maximum horizontal displacement in the downstream slope of the dyke. The maximum settlement and horizontal displacements of the filtered dry stacked tailings are 1.0 m and 2.5 m respectively. Regarding shear strains, three clear patterns can be seen in the filtered dry stacked tailings, the co-disposal dyke and the dyke’s foundation. These patterns are kinematically admissible and follow a non-circular slope instability failure mode reaching shear strains of 7.5% noticing a progressive failure through the foundation.

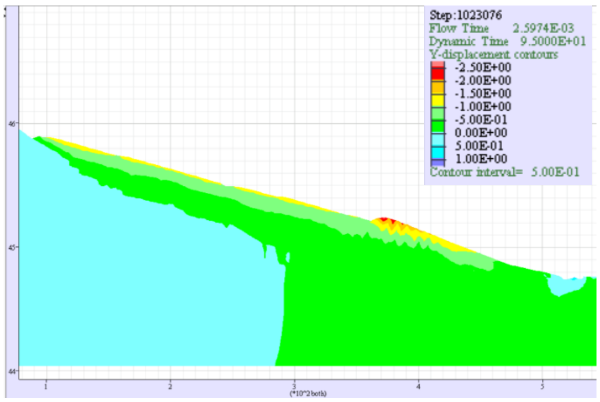

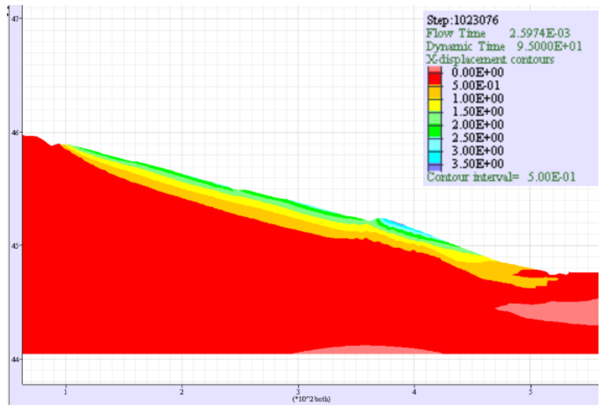

a **b**

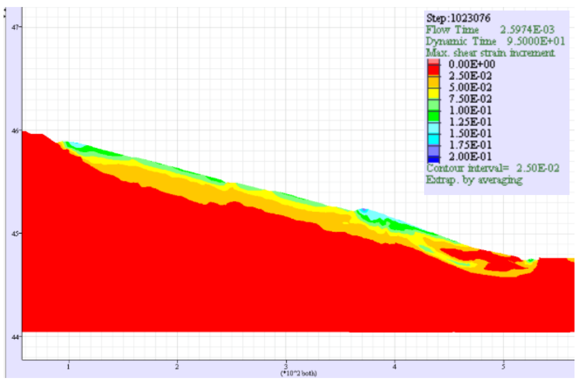

c

Figure 8: Contours of: a) vertical displacements, b) horizontal displacements and c) shear strains increments

Conclusion

The main findings obtained from the results of the NDA about the general seismic stability of the filtered dry stacked tailings facility are:

- 2D Plane strain conditions were deemed acceptable given the geometry and topography features of the filtered dry stacked tailings facility.
- The consequence classification defined for the filtered dry stacked tailings facility was "very high" according to GISTM principles which was used to define the controlling earthquake for the NDA.
- A set of seven spectrally matched earthquakes were applied at the base of the finite difference model for a filtered dry stacked tailing following recommendations for deconvolution. The results when applying the constitutive model SANISAND-Sf (Barrero, 2020) show that the highest values of displacements and shear strains were obtained for the Maule earthquake (Chile, 2010). This is

probably due to the higher values of parameters of the earthquake (long duration, higher Arias intensity, among others). This earthquake is representative of the tectonic setting of the site where the project is located.

- The model predicts deformations patterns in the filtered dry stacked tailings, the co-disposal dyke and through the foundation following a kinematically admissible non-circular progressive slope instability. Post-earthquake stability analysis can be conducted by reducing the available shear strengths of the units undergoing the highest shear strains.
- The highest displacements (vertical and horizontal) are higher than 1.0 m which indicates that the filtered dry stacked tailings facility will undergo important damages when subjected to the design earthquake loading although the facility is capable of withstand without reaching ground failure.
- The transient and permanent relative displacements predicted in the crest during the MCE scenario suggest the possible occurrence of longitudinal cracks along the crest of the co-disposal dyke as a result of seismic loading. However, the displacements induced by the MCE design earthquakes are finite and indicate that the crest of the dyke is stable in all the cases of seismic load analyzed.
- No liquefaction effects nor excess pore water pressures were taken into account given the high solids content of the units involved.
- The NDA shown are based on the most reasonable estimates of the geotechnical characterization of the materials. This characterization must be refined during construction and post-construction based on more advanced laboratory data, complementary site investigations and information from surveillance and monitoring.
- Despite being developed and calibrated for clean sands, the constitutive model SANISAND-Sf showed a fair match when calibrating the response of the triaxial and the CDSS test results. The filtered tailings are mainly low plasticity silts and therefore its behavior can be interpreted as sand-like. This low level of plasticity justifies the application of the SANISAND-Sf although effects of fabric and mineralogy play an important role and must be considered when evaluating the reliability of the model.

References

Barrero, A. (2020). “SANISAND-MSf: a sand plasticity model with memory surface and semi-fluidized state”. Géotechnique, 72(3):227-246

Bozorgnia et al (2020). “NGA-Subduction Project”. The Jhon Garrick Institute for the Risk Sciences. University of California at Los Angeles.

Dafalias, Y. F. and Manzari, M. T. (2004). “Simple plasticity sand model accounting for fabric change effects.” J. Engng Mech. 130, No. 6, 622–634.

Dafalias, Y. F. and Taiebat, M. (2016). SANISAND-Z: zero elastic range sand plasticity model. Géotechnique 66, No. 12, 999–1013

International Council of Mining and Metals (2020). Global International Standard on Tailings Management - GISTM

Kuhlemeyer, R.L. and Lysmer. J. (1973) “Finite Element Method Accuracy for Wave Propagation Problems”. Journal of the Soil Dynamics Division, 99, 421-427.

Groholski D, Hashash Y., Kim B., Musgrove M., Harmon J. and Stewart J. (2016). Simplified Model for Small-Strain Nonlinearity and Strength in 1D Seismic Site Response Analysis. Journal of Geotechnical and Geoenvironmental Engineering 142. 04016042. 10.1061/(ASCE)GT.1943-5606.0001496.

Davies, M.P. and S. Rice (2001), “An alternative to conventional tailing management – dry stack filtered tailings”. In proceedings of Tailings and Mine Waste 2001, Vancouver, Canada.

Davies, M.P. (2011). “Filtered Dry Stacked Tailings - The Fundamentals”. In Proceedings of Tailings and Mine Waste Conference 2011. Vancouver, Canada.

Hancock J., Watson-Lamprey J., Abrahamson N., Bommer J., Markatis A., Mccoyh E. and Mendis R. (2006). An improved method of matching response spectra of recorded earthquake ground motions using wavelets. Journal of earthquake engineering - J. Earthqu. Eng. 10.67-89. 10.1080.

Hynes M. and Franklin A. (1984). Rationalizing the Seismic Coefficient Method. Miscellaneous Paper GL-84-13, U.S. Army Waterways Experiment Station, Vicksburg, MS, 21 pp.

International Building Code (2015). 2015 International Building Code. International Code Council, INC (ICC) - USA.

Ishihara, K. (1993) Liquefaction and Flow Failure during Earthquake. Géotechnique, 43, 351-415.

Seed H. and Idriss, I.M. (1982). Ground Motions and Soil Liquefaction during Earthquakes. Earthquake Engineering Research Institute Monograph, Oakland.

Session 6:

Waste Piles

Compaction Performance of Iron Ore Tailings Mixture in the Iron Quadrangle

A. Freire, BVP Engenharia, Brasil
W. Pirete, BVP Engenharia, Brasil
P. Cella, BVP Engenharia, Brasil
D.Silva, BVP Engenharia, Brasil
P.Andrade, BVP Engenharia, Brasil
A. Oliveira, BVP Engenharia, Brasil
A. Risoli, Vale S.A, Brasil

Abstract

Due to regulatory policies that prohibit raising dams upstream in Brazil, research studies on alternative methods of disposal of filtered tailings in mining activities have been conducted in various mining companies, particularly in iron ore mines in the Iron Quadrangle. The objective of these studies is to reduce the need for slurry tailings disposal in dams, thereby minimizing the associated risks of downstream damage to tailings structures These studies involve experimental landfill tests to understand the behavior of compacted tailings and provide geotechnical parameters for design of Dry Stacking Tailings.

This paper presents the experiences obtained from the experimental landfill tests involving a mixture of filtered iron ore tailings (sandy and ultrafine mixtures). The study includes an evaluation of compaction performance by applying different energy variations, layer thicknesses and moisture content, as well as an analysis of the variabilities in physical characteristics and compaction curves of the tested iron ore tailings mixtures from Iron Quadrangle mines.

Introduction

For the disposal of tailings mixtures (sandy and ultrafine), a profound understanding of field compaction behavior is crucial to ensure optimal layer performance. In this context, in the experimental landfill tests of filtered tailings, referred to in this study as partial tailings (characterized by a composition of approximately 90% sandy and 10% ultrafine, by mass) and total tailings (characterized by a composition of approximately 80% sandy and 10% ultrafine, by mass), variations in moisture content representing operations during dry and wet seasons were tested. Additionally, variations in compaction energy (number of roller passes and vibration) and layer thicknesses were investigated.

The compaction performance results from the experimental landfill tests of the partial and total filtered tailings mixture were consolidated and interpreted to provide an integrated analysis of the mixtures. This analysis focused on behaviors related to void ratio reduction and variations in degree of saturation after compaction. Moisture content varied within the target range (close to optimum), as well as both below and above the target moisture range.

Methodology

The production of partial (90/10) and total (80/20) filtered tailings was achieved by incorporating ultrafine particles into the sandy tailings. In this process, the tailings generated from iron ore beneficiation are pumped to conditioners that supply a battery of hydrocyclones. These hydrocyclones separate the denser and coarser fractions (underflow) from the less dense and finer fractions (overflow) of the tailings.

The overflow stream from the cyclones proceeds to the slurry thickener, which also receives the filtered water from the tailings disc filtration system. The water resulting from the thickening process of the overflow is directed to a tailings dam, while the thickened material (ultrafine particles) is combined with the underflow from the cyclones (sandy tailings) for mixing in a conditioner. Subsequently, the mixture is fed into the disc filtration system, and the resulting filtered total tailings are directed to the experimental landfills. The unit filtration rate of the disk filter used in the experimental tests was 2.27 $t/h/m^3$ for partial tailings (90/10) and 1.53 $t/h/m^3$ for total tailings (80/20).

To assess the mechanical behavior of the filtered tailings, compaction was conducted using a smooth 20-ton roller (with and without vibration), as depicted in Figure 1a, b. Various layer thicknesses (30 cm, 50 cm, 70 cm, and 100 cm) and moisture contents (wet branch, dry branch, and near-optimal moisture content) were varied.

Figure 1: Compaction with a 20ton smooth roller of tailings mix (a) and sandy tailings (b)

Throughout the experimental tests, disturbed samples were collected for the purpose of conducting characterization tests, particle size analysis through sieving and sedimentation, following the guidelines of NBR 7181 (ABNT, 2018), as well as Proctor compaction tests according to NBR 7182 (ABNT, 2016).

For the evaluation of the compaction behavior of the tailings, the determination of in-situ bulk density was carried out using a drive cylinder, in accordance with the guidelines outlined in NBR 9813 (ABNT, 2016). The degree of compaction was determined using the Hilf Method - NBR 12102 (ABNT, 2020) - and subsequently confirmed through Proctor Compaction. Furthermore, the moisture content of the layers after compaction, void ratio, and degree of saturation were also examined.

Physical Characteristics and Compaction Curves of Filtered Tailings

In general, the characteristics of the filtered tailings are influenced by the raw ore and the industrial process used in beneficiation (Araújo, 2006; Ghose and Sen, 2001), for example, according Srivastava et al. (2001) an iron ore with a high clay content and which is softer generates more fine particles during mineral processing, which is reflected in the material's particle size curve.

Figure 2a, b depicts the grain size distribution curves of the tailing’s mixtures and the sandy tailings material tested, as well as the compaction curves for the three tested tailings typologies.

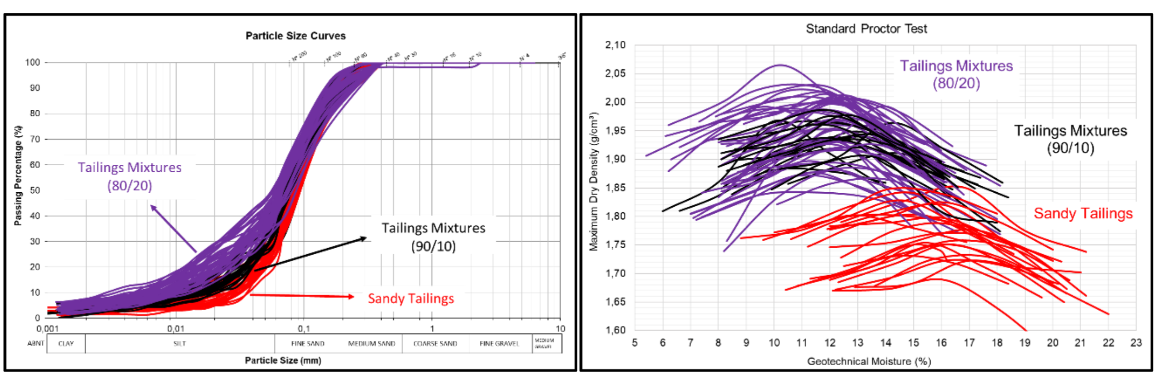

Figure 2: Particle size curves (a) and compaction curves of the tailings tested (b)

From the analysis of Figures 2a, there is an observed differentiation in the fine fraction of the tested tailings (below the #200 sieve), with notable percentages passing through 10µ and 45µ sieves, which are as follows:

- Sandy Tailings: Percentage passing through 10µ varied between 3% and 9%, and through 45µ ranged from 12% to 25%.
- 90/10 Tailings: Percentage passing through 10µ varied between 3% and 12%, and through 45µ ranged from 19% to 38%.
- 80/20 Tailings: Percentage passing through 10µ varied between 8% and 18%, and through 45µ varied from 25% to 45%.

Regarding the maximum dry densities and optimal moisture content obtained for the tailing's mixture (Fig. 2b), in comparison to the tailings without the addition of ultrafine, the following observations can be made:

- Tailings mixtures are more sensitive to variations in moisture content. Because of it, it's important to compact the tailings mixtures according to the " target Moisture Range " established in the "Base Case" in order to guarantee adequate compaction performance;
- Higher maximum Dry Density with the addition of ultrafine: This effect can be attributed to the concentration of iron fines in the ultrafine, which have a higher density than sandy tailings (approximately 3.6 to 3.9 g/cm³) with an increase in γs of the material;
- Lower Optimal Moisture Content with the addition of ultrafine: This effect can be attributed to greater packing of the tailing's mixtures, since the ultrafine fines occupy the empty spaces in the sandy matrix, reducing the amount of water needed to achieve maximum densification of the partial and total tailings, to the detriment of the sandy one. Figure 3 shows the optimum moisture variation as a function of the percentage of fines passing through 10µ.

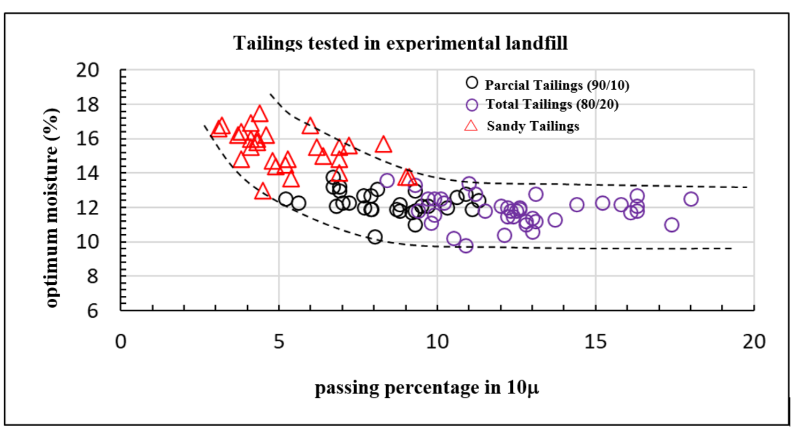

Figure 3: Optimum humidity vs percentage passing in 10 µ

The coefficients of uniformity (CU) and curvature (CC) of the tailing's mixtures tested, as well as the tailings without the addition of ultrafine, were obtained based on the particle size distributions of the materials. Table 1 shows the average CU and CC values for each type of tailings tested in the landfill.

Table 1 – Variation ranges of the Coefficients of Uniformity and Curvature of the Tailings Tested

Sample	Coefficient of Uniformity (CU)	Coefficient of Curvature (CC)
Sandy Tailings	3,8	1,4
90/10 Tailings	6,5	1,9
80/20 Tailings	11,4	2,1

From the comparative analysis of the coefficients of uniformity (CU) among the tailings types, there is an indication that in the sandy tailings, particle diameters are more similar when compared to the total and partial tailings, resulting in a lower coefficient of uniformity (CU<6).

Therefore, for the amount of fines used in experiments, it is suggested that the addition of ultrafine material to the sandy matrix contributes to a better particle size distribution of the material. This means that the spaces left by larger particles are filled by the smaller particles of the ultrafine tailings, promoting an improvement in the packing and interlocking condition of particles (partial fitting between adjacent particles). This leads to increased strength and reduced compressibility of the material when compacted close to the optimum moisture content.

Base Case Composition of Tailings Mixtures

Based on the interpretation of the tests conducted on the tested tailings in the experimental landfills, it was observed for both the partial tailings and the total tailings, a variability in the particle size distribution and compaction curves that represent each tailings typology. It was not possible to perform a test with a specific control that would accurately represent the exact proportion of a mixture.

This variability is linked to various operational causes, varying according to the type of ore processed in the plant or the influence on the filtering process, such as flocculant dosages, control of the proportion of ultrafine mass in the mixture, as in this case, as well as control of the pulp density in the disc filter feed.

Even though there were observed differences in particle sizes between the partial and total tailings, an overlap in optimal compaction densities and moisture content was noticeable, leading to similar compaction performance when compacted close to the target moisture levels.

Therefore, in a scenario where controlling a specific mixture type was challenging, an approach was taken to address the variations in tailings mixtures. This approach aimed to represent the material generated by the plant and incorporated mixture proportions ranging from 90/10 to 80/20, forming what is referred to as the "Base Case".

In addition to the delineation of granulometric limits, a treatment of the unified compaction curves of the tested tailings was also proposed, with a target moisture content for compaction being defined, resulting in degrees of saturation below 80%, void ratios below 0.60, and a degree of compaction above 95%, seeking to obtain the material's expansion behavior. Thus, for moisture control in tailings disposal, limits were identified between 10.5% and 12.5%. The granulometric limits and the desired humidity thresholds are shown in Figure 4a, b.

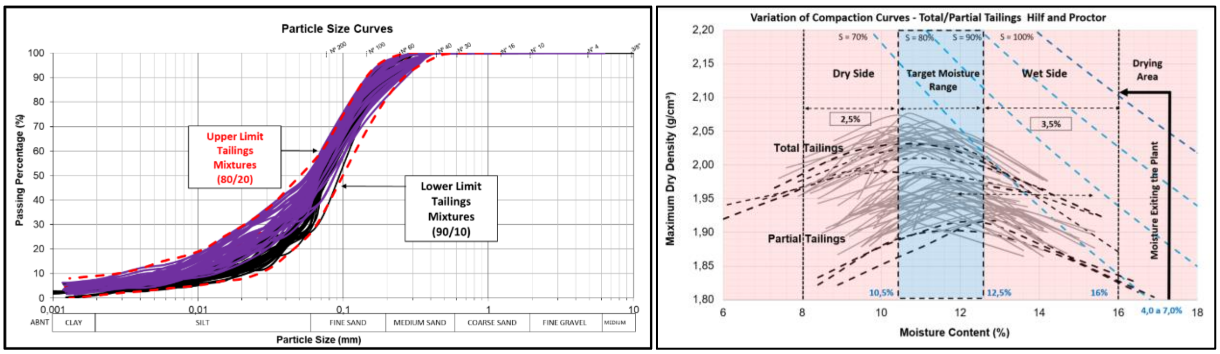

Figure 4: Base Case Grain Size Limits(a) Target moisture ranges for compaction (b)

As can be observed in Figure 4, several crucial pieces of information are interpreted and established as construction controls for achieving proper compaction performance and consequently low void ratios and low degrees of saturation below 80%. The key points are outlined as follows:

- Target moisture range: Moisture variation between 10.5% and 12.5%, interpreted as optimal compaction performance for both partial and total tailings (Base Case);
- Wet branch moisture range: Moisture variation between 12.5% and 16%, interpreted as moderate compaction performance for both partial and total tailings (baseline case), with the presence of "borrachudo" (a term often used in Brazilian mining for sticky, plastic clay-like materials);
- Dry branch moisture range: Moisture variation between 8% and 10.5%, interpreted as moderate compaction performance for both partial and total tailings (Base Case), requiring vibration for enhanced performance.

Thus, it can be observed that the compaction performance of the tailings mixtures in the field relies primarily on pre-compaction moisture control, avoiding reworking of layers due to inadequate compaction performance, as well as the effects of rubberization or water exudation.

The study then proceeds with an analysis of the compaction performance of the layers within the target moisture range, comparing them to the results of layers compacted in the wet and dry ranges. This analysis examines key technological controls such as in-situ dry density, void ratio, and degree of saturation.

Compaction performance as a function of field energies and moisture ranges

Regarding the compaction performance, the analyses were conducted with a focus on referencing the results obtained from Standard Proctor Tests. In total, 12 layers were constructed, varying in thickness, compaction energy (number of passes with and without vibration), and moisture content (dry, wet, and target for compaction). Figure 5 displays the layout of tracks within the experimental landfill.

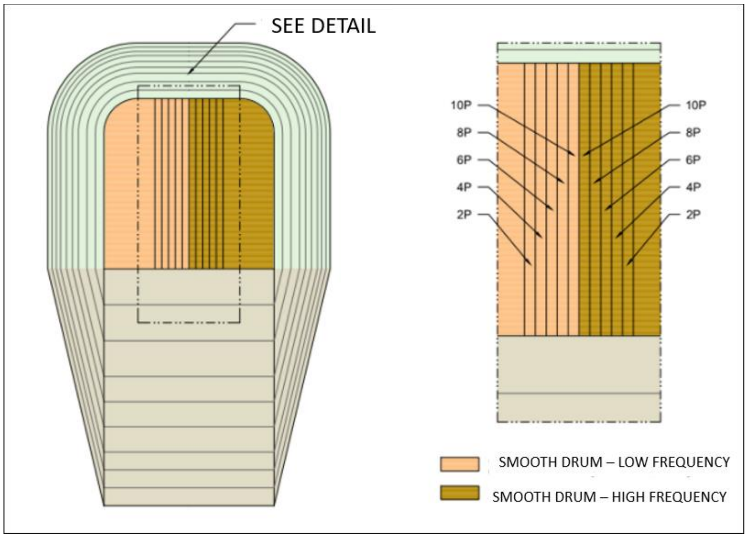

Figure 5: Layout of the experimental landfill: variation of energies and number of passes

In Figures 6a, b, as well as in Figures 7a, b, the compaction performance is illustrated as a function of the number of passes for the 50 cm layers of both partial and total top/base tailings. It's worth noting that layers above 50 cm did not exhibit satisfactory compaction performance due to challenges in achieving uniformity in thicker layers, achieving consistent moisture distribution top/base, and reducing compaction gradients. Hence, this study will primarily focus on analyzing the performance of the 50 cm layers.

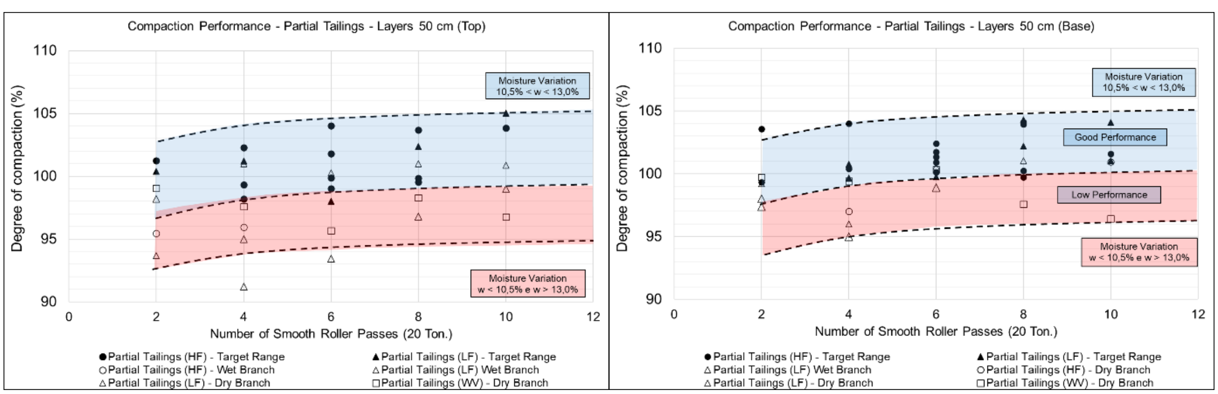

Figure 6: Compaction performance partial tailings top (a) and bottom (b)

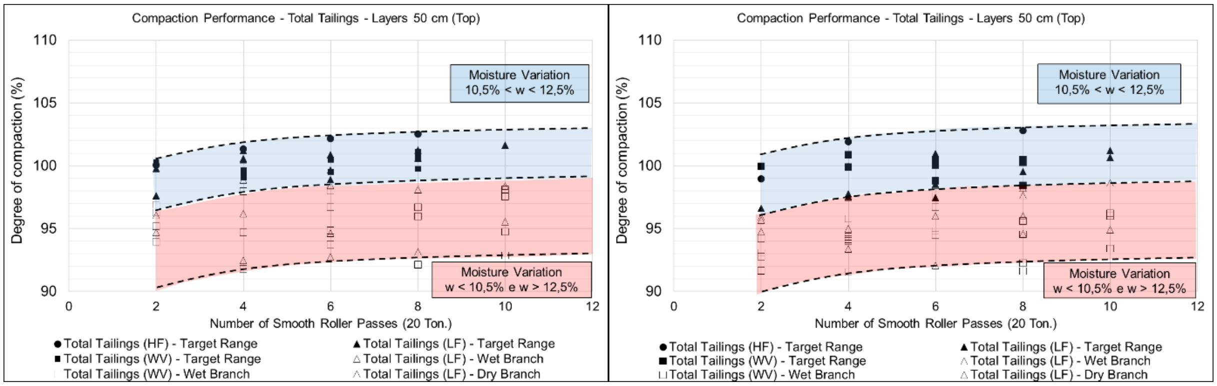

Figure 7: Compaction performance total tailings top (a) and base (b)

With regard to in situ performance, with variations in compaction energy, number of passes and humidity, the following points can be seen from the analysis of Figures 6 and 7 as a function of the energies applied and compaction humidity ranges:

- Partial and Total Tailings: Compaction degrees exceeding 95% were achieved after 2 passes, and over 98% after 4 passes using the 20-ton smooth roller at both low and high vibration frequencies. This was achieved for compacted layers within the optimal moisture range (between 10.5% and 13.0% for partial tailings, and between 10.5% and 12.5% for total tailings).
- Total Tailings: Sensitivity in the rubberized behavior was observed starting from a moisture content of 12.5%.
- Base Case Tailings: Moisture controls ranging from 10.5% to 12.5%, implemented after 4 passes, aimed to ensure uniformity at the top and base of the layer. This addresses potential moisture variations, operational fluctuations in compaction (roller speed), and potential discrepancies in technological control assays.

In both cases, a notable performance decrease was observed for the compacted layers with moisture content below 10.5% (dry branch) or above 12.5% to 13.0% (wet branch), with degrees of compaction falling below 95%. These findings underscore the necessity of moisture control near the optimum level, as under this condition, all tests involving passes of the 20-ton smooth roller exhibited satisfactory compaction performance.

Compaction performance as a function of in situ dry density

Figures 8a, b shows the overall distribution of compaction degrees for the tailings of the Base Case within the target moisture range (between 10.5% and 12.5%) and in the wet regime (above 12.5%).

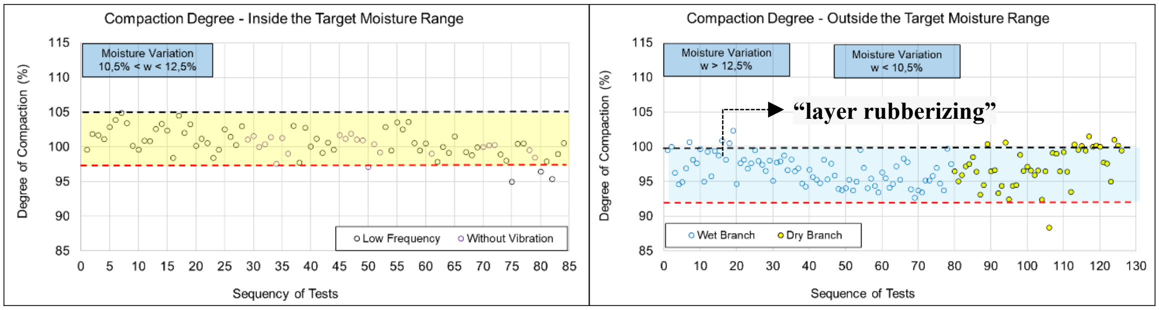

Figure 8: Degree of compaction Base Case tailings within the target moisture range (a) and outside the target moisture range (b)

In general, for compacted layers up to 50 cm thick using the 20-ton roller, compaction degrees (C.D) ranging from 100 to 105% are observed within the compaction moisture range of 10.5% to 12.5%. In the total tailing's material outside the target range, with moisture content in the wet regime, a rubbery behavior and water exudation on the surface were observed. Compaction degrees above 95% were noted, exhibiting a rubbery behavior that does not align with the macroscopic field response.

It was observed that, in this case, the compaction energy from the 20-ton roller after 2 passes was close to the intermediate energy range, resulting in compaction degrees above of 95% when using the Standard Proctor reference for layers exhibiting rubbery effects. The main focal points in the standardized compaction controls, based on the observed Hilf and Proctor tests, were as follows:

- Stringency in the timing of collecting the beveled samples, which should be done immediately after compaction, to avoid differences in wet density and moisture deviation between the moment of compaction and sample collection.
- Attention to the dispersion of results from the Standard Proctor tests compared to routine tests using the Hilf method.
- There will be outcomes with compaction degrees close to 100% in layers displaying rubbery behavior and dry densities below the minimum required.
- There will be results with compaction degrees above 100% in layers compacted within the Target Moisture Range.
- Greater uncertainty regarding the results and acceptance of compaction variations due to the variables presented, such as excessive compaction tests using the Hilf Method, routine repetitions, and changes in operators.

In this context, aiming to mitigate the uncertainties in compaction test routines, the technological monitoring of compacted layers in the experimental landfill was assessed using post-compaction dry density (γ_{dmin}). The minimum threshold for dry density (1.95 g/cm³) was established based on statistical analysis of the actual densities of tailings grains generated by the Plants (90th Percentile – 3.12) and the reference void ratio (0.60). Figure 9 displays the frequency distribution histogram of the obtained specific gravity.

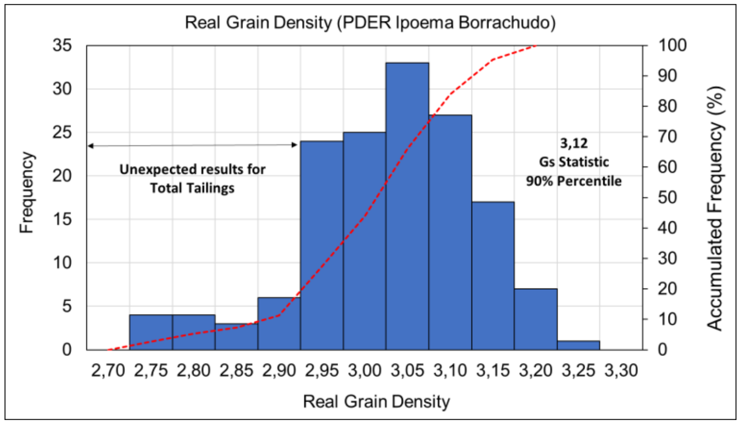

Figure 9: Frequency histogram Real Grain Density

Figures 10a, b as well as Figures 11a, b depicts the controls of dry density and void ratios obtained in the layers of the experimental landfill for the base case tailings compacted within the moisture target range and outside these limits.

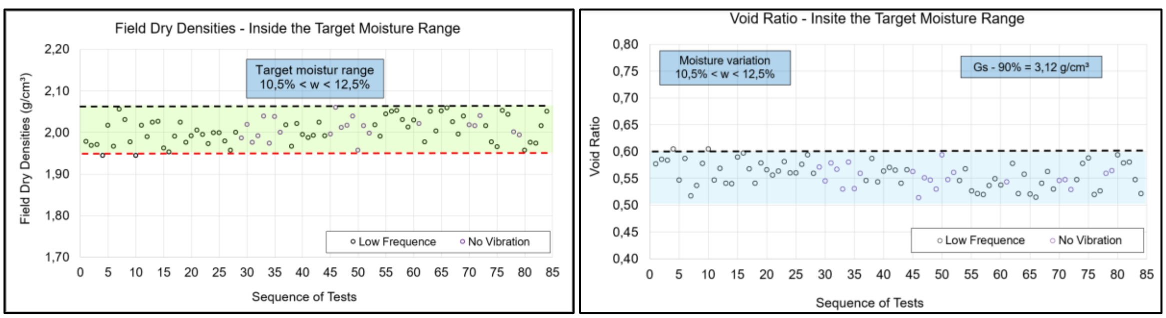

Figure 10: Field Dry Densities (a) and Index of Voids (b) - Within the Moisture Target

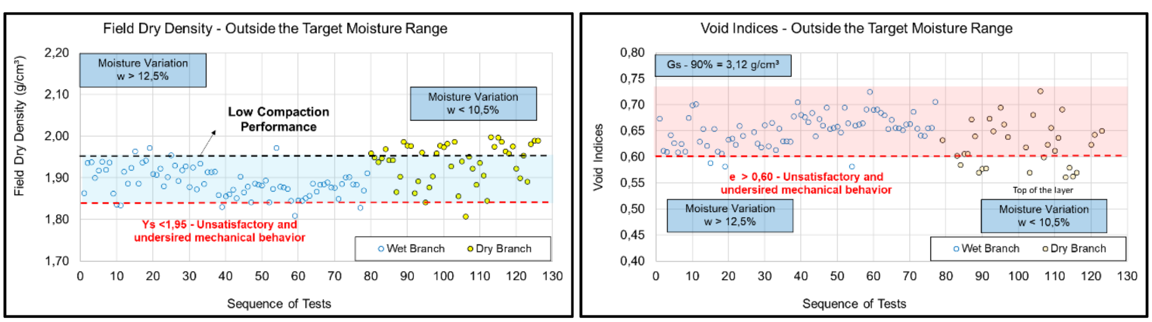

Figure 11: Field Dry Densities (a) and Void Indices (b) - Outside the Moisture Target

It is observed that the dry densities of the layers compacted within the moisture target thresholds (10.5% to 12.5%), exhibiting satisfactory behavior (void ratio below 0.60), exceeded the established statistical minimum threshold of 1.95 g/cm³. Conversely, for layers compacted outside the moisture target range (w < 10.5% or w > 12.5%), void ratios above 0.60 and dry densities below 1.95 g/cm³ were observed, reflecting the loss of mechanical performance in those layers.

It can be observed that the compaction control based on dry density exhibits strong representativeness and reliability compared to the Hilf and Proctor compaction control. Furthermore, the proposed approach of controlling by dry density eliminates the need for numerous Hilf/Proctor compaction tests during the tailing's storage facilities (T.S.F) operation, thereby reducing uncertainties within the approval process flow.

The control of minimum in-situ dry density can be carried out by collecting the cylinder and using a high-precision scale for weighing, along with moisture determination through methods like the sand bath or microwave techniques. These methods have demonstrated results with lower dispersion and greater convergence compared to moisture measurements taken in an oven within a timeframe of approximately 30 minutes (Fig.12a, b).

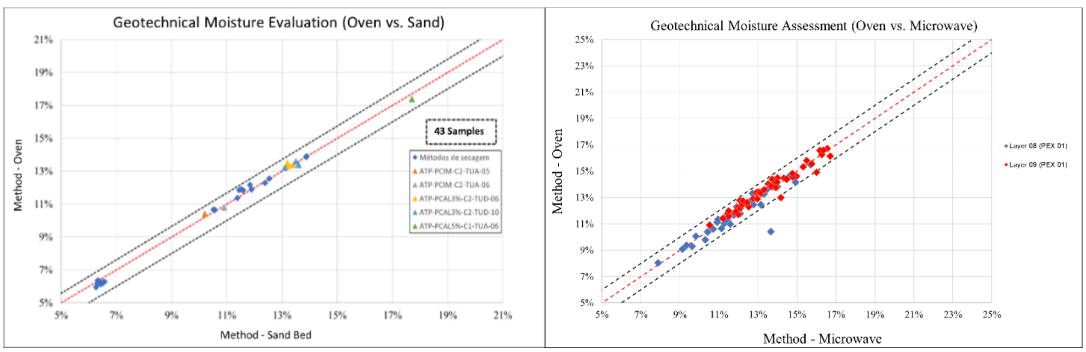

Figura 12: Tests for moisture measurement: Sand cushion (a) and microwave (b).

Conclusion

In this study, the objective was to assess the compaction performance of mixtures consisting of sandy and ultrafine tailings (partial and total tailings) in proportions of 90/10 and 80/20, within the optimal moisture range, both in the dry and wet regimes. This assessment was conducted at varying compaction energies and layer thicknesses.

In a general, satisfactory compaction performance was observed for 50 cm layers within the moisture range of 10.5% to 12.5%. For the wet regime (w > 12.5%), rubbery effects and water exudation were observed. However, when monitored using Hilf and Standard Proctor tests, compaction degrees above 95% were noted even for layers displaying rubbery behavior, in which compaction energy is transferred to the air and water system.

Given the variability of tailings produced on an industrial scale, influenced by mining fronts or filtration processes, as well as potential variations in Hilf tests during continuous execution, a statistical treatment of actual grain densities (P90) was performed. Using a reference void ratio, a minimum dry density value was established for monitoring the disposal of tailings.

It was observed that monitoring through statistical dry density obviates the need for multiple Hilf compaction tests, reducing uncertainties within the approval process flow. Additionally, it adequately represents the targeted compaction performance focusing on void ratios, always on the dilatant side, with a saturation degree below 80%. For this monitoring approach, it's recommended to continually update the statistical specific gravity through routine tests, reflecting possible variations in tailings production throughout the operation of the PDRs.

In summary, for monitoring the operation of tailings storage facilities, the following measurements can be carried out:

- Evaluation of tailings granulometries according to the Base Case thresholds;
- Target Moisture Range in accordance with the Base Case thresholds;
- Absence of “borrachudo” and Laminations;
- Statistical Minimum Dry Density and Maximum Void Ratio;
- Saturation Degree below 80%.

Acknowledgements

Special thanks to the team at BVP Geotechnics and Hydrogeotechnics, alongside the technical team from Vale's experimental landfill area, for their support during the development of experimental studies on filtered tailings. The results presented in this study have expanded our understanding of the compaction and mechanical behavior of filtered tailings mixtures.

References

Araújo, C.B. 2006. Contribuição ao estudo do comportamento de barragens de rejeito de mineração de ferro. Universidade Federal do Rio de Janeiro. Dissertação de Mestrado em Engenharia Civil. Rio de Janeiro. Disponível em: <http://www.coc.ufrj.br/index>. Acessado em: 04/10/2023

Associação Brasileira de Normas Técnicas. NBR 7181. 2016: Análise granulométrica. Rio de Janeiro, p. 12. 2016.

Associação Brasileira de Normas Técnicas. NBR 7182: Ensaio de Compactação. Rio de Janeiro, p. 09. 2020.

Associação Brasileira de Normas Técnicas. NBR 9813: Solo – Determinação da massa específica aparente in situ, com emprego de cilindro de cravação. Rio de Janeiro, p. 05. 2016.

Associação Brasileira de Normas Técnicas. NBR 12102: Solo – Controle de compactação pelo método de Hilf. Rio de Janeiro, p. 21. 2020.

BVP Engenharia e Hidrotecnia. 2023. Relatório Final Aterros Experimentais. p. 429.

Ghose, M.K. and sen, P.K. 2001. Characteristics of iron ore tailing slime in India and its test for required pond size. Environmental Monitoring and Assessment. v.68, p.51-61.

Srivastava, M.P., Pan, S.K., Prasad, N., Mishra, B.K. 2001. Characterization and processing of iron ore fines of Kiriburu deposit of Índia. International Journal of Mineral Processing. v.61, p. 93-107.

Characterisation of tailings for Dry Stacks

David Hight, Geotechnical Consulting Group LLP, UK
Angeliki Grammatikopoulou, Geotechnical Consulting Group LLP, UK
Tiago Dias, Geotechnical Consulting Group LLP, UK
Felix Schroeder, Geotechnical Consulting Group LLP, UK
Luiz Guilherme de Mello, Vecttor Projetos, Brazil.

Abstract

Tailings in Dry Stacks differ from tailings placed hydraulically behind tailings dams in terms of placement method and water content, density and state parameter, and resulting fabric and stress history. Characterisation of tailings for Dry Stacks which involves testing laboratory compacted samples requires a compaction method that ensures a fabric and density that matches that achieved in the field as closely as possible. The varying fines content of tailings, resulting from variations in geology and weathering of the mined ore, and variations in the beneficiation and flotation processes, introduce complications in both the characterisation and compliance testing. There is the need to identify transitional fines contents, and to investigate changing fabric, suction and permeability either side of optimum water content.

Index testing should be on different fractions and ideally should include identification of particle shape and surface texture, and maximum and minimum void ratio for different fines contents.

Compacted tailings are initially unsaturated and approach saturation as a result of infiltration and increasing overburden; this requires a stress path approach to mechanical testing. Stack construction involves principal stress rotation and stress levels can exceed 3MPa. Laboratory testing should enable an assessment of anisotropy of strength, stiffness and permeability, using triaxial compression and extension tests, simple shear and shear box tests, and ideally hollow cylinder tests, on samples compacted at different water contents and with different compaction energies, covering the range of expected fines contents.

Background

Most existing tailings storage facilities (TSFs) have been constructed with hydraulically deposited tailings. The characteristics of this type of construction have been widely documented. For example, it is known that once the tailings flow into TSFs, they have a tendency to segregate as the heavier particles sediment faster, resulting in particle size distributions (psds) that vary laterally and vertically. Once sedimented in place, the tailings have a very loose structure and are typically at full saturation. As construction advances, overburden causes these tailings to consolidate and develop a more compact structure. As the spigot position and/or the layout of such TSFs changes, the hydraulic conditions surrounding the tailings can cause them to desaturate, either seasonally or permanently.

A number of recent changes in the Brazilian regulations surrounding TSFs with hydraulically deposited tailings have pushed the industry to explore alternative methods to store tailings. One of these methods is to “filter” the tailings, which is essentially to remove most of the water used in the beneficiation process, through vacuum or mechanical press technologies, and to place them in, usually compacted, layers, forming embankments known as “dry stacks”. While the processes of dewatering and compaction are generally considered beneficial to increase the strength of the tailings within such TSFs, it is important to acknowledge the differences between this new approach and hydraulic deposition. Critical among these is the fact that filtered tailings that are transported to their placement sites are much less prone to suffer from segregation, so the fines present in the tailings at the filtration stage will most likely be part of the structure of these tailings when they are compacted. On top of that, it is critical to acknowledge that these tailings are placed and compacted in an unsaturated state, in which suctions can play a key role in preserving the particle structure, and that variations in these suctions during the life cycle of these Dry Stacks can lead to significant changes in this structure (e.g. saturation collapse).

This paper discusses the challenges to properly characterise filtered tailings that will be compacted in Dry Stacks, considering the elements outlined above. It is worth noting that the psds and mineralogy of the tailings vary between mines (Figure 1) and within a mine as the degree of weathering in the ore body changes, or when there are changes to the ore processing/beneficiation process, or when tailings from different mines are incorporated in the stack.

When considering the structural and hydraulic stability of the stacks, key questions arise regarding the behaviour of these sandy silts /silty sands, which are often non-plastic:

- What are the impacts of varying fines contents on strength, stiffness, volume change characteristics, permeability and erodibility of the placed material? At what fines content does the behaviour change from sand-dominated to silt-dominated? Is there a transitional fines content (see Figure 2)? Do the tailings of a particular grading behave as a transitional material, i.e. exhibiting non-converging Normal Consolidation and Critical State Lines?

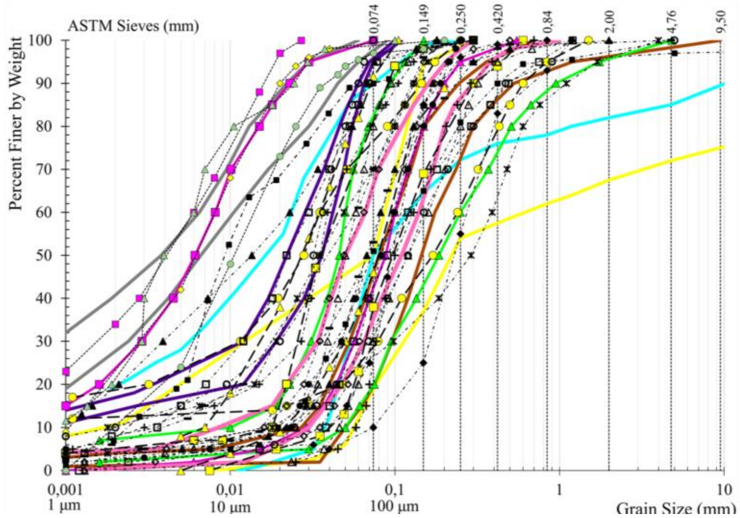

Figure 1: Grain size distribution curves of tailings stored in several tailings storage facilities of the Quadrilatero Ferrifero (Figure from Vieira Carneiro, 2023).

- Below what density and at what stress level can a collapse surface exist for different shearing directions? Can the tailings develop a potential to collapse under the extremely high stresses that will develop towards the base of the stack?
- How anisotropic are the strengths, stiffnesses, collapse potential and permeabilities of the tailings at increasing stress levels? While levels of initial anisotropy can be expected to be considerably less than in sedimented tailings, anisotropy will be induced by fabric changes accompanying the increase in mean and shear stresses and rotation of principal stress directions during construction of the stack.
- How important is fabric at the relatively high initial densities that will be achieved in the field? Is there complete breakdown of the filter cakes after compaction? Is there clustering/segregation in the field? Do the tailings have the characteristics of compacted silts and clayey silts, having markedly different micro-fabrics and macro-fabrics wet and dry of optimum[10]?
- After compaction in a Dry Stack, the tailings will be unsaturated initially. What wetting and drying cycles will the tailings experience (Figure 4b)? How important are suctions and their potential loss? Will the tailings exhibit collapse upon saturation? Over what height in the stack is unsaturated behaviour relevant?

[10] Compaction of silts on the dry side of the relevant optimum water content results in a soil with high suctions, and so high strength, and the presence of both macro-pores and micro-pores (Figure 3). The macro-pores give rise to high permeability to pore air, which is continuous, and a potential in less-well compacted soils for these pores to collapse on wetting. Compaction on the wet side of optimum results in low suctions, and so low constant water content strength, and the presence of only micro-pores. The pore air is discontinuous and in the form of occluded bubbles within the pore water (see Figure 4a for a summary of these points). The general absence of macro-pores means that a collapse potential upon wetting is much less likely. However, the low strength means that sliding and flow are potential failure mechanisms of the stack.

- What is the relationship between permeability and dry density, water content, suction and degree of saturation? When will undrained, rather than drained and partially drained behaviour be relevant?
- What risks have been identified from field trials and ongoing Dry Stack construction: segregation, development of wet layers, development of dried layers that are subsequently inundated under stress, development of a wet base as a result of infiltration or compression?

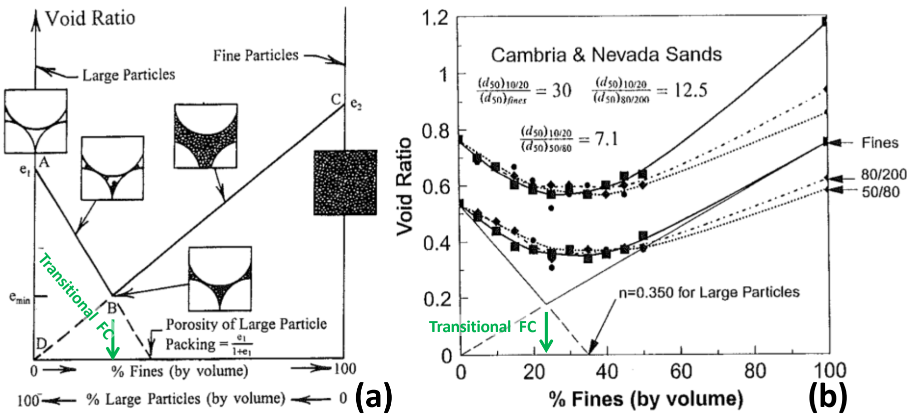

Figure 2: (a) Schematic diagram of theoretical variation of minimum void ratio in binary packings with % fines. (b) Variations of maximum and minimum void ratios for combinations of Cambria sand with 'fines' consisting of Nevada 50/80, Nevada 80/20, and Nevada fines. (From Lade et al, 1998).

Overall strategy

Characterisation of filtered tailings in Dry Stacks involves investigating the behaviour of the materials in their appropriate initial compacted state (composition, fabric, degree of saturation, dry density, suction), subject to relevant stress levels and stress paths that include the impact of wetting and drying history.

Properly designed field trials and the availability of undisturbed block samples[11] from these trials are the essential starting point for a comprehensive characterisation study. The behaviour of the material to be incorporated into Dry Stacks will depend to a large degree on the micro- and macro-fabric that is created by the filtration process and method of compaction, on the placement water content, and on the density that is achieved in layers, which may have different thicknesses and are subjected to different levels and methods of compaction. The fabric and the behaviour of the block samples in laboratory tests provides the database against which the laboratory compacted samples can be compared. Ideally, the database of block sample test results should be representative of the mineralogy, compaction at a range of initial water contents relative to the relevant optimum value, and representative of the range of particle size distributions that will be incorporated in Dry Stacks.

[11] Block samples have been taken successfully from a number of field trials and from ongoing dry stack constructions.

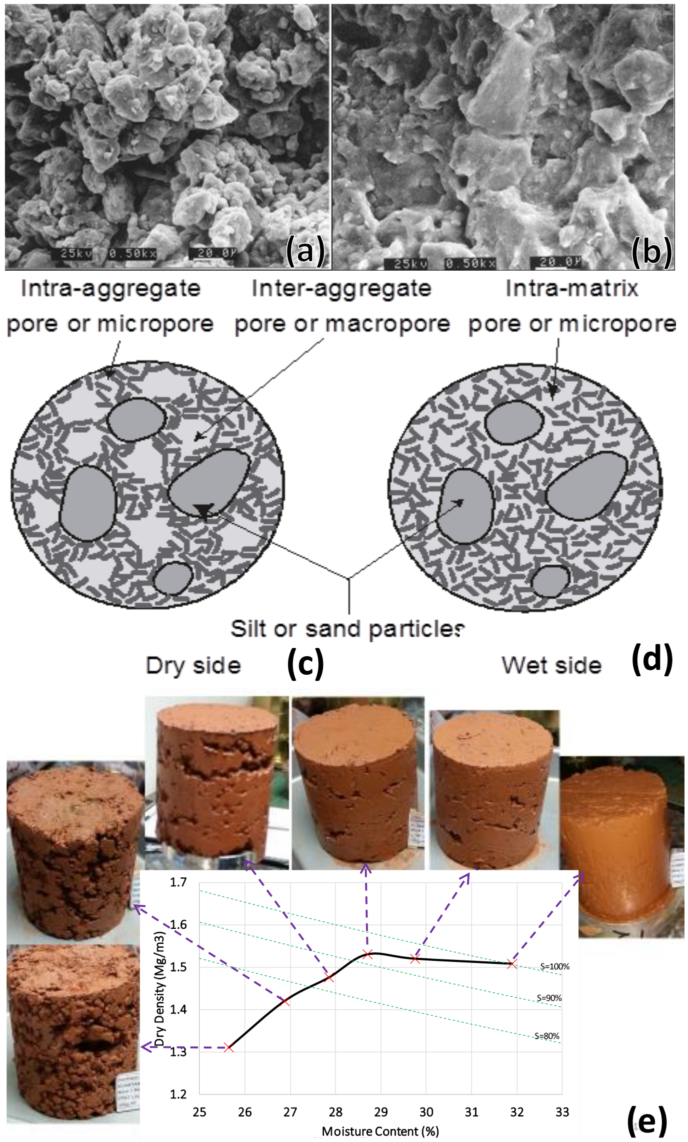

Figure 3: Changing micro- and macro-fabrics on dry and wet side of optimum water content in compacted soils. SEM photos (Delage et al. 1996) and schematic representation of a compacted Jossigny silt dry of optimum (a/c) and wet of optimum (b/d). Comparison of macro-fabrics of bauxite ore compacted at different water contents relative to optimum water content (e) (Menkiti, pers.comm.)

Testing of laboratory compacted samples is necessary to systematically investigate aspects of behaviour and supplement the findings from the block samples, e.g. to allow controlled variations in initial psd, compaction water content, compaction method and energy, stress history, stress path, and stress level, controls that cannot be achieved in the field trials. A stress path approach should be applied by working with initially unsaturated samples that may become saturated by compression or infiltration and may undergo wetting and drying. Numerical analyses of dry stack construction would be beneficial to identify relevant stress levels and stress paths.

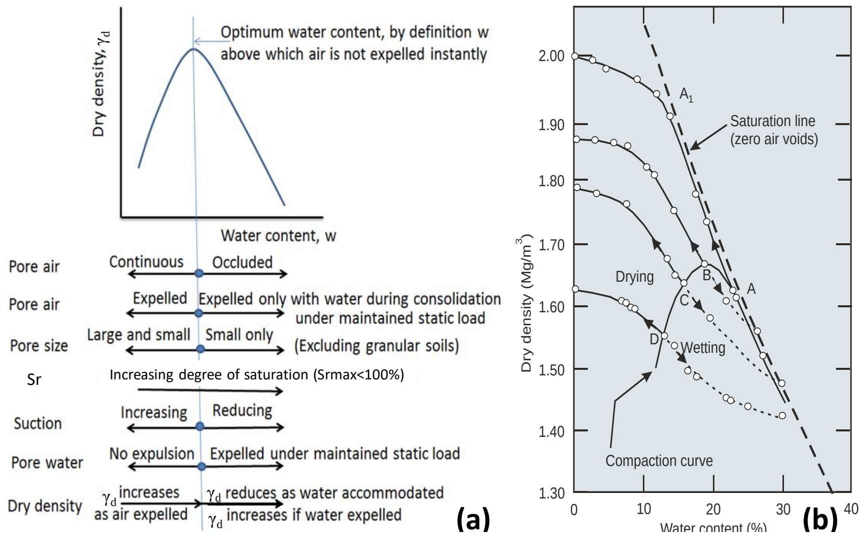

Figure 4: (a) Summary of differences in soil compacted on the wet and dry sides of optimum water content. (b) Relationship between dry density and moisture content of a sandy clay soil when allowed slowly to become drier or wetter (Croney, 1952)

The method of laboratory compaction must be shown to match, as closely as possible, the behaviour and fabric of the block samples in directly comparable tests in terms of compaction energy and compaction water content. Matching field and laboratory compaction curves does not guarantee matching fabrics. Different preparation methods may be required for different psds.

The characterisation programme and compliance testing need to take into account the variability in:

- particle size distribution, both at source (Figure 1) and after transport, spreading/segregation and compaction
- water content at placement (after filtration and stockpiling) and as a result of wetting and drying cycles
- density through layers and differences in compaction energy
- fabric and particle characteristics, linked to changes in mineralogy.

Overall aims

The paper does not address the contributions of trial embankments or their monitoring and in situ testing to the characterisation process. It sets out an idealised laboratory campaign that aims to:

- Identify the anisotropy of peak, large strain and residual strength, stiffness, collapse potential and permeability of materials subject to appropriate consolidation paths after compaction to relevant densities at relevant initial water contents. Consolidation paths include application of the increasing stress levels, including shear stresses and so changing principal stress directions. Triaxial compression, triaxial extension and simple shear tests (with and without shear stresses applied during consolidation) should be used. The possibility of testing in a hollow cylinder apparatus (HCA) should be considered bearing in mind its relevance and availability commercially, as highlighted by Reid et al (2022).

- Establish limits to the required placement conditions, including water contents, densities, fines contents, that will lead to dilatant or stable-contractant behaviour under the applied stress levels and stress paths, and so eliminate the risk of collapse due to inundation or shear, and provide sufficient drained strength.
- Establish a framework describing the behaviour of the range of materials to be incorporated into Dry Stacks.
- Provide the parameters required for analysis/assessment of trafficability, fill stability, including the potential for rainfall induced slope instability, infiltration, pore pressure build up and seepage, and erodibility.

The laboratory testing considered in this paper does not cover tests that may be required for analyses of earthquake loading and for derivation of specific parameters for constitutive models.

Detailed testing of block samples

Block samples should be accompanied by a detailed history of source, preparation, placement conditions (loose layer thickness, water content), compaction (plant, number of passes, uniformity of compaction within layers based on in situ testing), estimated wetting-drying history, sampling, storage and transport.

On bulk samples from each layer, adjacent to and at the same depth from which the block samples were taken, measure psd, specific gravity and maximum and minimum void ratios of full grading and of the separated sand and fines content, carry out Standard Proctor Compaction Tests on the representative mix.

On each block sample:

- Measure the profile of density and water content and measure suction. Where possible select specimens for testing which are uniform along the specimen height.
- Carry out oedometer tests without flooding and with flooding at different vertical stress levels. The aim is to identify conditions of placement and stress levels which could lead to a collapse potential under vertical loading.
- Measure the total stress strength of the unsaturated samples in triaxial compression, triaxial extension and simple shear in constant water content tests. The aim is to obtain a relationship between strength and water content and density for total stress stability analyses (refer to Seed & Chan, 1959).
- Carry out triaxial compression, triaxial extension and simple shear tests in which the unsaturated samples are loaded to a range of isotropic and anisotropic stress states under drained conditions. Drainage is then closed and the samples are saturated, measuring the resulting strains. Tests on

samples which do not collapse are then loaded to failure in the normal way. The aim is to identify the conditions under which there is a risk of collapse and flow after wetting up in the stack.

- Measure the soil water characteristic/ soil water retention curve (SWCC/SWRC), and air and water permeability, at the in situ state and after loading to represent construction of the stack.
- Identify the fabric of the field compacted tailings, taking micro- and macro-photographs (Figure 3), and carry out mercury intrusion porosimetry (MIP) and scanning electron microscopy (SEM) to evaluate the existence of the double-porosity structure (i.e. micro- and macro-pores). Measurements of air permeability under increasing stress levels provide a valuable insight to changes in fabric.

Detailed testing of laboratory compacted samples

PSDs to be tested

In order to deal with the varying psds (for a given mineralogy), it is suggested that a characterisation study should focus on representative psds that encompass the expected range (Figure 1); for instance 3 psds may be considered appropriate: a lower bound to the range, that represents the host sand; an upper bound that represents a likely maximum fines content; and a psd that lies midway between the upper and lower bounds. The study may benefit from selected tests on an increased range of fines contents.

Ensuring repeatable gradings of laboratory prepared samples

The challenge in all this work will be making sure tests are run on identical samples in terms of psd. Methods involving riffle boxes and quartering with thorough mixing are suggested. Checks on the psds achieved will be essential.

Index testing on each mix and fraction

- Particle size distribution including clay content, with and without the use of de-flocculants.
- Atterberg limits.
- Particle specific gravity of full mix grading and separately of the sand and silt fractions[12].
- Maximum and minimum void ratios of full grading and of each major fraction.

Particle characteristics

Mineralogical analysis of each major fraction using SEM, XRD, etc. to evaluate particle characteristics such as shape, aspect ratio, surface texture and crushability.

[12] The particle size for this boundary should be clearly defined. Standards vary between 60 and 75 μm.

Laboratory compaction

- Proctor Compaction Tests with varying levels of compaction energy, including Standard and Modified (Heavy) and less than Standard Proctor, following methods proposed by Fagerberg and Stavang (1971) for the shipping of ores. Compaction tests should include a minimum of 5 points and it is recommended that some tests are carried out with at least 7 different water contents to more fully define the compaction curve. It is possible that samples may dry or drain to some extent during testing, and it is therefore recommended that the specimen's water content is measured before and after compaction.
- Static compaction to dry densities achieved in Standard and Modified Proctor tests at equivalent water contents.
- Suctions should be measured after compaction in order to define suction – water content – dry density relationships for the representative mixes with different compaction energies and methods.
- On each compacted sample, determine the fabric following the same methods suggested for the block samples.
- Using the compaction curves applicable to the different compaction energies, define the line of optimums for the representative psds.

It is recommended that psd tests are run on the samples before and after compaction to understand the impact of compaction on the grading and the likelihood of particle breakage.

Comparison of fabric in field and laboratory compacted samples

The behaviour of the non-cohesive tailings is determined by the density of packing, the fabric, the stress history and current stress state, and the form of perturbation applied – i.e. the stress or strain path imposed. The fabric that is created by compaction of a particular tailings in the field and in the laboratory will depend on:

- the method of compaction – Field: vibrating or non-vibrating roller, impact compaction, trafficking by haulage trucks or dozers. Laboratory: dynamic, static, kneading;
- the placement water content and the void ratio achieved (layer thickness, number of passes) and, therefore the state of the tailings relative to its line of optimums - whether air is continuous (dry of optimum) or discontinuous (wet of optimum).

Void ratio is a global, but not local, indicator of packing density. Fabric provides detail of, inter alia, local packing, aggregation, variations in local pore size, shape and continuity, anisotropy of particle contact orientations and of particle alignment.

In the tailings, fabric must also consider the location of the silt component within the host sand, i.e. whether the voids are under-filled so that the fine sand provides the structural framework, or whether the voids are over-filled and the silt component is involved in or controls the structural framework. This will depend on the ratio of sand to silt and the compacted density or void size (Figure 5).

In the comparison between the fabric of field and laboratory compacted tailings, the comparison must be made on samples having the same water content and dry density (or void ratio if Gs is varying), which have been subject to similar levels of compaction energy. Ideally, the comparison should also be made between field and laboratory samples that are wet and dry of their line of optimums.

Select an appropriate method of compacting specimens in the laboratory which provides as close a match as possible to the fabric and behaviour observed in tests on block samples from the test fills. From hereon in, use the compaction method that provides the best representation of the field compacted tailings for each of the representative psds and prepare samples wet and dry of optimum and at optimum.

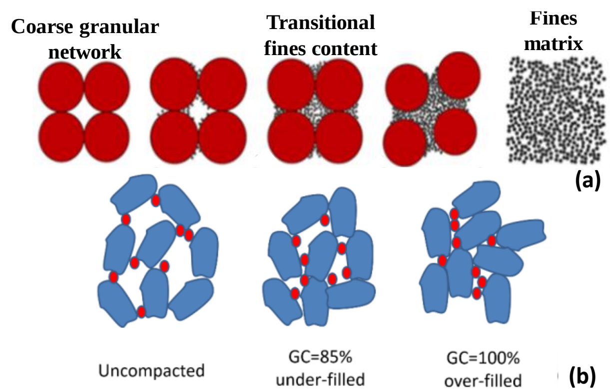

Figure 5: Illustration of (a) under- versus over-filled fabric and transitional fines content, and (b) impact of increasing density on fabric (GC is compacted dry density relative to Standard Proctor maximum dry density).

Tests for SWCC, air and water permeability

SWCC/SWRC curves (Figure 6) should be established, and air and water permeability should be measured, for the representative gradings on samples prepared wet and dry of optimum and at optimum water content, each under different stress levels, representing construction of the stack. Consider running column filtration tests to assess water content and void ratio redistribution, residual water content and field capacity.

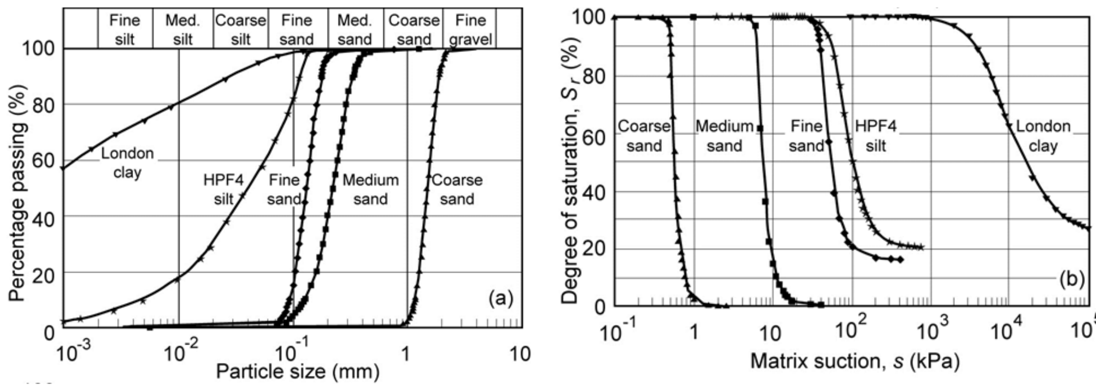

Figure 6: Psds and drying SWCCs for a range of soils (after Standing et al, 2013).

Tests for yield, compressibility, 1D collapse potential and check for transitional behaviour

Oedometer testing should be used to investigate yield stress levels on compacted samples and the potential for collapse on wetting under 1D conditions:

- One-dimensional compressibility of unsaturated specimens in oedometer tests, maintaining constant water content, so reducing suction; at what vertical stress do samples become saturated?
- One-dimensional compressibility and swelling with and without prior flooding in oedometer tests.
- Assessment of collapse potential in double oedometer tests with flooding at appropriate vertical stresses.
- Oedometer tests on samples of different initial void ratios taken to maximum stress levels to check for the existence of a unique normal compression line.

Tests for stiffness, strength and 3D collapse potential

- Stiffness and strength in triaxial compression and extension tests at constant water content, without prior saturation.
- Stiffness and strength in drained and undrained triaxial compression and extension tests, with prior saturation of the samples, and after isotropic and anisotropic consolidation.
- Constant volume simple shear tests, with prior saturation.
- Collapse potential in triaxial compression and extension tests, and simple shear or shear box tests, when flooded under selected isotropic and anisotropic stress states and suction levels.
- Identification of the load-collapse surface for the unsaturated and saturated material[13].
- Effects of different wetting-drying histories, including drying then wetting after compaction dry of, wet of and at optimum moisture content, and just wetting after the same three compaction conditions.

[13] A number of these tests will require the measurement or control of soil suction, directly, using osmotic systems or, indirectly, using axis translation techniques.

- Measurements of the angles of shearing resistance for the representative mixes and the individual fractions in drained triaxial compression, triaxial extension and shear box tests.

Tests for defining critical state parameters

To define critical state parameters for each mix, drained triaxial compression tests should be run on samples prepared in a loose state using moist tamping.

Erodibility

The risk of internal erosion due to water percolating through the material should be investigated. In particular, checks should be made as to whether percolating water can wash the smaller particles through the pores, that is the risk of suffusion between the two fractions should be investigated. This will probably be more instructive when carried out on block samples, i.e. samples in which there will be inhomogeneities and non-uniform distribution of the fines because of segregation, and in which internal erosion is more likely.

Concluding remark

Compaction of tailings in Dry Stacks will produce a much more stable end-product than hydraulically placed tailings, but characterisation of compacted tailings is a challenge, requiring consideration of, inter alia, fabric, unsaturated soil behaviour, anisotropy and the high stress levels associated with stacks of unprecedented heights.

References

Croney D. 1952. Soil Mechanics for Road Engineers. HMSO.

Delage P., Audiguier M., Cui Y.J., and Howat M. 1996. The microstructure of a compacted silt. Canadian Geotechnical Journal 33: 150-158.

Fagerberg, B. and Stavang, A. 1971. Determination of critical moisture contents in ore concentrates carried in cargo vessels. Proceedings of the 1st International Symposium on Transport and Handling of Minerals. Vancouver/

Lade, P.V., Liggio Jr., C.D. and Yamamuro, J.A. 1998. Effects of non-plastic fines on minimum and maximum void ratios of sand. Geotech. Test. J., ASTM 21(4): 336–347.

Reid D., Chiaro G., Fanni R. and Fourie A. 2022. Arguments for increasing the use of hollow cylinder testing in the characterisation of tailings. Tailings and Mine Waste Conference, Denver.

Seed, H.B. and Chan, C.K. 1959. Structure and strength characteristics of compacted clays. ASCE J. of Soil Mechanics and Foundations Div. 85(SM5): 87-128.

Standing J., Ghail R., Coyne D. (2013). Gas generation and accumulation by aquifer drawdown and recharge in the London Basin. Quarterly Journal of Engineering Geology and Hydrogeology, Vol. 46, 2013, pp. 293–302.

Vieira Carneiro J.J., Gomes Marques, E.A., Viana da Fonseca A.J.P. Lopes Ferraz, R. and Cruz Oliveira A.H. 2023. Characterisation of an iron ore tailing sample and the evaluation of its representativeness. Geotec. Geol Eng, 41: 2833-2852.

Disposal of filtered tailings and associated waste in Brazil – the PDER Alegria Sul (Samarco) case

Paulo Franca, F&Z Consultoria e Projetos, Brazil
Wanderson Silvério Silva, Samarco Mineração, Brazil
Viviane Aparecida Rezende, Samarco Mineração, Brazil

Abstract

This paper presents details of the final design, as well as the results of the tailings dry stack operation, being the new alternative strategy for tailings disposal of Samarco Mineração, five years after the failure of Fundão Tailings Dam, in November 2015. The tailings dry stack is being disposed for almost three years.

Introduction

Five years after the failure of Fundão Tailings Dam, in November 2015, Samarco has resumed its operation in December 2020, having an alternative strategy for tailings disposal. The finer portion of the tailings ("slimes"), which represents 20% of the total, are separated from the mass through a desliming circuit and disposed in an existing pit, the Alegria South pit. The coarser portion of the tailings mass that comes from flotation, is dewatered through vacuum disc filters, and placed with the associated mine waste cover, in the Alegria South Waste Dump (PDER Alegria Sul).

Tailings Characteristics

Tailings correspond to a silty-fine sand material obtained from flotation process. A typical particle size distribution of this material is shown in Figure 1. Tailings are a non-plastic material.

Loose tailings present contractive behavior, as shown in Figure 2. It can be noted that tailings with degree of compaction over 95% (Standard Proctor) shows dilatant behavior. This was the degree of compaction initially selected for the design, which was later changed to 98% to address the stress ranges.

Sieve (Mesh)	Openess Micrometer	Sandy tailings concentrator 3			
		Mass	% retida		% Passing
			Simple	Accumulative	
20	840	0,000	0,00	0,00	100,00
28	590	0,000	0,00	0,00	100,00
35	420	0,017	0,03	0,03	99,97
48	297	0,070	0,13	0,16	99,84
65	210	0,540	1,00	1,16	98,84
100	149	2,492	4,60	5,75	94,25
150	105	5,457	10,07	15,82	84,18
200	74	9,366	17,28	33,10	66,90
270	53	9,343	17,24	50,34	49,66
325	44	2,942	5,43	55,77	44,23
400	37	1,564	2,89	58,65	41,35
	35		2,64	61,30	38,70
	30		7,24	68,53	31,47
	25		7,84	76,37	23,63
	20		7,83	84,20	15,80
	15		6,79	91,00	9,00
	10		4,54	95,54	4,46
	5		2,36	97,90	2,10
	1		2,10	100,00	0,00
	< 1		0,00	100,00	0,00
Inicial Weigth		54,20			

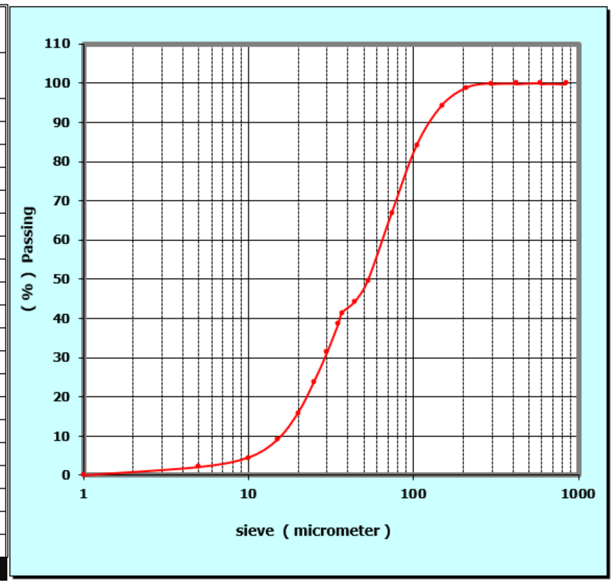

Figure 28: Typical particle size distribution

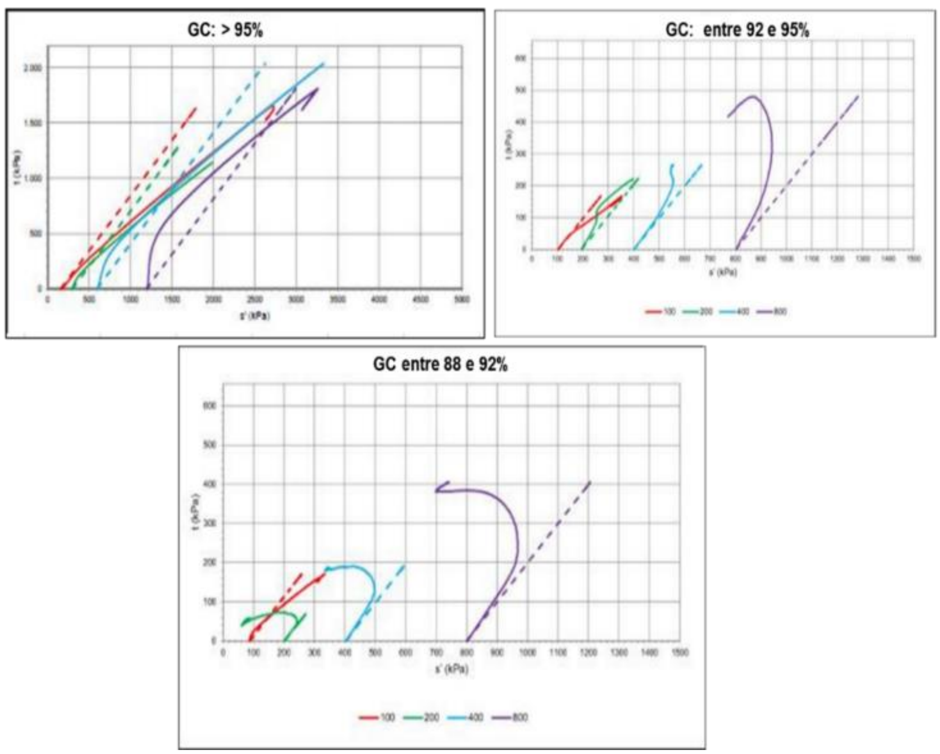

Figure 29: Triaxial CIU stress paths on filtered tailings, with different degrees of compaction (Standard Proctor)

The design considered compaction of the entire deposit. To evaluate the main characteristics of filtered flotation tailings, a representative large-scale sample of the material was delivered to a pilot plant, where it was re-pulped, filtered in vacuum disc filters and tested in three test fills, using loose layer with thickness of 0.6m, 1,0 m and 1.5m. Field testing involved density and moisture content tests in several depths and collection of undisturbed block samples for lab tests. Compaction was done with regular on road trucks and dozers (D6 size). A relationship between void ratio and degree of compaction was derived at all test fills, as shown in Figure 3.

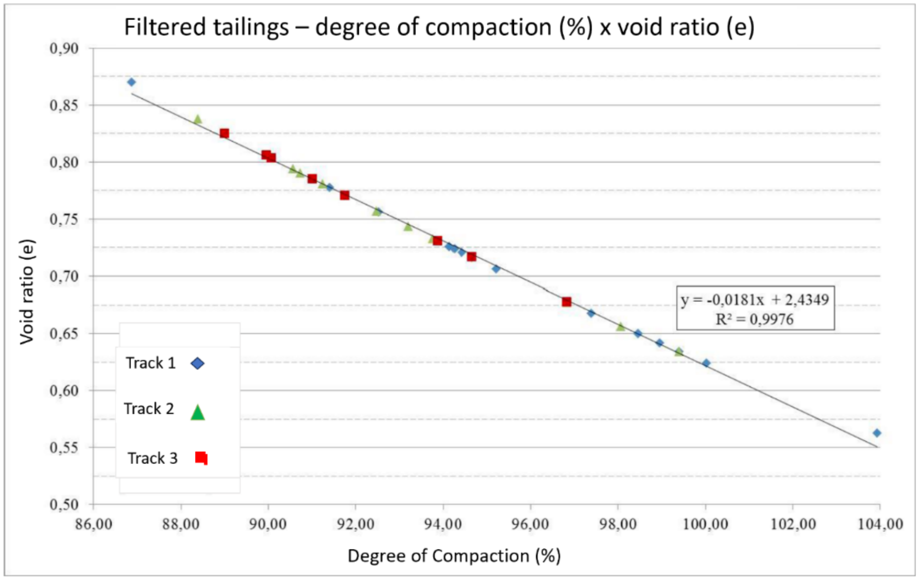

Figure 30: Void ratio vs. Compaction

A third test fill was carried out to verify the use of rollers, assessing its suitability and comparing its productivity with dozers. This test also considered the evaluation of different moisture ranges, layer thicknesses as well as the simulation of the full cycle (loading – hauling – unloading – spreading – compaction - quality control). The results showed that a 20-ton roller is more suitable for operation and that it is possible to adopt 0.75m thick loose layer in the deposit; tests have shown that the target degree of compaction (> 98% standard Proctor) is achieved in the whole layer depth.

Laboratory tests on samples collected in the test fills consisted of characterization tests (particle size, Atterberg Limits), degree of compaction, permeability tests, triaxial tests (CIU and CID) and consolidation. A typical result for a 1 m compacted layer (degree of compaction> 95% of Standard Proctor) is shown in Figure 4 (sample S17729). The stress paths show a dilatant material when compacted. Laboratory tests under higher confining stresses were also carried out for similar projects in Samarco, in labs in North America. Figure 5 shows the results of tests up to 6,000 kPa; in the range of Samarco's deposit (~2,000 kPa), with a compaction degree of 98% of the Standard Proctor, the void ratios will lie below the Critical State Line.

Based on the tests, final design considered:

- Use of off-road equipment in the dry stack construction.
- Loose layer thickness of 0.75 m.
- Minimum compaction degree of 98% of the Standard Proctor and a corresponding void ratio of 0.66.

- Optimum Moisture Content of 14%, with a ± 3% range.

Tailings shear strength parameters: c´= 0 kPa, f´= 33°.

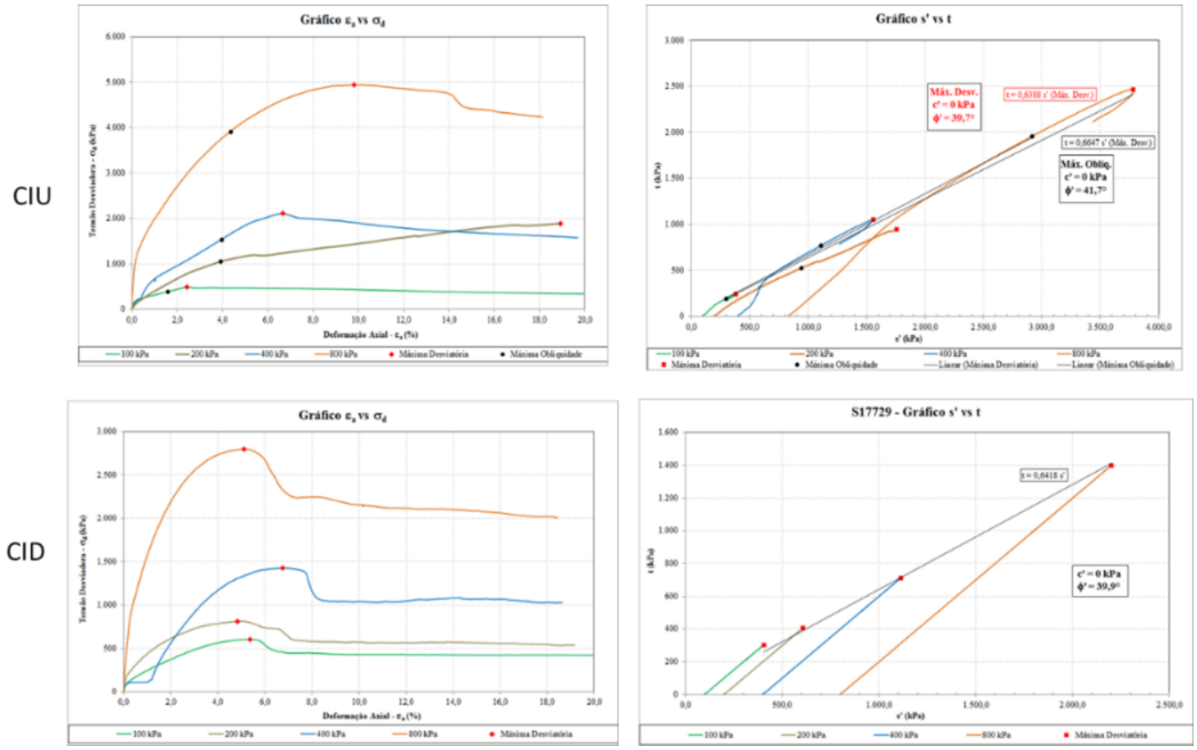

Figure 31: Triaxial tests results for filtered tailings

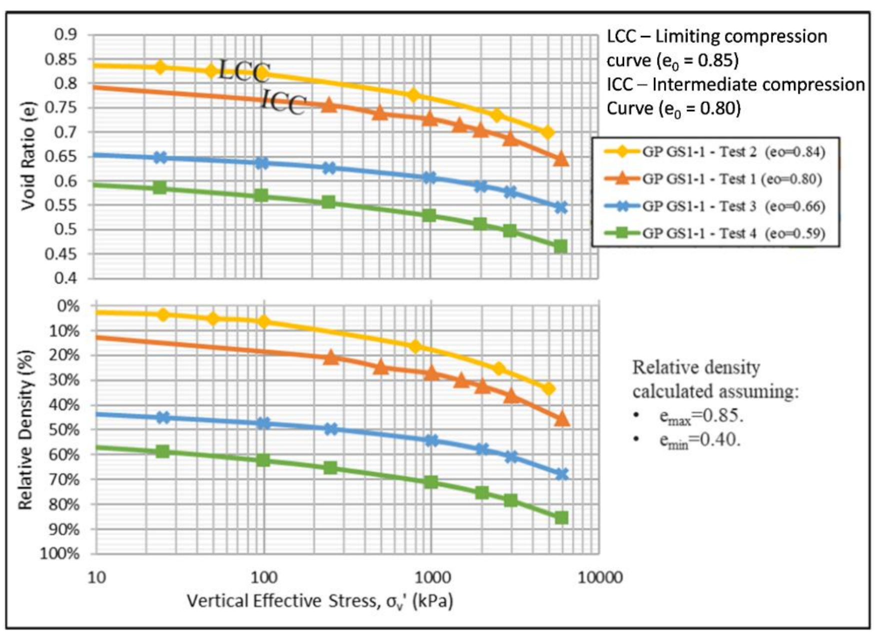

Figure 32: Compressibility versus Critical State Line (source: Stantec)

Design Details

Due to the physical restrictions of the licensed area for the Alegria South filtered stack facility and the need to use mining equipment, which require specific road geometries, design considered the construction of a levelling platform on the valleys, made with compacted waste borrowed from an adjacent dump. Underdrains were built under the platform to collect foundation water. Another set of underdrains were built over the levelling platform, in a herringbone fashion, with the objective of collecting water from the tailings deposits and to dissipate construction pore pressures. Figures 6 and 7 show a plan view of the underdrains scheme and a typical cross section of the tailing's underdrains. The geomembrane liner at the bottom was included to avoid infiltration, making it possible to measure flows from the tailings separately. The underdrains design was backed up by a hydrogeological model of the area.

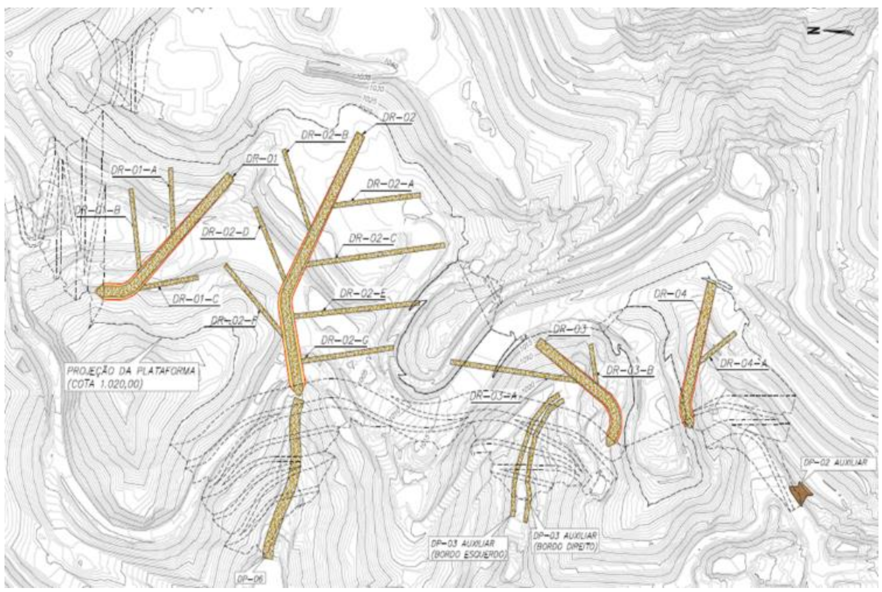

Figure 33: Underdrains plan view (DP – foundation drains; DR – tailings drains)

Figure 34: Tailings underdrains typical section

The stack geometry considered the use of compacted waste as an outer protective shell, with a minimum width of 15 meters, giving higher erosion resistance and minimizing infiltration. Tailings are disposed in the interior of the facility, compacted in the whole pile. Figure 8 shows a plan view and typical cross section of the design. Numerical analyses were carried out to evaluate excess pore pressure (and its dissipation) associated to the construction rates, as well as evaluation of vertical and horizontal displacements. Based on such analyses, raise rates of ~25 m/year (~ 2m/month) were adopted for construction.

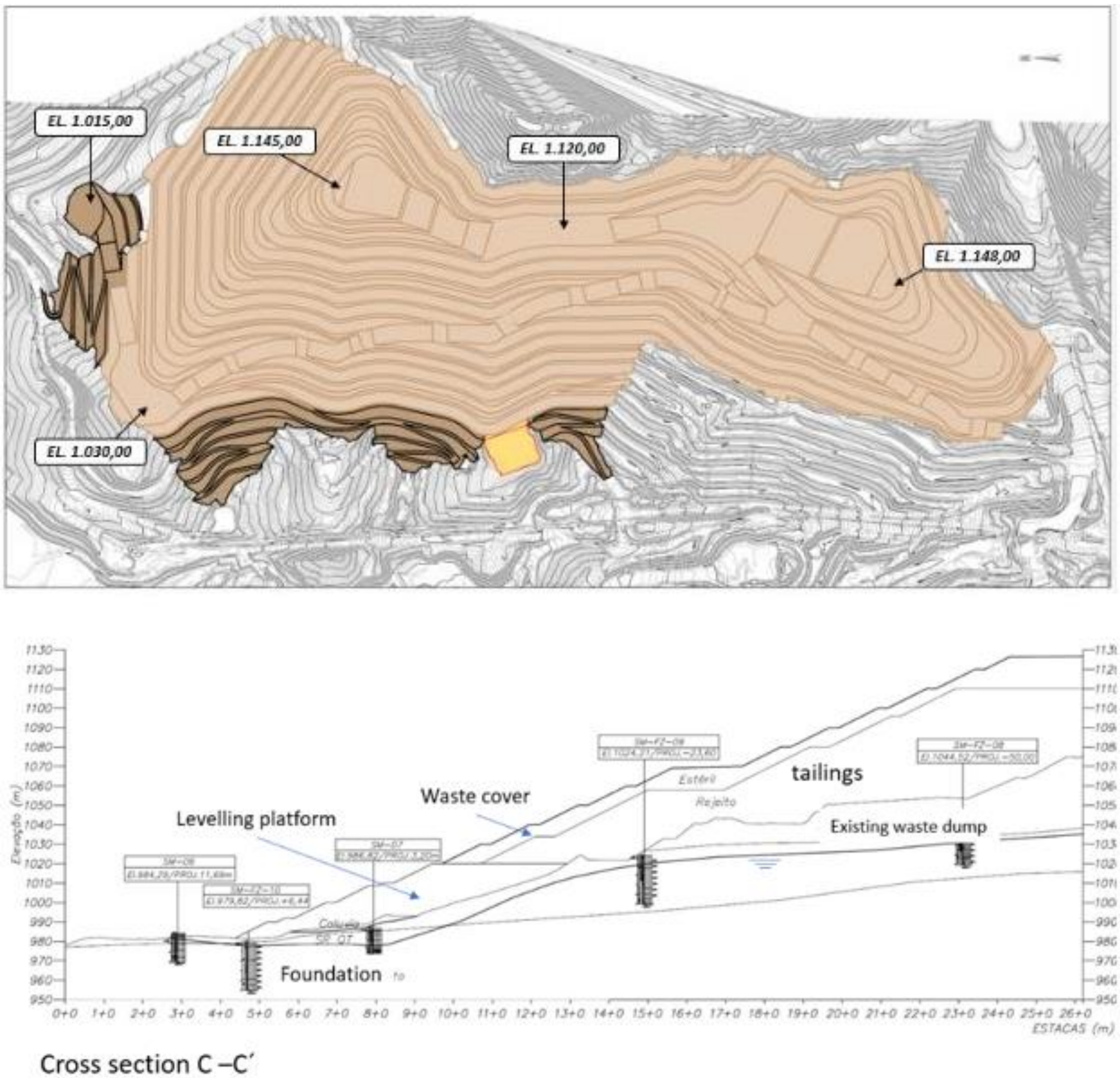

Figure 35: Plan view and typical cross section

Table 1 shows the standard design criteria used in Samarco, as a result of an agreement among designers, auditors, and the company´s Independent Tailings Review Board. All the stability analyses yielded Factors of Safety compliant with this standard. Post liquefaction analysis does not apply for this design, as tailings will be compacted to assure dilatant behavior.

Table 1: Criteria for stability analysis

Condition		Minimum FoS	Strength parameters			
			Tailings			Soil (CO/SR/SSAP)
			Contractive		Dilatant	
Water Table	Analysis		Saturated	Non saturated		
Normal	Drained	1,5	Effective	Effective	Effective	Effective
	Undrained	1,3	Undrained (peak)	Effective	Effective	Undrained
	Post liquefaction	1,2	Undrained (residual)	Effective	Effective	Undrained
	Pseudo-Static (*)	1,1	Undrained (peak)	Effective	Effective	Undrained (**)
Critical	Drained	1,3	Effective	Effective	Effective	Effective
	Post liquefaction	≥1,0	Undrained (residual)	Effective	Effective	Undrained

(*) seismic coefficient of 0,085, corresponding to ½ PGA (PGA = 0,168 for 10.000 years)

(**) with 20% reduction

The shear strength parameters were obtained as follows and Table 2 summarize the parameters adopted.

Foundation materials: based on existing design data and tests in similar materials, confirmed with additional undisturbed sampling and lab tests. Specific evaluation for the residual soil (verification of possible undrained behavior).

Waste: average parameters typically adopted in waste dump design, based on Samarco tests and peer review comments.

Filtered flotation tailings: lab and field tests carried out by diverse consultants, experimental fills, and comparison with similar tailings.

Table 2: Strength Parameters

Material	δ (kN/m³)	δ_{sat} (kN/m³)	Effective Strength Parameters	
			c' (kPa)	φ' (⁰)
Foundation – Quartzite/Phyllite	18	20	27	31
Foundation – residual soil	20	22	18	25
Waste	20	22	5 to 10	30
Filtered tailing	20	22	0	33

Instrumentation for pore pressure monitoring consisted of vibrating wire piezometers installed in the foundation, on the top of the levelling platform, in the tailings deposit and in the existing dump material. For displacement/deformation monitoring, the design considered inclinometers and magnetic extensometers. Load cells are installed at the base of the tailings deposit, along with piezometers. Flow measurement devices are installed for each drain.

The superficial drainage consists of channels at berms, water outlets at the slopes, peripheral channels, and windrows of compacted soil. The design considers critical storms with return periods as per Brazilian Standard NBR 13.029 (ABNT, 2017) – Return Period of 100 years for regular channels and 500 years for peripheral ones. Temporary diversion channels will be built to control water flow through the tailings area during the rainy season. These channels will contour the tailings deposit and divert water to the peripheral channels. The tailings plateau will be graded in 0.5 to the temporary channel.

Operation aspects

Operation of the stack facility started in December 2020, after commissioning the filtering plant and auxiliary facilities. From the filter plant, tailings are conveyed to a surge pile, where they are loaded in mining trucks and hauled to the disposal site.

Three rainy seasons have already been faced with no significant problems, due to the high permeability of the tailings (around 10-5m/s). Instrumentation readings shows no stability related problems, nor do the regular inspections. Design criteria and guidelines are being consistently met. Quality control/ Quality assurance includes compaction/moisture tests, with void ratio assessment for every 5,000 m3, as well as control of layer thickness, 24 hour/day, 7 days per week, done by a dedicated control crew. Special tests are also carried out every year, including collection of undisturbed samples for laboratory tests and CPTu drilling for verification. It is also considered the execution of geophysical tests to evaluate water infiltration and performance of the underdrainage. A similar control is also done for the waste shell. Some of QA/QC main results are depicted below.

The average layer thickness for tailings is 0.76 m, with a standard deviation of 0.052m; for waste is 0.78m with a standard deviation of 0.61m (data from December 2020 to April 2023).

Compaction rates and associated moisture content deviation are shown in Figures 9 and 10; the associated void ratios are presented in Figure 11. Moisture refers to values collected after the compaction. It is important to mention that tailings are filtered to moisture content of 15% (geotechnical) and lose 1% in the belt conveyor and another 2% during transportation. Wetting of the tailings is required for compaction.

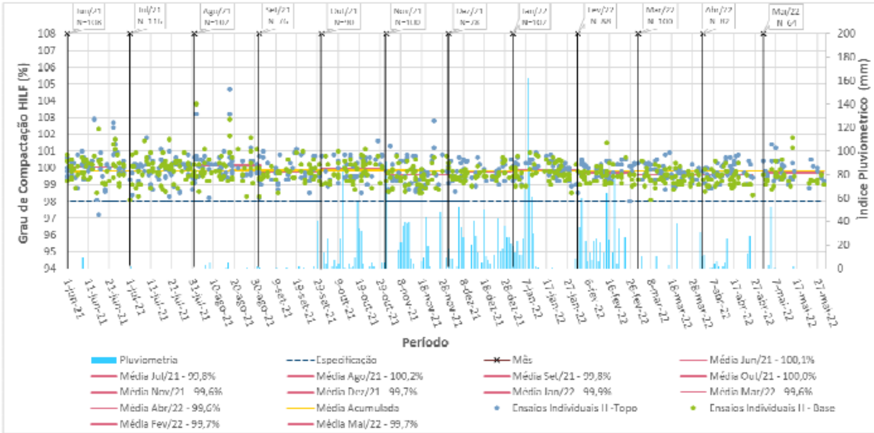

Figure 36: Degree of compaction

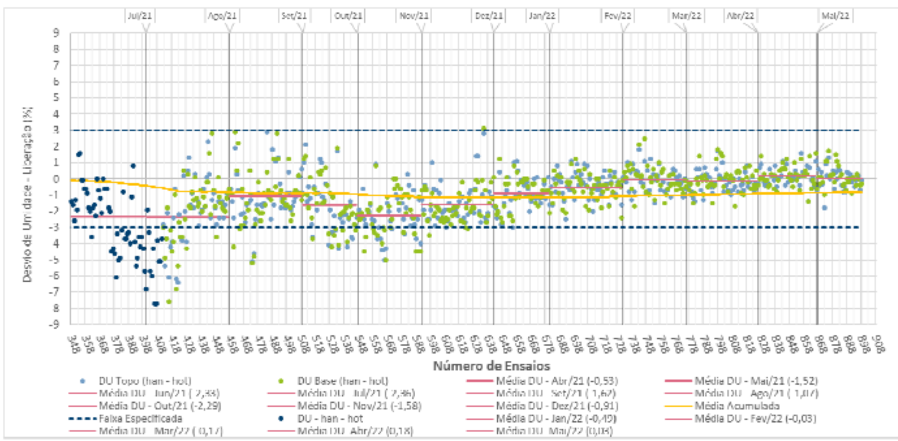

Figure 37: Moisture deviation

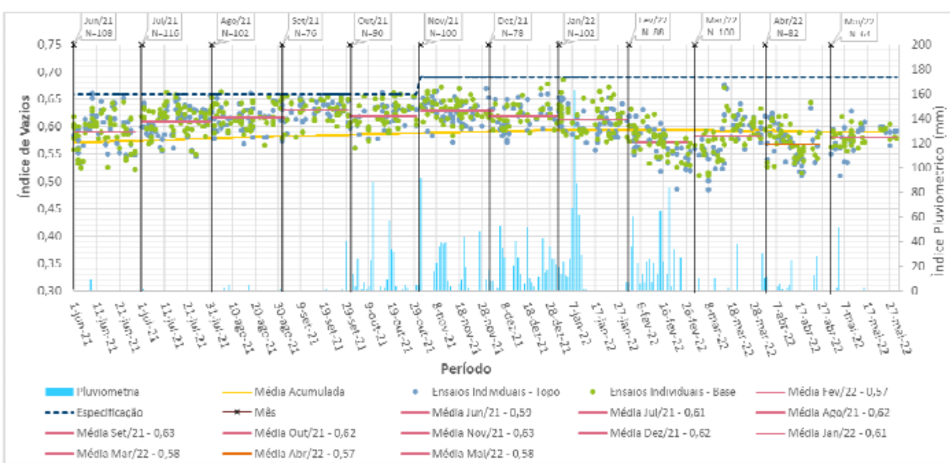

Figure 38: Void ratios

The designed instrumentation is being installed as the construction proceeds; instrumentation is automated and controlled from a Geotechnical Monitoring Center. As of April 2023, 71 piezometers, 8 water levels indicators, 3 inclinometers, 3 magnetic extensometers 1 load cell and 10 flow measurement devices have already been installed. Monitoring records do not show any significative variation that would impact stability. Field inspections are done weekly by the geotechnical staff, and once a month with the Engineer of Record.

Calibration of numerical analysis with field investigation, lab test results and instrumentation data are planned, as well as calibration of the hydrogeological model with instrumentation data. The following pictures show the present status and construction records of the stack.

Figure 39: Current situation of Alegria Sul Facility (May 2023)

Figure 40: View of the tailings underdrain construction

Figure 41: Disposal, spreading and compaction of tailings

Figure 42: Quality control soil testing activities

Conclusion

The paper shows an example of a filtered tailings stack in operation in Brazil. Nowadays this facility has the largest production rate amongst its kind in the country, with around 22,000 tones/day. Only coarser tailings are disposed in the area; the finer portion is disposed in a mine open pit.

Design criteria and construction infrastructure has been presented along the paper. Operation started in the end of 2020 and, until now, it has demonstrated that a rigorous control can guarantee the safety of the deposit.

Being a pioneering deposit of this kind in the country, it is serving as a benchmark for the mining industry.

Geomechanical Behaviour of an Iron Ore Tailings under High-Stress Levels for Disposal by Dry Stacking

Bruno Guimarães Delgado, CONSTRUCT-GEO, FEUP. Corporate Geotechnics Department, Vale S/A, Brazil.
António Viana da Fonseca, CONSTRUCT-GEO, University of Porto, Faculty of Engineering (FEUP), Portugal.
Rafael Jabur Bittar, Corporate Geotechnics Department, Vale S/A, Brazil.
Breno de Matos Castilho, Corporate Geotechnics Department, Vale S/A, Brazil.
Daniela Coelho, Geotechnical Laboratory, University of Porto, Faculty of Engineering (FEUP), Portugal

Abstract

Recent upstream tailings dam failures have driven, around the world, research for alternative and safer methods for mining tailings disposal. Dry stacking disposal with compacted tailings after the previous filtering (dry) process, instead of the traditional hydraulic disposal methods with successive upstream dam heightening, is being recently considered. In addition, the critical state soil mechanics (CSSM) approach is essential to understand the tailings' geomechanical behaviour under high-stress levels in order to design the maximum height of these stacking structures. Thus, this paper presents results of drained and undrained triaxial diversified stress path tests, that aimed to evaluate the behaviour of an iron ore tailings from the area known as 'Quadrilátero Ferrífero' (Minas Gerais State, Brazil), when subjected to mean effective stress levels (p') to represent confining pressures until 6400 kPa, value that exceeds the maximum design stresses involved in the highest stacking embankment. The results showed a relevant non-linearity in the critical state line (CSL) of the material for higher p' levels, which, given the importance of the critical state parameters for the material response pattern to different stress paths, can condition changes in their mechanical response during shearing, raising the need for further research about the microstructural properties (at particles level) that can explain this non-linearity of CSL.

Introduction

Recent tailings dam failures (Mt. Polley, Cadia, Fundão, and B1 in Brumadinho) have highlighted the particularity of the geomechanical behaviour of tailings deposited in these geotechnical structures and emphasized the importance of studying these peculiar materials in order to design safer tailings storage facilities (TSF). Although the structure design plays a major role, the nature of the tailings itself makes this material particularly sensitive to instability by liquefaction triggering. The characteristics of this type of material are highly influenced by its anthropic production, with none or hardly any chemical weathering, resulting in predominantly non-plastic silty or silty-sandy artificial soils. Together with the high-water content of the deposited material by conventional hydraulic disposal methods, tailings are highly susceptible to flow liquefaction.

Considering the difficulty of safely designing and maintaining upstream tailings dams, their construction and operation was recently banned in Brazil (ANM, 2019). The dry stacking disposal, with compacted tailings after the previous filtering process to ensure unsaturated tailings close to the optimum moisture content (OMC) from Proctor compaction standards (but not completely dry), appears as an alternative capable of better using the landform, as less storage space is required. However, the proper stacking design requires the knowledge of the geomechanical response of compacted filtered tailings under a variety of stress states, especially considering the high-stress levels to which the materials can be subjected, conditioning possible changes in its behaviour as the stress state increases.

The 'Quadrilátero Ferrífero' (‘Iron Quadrangle’, from Portuguese) is a mineral-rich region in the state of Minas Gerais, in Brazil known for its extensive deposits of minerals like gold, diamonds, and iron ore. Its long history of mining results in a large number of purpose-built TSF. In 2020, the National Mining Agency in Brazil registered 221 tailings dams in Minas Gerais.

The current paper will disclose an extensive and advanced laboratory program undertaken to investigate a non-plastic silty-sandy iron ore tailings from the region. This material is being studied for disposal by dry stacking. In this paper are presented the results of triaxial tests, allowing the definition of fundamental parameters for the entry of adequate constitutive models, based on the critical state soil mechanics (CSSM) framework, from a wide range of stress states (until 6400 kPa) and initial conditions of the material.

Background

Several researchers have studied the influence of stress states on the geomechanical behaviour of mining tailings (Schnaid et al., 2013; Viana da Fonseca et al., 2022).

From the CSSM, voids ratio (e) is recognized as a key parameter - together with stress state (mean effective stress, p', and deviator stress, q), which defines the mechanical behaviour of soils by means of the state parameter, Ψ (Jefferies & Been, 2016):

$$\Psi = e_0 - e_{cv} \tag{1}$$

where, e_0 and e_{cv} are respectively the current/initial void ratio and the critical state void ratio (at constant volume shearing) for the same stress level; this one is an intrinsic value for each type of soil and stress, independent of the loading condition (Schofield & Wroth, 1968).

The conventional CSSM framework defines a unique and straight critical state line (CSL) in both Cambridge $p' - q$ and $e - p'$ planes, given respectively by:

$$q = Mp' \tag{2}$$

and

$$e = \Gamma - \lambda \ln p' \tag{3}$$

where the constants M (critical state friction ratio), Γ (void ratio at reference pressure of 1 kPa) and λ (slope of the CSL) represent basic soil-material properties (Schofield & Wroth, 1968).

Several authors (Verdugo & Ishihara, 1996; Li & Wang, 1998) recognise that for cohesionless granular materials, a unique but curved CSL provides the best fit in the $e - \log p'$ plane, given by a power-law:

$$e = A - B(p'/100)^C \tag{4}$$

where A, B and C are fitted to match laboratory test results and 100 is the reference pressure taken as 1 atm ($\approx$ 100 kPa).

The CSL shape combined with the initial state of the material controls the static liquefaction potential. From undrained triaxial tests under axisymmetric stress conditions it is theoretically possible to evaluate the state of instability where to the onset of flow liquefaction induces sudden increases in strain and pore water pressure (PWP). The ratio of shearing at the instability line (η_{IL}) using the $p' - q$ plane is compared to in-situ conditions (η_0) in the same plane to ensure that:

$$\eta_0 < \eta_{IL} \tag{5}$$

with $\eta = q/p'$ as the stress ratio, where $q = \sigma'_1 - \sigma'_3$ and $p' = (\sigma'_1 + 2\sigma'_3)/3$); in which σ'_1 is the major effective principal stress and σ'_3 is the minor effective principal stress (confining pressure in the triaxial cell).

A flat trend of curved CSL in the $e - \log p'$ plane is usually observed at low stress levels and it is related to flow instability due to a loss of stiffness and strength of soils, which are characterized by effective stress close to zero (Yamamuro & Lade, 1998) or, in some cases, these differences can originate from compliance issues during testing, like unappropriated transducers for specific strain and stress levels that may induce significant errors in the test results (Figure 1a) (Viana da Fonseca, Cordeiro & Molina-Gómez, 2021).

Cohesionless materials, like mining tailings, will be prone to instability by flow liquefaction whenever the void ratio is above the CSL on its lower stress range. However, if the material has a lower void ratio, there will be a dilative response with increasing shear strain that inhibits a pronounced loss of strength under undrained shear loading.

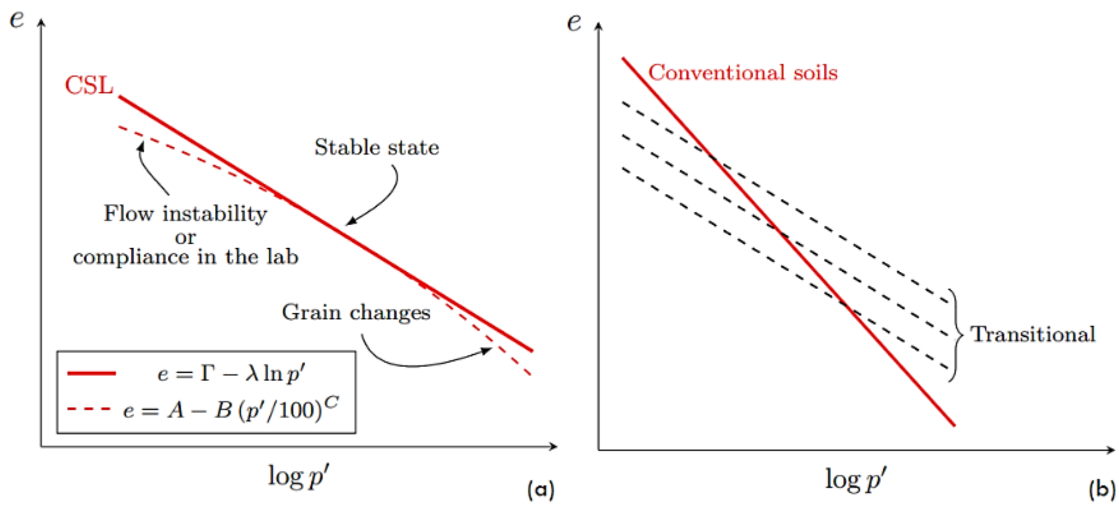

Figure 1: Schematic illustration of (a) non-linearity of CSL and (b) the transitional soil behaviour (Viana da Fonseca, Cordeiro & Molina-Gómez, 2021)

Marques et al. (2020) presented studies with iron ore tailings from the 'Quadrilátero Ferrífero', whose CLS presented a pronounced non-linearity for initial mean effective stress (p'_0) < 200 kPa, implying a higher brittleness of the material at low stresses under undrained shearing. Soares & Viana da Fonseca (2016), by extensive laboratory studies, shown similar behaviour for natural sands.

For high-stress levels, eventually, it was also possible to verify an increase in the non-linearity of CSL, which may be associated with particle breakage or with a relevant morphological particles' evolution (Figure 1a) (Schnaid et al., 2013; Soares & Viana da Fonseca, 2016) by changes in sphericity, angularity and/or superficial texture of individual soil particles (Delgado et al., 2022).

This microstructural approach (at particles level) can contribute to the understanding both the non-linearity of CSL and the transitional behaviours, characterized by non-unique, straight or curved, CSL (Figure 1b) their locations being highly dependent on the e_0, observed by some researchers (Coop, 2015; Velten et al., 2022) mainly for mixed grading and structured soils and less common for mining tailings.

Viana da Fonseca et al. (2022) studied some iron ore tailings from the B1 Dam in Brumadinho ('Quadrilátero Ferrífero') after dam failure, and showed a relevant non-linearity of CSL in the $e - \log p'$

plane at higher stress levels for the studied materials. This non-linearity was related by the authors to the material grading changes by morphological particles' evolution. This evolution behaviour was verified for p'_0 > 800 kPa. The CSL slope changes at higher stress level associated with increased grain angularity has also been reported by Soares & Viana da Fonseca (2016) and Lashkari et al. (2020). Further research, by quantification of morphological changes during laboratory tests and discrete element method (DEM) simulations, could help to validate this stress-strain behaviour at macro-scale.

Methodology

The material studied is a silty-sandy filtered tailings from iron ore processing of the 'Quadrilátero Ferrífero' to be disposed by dry stacking, here called AM3 (designation related to the origin in the mine). The mining tailings have a specific gravity (G_s) of 2.85 and its particle size distribution (PSD) curve will be show in the results section. The studies carried out aim to raise the knowledge level about the material as well as subsidize the dry stacking embankment design.

The Figure 2a shows one specimen prepared for one of the carried out triaxial tests (note the neoprene membrane and the copper pipes drainage to withstand the high pressures) and Figure 2b shows the detail of the embedded top-cap guided ram connection used in the tests.

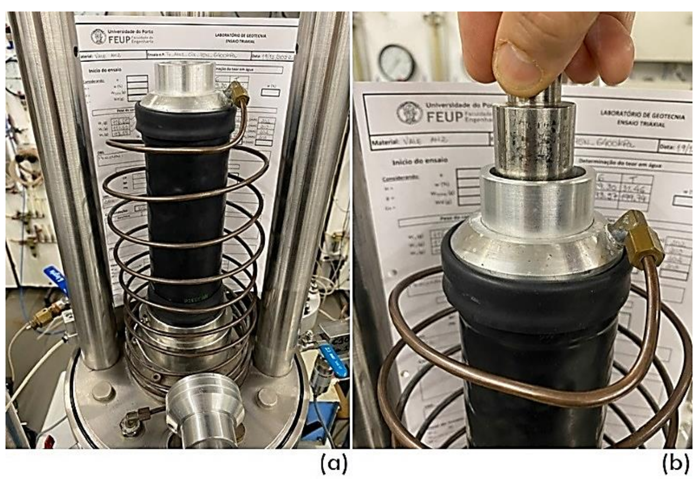

Figure 2: (a) Specimen for triaxial test and (b) Detail of the embedded top-cap guided ram connection

The triaxial compression tests were conducted at the Laboratory of Geotechnics (LabGeo) at the Faculty of Engineering of the University of Porto (FEUP), under saturated conditions, according to advanced laboratory procedures, such as: local internal instrumentation, embedded top-cap guided ram connection, oversized lubricated end platens, end-of-test soil freezing, etc. Such procedures, in current use at LabGeo/FEUP, and their importance for the determination of geomechanical parameters are widely discussed by Viana da Fonseca, Cordeiro & Molina-Gómez (2021).

The specimens were molded using two different effort levels from Proctor compaction standards with four degrees of compaction (75%, 97%, and 100% Standard Effort, 75N, 97N, 100N respectively, and 100% Modified Effort, 100M). Table 1 presents the different triaxial tests carried out and some results obtained from the tests.

Table 1: Triaxial compression tests (set-up and some results)

Test	p'_0 (kPa)	e_0	e_f	η_p	η_f	S_u/σ'_{vo}	State
Tx_AM3_CID_75N_200kPa	200	0.82	0.76	1.39	1.33	-	Loose
Tx_AM3_CID_75N_400kPa	400	0.82	0.73	1.38	1.37	-	Loose
Tx_AM3_CID_75N_800kPa	800	0.79	0.68	1.34	1.33	-	Loose
Tx_AM3_CID_75N_1600kPa	1,600	0.76	0.63	1.36	1.35	-	Loose
Tx_AM3_CID_75N_3200kPa	3,200	0.72	0.61	1.37	1.35	-	Loose
Tx_AM3_CID_75N_6400kPa	6,400	0.68	0.49	1.44	1.44	-	Loose
Tx_AM3_CID_100N_75kPa	75	0.63	0.69	1.74	1.52	-	Dense
Tx_AM3_CID_100N_150kPa	150	0.61	0.68	1.72	1.50	-	Dense
Tx_AM3_CID_100M_100kPa	100	0.60	0.67	1.79	1.48	-	Dense
Tx_AM3_CID_100M_200kPa	200	0.61	0.68	1.69	1.43	-	Dense
Tx_AM3_CIU_75N_400kPa	400	0.81	0.81	0.59	2.16	0.19	Loose
Tx_AM3_CIU_75N_1600kPa	1,600	0.75	0.75	0.66	1.35	0.20	Loose
Tx_AM3_CIU_75N_3200kPa	3,200	0.71	0.71	0.76	1.37	0.21	Loose
Tx_AM3_CIU_75N_6400kPa	6,400	0.66	0.66	0.83	1.44	0.24	Loose
Tx_AM3_CIU_97N_400kPa	400	0.67	0.67	1.39	1.30	2.33	Dense
Tx_AM3_CIU_97N_800kPa	800	0.64	0.64	1.41	1.33	1.70	Dense
Tx_AM3_CIU_97N_1600kPa	1,600	0.63	0.63	1.36	1.34	0.93	Dense
Tx_AM3_CIU_97N_3200kPa	3,200	0.62	0.62	1.39	1.32	0.57	Dense
Tx_AM3_CIU_97N_6400kPa	6,400	0.62	0.62	1.14	1.36	0.42	Dense

Note: Tx: Triaxial compression test; CID: Consolidated Isotropically Drained; CIU: Consolidated Isotropically Undrained; e_0: initial void ratio; e_f: final void ratio; η_p: peak shearing ratio; η_f: final shearing ratio; S_u/σ'_{vo}: undrained strength ratio, where S_u: undrained strength and σ'_{vo}: initial vertical effective stress.

Results and Discussion

From the results, it was possible to obtain a single CSL on the $p' - q$ plane (non-transitional behaviour) as shown in Figure 3, where all stress paths can be observed. It is noted that some specimens, as expected, went into flow liquefaction, given their initial state (Tx_AM3_CIU_75N_400kPa and Tx_AM3_CIU_75N_1600kPa). With the increase of the stress state and degree of compaction (initial state) an increase of stability under undrained condition was observed. The M parameter obtained was 1.42 with the friction angle at critical state, ϕ'_{cv} = 35˚.

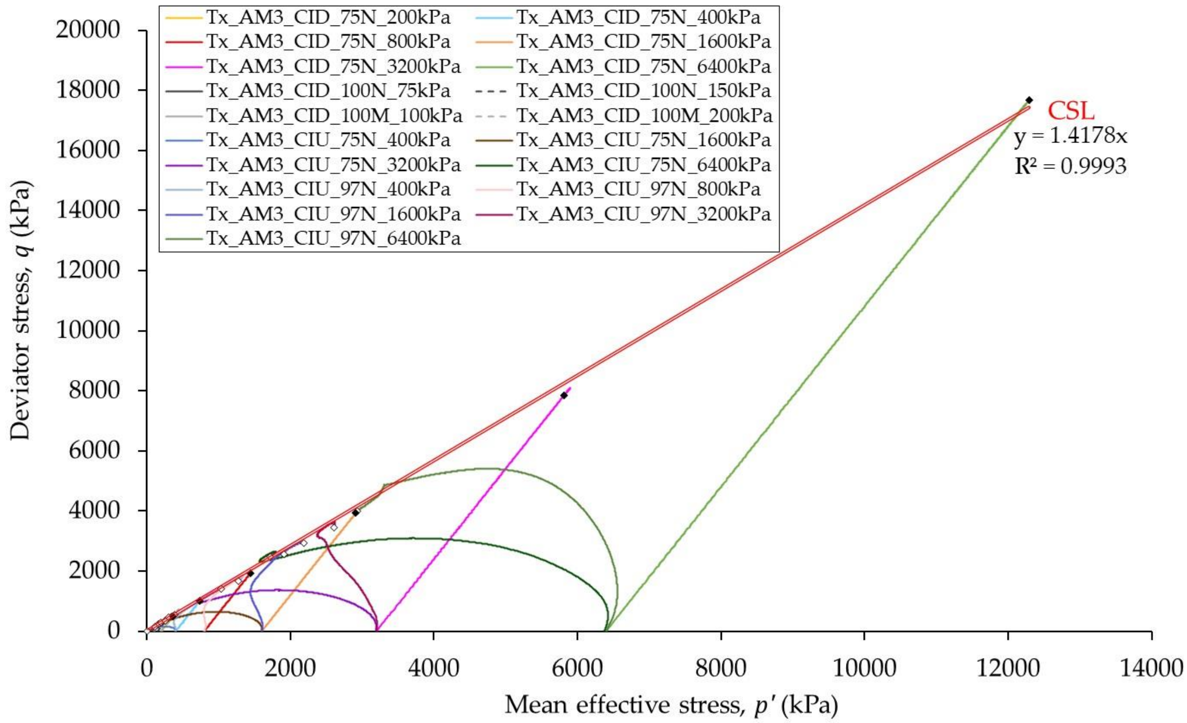

Figure 3: Triaxial compression tests results: stress paths and CSL in the $p' - q$ plane

Figure 4 shows the CSL fitted by a power-low given by Equation (4) just for loose specimens due to the best fiting, because for dense ones the formation of shear bands was observed making it difficult to accurately determine the critical state, together with an isotropic Normal Consolidation Line for 75% standard effort from Proctor compaction (NCL_{75N}) parallel to CSL. The triaxial tests' color code is the same from Figure 3. The parameters for the CSL fitted by power-law are A = 0.8291, B = 0.0494 and C = 0.4012.

The results showed a relevant non-linearity in the critical states line of the material in the $e - \log p'$ plane at higher stress levels (mainly observed from Tx_AM3_CID_75N_6400kPa test), which, given the importance of the critical state parameters for the material response pattern to different stress paths, raising the need for further research about the microstructural properties at particles level for explain this non-linearity behaviour (Viana da Fonseca et al., 2022). The Tx_AM3_CIU_97N_3200kPa test apparently did not reach the critical state and is certainly interfering slightly in the critical state parameters definition of the material, so it will be repeated.

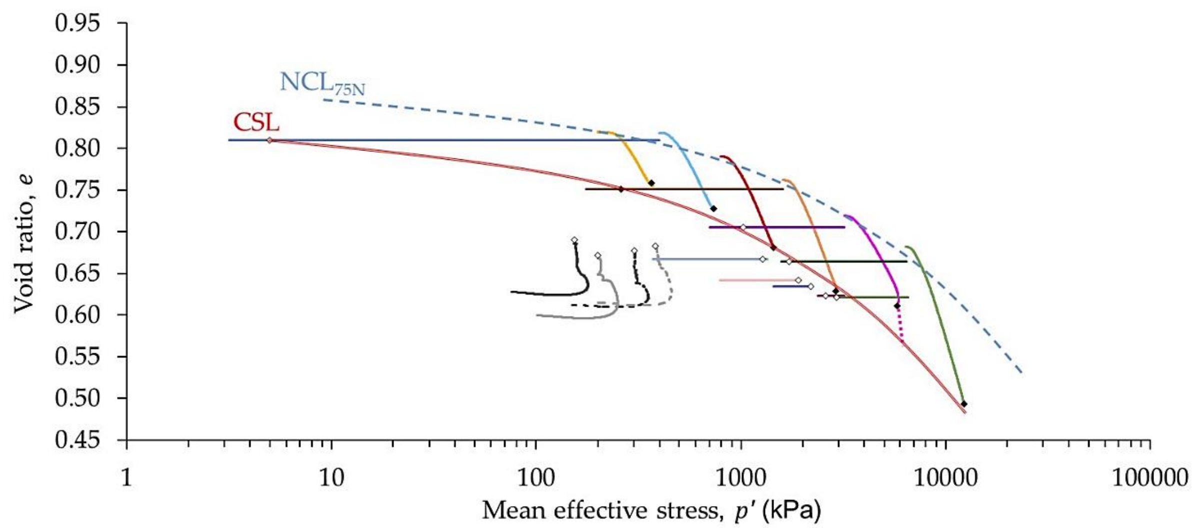

Figure 4: Triaxial compression tests results: CSL and NCL$_{75N}$ in the $e - \log p'$ plane

Figure 5 shows the original PSD curve of the material, as well as the PSD curves obtained after tests under high-stress levels (above 1600 kPa) making it possible to evaluate possible grain size evolutions due to particle breakage and/or morphological changes.

A considerable grain size evolution was noted, as expected, mainly for higher stress levels with specimens with a lower degree of compaction under drained shearing (Tx_AM3_CID_75N_3200kPa and Tx_AM3_CID_75N_6400kPa), which in the long-term could compromise the performance of the structure if it were subjected to at such stress levels, since changes in the state parameter, from dilatant to contractive behaviour (under drained shearing), can increase the susceptibility to liquefaction (in case of solicitations that induce stress-strain in undrained conditions). This possibility of liquefaction by state changes of the materials under high-stress levels should be studied during design and re-analyses while in construction by appropriate stress-strain constitutive models and numerical simulations.

Therefore, the filtered tailings mechanical behaviour under high-stress levels needs to be further investigated at the microstructural level (at the particle level), to try to understand more precisely what may be conditioning this non-linearity of CSL or its evolution, if transitional characteristics are envisage.

Conclusion

It could be concluded that the stress state increasing can impose uncertainties about the geomechanical behaviour of compacted filtered iron ore tailings due to a possible particle breakage and/or with relevant morphological particles' evolution, which added to the possibility of state changes under high-stress levels for stacking embankment. This investigation about non-linearity of CSL associated with evolution behaviour at the particles level should be an aspect to be considered and carefully studied during the design step.

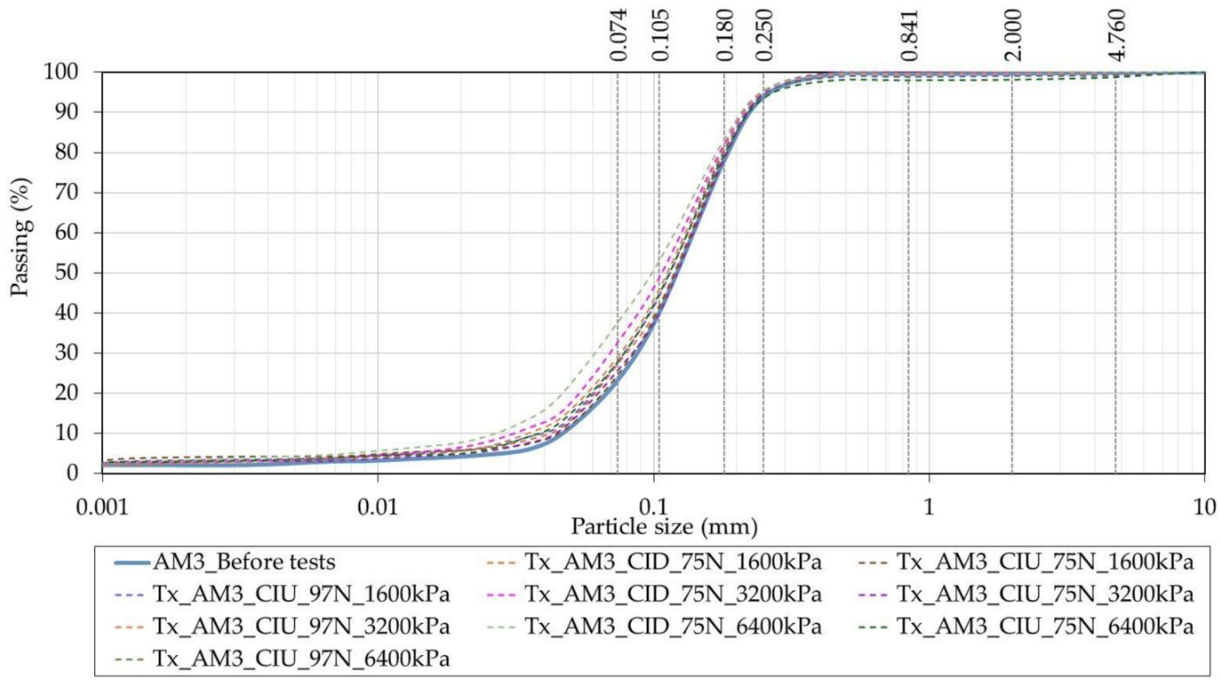

Figure 5: PSD curves before and after some triaxial tests

Acknowledgements

The authors would like to thank Vale S/A mining company for their continued support.

References

ANM, Agência Nacional de Mineração. 2019. *Diário Oficial da União, 2019. 6 p.*, Resolução Nº 13, January 6, 2023 [from Portuguese].

Coop, M.R. 2015. Limitations of a critical state framework applied to the behaviour of natural and 'transitional' soils. *Proc. of the 6th int. symp. on deformation characteristics of geomaterials*, 6. Netherlands. IOS Press: 115-155.

Delgado, B.G, Viana da Fonseca, A, Fortunato, E. and Motta, L.M.G. 2022. Particle morphology's influence on the rail ballast behaviour of a steel slag aggregate. *Environmental Geotechnics*. 9(6): 373-382.

Jefferies, M. and Been, K. 2016. *Soil liquefaction - A Critical State Approach*, 2nd edition. Boca Raton: CRC Press, Taylor & Francis.

Lashkari, A, Falsafizadeh, S.R., Shourijeh, P.T. and Alipour, M.J. 2020. Instability of loose sand in constant volume direct simple shear tests in relation to particle shape. *Acta Geotechnica*. 15(9): 2507–2527.

Li, X.S. and Wang, Y. 1998. Linear representation of steady-state line for sand. *Journal Of Geotechnical and Geoenvironmental Engineering*. 124(12): 1215–1217.

Marques, A., Oliveira, S., Paes, B., Paes, I. and Coelho, A. 2020. Evaluation of liquefaction susceptibility of filtered iron ore tailings from the Iron Quadrangle (Brazil). *Proc. of Paste 2020: 23rd International Conference on Paste, Thickened and Filtered Tailings*. Santiago. Gecamin Publications: 1-9.

Schnaid, F., Bedin, J., Viana da Fonseca, A. and Costa Filho, L.M. 2013. Stiffness and strength governing the static liquefaction of tailings. *Journal of Geotechnical and Geoenvironmental Engineering*. 139(12): 2136–2144.

Schofield, A.N. and Wroth, C.P. 1968. *Critical state soil mechanics*. London: McGraw Hill.

Soares, M. and Viana da Fonseca, A. 2016. Factors affecting steady state locus in triaxial tests. *Geotechnical Testing Journal*. 39(6): 1056–1078.

Velten, R., Consoli, N., Scheuermann Filho, H., Wagner, A., Schnaid, F. and Costa, J.P. 2022. Influence of grading and fabric arising from the initial compaction on the geomechanical characterisation of compacted copper tailings. *Géotechnique*, in Press, https://doi.org/10.1680/jgeot.22.00087.

Verdugo, R. and Ishihara, K. 1996. The steady state of sandy soils. *Soils and Foundations*. 36(2): 81–91.

Viana da Fonseca, A., Cordeiro, D. and Molina-Gómez, F. 2021. Recommended procedures to assess critical state locus from triaxial tests in cohesionless remoulded samples. *Geotechnics*. 1: 95–127.

Viana da Fonseca, A., Cordeiro, D., Molina-Gómez, F., Besenzon, D., Fonseca, A. and Ferreira, C. 2022. The mechanics of iron tailings from laboratory tests on reconstituted samples collected in post-mortem Dam I in Brumadinho. *Soils and Rocks*. 45(2): 1-20.

Yamamuro, J.A. and Lade, P.V. 1998. Steady-state concepts and static liquefaction of silty sands. *Journal of Geotechnical and Geoenvironmental Engineering*. 124(9): 868–877.

Stability Evaluation of Long-Standing Mining Waste Dumps – Case Studies

Paulo Roberto Costa Cella, BVP Engenharia, Brazil
Flávia Augusta Padovani, BVP Engenharia, Brazil
Fábio Marinho da Silva, Former BVP Engenharia, Brazil

Abstract

This article presents an in-depth appreciation of the factors that may affect mining waste dump stability several years after their final disposal geometry has been achieved. Changing conditions encountered in a large number of facilities call for prompt updates on their safety margins. Many dumps have been decommissioned recently or are in the final disposal stage, with transition works to meet Closure requirements being underway or about to get started.

Regarding dumps that remain inactive over decades, a trend to oversimplify earthy waste behavior has led Closure designers to perform stability analysis based on the classical undrained strength approach, even though dozens of years after the end of disposal, excess pore pressure would have been dissipated and slow GWT rising comes up as the only noticeable change in the vast majority of dumps in Brazil. For appropriate decision-making on whether Effective Strength and/or Undrained Strength analyses should be conducted in each case, long-term behavior must be taken into account, as well as mechanical material response and proper longevity stability scenarios.

In the authors' view, a more realistic approach is required for Factor of Safety estimation of long-standing waste dumps, based on the assumption that the facility's behavior in most cases may be governed by intermediate parameters residing somewhere between entirely undrained and effective strength. The proposed methods combine assumptions departing from maximum excess pore pressure, as recorded in undrained lab tests, and assuming a fraction of it potentially being remobilized as groundwater table gradually rises in a long-standing dump. Such approach is about firstly deriving anisotropic consolidation/dissipation paths associated with maximum obliquity of effective principal stresses ratio, based on both typical testing response and numerical modelling. This sounds more realistic for most long-standing waste dumps not having undergone significant prior deformation over post-construction phase.

Introduction

As society at large readily claimed for immediate measures to be taken to ensure mining activities could be safety performed, following the catastrophic failure of Fundão and Brumadinho tailings dams, Brazilian Authorities strove to set up a massive body of regulations within a rather short period of time. Yet to be well ordered, such body of regulations clearly tends to treat contractive soils as potentially responding in similar fashion to classical deformation-induced flow of brittle tailings. Such approach has raised relevant questioning by the mining community, once performing long-term undrained stability analysis was interpreted as a mandatory requirement, with no judicious consideration of soil type by the current set of regulations.

One of the unsuitable standards emerging from that not well-defined approach has considerably impacted Closure design, since it tends to oversimplify the issue by *a priori* considering undrained shear mechanism over long- term behavior of mining facilities, even when additional static loading is no longer expected to apply over the facility lifetime. This potential misconception disregards the substantial difference between the mechanical response of plain, yet contractive, soil and that of brittle, highly sensitive, mining tailings. As a result, reinforcement of a well-performing, long-standing waste dump may entail robust engineered embankments to wrap around the four or five lower benches (nearly 50 meters high), thus bringing about an excessive volume of controlled compaction works.

Undrained failure likelihood over the long term should clearly be part of Closure considerations in a regular basis, although careful efforts should be made to avoid applying an overly conservative engineering approach. This paper specifically discusses how to deal with long-term stability of waste dumps by approaching the effect of the most usual mechanism waste dumps experience over their lifetime: slow groundwater table rise over time.

Engineering Framework

The central idea upholds that a partially drained regime corresponds to the occurrence of some volume variation during actual *in situ* consolidation, that is to say, under the usual stacking rates. In other words, as per the dynamics of a layered waste dump construction, some pore pressure dissipation will take place, simultaneously to the facility formation, and few years later, following construction end, embankment pore pressure will most probably have thoroughly dissipated. Should construction not be resumed, slow and gradual ground water table rising as an isolated event, will not mobilize the classical undrained condition, especially for soils not bearing significant strength loss associated with moderate or large-strain.

However, for safety purposes, an applicable conceptual model cannot be reliably established owing to practical limitations to obtain a unique stress path that stands for a particular partially drained behaviour of a given dump.

Tunning laboratory tests to run tests with particular strain rates to match a particular velocity of pore pressure dissipation sounds far from the current standards. It is unknown which strain rate will comply with, let´s say, 50% pore pressure dissipation once the maximum pore pressure is not known *a priori*.

By verifiable empirical approximation, the dissipation path under the most oblique principal effective stress ratio i.e. the highest K ratio over the consolidation pathway, can be initially established to correspond to a particular solution for the delineation of the partially drained envelope, whose strength ratio will be further away from both the effective strength and the undrained strength (null volumetric variable) envelopes.

Based on this setting, a comprehensive approach for waste dump stability analysis is proposed, within several years following its completion as well as to the closure phase, taken into account the cases of absence of significant post-construction deformations, in which only phreatic surface rise takes place. This has been by far the most frequent long-term loading mechanism for earth-like waste in Brazil.

Mine waste is usually disposed of with low water content, and it is mostly thoroughly consolidated within a few years after dumping completion, most probably before slow GWT rising is completed. Concerning the geotechnical conditions, a fork-like approach applies here:

i) upon very slow saturation rate, it is assumed the soil may be assumed to follow a drained stress path (the CSD path, which keeps q constant with only hydrostatic loading remaining), or

ii) a partially drained condition; but never a fully undrained response (null volumetric strain) as with the laboratory undrained loading (ICU).

Since Type 3 waste is defined as quite frankly contractive material, we assume that some volume change occurs within the upward saturation zone during gradual GWT rise as a "partially drained regime", but not enough to mobilize the maximum excess pore pressure as it is the case with the fully undrained loading. Thus, the assumption made is that just a fraction of the maximum excess pore pressure in shear applies to compute the partially drained strength. An axiomatic generalization of empirical observations stands for the partially drained envelope residing someway between the effective and the fully undrained envelopes. Consequently, a selected fraction of pore pressure is projected onto a consolidation path, which represents a particular locus of effective stress state. On the other hand, the consolidation path is not unique and depends on the obliquity of effective principal stress ratio which varies significantly within a dump. A range of ratios has been detected with the numerical modeling in a Case Study named II, presented further in this paper.

For typical waste soils not undergoing post-peak strain softening, the worst scenario should a slow GWT rising occur, will be mobilization towards the lowest bound of partially drained strength, which in turn, will correspond to highest obliquity of effective stresses ratio. The other potential scenario will be the mobilization of the typically drained regime, consistent with virtually hydrostatic loading, which does not generate a shearing component (q remains constant). In such a drained case, the strength envelope is the effective one or that be associated with the Instability Line (Wan *et al*., 2011; 2013; Junaideen *et al*., 2021).

The approach discussed further in this paper aims at deriving partially drained strength envelope based on the assumption that this particular strength envelope articulates twofold i) with the consolidation path, according to a possible range of the 'obliquity of consolidation stress ratio' and ii) with positive pore pressure fraction (<100%) induced by a volume change resulting from slow rate of GWT rise in the dump.

Physical indexes and typical mechanical response of earthy wastes from Iron Quadrangle, MG

Mining waste are typically composed of earthy materials from iron ore mines, and they have predominantly shown particle size distributions in the silt-sand range and medium to low plastic indexes, as indicated the laboratory tests carried out on the waste dumps located in Brazilian's mining complex. The typical particle size distribution curves are shown in Figure 1.

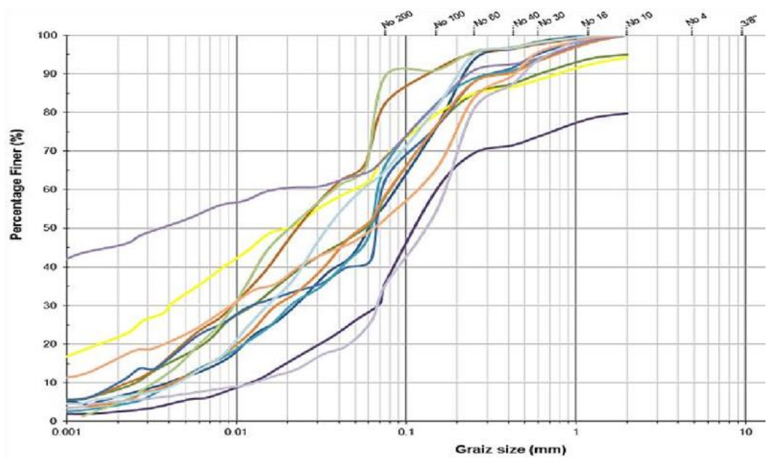

Figure 1. Particle size distribution curves of the mining waste

Conventional disposal methods predominantly comprise spreading thick layers – often more than a meter thick – of loose waste, whereas compaction is attained within the bounds of what the traffic of heavy trucks and dozers operating on site may provide. Water content is not controlled and tests on undisturbed samples usually show degrees of compaction within 80-90% range.

The void ratios found in undisturbed samples ranged between 0.6 and 0.8, with a maximum value of 1.24. In situ density was in the range of 16 to 19 kN/m³, which were consistent with low moisture contents of 0.6 – 7.0 % encountered in shallow depths. Table 1 summarizes the main typical physical properties of the mining waste samples.

Table 1. Typical physical properties of dominant mining waste (undisturbed samples)

Sample ID	Particle size distribution Sand (%)	Silt (%)	Clay (%)	Gravel (%)	Gs	γ_{nat} (kN/m^3)	W_{nat} (%)	LL (%)	PL (%)	PI (%)	e_0
S-01	44.0	43.0	9.0	5.0	2.775	21.03	5.07	41	21	20	0.39
S-02	52.0	26.0	2.0	20.0	2.675	19.27	5.99	30	14	16	0.47
S-03	32.0	41.0	22.0	6.0	2.816	21.71	1.70	45	22	23	0.32
S-04	33.0	59.0	9.0	0.0	2.913	16.77	3.23	36	21	15	0.79
S-05	58.0	31.0	11.0	0.0	2.886	17.69	3.48	35	16	19	0.69
S-06	52.0	43.0	5.0	0.0	2.888	14.03	0.54	28	16	12	1.07
S-07	48.0	47.0	5.0	0.0	2.742	16.72	0.57	36	20	16	0.65
S-08	33.0	62.0	5.0	0.0	2.858	17.99	0.62	40	21	19	0.60
S-07	36.0	19.0	46.0	0.0	2.693	14.25	18.76	59	34	25	1.24
S-10	50.0	44.0	6.0	0.0	2.615	16.19	7.07	34	18	16	0.73
S-11	74.0	21.0	5.0	0.0	3.073	19.18	0.28	19	11	8	0.61
S-12	38.0	55.0	7.0	0.0	2.964	17.25	2.07	34	16	18	0.75

The stress-strain curves and particularly the effective stress paths resulting from the isotropic consolidated, undrained triaxial compression (ICU) tests stands out three typical behaviors, which are pointed out in Figure 2.

Considering the MIT definition, p' is the mean effective stress, $p' = (\sigma'_1 + \sigma'_3)/2$,and q is the shear stress, $q = (\sigma'_1 - \sigma'_3)/2$.

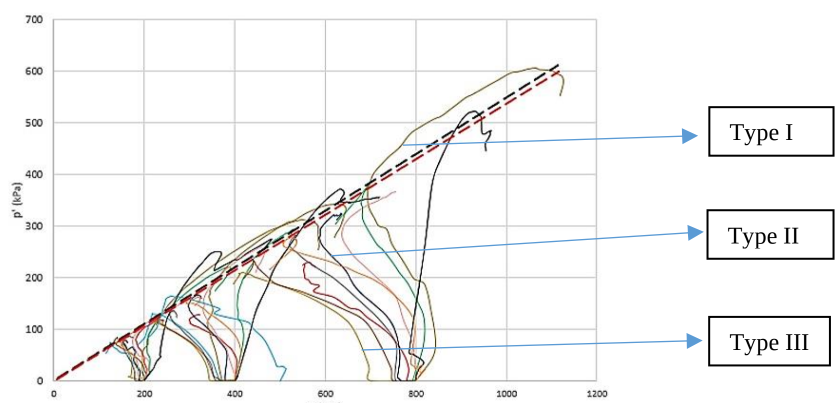

Figure 2. Tipos de comportamento em função das trajetórias de tensão I e II e III

Type I – Reversion from positive excess pore pressure to dissipative regime (pore pressure decrease) at medium axial strain, then increasing the maximum deviatoric strength at larger strain. There is almost no loss of strength in the post-peak, as can be seen in Figure 3.

Types II to III – Positive pore pressure generation almost to the maximum deviatoric strength and slightly brittle behavior at moderate to high confining stresses. Strength losses do not fall short than 10-15% strain as shown in Figure 4 and Figure 5, although pore pressure remains virtually steady to the highest strain attained in tests.

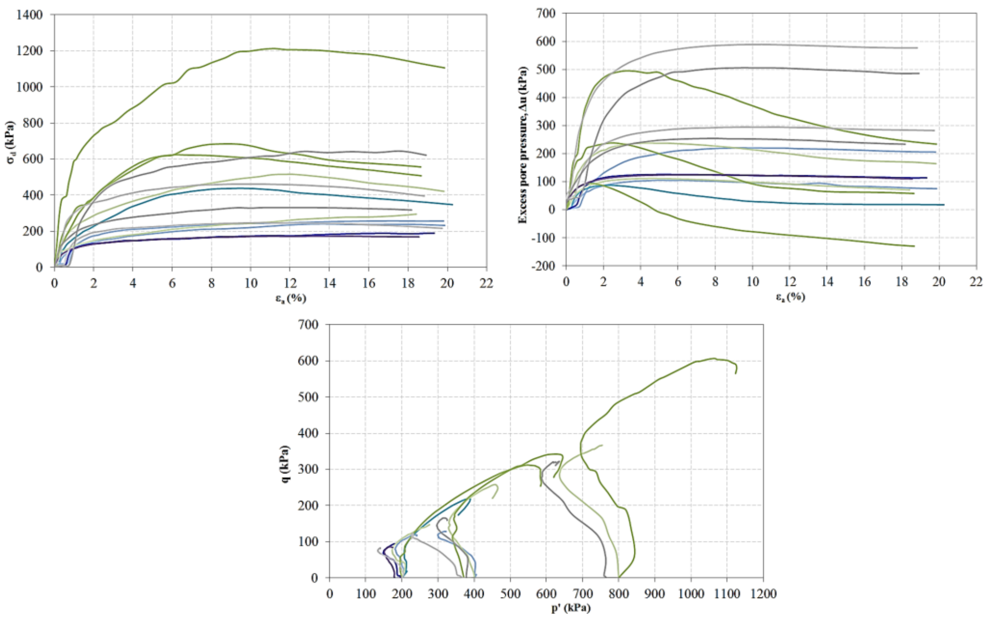

Figure 3. Results of ICU tests with mining waste – Type I

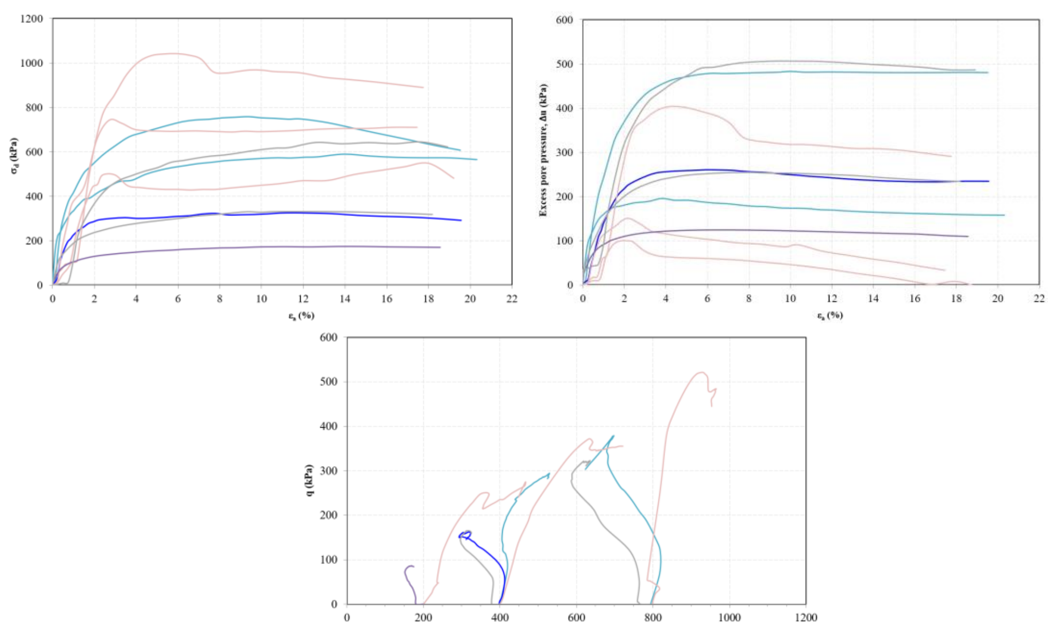

Figure 4. Results of ICU tests with mining waste – Type II

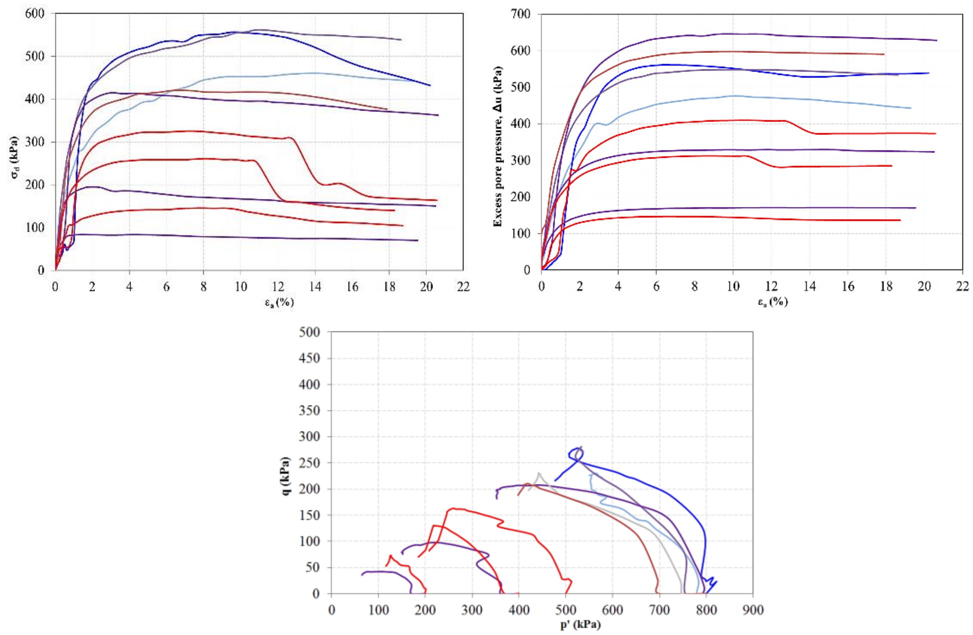

Figure 5. Results of ICU tests with mining waste – Type III

Table 2 summarizes the typical mechanical response of iron ore earthy wastes from a number of laboratory tests of undisturbed samples.

Table 2. Typical mechanical response of dominant mining waste from distinct effective stress paths

Type	Typical Mechanical Response	Notes associated with tests on compacted soils (*)
I	'S' stress paths. Initially positive pore pressure, later decreasing towards negative field. Sample tends to compress on the outset of the test, then expanding from the most oblique stress path point.	Favorable behavior of compacted embankments (Type IV – Cruz, 2004) 42% of the cases studied
II	Positive pore pressure throughout shearing phase. Peak deformations within 10 to 15% range. Well-defined elasto-plastic behavior, with minor post-peak strength loss in moderate to high deformations.	Still acceptable behavior (Type V – Cruz, 2004) 9% of the cases studied
III	Neutral pressure in the positive field throughout shearing phase. Peak deformations lower than 10%. Elasto-plastic behavior, with some post-peak strength loss at large-size deformations.	(Intermediate type, fairly unfavorable, between V and VI, more clayey soil (shale) compacted to lower density levels, Cruz, 2004) 33% of the cases studied, although higher peak deformations have been recorded

(*) Cruz, P. 2nd ed. (2004) – associated with compacted soils in dam sites in Brazil.

Typical mode of failure

For ascertaining the representative mode of failure, it was chosen the test in which the pore pressure reached its maximum value among the complete set of samples and showed no dissipation at large strain as well.

Table 3 shows details of the laboratory records, with particular attention to the onset of the deviatoric stress σ_d falling while the q/p' ratio of 0.53-0.54 sustains consistently near to its maximum value as pore pressure reach around 620 kPa (see ahead the point 1 in Figure 11) at a typical axial strain of 5%.

Table 3. Records of shearing phase of an ICU test

ε_a %	Δu kPa	σ_d kPa	Skempton´s parameter A	p kPa	p' kPa	q kPa	q/p'
0.00	0.0	0.0	0.0	800.0	800.0	0.0	0.00
⋮	⋮	⋮	⋮	⋮	⋮	⋮	⋮
4.35	607.9	413.8	0.73	1006.9	399.0	206.9	0.52
5.02	619.8	410.8	0.75	1005.4	385.7	205.4	0.53
5.70	630.2	408.8	0.77	1004.4	374.2	204.4	0.55
⋮	⋮	⋮	⋮	⋮	⋮	⋮	⋮
20.64	628.3	362.8	0.87	981.4	353.1	181.4	0.51

Focusing on characterizing the nature of the failure of the material, it can be seen that in the selected interval (bounded by dashed lines in Figure 6), the q/p' ratio and pore pressure were close to reaching a steady condition, while deviatoric stress was slightly decreasing. Skempton's parameter A increased smoothly to a high strain magnitude. Such mechanical response stands for a typical gradual failure mechanism. This is a very distinctive feature of earthy waste from loose, brittle tailings tested over a wide range of confining stresses.

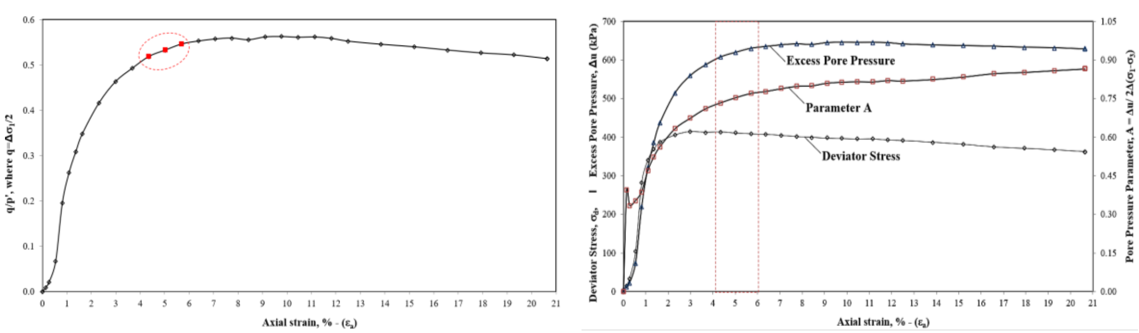

Figure 6. q/p' Chart – Deviatoric stress – Pore pressure – Parameter A vs. Axial strain

Incompatibility of applying undrained analysis to an old stack – Case study I

Stability analyses were performed to verify the validity of the undrained condition hypothesis, with the lower envelope, over each of three life phases of the reference mining waste dump. The first stage represents the end of construction in 2004, the second one eight years later, and the third at the 2021 condition. The stages consider differing changes to the groundwater table at different times. Results indicated that Factor of Safety (FoS) would have been acceptable only at the end of construction, when the GWT was still at its lowest. The increase in the GWT observed in 2012 would have shifted FoS to a marginal condition, and nowadays, the facility would render the dump at limit-equilibrium, as shown in Figure 7.

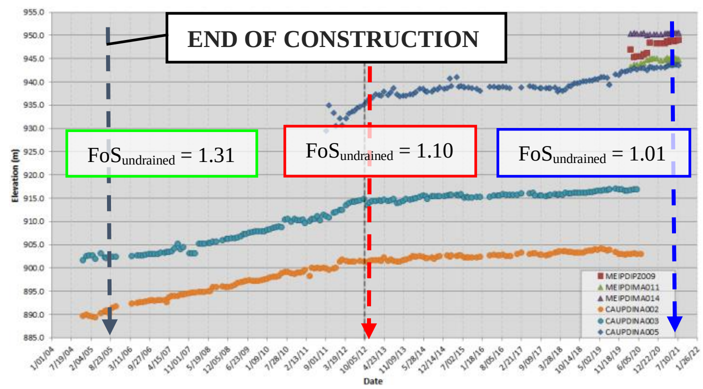

Figure 7. Historical groundwater table and corresponding factors of safety of the reference mining waste dump

This approach basically showed that if full undrained conditions were maintained until the present day, the stack would have stood for ten years under marginal FoS and would have possibly performed poorly, with signs of deformation and overall instability, which clearly was not the case. Under marginal FoS in 2012, Figure 8 shows that mobilized shear strength would have reached its limit on the base of slices 6 to 22, thus suggesting that fully undrained assumption is unlikely to stand eight years after the end of construction, considering the unobservable evidence of deformation or cracking to date.

Therefore, we are left with the analysis of alternative stability conditions consistent with the absence of poor structure performance in nearly 20 years, with the exception of shallow localized slips in non-regraded steep, 10-meter-high operational benches.

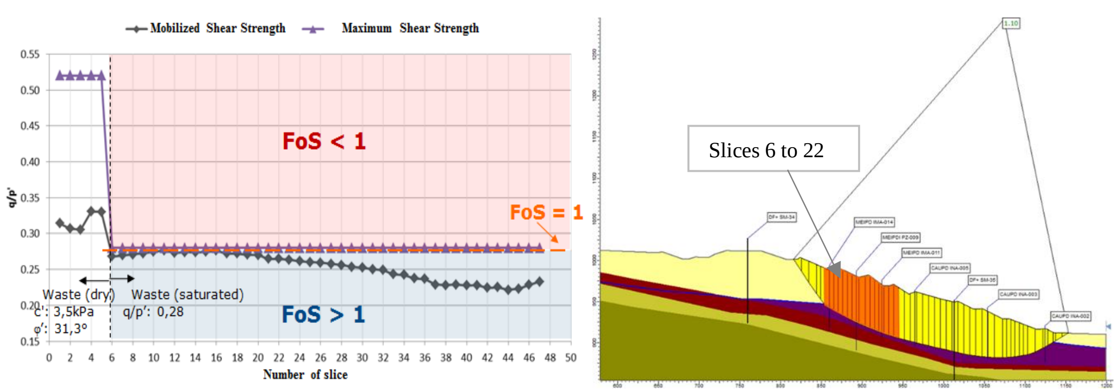

Figure 8. Mobilized vs. available shear strength across the critical slip surface

Raising groundwater table over time

According to the previous item, phreatic surface raise in the stack over time stands for an event occurring somewhat frequently. Consequently, two scenarios associated with hydrostatic loading are described as follows.

Scenario I – Drained behavior

This is about the drained behavior associated with slow phreatic surface rise, without shearing material deformation and no excess pore pressure generation. Only the hydrostatic component can be observed in this scenario at the stack structure, with potential occurrence of an instability zone for downright contractive soils. (Lade, 1992).

Wan et al (2010) discuss the application of a diffusional instability mechanism for porous soils when close to failure under a drained shearing. The authors consider that the stress path in these soils (starting from an initial condition of equilibrium) is represented by a reduction in the mean effective stress without an increase in the deviatoric stress, i.e., a condition in which q is kept constant. This stress path corresponds to a drained increase of the GWT analogous to the expected behavior of excavated and natural saprolitic soils. Such a stress path can be replicated in constant shear drained tests.

Figure 9 from Wan et al (2010) shows stress paths imposed in CSD tests with a progressive decrease in the mean effective stress (p'), while q is kept almost constant in: i) an initially loose soil (Loose #1) and ii) in initially more consolidated soil (Dense #1 and Dense #2), submitted to an initial loading stage under drained conditions.

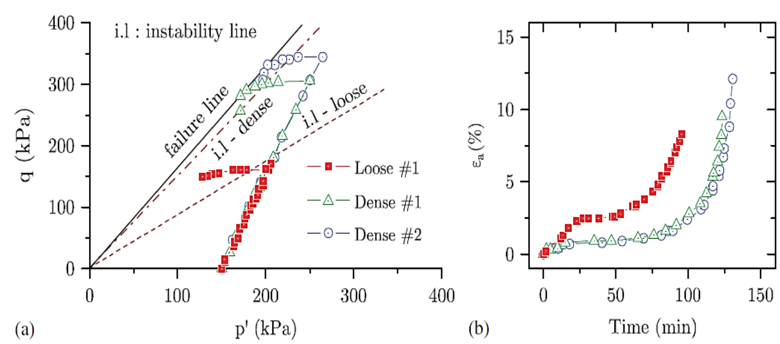

Figure 9. Stress paths of porous materials submitted to CSD tests (Wan, 2010)

Wan et al (2010) observed a trend showing a consistent drop in q as mean stresses p' in the CSD tests got closer to the Instability Line (maximum effective strength on rapid undrained loading from ICU tests), as shown in Figure 10. Notice that the IL can be tracked using quite normal undrained triaxial tests.

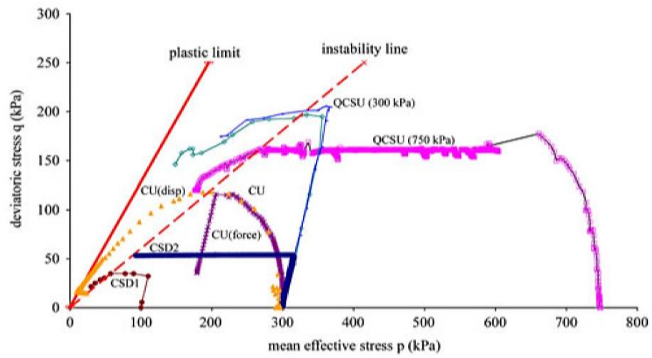

Figure 10. Typical stress paths of porous materials submitted to CSD and ICU tests (Wan, 2012)

Considering that the increase in the GWT under drained condition over long term might cause acceleration of axial strain in the vicinity of the instability point, the IL envelope should be utilized for verifying the Factor of Safety for closure purpose, as shown in Figure 11.

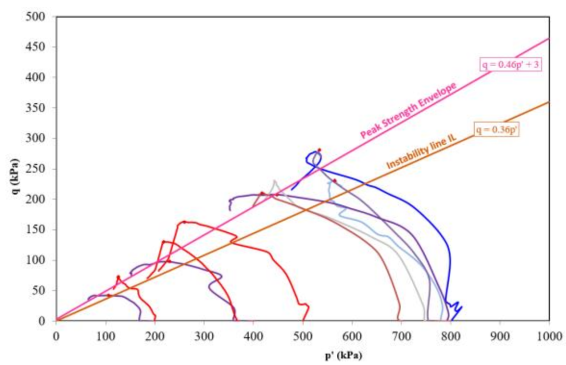

Figure 11. Strength envelopes of mining waste associated with peak (maximum deviatoric) stress and the instability boundary for ICU tests of Type III material

Scenario II – Partially drained behavior

It refers to a partially drained behavior, in which the occurrence of a certain contractive volumetric variation is admitted within the stack saturation area stemming from water level rise, whenever the material is not strain softening or highly sensitive tailings.

Partially drained strength envelope is derived based on the premise that such envelope locus articulates twofold i) with anisotropic consolidation path gradient defined due to potential ratios between major effective stresses of the consolidation process and ii) with an assumed pore pressure portion (lower than the maximum undrained loading) generated by slow material contraction (Type 2 and 3) during gradual water level rise.

Anisotropy in consolidation path – Laboratory tests and numerical modelling of a dump hypothesis

As previously alluded to in this article, classical undrained conditions are likely more strongly associated with the stacking stage, during which waste is placed as thick layers and compacted only partially by trucks and dozers moving in the area, without implementing more strict control to verify the actual compaction degree.

Standards correctly consider for the design phase the undrained envelope derived from ICU tests to ensure safety under a priorly assumed condition of rapid loading, without accounting for excess pore pressure dissipation alongside construction.

A rough assessment of the case study and typical earth-bearing waste showed that, whatever the magnitude of the excess pore pressures generated during stacking, it would take no longer than six years to dissipate the Δu, based on the typical consolidation coefficients, c_v, measured as 300 cm2/hour (fine silt/clayey soils) in consolidation tests.

In order to more closely estimate a Factor of Safety that represents the current condition of the long-standing waste dump, a partially drained strength ratio is expected to shape intermediate to the full undrained strength and the effective strength envelopes.

In connection to the field performance (see section 4), alongside the slow raising of the groundwater table, pore pressure generation may be null in case of fully drained path (see section 5.1) with mobilization of the effective strength or the instability line which has been defined in the most contractive waste samples of Type III. On the other hand, partial pore pressure might result from quasi-drained path, i.e., a combination of some contraction and further dissipation due to the low rate of water table raising, to falls short of the drained loading. Thus, a reference safety update for a long-standing dump should be conceived upon the assumption of partially drained behaviour. Let's assume a fraction of 50% pore pressure generation as a result. Of some slow volumetric change caused by the gradual raising of groundwater table.

In the definition of a 'partially drained' envelope, two hypotheses were considered to estimate a particular envelope at intermediate condition residing between the effective strength and classical undrained one, as described below:

- Hypothesis I: taking into account the maximum pore pressure equalized in a specimen out of the full set of the undrained triaxial tests Type 3 (least favorable), the consolidation path is assumed to occur in proportion to the highest ratio between the principal stresses ((σ'_1; σ'_3). So, for the reference test it is taken the one in which the highest pore pressure took place. The maximum obliquity of the effective principal stress ratio (maximum anisotropy) recorded in the tests was used to compute the slope of the 'line' of consolidation.

- Hypothesis II: uses a numerical model based on a well-documented real case, to compute a range of pore pressure dissipation paths intermediate to the maximum anisotropy ratio (as above but not necessarily the same as in the laboratory test) and a virtual isotropic path (K =1 i.e., parallel to the p' axis). Contrary to the hypothesis based on the well-controlled condition in laboratory, the slope of consolidation path in the field is not unique since it will depend on variables in the dump such as height and distortion effects at its base as connected to the foundation differential settlements. So, in the modelling, a range of effective horizontal to vertical stresses anisotropy bound around each monitored model location to control the slope of consolidation paths in each point. Hydraulic conductivities of the medium were derived from prior calibration of the model to the rate of the settlements measured by a close spaced net of prisms.

Based on the aforementioned hypotheses, a virtual partially drained strength can be derived according to the detected ratio of principal stress anisotropy and be further applied as lower bound strength envelope to supersede the overly conservative full undrained envelope in long-term stability analysis.

Hypothesis I – Laboratory test data

Figure 12 shows the diagram used in the approach employed to estimate the 'partially drained' envelope, considering an assumed 50% generation off the maximum pore pressure recorded in the tests with the Type III behaviour.

The effective stress paths were derived from the confining stresses of about 800 kPa seen in the ICU tests, which is comparable to the dominant effective stresses acting at the base of the slices, corresponding to a mobilized undrained strength of 0.28 (see Figure 7).

In Figure 12, excess pore pressure is represented by the 'distance' in axis p' between point 1, over the effective strength envelope, and point 2, taken over the total stress path (~1 to 1 slope). The effective stress difference between those points corresponds to the test pore pressure reading in the vicinity of soil failure/yielding. For the specimen with the highest pore pressure, the value was approximately 621 kPa.

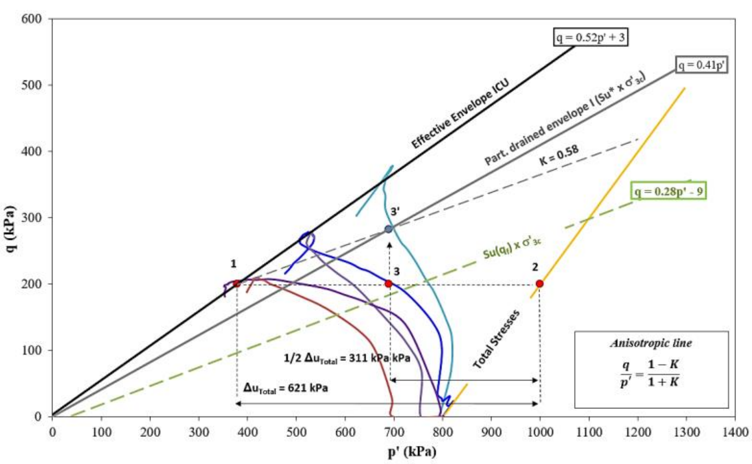

Figure 12. Partially drained strength envelope – Hypothesis I

In connection to the water table raising, an induced pore pressure assumed at 50% is delineated in the 'distance' between points 1 and 2 and corresponds to point 3 in Figure 12. Point 3' is the projection of point 3 onto the consolidation path corresponding to the maximum anisotropy σ'_3/σ'_1 ratio, K = 0.58, extracted over the loading stage from the triaxial laboratory test records. Such anisotropy ratio is assumed as invariable along way the full pore pressure dissipation.

The constant K is the anisotropic stress ratio and represents the ratio of effective minor to major principal stresses for loading condition, differing from the geostatic stress ratio, K_0, as the latter refers to the rest or normally consolidation conditions. In p' - q space, the relation between K and p'/q is:

$$\frac{q}{p'} = \left(\frac{\sigma'_1 - \sigma'_3}{\sigma'_1 + \sigma'_3}\right) = \left(\frac{1-K}{1+K}\right) \tag{1}$$

From point 3', the partially drained envelope starts from the origin to intersect the anisotropic consolidation path at the test highest K of 0.58. This fitting corresponds a q/p' stress ratio of 0.41, herein referred to as 'Partially Drained Strength Envelope I' according to the hypothesis I, seen in Figure 12.

Hypothesis II – Numerical model – Case study II

An alternative way of ascertaining the possible range of anisotropic consolidation paths so that a comparison with the envelope derived from hypothesis I can be made is a numerical model that has been prepared to explore the condition in which not only the dump fill matters but also how foundation features (settlements) may affect the pore pressure dissipation in the waste dump at the monitored near-base points. Thus, the results from the numerical model were also used to derive alternative envelopes for the partially drained condition.

The adopted waste stack cross-section for the numerical model is represented in Figure 13. To test limits of the approach proposed in this article, the numerical model has been developed to simulate the waste dump construction in two phases, applying loading rates deliberately much faster than the practice of ordinary waste dump raising to force stress states nearly to the effective strength envelope for quick, undrained loading.

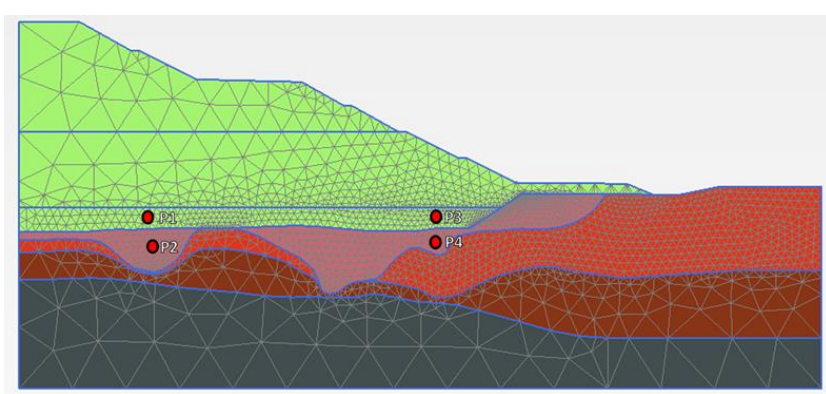

Figure 13. Adopted waste stack cross-section – Numerical model

The foundation of the dump was featured based on a very well-investigated real case, in which four geotechnical units of differential stiffnesses delineate interfaces stressed in shear and inducing considerable differential distortion across the dump base. The foundation model is composed of four materials of increasing strength and stiffness with depth, from soft and compressible saprolitic soil to hard soil, then saprolite, and bedrock along the weathering profile.

The deformational and strength parameters were determined from a number of laboratory testing on the waste and foundation materials, and they are presented in Table 4.

The calculation of in situ stresses in the model's first phase is done by means of gravitational loading, in which the load corresponding to the weight of the materials is applied in small fractions of the soil's volumetric weight and, at the end of the procedure, the stress field equilibrium is checked for unbalanced forces.

After establishing the geostatic stresses, the model simulates the construction of a hypothetical Stockpile over the previously described foundation, with two loading stages. In each stage, the foundation is subjected to a maximum total stress increment ($\Delta\sigma_v$) of approximately 500 kPa. The loading rates were deliberately high in order to induce, in response, a generation of excess pore pressure approximately equal to the applied total stress increment ($\overline{B} \cong 1$).

Table 4. Input parameters of the numerical model

Parameter	Symbol	Material				
		Embankment (mine waste)	Residual soil	Saprolite soil	Saprolite	Weathered Rock
Constitutive Model	-	Hardening Soil	Hardening Soil	Hardening Soil	Hardening Soil	Mohr-Coulomb
Unsaturated unit weight	δ_{unsat} (kN/m^3)	17	16.5	16.5	22	26.5
Drainage type	-	Undrained (A)	Undrained (A)	Undrained (A)	Undrained (A)	Drained
Young's Modulus	E' (kPa)	-	-	-	-	1000000
Poisson's ratio	n	-	-	-	-	0.3
Secant modulus	E_{50} (kPa)	13000	1881	7416	50000	-
Constrained modulus	E_{oed} (kPa)	8000	1506	5939	50000	-

Unloading/reloading modulus	E_{ur} (kPa)	39000	13230	53420	150000	-
Exponent	m	0.5	1	0.65	0.5	-
Initial void ratio	e_i	1.19	1.4	1.15	0.5	-
Effective cohesion	c' (kPa)	3.5	11	11	50	500
Effective friction angle	φ' (°)	31	24	27	28	50
Hydraulic conductivity	k_x (cm/s)	4,50E-05	9,00E-07	1,40E-05	1,90E-03	5,00E-05
	k_y (cm/s)	9,00E-06	9,00E-07	1,40E-05	1,90E-03	5,00E-05

After each loading phase, a stage of consolidation follows, in which all nodal values of excess pore pressure generated during the undrained loading are allowed to dissipate. The consolidation paths are established as the ratio of horizontal to vertical effective stresses σ'_h/σ'_v over the pore pressure dissipation. Table 5 shows the implemented sequence of the numerical model.

In order to evaluate consolidation paths in elements subjected to different stress states, four monitoring points were selected close to the center of the dump as well as in the less confined toe. For these points, the total principal stresses and pore pressures were associated with each time interval (Δt), allowing to the extraction of the effective stress paths (ESP) for each model phase.

It has been shown that slopes of the modelled consolidation paths (in, q/p' space) vary, reflecting horizontal to vertical stress ratios K within 0.53 and 0.78 in the foundation, as shown in Figure 14a. In the dump, the K variation was from 0.46 to 0.60 for a wide range of angular distortion at the base of the dump as represented in Figure 14b.

Table 5. Modelling staged construction

Model phase	Type	Description	Loading rate (m/day)	Flow conditions
Initial	Gravity loading	Generation of in situ stresses	-	Steady State Groundwater flow
Phase 1	Consolidation / Staged construction	1st undrained loading	6,00	Previous Phase
Phase 2	Consolidation / Minimum pore pressure	Dissipation of excess pore pressure generated in Phase 1	-	Minimum pore pressure
Phase 3	Consolidation / Staged construction	2nd undrained loading	6,00	Previous Phase
Phase 4	Consolidation / Minimum pore pressure	Dissipation of excess pore pressure generated in Phase 3	-	Minimum pore pressure

Among those modelled consolidation paths, the K stress ratio that renders the more conservative partially drained strength envelope corresponds to 0.60 and it is delineated alongside the Hypothesis I-derived envelope, in Figure 15. Moreover, for all the monitored points, in each rapid loading cycle, the equilibrium state lies far away from the effective strength envelopes and even mostly beyond the K dashed line.

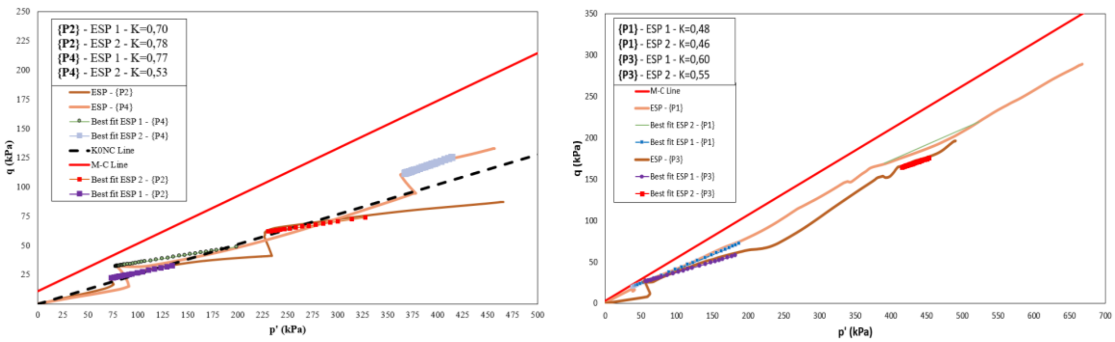

(a) (b)

Figure 14. Consolidation paths and K best fit adjustments at 50% pore pressure dissipation (a) Foundation, with K_0 (dashed line); and (b) Waste dump materials

Looking at the Figure 15, it is also clear that any potential static trigger for undrained behavior, namely the deformation flow, i.e., with no incremental rapid loading, would only be plausible if the materials were strongly brittle, with remarkable softening at large strain, which has been proved not to be the case for the vast majority of the mining waste tested from iron ore mines in Brazil.

It must be emphasized that the required magnitude of any possible static trigger after the consolidation is completed should be even larger than the magnitude of the undrained loading brought about by the rapid construction rate itself.

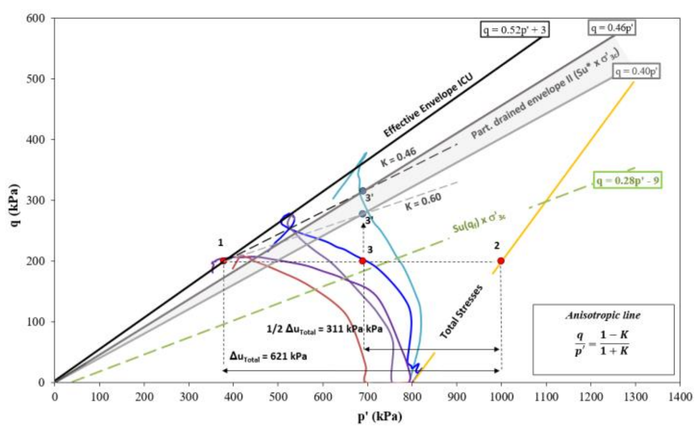

Figure 15. Range of Partially drained strength envelope as a function of distinct anisotropy consolidation paths – Hypothesis II

Scenarios to be considered in stability analysis for Closure

The analysis scenarios presented in Table 6 were used for the safety review of the reference mining waste dump.

The results of the stability analysis performed for the mining waste dump described in this article are also summarized in Table 6.

The minimum Factors of Safety met the requirements stipulated in Brazilian standard NBR 13.029/2017 and in National Mining Agency (ANM) Resolution 130/2022 for mining waste dump.

The summary of the strength envelopes considered for the mining waste in this analysis is represented in Figure 16.

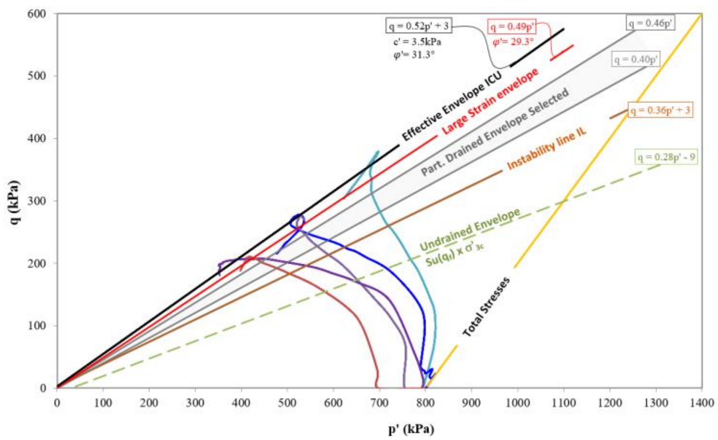

Figure 16. All-around strength envelope scenarios concerning the slow rise of the GWT over time for waste dump stability

Table 6. Stability analysis scenarios considered for the Case Study Dump

Scenario			Waste Strength		Objective	Factor of Safety	
#	**Analysis**	**GWT**	**Saturated**	**Non Saturated**		**Min.**	**Obtained**
0	End of construction	GWT 2004	Undrained envelope S_u/σ'_{3c}: 0.28	ICU Effective Envelope c'= 3.5kPa φ'= 31.3°	Estimate the FoS at maximum pore pressure induced by the construction of the waste dump.	1.3	1.31
1	10 years back	GWT 2012	Undrained envelope S_u/σ'_{3c}: 0.28	c'= 3.5kPa φ'= 31.3°	Estimate the FoS if a condition of maximum pore pressure induced by the construction of the waste dump is sustained.	1.3	1.10
2	Long term	Current GWT	Partially drained envelope (1) S_u/σ'_{3c}: 0.40-0.46	c'= 3.5kPa φ'= 31.3°	Estimate the FoS considering a condition of partial dissipation (50%) of the maximum pore pressure seen in ICU tests.	-	1.42-1.60

3	Long term	Current GWT	ICU Effective Envelope c' = 3.5 kPa φ' = 31°	c'= 3.5kPa φ'= 31.3°	Condition in which the waste dump would find itself with excess pore pressure almost entirely dissipated and current GWT as hydrostatic head.	1.3	1.84
4	Long term	Current GWT	Large Strain Envelope c' = 0 kPa φ' = 29.3°	c'= 3.5kPa φ'= 31.3°	Simulation covering the hypothetical large strain scenario.	1.5	1.80
5	Long term	GWT 2012 / current	Instability Line (2) S_u/σ'_{3c}: 0.39	c'= 3.5kPa φ'= 31.3°	Estimate the FoS considering a mechanism of diffusional instability in the waste embankment, a case in which mean effective stress nears the IL.	1.2-1.3 (3)	1.45

Notes

1. Prior to decide for the partially drained approach it is strongly suggested to pay careful attention to the past performance of the dump. In presence of strain softening materials, even a small increment in strain after construction may allow a previously overstressed material to resume undrained shearing along a pre-formed potential slide surface. In this case, the authors highly recommend checking the factor of safety using the classical undrained analysis.

2. Case in which failure might be triggered by slow increases in the groundwater table under drained conditions assuming the potential for Diffusional Instability of the Type 3 material. The verification was performed considering the ground water level conditions in effect in 2012 and 2021, as illustrated in scenario 5.

3. Source: Hawley and Cunning (2017). Depend on the consequence

Final Remarks and Conclusions

The present article has discussed the main design aspects to be taken into account for the safety assessment of long-standing waste dumps. Two cases studies involving waste dumps located in Brazil's mining complex were used as the basis.

The chances of achieving full undrained strength mobilization, as observed in rapid undrained loading test, occurring in a waste dump in which construction ended decades ago, is very remote, especially when the materials are not undergoing strain-softening or are not highly sensitive. Alternative scenarios of mobilized strength involving drained, effective or partially drained conditions are more realistic, whether dealing with earthy wastes, although contractive, are each featured by non-strength loss after their peak resistance.

Partially drained strength envelopes can be addressed consistently with assumptions on fractions of pore pressure generation due to some contraction of the soil in depths slowly saturated by raising of the groundwater table over time. Further on, hypotheses comprising a range of predicted anisotropic consolidation paths under distinct principal stresses obliquity are required to enable delineation of the partially drained strength envelopes.

In short, if the groundwater table raises alongside the aging of the mining waste dump, the following scenarios presented in Table7 must be considered. The terms USA and ESA in Table 7 correspond to undrained and effective strength analysis, respectively.

Table 7. Authors' recommendations for long-standing mining waste dump stability analysis

Previous signs of a poor performance	Factor of Safety at the end of construction	Scenario applicable over post-construction / closure (minimum FoS according to existing regulations)	Comments
Absent, but slow raise of the groundwater table	USA – Minimum 1,3 ESA – Minimum 1,5	Long term, drained diffuse instability (LI) – if full contractive Long term, partially drained with hypothesis of partial pore pressure generation in slowly saturated zone Long term, drained (effective) Seismic trigger, undrained	Check for large strain if some loss of strength after peak occurs; Use the lowest static FoS for checking drainage works, if decided for adjoining that with a buttress
Cracking; evidence of deformation; bulging of the toe of the dump, relevant displacements from monitoring or visually observable	Review strength parameters for either ESA and USA scenarios	Long term (drained w/ Ru) Long term (USA – full undrained analysis) Residual strength scenario Seismic trigger (undrained)	Use FoS fully undrained strength for buttress sizing

It must be emphasized that the approach is not suitable for highly brittle soils or those showing strain-softening at large strains. Rather, it complies well with materials that undergo gradual failure, which, in turn, are more prone to develop partially drained shearing. It has been verified that materials like these are dominant in most existing earthy waste dumps in iron mines in Brazil.

It is important to apply a rigorous evaluation on the potential of static triggers to set off undrained shear mechanism. In the Case Study I, the mining waste has shown no tendency, in the full campaign of triaxial undrained strength tests, to present meaningful loss of strength after the peak, even when contraction took place all over the tests strain range. In such a condition, once excess pore pressure is fully dissipated to the effective stress condition, a static trigger would require stress changes potentially higher in magnitude as compared to the stresses imposed by extra-rapid construction stage modelled as nearly ten times faster of the usual rates.

This paper does not presume to have the final say on the safety assessment of long-standing mining waste dumps or for closure scenario; rather, it intends to draw attention to and deepen discussions about the complex choice of representative scenarios and respective strength parameters applicable to the stability analysis of old mining waste dumps that have shown no prior signs of instability spanning the life of these facilities.

If, for the sake of simplicity, only the USA scenario is chosen, it can result oversized reinforcements through engineered embankments to wrap around the four or five lower benches (perhaps 50 meters high), thus rendering exaggerated volume of controlled compaction.

Hence, a meticulous selection of representative analysis scenarios of the current stack status, in view of its operational and post-construction history, may result in reduced requirement for mobilization of additional borrow material and constructed footprint during the Facility Decharacterization phase.

References

ABNT NBR 13029. 2017. Mineração – Elaboração e apresentação de projeto de disposição de estéril em pilha. (in Portuguese).

ANM Resolution 13. 2017. (in Portuguese).

Cella, P. R. C. and Padovani, F. A. 2021. Five Brazilian tailings – from laboratory and field data towards safer design criteria. *Proceedings of the Tailings 2021 conference*.

Cruz, P. T. D. 2004. *100 barragens brasileiras: casos históricos, materiais de construção, projeto*. Oficina de Textos (in Portuguese)

Duncan J. M., Wright S. G. and Brandon T. L. 2014. *Soil Strength and Slope Stability*. Hoboken: John Wiley & Sons.

Hawley, M. and Cunning, J. 2017. *Guidelines for mine waste dump and stockpile design*. CSIRO Publishing.

Junaideen, S. M., Tham, L. G., and Lee, C. F. 2021. Instability of compacted residual soil. *J. of Geosciences*. 11(10): 403.

Lade, P.V. 1992. Static instability and liquefaction of loose fine sandy slopes. ASCE J. Geotechnical. Eng. 1992, 118, 51–71.

Wan, R. G., Pinheiro, M. and Guo, P. J. 2011. Elastoplastic modelling of diffuse instability response of geomaterials. *International Journal for Numerical and Analytical Methods in Geomechanics*. 35(2), 140-160.

Wan, R., Pinheiro, M., Daouadji, A., Jrad, M. and Darve, F. 2013. Diffuse instabilities with transition to localization in loose granular. *International Journal for numerical and analytical methods in geomechanics*. 37(10): 1292–1311.